Radboud Repository

Radboud University Nijmegen

PDF hosted at the Radboud Repository of the Radboud University Nijmegen

The following full text is a publisher's version.

For additional information about this publication click this link.
http://hdl.handle.net/2066/201606

Please be advised that this information was generated on 2019-06-02 and may be subject to change.

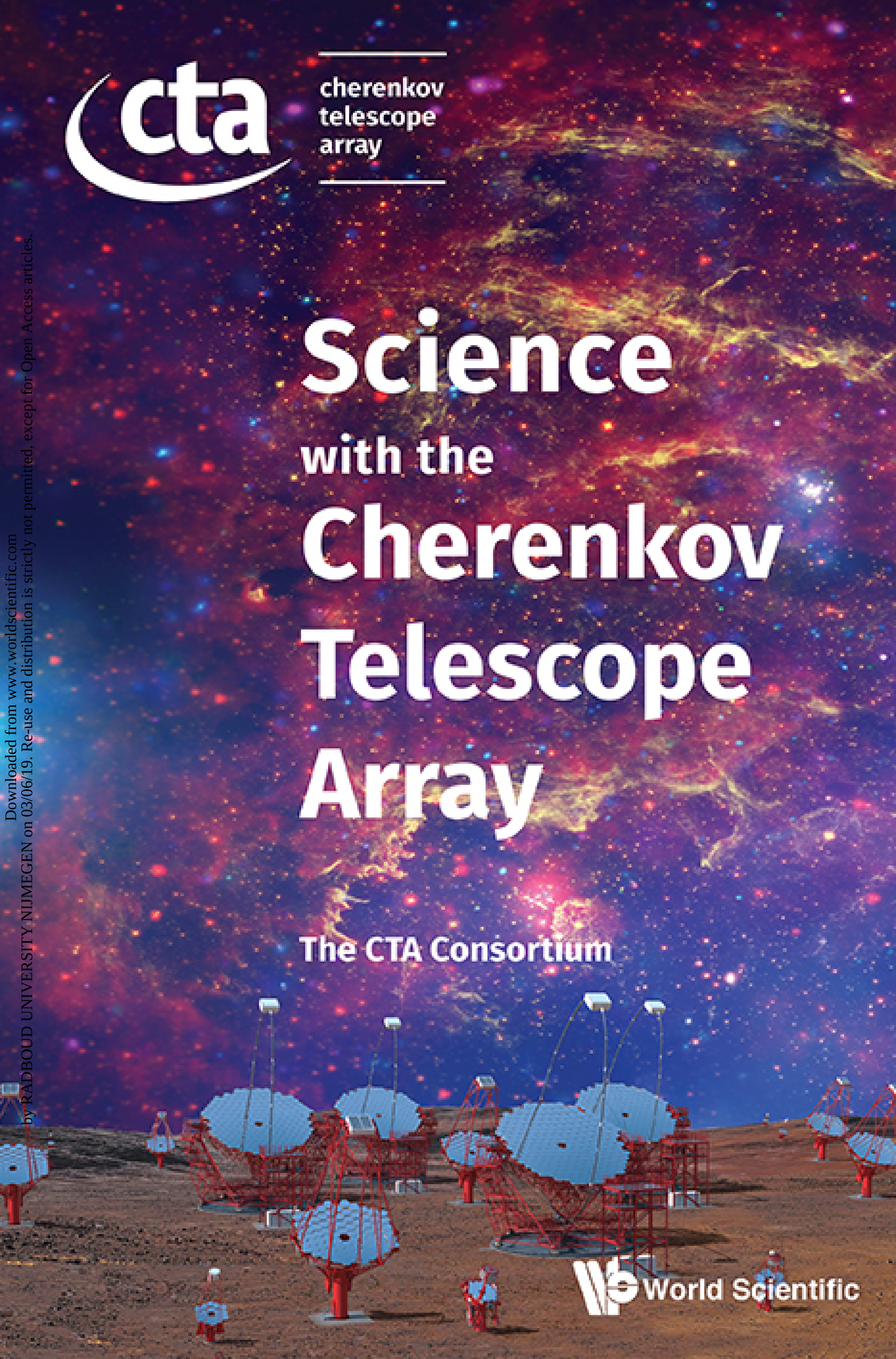

cta
cherenkov
telescope
array

Science with the Cherenkov Telescope Array

The CTA Consortium

World Scientific

Science
with the
Cherenkov
Telescope
Array

Other Related Titles from World Scientific

Cherenkov Reflections: Gamma-Ray Imaging and the Evolution of TeV Astronomy
by David Fegan
ISBN: 978-981-3276-85-7

Neutrino Astronomy: Current Status, Future Prospects
edited by Thomas Gaisser and Albrecht Karle
ISBN: 978-981-4759-40-3

An Overview of Gravitational Waves: Theory, Sources and Detection
edited by Gerard Auger and Eric Plagnol
ISBN: 978-981-3141-75-9

The Encyclopedia of Cosmology
(In 4 Volumes)
Volume 1: Galaxy Formation and Evolution
Volume 2: Numerical Simulations in Cosmology
Volume 3: Dark Energy
Volume 4: Dark Matter
Editor-in-chief: Giovanni G Fazio
by Rennan Barkana, Shinji Tsujikawa and Jihn E Kim
edited by Kentaro Nagamine
ISBN: 978-981-4656-19-1 (Set)
ISBN: 978-981-4656-22-1 (Vol. 1)
ISBN: 978-981-4656-23-8 (Vol. 2)
ISBN: 978-981-4656-24-5 (Vol. 3)
ISBN: 978-981-4656-25-2 (vol. 4)

Science with the Cherenkov Telescope Array

The CTA Consortium

World Scientific

NEW JERSEY • LONDON • SINGAPORE • BEIJING • SHANGHAI • HONG KONG • TAIPEI • CHENNAI • TOKYO

Published by

World Scientific Publishing Co. Pte. Ltd.
5 Toh Tuck Link, Singapore 596224
USA office: 27 Warren Street, Suite 401-402, Hackensack, NJ 07601
UK office: 57 Shelton Street, Covent Garden, London WC2H 9HE

Library of Congress Cataloging-in-Publication Data
Names: CTA Consortium (Organization)
Title: Science with the Cherenkov Telescope Array / by The CTA Consortium.
Description: New Jersey : World Scientific, 2018. | Includes bibliographical references.
Identifiers: LCCN 2018017444| ISBN 9789813270084 (hardcover : alk. paper) |
ISBN 981327008X (hardcover : alk. paper)
Subjects: LCSH: Gamma ray astronomy. | Astronomy. | Cherenkov Telescope Array (Observatory)
Classification: LCC QB471 .S35 2018 | DDC 522/.6862--dc23
LC record available at https://lccn.loc.gov/2018017444

British Library Cataloguing-in-Publication Data
A catalogue record for this book is available from the British Library.

Copyright © 2019 by The CTA Consortium

This is an Open Access book published by World Scientific Publishing Company. It is distributed under the terms of the Creative Commons Attribution-Non Commercial 4.0 (CC BY-NC) License. Further distribution of this work is permitted, provided the original work is properly cited.

For any available supplementary material, please visit
https://www.worldscientific.com/worldscibooks/10.1142/10986#t=suppl

Desk Editor: Ng Kah Fee

Typeset by Stallion Press
Email: enquiries@stallionpress.com

Printed in Singapore

Executive Summary

The Cherenkov Telescope Array (CTA), will be the major global observatory for very high-energy (VHE) gamma-ray astronomy over the next decade and beyond. The scientific potential of CTA is extremely broad: from understanding the role of relativistic cosmic particles to the search for dark matter. CTA is an explorer of the extreme universe, probing environments from the immediate neighbourhood of black holes to cosmic voids on the largest scales. Covering a huge range in photon energy from 20 GeV to 300 TeV, CTA will improve on all aspects of performance with respect to current instruments. Wider field of view and improved sensitivity will enable CTA to survey hundreds of times faster than previous TeV telescopes. The angular resolution of CTA will approach 1 arc-minute at high energies — the best resolution of any instrument operating above the X-ray band — allowing detailed imaging of a large number of gamma-ray sources. A one to two order-of-magnitude collection area improvement makes CTA a powerful instrument for time-domain astrophysics, three orders of magnitude more sensitive on hour timescales than Fermi-LAT at 30 GeV. The observatory will operate arrays on sites in both hemispheres to provide full sky coverage and will hence maximise the potential for the rarest phenomena such as very nearby supernovae, gamma-ray bursts, or gravitational wave transients. With 99 telescopes on the southern site and 19 telescopes on the northern site, flexible operation will be possible, with sub-arrays available for specific tasks.

CTA will have important synergies with many of the new generation of major astronomical and astroparticle observatories. Multi-wavelength (MWL) and multi-messenger (MM) approaches combining CTA data with those from other instruments will lead to a deeper understanding of the broad-band non-thermal properties of target sources, elucidating the nature, environment, and distance of gamma-ray emitters. Details of synergies in each waveband are presented.

The CTA Observatory will be operated as an open, proposal-driven observatory, with all data available on a public archive after a predefined proprietary period (of typically one year). Scientists from institutions worldwide have combined together to form the CTA Consortium. This Consortium has prepared a proposal for a Core Programme of highly motivated observations. The programme, encompassing approximately 40% of the available observing time over the first 10 years of CTA operation, is made up of individual Key Science Projects (KSPs), which are presented in the subsequent chapters. The science cases have been prepared over several years by the CTA Consortium, with community input gathered via a series of workshops connecting CTA to neighbouring communities. A major element of the programme is the search for dark matter via the annihilation signature of weakly interacting massive particles (WIMPs). The strategy for dark matter detection presented here places the expected cross-section for a thermal relic within reach of CTA for a wide range of WIMP masses from ∼200 GeV to 20 TeV. This makes CTA extremely complementary to other approaches, such as high-energy particle collider and direct-detection experiments. CTA will also conduct a census of particle acceleration over a wide range of astrophysical objects, with quarter-sky extragalactic, full-plane Galactic, and Large Magellanic Cloud surveys planned. Additional KSPs are focused on transients, acceleration up to PeV energies in our own Galaxy, active galactic nuclei, star-forming systems on a wide range of scales, and the Perseus cluster of galaxies. All provide high-level data products which will benefit a wide community, and together they will provide a long-lasting legacy for CTA.

Finally, while designed for the detection of gamma rays, CTA has considerable potential for a range of astrophysics and astroparticle physics based on charged cosmic-ray observations and the use of the CTA telescopes for optical measurements.

Authors

The Cherenkov Telescope Array Consortium:

B.S. Acharya[1], I. Agudo[2], I. Al Samarai[3], R. Alfaro[4], J. Alfaro[5], C. Alispach[3], R. Alves Batista[6], J.-P. Amans[7], E. Amato[8], G. Ambrosi[9], E. Antolini[10], L.A. Antonelli[11], C. Aramo[12], M. Araya[13], T. Armstrong[6], F. Arqueros[14], L. Arrabito[15], K. Asano[16], M. Ashley[17], M. Backes[18], C. Balazs[19], M. Balbo[20], O. Ballester[21], J. Ballet[22], A. Bamba[23], M. Barkov[24], U. Barres de Almeida[25], J.A. Barrio[14], D. Bastieri[26], Y. Becherini[27], A. Belfiore[28], W. Benbow[29], D. Berge[30], E. Bernardini[30], M.G. Bernardini[15], M. Bernardos[31], K. Bernlöhr[32], B. Bertucci[9], B. Biasuzzi[33], C. Bigongiari[11], A. Biland[34], E. Bissaldi[35], J. Biteau[33], O. Blanch[21], J. Blazek[36], C. Boisson[7], J. Bolmont[37], G. Bonanno[38], A. Bonardi[39], C. Bonavolontà[12], G. Bonnoli[10], Z. Bosnjak[40], M. Böttcher[41], C. Braiding[17], J. Bregeon[15], A. Brill[42], A.M. Brown[43], P. Brun[15], G. Brunetti[44], T. Buanes[45], J. Buckley[46], V. Bugaev[46], R. Bühler[30], A. Bulgarelli[47], T. Bulik[48], M. Burton[49], A. Burtovoi[50], G. Busetto[26], R. Canestrari[10], M. Capalbi[51], F. Capitanio[52], A. Caproni[53], P. Caraveo[28], V. Cárdenas[54], C. Carlile[55], R. Carosi[56], E. Carquín[13], J. Carr[57], S. Casanova[58,32], E. Cascone[59], F. Catalani[60], O. Catalano[51], D. Cauz[61], M. Cerruti[37], P. Chadwick[43], S. Chaty[22], R.C.G. Chaves[15], A. Chen[62], X. Chen[5], M. Chernyakova[63], M. Chikawa[64], A. Christov[3], J. Chudoba[36], M. Cieślar[48], V. Coco[3], S. Colafrancesco[62], P. Colin[65], V. Conforti[47], V. Connaughton[177], J. Conrad[66], J.L. Contreras[14], J. Cortina[21], A. Costa[38], H. Costantini[57], G. Cotter[6], S. Covino[10], R. Crocker[67], J. Cuadra[5], O. Cuevas[54], P. Cumani[21], A. D'Aì[51],

F. D'Ammando[44], P. D'Avanzo[10], D. D'Urso[9], M. Daniel[29], I. Davids[18], B. Dawson[68], F. Dazzi[69], A. De Angelis[26], R. de Cássia dos Anjos[70], G. De Cesare[47], A. De Franco[6], E.M. de Gouveia Dal Pino[71], I. de la Calle[14], R. de los Reyes Lopez[32,a], B. De Lotto[61], A. De Luca[28], M. De Lucia[12], M. de Naurois[72], E. de Oña Wilhelmi[73], F. De Palma[74], F. De Persio[75], V. de Souza[76], C. Deil[32], M. Del Santo[51], C. Delgado[31], D. della Volpe[3], T. Di Girolamo[12], F. Di Pierro[77], L. Di Venere[78], C. Díaz[31], C. Dib[13], S. Diebold[79], A. Djannati-Ataï[80], A. Domínguez[14], D. Dominis Prester[40], D. Dorner[81], M. Doro[26], H. Drass[5], D. Dravins[55], G. Dubus[82], V.V. Dwarkadas[83], J. Ebr[36], C. Eckner[84], K. Egberts[85], S. Einecke[86], T.R.N. Ekoume[3], D. Elsässer[86], J.-P. Ernenwein[57], C. Espinoza[5], C. Evoli[87], M. Fairbairn[88], D. Falceta-Goncalves[89], A. Falcone[90], C. Farnier[66], G. Fasola[7], E. Fedorova[91], S. Fegan[72], M. Fernandez-Alonso[92], A. Fernández-Barral[21], G. Ferrand[24], M. Fesquet[93], M. Filipovic[94], V. Fioretti[47], G. Fontaine[72], M. Fornasa[95], L. Fortson[96], L. Freixas Coromina[31], C. Fruck[65], Y. Fujita[97], Y. Fukazawa[98], S. Funk[99], M. Füßling[30], S. Gabici[80], A. Gadola[100], Y. Gallant[15], B. Garcia[101], R. Garcia López[102], M. Garczarczyk[30], J. Gaskins[95], T. Gasparetto[103], M. Gaug[104], L. Gerard[30], G. Giavitto[30], N. Giglietto[35], P. Giommi[11], F. Giordano[78], E. Giro[50], M. Giroletti[44], A. Giuliani[28], J.-F. Glicenstein[105], R. Gnatyk[91], N. Godinovic[106], P. Goldoni[80], G. Gómez-Vargas[5], M.M. González[4], J.M. González[107], D. Götz[22], J. Graham[43], P. Grandi[47], J. Granot[108], A.J. Green[109], T. Greenshaw[110], S. Griffiths[21], S. Gunji[111], D. Hadasch[16], S. Hara[112], M.J. Hardcastle[113], T. Hassan[21], K. Hayashi[114], M. Hayashida[16], M. Heller[3], J.C. Helo[13], G. Hermann[32], J. Hinton[32,*], B. Hnatyk[91], W. Hofmann[32], J. Holder[115], D. Horan[72], J. Hörandel[39], D. Horns[116], P. Horvath[117], T. Hovatta[118], M. Hrabovsky[117], D. Hrupec[119], T.B. Humensky[42], M. Hütten[30], M. Iarlori[87], T. Inada[16], Y. Inome[120], S. Inoue[24], T. Inoue[114], Y. Inoue[121], F. Iocco[122], K. Ioka[123], M. Iori[75], K. Ishio[65], Y. Iwamura[16], M. Jamrozy[124], P. Janecek[36], D. Jankowsky[99], P. Jean[125], I. Jung-Richardt[99], J. Jurysek[36], P. Kaaret[126], S. Karkar[37], H. Katagiri[127], U. Katz[99], N. Kawanaka[128], D. Kazanas[129], B. Khélifi[80], D.B. Kieda[130], S. Kimeswenger[131], S. Kimura[132], S. Kisaka[133], J. Knapp[30], J. Knödlseder[125], B. Koch[5], K. Kohri[134], N. Komin[62], K. Kosack[22], M. Kraus[99], M. Krause[30], F. Krauß[95], H. Kubo[128], G. Kukec Mezek[84], H. Kuroda[16], J. Kushida[132], N. La Palombara[28], G. Lamanna[135], R.G. Lang[76], J. Lapington[136], O. Le Blanc[7], S. Leach[136], J.-P. Lees[135], J. Lefaucheur[7], M.A. Leigui de Oliveira[137], J.-P. Lenain[37], R. Lico[44], M. Limon[42], E. Lindfors[118], T. Lohse[138], S. Lombardi[11], F. Longo[103],

M. López[14], R. López-Coto[32], C.-C. Lu[32], F. Lucarelli[11],
P.L. Luque-Escamilla[139], E. Lyard[20], M.C. Maccarone[51], G. Maier[30],
P. Majumdar[140], G. Malaguti[47], D. Mandat[36], G. Maneva[141],
M. Manganaro[102], S. Mangano[31], A. Marcowith[15], J. Marín[54], S. Markoff[95],
J. Martí[139], P. Martin[125], M. Martínez[21], G. Martínez[31], N. Masetti[47,107],
S. Masuda[128], G. Maurin[135], N. Maxted[17], D. Mazin[16,65], C. Medina[142],
A. Melandri[10], S. Mereghetti[28], M. Meyer[143], I.A. Minaya[110], N. Mirabal[14],
R. Mirzoyan[65], A. Mitchell[32], T. Mizuno[144], R. Moderski[145],
M. Mohammed[146], L. Mohrmann[99], T. Montaruli[3], A. Moralejo[21],
D. Morcuende-Parrilla[14], K. Mori[147], G. Morlino[87], P. Morris[6],
A. Morselli[148], E. Moulin[105], R. Mukherjee[42], C. Mundell[149], T. Murach[30],
H. Muraishi[150], K. Murase[16], A. Nagai[3], S. Nagataki[24], T. Nagayoshi[151],
T. Naito[112], T. Nakamori[111], Y. Nakamura[152], J. Niemiec[58], D. Nieto[14],
M. Nikołajuk[153], K. Nishijima[132], K. Noda[21], D. Nosek[154],
B. Novosyadlyj[155], S. Nozaki[128], P. O'Brien[136], L. Oakes[138], Y. Ohira[133],
M. Ohishi[16], S. Ohm[30], N. Okazaki[16], A. Okumura[152], R.A. Ong[156,*],
M. Orienti[44], R. Orito[157], J.P. Osborne[136], M. Ostrowski[124], N. Otte[158],
I. Oya[30], M. Padovani[15], A. Paizis[28], M. Palatiello[103], M. Palatka[36],
R. Paoletti[56], J.M. Paredes[159], G. Pareschi[10], R.D. Parsons[32], A. Pe'er[65],
M. Pech[36], G. Pedaletti[30], M. Perri[11], M. Persic[160,61], A. Petrashyk[42],
P. Petrucci[82], O. Petruk[161], B. Peyaud[105], M. Pfeifer[99], G. Piano[52],
A. Pisarski[153], S. Pita[80], M. Pohl[85], M. Polo[31], D. Pozo[54], E. Prandini[26],
J. Prast[135], G. Principe[99], D. Prokhorov[27], H. Prokoph[95], M. Prouza[36],
G. Pühlhofer[79], M. Punch[80,27], S. Pürckhauer[32], F. Queiroz[32],
A. Quirrenbach[146], S. Rainò[78], S. Razzaque[162], O. Reimer[163],
A. Reimer[163], A. Reisenegger[5], M. Renaud[15], A.H. Rezaeian[13],
W. Rhode[86], D. Ribeiro[42], M. Ribó[159], T. Richtler[164], J. Rico[21],
F. Rieger[32], M. Riquelme[165], S. Rivoire[15], V. Rizi[87], J. Rodriguez[22],
G. Rodriguez Fernandez[148], J.J. Rodríguez Vázquez[31], G. Rojas[166],
P. Romano[10], G. Romeo[38], J. Rosado[14], A.C. Rovero[92], G. Rowell[68],
B. Rudak[145], A. Rugliancich[56], C. Rulten[96], I. Sadeh[30], S. Safi-Harb[167],
T. Saito[16], N. Sakaki[16], S. Sakurai[16], G. Salina[148], M. Sánchez-Conde[66],
H. Sandaker[168], A. Sandoval[4], P. Sangiorgi[51], M. Sanguillon[15], H. Sano[114],
M. Santander[42], S. Sarkar[6], K. Satalecka[30], F.G. Saturni[11], E.J. Schioppa[3],
S. Schlenstedt[30], M. Schneider[169], H. Schoorlemmer[32], P. Schovanek[36],
A. Schulz[30], F. Schussler[105], U. Schwanke[138], E. Sciacca[38], S. Scuderi[38],
I. Seitenzahl[17], D. Semikoz[80], O. Sergijenko[155], M. Servillat[7], A. Shalchi[167],
R.C. Shellard[25], L. Sidoli[28], H. Siejkowski[170], A. Sillanpää[118], G. Sironi[10],
J. Sitarek[171], V. Sliusar[20], A. Slowikowska[172], H. Sol[7], A. Stamerra[173],

S. Stanič[84], R. Starling[136], Ł. Stawarz[124], S. Stefanik[154], M. Stephan[95], T. Stolarczyk[22], G. Stratta[47], U. Straumann[100], T. Suomijarvi[33], A.D. Supanitsky[92], G. Tagliaferri[10], H. Tajima[152], M. Tavani[52], F. Tavecchio[10], J.-P. Tavernet[37], K. Tayabaly[10], L.A. Tejedor[14], P. Temnikov[141], Y. Terada[151], R. Terrier[80], T. Terzic[40], M. Teshima[65,16], V. Testa[11], S. Thoudam[27], W. Tian[16], L. Tibaldo[32], M. Tluczykont[116], C.J. Todero Peixoto[60], F. Tokanai[111], J. Tomastik[117], D. Tonev[141], M. Tornikoski[174], D.F. Torres[73,*], E. Torresi[47], G. Tosti[10], N. Tothill[94], G. Tovmassian[4], P. Travnicek[36], C. Trichard[57], M. Trifoglio[47], I. Troyano Pujadas[3], S. Tsujimoto[132], G. Umana[38], V. Vagelli[9], F. Vagnetti[148], M. Valentino[12], P. Vallania[173], L. Valore[12], C. van Eldik[99], J. Vandenbroucke[175], G.S. Varner[176], G. Vasileiadis[15], V. Vassiliev[156], M. Vázquez Acosta[102], M. Vecchi[76], A. Vega[54], S. Vercellone[10], P. Veres[177], S. Vergani[7], V. Verzi[148], G.P. Vettolani[44], A. Viana[32], C. Vigorito[77], J. Villanueva[54], H. Voelk[32], A. Vollhardt[100], S. Vorobiov[84], M. Vrastil[36], T. Vuillaume[135], S.J. Wagner[146], R. Wagner[65,66], R. Walter[20], J.E. Ward[21], D. Warren[24], J.J. Watson[6], F. Werner[32], M. White[68], R. White[32], A. Wierzcholska[58], P. Wilcox[126], M. Will[102], D.A. Williams[169], R. Wischnewski[30], M. Wood[143], T. Yamamoto[120], R. Yamazaki[133], S. Yanagita[127], L. Yang[84], T. Yoshida[127], S. Yoshiike[114], T. Yoshikoshi[16], M. Zacharias[41], G. Zaharijas[84], L. Zampieri[50], F. Zandanel[95], R. Zanin[32], M. Zavrtanik[84], D. Zavrtanik[84], A.A. Zdziarski[145], A. Zech[7], H. Zechlin[77], V.I. Zhdanov[91], A. Ziegler[99], J. Zorn[32]

[1]Tata Institute of Fundamental Research, Homi Bhabha Road, Colaba, Mumbai 400005, India

[2]Instituto de Astrofísica de Andalucía-CSIC, Glorieta de la Astronomía s/n, E-18008, Granada, Spain

[3]University of Geneva - Département de physique nucléaire et corpusculaire, 24 rue du Général-Dufour, 1211 Genève 4, Switzerland

[4]Universidad Nacional Autónoma de México, Delegación Coyoacán, 04510 Ciudad de México, Mexico

[5]Pontificia Universidad Católica de Chile, Avda. Libertador Bernardo O' Higgins No 340, borough and city of Santiago, Chile

[6]University of Oxford, Department of Physics, Denys Wilkinson Building, Keble Road, Oxford OX1 3RH, United Kingdom

[7]LUTH and GEPI, Observatoire de Paris, CNRS, PSL Research University, 5 place Jules Janssen, 92190, Meudon, France

[8]INAF - Osservatorio Astrofisico di Arcetri, Largo E. Fermi, 5 - 50125 Firenze, Italy

[9]INFN Sezione di Perugia and Università degli Studi di Perugia, Via A. Pascoli, 06123 Perugia, Italy

[10]INAF - Osservatorio Astronomico di Brera, Via Brera 28, 20121 Milano, Italy

[11]INAF - Osservatorio Astronomico di Roma, Via di Frascati 33, 00040, Monteporzio Catone, Italy

[12]INFN Sezione di Napoli, Via Cintia, ed. G, 80126 Napoli, Italy

[13]CCTVal Universidad Técnica Federico Santa María, Avenida España 1680, Valparaíso, Chile

[14]Grupo de Altas Energías and UPARCOS, Universidad Complutense de Madrid, Av Complutense s/n, 28040 Madrid, Spain

[15]Laboratoire Univers et Particules de Montpellier, Université de Montpellier, CNRS/IN2P3, CC 72, Place Eugène Bataillon, F-34095 Montpellier Cedex 5, France

[16]Institute for Cosmic Ray Research, University of Tokyo, 5-1-5, Kashiwa-no-ha, Kashiwa, Chiba 277-8582, Japan

[17]School of Physics, University of New South Wales, Sydney NSW 2052, Australia

[18]University of Namibia, Department of Physics, 340 Mandume Ndemufayo Ave., Pioneerspark, Windhoek, Namibia

[19]School of Physics and Astronomy, Monash University, Melbourne, Victoria 3800, Australia

[20]ISDC Data Centre for Astrophysics, Observatory of Geneva, University of Geneva, Chemin d'Ecogia 16, CH-1290 Versoix, Switzerland

[21]Institut de Fisica d'Altes Energies (IFAE), The Barcelona Institute of Science and Technology, Campus UAB, 08193 Bellaterra (Barcelona), Spain

[22]CEA/IRFU/SAp, CEA Saclay, Bat 709, Orme des Merisiers, 91191 Gif-sur-Yvette, France

[23]Department of Physics, Graduate School of Science, University of Tokyo, 7-3-1 Hongo, Bunkyo-ku, Tokyo 113-0033, Japan

[24]RIKEN, Institute of Physical and Chemical Research, 2-1 Hirosawa, Wako, Saitama, 351-0198, Japan

[25]Centro Brasileiro de Pesquisas Físicas, Rua Xavier Sigaud 150, RJ 22290-180, Rio de Janeiro, Brazil

[26]INFN Sezione di Padova and Università degli Studi di Padova, Via Marzolo 8, 35131 Padova, Italy

[27]Department of Physics and Electrical Engineering, Linnaeus University, 351 95 Växjö, Sweden

[28]INAF - Istituto di Astrofisica Spaziale e Fisica Cosmica di Milano, Via Bassini 15, 20133 Milano, Italy

[29]Harvard-Smithsonian Center for Astrophysics, 60 Garden St, Cambridge, MA 02180, USA

[30]Deutsches Elektronen-Synchrotron, Platanenallee 6, 15738 Zeuthen, Germany

[31]CIEMAT, Avda. Complutense 40, 28040 Madrid, Spain

[32]Max-Planck-Institut für Kernphysik, Saupfercheckweg 1, 69117 Heidelberg, Germany

[33]Institut de Physique Nucléaire, IN2P3/CNRS, Université Paris-Sud, Université Paris-Saclay, 15 rue Georges Clemenceau, 91406 Orsay, Cedex, France

[34]ETH Zurich, Institute for Particle Physics, Schafmattstr. 20, CH-8093 Zurich, Switzerland

[35]INFN Sezione di Bari and Politecnico di Bari, via Orabona 4, 70124 Bari, Italy

[36]Institute of Physics of the Academy of Sciences of the Czech Republic, Na Slovance 1999/2, 182 21 Praha 8, Czech Republic

[37]Sorbonne Universités, UPMC Université Paris 06, Université Paris Diderot, Sorbonne Paris Cité, CNRS, Laboratoire de Physique Nucléaire et

de Hautes Energies (LPNHE), 4 Place Jussieu, 75252, Paris Cedex 5, France

[38]INAF - Osservatorio Astrofisico di Catania, Via S. Sofia, 78, 95123 Catania, Italy

[39]Radboud University Nijmegen, P.O. Box 9010, 6500 GL Nijmegen, The Netherlands

[40]University of Rijeka, Department of Physics, Radmile Matejcic 2, 51000 Rijeka, Croatia

[41]Centre for Space Research, North-West University, Potchefstroom Campus, 2531, South Africa

[42]Department of Physics, Columbia University, 538 West 120th Street, New York, NY 10027, USA

[43]Dept. of Physics and Centre for Advanced Instrumentation, Durham University, South Road, Durham DH1 3LE, United Kingdom

[44]INAF - Istituto di Radioastronomia, Via Gobetti 101, 40129 Bologna, Italy

[45]Department of Physics and Technology, University of Bergen, Museplass 1, 5007 Bergen, Norway

[46]Department of Physics, Washington University, St. Louis, MO 63130, USA

[47]INAF - Istituto di Astrofisica Spaziale e Fisica Cosmica di Bologna, Via Piero Gobetti 101, 40129 Bologna, Italy

[48]Astronomical Observatory, Department of Physics, University of Warsaw, Aleje Ujazdowskie 4, 00478 Warsaw, Poland

[49]Armagh Observatory and Planetarium, College Hill, Armagh BT61 9DG, United Kingdom

[50]INAF - Osservatorio Astronomico di Padova, Vicolo dell'Osservatorio 5, 35122 Padova, Italy

[51]INAF - Istituto di Astrofisica Spaziale e Fisica Cosmica di Palermo, Via U. La Malfa 153, 90146 Palermo, Italy

[52]INAF - Istituto di Astrofisica e Planetologia Spaziali (IAPS), Via del Fosso del Cavaliere 100, 00133 Roma, Italy

[53]Universidade Cruzeiro do Sul, Núcleo de Astrofísica Teórica (NAT/UCS), Rua Galvão Bueno 8687, Bloco B, sala 16, Libertade 01506-000 - São Paulo, Brazil

[54]Universidad de Valparaíso, Blanco 951, Valparaiso, Chile

[55]Lund Observatory, Lund University, Box 43, SE-22100 Lund, Sweden

[56]INFN Sezione di Pisa, Largo Pontecorvo 3, 56217 Pisa, Italy

[57]Aix Marseille Univ, CNRS/IN2P3, CPPM, Marseille, France, 163 Avenue de Luminy, 13288 Marseille cedex 09, France

[58]The Henryk Niewodniczański Institute of Nuclear Physics, Polish Academy of Sciences, ul. Radzikowskiego 152, 31-342 Cracow, Poland

[59]INAF - Osservatorio Astronomico di Capodimonte, Via Salita Moiariello 16, 80131 Napoli, Italy

[60]Escola de Engenharia de Lorena, Universidade de São Paulo, Área I - Estrada Municipal do Campinho, s/n°, CEP 12602-810, Brazil

[61]INFN Sezione di Trieste and Università degli Studi di Udine, Via delle Scienze 208, 33100 Udine, Italy

[62]University of the Witwatersrand, 1 Jan Smuts Avenue, Braamfontein, 2000 Johannesburg, South Africa

[63]Dublin City University, Glasnevin, Dublin 9, Ireland

[64]Dept. of Physics, Kindai University, Kowakae, Higashi-Osaka 577-8502, Japan

[65]Max-Planck-Institut für Physik, Föhringer Ring 6, 80805 München, Germany

[66]Oskar Klein Centre, Department of Physics, University of Stockholm, Albanova, SE-10691, Sweden

[67]Research School of Astronomy and Astrophysics, Australian National University, Canberra ACT 0200, Australia

[68]School of Physical Sciences, University of Adelaide, Adelaide SA 5005, Australia

[69]Cherenkov Telescope Array Observatory, Saupfercheckweg 1, 69117 Heidelberg, Germany

[70]Universidade Federal Do Paraná - Setor Palotina, Departamento de Engenharias e Exatas, Rua Pioneiro, 2153, Jardim Dallas, CEP: 85950-000 Palotina, Paraná, Brazil

[71]Instituto de Astronomia, Geofísico, e Ciências Atmosféricas - Universidade de São Paulo, Cidade Universitária, R. do Matão, 1226, CEP 05508-090, São Paulo, SP, Brazil

[72]Laboratoire Leprince-Ringuet, École Polytechnique (UMR 7638, CNRS/IN2P3, Université Paris-Saclay), 91128 Palaiseau, France

[73]Institute of Space Sciences (IEEC-CSIC) and Institució Catalana de Recerca I Estudis Avançats (ICREA), Campus UAB, Carrer de Can Magrans, s/n 08193 Cerdanyola del Vallés, Spain

[74]INFN Sezione di Bari, via Orabona 4, 70126 Bari, Italy

[75]INFN Sezione di Roma La Sapienza, P.le Aldo Moro, 2 - 00185 Roma, Italy

[76]Instituto de Física de São Carlos, Universidade de São Paulo, Av. Trabalhador São-carlense, 400 - CEP 13566-590, São Carlos, SP, Brazil

[77]INFN Sezione di Torino, Via P. Giuria 1, 10125 Torino, Italy

[78]INFN Sezione di Bari and Università degli Studi di Bari, via Orabona 4, 70124 Bari, Italy

[79]Institut für Astronomie und Astrophysik, Universität Tübingen, Sand 1, 72076 Tübingen, Germany

[80]APC, Univ Paris Diderot, CNRS/IN2P3, CEA/lrfu, Obs de Paris, Sorbonne Paris Cité, France, 10, rue Alice Domon et Léonie Duquet, 75205 Paris Cedex 13, France

[81]Institute for Theoretical Physics and Astrophysics, Universität Würzburg, Campus Hubland Nord, Emil-Fischer-Str. 31, 97074 Würzburg, Germany

[82]Université Grenoble Alpes, CNRS, Institut de Planétologie et d'Astrophysique de Grenoble, 414 rue de la Piscine, Domaine Universitaire, 38041 Grenoble Cedex 9, France

[83]Enrico Fermi Institute, University of Chicago, 5640 South Ellis Avenue, Chicago, IL 60637, USA

[84]Center for Astrophysics and Cosmology, University of Nova Gorica,
Vipavska 11c, 5270 Ajdovščina, Slovenia

[85]Institut für Physik & Astronomie, Universität Potsdam,
Karl-Liebknecht-Strasse 24/25, 14476 Potsdam, Germany

[86]Department of Physics, TU Dortmund University, Otto-Hahn-Str. 4,
44221 Dortmund, Germany

[87]INFN Dipartimento di Scienze Fisiche e Chimiche - Università degli
Studi dell'Aquila and Gran Sasso Science Institute, Via Vetoio 1, Viale
Crispi 7, 67100 L'Aquila, Italy

[88]King's College London, Strand, London, WC2R 2LS, United Kingdom

[89]Escola de Artes, Ciências e Humanidades, Universidade de São Paulo,
Rua Arlindo Bettio, 1000 São Paulo, CEP 03828-000, Brazil

[90]Dept. of Astronomy & Astrophysics, Pennsylvania State University,
University Park, PA 16802, USA

[91]Astronomical Observatory of Taras Shevchenko National University of
Kyiv, 3 Observatorna Street, Kyiv, 04053, Ukraine

[92]Instituto de Astronomía y Física del Espacio (IAFE CONICET-UBA),
CC 67, Suc. 28, (C1428ZAA), Ciudad de Buenos Aires, Argentina

[93]CEA/IRFU/SEDI, CEA Saclay, Bat 141, 91191 Gif-sur-Yvette, France

[94]Western Sydney University, Locked Bag 1797, Penrith, NSW 2751,
Australia

[95]GRAPPA, University of Amsterdam, Science Park 904 1098 XH
Amsterdam, The Netherlands

[96]School of Physics and Astronomy, University of Minnesota, 116 Church
Street S.E. Minneapolis, Minnesota 55455-0112, USA

[97]Department of Earth and Space Science, Graduate School of Science,
Osaka University, Toyonaka 560-0043, Japan

[98]Department of Physical Science, Hiroshima University,
Higashi-Hiroshima, Hiroshima 739-8526, Japan

[99]Universität Erlangen-Nürnberg, Physikalisches Institut,
Erwin-Rommel-Str. 1, 91058 Erlangen, Germany

[100]Physik-Institut, Universität Zürich, Winterthurerstrasse 190, 8057 Zürich, Switzerland

[101]Instituto de Tecnologias en Deteccion y Astroparticulas (CNEA/CONICET/UNSAM), Av. Gral. Paz 1499, (B1650KNA) San Martin, Prov. Buenos Aires, Argentina

[102]Instituto de Astrofísica de Canarias and Departamento de Astrofísica, Universidad de La Laguna, La Laguna, Tenerife, Spain

[103]INFN Sezione di Trieste and Università degli Studi di Trieste, Via Valerio 2, 34127 Trieste, Italy

[104]Unitat de Física de les Radiacions, Departament de Física, and CERES-IEEC, Universitat Autònoma de Barcelona, E-08193 Bellaterra, Spain, Edifici C3, Campus UAB, 08193 Bellaterra, Spain

[105]CEA/IRFU/SPP, CEA-Saclay, Bât 141, 91191 Gif-sur-Yvette, France

[106]University of Split - FESB, R. Boskovica 32, 21 000 Split, Croatia

[107]Universidad Andrés Bello UNAB, República N° 252, Santiago, Región Metropolitana, Chile

[108]Department of Natural Sciences, The Open University of Israel, 1 University Road, POB 808, Raanana 43537, Israel

[109]School of Physics, University of Sydney, Sydney NSW 2006, Australia

[110]University of Liverpool, Oliver Lodge Laboratory, Liverpool L69 7ZE, United Kingdom

[111]Department of Physics, Yamagata University, Yamagata, Yamagata 990-8560, Japan

[112]Faculty of Management Information, Yamanashi-Gakuin University, Kofu, Yamanashi 400-8575, Japan

[113]Centre for Astrophysics Research, Science & Technology Research Institute, University of Hertfordshire, College Lane, Hertfordshire AL10 9AB, United Kingdom

[114]Department of Physics, Nagoya University, Chikusa-ku, Nagoya, 464-8602, Japan

[115]Department of Physics and Astronomy and the Bartol Research Institute, University of Delaware, Newark, DE 19716, USA

[116]Universität Hamburg, Institut für Experimentalphysik, Luruper Chaussee 149, 22761 Hamburg, Germany

[117]Palacky University Olomouc, Faculty of Science, RCPTM, 17. listopadu 1192/12, 771 46 Olomouc, Czech Republic

[118]Tuorla Observatory, Department of Physics and Astronomy, University of Turku, FI-21500 Piikkiő, Finland

[119]Rudjer Boskovic Institute, Bijenicka 54, 10 000 Zagreb, Croatia

[120]Department of Physics, Konan University, Kobe, Hyogo, 658-8501, Japan

[121]Institute of Space and Astronautical Sciences, Japan Aerospace Exploration Agency, 3-1-1 Yoshinodai, Chuo-ku, Sagamihara, Kanagawa 252-5210, Japan

[122]ICTP-South American Institute for Fundamental Research - Instítuto de Fisica Teorica da UNESP, Rua Dr. Bento Teobaldo Ferraz 271, 01140-070 Sao Paulo, Brazil

[123]Yukawa Institute for Theoretical Physics, Kyoto University, Kyoto 606-8502, Japan

[124]Faculty of Physics, Astronomy and Applied Computer Science, Jagiellonian University, ul. prof. Stanisława Łojasiewicza 11, 30-348 Kraków, Poland

[125]Institut de Recherche en Astrophysique et Planétologie, CNRS-INSU, Université Paul Sabatier, 9 avenue Colonel Roche, BP 44346, 31028 Toulouse Cedex 4, France

[126]University of Iowa, Department of Physics and Astronomy, Van Allen Hall, Iowa City, IA 52242, USA

[127]Faculty of Science, Ibaraki University, Mito, Ibaraki, 310-8512, Japan

[128]Division of Physics and Astronomy, Graduate School of Science, Kyoto University, Sakyo-ku, Kyoto, 606-8502, Japan

[129]School of Physics, Aristotle University, Thessaloniki, 54124 Thessaloniki, Greece

[130]Department of Physics and Astronomy, University of Utah, Salt Lake City, UT 84112-0830, USA

[131]Universidad Católica del Norte, Av. Angamos 0610, Antofagasta, Chile

[132]Department of Physics, Tokai University, 4-1-1, Kita-Kaname,
Hiratsuka, Kanagawa 259-1292, Japan

[133]Department of Physics and Mathematics, Aoyama Gakuin University,
Fuchinobe, Sagamihara, Kanagawa, 252-5258, Japan

[134]Institute of Particle and Nuclear Studies, KEK (High Energy
Accelerator Research Organization), 1-1 Oho, Tsukuba, 305-0801, Japan

[135]Laboratoire d'Annecy-le-Vieux de Physique des Particules, Université
de Savoie Mont-Blanc, CNRS/IN2P3, 9 Chemin de Bellevue - BP 110,
74941 Annecy-le-Vieux Cedex, France

[136]Dept. of Physics and Astronomy, University of Leicester, Leicester, LE1
7RH, United Kingdom

[137]Centro de Ciências Naturais e Humanas - Universidade Federal do
ABC, Rua Santa Adélia, 166. Bairro Bangu. Santo André - SP - Brasil.
CEP 09.210-170, Brazil

[138]Department of Physics, Humboldt University Berlin, Newtonstr. 15,
12489 Berlin, Germany

[139]Escuela Politécnica Superior de Jaén, Universidad de Jaén, Campus Las
Lagunillas s/n, Edif. A3, 23071 Jaén, Spain

[140]Saha Institute of Nuclear Physics, Bidhannagar, Kolkata-700 064, India

[141]Institute for Nuclear Research and Nuclear Energy, Bulgarian Academy
of Sciences, 72 boul. Tsarigradsko chaussee, 1784 Sofia, Bulgaria

[142]Instituto Argentino de Radioastronomía (CCT La Plata - CONICET),
Camino Gral. Belgrano Km 40, Berazategui, Prov. Buenos Aires,
Argentina

[143]Kavli Institute for Particle Astrophysics and Cosmology, Department of
Physics and SLAC National Accelerator Laboratory, Stanford University,
2575 Sand Hill Road, Menlo Park, CA 94025, USA

[144]Hiroshima Astrophysical Science Center, Hiroshima University,
Higashi-Hiroshima, Hiroshima 739-8526, Japan

[145]Nicolaus Copernicus Astronomical Center, Polish Academy of Sciences,
ul. Bartycka 18, 00-716 Warsaw, Poland

[146]Landessternwarte, Universität Heidelberg, Königstuhl, 69117
Heidelberg, Germany

[147]Department of Applied Physics, University of Miyazaki, 1-1 Gakuen
Kibana-dai Nishi, Miyazaki, 889-2192, Japan

[148]INFN Sezione di Roma Tor Vergata, Via della Ricerca Scientifica 1,
00133 Rome, Italy

[149]Department of Physics, University of Bath, Claverton Down, Bath BA2
7AY, United Kingdom

[150]School of Allied Health Sciences, Kitasato University, Sagamihara,
Kanagawa 228-8555, Japan

[151]Graduate School of Science and Engineering, Saitama University, 255
Simo-Ohkubo, Sakura-ku, Saitama city, Saitama 338-8570, Japan

[152]Institute for Space-Earth Environmental Research, Nagoya University,
Chikusa-ku, Nagoya 464-8601, Japan

[153]University of Białystok, Faculty of Physics, ul. K. Ciołkowskiego 1L,
15-254 Białystok, Poland

[154]Charles University, Institute of Particle & Nuclear Physics,
V Holešovičkách 2, 180 00 Prague 8, Czech Republic

[155]Astronomical Observatory of Ivan Franko National University of Lviv,
8 Kyryla i Mephodia Street, Lviv, 79005, Ukraine

[156]Department of Physics and Astronomy, University of California,
Los Angeles, CA 90095, USA

[157]Graduate School of Technology, Industrial and Social Sciences,
Tokushima University, Tokushima 770-8506, Japan

[158]School of Physics & Center for Relativistic Astrophysics, Georgia
Institute of Technology, 837 State Street, Atlanta, Georgia, 30332-0430,
USA

[159]Departament de Física Quàntica i Astrofísica, Institut de Ciències del
Cosmos, Universitat de Barcelona, IEEC-UB, Martí i Franquès, 1, 08028,
Barcelona, Spain

[160]INAF - Osservatorio Astronomico di Trieste and INFN Sezione di
Trieste, Via delle Scienze 208 I-33100 Udine, Italy

[161]Pidstryhach Institute for Applied Problems in Mechanics and Mathematics NASU, 3B Naukova Street, Lviv, 79060, Ukraine

[162]University of Johannesburg, Department of Physics, University Road, PO Box 524, Auckland Park 2006, South Africa

[163]Institut für Astro- und Teilchenphysik, Leopold-Franzens-Universität, Technikerstr. 25/8, 6020 Innsbruck, Austria

[164]Universidad de Concepción, Barrio Universitario S/N, Concepción, Chile

[165]Facultad de ciencias físicas y matemáticas, Universidad de Chile, Beauchef 850, comuna y ciudad de Santiago, Chile

[166]Núcleo de Formação de Professores - Universidade Federal de São Carlos, Rodovia Washington Luís, km 235 - SP-310 São Carlos - São Paulo - Brasil CEP 13565-905, Brazil

[167]The University of Manitoba, Dept of Physics and Astronomy, Winnipeg, Manitoba R3T 2N2, Canada

[168]University of Oslo, Department of Physics, Sem Saelandsvei 24 - PO Box 1048 Blindern, N-0316 Oslo, Norway

[169]Santa Cruz Institute for Particle Physics and Department of Physics, University of California, Santa Cruz, 1156 High Street, Santa Cruz, CA 95064, USA

[170]Academic Computer Centre CYFRONET AGH, ul. Nawojki 11, 30-950 Cracow, Poland

[171]Faculty of Physics and Applied Computer Science, University of Lódź, ul. Pomorska 149-153, 90-236 Lódź, Poland

[172]University of Zielona Góra, ul. Licealna 9, 65-417 Zielona Góra, Poland

[173]INAF - Osservatorio Astrofisico di Torino, Strada Osservatorio 20, 10025 Pino Torinese (TO), Italy

[174]Aalto University, Otakaari 1, 00076 Aalto, Finland

[175]University of Wisconsin, Madison, 500 Lincoln Drive, Madison, WI, 53706, USA

[176]University of Hawai'i at Manoa, 2500 Campus Rd, Honolulu, HI, 96822, USA

[177]University of Alabama in Huntsville - Center for Space Physics and Aeronomic Research, 320 Sparkman Dr, Huntsville AL 35805, USA

[a]Currently at the German Aerospace Center (DLR), Earth Observation Center (EOC), 82234 Wessling, Germany

*Overall editors

Acknowledgements

We gratefully acknowledge financial support from the following agencies and organisations:

Ministerio de Ciencia, Tecnología e Innovación Productiva (MinCyT), Comisión Nacional de Energía Atómica (CNEA), Consejo Nacional de Investigaciones Científicas y Técnicas (CONICET), Argentina; State Committee of Science of Armenia, Armenia; The Australian Research Council, Astronomy Australia Ltd, The University of Adelaide, Australian National University, Monash University, The University of New South Wales, The University of Sydney, Western Sydney University, Australia; Federal Ministry of Science, Research and Economy, and Innsbruck University, Austria; Conselho Nacional de Desenvolvimento Científico e Tecnológico (CNPq), Fundação de Amparo à Pesquisa do Estado do Rio de Janeiro (FAPERJ), Fundação de Amparo à Pesquisa do Estado de São Paulo (FAPESP), Brasil; The Natural Sciences and Engineering Research Council of Canada and the Canadian Space Agency, Canada; CONICYT-Chile grants PFB-06, FB0821, ACT 1406, FONDECYT-Chile grants 3160153, 3150314, 1150411, 1161463, 1170171, Pontificia Universidad Católica de Chile Vice-Rectory of Research internationalization grant under MINEDUC agreement PUC1566, Chile; Croatian Science Foundation, Rudjer Boskovic Institute, University of Osijek, University of Rijeka, University of Split, Faculty of Electrical Engineering, Mechanical Engineering and Naval Architecture, University of Zagreb, Faculty of Electrical Engineering and Computing, Croatia; Ministry of Education, Youth and Sports, MEYS LE13012, LG14019, LM2015046, LO1305, LTT17006 and EU/MEYS CZ.02.1.01/0.0/0.0/16_013/0001403, Czech Republic; Ministry of Higher Education and Research, CNRS-INSU and CNRS-IN2P3, CEA-Irfu, ANR, Regional Council Ile de France, Labex ENIGMASS, OSUG2020, P2IO and OCEVU, France; Max Planck Society, BMBF, DESY, Helmholtz Association, Germany; Department of Atomic Energy, Department of Science and Technology, India; Istituto Nazionale di Astrofisica (INAF), Istituto Nazionale di Fisica Nucleare (INFN), MIUR, Istituto Nazionale di Astrofisica (INAF-OABRERA) Grant Fondazione Cariplo/Regione Lombardia ID 2014-1980/RST_ERC, Italy; ICRR, University of Tokyo, JSPS, MEXT, Japan; Netherlands Research School for Astronomy (NOVA), Netherlands Organization for Scientific Research (NWO), Netherlands; The Bergen Research Foundation, Norway; Ministry of Science and Higher Education, the National Centre for Research and Development and the National Science Centre, UMO-2016/22/M/ST9/00583 and UMO-2014/13/B/ST9/00945, Poland; Slovenian Research Agency, Slovenia; South African Department of Science and Technology and National Research Foundation through the South African Gamma-Ray Astronomy Programme, South Africa; MINECO National R+D+I, Severo Ochoa, Maria de Maeztu, CDTI, MultiDark Consolider-Ingenio 2010, PAIDI, UJA, Spain; Swedish Research Council, Royal Physiographic Society of Lund, Royal Swedish Academy of Sciences, The Swedish National Infrastructure for Computing (SNIC) at Lunarc (Lund), Sweden; Swiss National Science Foundation (SNSF), Ernest Boninchi Foundation, Switzerland; Durham University, Leverhulme Trust, Liverpool University, University of Leicester, University of Oxford, Royal Society, Science and Technology Facilities Council, UK; U.S. National Science Foundation, U.S. Department of Energy, Argonne National Laboratory, Barnard College, University of California, University of Chicago, Columbia University, Georgia Institute of Technology, Institute for Nuclear and Particle Astrophysics (INPAC-MRPI program), Iowa State University, the Smithsonian Institution, Washington University McDonnell Center for the Space Sciences, The University of Wisconsin and the Wisconsin Alumni Research Foundation, USA.

The research leading to these results has received funding from the European Union's Seventh Framework Programme (FP7/2007-2013) under grant agreements No 262053, 317446, and 332350. This project is receiving funding from the European Union's Horizon 2020 research and innovation programs under agreement No 676134.

We gratefully acknowledge the critical efforts of the late Professor Giovanni Bignami in the development of CTA.

Contents

Executive Summary v

Authors vii

Acknowledgements xxiii

Chapters and Corresponding Authors

Chapter 1. Introduction to CTA Science 1
J.A. Hinton, R.A. Ong, D. Torres

Chapter 2. Synergies 27
S. Markoff, J.A. Hinton, R.A. Ong, D. Torres

Chapter 3. Core Programme Overview 41
J.A. Hinton, R.A. Ong, D. Torres

Chapter 4. Dark Matter Programme 45
E. Moulin, J. Carr, J. Gaskins, M. Doro, C. Farnier, M. Wood, H. Zechlin

Chapter 5. KSP: Galactic Centre 83
C. Farnier, K. Kosack, R. Terrier

Chapter 6. KSP: Galactic Plane Survey 101
R.C.G. Chaves, R. Mukherjee, R.A. Ong

Chapter 7. KSP: Large Magellanic Cloud Survey 125
P. Martin, C.-C. Lu, H. Voelk, M. Renaud, M. Filipovic

Chapter 8. KSP: Extragalactic Survey 143
D. Mazin, L. Gerard, J.E. Ward, P. Giommi, A.M. Brown

Chapter 9. KSP: Transients 163
S. Inoue, M. Ribó, E. Bernardini, V. Connaughton, J. Granot, S. Markoff, P. O Brien, F. Schussler

Chapter 10. KSP: Cosmic Ray PeVatrons 199
R.C.G. Chaves, E. De Oña Wilhelmi, S. Gabici, M. Renaud

Chapter 11. KSP: Star Forming Systems 211
S. Casanova, S. Ohm, L. Tibaldo

Chapter 12. KSP: Active Galactic Nuclei 231
A. Zech, D. Mazin, J. Biteau, M. Daniel, T. Hassan, E. Lindfors, M. Meyer

Chapter 13. KSP: Clusters of Galaxies 273
F. Zandanel, M Fornasa

Chapter 14. Capabilities beyond Gamma Rays 291
R. Bühler, D. Dravins, K. Egberts, J.A. Hinton, R.D. Parsons

Chapter 15. Appendix: Simulating CTA 299
G. Maier

References 301

Glossary 333

1

Introduction to CTA Science

Ground-based gamma-ray astronomy is a young field with enormous scientific potential. The possibility of astrophysical measurements at tera-electronvolt (TeV) energies was demonstrated in 1989 with the detection of a clear signal from the Crab nebula above 1 TeV with the Whipple 10 m imaging atmospheric Cherenkov telescope (IACT). Since then, the instrumentation for, and techniques of, astronomy with IACTs have evolved to the extent that a flourishing new scientific discipline has been established, with the detection of more than 150 sources and a major impact in astrophysics and more widely in physics. The current major arrays of IACTs, H.E.S.S., MAGIC, and VERITAS, have demonstrated the huge physics potential at these energies as well as the maturity of the detection technique. Many astrophysical source classes have been established, some with many well-studied individual objects, but there are indications that the known sources represent the tip of the iceberg in terms of both individual objects and source classes. The Cherenkov Telescope Array (CTA) will transform our understanding of the high-energy universe and will explore questions in physics of fundamental importance. As a key member of the suite of new and upcoming major astroparticle physics experiments and observatories, CTA will exploit synergies with gravitational wave and neutrino observatories as well as with classical photon observatories. CTA will address a wide range of major questions in and beyond astrophysics, which can be grouped into three broad themes:

Theme 1: Understanding the Origin and Role of Relativistic Cosmic Particles

- What are the sites of high-energy particle acceleration in the universe?
- What are the mechanisms for cosmic particle acceleration?
- What role do accelerated particles play in feedback on star formation and galaxy evolution?

Theme 2: Probing Extreme Environments

- What physical processes are at work close to neutron stars and black holes?
- What are the characteristics of relativistic jets, winds, and explosions?
- How intense are radiation fields and magnetic fields in cosmic voids, and how do these evolve over cosmic time?

Theme 3: Exploring Frontiers in Physics

- What is the nature of dark matter? How is it distributed?
- Are there quantum gravitational effects on photon propagation?
- Do axion-like particles exist?

This chapter introduces the key characteristics of the observatory and describes the involvement of the wider scientific community in the derivation of the scientific requirements for CTA. The broader multi-wavelength and multi-messenger context is presented in the following chapter and the scientific programme proposed for the Key Science Projects, to be carried out by the CTA Consortium using guaranteed time, is presented in later chapters of this document.

1.1 Key Characteristics and Capabilities

CTA will be an observatory with arrays of IACTs on two sites aiming to:

- improve the sensitivity level of current instruments by an order of magnitude at 1 TeV,
- significantly boost detection area, and hence photon rate, providing access to the shortest timescale phenomena,
- substantially improve angular resolution and field of view and hence ability to image extended sources,

- provide energy coverage for photons from 20 GeV to at least 300 TeV, to give CTA reach to high-redshifts and extreme accelerators,
- dramatically enhance surveying capability, monitoring capability, and flexibility of operation, allowing for simultaneous observations of objects in multiple fields,
- serve a wide user community, with provision of data products and tools suitable for non-expert users, and
- provide access to the entire sky, with sites in two hemispheres. (In this document, the two sites are referred to as CTA-South and CTA-North).

CTA will be operated as an open, proposal-driven observatory for the first time in very high-energy (VHE, $E > 20\,\mathrm{GeV}$) astronomy. The observatory-mode operation of CTA is expected to significantly boost scientific output by engaging a research community much wider than the historical ground-based gamma-ray astronomy community.

The very wide energy range covered by the southern CTA array necessitates the use of at least three different telescope types: referred to as Large, Medium, and Small-Sized Telescopes (LSTs, MSTs, and SSTs). The LSTs provide sensitivity at the lowest energies and the SSTs at the highest. There are multiple strong motivations for the wide CTA energy range: the lowest energies provide access to the whole universe (avoiding significant gamma–gamma absorption on the extragalactic background light); the highest energies are needed to study the extreme accelerators which we know from direct cosmic-ray measurements are present in our Galaxy; a wide energy range maximises the chances of serendipitous detection of new source classes with unknown spectral characteristics, for example in the search for dark matter with an unknown WIMP mass; a wide energy range is key for discrimination between scenarios and to identify features. All objects which have been studied over a wide energy range with good signal to noise using current IACT arrays exhibit features in their gamma-ray spectra. Conversely, the narrow energy range and lower signal to noise measurements more typical of current generation instruments invariably result in spectra which are consistent with power-law forms. In the north, where the inner regions of the Galaxy are not visible, there will be a greater emphasis on extragalactic targets. Therefore, in the interest of optimisation of the observatory, the northern CTA array will be implemented with only LSTs and MSTs.

Access to the full sky is necessary as many of the phenomena to be studied by CTA are rare and individual objects can be very important. For example, the most promising galaxy cluster, the brightest starburst galaxy, and the only known gravitationally lensed TeV source are located in the north. The inner Galaxy and the Galactic Centre are key CTA targets (see, e.g. Chapter 5) and are located in the south. Full sky coverage ensures that extremely rare but critically important events (for example a Galactic supernova explosion, bright gravitational wave transient, or nearby gamma-ray burst) will be accessible to CTA.

Individual CTA telescopes will have Cherenkov cameras with wide fields of view: $>4.5°$ for the LSTs, $>7°$ for the MSTs, and $>8°$ for the SSTs. The wide camera field serves a dual purpose: to provide contained shower images up to large impact distance (improving collection area and resolution) for on-axis gamma rays and to increase the gamma-ray field of view of the system as a whole. This characteristic of CTA is critical for the observation of very extended objects and regions of diffuse emission, as well as for surveys. Furthermore, the wide field provides reduced systematic errors, with a uniform response over regions much larger than the point-spread-function size (not always the case for current generation instruments).

The large telescope number ($\sim$100 in the south) and individual wide telescope fields of view result in a CTA collection area which is one or more orders of magnitude larger than current generation instruments at essentially all energies, with substantial benefits for imaging, spectroscopy, and light-curve generation. Multi-square-kilometre collection area is essential at the highest energies where there is essentially zero background even in long exposures and sensitivity is limited by the collection of sufficient signal photons. For very short timescale phenomena, CTA is background free over much of its energy range and the large collection area is the key performance driver.

For events incident in the central parts of the CTA arrays, the number of recorded shower images will be large ($>$10) for all but the lowest energies. These high image multiplicities, combined with the contained nature of events and superior image information to existing instruments, provide excellent energy and angular resolution. A precision of 1 arc-minute on individual photons will be obtained for the upper end of the CTA energy range, which is the best resolution achieved anywhere above the X-ray domain.

The ability to rapidly respond to external alerts, and to rapidly issue its own alerts, is built into the CTA design. In particular the LSTs, where the energy range covered provides access to essentially the whole universe, are optimised for rapid movement, with a goal slewing time of 20 s (minimum requirement 50 s) to anywhere in the observable sky. A real-time analysis pipeline will enable the identification of significant gamma-ray activity in any part of the field of view and the issuing of alerts to other instruments within one minute.

The dramatic improvement in the point-source sensitivity of CTA with respect to current instruments is a consequence of the combination of improved background rejection power, increased collection area, and improved angular resolution. The improved background rejection power is achieved primarily through high image multiplicity and is particularly important for the study of extended, low-surface brightness objects and for low-flux objects where deep exposures are required. Figures 1.1 and 1.2 compare the sensitivity and angular resolution of the CTA arrays to a selection of existing gamma-ray detectors.

Finally, the number of individual telescopes in the CTA arrays, and the ability to operate multiple sub-arrays independently, provides enormous flexibility of operation. CTA will operate with different pointing directions

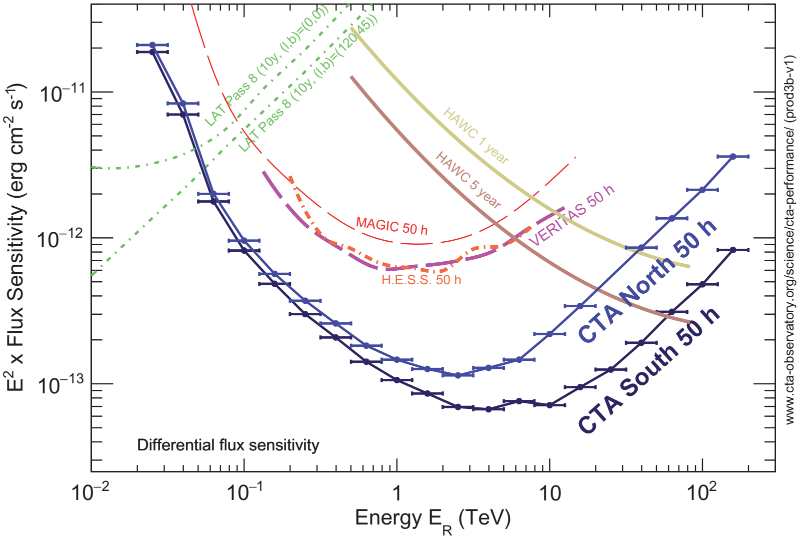

www.cta-observatory.org/science/cta-performance/ (prod3b-v1)

Figure 1.1: Comparisons of the performance of CTA with selected existing gamma-ray instruments. Differential energy flux sensitivities for CTA (south and north) are shown for five standard deviation detections in five independent logarithmic bins per decade in energy. For the CTA sensitivities, additional criteria are applied to require at least ten detected gamma rays per energy bin and a signal/background ratio of at least 1/20. The curves for Fermi-LAT and HAWC are scaled by a factor of 1.2 to account for the different energy binning. The curves shown give only an indicative comparison of the sensitivity of the different instruments, as the method of calculation and the criteria applied are different. In particular, the definition of the differential sensitivity for HAWC is rather different due to the lack of energy reconstruction for individual photons in the HAWC analysis. See Figure 1.2 for references.

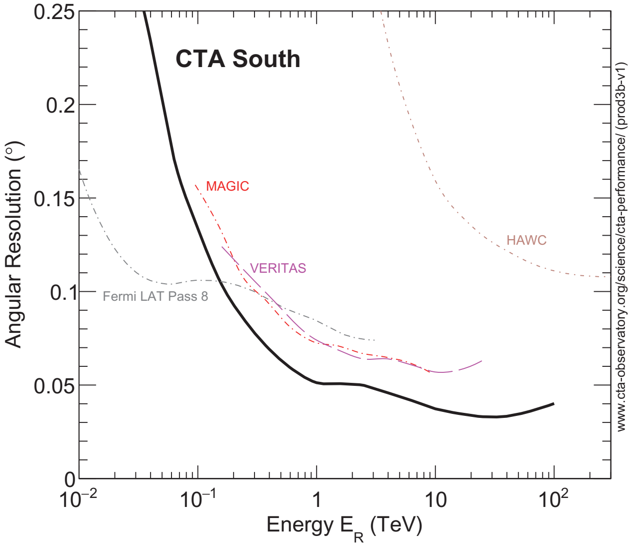

Figure 1.2: Angular resolution expressed as the 68% containment radius of reconstructed gamma rays (the resolution for CTA-North is similar). The sensitivity (Figure 1.1) and angular resolution curves are based on the following references: Fermi-LAT [1], HAWC [2], H.E.S.S. [3], MAGIC [4], and VERITAS [5]. The CTA curves represent the understanding of the performance of CTA at the time of completion of this document; for the latest CTA performance plots, see https://www.cta-observatory.org/science/cta-performance.

for different sub-systems, for example with the LSTs pointed to a distant active galaxy and the MSTs and SSTs observing a hard-spectrum Galactic source. Furthermore, small groups of MSTs or SSTs may be used to monitor up to 10 variable sources simultaneously. The pointing pattern of the CTA telescopes may also be optimised for the purpose of surveying an extended region of arbitrary shape, for example the error box from a gravitational wave alert [6, 7]. Preliminary CTA performance curves are available publicly at [8]. Below, we highlight two key aspects of the unique instrumental reach of CTA.

1.1.1 *Surveying Capabilities*

CTA will conduct a census of particle acceleration in our universe by performing surveys of the sky at unprecedented sensitivity at very high energies. Deep fields will be obtained for some key regions hosting prominent targets, while wider and shallower surveys will be conducted to build up unbiased population samples and to search for the unexpected. The combination of the wide CTA field of view with unprecedented sensitivity ensures that CTA can deliver surveys one to two orders of magnitude deeper than existing surveys early in the life of the observatory. Indeed, over much of the sky and much of the energy range of CTA, no sensitive survey exists and CTA measurements will be revolutionary. The CTA surveys will open up discovery space in an unbiased way and generate legacy datasets of long-lasting value.

The potential for surveys with CTA is described in Ref. [9]. To ensure that essential surveys will be conducted by CTA early on in the observing programme, and to accommodate the related observing time demands, surveys will be part of CTA's Core Programme and are described in the Key Science Project (KSP) chapters that follow.

- **Extragalactic Survey** (Chapter 8): Covering 1/4 of the sky to a depth of $\sim$6 mCrab. No extragalactic survey has ever been performed using IACTs, and the existing VHE surveys using ground-level particle detectors [10, 11] have modest sensitivity, limited angular and energy resolution, and limited energy range. A 1000 h CTA survey of such a region will reach the same sensitivity as the decade long H.E.S.S. programme of inner Galaxy observations and will cover a solid angle $\sim$40 times larger, providing a snapshot of activity in an unbiased sample of active galactic nuclei (AGN) (see Figure 1.4).
- **Galactic Plane Survey (GPS)** (Chapter 6): Consisting of a deep survey ($\sim$2 mCrab) of the inner Galaxy and the Cygnus region, coupled with a somewhat shallower survey ($\sim$4 mCrab) of the entire Galactic plane. For the typical luminosity of known Milky Way TeV sources of 10^{33-34} erg/s, the CTA GPS will provide a distance reach of $\sim$20 kpc, detecting essentially the entire population of such objects in our Galaxy and providing a large sample of objects one order of magnitude fainter. The excellent angular resolution of CTA is critical here to avoid being limited by source confusion rather than flux (see Figure 1.3).
- **Survey of the Large Magellanic Cloud (LMC)** (Chapter 7): Providing a face-on view of an entire star-forming galaxy, resolving regions down to 20 pc in size with sensitivity down to luminosities of $\sim 10^{34}$ erg/s. CTA aims to map the diffuse LMC emission as well as individual objects, providing information on relativistic particle transport.

These surveys will establish the populations of VHE emitters in Galactic and extragalactic space and provide large enough samples of objects to understand source evolution and/or duty cycle. Data products from the survey KSPs include catalogues and flux maps which will serve as valuable long-term resources to a wide community.

Some other KSPs are also effectively surveys due to the wide field of view. For example, a deep observation of the Perseus Cluster is envisaged (see Chapter 13) to provide a sample of low redshift galaxies and to have

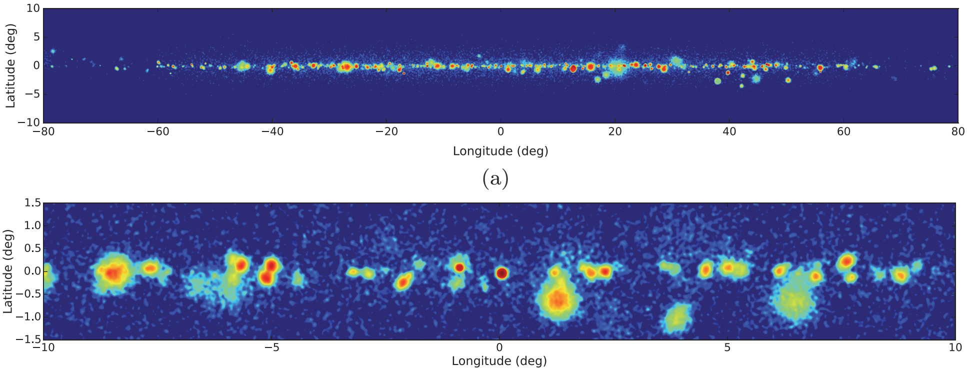

(a)

(b)

Figure 1.3: (a) Simulated CTA image of the Galactic plane for the inner region, $-80^\circ < l < 80^\circ$, adopting the proposed GPS KSP observation strategy and a source model incorporating both supernova remnant and pulsar wind nebula populations, as well as diffuse emission. (b) A zoomed image of an example 20° region in Galactic longitude.

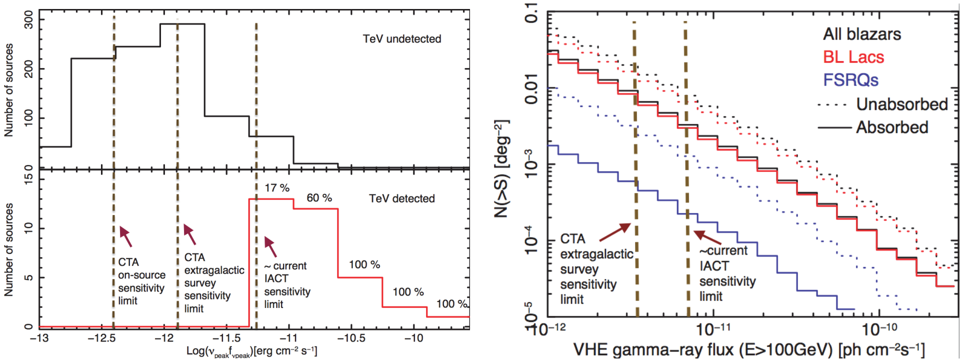

(a) (b)

Figure 1.4: Predictions for the number of blazars on the sky in the GeV–TeV domain. (a) Source counts versus peak synchrotron flux. The upper panel shows predictions by [12] together with the current and envisioned sensitivity limits of IACTs. The lower panel shows detected AGN with current instruments. (b) Expected source counts as a function of the integral gamma-ray flux above 100 GeV, from Ref. [13].

sensitivity to the low end of the luminosity function of active galaxies as well as to diffuse emission associated with accelerated hadrons or dark matter annihilation.

The search for an annihilation signature of dark matter, throwing light on the nature of the dark matter particles, is a key part of the CTA research programme. The prime targets are the Galactic Centre (Chapter 5) and Milky Way satellite galaxies, but the surveys introduced above will probe concentrations of dark matter in the LMC and Milky Way, providing complementary datasets. The strategy for dark matter detection with CTA is introduced in Chapter 4.

Surveys will in general be conducted in a mode with telescopes co-pointed, but a *divergent mode* is also possible and under consideration for the Extragalactic Survey, offering increased instantaneous field of view (∼20° × 20°) and survey depth at the expense of angular and energy resolution.

1.1.2 *Short Timescale Capabilities*

CTA is a uniquely powerful instrument for the exploration of the violent and variable universe. It has unprecedented potential both in terms of energy reach and sensitivity to short timescale phenomena. Figure 1.5 compares the sensitivity of CTA to that of Fermi-LAT as a function of observation time. CTA has four orders of magnitude better sensitivity to minute timescale phenomena at energies around 25 GeV. Even at variability timescales of 1 month, CTA will be a factor 100 more sensitive than Fermi-LAT. Only for emission which is stable over the full mission lifetime of Fermi are the

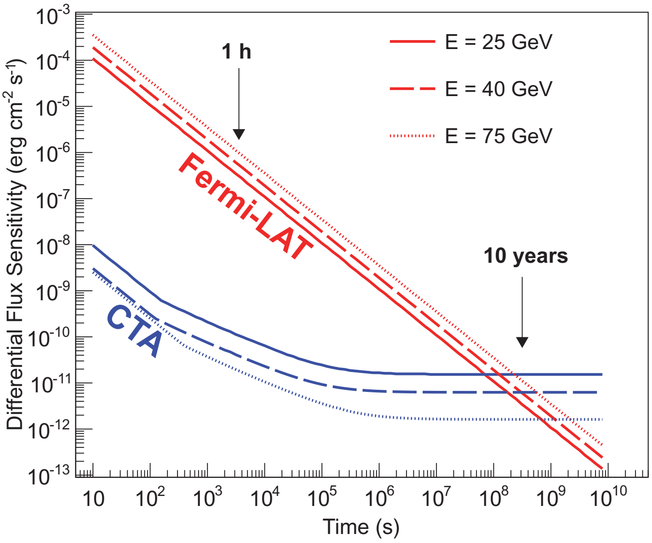

Figure 1.5: Comparison of the sensitivities of CTA and Fermi-LAT in the energy range of overlap versus observation timescale. Differential flux sensitivities at three energies are compared. Adapted from Ref. [18]. Note that the Pass 6 sensitivity is shown for Fermi-LAT and the CTA sensitivity is calculated using an early model of the arrays; thus, better sensitivities for both Fermi-LAT and CTA are now expected.

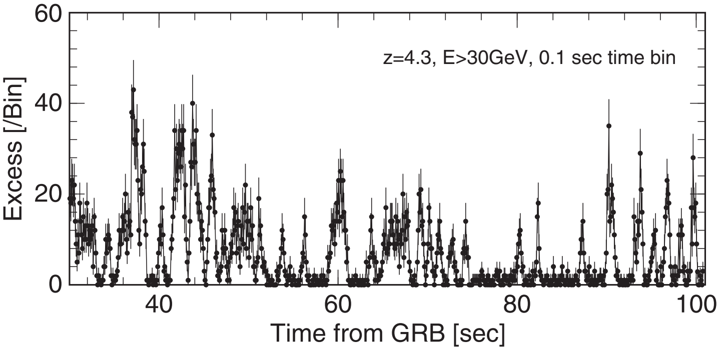

Figure 1.6: Simulated CTA GRB light curve, based on the Fermi-LAT-detected GRB 080916C at $z = 4.3$. See Figure 9.1 for more details.

sensitivities of the two instruments comparable in the lowest part of the CTA energy range. Instruments such as HAWC, which have sensitivity in the higher part of the CTA range, are also limited at short timescales by (relative to CTA) small collection areas, as well as low signal to noise.

The ability to probe short timescales at the highest energies will allow CTA to explore the connection between accretion and ejection phenomena surrounding compact objects, study phenomena occurring in relativistic outflows, and open up significant phase space for serendipitous discovery. Particularly important targets for CTA are gamma-ray bursts (GRBs), AGN, and Galactic compact object binary systems. The most dramatic case is that of GRBs where CTA will make high-statistics measurements for the first time above ∼10 GeV, probing new spectral components which will shed light on the physical processes at work in these systems [14] (see Figure 1.6).

CTA's reach to ultra high energies also provides access to a regime where cooling times for electrons are extremely short and variability is expected even for objects which are currently considered as stable sources (for example the Crab pulsar wind nebula [15] and the supernova remnant RX J1713−3946 [16]).

As well as having unprecedented sensitivity to emission on short timescales, CTA will be able to respond very rapidly both to external alerts and in delivery of alerts to other observatories. The absolute maximum repointing times for the CTA telescopes (to and from anywhere in the observable sky) will be 50 seconds for the LSTs and 90 seconds for the MSTs and SSTs, with the goal to reach shorter slewing times. This fast slewing capability is particularly important for capturing transient phenomena such as GRBs.

The wide field of view and unprecedented sensitivity of CTA make the serendipitous detection of transient or variable VHE emission likely. To maximise the scientific return, CTA will be equipped with a low-latency (effectively real-time) analysis pipeline which will monitor the field of view for variability on a wide range of timescales. The detection of a gamma-ray flare in the field and the issuing of an alert will be possible within 60 seconds. CTA will itself respond to such alerts by repositioning the telescopes, by modifying the observing schedule and by alerting other observatories to allow rapid follow-up. See Ref. [17] for details.

The KSPs which rely on the short-timescale capabilities of CTA include:

- **Transients** (Chapter 9): Comprising a programme responding to a broad range of multi-wavelength and multi-messenger alerts, including GRBs, gravitational wave transients, and high-energy neutrino transients. Rapid feedback to the wider community on the VHE gamma-ray properties of transients is a key element of the KSP.
- **Active Galactic Nuclei** (Chapter 12): Where flaring activity forms a key part of the science case, with rapid bi-directional information flow again critical. Blazars exhibit the fastest known variability (1 minute timescales) at TeV energies and blazar flares can be used to search for Lorentz invariance violation, as well as to cast light on the physics of the ultra-relativistic inner jets of these systems (see for example [19]).
- **Galactic Plane Survey** (Chapter 6): With multiple observations of every part of the Plane allowing the identification of objects variable on timescales from seconds to months, including the expected discovery of many new gamma-ray binaries [20]. Real-time alert generation from CTA will maximise the scientific return from short-timescale transients.

1.1.3 *Capabilities Beyond Gamma Rays*

While CTA is designed as a gamma-ray observatory it will, as part of its normal operation, collect an enormous quantity of valuable information on charged cosmic rays. Of particular interest are the highest energy cosmic-ray electrons, which must be associated with nearby particle accelerators (which can therefore be studied using CTA data in both the gamma-ray and electron channels), and heavy nuclei, which can be separated using their direct Cherenkov emissions (i.e. from the primary cosmic ray, rather than from the secondary products in an air shower). Cosmic-ray observations with CTA are discussed in Ref. [21] and in Chapter 14.

Both gamma-ray and cosmic-ray observations with CTA rely on nanosecond-timescale cameras to detect Cherenkov light. Other uses for the very large optical-photon collection area of the CTA telescopes do exist. Longer integration time observations of *optical* targets with CTA could include the use of intensity interferometry, to provide unprecedented angular resolution at blue wavelengths for bright sources (see [22] and Chapter 14).

1.2 Overview of CTA Science Themes

Here, we provide a brief overview of the main scientific questions and topics addressed by CTA, referring forward where relevant to the KSP chapter for details.

1.2.1 *Understanding the Origin and Role of Relativistic Cosmic Particles*

Relativistic particles appear to play a major role in a wide range of astrophysical systems, from pulsars and supernova remnants to active galactic nuclei and clusters of galaxies. Within the interstellar medium of our own Galaxy, these cosmic rays are close to pressure equilibrium with turbulent motions of gas and magnetic fields, yet the relationship between these three components, and the overall impact on the star-formation process and the evolution of galaxies, is very poorly understood. CTA will provide the first high angular resolution measurements of cosmic-ray protons and nuclei (rather than the energetically sub-dominant electrons that produce the non-thermal emission seen at radio and X-ray wavelengths) in astrophysical systems, providing insights into the process(es) of acceleration, transport, and the cosmic-ray-mode feedback mechanisms in these systems. Historically, non-thermal effects in astrophysical systems have largely been ignored or parametrised away due to a lack of high-quality data. The insights from CTA will therefore represent a major contribution to our deepening understanding of the processes by which galaxies and clusters of galaxies evolve, in the era of precision astrophysics with major instruments across all wavebands from radio (SKA) to VHE gamma ray (CTA).

Below, we introduce the main elements of this theme, moving from the accelerators themselves to the impact of accelerated particles.

1.2.1.1 *Cosmic accelerators*

The primary goal of gamma-ray astrophysics thus far has been to establish in which cosmic sources particle acceleration takes place and, in particular, to establish the dominant contributors to the locally measured ‘cosmic rays’ which are 99% protons and nuclei (collectively referred to as ‘hadrons’). Much progress has been made in the last decade in this area, with the combination of Fermi-LAT and IACT data proving extremely effective in identifying the brightest Galactic accelerators and providing strong evidence of hadron acceleration in a handful of sources. However, key questions remain unanswered: are supernova remnants (SNR) the only major contributor to the Galactic cosmic rays? Where in our Galaxy are particles accelerated up to PeV energies? What are the sources of high-energy cosmic electrons? What are the sources of the ultra high-energy cosmic rays (UHECRs)?

CTA will address all of these questions and also the critical issue of the mechanism(s) for particle acceleration at work in cosmic sources, through two main approaches:

- **a census of particle accelerators in the universe**, with Galactic and extragalactic surveys and deep observations of key nearby galaxies and clusters and
- **precision measurements of archetypal sources**, where bright nearby sources will be targeted to obtain resolved spectroscopy or very high statistics light curves, to provide a deeper physical understanding of the processes at work in cosmic accelerators.

A general census is required to understand the populations of accelerators and the evolution/life cycle of these source classes. Deep observations of individual sources are required to acquire the very broad-band spectra needed to unambiguously separate lepton and hadron acceleration and to test acceleration to the highest energies possible for Galactic accelerators.

While the main resources for the census are the KSP survey observations introduced above, the Guest Observer (GO) programme will provide most of the deep observations of individual sources. For example, the deep observation of the TeV-bright pulsar wind nebula (PWN) HESS J1825-137, mapping in detail its energy-dependent morphology and studying particle propagation and cooling in the post-shock flow [15], is anticipated as a GO proposal.

One key object that is included in the proposed KSPs is the TeV-bright, young supernova remnant (SNR) RX J1713-3946 (see Figure 1.7 and Chapter 10), where the dominant gamma-ray emission mechanism is unclear from current measurements [23, 24], but where CTA can resolve the ambiguity between electron- and proton-dominated emission and resolve sub-structure

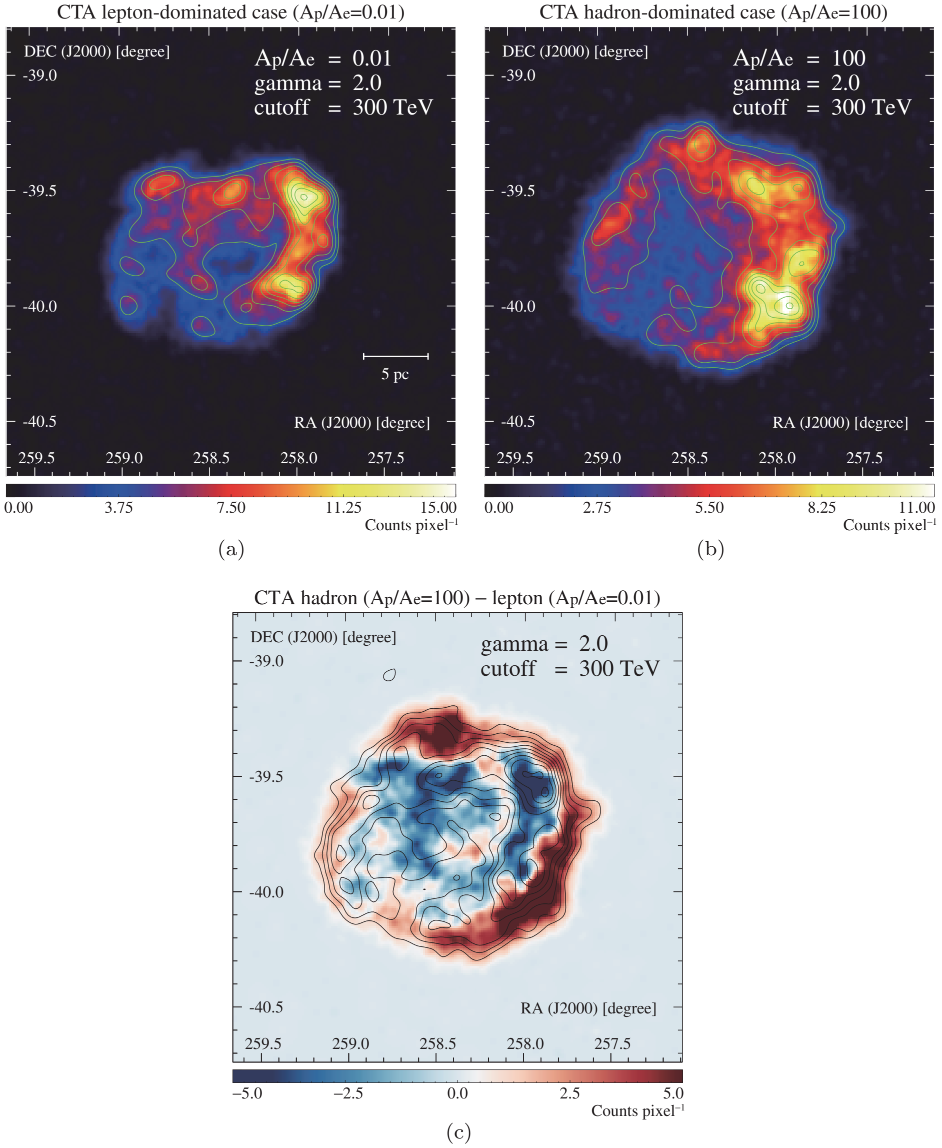

Figure 1.7: Simulated CTA images of the TeV-bright supernova remnant RX J1713-3946 for different emission scenarios, showing the power of CTA to differentiate between these scenarios. Reproduced from Ref. [25].

within the SNR shell on scales that are important for our understanding of the acceleration process.

Known TeV-emitting source classes where CTA data will have a transformational impact on our understanding include PWNe, gamma-ray binaries, colliding-wind binaries, massive stellar clusters, starburst galaxies, and active galaxies. There is clearly huge potential for the discovery of new classes of accelerators, with emission from clusters of galaxies (see Chapter 13) as one of the most exciting possibilities.

1.2.1.2 *Propagation and influence of accelerated particles*

Beyond the question of how and where particles are accelerated in the universe is the question of what role these particles play in the evolution of their host objects and how they are transported out to large distances. On the scale of clusters of galaxies, cosmic rays with TeV–PeV energies are thought to be confined over a Hubble time [26]. On smaller scales, they typically escape from their acceleration sites and may impact upon their environments in a number of ways:

1. as a dynamical constituent of the medium,
2. through generation / amplification of magnetic fields, and
3. through ionisation and subsequent impact on the chemical evolution of, for example, dense cloud cores.

All these effects are relevant for the interstellar medium of our own Galaxy and are likely to be important in star-forming systems on all scales (see, e.g. Chapters 11 and 7). The first aspect is also likely to be important for the process of AGN feedback on the host galaxy cluster and growth of massive galaxies (see, e.g. Chapter 12 and 13).

CTA will map extended emission around many gamma-ray sources and look for energy-dependent morphology associated with diffusion (in the case of hadrons) or cooling (in the case of electrons). As the energy dependence is expected to be opposite in the two cases, such mapping provides another means to separate emission from these two populations. It is CTA's unprecedented (in the gamma-ray domain) angular resolution, energy resolution, and background rejection power that make this possible (see, e.g. Chapter 10).

There are important synergies here with THz instruments capable of mapping molecular material and deriving the physical conditions in the TeV-emitting regions (see Chapter 2).

Again, many of the key targets for this topic are left for GO proposals, with the expectation that teams with access to key data sets at other wavelengths will propose CTA observations. For example, although there are a number of galaxy clusters and AGN with cluster-scale impact that are potentially detectable with CTA, the KSP on galaxy clusters targets only a single object (Perseus, see Chapter 13).

1.2.2 *Probing Extreme Environments*

Particle acceleration to very high energies is typically associated with extreme environments, such as those close to neutron stars and black holes, or in relativistic outflows or explosions. VHE emission from accelerated particles can therefore act as a probe of these environments, providing access to time and distance scales which are inaccessible in other wavebands. VHE emission often escapes from systems where UV and X-ray emission is absorbed, and it provides information independent of assumptions on magnetic field strengths. In addition, VHE photons from distant objects can be used as a probe of the intervening space. Gamma–gamma pair production signatures will allow us to measure the redshift evolution of the UV–IR background, and hence the star-formation history of the universe, to probe magnetic fields in cosmic voids down to values many orders of magnitude below the reach of any other technique. CTA will also establish if VHE photons heat the gas in these under-dense regions, suppressing the formation of dwarf satellite galaxies.

Below, we consider three key areas within this theme where CTA data will have a transformational impact, referring forward to the Key Science Projects that will address them and to potential major GO observations.

1.2.2.1 *Black holes and jets*

Active galactic nuclei are thought to harbour supermassive black holes (SMBHs), accreting material and producing collimated relativistic outflows by a still poorly understood process. Similarly, accreting stellar mass black holes are known to produce jets, and particle acceleration seems to be universally associated with BH-powered jets. Acceleration may occur extremely close to the SMBH (and must do so in some systems to explain the remarkably short variability timescales, see Figure 1.8) or up to Mpc scales, where the largest AGN jets finally terminate. Active galaxies are seen as one of the most likely sites of the acceleration of the UHECRs, with energies up to around 10^{20} eV, but so far there is no strong evidence for hadronic acceleration in AGN jets.

Simultaneous broad-band data (see Chapter 2) is needed to study variable jet emission in both Galactic and extragalactic systems, with CTA data playing a key role: establishing the presence of very high energy particles, identifying the presence of hadrons, and studying extremely

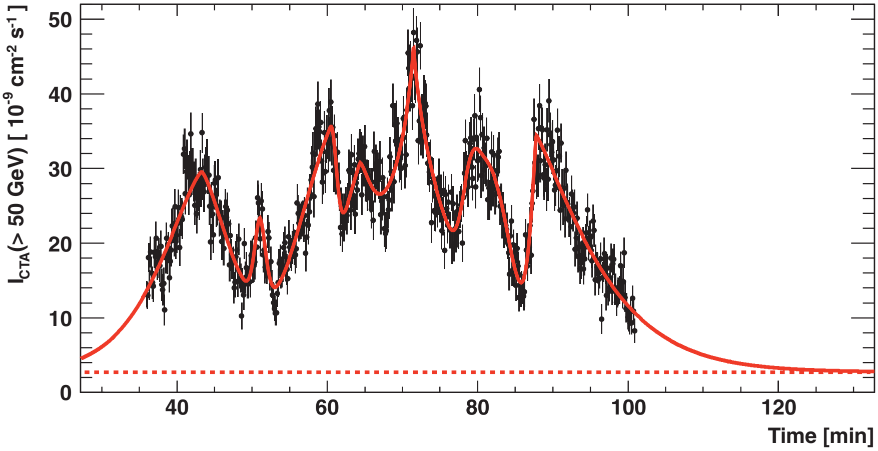

Figure 1.8: Probing ultra-fast variability in the inner jet of an active galaxy: simulated CTA light curve for the 2006 flare of PKS 2155-304 (reproduced from Ref. [30]). Such observations provide access to timescales much shorter than the light-crossing time of the supermassive black hole.

short-timescale variability that provides information on the smallest spatial scales and probes the bulk ultra-relativistic motions of the inner jet. Time-resolved VHE spectral measurements are key to disentangling leptonic and hadronic emission scenarios, to study jet power and dynamics, and to probe magnetic fields in this extreme environment. While a significant sample of AGN will be targeted in the Active Galactic Nuclei KSP (see Chapter 12) and discovered in the CTA survey KSPs, it is anticipated that the majority of targeted AGN observations with CTA will occur in the open time, with many as target-of-opportunity (ToO) proposals associated with triggers from other wavelengths.

The low luminosity AGN at the heart of our own Galaxy, Sgr A*, is coincident with a TeV source and has associated non-thermal emission in the radio and X-ray bands. However, the sensitivity, resolution, and pointing precision of current gamma-ray telescopes are insufficient to separate the emission from very nearby sources from the diffuse emission around the Galactic Centre. CTA will map this region in unprecedented detail (see Chapter 5), probing the relationship between the central source and the diffuse emission and, on much larger scales, up to the Fermi bubbles.

There is evidence from current IACTs for TeV emission from a single system hosting a stellar mass black hole: Cygnus X-1. The sensitivity of CTA should allow this object to be studied in detail, opening the door to studies of high-energy non-thermal processes associated with stellar mass black holes and allowing the first comparisons to be made with SMBH systems. While the Core Programme will cover the Cygnus region as part of the GPS and black hole binary activity will be used to trigger the Transients KSP (see Chapters 9 and 6), the bulk of observations of such objects, including deep observations of Cygnus X-1, are expected throughout the GO programme, again likely from proposers with access to data from other wavelength bands.

The recent discovery of gravitational wave (GW) emission associated with the mergers of massive compact objects [7, 27, 28] raises many exciting new possibilities in observational astrophysics and many questions about the evolution of high mass binary systems [27, 29]. Clearly, the possibility for jet formation and acceleration of particles to TeV energies in such systems exists, and as GW detections will, for the foreseeable future, all originate within the TeV gamma-ray horizon; such alerts will form a key target for CTA (see Chapter 9).

1.2.2.2 *Neutron stars and relativistic outflows*

CTA will probe the environment around neutron stars via pulsed gamma-ray emission from the magnetosphere of pulsars and study the ultra-relativistic outflows of these systems via mapping and spectral measurements of the associated synchrotron/inverse-Compton nebula and (possibly and uniquely) the unshocked pulsar wind. Young and energetic (in terms of available rotational energy) pulsars cluster tightly along the Galactic plane, and hence the majority of objects will be covered by the CTA Galactic Plane Survey (see Chapter 6). Two key objects, HESS J1825-137 and the Vela pulsar (and the associated Vela X nebula), are very promising targets and are expected to be targeted by GO proposals.

Binary systems including a pulsar provide a unique opportunity to study a relativistic outflow under changing physical conditions as the orbit progresses, via energy-dependent light-curve measurements. Several such systems will be covered by the CTA Galactic Plane Survey, but deep observations are again expected as GO proposals.

Merging neutron stars and other compact object mergers are the likely counterparts of short GRBs and are of course the targets of the young field of gravitational wave astronomy. CTA will be able to respond rapidly to triggers from GRB or GW instruments and hence probe the highest energy processes associated with such events.

1.2.2.3 *Cosmic voids*

Much of the universe consists of extremely under-dense regions known as cosmic voids. Very high-energy photons interact within these voids and allow us to probe the radiation fields and magnetic fields that they contain. The extragalactic background light (EBL) is the integrated emission from stars and galaxies of all types throughout the evolution of the universe. As such, it is an important tool for cosmology, but it is extremely difficult to measure directly due to very strong foregrounds from the Solar System and the Milky Way. However, the EBL leaves an imprint on the measured spectra of gamma-ray sources, via the process of gamma–gamma pair production. The wide-band, high-quality spectra measured with CTA for a large number of objects will allow the EBL spectrum from the optical to the far infrared to be precisely measured at redshift zero. Furthermore, with the expected large sample of blazars up to redshift $\sim$1 detected with CTA, the evolution of the EBL with cosmic time can be probed for the first time. See Ref. [31] and Chapter 12 for more details.

Pair production by TeV photons interacting in voids also offers the prospect of measuring the extremely weak magnetic fields thought to exist in these regions. Secondary gamma rays are produced by the primary $e^{\pm}$ pairs via inverse Compton scattering on the EBL. A cascade can then develop from further pair and inverse Compton interactions. Depending on the typical value of the intergalactic magnetic field (IGMF), deflections of the secondary particles may either be small enough that secondary components may be observable as *pair echoes*, which arrive with a time delay relative to the primary emission, or as a *pair halo*, potentially resolvable extended emission around the primary source. The properties of the extended emission depend on the IGMF strength. A strong enough IGMF ($>10^{-12}$ G) leads to full isotropisation of the cascade emission and formation of a physical pair halo, while a weaker magnetic field leads to the appearance of an extended emission with an IGMF-dependent size. If the IGMF strength is in the range of $B \sim 10^{-16} - 10^{-12}$ G, the spatially extended emission may be detectable and resolvable by CTA by virtue of its high sensitivity and angular resolution; e.g. for a source at a distance of 100 Mpc, the extended emission would be on the $\sim 1^{\circ}$ scale and would be comfortably contained within the CTA field of view. See Ref. [30] and Chapter 12 for details.

If, as has been recently suggested, TeV electrons produced in gamma–gamma interactions in the voids do not initiate cascades but rather *heat* the ultra-low dense plasma [32], CTA will allow this hypothesis to be proven and the heating rate to be very well constrained. As such, heating could be the dominant means of heating in low density regions after redshift ∼2 and could solve the problem of the missing dwarf satellite galaxies; this measurement would be a very valuable addition to cosmology.

1.2.3 *Exploring Frontiers in Physics*

The reach of CTA encompasses considerable discovery space in the area of fundamental physics. CTA will reach the expected thermal relic cross-section for self-annihilating dark matter for a wide range of dark matter masses, including those inaccessible to the Large Hadron Collider (LHC). The long travel times of gamma rays from extragalactic sources combined with their short wavelength make them a sensitive probe for energy-dependent variation of the speed of light due to quantum-gravity induced fluctuations of the metric. CTA will be sensitive to such effects on their expected characteristic scale: the Planck scale. On their long journey, gamma rays may couple to other light particles such as axion-like particles (ALPs), under the influence of intergalactic magnetic fields. Such photon-ALP oscillations effectively make the universe more transparent to gamma rays and, akin to neutrino oscillations, introduce a spectral modulation. Each of these effects would represent a very major discovery, alone worth the effort of constructing and operating CTA. The major step in sensitivity and energy coverage that CTA represents brings such effects within reach and could well allow further issues in fundamental physics to be addressed.

Below, we briefly consider each of these fundamental physics probes in turn, referring forward to the Key Science Projects which will address them in detail.

1.2.3.1 *Dark matter*

A major open question for modern physics is the nature of dark matter. On scales from kpc to Mpc, there are numerous lines of evidence for the presence of an unknown form of gravitating matter that cannot be accounted for by the Standard Model of particle physics. The observation of the acoustic oscillations imprinted into the cosmic microwave background quantifies this dark component as making up about 27% of the total universe energy budget. Being dominant with respect to the baryonic component, which accounts for only about 5% of the total energy density, dark matter shaped the growth of cosmic structures through gravitational instability. By comparing the observed distribution in large galaxy redshift surveys with computer simulations of structure formation, it emerges that the particles constituting the dark matter had to be moving non-relativistically when they stopped scattering in the early universe, hence the term cold dark matter (CDM). The observational evidence has led to the establishment of a concordance cosmological model, dubbed ΛCDM. Despite the fact that the standard cosmology rests on the dark matter paradigm, we still have no clue as to its particle nature. One of the most popular scenarios for CDM is that of weakly interacting massive particles (WIMPs) that comprise a large class of non-baryonic candidates with a mass typically between few tens of GeV and a few TeV and an annihilation cross-section of the order of the weak interaction. Natural WIMP candidates are found in many models, for example, in supersymmetric extensions of the Standard Model and indeed in any model incorporating the breaking of electroweak symmetry by the Higgs mechanism. The success of the WIMP scenario relies on the observation that weak scale masses (GeV–TeV) and couplings yield a self-annihilation cross-section that generically implies their relic abundance to be close to the currently observed value for dark matter. This (velocity-weighted) cross-section ($\sim 3 \times 10^{-26}\,\mathrm{cm}^3\,\mathrm{s}^{-1}$) is therefore a benchmark value that CTA aims to reach through searches for the gamma rays arising from annihilation of dark matter in the Galaxy, as has been attempted already by all operating IACTs. Note that CTA is also sensitive to particle physics models in which gamma rays result from the decay of dark matter particles.

Obtaining convincing evidence for dark matter from excesses in the measured energy spectrum of gamma rays needs careful assessment of (uncertain) astrophysical backgrounds as well as a good understanding of the Galactic dynamics of dark matter. There is a major complementary effort at the LHC in attempting to create dark matter directly in the laboratory or in detecting its virtual traces on Standard Model signals. Some underground direct-detection experiments that measure the recoil energy of nuclei in a well-shielded detector when hit by a passing dark matter particle have reported events in their signal region (e.g. CDMS-Si, CRESST, and EDELWEISS-II) although these are all consistent with being residual background and are in tension with stronger limits placed by other experiments (e.g. XENON100, LUX, and CDMS II-Ge). Moreover, controversial evidence has been presented of an annual modulation signal (due to our motion around the Sun) of dark matter with mass around 10 GeV (presented originally by DAMA/LIBRA but, more recently, also by CoGeNT). Concerning indirect detection, CTA will have a much greater potential for dark matter detection than the current generation of VHE telescopes, for a number or reasons: (1) CTA's extended energy range will allow searches for WIMPs with lower mass, (2) the improved sensitivity in the entire energy range will improve the probability of detection of dark matter, (3) the increased field of view with a homogeneous sensitivity as well as the improved angular resolution will allow for more efficient searches for extended sources and spatial anisotropies, and (4) the improved energy resolution will increase the chances of detecting a possible spectral feature in the dark matter induced photon spectrum.

By observing the region around the Galactic Centre and by adopting dedicated observational strategies (see Chapter 5 and Figure 1.9), CTA will indeed reach the canonical velocity-averaged annihilation cross-section of $\sim 3 \times 10^{-26}\,\mathrm{cm}^3\,\mathrm{s}^{-1}$ for a dark matter mass in the range ∼200 GeV to 20 TeV — something which is not possible with current instruments for any exposure time. Together with the constraints from Fermi-LAT on dark

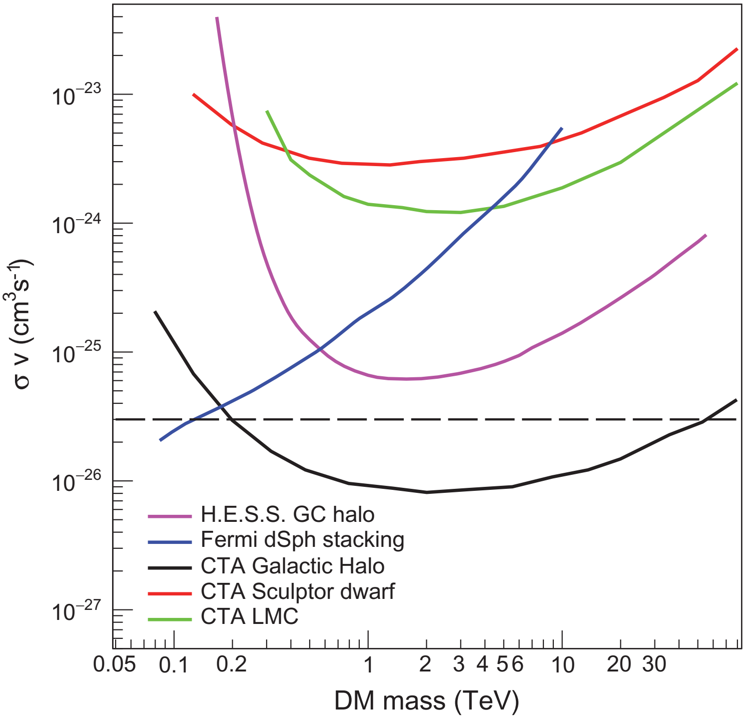

Figure 1.9: CTA sensitivity to a WIMP annihilation signature as a function of WIMP mass, for nominal parametres and for the multiple CTA observations described in Chapter 4. The dashed horizontal line indicates the likely cross-section for a WIMP which is a thermal relic of the Big Bang. See Figure 4.1 for a discussion of the various sensitivities.

matter lighter than a few hundred GeV, this will seriously constrain the WIMP paradigm for CDM in the case of non-detection. Models with a large photon yield from dark matter annihilation will be constrained to even smaller cross-sections. In conclusion, the WIMP paradigm, either through detection or non-detection will be significantly impacted upon during the first years of operation of CTA. Additional targets, including Milky Way satellites (see Chapters 4 and 7), complement the primary Galactic Centre observation, with considerable scope for Guest Observer observations.

If signatures of dark matter do appear in direct-detection experiments or at the LHC, gamma-ray observations will provide a complementary approach to identify dark matter, while the typical cutoff of the energy spectrum will allow for a precise mass determination. If such experiments do not detect dark matter, as may be the case for sufficiently heavy dark matter candidates, CTA may be the only way to look for such particles over the next decade.

1.2.3.2 *Quantum gravity and axion-like particle search*

Photons of energy extending up to hundreds of TeV which will be detected by CTA from distant cosmic sources provide a powerful tool to search for possible new physics beyond the Standard Model. Apart from the search for annihilation/decay signals from dark matter, there is the exciting possibility of detecting ALPs and finding evidence of Lorentz invariance violation (LIV) associated with possible quantum gravity effects on space-time at the Planck scale. Blazars (Chapter 12) and GRBs (Chapter 9) have been identified as the most promising (bright and distant) target classes for both these searches. It has been suggested that quantum gravity effects may induce time delays between photons with different energies travelling over large distances, corresponding to a non-trivial refractive index of the vacuum. High statistics measurements of GRBs and blazars over a wide energy range (see e.g. Figures 1.8 and 1.6) will allow CTA to probe this possibility significantly better than is possible with current IACTs. Even a negative result is rather important in this context to guide theoretical work.

Axions are a proposed solution to the strong-CP problem of quantum chromodynamics and also well-motivated candidates to constitute a part or all of CDM. ALPs would not have the correct properties (i.e. mass and coupling) to explain the strong-CP problem, but they could potentially be an important component of the dark matter. ALPs are expected to convert into photons (and vice versa) as they traverse cosmic magnetic fields. In the case of a very distant AGN, the ALP/photon coupling can result in a detectable enhancement of the TeV photon flux (which competes with the absorption on the EBL), dependent on the ALP mass. The search for ALPs by CTA will complement dedicated laboratory experiments and studies using indirect astrophysical tests and X-ray telescopes. See Chapter 12.1.3 for more details.

1.3 Community Input to the Science Case

The scientific motivations and requirements for CTA have been developed by the CTA Consortium with the engagement of the much wider community of scientists working in astrophysics and astroparticle physics. A dedicated work package (LINK) of the FP7-funded Preparatory Phase of CTA was created to provide this community engagement. A series of workshops provided the main basis for reaching out to the broader community, gathering input to refine the science goals, to perform the scientific optimisation of the instrument, and to develop user interfaces and services to provide the best possible scientific exploitation of the observatory.
Three FP7-supported LINK workshops took place:

- 1st: *Probing physics beyond the Standard Model with CTA*, Oxford, UK, November 11–12, 2010.
- 2nd: *Links between CTA science and cosmic ray physics at high energies*, Buenos Aires, Argentina, November 19–21, 2012.
- 3rd: *X-raying the gamma-ray Universe*, Hakone, Japan, November 4–6, 2013.

Additional symposia and workshops included:

- *AGN physics in the CTA era*, Toulouse, France, May 16–17, 2011.
- *The highest-energy gamma-ray Universe*, A Joint Discussion Session of the International Astronomical Union General Assembly, Beijing, China, August 20–21, 2012.
- *Extragalactic gamma-ray astronomy with CTA*, Muonio, Finland, March 18–21, 2013.
- *The gamma-ray sky in the era of Fermi & CTA*, Symposium at the European Week of Astronomy & Space Science (EWASS), Turku, Finland, July 11–12, 2013.

These meetings were all targeted at different communities, where links to CTA were apparent, but needed to be developed. In addition, a number of national-level meetings took place, exploring links to existing strong theoretical and experimental activities in individual CTA member countries.

As part of these activities, a special issue of the journal Astroparticle Physics was also produced: *Seeing the High-Energy Universe with the Cherenkov Telescope Array* [33], dedicated to CTA and with seven articles by prominent scientists outside of the CTA Consortium, as well as detailed studies and highlight articles written by the Consortium science teams.

This page intentionally left blank

2

Synergies

CTA will have important synergies with many of the new generation of astronomical and astroparticle observatories. As the flagship VHE gamma-ray observatory for the coming decades, CTA plays a similar role in the VHE waveband as the SKA in radio, ALMA at millimetre, or E-ELT/TMT/GMT in the optical wavebands, providing excellent sensitivity and resolution compared to prior facilities. At the same time, the scientific output of CTA will be enhanced by the additional capabilities provided by these instruments (and vice-versa). MWL and MM studies using CTA provide added value to the science cases in two main ways:

Non-thermal emission: To understand the origin of cosmic rays and the extreme physical environments that produce them, it is necessary to study non-thermal signatures that span many orders of magnitude in frequency in the broad-band spectral energy distribution (SED) of a given object. In the case of time-variable emission, such studies require simultaneous observations and/or alerts and triggers between observatories.
Source properties: Information on the nature of gamma-ray emitting sources can be provided by MWL observations, enabling, for example, the object class, environmental conditions, or the distance to be established. For this purpose, simultaneous observations are in general not required, except for the need to characterise transient sources, for example in the case of gamma-ray burst redshift measurements.

The need for (simultaneous) MWL and MM observations has been considered as a factor in the site selection process for CTA and in the preparations for CTA science. Below, we describe the main areas in which synergies exist by

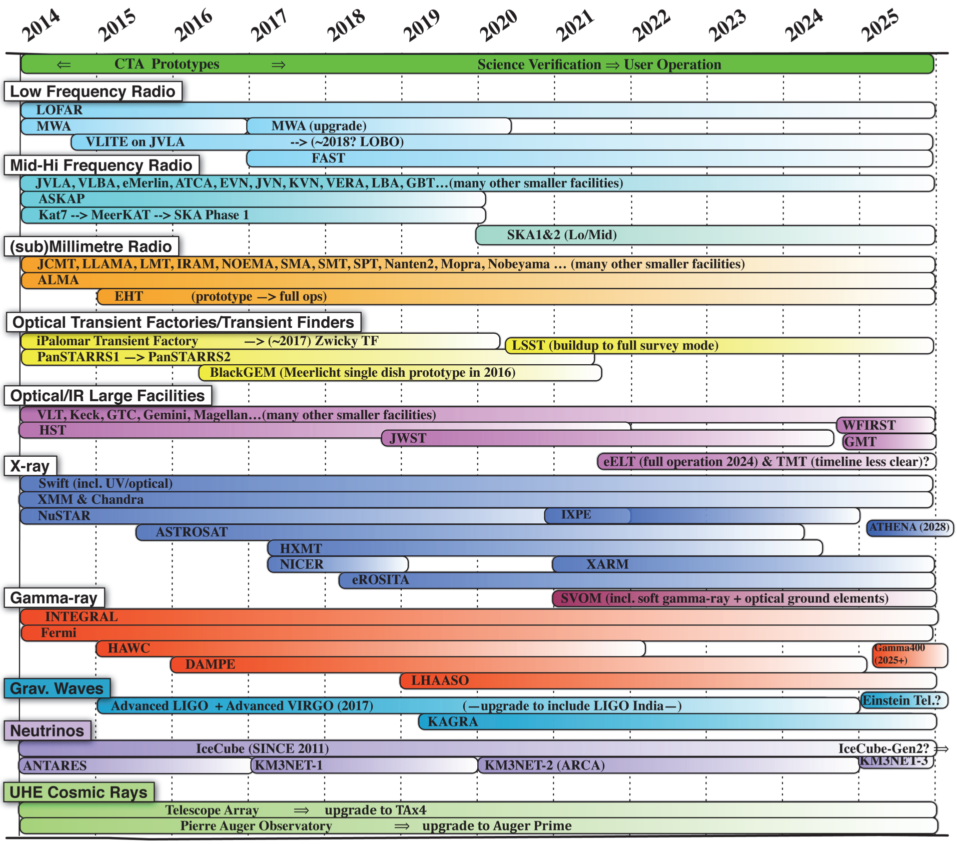

Figure 2.1: Timeline of major MWL/MM facilities over the next decade. Note that the lifetimes of many facilities are uncertain, contingent on performance and funding. We indicate this uncertainty via the gradient, but have chosen timelines based on the best information currently available. Instruments still in the proposal phase have been omitted, as have many relevant survey instruments mentioned in the text, for the sake of space.

waveband; see also a summary timeline of major facilities in Figure 2.1. We also discuss cases where agreements between CTA (Consortium or Observatory) are desirable, as well as cases where data can be obtained without agreement via publicly accessible archives. Detailed MWL/MM plans can be found in the individual KSP chapters. Please note that there are many important and complementary facilities to CTA the world over, and for the sake of space we cannot list them all, particularly the many existing survey instruments. We thus focus primarily on the newest developments, and this chapter is representative rather than exhaustive.

2.1 Radio to (Sub)Millimetre

Until a few decades ago, the radio band provided our main window to the non-thermal universe, via the cyclo-synchrotron emission of relativistic electrons that often dominates over thermal processes below ∼10 GHz. Synchrotron emission goes hand in hand with particle acceleration, due to the inferred presence of magnetic fields and the presence of relativistic electrons, either directly accelerated or produced as secondaries. In addition, dark matter annihilation scenarios usually lead to the production of synchrotron-emitting secondaries along with gamma-ray emission.[a]

The radio bands also have tremendous advantages for localising acceleration zones, because of the high angular resolution (e.g., down to tens of microarcseconds with VLBI) and the ability to observe in daylight. The combination of radio measurements with those at very high energies can provide limits on the electron density independent of assumptions about magnetic field strengths and can help determine which of several competing non-thermal processes dominate at the highest energies. Radio measurements also provide important magnetic field constraints via Faraday rotation and provide the ephemerides of known pulsars, to guide the search for potential gamma-ray pulsations with CTA. The success of Fermi-LAT in this regard relied on close cooperation with radio observatories [35]. An exciting recent development in the radio domain is the discovery of fast radio bursts [36, 37], with the possibility of high energy counterparts and potential synergies due to the wide field of view of CTA.

After decades of incremental improvements, radio astronomy has now again entered a rapid development phase. Many existing facilities have recently received major upgrades, providing much improved bandwidth and sensitivity (e.g., JVLA, e-MERLIN). At the same time, windows to entirely new parts of the radio spectrum at both low and high frequencies are finally being opened. In particular, the low-frequency bands (30–80, 120–240 MHz) are now being explored using LOFAR, which can monitor 2/3 of the sky nightly in Radio Sky Monitor mode and has a Transients Key Project dedicated to the detection, triggering, and cataloguing of new radio transients. In China, the Five-hundred-metre Aperture Spherical radio Telescope (FAST, 70 MHz to 3 GHz), the largest radio telescope ever built, had first light in 2016 and is now undergoing commissioning tests. A key new radio project is the Square Kilometre Array (SKA), whose phase 1 will come online during CTA's science verification phase, followed by a ramp up to full operation with phase 2 by about 2024. SKA will have unprecedented sensitivity and excellent angular resolution, and the use of phased-array technology allows for a very large field of view, ideal for survey studies and transient detection (see Section 2.2). The pathfinders for SKA are very powerful instruments in their own right and will be important for early multi-frequency work involving CTA. A low-frequency pathfinder (MWA; 80–300 MHz) is well into its early science phase in Australia with upgrades in progress, and new projects at somewhat higher frequencies are under development in Australia (ASKAP; 700–1800 MHz and UTMOST; 843 MHz) and South Africa (MeerKAT; eventually 3 bands between 0.6 and 14.5 GHz). The ThunderKAT programme for transients with 3000 h of MeerKAT plus matching optical coverage (2017–2021) is particularly interesting for CTA. Finally, while not strictly a pathfinder for SKA, VLITE has just been commissioned with a wide bandwidth 330 MHz channel and large field of view (FoV) to conduct a new low-band survey of the sky, as well as detect new transients in real time. VLITE is a three-year pathfinder for the proposed LOBO project, a more extensive low-frequency radio monitoring project using the full JVLA. Having radio facilities in both hemispheres provides important complementarity for the two CTA sites.

---

[a] See [34] for many examples.

CTA's sensitivity to diffuse emission around accelerators makes mapping of the interstellar gas over wide areas absolutely essential to enable identification of sources in the Galactic plane and within other large-scale surveys such as that of the LMC. (Sub)-millimetre wavelengths thus complement CTA science by offering a detailed understanding of the environment into which shock waves propagate and through which accelerated particles are transported and interact. Most relevant to CTA are the facilities geared to degree-scale surveys such as Mopra (Australia), APEX and Nanten2 (Chile), and Nobeyama 45 m (Japan), whose beam sizes are well-matched to CTA's arc-minute resolution. These telescopes measure molecular gas via a variety of molecular lines that trace the matter density over a wide range of scales. Of particular interest is the missing "dark" molecular gas now attracting serious attention in the ISM community, traced by THz lines, with pathfinder telescopes in Antarctica such as HEAT (USA/Australia) paving the way for large-scale survey instruments such as the proposed DATE5 project led by China.

The recently completed Atacama Large Millimetre/sub-millimetre Array (ALMA) represents a huge leap forward for (sub)-millimetre interferometry. With sub-arcsecond resolution and the sensitivity to probe a very wide range of interstellar molecules, ALMA can carry out high fidelity probes of the density, temperature and ionisation level of material towards many CTA sources (including the LMC and nearby starburst galaxies), helping to understand the environments in which particles are accelerated and interact.

Furthermore, in recent years it has become clear that the sub-millimetre range is of particular interest for studying the particle acceleration processes in the jets of Galactic black hole transients (microquasars), as well as in the innermost regions of nearby AGN. For the former, there are many new small arrays and single-dish facilities in both hemispheres available. For the latter, the upcoming Event Horizon Telescope will link ALMA and other facilities in the first global VLBI array at millimetre/sub-millimetre frequencies, offering direct imaging of the jet-launching regions of key sources such as Sgr $A^\star$ and M 87. Eventually mm/sub-mm observations together with CTA can be used to directly study the relation between near event horizon physics and cosmic-ray acceleration and non-thermal processes in astrophysical jets.

At higher frequencies, the microwave all-sky survey by the Planck mission (decommissioned in 2013) has produced a legacy archive that can be searched for very extended microwave counterparts to CTA sources within our Galaxy, complementary information on the lobes of nearby radio galaxies and nearby clusters, and constraints on Galactic magnetic fields.

2.2 Infrared/Optical through Ultraviolet and Transient Factories

Traditionally, the overlap between optical/infrared (OIR) astronomy and gamma-ray astronomy has been considered to be fairly small. Indeed much OIR emission has a thermal origin, such as stellar light, heated dust, or emission from HII regions. However, the last few years have revealed that many compact, high-energy sources emit detectable levels of synchrotron emission in the OIR, which can also display very fast variability. Some examples include blazars, microquasars, and pulsar-wind nebulae, all of which are high energy gamma-ray emitters, making OIR a new frontier also for MWL exploration, and especially for producing transient alerts. Some steady gamma-ray sources also display mixed OIR emission, such as the supernova remnant Cas A, which emits strong thermal emission but also has IR synchrotron-emitting regions. In addition, OIR studies of non-radiative shocks in supernova remnants can provide useful constraints on nonlinear particle acceleration and its influence on shock heating. Finally, OIR observations provide an interesting perspective in the case of gamma-ray binaries, as properties of circumstellar discs may directly affect inter-wind shocks and lead to light-curve evolution.

There are too many existing smaller facilities to list here that will likely be useful for follow-up of CTA results, so we focus only on the larger developments. The high sensitivity of future telescopes will increase the number of sources for which one can identify non-thermal emission, or for which one can detect faint line emission from non-radiative shocks. By the time that CTA is operational, several very large, ground-based facilities will also come online. Already quite advanced is the project to build the European Extremely Large Telescope (E-ELT) in Chile, which will have diameter of 39 m and is expected to start operation by ∼2024. A similar project on the US side, the Thirty Meter Telescope (TMT) meant for Hawaii has run into some uncertainty with the site, but has enough momentum that it is likely to continue with a somewhat delayed timescale. The Giant Magellan Telescope (GMT) in Chile also begins commissioning in 2021, with diameter of 24.5 m. In space, the follow-up for the Hubble Space Telescope (HST) is the James Webb Space Telescope (JWST), launching in 2018. Similar to HST, the emphasis for JWST will be more on thermal sources, however HST has made some important progress for IR synchrotron-emitting sources and JWST's improved sensitivity will likely prove relevant for constraining several TeV-emitting sources. On the longer timescale, NASA has just placed highest priority on the O/NIR WFIRST mission, a wide-field survey instrument.

Optical polarimetry, as compared for example to radio, has not historically been of interest for MWL studies of VHE sources. It is becoming apparent, however, that polarisation offers an ideal way of isolating the synchrotron/non-thermal component in cases of mixed emission. This technique can be employed to provide new insights in broad-band SED correlations, for example to reveal potential low-energy signatures of otherwise orphan VHE flares. Additionally, polarisation studies of jets allow direct derivation of magnetic field parameters that can be used to improve SED modeling and emission-region localisation.

In general, the technical requirements for basic, but valuable, optical studies can be met at modest cost, suggesting that the installation of a small on-site (or nearby) optical telescope with polarimetric capability could significantly benefit the CTA science case. Having a dedicated facility for simultaneous, high cadence monitoring of AGN sources, as well as to follow-up transients or help trigger CTA programmes, could be an important addition to the Observatory capabilities. For example, several new VHE blazars were discovered from triggers based on high optical emission states

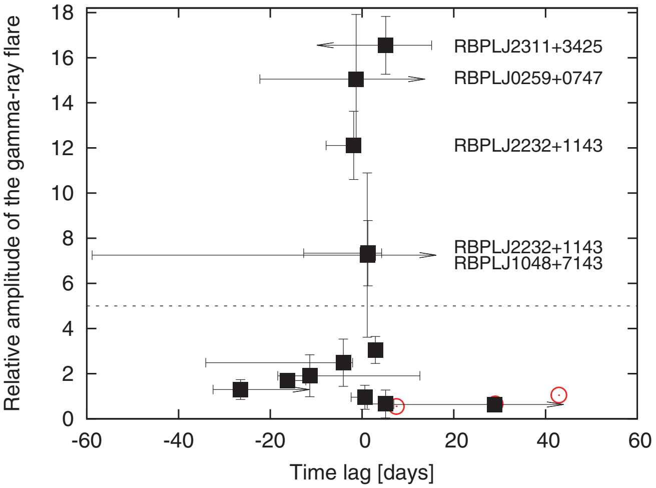

Figure 2.2: Results from the first season of RoboPol [38] blazar monitoring, simultaneously with Fermi observations in the GeV gamma-ray range. The fractional amplitude of a gamma-ray flare is plotted against the time delay between the gamma-ray flare and observed rotation in the optical polarisation angle. The length of the delay seems to be correlated with the gamma-ray flare amplitude. Red symbols show values prior to redshift correction. Reproduced from Ref. [39].

(see e.g. [40–42]), and optical polarisation shows interesting correlations with gamma-ray flares (see Figure 2.2). The addition of a dedicated optical telescope to the CTA baseline is under discussion within the project.

The newest development in the CTA context are the multiple initiatives for increasingly more sensitive, wide-field optical transient monitoring, collectively referred to as "Transient Factories". Currently in operation are two ground-based facilities with $\sim 7-8\,\mathrm{deg}^2$ FoV, the Panoramic Survey Telescope and Rapid Response System (Pan-STARRS), and the "intermediate" Palomar Transient Factory (iPTF). The latter is itself a pathfinder for the Zwicky Transient Facility (ZTF) that will have a very large $50\,\mathrm{deg}^2$ FoV, a survey speed of 3750 deg^2/hr, and be online in 2017. On a similar timescale, the BlackGEM project, aimed to identify counterparts of gravitational wave (GW) sources, will focus on transient detection, particularly before GW sources are discovered, and will start operation in ∼2018 with an initial deployment of three telescopes. All of these facilities use $< 1\,\mathrm{m}$ telescopes and in some sense pave the way for the Large Synoptic Survey Telescope (LSST), an 8 metre class telescope with a $9.6\,\mathrm{deg}^2$ FoV that will scan the available sky every three nights with much higher sensitivity. By the time CTA is starting science verification, these facilities together with SKA and its prototypes will generate overwhelming numbers of triggers (e.g., thousands each of GRBs and tidal disruption events, and likely hundreds of Galactic transients per year). Thus in the coming years, it is key to understand the potential for VHE follow-up and define appropriate response criteria, in order to select from the many transient alerts that will be supplied via subscribable streams such as VOEvent.[b] Particularly, the earliest of these facilities will be proprietary in terms of sharing their transients alerts, exactly when the response modes of CTA need to be trained. To that end, agreements between CTA and some of these collaborations are likely to be beneficial and could also include triggering of the external facilities on CTA-detected transients.

Finally, the ultraviolet (UV) domain probes synchrotron emission of electrons which have comparable energies to those emitting inverse-Compton emission detected by CTA. As such, simultaneous UV observations of bright AGN, blazars and other variable objects can be extremely useful, as long as their emission is not too absorbed by interstellar gas. Swift, XMM-Newton, and ASTROSAT all have UV capabilities, and other missions are being proposed, but at the time of writing there are no definitive plans for a UV-capable space mission on the timescale of CTA.

2.3 X-ray

There is an obvious synergy between gamma-ray astronomy and X-ray astronomy. Phenomena which result in high enough temperatures for thermal X-rays to be produced are very often associated with shock waves, accretion, or high velocity outflows, and hence with particle acceleration and gamma-ray emission. In addition, studies of synchrotron and inverse-Compton emission in the X-ray domain have become increasingly important as missions capable of higher spatial resolution and sensitivity have been launched. In supernova remnants for example, the X-ray emitting electrons have ∼100 TeV energies, making the combination of VHE gamma-ray and X-rays extremely powerful for constraining magnetic field strengths, the electron to proton ratio of the accelerated particles, and the particle energy distributions. The thermal X-ray emission from gamma-ray sources provides valuable information about plasma properties (e.g., temperatures, densities) and energetics (e.g., outflow/shock velocities). Non-thermal X-ray emission also provides a natural tracer of locations of extreme particle acceleration.

---

[b] http://wiki.ivoa.net/twiki/bin/view/IVOA/IvoaVOEvent

Over the last decade X-ray astronomy has been very successful thanks to large missions such as Chandra and XMM-Newton, both spectro-imaging missions, plus several medium missions such as the Rossi X-ray Timing Explorer (RXTE, which pioneered many timing and monitoring studies), Suzaku (imaging-spectroscopy), and Swift (which continues to be extremely successful for transient detection and follow-up, including in the UV). NuSTAR, launched in 2012 and with a guest-observer programme started in 2015, is the first focusing telescope at hard X-rays and is currently making many exciting discoveries about extreme particle accelerators in the energy range 10–80 keV. MAXI, a Japanese all sky monitor, is currently in operation on the International Space Station, and the main X-ray transient detector besides Swift. More recently, CALET and the UFFO pathfinder have added additional hard X-ray/soft gamma-ray transient capabilities.

Chandra, XMM-Newton, and Swift will likely continue to operate throughout the early years of CTA operation, if not beyond. Several new missions have recently been launched or are funded, and will be very relevant for CTA science during its operation. For example, the German/Russian mission eROSITA (launch 2018; 0.3–10 keV imaging spectroscopy survey) will overlap with CTA's early operation years and further. eROSITA in particular will be the first imaging all-sky survey in the 2–10 keV range and, as such, it can be expected to provide a primary reference for CTA source identification and multi-wavelength correspondences. The data however will be proprietary, with the German side planning two data releases, one around 2021 and the other two years later at the end of the survey, $\sim$2023. The Russian side will likely join in at least the final data release, but if CTA wants earlier access to survey data, as well as first pick of transients discovered in their offline (not real-time) pipeline analysis, a memorandum of understanding may be necessary. The loss of the Hitomi (earlier Astro-H) mission is clearly a major blow, but a replacement mission (XARM) has now been approved by JAXA.

Instruments with more focused capabilities include the recently launched (2015) Indian UV/X-ray satellite ASTROSAT, which features an all-sky monitor that will be very valuable for triggering CTA. An agreement may be necessary here as well. In June 2017, NICER was installed on the International Space Station (ISS) for soft X-ray timing focusing on primarily neutron stars and will be open for proposals in the second year. Also recently launched by China is the Hard X-ray Modulation Telescope (HXMT), a "super RXTE" operating in the 20–200 keV band with a 3600 deg^2 FoV.

Beyond that, the landscape for future X-ray missions is not yet fully determined but is looking very promising. SVOM is an optical/X-ray mission primarily for discovering GRBs, planned for launch in 2021. SVOM has similarities with Swift, triggering on bursts in both softer and harder bands, and following them in the X-ray and optical on-board. SVOM also includes a dedicated group of ground-based optical telescopes for wide FoV coverage before and after transient events.

Concepts under development which could provide synergies with CTA include the Chinese enhanced X-ray Timing and Polarimetry mission (eXTP), which incorporates large-area soft and hard X-ray telescopes, a wide-field monitor and a polarimeter, and would be launched around 2025. Several concepts related to Lobster-eye wide-field X-ray optics are being explored in the US, Europe, and in China. Such instruments could provide a major source of triggers for CTA transient observations.

The Athena+ project due for 2028 launch is, however, the next major observatory class mission, with good spatial resolution (∼10”), high sensitivity and energy resolution, and excellent spectroscopic capabilities. This mission will be the key X-ray facility for the 2030 decade and is designed for complementarity with radio/optical facilities and a large scientific breadth, providing additional high-energy constraints for CTA-detected sources.

One final development is the potential for X-ray polarimetry, a sure-fire way to isolate X-ray synchrotron from other components and to constrain the presence of accelerated particles. The IXPE mission has recently been selected by NASA as part of the SMEX programme. In the M4 ESA call, the X-ray Imaging Polarimetry Explorer (XIPE) was selected for a two-year design study as part of the Cosmic Vision programme. By the time of CTA’s early science verification, the future for this exciting new capability should be clear.

2.4 Sub-VHE Gamma-ray Energies

The hard X-ray/soft gamma-ray domain (0.1–10 MeV) represents a very useful window on the non-thermal spectra of astrophysical sources, but is extremely challenging experimentally. Three main instruments currently contribute here: INTEGRAL, Swift-BAT, and Fermi-GBM. INTEGRAL was launched in 2002 and its lifetime has been extended through to 2018, and it may be extended further into the CTA early science period. The Fermi-GBM and Swift-BAT detectors are the critical current instruments for the detection of high-energy transients. Swift was launched in 2004 with a nominal 10-year lifetime that has already been extended. In the 2016 NASA Senior Review, it reviewed first out of six missions, with operations confirmed through 2018 and recommended for extension at least until 2020. With an orbital lifetime stated as 2025 or beyond, it will likely continue to be a resource for transient detection during the CTA period.

At higher gamma-ray energies, the synergies with CTA are stronger and the instrumental performance is better matched to CTA. The GeV domain is dominated by pion decay, bremsstrahlung, and inverse-Compton emission, and in combination with the TeV range can help identify the dominant radiative mechanisms. CTA's lowest energy range overlaps with that of the two current instruments: the Fermi Large Area Telescope (Fermi-LAT) and AGILE. The Fermi mission has been so successful that its lifetime has been extended through 2018, and it will likely continue operating through 2020 and potentially beyond. NASA does not generally decommission fully operational missions, especially those with no clear successors, and Fermi's science performance continues to improve while having no consumables. The 2016 NASA Senior Review panel explicitly acknowledged the added scientific value of extending Fermi's lifetime so that it overlaps with CTA operations. Thus, it seems likely that Fermi will still be able to provide triggers and complementary coverage for a number of years of the CTA era. Fermi will continue to provide the main reservoir of extragalactic targets for CTA.

On the horizon, there are several missions upcoming or proposed to advance the observations of gamma rays from space in diverse domains. The Chinese Academy of Science's DAMPE (launched in 2015) and HERD (proposed for launch in the 2020's) are going to explore the energy range from hundreds of GeV to 10 TeV with an energy resolution approaching 1%. A few missions currently in the concept development phase (AMEGO in the U.S. and PANGU in China/Europe) aim at exploring the energy range from 0.5 MeV to 1 GeV with much improved sensitivity, point spread function, and polarisation capabilities thanks to the first-time ever combination of detection techniques based on pair production and Compton scattering in the same instrument. An alternative concept for a high-sensitivity, high-angular-resolution instrument with polarisation capabilities in the MeV to GeV domain uses gas time projection chambers. The concept is substantiated in two ongoing R&D projects, AdePT and HARPO. All of these future (potential) missions offer new and interesting synergies with CTA.

2.5 Complementary VHE Gamma-ray Instruments

Several ground-based VHE gamma-ray instruments may be operational at the same time as CTA. None of these instruments are direct competitors, but rather provide complementary performance. In particular, the High Altitude Water Cherenkov (HAWC) detector is a 100% duty cycle and very wide field of view ($\sim$1 sr) TeV range instrument [43]. Seated at a high-altitude site in Mexico, HAWC is capable of detecting the brightest known TeV sources in $\sim$1 day and will be able to provide alerts to CTA for active/flaring states of blazars and transients. HAWC's modest ($\sim$0.5°) angular resolution and somewhat limited energy resolution gives it competitive sensitivity for very extended emission, and by the time of CTA, it will have mapped the northern sky to intermediate depth (see Chapter 6), identifying many interesting steady sources for CTA to investigate.

LHAASO [44], is an ambitious multi-component project incorporating HAWC-like water Cherenkov detectors and a very large array of scintillators at a site in China. LHAASO will complement CTA at higher energies in a similar way to HAWC, with modest resolution and background rejection power offset by high duty cycle, wide field of view, and large area. A number of concepts now also exist for a ground-particle-based detector for VHE gamma rays in the southern hemisphere, strongly complementing CTA-South by providing triggers and additional information on very extended emission regions.

One or more of the current generation of IACT arrays — H.E.S.S.-2, MAGIC and VERITAS — may continue operations into the CTA era. Use of these telescopes for monitoring could be considered, under suitable agreement between the telescope and CTA. In particular for cases when the CTA sites are at different longitudes than current IACTs, these can extend monitoring of bright flaring sources to periods before and after the CTA observations.

2.6 VHE and UHE Neutrinos

Essentially all mechanisms invoked for the production of high-energy neutrinos will also produce gamma rays of similar energies, and unlike charged cosmic rays, both point back to their sources. There is thus strong complementarity to observations with these two messengers. Gamma-ray telescopes, using e.g., the atmospheric Cherenkov technique, achieve the precision pointing and sensitivity to identify and understand populations of accelerators and to even localise acceleration sites in nearby objects.

Neutrino telescopes, using e.g., reconstructed muon tracks, are less able to precisely pinpoint the origin of neutrinos, but the neutrinos they detect are the only completely unambiguous tracers of hadronic acceleration, even out to high redshifts and beyond PeV energies, a combination that is not possible for gamma-ray telescopes due to photon–photon absorption.

The experimental situation in the VHE neutrino domain has recently dramatically altered, with the first strong evidence for astrophysical neutrinos above the MeV band. The IceCube collaboration has announced the detection of a diffuse astrophysical neutrino signal at 0.1–1 PeV energies [45]. Individual neutrino sources with a flux corresponding to O(1) neutrino per IceCube exposure will be very easily detectable with CTA up to 1 PeV if they are Galactic in nature[c] as has been suggested [46].

With the construction of KM3Net [47] and several upgrades to IceCube in the planning, the detection of individual neutrino sources is a distinct possibility. CTA is the ideal instrument to follow-up on any VHE neutrino clustering, necessary to localise and characterise the VHE accelerators. An important new aspect therein will be the follow-up of neutrino-generated triggers as ToOs, in order to localise and identify the hadronic accelerators.

2.7 Gravitational Waves

Now that gravitational waves from compact object merger events have unambiguously been detected by Advanced LIGO [7, 27, 28], a new and exciting field is opening up for electromagnetic follow-up and identification. Mergers of binary black holes and neutrons stars (or mixed systems) should be detectable out to a few hundred Mpc [48], with expectations of several to hundreds of GW transients per year after 2018 [49]. However, until the advent of third-generation detectors such as the Einstein Telescope [50], the localisation errors on these transients will be relatively large and asymmetric. For follow-up of GW alerts, CTA has huge advantages with respect to most other instruments and wavebands. These advantages include the large field of view and the flexibility to map very large and non-circular error boxes (which comes from the large telescope number [6] and potential divergent pointing modes), the rapid response time, and the less ambiguous nature of counterpart identification (when compared, for example, to the optical band).

---

[c] Unless there is very strong internal gamma-gamma absorption, as might be the case for some binary systems.

This page intentionally left blank

3

Core Programme Overview

Over the lifetime of CTA, most of the available observation time at both of the CTA sites will be divided into open time, based on scientific merit and awarded by a Time Allocation Committee to Guest Observer proposers, and a Core Programme consisting of a number of major legacy projects. Smaller fractions of observation time will be allocated to Director's Discretionary time and host reserved time. The Core Programme, corresponding to approximately 40% of the total observation time over the first 10 years of CTA operations, will be comprised of Key Science Projects (KSPs) to be carried out by the CTA Consortium. Here, we introduce the KSPs; in the following chapters, they are described in more detail.

The CTA KSPs have been defined through a multi-year process of discussion within the CTA Consortium and in interaction with the wider community. They are ambitious projects with very significant scientific promise that also require considerable observation time. As such, they are suitable for execution in the guaranteed time of the CTA Consortium. Figure 3.1 provides a matrix of the main science questions within the CTA themes versus KSPs. The KSPs are multi-purpose observations designed to efficiently address the broad-ranging science questions of CTA. An internal review of the KSPs was conducted in late 2014, followed by a presentation in 2015 to the CTA Scientific and Technical Advisory Committee (STAC). The projects were refined and optimised accordingly.

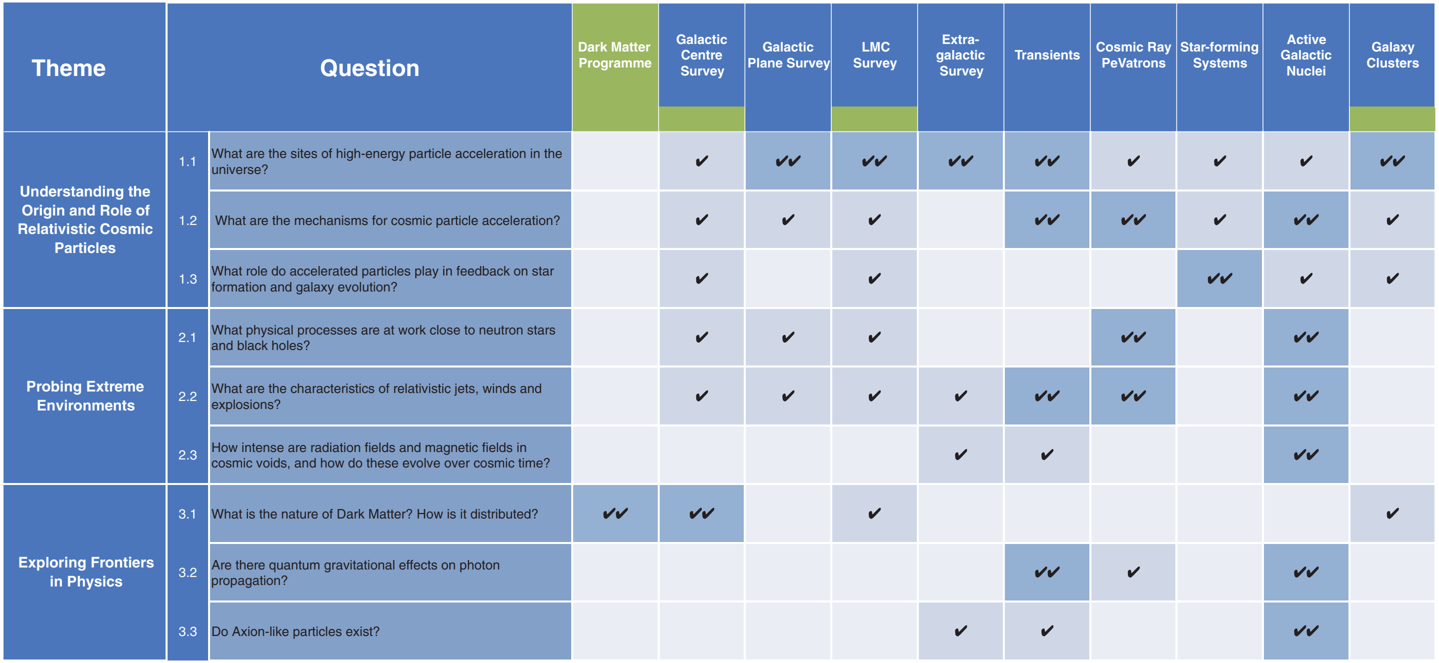

Theme	Question		Dark Matter Programme	Galactic Centre Survey	Galactic Plane Survey	LMC Survey	Extra-galactic Survey	Transients	Cosmic Ray PeVatrons	Star-forming Systems	Active Galactic Nuclei	Galaxy Clusters
Understanding the Origin and Role of Relativistic Cosmic Particles	1.1	What are the sites of high-energy particle acceleration in the universe?		✔	✔✔	✔✔	✔✔	✔✔	✔	✔	✔	✔✔
	1.2	What are the mechanisms for cosmic particle acceleration?		✔	✔	✔		✔✔	✔✔	✔	✔✔	✔
	1.3	What role do accelerated particles play in feedback on star formation and galaxy evolution?		✔		✔				✔✔	✔	✔
Probing Extreme Environments	2.1	What physical processes are at work close to neutron stars and black holes?		✔	✔	✔			✔✔		✔✔	
	2.2	What are the characteristics of relativistic jets, winds and explosions?		✔	✔	✔	✔	✔✔	✔✔		✔✔	
	2.3	How intense are radiation fields and magnetic fields in cosmic voids, and how do these evolve over cosmic time?					✔	✔			✔✔	
Exploring Frontiers in Physics	3.1	What is the nature of Dark Matter? How is it distributed?	✔✔	✔✔		✔						✔
	3.2	Are there quantum gravitational effects on photon propagation?						✔✔	✔		✔✔	
	3.3	Do Axion-like particles exist?					✔	✔			✔✔	

Figure 3.1: Matrix of CTA science questions and proposed Key Science Projects (KSPs). The KSPs are sets of observations addressing multiple science questions within the CTA themes. KSPs which contribute to the programme aimed at dark matter detection are indicated in green, with the exclusively dark-matter-oriented targets described entirely within the Dark Matter Programme in Chapter 4. For KSPs simultaneously addressing dark matter and other physics/astrophysics, the motivation and context for the dark matter element is again described in Chapter 4. The order of the KSPs in this table starts with dark matter due to its importance and transversal nature and follows with surveys and more focused KSPs by increasing distance scale. The check marks are intended to give a qualitative assessment of the impact of each KSP on a particular science question.

The criteria used for selection of the KSPs were:

1. excellent scientific case and clear advance beyond the state of the art,
2. the production of legacy datasets of high value to the wider community, and
3. clear added value of the project as a KSP rather than as part of the Guest Observer Programme, including:
   - the scale of the project in terms of observing hours — very large projects will be difficult to accommodate in the open time early in the lifetime of the observatory,
   - the need of a coherent approach across multiple targets or pointings, and
   - the technical difficulty of performing the required analysis, and hence reliance on Consortium expertise.

As a demonstration of feasibility, this programme has been scheduled in detail using the prototype software for final CTA observation scheduling, under the assumption of an approximate 40% share of the observation time during the first 10 years. The preliminary conclusions of this exercise are that the presented programme is feasible overall, with some adjustments needed on the total observation hours and on the relative hours among the KSPs.

The following chapters present each KSP in turn. The Dark Matter Programme, being of particular importance to CTA and overlapping considerably in terms of observation fields with other science topics, is dealt with somewhat differently, with a dedicated Chapter 4 describing the complete strategy.

We note that the Core Programme described below was developed over a period of several years and was largely finalised in 2016. It is expected to evolve before it is implemented, due to changes in theoretical understanding and new observational insights. It is envisaged that working groups within the CTA Consortium will continuously improve and update the programme and that feedback from the broader astronomical community will be essential in refining the KSPs.

This page intentionally left blank

4

Dark Matter Programme

The existence of dark matter as the dominant gravitational mass in the universe is by now well established, but the detailed nature of dark matter is still unknown. Multiple hypotheses endure as to the character of dark matter, and for the most popular models discussed the Cherenkov Telescope Array (CTA) has a unique chance of discovery. In the form of weakly interacting massive particles (WIMPs), dark matter particles can self-annihilate, converting their large rest masses into other Standard Model particles, including gamma rays. Indirect detection from such annihilations provides a unique test of the particle nature of dark matter, *in situ* in the Cosmos. Observations of the gamma rays provide the probe for the "indirect" detection of dark matter employed by CTA. In the standard thermal history of the early universe, the annihilation cross-section has a natural value, the "thermal cross-section", which provides the scale for the sensitivity needed to discover dark matter in this way. Particular models for WIMPs such as supersymmetry (SUSY) and theories with extra dimensions give predictions for gamma-ray energy spectra from the annihilations which are essential ingredients towards the predictions of the sensitivity of the indirect searches. Another vital ingredient in the CTA sensitivity predictions is the distribution of dark matter in the targets observed for the search.

The priority for the CTA dark matter program is to discover the nature of dark matter with a positive detection. The publication of limits following non-detections would certainly happen, but in planning the observational strategy the priority of discovery drives the programme. The possibility of discovery should be considered in the light of model predictions where the minimum goal for searches within the most widely considered models is the velocity-weighted thermal cross-section of $3 \times 10^{-26}\,\mathrm{cm}^3\,\mathrm{s}^{-1}$. The principal target for dark matter observations in CTA is the Galactic halo. These observations will be taken within several degrees of the Galactic Centre with the Galactic Centre itself and the most intense diffuse emission regions removed from the analysis. With a cuspy dark matter profile, observations of 500 hours in this region provide sensitivities below the thermal cross-section and give a significant chance of discovery in some of the most popular models for WIMPs. Since the dark matter density in the Galactic halo is far from certain, other targets are also proposed for observation. Among these secondary targets, the first to be observed will be ultra-faint dwarf galaxies with 100 h/yr proposed.

Beyond these two observational targets, alternatives will be considered closer to the actual date of CTA operations. New star surveys will extend the knowledge of possible sites of large dark matter concentrations, and a detailed study of the latest data will be made to continuously select the best targets for dark matter searches in CTA. Among these new possible targets are newly discovered candidate dwarf galaxies and dark matter clumps which could be very promising sources if their locations are identified *a priori*. Beyond the targets proposed for observations in the present KSP, the data for the Large Magellanic Cloud (LMC) KSP will also be used to search for dark matter. Furthermore, the data from the Galactic Plane and Extragalactic surveys might give hints of gamma-ray sources which do not have counterparts in MWL data and which could be pursued as dark matter targets. The sensitivity predictions for the Galactic halo, the dwarf galaxy Sculptor, and the LMC are summarised in Figures 4.1 and 4.2. Figure 4.1 shows that the sensitivity possible with the Galactic halo observation is much better than what is possible with a single dwarf galaxy or the LMC.

The Dark Matter Programme is very well suited to being carried out in the Core Programme by the CTA Consortium. The observations require a large amount of time with a significant chance of major discovery but with a clear risk of a null detection. For the Galactic halo, the observation time used will also be of great use for astrophysics, but the time on dwarf galaxies may be of lesser use. In the time period before the actual operation of CTA, much will evolve in the knowledge of dark matter distributions in the various targets. Further detailed work is needed to understand the systematics in the backgrounds; however, it is very likely that to have a chance of discovery the emphasis of observation should be on the Galactic halo. To have the best opportunity to discover the nature of dark matter, CTA must probe TeV scale masses with annihilation cross-sections in the range 5×10^{-27}

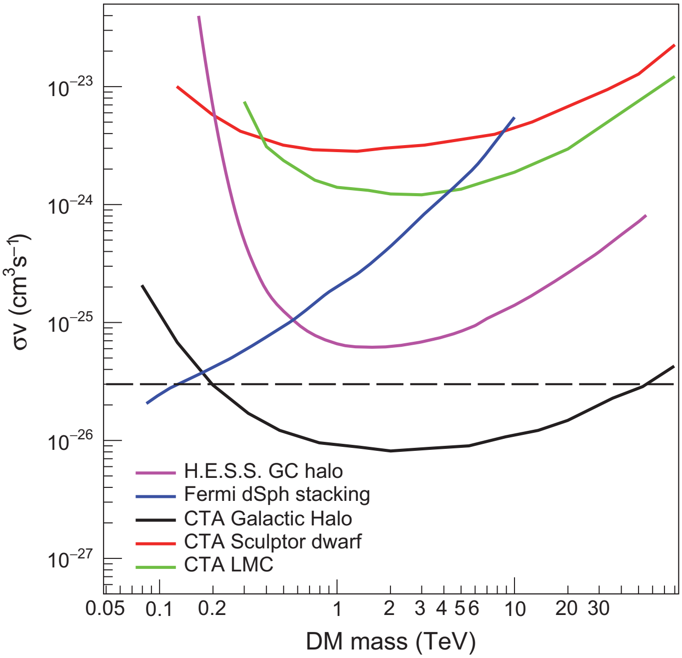

Figure 4.1: Comparison of predicted sensitivities in $\langle\sigma v\rangle$ for the following targets: the Milky Way Galactic halo, the LMC, and the dwarf galaxy Sculptor. The CTA sensitivity curves use the same method and W^+W^- annihilation modes for each target and the Einasto dark matter profile. The sensitivities for the three targets are all for 500 h taking into account the statistical errors only; for the Milky Way and the LMC, the systematics of backgrounds must be well controlled to achieve this statistically possible sensitivity. The H.E.S.S. results come from the Galactic halo for the W^+W^- channel [51] and the Fermi-LAT results come from dwarf spheroidal galaxies for the W^+W^- channel [52]. The horizontal dashed line indicates the thermal cross-section at 3×10^{-26} $\mathrm{cm^3 s^{-1}}$. Note that the Fermi-LAT results come from a stacked analysis of many dwarf spheroidal galaxies and the CTA curves are for specific individual sources.

to $3 \times 10^{-26}\,\mathrm{cm^3 s^{-1}}$. This seems possible if adequate observation time is allocated to the Dark Matter Programme as well as sufficient resources to develop methods to control the systematic errors.

Although there are great expectations for the search of new particles at the Large Hadron Collider (LHC), collider experiments will most probably not *on their own* be able to assess if any discovered particles are the whole constituent of the dark matter in the universe. Complementary searches, by means of direct nuclear recoil measurements and indirect searches such as the one CTA will perform, could allow an important breakthrough in the identification of the true nature of dark matter. The combination of results obtained from the three major axes of dark matter searches, production at colliders,

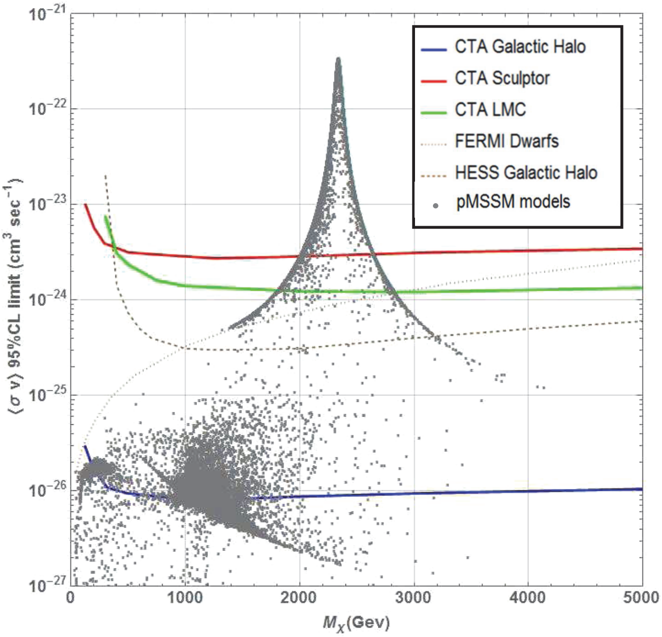

Figure 4.2: The zoomed sensitivities in the TeV mass range together with model points from the phenomenological minimal supersymmetric model (pMSSM), extracted from Ref. [53] (see also Ref. [54]). The H.E.S.S. results come from the Galactic halo for the Tasitsiomi parametrisation (close to the W^+W^- channel without electroweak correction) [55], and the Fermi-LAT results come from dwarf spheroidal galaxies for the W^+W^- channel [52].

direct detection of nuclear recoil, and indirect detection, will be essential to refine our understanding of the physics beyond the Standard Model. The dark matter parameter space in reach for CTA is unique and will benefit the entire scientific community. The release of multi-dimensional likelihood functions enabling model-independent searches for new particles is foreseen.

4.1 Science Targeted

The nature of dark matter in the universe is one of the most compelling questions facing physics and astronomy at the present time. There are many programmes around the world that have capabilities or are devoted to searching for non-gravitational signals of dark matter. Among these, CTA has an almost unique capability during the next decade to explore the WIMP mass region in the few hundreds of GeV to the 10 TeV regime, above the reach of the LHC and ton-scale direct detection experiments. To capitalise on this remarkable opportunity, it is imperative for CTA to devote substantial resources (both observing time and analysis effort) towards a comprehensive and integrated Dark Matter Programme. If this is done, CTA will be a cornerstone of the global, multi-faceted line of attack from different experiments probing with different methods to understand the nature of the dominant gravitational matter in the universe.

4.1.1 *Existence of Dark Matter*

The existence of dark matter in the universe was first proposed by Zwicky [56] in the 1930s to explain the dynamics of the Coma galaxy cluster where the observed luminous matter was insufficient to provide gravitational stability. More recent studies have confirmed the presence of dark matter in galaxy clusters by gravitational lensing, for instance in the galaxy cluster Abell 1689 shown in Figure 4.3(a). Evidence for dark matter now exists on many scales. In spiral galaxies, composed of a central bulge surrounded by a luminous disk, stellar motions are dominated by rotation within the disk. The luminous component of such a galaxy decreases exponentially from the centre giving the expectation that the star rotation velocities would scale

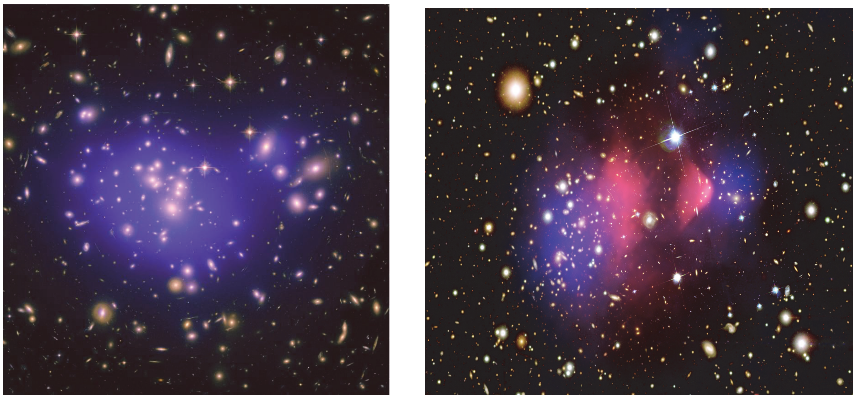
(a) (b)

Figure 4.3: (a) Hubble Space Telescope image of the inner region of the galaxy cluster Abell 1689. The blue overlay shows the dark matter distribution reconstructed by gravitational lensing using the multiple galaxy images seen in the telescope image. Credit: NASA, ESA, E. Jullo (JPL), P. Natarajan (Yale), and J.-P. Kneib (LAM, CNRS). (b) Composite image of the galaxy cluster 1E 0657-56 (also known as the Bullet cluster) [59]. Hot X-ray emitting gas is shown in red, and the blue hue shows the dark matter distribution in the cluster deduced from gravitational lensing. Credit: X-ray: NASA/CXC/CfA/M.Markevitch *et al.*; Optical: NASA/STScI; Magellan/U.Arizona/D.Clowe *et al.*; Lensing Map: NASA/STScI; ESO WFI; Magellan/U.Arizona/D.Clowe *et al.*

as $r^{-1/2}$ according to Kepler's laws; however, galaxy rotation curves usually remain flat far from galactic centres, typically beyond 30–40 kpc, where gas and stars are not dominant, implying a massive dark component. In elliptical galaxies, where the dynamical equilibrium is dominated by random motion of dark matter and stars rather than the rotational motion, observations also indicate a large contribution of dark matter. Two galaxy types are particularly dominated by dark matter: low surface brightness galaxies and dwarf spheroidal galaxies. In galaxy clusters, about 80% of the total mass is composed of dark matter. Recently, gravitational lensing studies of colliding galaxy clusters have shown different behaviours of the major components of the cluster pair during collision [57, 58] and provide one of the strongest pieces of evidence to date for the existence of dark matter (Figure 4.3(b)).

Numerous observational cosmology experiments performed over the past two decades, such as observations of the cosmic microwave background, baryonic acoustic oscillations, large-scale structures and supernovae, combine to give the standard picture of the composition of matter/energy in the universe as: ∼68% dark energy, ∼27% dark matter and ∼5% baryonic matter, and a small fraction of radiation in various forms. Only ∼1% of the universe is normal matter in luminous star systems. The limited amount of normal matter in the form of baryons and luminous stars is given in independent ways from the predictions of primordial nucleosynthesis and the measurements of the spectrum of fluctuations of the cosmic microwave background. The total amount of matter, baryonic plus non-baryonic, comes again from two independent sets of measurements: in galaxy clusters and the cosmic microwave background. It is simulations of structure formation which indicate that the non-baryonic dark matter is "cold" rather than "hot" in the sense that to explain the observed structures in the universe the dark matter must behave in a non-relativistic manner. The baryonic dark matter could be concentrated in molecular clouds or small stellar objects with masses too low to be luminous, although searches for these latter objects have not proved fruitful [60, 61]. With this broad set of observations, it is now well established that the dominant gravitation mass in the universe is non-baryonic dark matter with a global density of $\Omega_{\mathrm{DM}}h^2 = 0.120 \pm 0.003$ [62, 63], where Ω_{DM} is the ratio of the dark matter density to the critical density and h is the dimensionless Hubble parameter in units of $100\,\mathrm{km\,s^{-1}\,Mpc^{-1}}$. Independently, Big Bang nucleosynthesis measurements indicate that most of the dark matter is non-baryonic. However despite this precise knowledge on the global amount of dark matter, its nature is still elusive and remains to be discovered.

4.1.2 *Distribution of Dark Matter*

The hierarchical formation of structures in the universe is due to the gravitational amplification of primordial density fluctuations during its expansion. Due to the complexity of the physical processes that play a role in the structure formation, large-scale cosmological N-body simulations are used for modelling of the evolution from density fluctuations in a non-linear regime. These simulations give predictions for the dark matter halos that are observed to surround all systems, from galactic scale to galaxy cluster scale. Among the groups performing simulations are the Aquarius Project [64] and the Via Lactea Project [65]. Until recently, simulations used only cold dark matter (CDM), included only the gravitational force, and usually predicted the dark matter density to go approximately as $1/r$ towards the centre of the dark matter halos. Standard parametrisations of these simulated dark matter halos are the Navarro, Frenk, and White (NFW) [66] and the Einasto [67, 68] profiles. The latter one is moderately shallower on small spatial scales compared to the NFW profile. N-body simulations showed dark matter profiles that can be both steeper and shallower [64, 65]. Steeper profiles are usually referred to as cuspy profiles. All the dark matter simulations agree on the main halo structure at large distances, but the predictive power is limited by the spatial resolution of the simulation, and the shape and density of the profile in the inner part of the halo relies on extrapolation of the simulation prediction. The existence of such a cuspy density profile is in disagreement with observations of disc and dwarf galaxies where detailed mass modelling using rotation curves suggests a flatter or cored dark matter density profile in the central region. The study of velocity dispersions of stars in dwarf galaxies suggest that they can be equally accommodated by cuspy and cored profiles [69]. Recently, it has been shown that the detection of distinct stellar populations in dwarf galaxies allows for measurements of the inner slope of the dark matter profile and may allow cored and cuspy profiles to be distinguished [70].

Incorporating baryons into the N-body simulations dramatically increases their complexity. Predictions on the dark matter and total mass distribution require a realistic treatment of the baryons and their dynamical interactions with the dark matter. Extensive work is being done to quantify the effects of baryons [71–74] and black holes [75, 76] in modifying the dark matter distribution. The centre of galaxies are complex environments, and a number of astrophysical processes may likely change the initial dark matter density distribution. Because baryons dissipate energy and so collapse to smaller scales than dark matter, they constitute a sizeable fraction of the mass in the central regions. In the central regions of galaxies, the gravitational potential is dominated by baryons and the dark matter distribution is expected to evolve due to interaction with these components. Collisionless dark matter simulations have reached maturity, and much effort has been devoted recently to implement gas hydrodynamics and a description of star formation within simulations [77–80]. Feedback processes including supernova winds, radiation from young stars, and radiation and heat from black hole accretion play a crucial role in galaxy formation. These processes have an impact on the scaffolding of dark matter during galaxy formation; cuspy dark matter distributions in halos may be altered and tend to produce core-like dark matter distributions, reducing the potential for a CTA discovery of dark matter.

4.1.3 *The Nature of Dark Matter*

Present information indicates dark matter is non-baryonic and is compatible with a collisionless fluid of cold and WIMPs. A major motivation for WIMPs is that in the standard thermal picture of the early universe a particle with annihilation cross-section and mass of the order of the weak interaction leads to the observed dark matter relic density [62]. To be dark matter, WIMPs have an average annihilation cross-section (multiplied by the relative velocity of the annihilating WIMPs) of $\langle\sigma \mathrm{v}\rangle = 3 \times 10^{-26}\mathrm{cm}^3\mathrm{s}^{-1}$. This point is discussed further in Section 4.1.6. The dark matter particle is necessarily neutral of charge and colour and must be stable on cosmological time scales. For the discussion in this document, it is assumed that there is only one type of non-baryonic dark matter which makes up the full amount of the relic density $\Omega_{\mathrm{DM}}h^2$. Latest results from Fermi-LAT [81] and Planck [63] satellites are starting to probe thermal WIMPs with masses up to ∼100 GeV.

No candidate exhibits the necessary properties within the Standard Model of particle physics. However, theories beyond the Standard Model, mainly built in order to solve problems inherent to particle physics, like the unification of couplings at high energy and the hierarchy and naturalness problems [82], do have dark matter candidates. The currently most popular candidates for WIMPs with masses from a few GeV to a several tens of TeV come from the supersymmetric and extra-dimensional theories. In many SUSY models, the lightest supersymmetric particle is the lightest neutralino. In models with extra dimensions, the dark matter candidates include the first Kaluza–Klein excitation of the $B^{(1)}$ boson and the neutrino $\nu^{(1)}$. Axion-like particles are also among the popular candidates. A review of particle physics candidates can be found in Ref. [83].

4.1.4 *Search Methods for Dark Matter*

Different complementary approaches are required to establish and corroborate a dark matter signal and to extrapolate from a discovery to understanding the properties of dark matter in the universe. The four searches to carry out for non-gravitational signatures of dark matter in the form of WIMPs are: direct detection, indirect detection, collider experiments, and astrophysical probes sensitive to non-gravitational interactions of dark matter. The direct detection method looks for interactions of dark matter particles embedded in the Milky Way's dark matter halo in Earth-based detectors (see Ref. [84] for a recent review) while the indirect detection method looks for secondary particles emanating from dark matter annihilations or decays in our own and other galaxies. The two methods are complementary; positive evidence seen with distinct methods would provide convincing confirmation of the discovery of dark matter. To elucidate the particle properties of the dark matter, collider experiments have searched for evidence of dark matter particle candidates over the past three decades. Many searches for direct production of supersymmetric particles (sparticles) have been made at the LEP, TeVatron, and LHC colliders as well as various fixed target experiments. All such searches have led to negative results. Many parameters and branching ratios measured in accelerator experiments do, however, lead to strong constraints and indications of where the dark matter particles may lie. The particle properties of dark matter can be also constrained through its impact on astrophysical observables. In particular, non-gravitational interactions of dark matter can affect the densities of dark matter present in the central regions of galaxies or the amount of dark matter substructure found in galactic halos [85]. Such interactions may also alter the cooling rates of stars and influence the pattern of temperature fluctuations observed in the cosmic microwave background.

The indirect search method looks for cosmic radiation emitted from annihilations of pairs of WIMPs in regions of the surrounding universe with a high dark matter density. Different experiments search for different annihilation products, and currently searches are in progress with charged cosmic rays, gamma rays, and neutrinos. Experiments with neutral particle probes (gamma rays and neutrinos) can point directly to the annihilation sources, while charged cosmic rays, at least below energies of $\sim 10^{19}$ eV, are deflected considerably by Galactic and intergalactic magnetic fields and cannot be used to trace back to any particular location. Indirect detection of dark matter annihilations through gamma rays has attracted much interest due to several unique properties of gamma rays. First of all, they do not scatter appreciably during their travel through the Galaxy, but rather point back to the site where the annihilation took place. Also, absorption can generally be neglected, as the cross-section for scattering on electrons and nuclei for GeV to TeV photons is small. This means that one may use properties of the energy distribution resulting from these processes to separate a signal from astrophysical foreground or backgrounds. And, as the electromagnetic cross-section of gamma rays is so much higher than the weak interaction cross-section for neutrinos, they are relatively easy to detect.

These different search methods are sensitive to different couplings and different dark matter candidates. Also, the diverse experiments are sensitive to different dark matter particle masses. For a complete understanding of the nature of dark matter, these different techniques are complementary and essential. Figure 4.4 shows the survival and exclusion rates from the direct, indirect, and LHC searches and their combinations in the plane of scaled spin-independent cross-section versus lightest supersymmetric particle (LSP) mass [86]. The spin-independent cross-section is scaled to the fraction of dark matter provided by the WIMPs. The relative contributions arising from the LHC and CTA searches to the model survival/exclusion are shown. It is clear that CTA dominates for large LSP masses, which correspond mostly to the neutral wino and Higgsino LSPs, and it also competes with the LHC throughout the band along the top of the distribution.

4.1.5 *Annihilation of Dark Matter Particles*

For the indirect search experiments, complete rate predictions rely on calculations of the numbers and spectra of the relevant particle species in the annihilation reaction final state. To be able to self-annihilate, the dark matter candidate is most often a Majorana particle or a Dirac particle with no matter–antimatter asymmetry, but a complex scalar, or even a vector-like particle, could be a possibility. In all annihilation locations, the relative velocity of the WIMPs is low and usually annihilation rates are calculated in the null velocity limit where only the s-wave term contributes. In this limit, the annihilation products in the leading order of perturbation theory are mostly pairs of Standard Model fermions/anti-fermions and neutral pair combinations of gauge or Higgs bosons.

Three types of dark matter annihilation spectra are expected in the final state: (i) a continuum of gamma rays up to the dark matter mass from the decays of neutral pions produced by hadronisation and/or decays of the annihilation products; (ii) a monochromatic gamma-ray signal produced

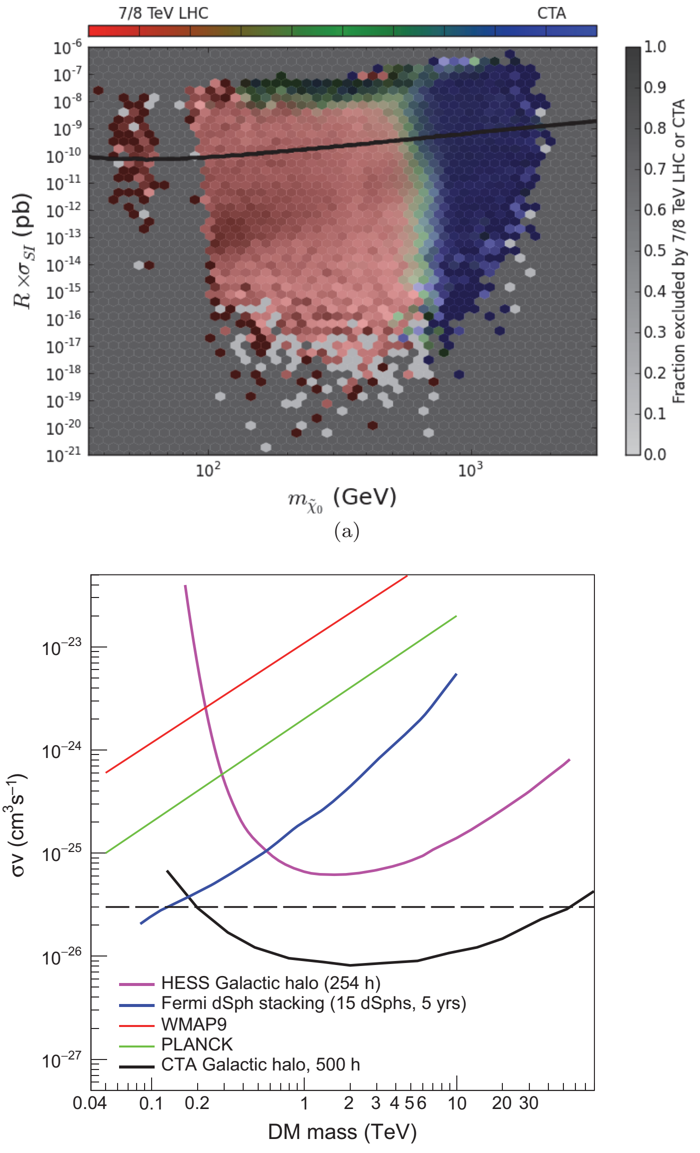

(a)

(b)

Figure 4.4: (a) Comparisons of models from the phenomenological minimal supersymmetric model (pMSSM) surviving or being excluded by future direct detection, indirect detection, and collider searches in the neutralino mass-scaled spin-independent cross-section plane. The spin-independent XENON1T exclusion is shown as a solid black line. The models accessible to CTA (blue) and LHC (red) are shown. Figure extracted from Ref. [86]. (b) Current best limits on the annihilation cross-section from indirect detection (Fermi-LAT dwarf spheroidal galaxies stacking analysis, W^+ W^- channel [52] and H.E.S.S. Galactic halo, W^+ W^- channel [51]) and cosmic microwave background experiments (WMAP and Planck, $b\bar{b}$ channel [63]) compared to the projected sensitivity for CTA from observations of the Galactic halo for the Einasto profile and W^+ W^- channel.

by loop-order induced processes at $E_\gamma = m_{\rm DM}$; and (iii) line-like features close to the dark matter mass from radiative corrections to processes with charged final states (e.g. virtual internal bremsstrahlung). These spectral features provide powerful discrimination against the more smooth spectra expected for standard astrophysical sources. Figure 4.5(a) shows typical spectra arising from the above-mentioned processes. Figure 4.5(b) indicates the dominant annihilation modes as a function of the neutralino mass M_χ for the allowed models in the pMSSM scan of Ref. [54]. From this plot, it can be seen that above 800 GeV the $\rm W^+W^-$ channel is always the dominant annihilation mode (meaning that for the particular model, it is the mode with the largest branching fraction). Between 200 and 800 GeV, the $t\bar{t}$ and the $b\bar{b}$ modes dominate in different regions. The $\tau^+\tau^-$ mode is only significant below 200 GeV.

The gamma-ray continuum from dark matter annihilation discussed in the previous section typically vastly dominates the total photon count, at least for energies $E_\gamma \leq 0.1\ M_\chi$. However, the resulting spectrum is rather soft and does not contain any specific features that would unambiguously point to its dark matter origin. Higher-order processes, on the other hand, can add sharp spectral features to the high-end part of the spectrum, $E_\gamma \sim M_\chi$, and would provide potential smoking-gun signatures for the detection of particle dark matter. In fact, the detection of such features would not only help to discriminate a signal from the background [87], but would also provide valuable information about the particle nature of the annihilating dark matter.

The first signal considered historically of this type is the direct annihilation of dark matter pairs into γX (where X = γ, Z, H, or some new neutral state). This process is necessarily loop-suppressed because the dark matter particles carry no charge, but it leads to the striking signature of monochromatic photons with an energy of $E_\gamma = M_\chi(1 - M_X^2/4M_\chi^2)$. The discrimination of these lines is generally challenging, though annihilating Kaluza–Klein dark matter may provide a noteworthy exception in that it can lead to the fascinating signature of several equidistant lines at TeV energies. For thermally produced dark matter, one would naively expect that the process $\chi\chi \to \gamma\gamma$ happens at a rate of $\alpha^2\langle\sigma v\rangle_{\rm thermal} \sim 10^{-31}\ {\rm cm^3 s^{-1}}$, where α is the fine structure constant. While this naive estimate falls well below the sensitivity of CTA, there are several mechanisms that can significantly enhance line signals — in particular at the high energies accessible by CTA, see, e.g. Ref. [88].

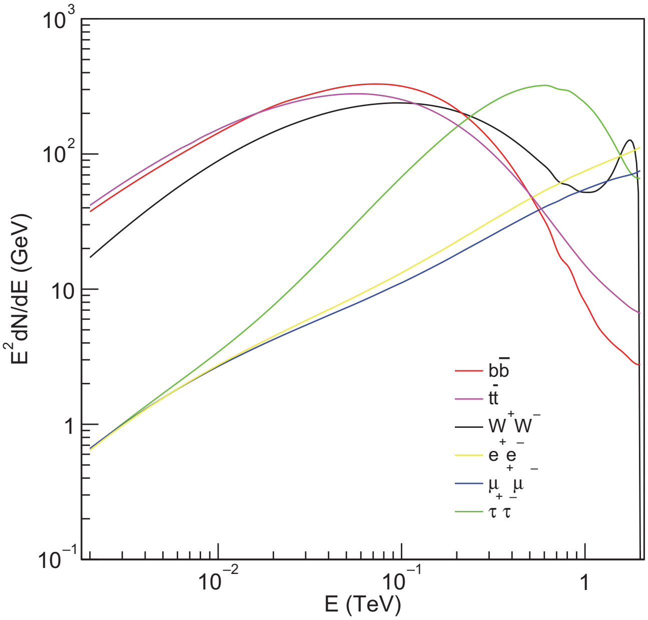

(a)

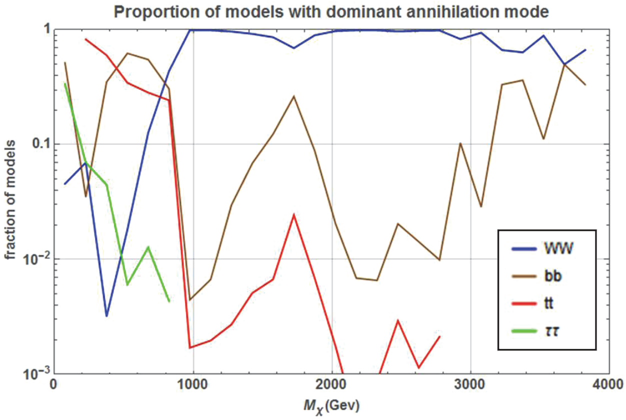

(b)

Figure 4.5: (a) Annihilation spectra for the continuum signals from the quark, lepton, and gauge boson primary channels for a 2 TeV dark matter mass. The line-like feature expected from the virtual internal bremsstrahlung process contribution is particularly prominent for the W^+W^- channel. (b) The dominant annihilation modes in the pMSSM scan of Ref. [54]. As a function of neutralino mass, the plot shows the fraction of models with each of the annihilation modes as indicated. It should be noted that in general for any particular model more than one mode contributes and the dominant mode is the one with the largest branching fraction.

At first order in α, pronounced spectral features can also be generated by an additional photon in the final state whenever dark matter annihilates to charged particles. This process is known as internal bremsstrahlung and one may further distinguish between final state radiation and virtual internal bremsstrahlung, VIB [89]. The former produces a model-independent hard spectrum with a sharp step-like cutoff at $E_\gamma = M_\chi$ [90], like in the case of Kaluza–Klein dark matter [91]. VIB, on the other hand, dominates for TeV dark matter annihilating into W bosons [92] or if the tree-level annihilation of dark matter into light fermions is suppressed by a symmetry [93, 94], such as the helicity suppression for neutralino dark matter. Given the energy resolution of CTA, VIB features are essentially indistinguishable from a monochromatic line (though in principle the exact spectral shape is highly model-dependent). At lower energies, internal bremsstrahlung of gluons or electroweak gauge bosons may also both change and significantly enhance the photon spectrum.

4.1.6 *Parameters Expected for WIMP Dark Matter*

For a standard thermal history of the early universe, the abundance of a particle is related to the thermally averaged annihilation cross-section times relative velocity ($\langle\sigma_{\chi\chi}v\rangle$). Initially, the WIMPs were in thermal and chemical equilibrium with the hot "soup" of Standard Model particles. The WIMPs dropped out of thermal equilibrium ("freezed-out") once the rate of interactions that change Standard Model particles into WIMPs, or vice-versa, became smaller than the Hubble expansion rate of the universe. After freeze-out, the co-moving WIMP density remained essentially constant and the dark matter relic density and the annihilation cross-section are thus inversely proportional (neglecting the logarithmic dependency on the dark matter mass): $\Omega_{\mathrm{DM}}h^2 \simeq K/\langle\sigma_{\chi\chi}v\rangle$, where the proportionality constant is $\mathrm{K} \simeq 3 \times 10^{-27}\mathrm{cm}^3\mathrm{s}^{-1}$ and is related to the cosmic microwave background temperature and the Planck mass. For $\Omega_{\mathrm{DM}}\mathrm{h}^2 \sim 0.1$, this gives $\langle\sigma_{\chi\chi}\mathrm{v}\rangle \sim 3 \times 10^{-26}\mathrm{cm}^3\mathrm{s}^{-1}$, which is referred to as the thermal cross-section. The fact that this cross-section is of the order of magnitude of the weak interaction is often referred to as the "WIMP miracle".

This thermal value of the cross-section is often used as a sensitivity goal for indirect searches; however, this value cannot be taken as a strict expectation, in general, since the cross-section in the early universe is not identical to the cross-section applicable to indirect searches at the present time. Detailed discussions of the differences can be found in Ref. [54]. In

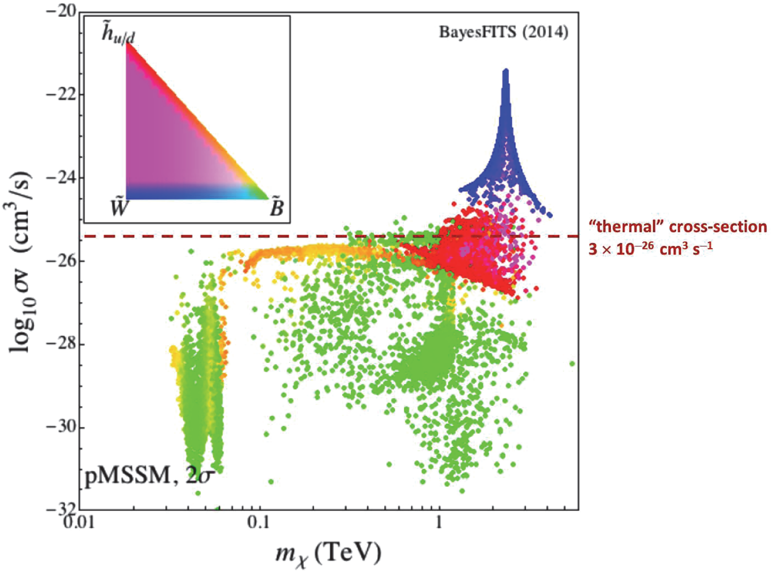

Figure 4.6: Annihilation cross-section points from a 19-dimensional pMSSM fit from Ref. [53] which contains a set of basic constraints and direct search limits as explained in the reference. The colour coding identifies the composition of the lightest neutralino. Pure states are shown for the supersymmetric electroweak gauge bosons (green for the bino and blue for the wino) and for the Higgsino (supersymmetric partner of the Higgs boson) in red. Admixtures are shown with intermediate colours in accordance with the legend.

the early universe, the relic density is obtained by using a momentum-dependent cross-section including both annihilation of the LSP neutralino and co-annihilation with close-in-mass neutralinos and other sparticles. Due to the high temperature at freeze-out, the momentum dependence is different from present day annihilation, which takes place essentially at rest. Furthermore, the present-day cross-section contains no contribution from co-annihilation since the co-partners have all decayed away. Figure 4.6 shows example points from a pMSSM model scan showing that many specific points are below the thermal cross-section and some are above, and hence searches should encompass a wider range of annihilation cross-sections. A strong enhancement of the annihilation cross-section occurs for winos around 2–3 TeV due to Sommerfeld enhancement.

4.1.7 *Rate of Gamma Rays in Detector*

The rate of gamma rays from dark matter is usually expressed as a separation into two terms which characterise the astrophysical properties of the source and the particle physics contribution to the rate. The astrophysical terms are combined in a so-called J-factor term defined as

$$J_{\Delta\Omega} = \int_{\Delta\Omega} d\Omega \int_{\mathrm{los}} dl \times \rho^2[r(l)]. \tag{4.1}$$

The J-factor reflects the integral of the squared dark matter density distribution, ρ^2, over the line of sight (los) and inside the observing angle $\Delta\Omega$. The dark matter density is conveniently parametrised as a function of the radial distance r from the centre of the astrophysical object under consideration. Depending on the dark matter targets, the J-factors range from $\sim 10^{21}$ to $\sim 10^{24}$ $\mathrm{GeV}^2\mathrm{cm}^{-5}$. The number of observable events is then expressed as

$$N_{\mathrm{DM}} = \frac{T_{\mathrm{obs}}\ J_{\Delta\Omega}\ \langle\sigma v\rangle}{8\pi M_\chi^2} \int_{E_{\mathrm{min}}}^{E_{\mathrm{max}}} \frac{dN_{\mathrm{DM}}}{dE}(E) A_{\mathrm{eff}}(E) dE, \tag{4.2}$$

where

- T_{obs} is the live time of observation,
- $\langle\sigma v\rangle$ is the thermally averaged velocity-weighted annihilation cross-section,
- M_χ is the dark matter particle mass,
- $dN_{\mathrm{DM}}(E)/dE$ is the energy spectrum of the gamma rays produced in the annihilation,
- A_{eff} is the detector effective area, and
- E_{min} and E_{max} are the energy limits for the measurement.

4.2 Strategy

The indirect dark matter search with CTA has several possible astrophysical targets, each with its own inherent advantages and disadvantages. The Milky Way represents a natural place to look for dark matter signatures, and its centre is expected to be the brightest known source in the dark matter induced gamma-ray sky, although the exact magnitude is rather uncertain. The dark matter density profile in the Milky Way should lead to an annihilation signal observable on large angular scales; however, astrophysical Galactic foregrounds coupled with the enormous spatial extent and the truly diffuse nature of this Galactic dark matter emission make separation between signal and background challenging. On the other hand, nearby dwarf spheroidal galaxies should provide easier separation of signal and background but yield comparatively lower signals because of both the distance and lower dark matter content compared to the Milky Way.

The concordance cosmological ΛCDM model predicts that the formation of visible structures has been guided by gravitational accretion of baryons onto previously formed dark matter over-densities. The astrophysical structures of interest result from the hierarchical formation of dark matter halos from primordial dark matter over-densities. The subsequent evolution of these dark matter halos occurred in many different ways. In particular, on galactic and sub-galactic scales, the process depended on halo parameters such as the halo mass and the mass density profile, the evolution history, and the conditions set by the local galactic evolution environment. Some of the resulting halos could have been sufficiently massive to accrete enough baryons to initiate star formation and form galaxies, including the variety of satellite galaxies we actually observe in the Milky Way halo. In-falling dwarf galaxies (e.g. dwarf irregular galaxies) approaching more central parts of their host halo could have evolved to dwarf spheroidal galaxies (dSphs), see e.g. Ref. [95]. These dwarf galaxies, being highly dark matter dominated and comparatively close by, form one of the primary targets for CTA observations of this programme. However, for various reasons, including the halo size, location, encounters, the baryonic content of the environment, or the presence of a central black hole, less massive dark matter clumps could have evolved differently and not into a visible dSph. They would constitute dark matter-dominated over-densities purely observable in gamma rays or cosmic rays emerging from dark matter annihilations. Such objects are commonly known as dark matter subhalos or dark matter clumps.

It is clear that the scientific interpretation of any dark matter signal detected by CTA (or indeed a non-detection) in terms of a constraint on the properties of dark matter particles depends sensitively on our knowledge of the dark matter distribution within the targeted systems. This section considers the likely impact of observations and modelling over the next 5–10 years on our knowledge of the dark matter profiles of dSphs, the LMC, and the central regions of the Milky Way.

Observations with the fully operational CTA are required in order to maximise the sensitivity and to take advantage of the best energy and angular resolutions. In particular, the energy resolution is of utmost importance to identify possible spectral features, e.g. bumps and the cutoff. If detected, these will provide crucial information in the identification of the dark matter particles. In case of massive dark matter candidates, the continuous dark matter-induced gamma-ray spectra extends down to the GeV scale. A low energy threshold is therefore mandatory to probe the largest energy range and to be sensitive to dark matter candidates with low masses. Observations at the lowest possible zenith angle are preferred, since they provide access to the lowest possible energies. Good weather conditions are also required to keep an optimal energy resolution and to reduce systematic effects.

The observational strategy proposed for the CTA Dark Matter Programme is focused first on collecting a significant amount of data on the Galactic Centre. Complementary observations of a dSph galaxy will be conducted to extend the search. The Galactic Centre, the LMC, and galaxy clusters are valuable targets both for dark matter searches and for studies of non-thermal processes in astrophysical sources. Data will be searched for continuum emission and line features, and strategies will be adopted according to the findings. Discoveries will modify any strategies defined *a priori*.

Below, we outline the strategy for CTA observations of the Galactic halo, dwarf galaxies, the LMC, and the Perseus cluster, respectively, followed by an overall summary of the targets.

4.2.1 *Milky Way*

4.2.1.1 *Description*

The centre of the Milky Way has in the past been considered as a target for dark matter searches [96]. More recently, because of the rich field of VHE gamma-ray astrophysical sources in the region, the searches focus on the Galactic halo excluding the central region of Galactic latitude $b < 0.3^\circ$ [55]. Even excluding the very central region, the total mass of dark matter in the Galactic halo together with its proximity to Earth make it the most promising source for dark matter searches with CTA. The inconvenience of this target, however, is the fact that being a diffuse source, the integration over the inner halo, while yielding a large signal, gives a very large instrumental background from misidentified charged cosmic rays. Furthermore, there are astrophysical backgrounds from various sources which must be understood, even with the very central region excluded from the analysis. It is believed that the disadvantages of the Milky Way target can be overcome with sufficient experimental effort to control systematic effects in the background subtraction and modelling. The expertise required for this analysis strengthens the case for this programme to be conducted by the CTA Consortium.

Standard astrophysical processes typically have steeper VHE spectra than the expected dark matter-induced gamma-ray continuum emission.

Given the wealth of other high-energy emitters expected in this region, the search for a dark matter component requires a very deep exposure to enable detection and detailed spectromorphological studies, a good understanding of the instrumental and observational systematics, and accurate measurements of other astrophysical emission in the region to be able to reduce any contamination to the dark matter signal. A deep exposure for the Galactic Centre observation will provide the means for an in-depth study and better understanding of the astrophysical emissions in this region.

Stellar dynamics in the Milky Way is dominated by the gravitational potential of baryons up to the kpc scale, and the dark matter density distribution in the inner kpc region can thus be accommodated by both cuspy (NFW, Einasto) profiles and cored (isothermal, Burkert) profiles. Important efforts are ongoing to accurately simulate the baryon impact on dark matter distribution in the central region of galaxies. With rapid progress being made in the field, a more comprehensive picture for the central region of the Milky Way is expected by the time of CTA observations with reduced theoretical uncertainties on dark matter distribution. Although the observation strategy may substantially differ for a kpc-size core profile compared to a cuspy profile, the detection of a dark matter signal and the detailed study of its morphology would help to resolve this important question.

4.2.1.2 *Evolution of knowledge*

The inner region of the Milky Way presents a very complex environment in which to determine the distribution of dark matter. Present kinematic and microlensing data are consistent with an inner log slope for the halo of −1.0 [97], the value predicted by dark matter-only simulations of structure formation, although the observational constraints are very broad. Simulations including baryonic physics can produce steeper profiles through adiabatic contraction of gas and supermassive black hole formation. However, outflows produced by AGN activity and/or star formation have the opposite effect. The theoretically expected value is therefore almost as uncertain as the observationally determined one. Given the high level of activity in the field of galaxy formation, it is expected that improved simulations, e.g. EAGLE [98], will provide further insights into theoretical expectations over the coming years. However, the interpretation of CTA observations requires tighter observational constraints. The two likely avenues for improvement on this front are from microlensing and large-scale radial velocity surveys. Microlensing surveys can be used to probe the baryonic mass function towards the Galactic Centre and hence place limits on the baryonic contributions to the mass distribution of the inner Galaxy, e.g. Ref. [99]. Kinematic surveys such as ARGOS [100], BRAVA [101], GAIA [102], and GIBS [103] are collecting samples of thousands of radial velocities which will be used to map the dynamical structure of the bulge and bar regions. Together, the microlensing and kinematic data have the potential to provide improvements on the constraints in the mass profile of the inner Galaxy.

4.2.1.3 *Observational strategy*

The Galactic Centre observations will be taken with multiple grid pointings with offsets from the Galactic Centre position of about ±1.3° to cover the central 4° as uniformly as possible. The observation strategy defined explicitly to search for dark matter will require 525 h to probe cuspy profile dark matter distributions. In the Galactic Centre KSP, a further 300 h are proposed for astrophysics covering up to latitudes ±10°. These data will also be included in the analysis for dark matter to improve the sensitivity for cored dark matter density profiles. Given the major scientific impact of a positive result, we propose that the initial 525 h exposure be done in the first three years of CTA operation with high priority.

4.2.1.4 *Performance*

The quest for dark matter requires a deep and uniform exposure over several degrees around the central black hole Sgr A* to allow for both spectral and spatial morphological studies, a deep understanding of the instrumental and observational systematics, and precise determinations of the standard astrophysical emissions. The expected CTA energy and angular resolutions are key ingredients to disentangle a dark matter signal from standard astrophysical background. The sensitivity predictions for observations in the Galactic Halo are shown in Figure 4.7. Figure 4.7(a) shows the sensitivity for different annihilation modes ($b\bar{b}$, $\tau^+\tau^-$, $\mathrm{W}^+\mathrm{W}^-$, $t\bar{t}$) and Figure 4.7(b) for different observation times with a method [104] to include systematic uncertainties on the residual cosmic ray background as indicated in the caption. Figure 4.8 shows the CTA sensitivity for various dark matter halo profiles satisfying stellar dynamics. Even in the case of a pessimistic dark matter distribution at the Galactic Centre, e.g. a Burkert profile, the sensitivity of CTA is comparable to what is expected for a classical dwarf galaxy (see Figure 4.11). Figure 4.9 compares the CTA Galactic halo sensitivity limit predictions with the pMSSM model scan of Ref. [54]. Each

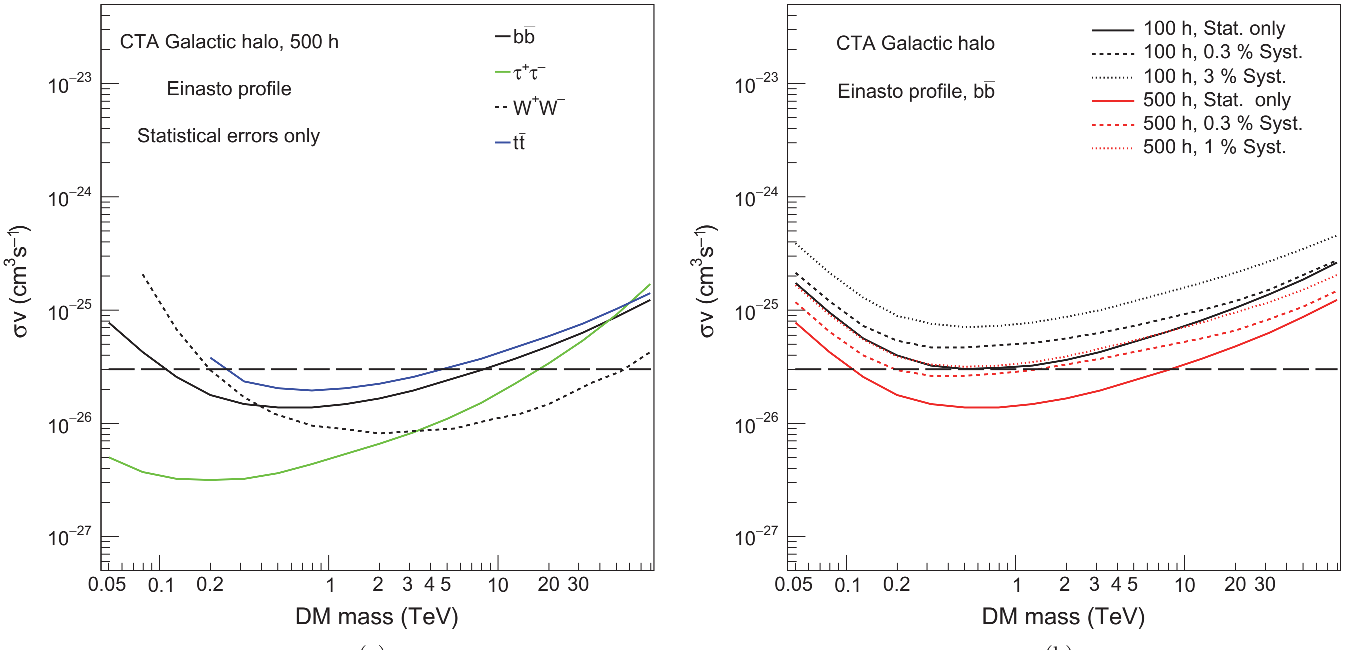

(a)

(b)

Figure 4.7: (a) CTA sensitivity for $\langle\sigma v\rangle$ from observation of the Galactic halo for different annihilation modes as indicated. (b) CTA sensitivity for $b\bar{b}$ annihilation modes for different conditions; black is for 100 h of observation and red is for 500 h. The solid lines are the sensitivities only taking into account the statistical errors, while the dashed and dotted curves take into account systematics as indicated. The dashed horizontal lines approximate the level of the thermal cross-section of $3 \times 10^{-26}\mathrm{cm}^3\mathrm{s}^{-1}$.

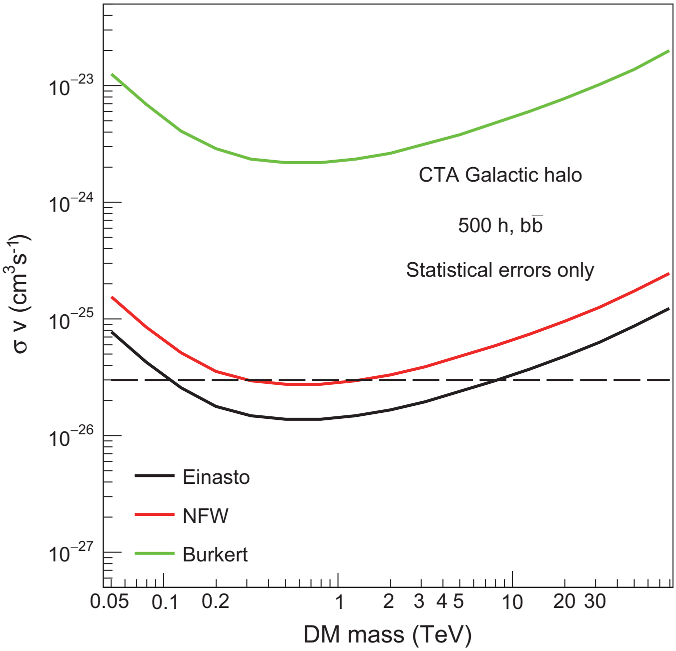

Figure 4.8: CTA sensitivity for $\langle \sigma v \rangle$ on the Galactic halo for cuspy (NFW, Einasto) and cored (Burkert) dark matter halo profiles. The sensitivities are plotted for 500 h observation, the $b\bar{b}$ annihilation channel, and for statistical errors only. The dashed horizontal lines indicate the level of the thermal cross-section of $3 \times 10^{-26}\text{cm}^3\text{s}^{-1}$.

panel shows the branching fraction of the primary annihilation channels for a given model. Similar studies can be found in Refs. [86, 105]. It can be seen that for models with $M_\chi > 500$ GeV, CTA will be the only experiment able to probe the vast majority of models.

Similar studies have been carried out in the recent literature on the CTA sensitivity prospects towards the Galactic Centre [104, 106, 107]. A careful examination of these works reveals differences in the dark matter distribution modelling and/or in the sensitivity computation that significantly impact the expected sensitivity. Among the differences are the instrument's response functions together with the residual background used for CTA and the dark matter distribution in the innermost kpc of the Galactic Centre. A description of the instrument response functions used for this study can be found in the appendix.

The estimate of CTA sensitivity in the monochromatic line search is shown in Figure 4.10, where the data are analysed in a circle of 1° radius encompassing the Galactic Centre position assuming two different dark

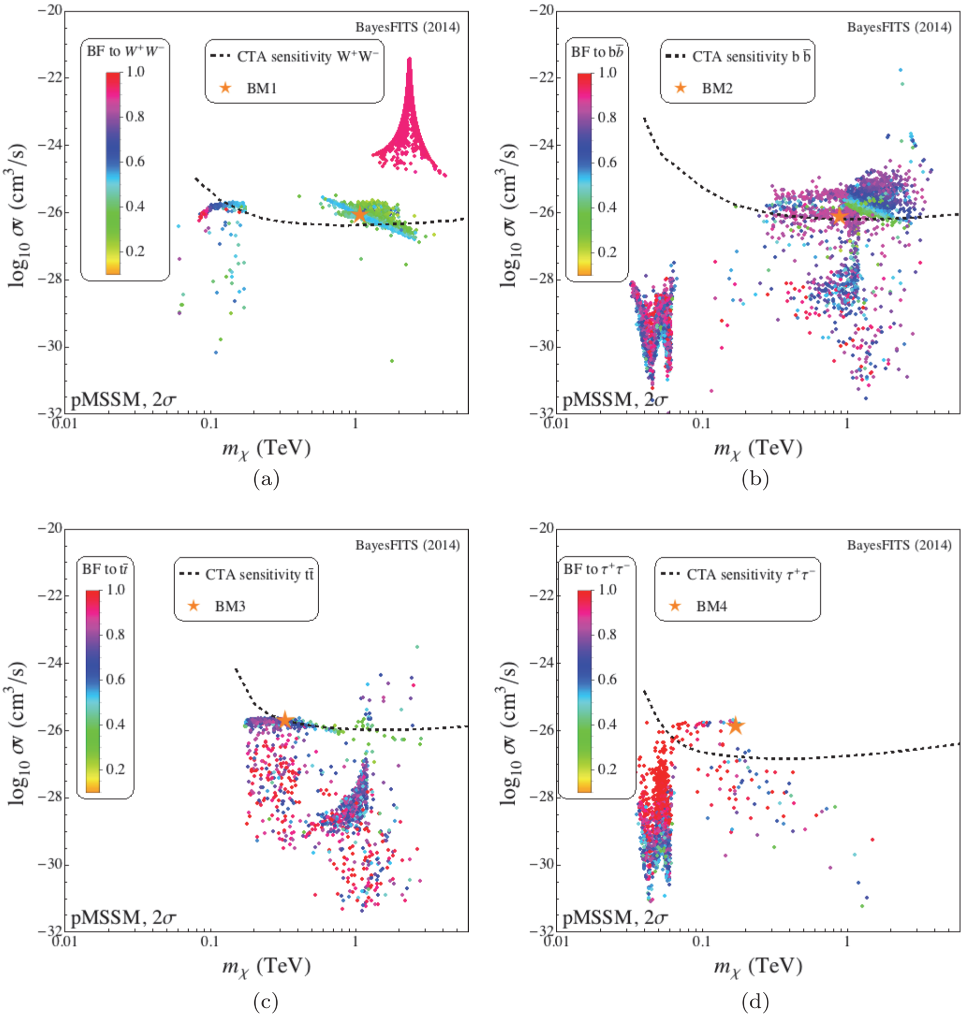

(a) (b) (c) (d)

Figure 4.9: Comparison of allowed models from Ref. [53] for each the dominant modes: W^+W^-, $b\bar{b}$, $t\bar{t}$ and $\tau^+\tau^-$ in (a)–(d) as indicated with the corresponding sensitivities as calculated in their paper. The colour code shows the value of dominant branching fraction for each point (the stars mark the particular benchmark points discussed in Ref. [54]).

matter distribution profiles (Einasto and isothermal). The modelling of the standard astrophysical emission is obtained by taking into account the already detected gamma-ray emission by H.E.S.S. in that region convolved with the instrument response functions as well as the residual rate of charged cosmic rays. Using the energy-dependent variation of the energy resolution, an unbinned analysis of Monte Carlo simulations was performed. A sliding search window of four times the size of the energy resolution centred at the

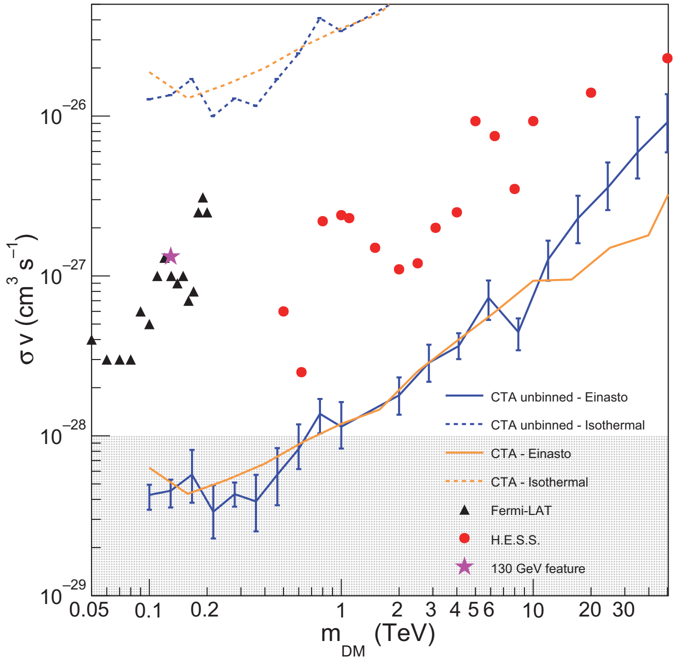

Figure 4.10: Sensitivity of CTA to monochromatic gamma-ray signals from dark matter annihilation, with $E = M_\chi$, after 500 h of observation of a region with 1° radius around the Galactic Centre using an unbinned likelihood analysis (blue line) and a differential sensitivity analysis (orange curve) assuming an Einasto profile. For comparison, the currently best limits from Fermi [108] (black triangles) and H.E.S.S. [109] (red dots) are also shown, along with the much discussed line-like feature at around 130 GeV [110, 111] (magenta star). The dashed lines also show the mean upper limits obtained in case of a Burkert profile. The natural scale for monochromatic gamma-ray signal is highlighted as a black shaded area.

position of the expected line is used. The results in Figure 4.10 show this method as well as an analysis cross-check, assuming a 500 h exposure and an Einasto dark matter distribution profile. While the current analyses do not include systematic uncertainties, these are expected to be small. As no known standard astrophysical sources would produce such sharp energetic features, the discrimination against background is easier in line searches compared to the continuum emission search.

4.2.2 *Dwarf Spheroidal Galaxies and Dark Clumps*

4.2.2.1 *Description*

The dwarf spheroidal galaxies (dSphs) of the Local Group could give a clear and unambiguous detection of dark matter. They are gravitationally bound objects and are believed to contain up to $\mathcal{O}(10^3)$ times more mass in dark matter than in visible matter, making them widely discussed as potential targets. Being small and distant, many of the dwarf galaxies will appear as point sources to CTA, and hence the nuisance of the instrumental background is much reduced. Although less massive than the Milky Way or the LMC, they are also environments with a favourably low astrophysical gamma-ray background making the unambiguous identification of a dark matter signal easier compared to the Galactic Centre or LMC. Neither astrophysical gamma-ray sources (supernova remnants, pulsar wind nebulae, etc.) nor gas acting as target material for cosmic rays have been observed in these systems.

The search program selects dwarf galaxy targets on the basis of both their J-factors and relative J-factor uncertainties. Due to the larger available sample of spectroscopically measured stars, the classical dwarf galaxies such as Draco, Ursa Minor, Sculptor, and Fornax have significantly smaller uncertainties on the J-factor than the ultra-faint dwarf galaxies [81]. However, several of the ultra-faint galaxies (e.g. Ursa Major 2) have J-factors which are larger than the J-factors of the best classical dwarfs which, to some degree, outweighs the larger J-factor uncertainties for these objects. A recent evaluation of dwarf galaxy J-factors was presented in Ref. [112] which used a Bayesian hierarchical modelling analysis to constrain the dark matter mass and scale radius in 18 dSph galaxies with good spectroscopic data. Using these mass models, we can compare the CTA detection prospects of the dwarf galaxies in this sample on the basis of the J-factor integrated within an angular region of radius 0.1° ($J_{0.1}$), where the angular scale of the integration region has been chosen to match the CTA point spread function at 100 GeV. This study shows that two of the best classical dwarf candidates are Draco in the northern hemisphere with $\log_{10}(J_{0.1}/\mathrm{GeV}^2\mathrm{cm}^{-5}) = 18.69 \pm 0.16$ and Sculptor in the southern hemisphere with $\log_{10}(J_{0.1}/\mathrm{GeV}^2\mathrm{cm}^{-5}) = 18.47 \pm 0.18$. The most promising known ultra-faint galaxies are best observed from the northern hemisphere, although discovery of new ultra-faints in the southern hemisphere is anticipated within the next 5–10 years as new optical surveys come online. Ultra-faint dwarf candidates observable from the northern hemisphere include Segue 1, Coma Berenices, and Ursa Major 2. Very recently, the Dark Energy Survey (DES) data revealed eight Milky Way satellites [113, 114] in the southern hemisphere likely to be ultra-faint dwarf galaxies. In particular, Reticulum II is the most attractive of these, given both its proximity and high dark matter content [115]. With forthcoming in-depth studies of their dark matter content and distribution, these ultra-faint dSph candidates may be well-motivated targets for CTA.

Structure formation predicts gravitationally bound dark matter clumps down to much lower masses than observed for dSph galaxies. The low-mass cutoff of the clump distribution is related to the free-streaming scale of dark matter particles in the early universe and is expected to be between 10^{-12} $M_\odot$ and 10^{-3} $M_\odot$ for typical WIMP scenarios [116]. The number-counts distribution of clumps in Milky Way-like galaxies has been investigated with numerical N-body simulations, finding a power law: $\mathrm{dN/dM} \propto \mathrm{M}^\alpha$ in clump mass M, with a high-mass cutoff at $M \sim 10^{10}$ $M_\odot$ and an index α between -1.9 and -2.0 [64, 65]. For the Milky Way, this would imply a clumpiness factor of ∼18% (referring to the relative contribution of the total mass in clumps to the total mass of the main halo). The spatial distribution of dark matter clumps is biased away from the smooth central dark matter distribution of the host halo, i.e. the majority of clumps populate outer halo regions ($r > 100$ kpc).

In the near future, experiments will be able to probe the subhalo population above 10^5 $M_\odot$ using gravitational millilensing of background objects [117], while the statistical properties of lighter clumps (down to mass scales below a Solar mass) in the Solar neighbourhood can be measured from gravitational nanolensing [118, 119]. Additional statistical techniques to estimate the presence and properties of moving sources contributing to a diffuse background emission are being investigated as well [120]. Dark clumps orbiting in the solar vicinity also affect the kinematics of stellar streams. A peculiar distribution of gaps would be imposed on local stellar streams by impacting clumps of all mass scales. First studies of local streams have already hinted at clump impacts [121], while further studies are ongoing or proposed [122–126].

Lacking identification in optical surveys, the prime channels of detecting dark clumps are VHE gamma rays emerging from annihilations or decays of dark matter particles in the clump. Clumps would show the unique spectral gamma-ray signature of dark matter annihilation or decay [127–129]. The Smith Cloud is a unique nearby Galactic substructure which was detected as a cold cloud of neutral hydrogen (HI) and is characterised by its large peculiar velocity [130]. The dark matter content of such objects is still under debate [131, 132], but it is plausible that the Smith Cloud hosts a large dark matter halo.

4.2.2.2 *Evolution of knowledge*

Our knowledge of the dark matter distribution in the so-called "classical" dSph satellites of the Milky Way is based on dynamical modelling of their internal stellar kinematics (for recent works, see, e.g. Refs. [133, 134]). The availability of multi-object spectrographs on a number of large telescopes combined with the dSphs' proximity to Earth has made it possible to obtain data sets of individual stellar velocities ranging in size from ∼170 (Leo II [135]) up to ∼2500 (Fornax [136]) stars. Reference [137] provides an excellent review of the currently available data.

The next step change in the size of dSph kinematic data sets is expected once instruments such as the Prime Focus Spectrograph [138] mounted on the 8.2-m Subaru telescope are available, providing thousands of fibres over a large field of view. Based on the numbers of red giant stars in the classical dSphs down to magnitude 22, it is reasonable to expect that on a 5–10-year timescale there will be samples of at least 1000 stars for all of the classical dSphs, with Sculptor and Fornax yielding particularly rich samples of ∼5,000 and ∼10,000 stars, respectively. These new data will need to be complemented by more advanced modelling in order to constrain their dark matter profiles. A number of groups are working on a range of approaches, and there is reason to be optimistic that community efforts such as the Gaia Challenge will drive further developments in this area by comparing existing modelling techniques, identifying systematic errors and biases in current algorithms, and facilitating the development of new ones. Studies are underway to estimate the impact that increased data sets and improved modelling can be expected to have on the ability of CTA to constrain the nature of dark matter, building on the earlier work of Ref. [139].

Since the recent discovery of a new population of satellite galaxies around the Milky Way, the ultra-faint dSphs, significant attention has been focused on their potential as targets in which to search for dark matter annihilation signals [140]. The paucity of stars in these objects means that current sample sizes range from ∼200 stars in CVnI to ∼70 in Segue 1 and as low as 5 in the case of Leo V (see Ref. [137] for references), with limited prospects for significantly larger samples in the near future. These objects with a limited number of stars are prone to higher systematic uncertainties when modelling their dark matter content (see, for instance, Ref. [133]). An additional complication is that the nature of these objects is still uncertain. If they represent a population of objects which have been strongly affected by the tidal field of the Milky Way, their dark matter content may have been over-estimated by simple equilibrium models. Further work is required to establish whether the potential constraints which these satellites may place on dark matter, see e.g. [141], justify the risk that they may not contain sufficient dark matter to be detectable. New surveys such as Pan-STARRS and SkyMapper are expected to yield numerous additional ultra-faint dSphs, e.g. [142, 143]. Indeed, a new population of low-luminosity dSphs with a peak surface brightness lower than 30 mag arcsec^{-2} (i.e. below current detection thresholds) is expected [144]. Toy models applied to numerical N-body simulations predict the discovery of 3−13 $L \gtrsim 10^3\ L_\odot$ and 9−99 $L \lesssim 10^3\ L_\odot$ (i.e. ultra-faint) dwarfs with DES, and 18−53 $L \gtrsim 10^3\ L_\odot$ and 53−307 $L \lesssim 10^3\ L_\odot$ dwarfs with LSST [145]. Ultra-faint dSphs are likely to be hosted by light dark subhalos ($\lesssim 10^6\ M_\odot$) which could be orbiting in the vicinity of the Solar System. These future surveys will extend significantly the knowledge of dwarf galaxies in the southern sky where CTA will have the highest sensitivity.

4.2.2.3 *Observational strategy*

The observations of a dwarf spheroidal galaxy will be started in the first year of the Dark Matter Programme. Any hints of dark matter signals or unknown sources would guide the plans for future observations. In the absence of signals, a programme of observation on the most promising dSph would be taken. As discussed earlier, according to existing data, the ultra-faint dwarf galaxies have the highest J-factors, and so the best of these at the time would be adopted with the criterion of maximising the chance of discovery. In the time before full CTA operations, it is expected, as discussed previously, that much more information will be available to make the final choice. If new astrophysical data on stellar dynamics for a given dSph provide further motivation for pursuing the search, the observation strategy will be modified accordingly. Following a full evaluation of all results, the observing strategy is to acquire 100 h of observations per year on the best candidate dSph at that time.

4.2.2.4 *Performance*

Dwarf Galaxies have been principle targets for dark matter searches in existing gamma-ray experiments. Many strategies are considered for CTA with the spirit of being flexible to observe the most promising targets known when CTA is operational following information from the new surveys discussed previously or from any other resource.

An example of the sensitivity which could be obtained by observations of a classical dwarf galaxy is shown in Figure 4.11, using the same analysis methodology [104] as that performed for the Galactic halo so the results can be directly compared. In making this comparison with Figure 4.7, it can be seen that the sensitivity is a factor 100 worse for this classical dwarf galaxy; however, the effect of systematics is drastically reduced for this small source compared to the extended Galactic halo, explaining the significant interest in observations of dwarfs. Interestingly, observations of a classical dSph provide comparable sensitivity to the Galactic Centre for the cored dark matter profile.

Figure 4.12 compares the sensitivity in the $b\bar{b}$ annihilation channel for 500 h observation time on the ultra-faint dSph Segue 1 and Coma Berenices to the sensitivity on classical dSphs Draco and Sculptor. Ultra-faint dSphs provide stronger constraints compared to classical dSphs though higher uncertainties are expected in the dark matter distribution. One standard deviation uncertainties are shown as dashed lines [81].

4.2.3 *Large Magellanic Cloud*

4.2.3.1 *Description*

The LMC is a nearby satellite galaxy at high Galactic latitude, and it has the shape of a disk seen nearly face-on. At a distance of only ∼50 kpc, and with a large dark matter mass of $\sim 10^{10}\ M_\odot$, the LMC is a candidate for indirect dark matter searches which has long been recognised as a potentially favourable target [146]. The mass of the LMC of 1% of the Milky Way makes it interesting even though its distance, at six times further away than the Galactic Centre, gives a large signal reduction. The LMC is an extended source for CTA. Most of the emission lies within the CTA field of view, enabling the full galaxy to be observed in detail. Like the Milky Way Galactic halo, astrophysical backgrounds are a significant challenge for the LMC. However, the J-factor of the LMC has been claimed to be as high as $\log_{10}(\mathrm{J/GeV^2cm^{-5}}) \sim 20.5$ [146, 147], making it an attractive target for indirect searches. However, the spatial extent of the LMC and its significant astrophysical gamma-ray emission lead to both analysis uncertainties and systematics.

The LMC hosts many interesting astrophysical sources: the largest star-forming region in the Local Group of galaxies, one of the densest stellar clusters known, the most massive stars ever observed, several tens of HII regions, more than a dozen super-bubbles, numerous giant shells, more than

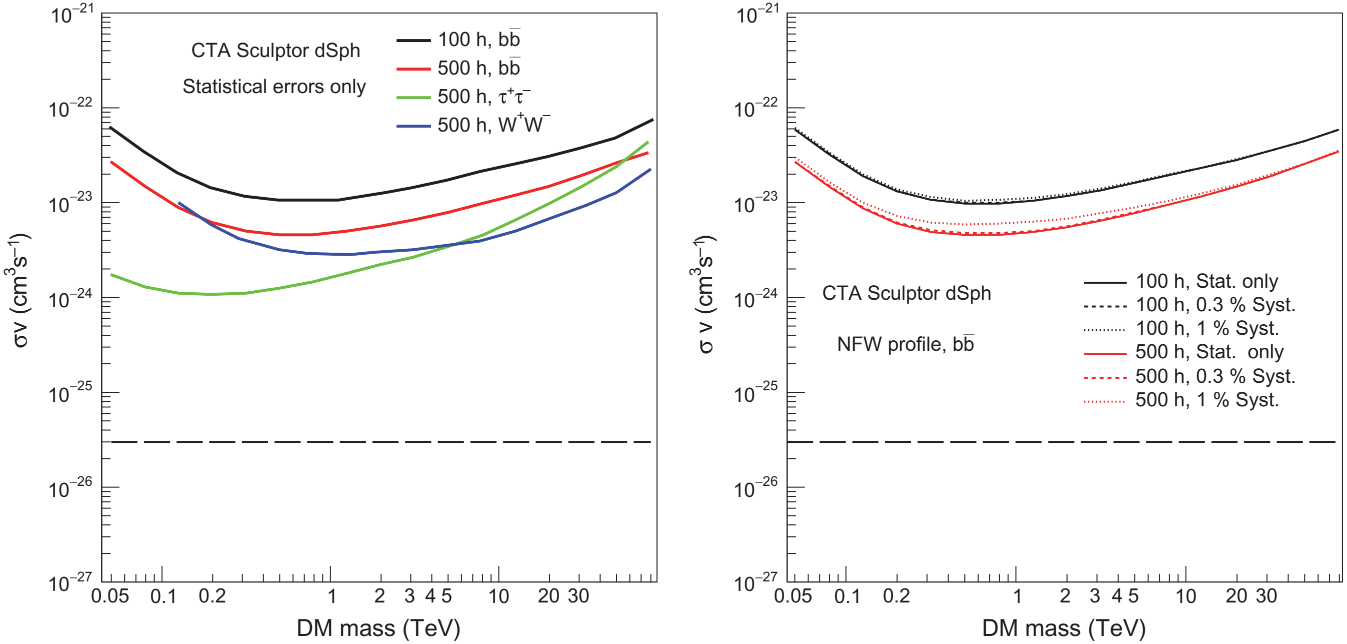

(a) (b)

Figure 4.11: (a) CTA sensitivity for $\langle \sigma v \rangle$ from observation of the classical dwarf galaxy Sculptor for different annihilation modes as indicated. (b) CTA sensitivity for $b\bar{b}$ annihilation modes for different conditions; black line is for 100 h of observation and red line for 500 h. The solid lines are the sensitivities only taking into statistical errors, while dashed and dotted curves take into account systematics as indicated in the figure. The dashed horizontal line shows the thermal cross-section of 3×10^{-26}cm^{3}s^{-1}.

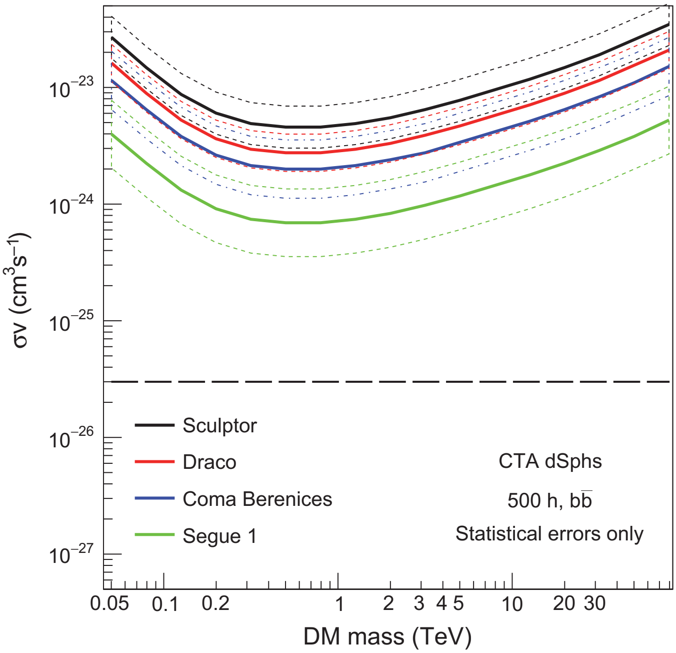

Figure 4.12: CTA sensitivity for $\langle\sigma v\rangle$ from 500 h observation of the classical dSphs Draco and Sculptor, and the ultra-faint dwarf galaxies Segue 1 and Coma Berenices as indicated. Dashed lines correspond to one standard deviation uncertainties on the J-factors. Sensitivity is computed assuming the $b\bar{b}$ annihilation mode and statistical errors only are taken into account. The dashed horizontal line shows the thermal cross-section of $3 \times 10^{-26}\mathrm{cm}^3\mathrm{s}^{-1}$.

50 catalogued supernova remnants, and the remnant of the recent naked-eye supernova SN 1987A. The LMC was detected in high-energy gamma rays and characterised by Fermi-LAT after just one year of data [148]. Recently, powerful VHE emitters have been detected by H.E.S.S. [149]. The astrophysical motivation for observations of the LMC are discussed in the LMC Key Science Project.

The dark matter distribution uses benchmark halo models of the LMC for which updated modelling was performed in Ref. [147] using HI rotation curve data [150] and stellar velocity data [151]. The rotation curve was decomposed into a dark matter component, the HI mass, and the stellar mass. At all stages of the analysis, choices were made to maximise the baryonic contribution to the rotation curve and to minimise the dark matter contribution, leading to conservative estimates of the dark matter content. The dark matter distribution was fit to an isothermal profile, representing the conservative case of a cored inner density profile, and an NFW profile, representing a more typical choice for the assumed dark matter distribution. The analysis was performed assuming the best-fit position for the LMC centre based on HI and proper motion studies. The largest source of uncertainty in the rotation curve determination is the inclination of the LMC, so the fit for each profile was performed for extreme values of the inclination angle to bracket this source of uncertainty.

The rotation curve data place a robust lower limit on the J-factor of the LMC of $\sim 5 \times 10^{19}$ $\mathrm{GeV^2\,cm^{-5}}$ (integrated over the LMC), although we emphasise that the rotation curves are also consistent with much larger J-factors. The J-factor values integrated within 15° of the LMC centre range from $\sim 5\times 10^{19}$ to $\sim 5\times 10^{20}$ $\mathrm{GeV^2\,cm^{-5}}$ and, for both profiles, the emission profile is peaked towards the centre with more than half of the emission originating from within a few degrees of the centre. Eventually, detectability depends not only on the J-factor but also the dark matter distribution and on how well it can be discriminated from instrumental background and astrophysical emission. The level of expertise for this analysis motivates this program to be conducted by the CTA Consortium.

4.2.3.2 *Evolution of knowledge*

The complexity of the dynamical state of the LMC, and the associated difficulty of modelling it, is reflected in the relatively few attempts at building a comprehensive picture of the mass distribution in its inner regions. Reference [152] presented a detailed study of the stellar kinematics in the LMC, and recently updated modelling was performed in Ref. [147]. As in the case of spiral galaxies, the baryonic mass in the disk and bar of the LMC contributes a significant fraction of the gravitational potential in the inner regions, making the LMC more difficult to model than the dSphs in which the stellar component can, to first order at least, be treated as a massless tracer population. Furthermore, the LMC is interacting with the Small Magellanic Cloud and has a central stellar bar which is not properly understood dynamically. Both these complications, coupled with the $>20°$ extension of the LMC on the sky, make it very challenging to construct a precise picture of its inner mass distribution. Interestingly, despite all the uncertainties and complications noted above, the range of J values for the LMC is just a factor of 20 when the halo profile is varied from NFW to cored isothermal. By comparison, in the centre of the Milky Way, the J-factor varies by a factor of 100 when the halo is varied over the narrower range of an NFW halo and a halo with inner log slope of 0.5 [106]. Under such consideration, the LMC appears to be a robust target, despite the lower nominal value of J relative to that of the Milky Way.

Spectroscopic studies continue to expand the size of radial velocity samples in the LMC (see e.g. Ref. [151] for an overview with new instruments (e.g. MUSE on the VLT)) providing opportunities for detailed studies of the stellar kinematics of the inner degree. Proper motions obtained using Hubble Space Telescope observations [151] have complemented the line-of-sight velocities, and it is the Gaia satellite that promises the next major step in understanding by mapping out the proper motion velocity field in much greater detail. With 3D velocities, it may become possible to unravel the inner dark halo slope, although considerable further modelling effort for the stellar and gas components will be needed. Finally, gravitational microlensing studies may assist in this by constraining the line of sight depth of the LMC.

4.2.3.3 *Observational strategy*

For the LMC, observations will be taken with several pointings to cover the full galaxy. A total of 340 h of observations are proposed for both dark matter and astrophysical motivations (see LMC Key Science Project).

4.2.3.4 *Performance*

The sensitivity is computed for two benchmark annihilation channels, $b\bar{b}$ and $\mathrm{W}^+\mathrm{W}^-$, with the results shown in Figure 4.13. The curves represent the 95% confidence level upper limits that would be obtained on the dark matter annihilation cross-section as a function of dark matter particle mass in the case that no emission associated with a dark matter spatial template is detected. The minimum energy considered in the analyses is 200 GeV due to the minimum zenith angles allowed for LMC observations. The strongest sensitivity is achieved for the NFW profile with the maximum rotation curve and maximum allowed density within uncertainties in the inclination angle of the LMC, while the minimum rotation curve with the isothermal profile yields the weakest sensitivity. In the most optimistic case, the expected sensitivity is about a factor of 20 above the natural cross-section. The difference in the testable annihilation cross-section between the extreme cases is a factor of ~ 10. The astrophysical backgrounds in the LMC and their uncertainties differ from those in the Galactic Centre, making it a complementary dark matter search target.

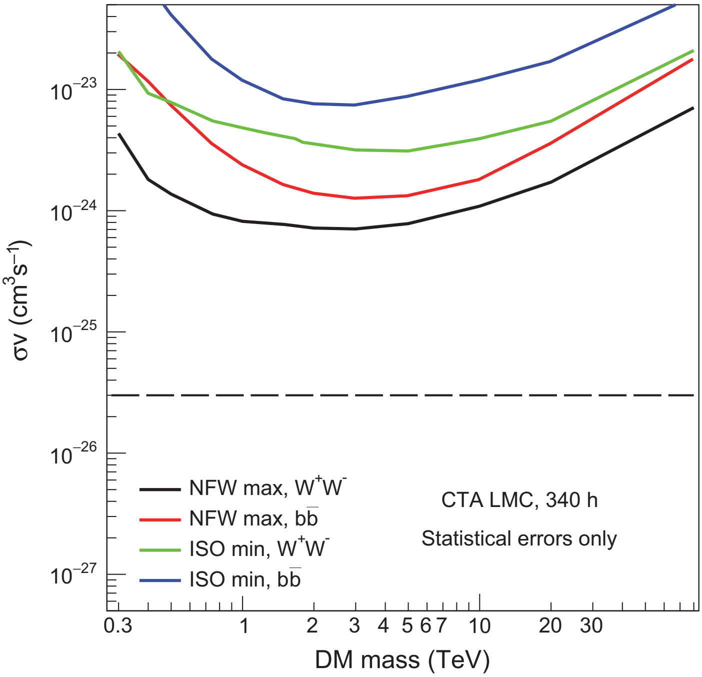

Figure 4.13: CTA sensitivity on $\langle \sigma v \rangle$ from observation of the LMC for 340 hours of observation in the $b\bar{b}$ and W^+W^- annihilation channels for both NFW and isothermal (ISO) dark matter profiles, as shown in the legend. The sensitivities are computed with a 200 GeV energy threshold assuming statistical errors only.

4.2.4 *Clusters of Galaxies*

Clusters of galaxies are the largest and most massive gravitationally bound systems in the universe, with radii of a few Mpc and total masses of 10^{14} to 10^{15} $M_\odot$, of which galaxies, gas, and dark matter contribute roughly 5%, 15%, and 80%, respectively. They present very high mass-to-light ratio environments and should be also considered promising targets for indirect dark matter searches, both for decay and annihilation. In particular, the dark matter decay rate is directly proportional to the enclosed mass, making clusters the best targets together with our Galactic Centre [153]. The dark matter halo of galaxy clusters harbour an abundance of dark matter substructures which contribute to the overall dark matter luminosity of the clusters. In principle, they provide substantial contribution to the dark matter annihilation signal. However, large uncertainties in the substructure boost factors remain [154], making them less favoured environments for annihilating dark matter than previously thought [155, 156].

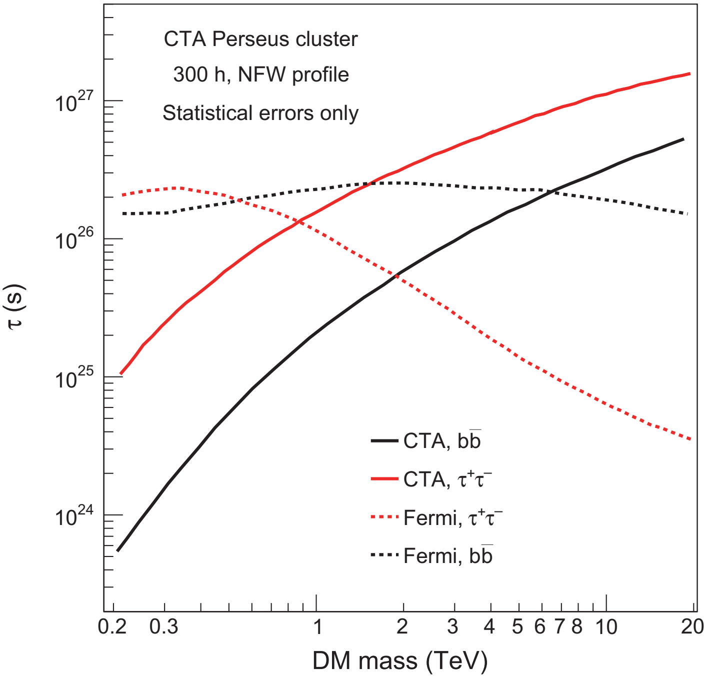

Figure 4.14: Expected CTA sensitivity to the dark matter decay lifetime for 300 h of observation of the Perseus cluster. We assume a dark matter profile as in Ref. [158] and adopt the full-likelihood analysis of Ref. [159], while the adopted dark matter spectra are from Ref. [161]. The size of the signal integration region (0.3° radius) has been optimised taking into account the expected source extension and the performance for off-axis observations. We assume five off regions. We compare our CTA predictions with the results from the Galactic halo by Fermi [160].

Galaxy clusters are a promising target for decaying dark matter (see, for instance, Ref. [157]). While the signal originating from annihilating dark matter is proportional to the square of the dark matter density, for decaying dark matter the dependence is on the first power. As a consequence, dense dark matter concentrations outshine the astrophysical backgrounds if annihilation is at play, but remain comparatively dim if dark matter is decaying. Decaying dark matter wins instead, generally speaking, when large volumes are considered. Figure 4.14 shows predictions for the case of the Perseus cluster for 300 h of observation. We assume a dark matter profile in the cluster as in Ref. [158] while adopting the full-likelihood analysis of Ref. [159]. We consider an integration radius of 0.3°. As is clear from the figure, CTA can do much better than Fermi [160] at the TeV scale.

The astrophysical motivations for observation of Perseus presented in the Galaxy Cluster KSP complement and extend the science case for dark matter presented here.

4.2.5 *Summary of Targets*

The Dark Matter Programme comprises 10 years of observations dedicated to dark matter targets. The calendar for the observations is shown in Table 4.1. The first three years are devoted to deep observations of the Galactic Centre together with observation of the best ultra-faint dwarf galaxy. The observations towards the Galactic Centre will represent an important achievement and the result, eagerly awaited by the scientific community, is an expected deliverable of CTA.

Two different observation scenarios are considered depending on the outcome of the first three years of observations, i.e. whether there is a detection of a signal or not in the Galactic Centre dataset:

- In case of a detection and a relatively high annihilation cross-section (a few times 10^{-25} cm^{3}s^{-1}), the schedule will focus the observation time on the ultra-faint dwarf galaxy with a high J-factor to probe the annihilation cross-section in a cleaner environment. Simultaneously, follow-up observations of the Galactic halo would be scheduled to allow

Table 4.1: Strategy for dark matter observations over 10 years with CTA.

Year	1	2	3	4	5	6	7	8	9	10
Galactic halo	175 h	175 h	175 h							
Best dSph	100 h	100 h	100 h							
				In case of detection at GC, large σv						
Best dSph				150 h	150 h	150 h	150 h	150 h	150 h	150 h
Galactic halo				100 h	100 h	100 h	100 h	100 h	100 h	100 h
				In case of detection at GC, small σv						
Galactic halo				100 h	100 h	100 h	100 h	100 h	100 h	100 h
				In case of no detection at GC						
Best Target				100 h	100 h	100 h	100 h	100 h	100 h	100 h

Note: The first three years are devoted to the deep observation of the Galactic Centre (GC) together with the observation of the best ultra-faint dwarf galaxy. In case of non-detection of the GC, observations starting in the fourth year focus on the most promising target at that time to provide legacy constraints.

for in-depth study of the morphology of the dark matter distribution. For a relatively small annihilation cross-section (a few times 10^{-26} cm^{3}s^{-1}), the following years will be devoted to follow-up observations of the Galactic Centre in order to double at least the photon statistics to accurately characterise the faint detected signal.

- In case of no detection at the Galactic Centre, we will focus our observation time towards the *best target* at that time, on e.g. an ultra-faint dwarf galaxy or dark clump target, from years 4 to 10. This observation time will be devoted to provide long-standing legacy constraints.

4.3 Data Products

The following data products will be provided to the community:

- For each target: Data-cubes (binned in the two spatial dimensions around the source and in energy) with the measured number of excess events over the background, together with the statistical significance of the excess.
- For each detected source: Energy spectrum and surface brightness of the emission, with a binning determined by its intensity and spatial extension.
- A model of diffuse VHE gamma-ray emission in the field of view of each target.
- For each target: The value of the likelihood function versus gamma-ray flux, in bins of energy, following the prescription used in Ref. [81]. This information is sufficient to compute the total likelihood (individually for each source or globally for all of them) for any given dark matter model.
- Using the previous information, constraints will be placed on the parameters of a set of dark matter annihilation and decay channels, including those producing gauge boson, quark, lepton, and photon pairs, and any other channels favoured by the theory and other experimental constraints at the time of the data analysis.

These results will be produced and released whenever a new source will be observed and/or when a significant amount of new data will justify an update of the results. In the case of no signal, we will publish our results after 100 h and 500 h of observations (for any given source).

This page intentionally left blank

5

KSP: Galactic Centre

The Galactic Centre Key Science Project is comprised of a deep exposure of the inner few degrees of our Galaxy, complemented by an extended survey to explore the regions not yet covered by existing very high-energy (VHE) instruments at high latitudes to the edge of the bulge emission. A schematic representation is shown in Figure 5.1, with details of the observation strategy and possible options given in Section 5.2.

The region within a few degrees of the Galactic Centre contains a wide variety of possible high-energy emitters, including the closest supermassive black hole, dense molecular clouds, strong star-forming activity, multiple supernova remnants and pulsar-wind nebulae, arc-like radio structures, as well as the base of what may be large-scale Galactic outflows (commonly referred to as the *Fermi bubbles*); it is also one of the best places to look for dark matter, as outlined in Chapter 4. The central few degrees of our Galaxy is arguably one of the most studied regions of the sky in nearly every waveband (see Figure 5.2). In VHE gamma rays alone (for a review see Ref. [165]), the region has yielded major scientific discoveries including an unidentified central point-like gamma-ray source [166, 167] that may be associated with Sgr A* and a complex pattern of diffuse emission [168, 169] that may be an indication of local PeV cosmic-ray acceleration in the recent past [170]. Precision measurements with CTA will allow us to study this complex region in unprecedented spatial and spectral detail, and may allow for the identification of the central source, the disentangling of models that have been put forth to explain the extended emission, and perhaps the deeper understanding of the capability for cosmic ray acceleration in our Galaxy and the history thereof. A simulated CTA view of the Galactic Centre region

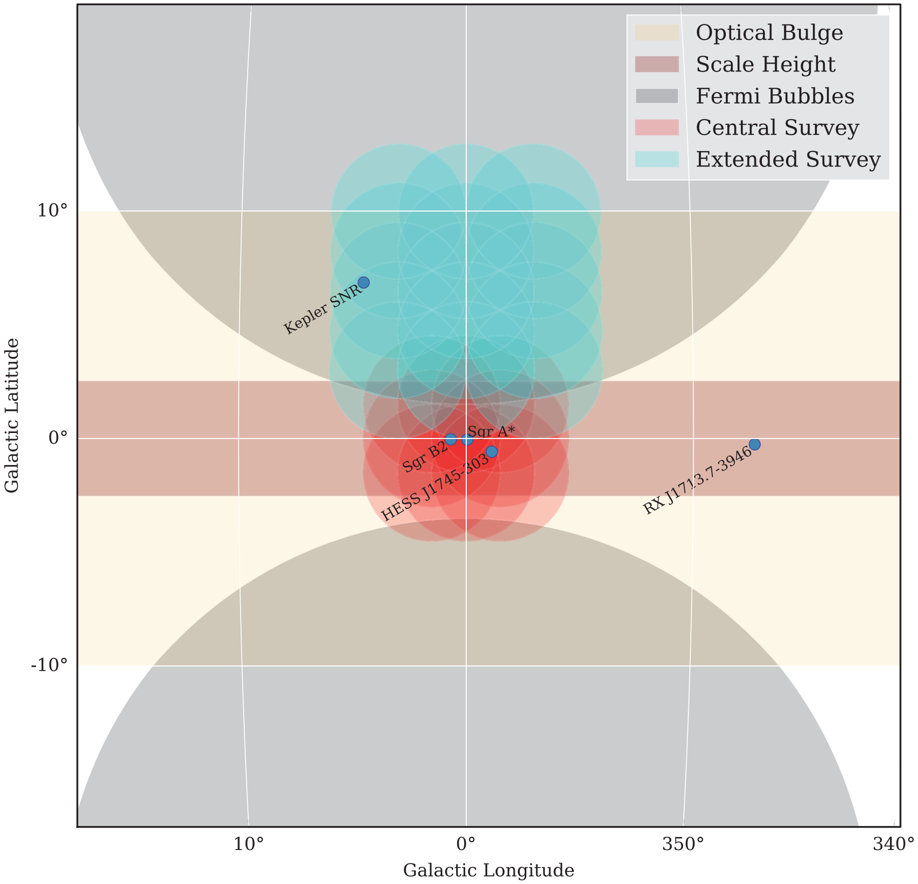
Optical Bulge
Scale Height
Fermi Bubbles
Central Survey
Extended Survey
Kepler SNR
Sgr A*
Sgr B2
HESS J1745-303
RX J1713.7-3946
10°
0°
-10°
Galactic Latitude
10°
0°
350°
340°
Galactic Longitude

Figure 5.1: A schematic representation of the Galactic Centre KSP. This figure shows one possible observation strategy for CTA. The deep survey region is shown in red, with the Galactic bulge extension shown in cyan (with each circle representing a 6° field of view for a typical CTA configuration). Several object positions are overlaid with blue dots for reference, in particular Sgr A*, the supermassive black hole that lies at the geometric center of the Galaxy.

that could be accomplished with the observations proposed in this KSP is shown in Figure 5.3 for various astrophysical scenarios; the differences among the scenarios can be clearly identified. Note that the angular resolution of the diffuse template used in these simulations is poorer than that of CTA; therefore, small-scale features possible with CTA are not well represented beyond the included point-like sources.

A deep Galactic Centre survey is considered key science for both scientific and technical reasons. The scientific results will encompass a wide variety of targets and topics and will require a large time commitment spread over

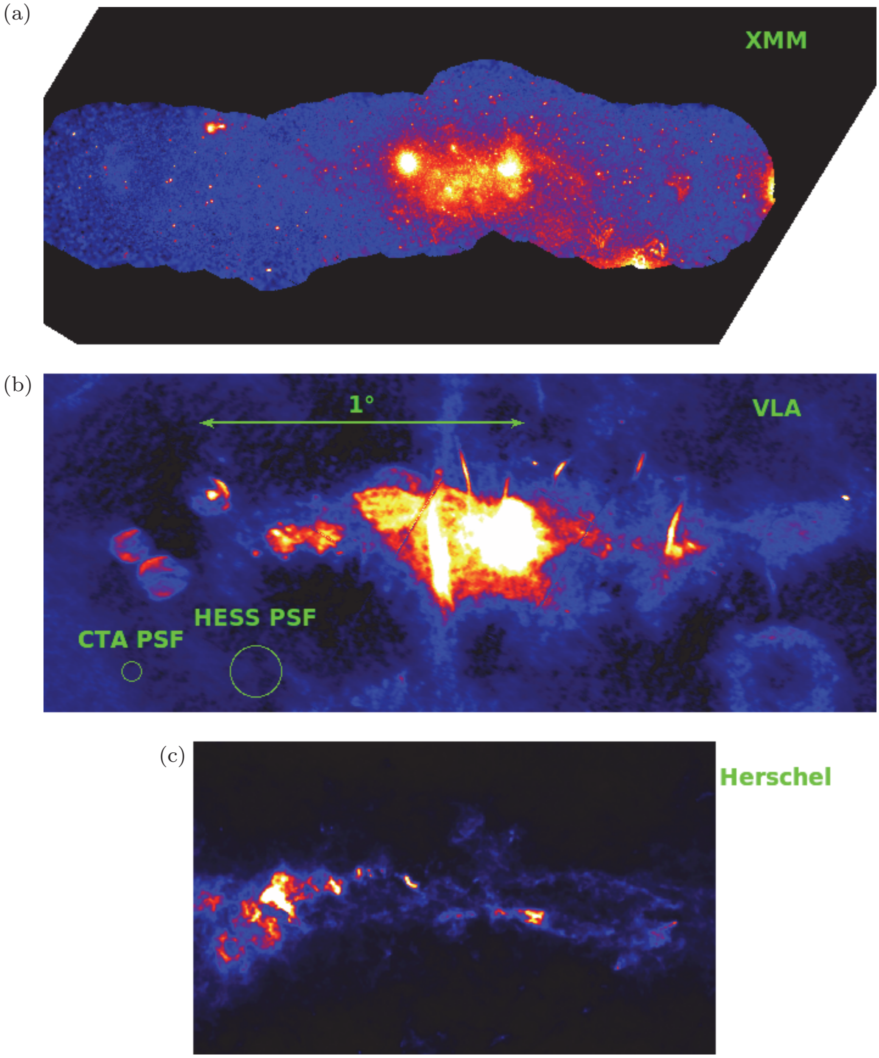

Figure 5.2: Multi-waveband view of the inner Galactic Centre region, showing the wide variety of diffuse emission. The scale is set such that the bright point source associated with Sgr A* in radio and X-rays is clipped to accentuate the surrounding emission. (a) The X-ray emission detected by XMM-Newton, from Ref. [162]. (b) The radio view, showing diffuse emission, SNR shells, and various arc-like radio features, from Ref. [163]. The CTA point spread function is shown in comparison with that of the presently operating H.E.S.S. telescope to illustrate the possibility of resolving structures with CTA that are point-like with existing instruments. (c) Infrared (IR) view of the gas (target material for cosmic rays to produce pion-decay gamma rays), showing the toroidal feature in the central molecular zone, from Ref. [164].

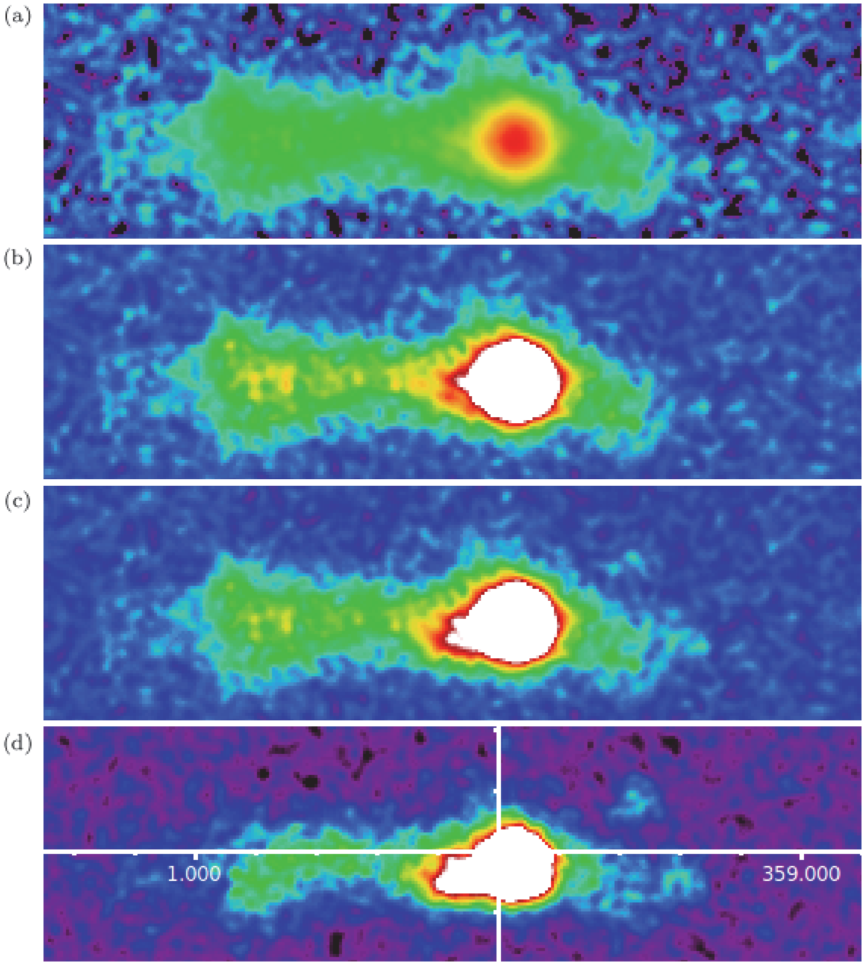

Figure 5.3: A simulated view of the Galactic Centre region as seen by CTA (excess events above 800 GeV after cosmic-ray background subtraction, with Gaussian smoothing). (a) and (b) The reference model that includes a point-like source at the position of Sgr A* with an exponential-cutoff power-law spectrum matching H.E.S.S. measurements [166], a similarly modelled point-like supernova remnant G0.9+0.1 [171], diffuse emission from a template based on the dense matter distribution deduced from HCN molecule observations [172], and an extended circumnuclear ring template. (a) is in log scale and (b) is clipped to show the details of the diffuse emission (thus the point-like central source which is an order of magnitude brighter is washed out). (c) The reference model plus a catalogue of energetic pulsar-wind-nebulae [173]; here the central source clearly appears extending towards the left. (d) An alternative model consisting of an extended circumnuclear ring model assuming the source is produced by the interaction of isotropic cosmic rays with the circumnuclear ring gas (which has a $1.5'$ diameter), diffuse emission from HCN maps as above, and close-by pulsar-wind nebulae [173] (modelled as point-sources). The central source and G 0.9+0.1 are excluded. Cosmic-ray background is subtracted using a model generated from cosmic-ray events; the same background model is used in all cases.

multiple years. The proposed observations will provide the deepest exposure of the Galactic Centre region ever produced in the TeV domain and will provide significant scientific output on a variety of topics for years to come. As part of this project, the CTA Consortium will organise coordinated observations in other wavebands that will permit detailed variability studies and constitute an invaluable legacy data set.

The realisation of an extremely deep and high-precision survey of the Galactic Centre region is non-trivial from a technical standpoint due to the complexity and confusion of the gamma-ray and optical emission in the region, the difficulty of modelling the background when there is an expectation of sources that are larger or similar to the instrumental field of view, the necessity to handle strong background optical light that varies by a factor of over ten within the field of view, and the need to push the systematic errors to extremely low levels to produce meaningful limits on models. Such a study will therefore require a deep knowledge of the instrument and atmosphere and will perhaps even require specialised knowledge of the calibration, reconstruction, and discrimination of Cherenkov events that only the CTA Consortium can readily provide.

The main science topics that can be explored with this rich data set are described below, followed by the observational strategy, data products, and expected return.

5.1 Science Targeted

This key science program of the Galactic Centre region covers a wide range of scientific topics due to the rich environment within the central few degrees of our Galaxy.

5.1.1 *Scientific Objectives*

5.1.1.1 *Revealing the nature of the central gamma-ray source*

CTA can provide the answer to what is producing the point-like source of the VHE gamma-ray emission at the dynamic centre of the Milky Way.

The central VHE source was first detected in 2004 [174, 175], and although well studied by current-generation atmospheric Cherenkov telescopes (H.E.S.S. and VERITAS), it still remains unidentified due to source confusion and limited sensitivity to variability and small-scale morphology. The emission may originate from close to the supermassive black hole Sgr A*, from winds driven out from it, from a background pulsar-wind nebula, or from a variety of other possibilities. CTA, with its arc-minute resolution at high energies and dramatic improvement in sensitivity for rapidly variable phenomena, will have the opportunity to resolve this question.

5.1.1.2 *Diffuse VHE emission: Particle acceleration in the vicinity of the Galactic Centre*

The diffuse gamma-ray emission along the Galactic ridge provides the best case for studying both gamma rays produced by hadronic interactions and to understand the acceleration history of the central engine. This diffuse region is the sole VHE source presently known that is generally acknowledged to be predominantly hadronic in nature. H.E.S.S. observations revealed the presence of a ridge of hard (photon spectral index, $\Gamma \sim 2.3$) VHE emission, extending over 1.5° along the Galactic plane [168]. The spectrum is similar to that of the central source implying a possible connection, but it so far shows no evidence of a high-energy cutoff — a fact that may be explained by the diffusion of cosmic rays from a central accelerator [170] that reaches PeV energies. The diffuse emission spatially correlates with the inner dense clouds, and although it establishes that active or recently active cosmic-ray accelerators are present in the central degree, the origin remains uncertain. All current studies are limited by statistics and field of view, and CTA will thus provide in an incredible wealth of new information.

Detailed spectro-morphological analyses of the diffuse VHE emission are required. CTA deep coverage will enable us to properly determine the level of hadronic cosmic-ray-induced emission by distinguishing clouds from individual sources seen at other wavelengths, thanks to a largely improved angular resolution with respect to current experiments. It will provide a unique measure of cosmic-ray propagation in the central molecular zone (CMZ), a region rich in molecules that contains the Galactic Central Radio Arc. The large number of photons that can be detected across this region — particularly at high energies where current instruments suffer from low statistics — will allow detailed spectral characterisation. The improved statistics with CTA will allow, in particular, the study of spectral changes associated with diffusion from a central accelerator that are hinted at with current observations [170].

5.1.1.3 *Exploring large-scale outflows*

An extended exposure with CTA will provide, for the first time, the ability to search for VHE diffuse emission away from the Galactic plane ($|b| > 0.3°$) in the region of the Galactic Centre.

Beyond the supermassive black hole (SMBH) at the gravitational centre, the central 30 pc region harbours up to 10% of the massive stars ($>20M_\odot$) in the Galaxy [176], implying a star-formation rate per unit volume two orders of magnitude larger than that in the rest of the disk. The kinetic power released by supernova explosions is therefore expected to be as large as 10^{40} erg/s [177]. This should produce very sustained particle acceleration as well as a strong outflow advecting cosmic rays into the Galactic halo, thus possibly feeding the large Fermi bubbles (e.g. [177, 178]). A presumed period of high activity of the SMBH has also been invoked to explain the bubbles (e.g. [179] and others). Evidence of on-going cosmic-ray escape from the Galactic Centre region would support this picture.

An interesting feature in this respect is the Galactic Centre lobe which extends over 150 pc north of the Galactic Centre. It is an energetic outflow from the inner regions. The energy required to inflate it is similar to that released by 50 supernovae, and the outflow is presumably powered by the sustained star formation activity in the Galactic Centre [180]. Similarly, a bright extended region of recombining plasma has been recently discovered at $b = -1.4^\circ$ which might be the relic of an energetic event at the Galactic Centre some 10^5 years ago [181]. Detection of gamma-ray emission associated with these features might help understand the connection between the activity in the central 100 pc and the large-scale Fermi bubbles.

5.1.1.4 *Supernova remnants, pulsar-wind nebulae, and molecular clouds*

A large number of supernova remnants (SNRs) and pulsar-wind nebulae (PWNe) will be covered by a deep exposure of the Galactic Centre region (see the radio image in Figure 5.2), providing a significant increase in the number detected of these objects, which are known VHE accelerators. Though some nearby SNRs like G 0.9+0.1 have already been detected and studied at very high energies [171], others remain too weak for current instruments or suffer from significant source confusion that could be mitigated by the improved sensitivity and smaller point spread function of CTA. For example, the inner Galactic Centre field of view contains G 1.9+0.3, which may be the youngest Galactic SNR, the expansion of which can be seen in radio and X-rays, see e.g. [182]. Since very young SNRs are thought to be the most likely objects to be producing TeV cosmic rays, G 1.9+0.3 is definitely a major target for CTA observation. The region also harbours a number of older SNRs, some of which may be interacting with molecular clouds and producing the gamma-ray emission, e.g. the source known as H.E.S.S. J1745-303 [183, 184].

The improved point spread function of CTA will allow morphological studies of some of these objects that are currently seen as point-like (see Figure 5.2). In particular, about 20 filaments of non-thermal X-ray emission are visible in the central degree. A significant number of them appear to be PWNe and could therefore have non-negligible TeV emission. CTA will be able to resolve several of them from the truly interstellar emission.

5.1.2 *Context/Advance beyond State of the Art*

While the Galactic Centre Key Science Project will allow us to explore new domains in both space and energy, it will also drastically improve upon the existing observations from current or past gamma-ray telescopes. In particular, it will build upon the knowledge gained from Fermi-LAT at GeV energies and from H.E.S.S. and VERITAS observations at higher energies.

Fermi-LAT has successfully explored the entire gamma-ray sky from 100 MeV up to ~100 GeV. In particular, it has measured the diffuse emission in the Galactic Centre region. At higher energies above 100 GeV, however, the limited size of Fermi-LAT severely constrains the number of detected gamma rays. Moreover, the instrument suffers from high source confusion due to its limited angular resolution and from poor sensitivity to short-term variability.

Above 100 GeV, the discovery by imaging atmospheric Cherenkov telescopes of VHE gamma-ray emission from the region was a major success [165–167], highlighted by the strong detection of an unknown point-like source coincident with the supermassive black hole Sgr A* that was inconsistent with a dark matter interpretation [185]. H.E.S.S. [168], and later VERITAS [169], further identified significant extended VHE diffuse emission in the inner ±1°. The apparent correlation of this emission with dense molecular clouds suggests an illumination of the gas from recently accelerated hadrons. However, these results are limited by the sensitivity, angular resolution, and systematics of current instruments; further exploring the science of this region requires an improvement in all three.

5.1.2.1 *Central engine*

The central VHE source has been well studied with existing atmospheric Cherenkov telescopes, but still remains unidentified due to source confusion and limited sensitivity to variability and small-scale morphology. It is coincident with Sgr A* within the pointing accuracy of H.E.S.S. ($<7''$), but it cannot be definitively associated with the SMBH; for example, there is an

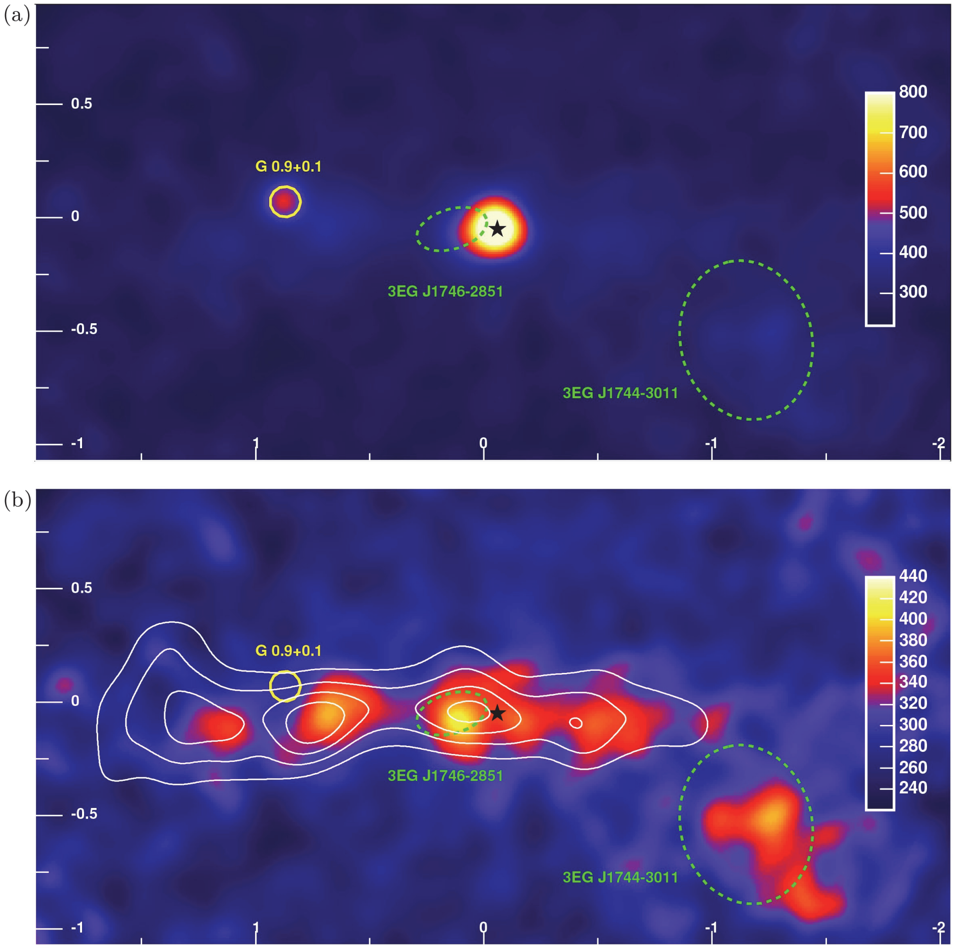

Figure 5.4: The VHE gamma-ray view of the Galactic Centre with H.E.S.S., reproduced from Ref. [168]. (a) is the total emission, dominated by the central unidentified point source, while (b) shows the emission after the point-source and SNR G 0.9+0.1 have been subtracted. The residual signal shows the diffuse gamma-ray emission along the ridge, which roughly matches the morphology of local molecular clouds (white contours).

X-ray emitting pulsar-wind nebula detected by Chandra that is within the same error circle.

If the central VHE source can be associated with accretion-related processes around Sgr A*, it will provide the best laboratory for studying the details of particle acceleration from accretion or jet emission in a SMBH that is not just nearby, but covered better with multi-waveband instruments than any other similar source. Sgr A* is seen as a bright point-source in radio, near-IR, and X-ray wavelengths, and it exhibits flaring activity on half-hour timescales in both IR and X-rays, pointing to rapid changes in accretion rate, caused by anything from clumps in the surrounding gas to an Oort cloud of asteroids [186]. The dynamics of the region are extremely well measured, with the orbits of stars around the black hole tracked with high precision.

Starting in 2013, the approach and tidal disruption of a dense gas cloud (G2) on a trajectory towards the black hole has been tracked with IR observatories, possibly leading to a detectable, long-term increase in accretion. So far, no variability of the VHE source has been seen on short or long timescales. However, current instruments are only sensitive to changes of flux of roughly a factor of two, and systematics may limit long-timescale studies.

Deep observations of this object with CTA will provide:

- an angular resolution sufficient to image the arc-minute scale VHE source, helping to resolve its nature (Figure 5.5 shows the ability of CTA to measure the size of the central source),
- the possibility to search for variability of the central source, coinciding with X-ray or IR flaring, which would enhance our understanding of the emission processes in SMBH, and

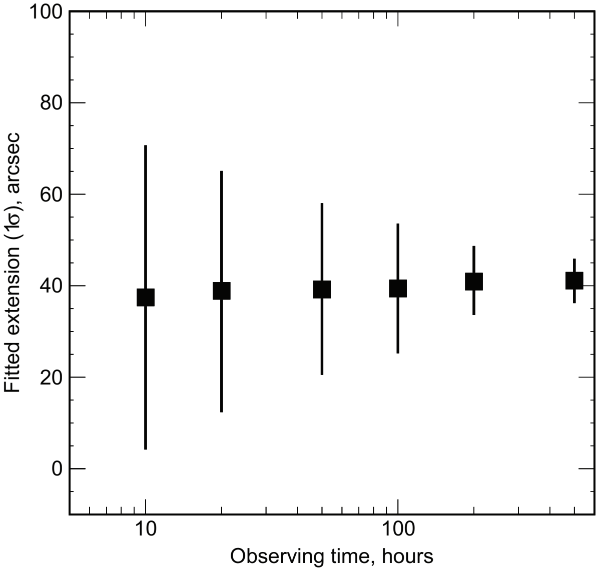

Figure 5.5: Expectation for the fitted size of the central source (assuming a Gaussian shape) made by CTA as a function of observing time. Each point in the curve is generated by 100 Monte Carlo simulations. The error bars show the typical spread of the simulated measurements. With 200 h, CTA should reach a detection of the source extent with a statistical significance of approximately four standard deviations. The error bars are accurate to within ±10%.

- sufficient spectral sensitivity and energy coverage to determine the maximum energy reached by accelerated cosmic rays in this region and to measure any possible spectral variation during accretion events.

5.1.2.2 *Advances in the study of diffuse emission*

The ridge of hard (photon spectral index, $\Gamma \sim 2.3$) VHE emission at the Galactic Centre extending over 1.5° along the Galactic plane (seen modeled in Figure 5.3 and in reality in Figure 5.4) is well correlated with the dense clouds present in the central 200 pc that are traced with line emission from CS molecules [168]. The photon spectral index of this emission is somewhat harder than the cosmic-ray spectrum measured at Earth. Under the hadronic origin assumption, the density of multi-TeV cosmic rays is significantly larger in the central region than in the local medium. Therefore, active or recently active cosmic-ray accelerators are likely present in the central degree, but their nature is still very uncertain.

SNR Sgr A East was seen as a possible source of these cosmic rays [168], but the influences of the starburst environment of the central 200 pc, or of the supermassive black hole itself, have to be understood. A key question here is to determine how cosmic rays propagate in the complex environment of the CMZ. For instance, the large poloidal magnetic fields traced by non-thermal filaments might limit the diffusion of particles along the Galactic plane. Similarly, the presence of an advecting wind is required by several models of the star formation activity of the CMZ [177, 178]. The idea of a single accelerator injecting cosmic rays in the Galactic Centre has therefore been questioned (see, for example [187]), and distributed turbulent acceleration in the inter-cloud medium has been proposed by several authors [188, 189]. The starburst activity and the associated supernovae should also provide enough energy to create the observed excess and even power the large-scale Fermi bubbles [177]. It is therefore fundamental to properly measure how cosmic rays are distributed and how they diffuse in the central 200 pc. This requires a detailed spatially resolved spectral analysis of the region that only CTA can provide.

Deep observations of the CMZ with CTA will provide:

- an angular resolution sufficient to resolve diffuse emission down to the arc-minute scale. Comparing with molecular matter surveys, this will help resolve the truly interstellar emission from distinct features in the region and thus precisely measure the level of hadronic cosmic rays in the CMZ. The ability of specific objects (e.g. the young and massive Arches cluster, the radio arc, etc.) to accelerate particles to very high energies and emit gamma rays will be precisely tested;

- very high photon statistics, making spectral extraction possible on scales of a few arc-minutes and for energies above 10 TeV. This will allow a detailed study of the cosmic-ray distribution in the region that will provide invaluable information on cosmic-ray propagation and their penetration into very dense clouds. The Galactic Centre region is probably one of the very few regions in the Galaxy where such a study will be possible;
- excellent spectral sensitivity at very high energy to determine the maximum energy reached by cosmic rays in the central 200 pc.

5.2 Strategy

There are several possible observation strategies to achieve the goals outlined earlier. In general, the exposure can be broken into two small survey regions: a deep exposure close in to the central source, centred on Sgr A*, and an extended region starting at the edge of the deep exposure and extending to the edge of the Galactic bulge as delineated by optical emission (approximately ±10° in Galactic latitude). This strategy is shown schematically in 5.1. The exact pointing strategy will be optimised once the final characteristics of CTA are known, and it may also be adjusted to provide, for example, better coverage of interesting features of the Fermi bubbles based on new analyses of GeV data.

Nominally, the exposures can be described as follows (see also Table 5.1):

- **Central survey region:** A deep exposure of 525 h, centred on Sgr A*, with pointings centred on grid points covering all combinations of $l = \pm 1.0^\circ$, 0° and $b = \pm 1.0^\circ$, 0°. The grid spacing of this survey

Table 5.1: Exposure summary for the Galactic Centre KSP.

	Deep exposure	Extended survey	Monitoring+multi-waveband
Time requested	525 h	300 h	(Co-ordinated with other instruments)
Priority	1	3	2
Strategy	survey	survey	Periodic + coordinated
Site	S	S	S
Sub-array	Full	Full	Full
Zenith Range	<40°	<50°	<40°
Atmosphere Quality	high	high	Medium
Targets Covered	multiple	multiple	Multiple

may be optimised depending on the final field of view and acceptance characteristics of CTA. These observations should be completed in the first three years of operation because of the high importance of the dark matter search (see Chapter 4). In the first year, the data should be sufficient to publish an updated analysis of the central source. After three years, a detailed study of the extended/diffuse emission will be possible. This exposure covers the:

- Galactic Centre central source,
- centre of the dark matter halo,
- all of the known diffuse emission, including H.E.S.S. J1745-303,
- multiple SNRs (G 0.9+0.1, G 1.9+0.3, ...),
- multiple PWNe (Mouse G359.2-0.8), and
- central radio lobes (central ±1°) and arc features.

- **Extended survey region:** 300 h of exposure covering a large region to the south or north of the Galactic Plane Survey (Chapter 6) region out to 10° in latitude. Since large-scale emission is expected to be symmetric, it is likely not necessary to extend observations to both north and south, with north being preferred due to lower optical brightness. These observations can be taken after the deep exposure, i.e. after the third year of operation, though a first pass may be interleaved into the first few years to help develop the analysis and to look for new bright targets. Note that the observations are shown currently as a box, but could be skewed to better cover interesting regions like the edge of a bubble. This exposure covers the:
  - edge of the Galactic bulge,
  - base of Fermi bubbles,
  - radio "spurs", and
  - the Kepler SNR.

5.2.1 *Timeline and Sub-array Choice*

The Galactic Centre observations should be taken primarily with the southern array due to the declination of the region of interest $\simeq -30°$. Some fraction of the observation time should be coordinated with other instruments (e.g. X-ray or radio) to facilitate variability studies. Small zenith angle observations should be prioritised to give the low-energy threshold needed for variability studies. However, since high-energy observations are also useful, a fraction of the time could be taken with the northern array, using large zenith angle observations. Taking data with the full array (i.e. LST+MST+SST) is also recommended, since the interesting energies span the full CTA energy range. LST data are required to search for variability at low energies, where CTA will have a large advantage in sensitivity over Fermi. In addition, the study of outflows related to the Fermi bubbles requires low-energy response, since the spectrum exhibits a cutoff around 100 GeV in the Fermi data. Conversely, the high-energy response is important for mapping the diffuse emission and for determining the maximum energy of the various accelerators in the region. One caveat is that since there is more signal at low energies and thus the low-energy sensitivity may be achieved faster, it may be possible to optimise the energy coverage by taking some data with the MST/SST sub-array only. This must be studied once the final configuration of CTA is known.

The Galactic Plane Survey (Chapter 6) will contribute to observations needed in this KSP in the first two years, providing a depth of approximately 15 h in survey mode. The deep observations required for this KSP imply the need to take an additional 160 h every year during the first three years, followed by 45 h/yr during the following seven years. Figure 5.6 shows

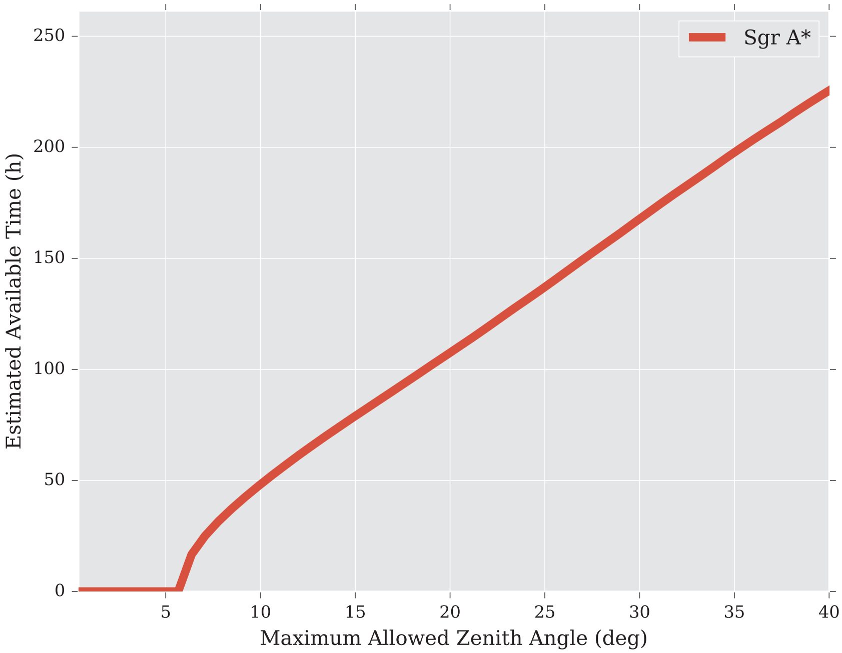

Figure 5.6: Available time at the position of Sgr A* as a function of zenith angle for CTA-South. The available time includes only moonless dark time and is adjusted for a typical data taking efficiency of 70%. In order to achieve the time needed per year, the maximum allowed zenith angle must be at least 35°.

the estimated observation time available for a single year as a function of zenith angle, which typically should be as low as possible. Restricting the zenith angle to under 35° provides enough time per year for this KSP, under the assumption of no other competing sources in the same band of right ascension.

5.2.2 *Relation to other KSPs*

The Galactic Centre KSP is closely connected to the Dark Matter Programme (Chapter 4), the Galactic Plane Survey (Chapter 6), and the Extragalactic Survey (Chapter 8), in the case that the region of interest is connected to the Galactic Centre. For this reason, some coordination between these KSPs will be useful when determining the detailed observation strategy.

5.2.3 *Analysis Strategy*

Due to the complexity of this region, careful consideration will be required for the analysis. Several different analysis approaches will be applied to the data, particularly because each science case has different goals. This includes standard survey-like analyses, along with searches for time variability at multiple scales. It implies both imaging, likelihood modelling, and spatial/temporal region-based signal extraction. All science cases require extremely low systematic errors, ideally better than those required by CTA as a whole, which may be difficult to achieve without detailed knowledge of the system.

The analysis challenges and possible solutions are as follows:

- **Exposures near systematic limits** are likely in the central survey region, where the goals include a search for weak variability, and detailed spectral and morphological studies. This is particularly challenging in this region where the optical brightness can vary over an order of magnitude, requiring careful consideration in the background determination to avoid biasing. CTA should provide sufficient information to correct for observation-to-observation atmosphere variations (i.e. seeing and transparency), but this KSP will be one of the first to push them to their limits.
- **Strong source confusion** is already a known challenge for this region with current telescopes. A detailed likelihood modelling analysis will be required in order to disentangle emission components, implying the need for iterative modelling.

- **Emission that is of similar scale or larger than the field of view** is a key part of several of the science goals, namely large-scale outflows and the diffuse emission. In all current analysis techniques where background is normalised using off-source regions in the field of view, such emission is subtracted due to the methodology. Therefore new techniques will need to be developed to deal with large-scale targets, requiring better methods for using external information to normalise background rates and the detailed spatial shape of the detection efficiency.
- **Development of a robust high-energy diffuse model** will be required at the lowest energies to separate emission from local acceleration from emission from cosmic-ray interactions that is seen at GeV energies. To date, there is no good model for this emission that extends to the core CTA energies in the Galactic Centre region.

These challenges imply considerable work to be done by the CTA Consortium, which may require the development of new science tools and techniques that should eventually be propagated to Guest Observers.

5.3 Data Products

The data products produced by this KSP will include:

- maps/data-cubes of the full region of interest (excess, flux, spectral hardness),
- spectra of the central source, at various regions in the diffuse emission, and at the position of known SNRs, PWNs, and interesting sources within the field of view,
- light curves of the Galactic Centre central source and any other point-like sources,
- a catalogue of the Galactic Central region, including all detected sources with morphological, spectral, and variability measures; this may require special consideration above what is in a general CTA catalogue or for the Galactic Plane Survey due to the complexity of the emission region, and
- a model of diffuse VHE gamma-ray emission in the region (needed for dark matter, central source, or background object studies); ideally, this should provide components expected from cosmic-ray interactions and from local acceleration.

These data products will be produced by the CTA Consortium and will be made available to the public when the results are published.

5.4 Expected Performance/Return

5.4.1 *Determination of the Nature of the Central Source*

The angular resolution and source localisation capabilities of CTA will provide strong constraints on the extension of the central source (see Figure 5.5). This will help discard many scenarios regarding its nature. For example, if the emission arises from cosmic rays interacting with the circumnuclear ring (CMR) about Sgr A*, then we expect a larger extension (up to $1.5'$, ignoring ballistic propagation) than that produced by the possible counterpart PWN G359, which would give an extension of $<10''$ given the magnetic and radiation fields near the black hole. The proposed observations will very clearly discriminate between these two options.

5.4.2 *A Detailed View of the Diffuse VHE Emission*

The increase in sensitivity over existing instruments will also provide the ability to study the energy-dependent morphology of the diffuse region and will enable the extraction of detailed spectra at various points, possibly showing spectral variations expected if the diffuse emission was caused by a past, point-like outburst. The comparison of spectra in various regions of the central 100 pc will also help in evaluating whether cosmic rays can penetrate the densest cloud cores present in the CMZ, such as Sgr B2, and will provide more information about possible PeV cosmic-ray production in the region.

5.4.3 *Resolving New, Previously Undetectable Sources*

Simulations carried out verify that with the exposure proposed here, CTA will be able to resolve point sources above the diffuse VHE emission at flux levels from 2 to 5 mCrab, depending on their location in the region. This will likely lead to the discovery of new sources that are presently not resolvable, including young massive stellar clusters such as the Arches and Quintuplet clusters, known SNRs such as Sgr C and SNR G 1.9+0.3, and over 10 PWN candidates.

5.4.4 *Search for Variability in the VHE Source Near Sgr A**

The X-ray variability of Sgr A* is on timescales down to an hour, which are too short for current VHE instruments to resolve. CTA will provide sensitivity to detect the central source on minute timescales, allowing for the detection of strong variability on similar scales and for weaker variability over hour timescales. Therefore, it should be possible to detect a flare and measure spectral variability on <30 min scales. The monitoring involved in this KSP will also allow CTA to study any long-term flux variations that may be due to changes in accretion around the black hole.

5.4.5 *Studying the Interaction of the Central Source with Neighbouring Clouds*

Simulations show that the improvement in the point spread function and in sensitivity over current instruments will allow CTA to resolve the Galactic Centre source from neighbouring clouds and to provide a detailed view of clumps in the central molecular zone. The CTA point-source localisation accuracy of $<3''$ will be sufficient to rule out some counterparts, and CTA's excellent angular resolution will enable the search for an extension of the central source that might be expected in a PWN scenario or in the case of hadronic interactions with nearby gas.

5.4.6 *Science Impact*

This KSP will produce the deepest exposure of the Galactic Centre region, the richest known environment of VHE gamma-ray emission. The scientific outcome on the different scientific cases discussed here is enormous. The legacy data set provided by this KSP will benefit many multi-wavelength and multi-messenger studies.

6

KSP: Galactic Plane Survey

Astronomical surveys of the Galaxy provide essential, large-scale data sets that form the foundation for Galactic science at all photon energies. Here, we introduce a Galactic Plane Survey (GPS) for CTA that will fulfil a number of important science goals, including: (1) providing a census of Galactic very high-energy (VHE) gamma-ray source populations, namely supernova remnants (SNRs), pulsar-wind nebulae (PWNe), and binary systems, through the detection of hundreds of new sources, substantially increasing the Galactic source count and permitting more advanced population studies, (2) identifying a list of promising targets for follow-up observations, such as new gamma-ray binaries and PeVatron candidates, to be carried out by the Consortium within the Key Science Projects (KSPs) or to be proposed through the Guest Observer (GO) programme, (3) determining the properties of the diffuse emission from the Galactic plane, (4) producing a multipurpose, legacy data set, comprising the complete Galactic plane at very high energies, that will have long-lasting value to the entire astronomical and astroparticle physics communities, and (5) discovering new and unexpected phenomena in the Galaxy, such as new source classes and new types of transient and variable behaviour.

The GPS KSP will carry out a survey of the full Galactic plane using both the southern and northern CTA observatories; the survey will be graded so that more promising regions (especially the inner Galactic region of $-60^\circ < l < 60^\circ$) will receive significantly more observation time than other regions. Our knowledge from the current Galactic VHE source population (e.g., $\log N - \log S$ extrapolations) and from other high-energy (HE) surveys (e.g., Fermi-LAT) motivate a target sensitivity for the CTA GPS at the level of a few mCrab (1 mCrab = 5.07×10^{-13} cm^{-2} s^{-1} for a minimum energy threshold of 125 GeV) in order to achieve the aforementioned science goals. As demonstrated here, the GPS will achieve a sensitivity[a] (for detecting a point-like source at a statistical significance of 5σ) better than 4.2 mCrab over the entire Galactic plane and 1.8 mCrab in the inner Galactic region. Thus, the CTA GPS will be a factor of 5–20 more sensitive than surveys carried out by earlier or existing atmospheric Cherenkov telescopes (HEGRA, H.E.S.S., and VERITAS). In the northern hemisphere, CTA will complement and extend observations made by the water Cherenkov telescope HAWC; CTA will go deeper by a factor of 5–10 in the core energy range of 100 GeV to 10 TeV compared to the HAWC five-year sensitivity [2, 190], at much lower energy and with substantially better angular resolution (e.g., factor of 5 better at 1 TeV). A comparison of the instrumental differential sensitivities is shown in Figure 1.1.

There are several strong motivations to carry out the GPS as a KSP of CTA. The GPS will provide a valuable legacy product to the entire astronomical community — the first sensitive VHE scan of the entire Galactic plane. It is expected that many sources will be discovered, resulting in follow-up observations and a large scientific output. The periodic data releases, comprising sky images (maps) and source catalogues, will strongly shape the observing programme of CTA as well as other observatories, both in space and on the ground. In addition, the GPS will have significant synergies with other MM facilities to enhance the scientific profile and output of CTA (see Section 6.1.3). The Consortium, with its detailed knowledge of the atmospheric Cherenkov technique and CTA-specific technical information, will be in a good position to develop the non-standard data analysis tools to account for a variety of observational and instrumental effects present in exceptionally large data sets. Of particular importance will be the issues of analysis of sources extended beyond the CTA point spread function (PSF), proper treatment of diffuse emission and source confusion, and the production of a coherent source catalogue.

The GPS will provide important pathfinder information for other CTA KSPs, including the *Galactic Centre KSP* (Chapter 5), the *Transients KSP* (Chapter 9), the *Cosmic Ray PeVatrons KSP* (Chapter 10), and the *Star Forming Systems KSP* (Chapter 11). It will also support the preparation of the GO programme since it will guide the community towards interesting targets via the production of source catalogues and sky maps.

---

[a] All target sensitivities presented in this KSP are a result of the combined simulations of individual telescope sub-arrays: small-sized telescopes (SSTs), medium-sized telescopes (MSTs), and large-sized telescopes (LSTs).

The GPS is divided into an early-phase programme (years 1–2) and a long-term programme (years 3–10) with a total requested observation time of 1020 h (CTA-South) and 600 h (CTA-North). For comparison, the total amount of dark time available for all CTA observations will be 1100–1300 h/year at each site. Observations will be done during dark time, under good weather conditions, and at zenith angles less than 45°. A double-row pointing strategy will be utilised, with a nominal pointing separation distance of 3° and with a cadence set to optimise sensitivity to periodic phenomena on a variety of time scales. Follow-up observations of promising regions and sources revealed by the GPS will mostly be carried out in the GO programme. Because of their scientific importance and timeliness, follow-up observations of transients and PeVatron candidates will be done in the context of the relevant KSPs.

Since the GPS will be carried out over the entire 10-year nominal lifetime of CTA, it is of high importance that regular data releases to the community are made. In the early phase, we expect an intermediate data release on a time scale of 12–18 months after the start of data taking, with the main data release for the first two years of observations to be made at the end of year 3. Successive data releases during the long-term programme will take place every ∼2 years. The data products available to the community via a searchable online archive will include: source catalogue(s), sky maps, scientific analysis tools and GO tools (e.g., exposure maps, observation schedules, etc.).

With the uniform, comprehensive, and mCrab-deep survey proposed here, the GPS will greatly expand the discovery potential of CTA and will also produce a great deal of guaranteed science. Hundreds of sources[b] will be detected. For each of these sources, the GPS will provide spectral and morphological information which can be used in conjunction with MWL data and comparison to theoretical models to identify the origin of the VHE gamma rays as well as the favoured scenarios for particle acceleration ultimately responsible for the gamma-ray production. With data taken over 10 years, the GPS will also be an important source of serendipitous discoveries. The sensitivity achieved by the GPS compared to the current state of the art will enable a major step forward in understanding the VHE

---

[b] In this KSP, a “source” is defined as an astrophysical source, i.e., a discrete source of VHE gamma rays which have a common astrophysical origin.

Galactic source population and will thus permit a better understanding of the origin of cosmic rays.

6.1 Science Targeted

6.1.1 *Scientific Objectives*

Galactic plane surveys have been carried out in practically every wavelength band, and new observatories regularly incorporate a GPS into their core observation programme to take advantage of improvements in telescope capabilities compared to previous generations and as an efficient way of achieving their diverse scientific objectives.

Generally speaking, a GPS provides:

- important source discovery potential,
- the critical, first-look data which guide deeper, more specific observations,
- a complete and systematic view of the Galaxy to facilitate our understanding of Galactic source populations and diffuse emission,
- a comprehensive data set and catalogue which comprise a key part of the scientific legacy of an observatory, and
- upper limits where no significant emission is detected, to constrain theoretical emission models.

The major scientific objectives for the CTA GPS include the following:

- Discovery of new and unexpected phenomena in the Galaxy. These would include completely new source classes, new types of transient and variability behaviour, or new forms of diffuse emission.
- Discovery of PeVatron candidates that are of key importance in our search for the origin of cosmic rays. These candidates will likely require deeper, follow-up observations to confirm and characterise their PeVatron nature.
- Detection of many new VHE Galactic sources (of order 300–500, see Section 6.1.2), particularly PWNe and SNRs, to increase the Galactic source count by a factor of five or more. The substantially increased statistics and more uniform sensitivity will allow more advanced population studies to be performed. The ultimate goal is to significantly advance our understanding of the origin of cosmic rays.
- Measurement of the large-scale diffuse VHE gamma-ray emission [198], to better understand its origin in terms of inverse-Compton, π^0 decay, and unresolved source components.

- Discovery of new VHE gamma-ray binary systems, a unique class of objects with periodic emission on varying timescales, where physical processes are observed from different vantage points depending on each system's orbital inclination. Only five such systems are currently known in the Galaxy.
- Production of a multi-purpose legacy data set comprising sky images and source catalogues of the complete Galactic plane at very high energies. This dataset will have long-lasting value to the entire astronomical and astroparticle physics communities, far beyond the lifetime of CTA.
- The GPS will produce and periodically release sky maps and catalogues. These will be important road maps to guide further Galactic observations made by:
  - the CTA GO community,
  - the broader astronomical communities, and
  - the CTA Consortium via other KSPs.

In the context of the defined science themes of CTA (Figure 3.1), the goal of the GPS is to substantially improve our understanding of the origin of cosmic rays by answering the following distinct questions:

1.1 How and where are protons and nuclei accelerated to PeV energies?
1.2 How are particles accelerated in relativistic shocks?
2.1 What is the role of external photon fields, jet content, and geometry in distinguishing jet sources, such as pulsars and microquasars?
2.2 Where and how do pulsar complexes accelerate high-energy particles?

The current motivation for the CTA GPS builds upon the published work of others, in particular Dubus *et al.* [9]. This KSP document is consistent with that work, but has gone further by using up-to-date sensitivity calculations, simulations, and observation planning. Additional comparisons with observatories at complementary energies, namely Fermi-LAT and HAWC, have also been carried out.

6.1.2 *Context/Advance beyond State of the Art*

Our current knowledge of the Galaxy at very high energies is based on both surveys and pointed observations made by ground-based gamma-ray telescopes using the atmospheric Cherenkov, water Cherenkov, and air-shower techniques as well as space-based gamma-ray telescopes, such as Fermi-LAT

Table 6.1: Compilation of previous VHE surveys of the Galactic plane. For each telescope, the spatial coverage, energy threshold, approximate point-source sensitivity, and reference are given. The telescopes are listed in order of increasing energy threshold.

Telescope	Hemisphere	Galactic Plane Coverage	Energy (GeV)	Sensitivity (mCrab)	Reference
Fermi-LAT 2FHL	(space)	full plane	>50	∼30–40	[191]
H.E.S.S.-I	S	$-95° < l < 60°$, $\lvert b\rvert \lesssim 2°$	$\gtrsim$300	4–20	[192]
VERITAS	N	$67° < l < 83°$, $-1° < b < 4°$	$\gtrsim$300	20–30	[193]
ARGO-YBJ	N	northern sky	>300	240–1000	[194]
HEGRA	N	$-2° < l < 85°$, $\lvert b\rvert < 1°$	>600	150–250	[195]
Milagro	N	northern sky	>10,000	300–500	[196]

Notes: For a discussion of the "mCrab" unit of flux sensitivity, see Section 6.4.1.

and AGILE. Specifically, surveys have had a major impact on VHE source detections in the Galactic plane, including the H.E.S.S. GPS, the Milagro survey of the northern sky, the HEGRA survey of the northern Galactic plane, the VERITAS survey of the Cygnus region, and the Fermi-LAT catalogue of hard sources. Table 6.1 provides a compilation of the previous VHE surveys of the Galactic plane.

A total of ∼100 Galactic sources of VHE gamma rays have now been detected. Their distribution in Galactic latitude peaks sharply along the Galactic plane ($b \simeq 0°$), with more than 90% located at latitudes $b < 2.0°$, although there may be some bias due to the worsening sensitivity of the H.E.S.S. survey off-plane. The largest source class is that of PWNe, followed by SNRs and gamma-ray binaries. About two-thirds of known sources are not yet firmly identified; most have multiple plausible associations that are challenging to disentangle, although some appear to be dark accelerators that are not detected at lower energies. Only a handful of the VHE Galactic sources are point-like in nature (largely binary systems). The large majority of sources have extended VHE emission, with a typical angular size of ∼ 0.1–0.2° (in radius), and a few are considerably larger than this. The reconstructed spectra are generally well fit by power-law spectral models, with typical differential spectral indices in the range of $\Gamma \sim 2.3$–2.7.

We can estimate the expected number of VHE sources (predominantly PWNe and SNRs) to be detected in the CTA GPS from the known population of ∼100 VHE Galactic sources. For example, in Renaud 2009 [199], the $\log N-\log S$ distribution of the VHE Galactic population (including all detections made by imaging atmospheric Cherenkov telescopes but

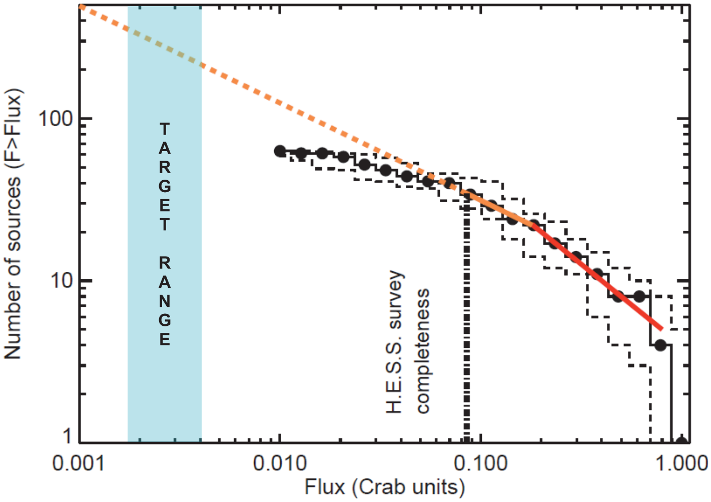

Figure 6.1: Cumulative Galactic source count as a function of VHE gamma-ray flux. Adapted from Renaud 2009 [199] to show the target CTA GPS sensitivity range (cyan-shaded region).

dominated by H.E.S.S. detections) was used to predict 300–500 sources for an instrument achieving a sensitivity of 1–3 mCrab. Figure 6.1 shows the cumulative source count as a function of VHE flux. Similarly, a few different source population models were used in Dubus *et al.* [9] to estimate the source count for the CTA GPS at 20–70 SNRs and 300–600 PWNe; however, in this case the models assume point-source sensitivities. It is important to note that sensitivity will be worse for extended sources (see Section 6.2.2) and the actual detected numbers of sources may be correspondingly reduced. Alternatively, these extrapolations could also be viewed as conservative, since they are based on the currently known VHE source populations. The discovery of new source classes would increase the total number of Galactic sources detectable by CTA.

Figure 6.2 shows a simulated image of what could result from a CTA survey of a portion of the Galactic plane using a model that incorporates SNR and PWN source populations as well as diffuse emission. The current work is an extension of earlier simulations described in Ref. [9]. As can be seen in this figure, the source density in the innermost regions of the Galaxy ($|l| < 30°$) could approach 3–4 sources per square degree, and thus source confusion is likely to be a concern (see Section 6.4.2). Preliminary work has estimated the number of sources expected by calculating the intrinsic VHE luminosities of the existing sources (with known distances) and then

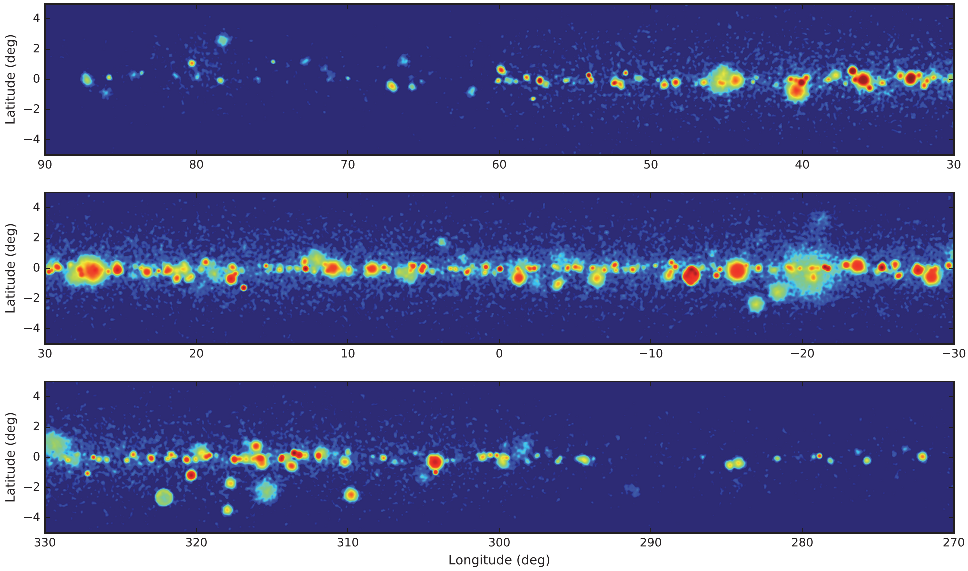

Figure 6.2: Simulated CTA image of the Galactic plane for the inner region $-90^\circ < l < 90^\circ$, adopting the actual proposed GPS observation strategy, a source model incorporating both supernova remnant and pulsar wind nebula populations and diffuse emission.

assuming a disc-like distribution of sources to estimate the increased number of more distant sources with comparable intrinsic luminosities detectable by CTA. This relatively simplistic but straightforward estimate yields ∼300 sources and is likely conservative because it does not consider possible sources that are intrinsically dim, i.e., those sources with intrinsic luminosities comparable or dimmer than Geminga, the source that currently has the lowest intrinsic VHE luminosity [200]. *The conclusion that can be drawn from these population estimates is that CTA can expect the detection of many hundreds of Galactic sources that would follow from a survey of the plane with a sensitivity at the level of a few mCrab.*

For a somewhat different approach, one can use knowledge from Fermi-LAT to estimate sources that could be expected in the VHE band. In one study, the spectra of probable Galactic sources from the Fermi-LAT 2FGL catalogue were extrapolated to VHE to predict that CTA would detect more than 70 of the Galactic 2FGL sources [9]. The spatial (Galactic coordinate) distribution of the Fermi-LAT sources has been studied further for this KSP, using primarily the 2FHL [191] catalogue. Increased exposure by Fermi-LAT has enabled the production of the latter catalogue, containing sources of gamma rays with energies $E > 50$ GeV, of which 62 are within $|b| < 5^\circ$.

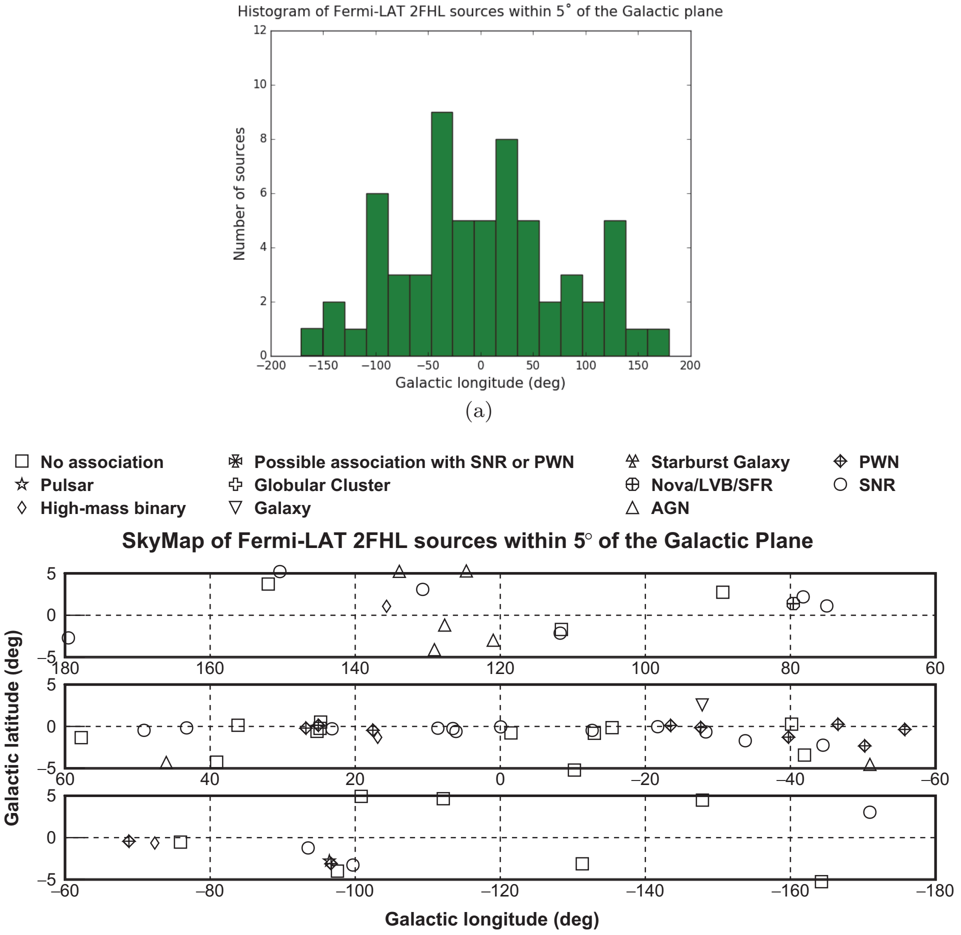

(a)

(b)

Figure 6.3: (a) histogram of Galactic longitude of Fermi-LAT 2FHL sources (from Ref. [191]) within 5° of the Galactic plane; (b) sky map of Fermi-LAT 2FHL sources within 5° of the Galactic plane.

Of these, 15 are spatially coincident with SNRs, 13 with PWNe, 6 with SNR/PWN complexes, three with X-ray binaries, one with a pulsar, and one with the Cygnus region [191]. Figure 6.3 shows a projection in Galactic coordinates of the 2FHL sources, along with a histogram of the distribution in Galactic longitude.

It can be seen that the 2FHL source distribution is relatively broad in longitude, which provides support for a VHE survey that is likewise broad. It is important to mention several caveats when considering extrapolations from the Fermi-LAT catalogues to higher energies: (a) the extrapolations assume continuous HE-VHE source spectra with no cutoff or break, (b) the largest VHE source class, PWNe, are bright at VHE but generally faint at HE (therefore suggesting that extrapolation from the HE regime may not be a fair indicator of VHE source numbers), (c) the second largest source class of SNRs often exhibit spectral breaks between the HE and VHE regimes, and (d) the Fermi-LAT catalogues have reduced sensitivity in the inner regions of the Galaxy where source confusion is significant. Thus, we conclude that information from Fermi-LAT is a useful indicator from an adjacent energy band but does not provide unambiguous predictions.

It is challenging to predict with better precision the number of sources that CTA can expect to detect in the GPS. While there may be larger-than-expected source populations in the outer Galaxy and at higher latitudes, it is clear that the highest concentration of VHE sources lies in the inner Galaxy. Therefore, a full-plane GPS, with graded sensitivity goals that peak in the inner Galaxy, is the most efficient way to probe the VHE source population. Aiming for a factor of approximately ten improvement in sensitivity compared to the current state of the art will:

1. enable a major step forward in understanding the VHE Galactic source population (and hence the origin of cosmic rays),
2. open a large amount of discovery space for new and unexpected phenomena, and
3. provide an excellent baseline sensitivity in regions of the plane of great interest to CTA and the overall community (e.g., the Galactic Centre, Cygnus, Vela, etc.) that will set the stage for even deeper follow-up observations.

All of these various considerations motivate a target sensitivity for the GPS at the level of a few mCrab, approximately a factor of ten better than the H.E.S.S. and VERITAS surveys.

Thus, to summarise the advances that the CTA GPS will bring to the state of the art:

- in the south, CTA will go deeper in the inner region ($|l| < 60^\circ$) by a factor of 5–20 compared to H.E.S.S., and CTA will cover the entire accessible Galactic plane, and
- in the north, CTA will go deeper by a factor 5–10 compared to HAWC in the energy range 100 GeV–10 TeV and with a factor of five better angular resolution (at 1 TeV). In Cygnus, CTA will reach a factor of ten better sensitivity than that achieved by VERITAS.

6.1.3 *Multi-wavelength/Multi-messenger Context*

6.1.3.1 *Synergy with HAWC*

The HAWC water Cherenkov array [2, 190] has recently started operation at Sierra Negra, Mexico. Larger than its predecessor, Milagro, and at a higher altitude of 4,100 m, it is substantially more sensitive. It is also farther south (latitude = 19° N) than Milagro (latitude = 36° N), which will permit a better view of the inner regions of the Galaxy. Table 6.2 shows a comparison of the relevant capabilities of HAWC and CTA for surveying the Galactic plane. The table shows that CTA and HAWC are complementary telescopes. HAWC will survey the entire (northern) sky above an energy threshold of ∼2 TeV. CTA will survey the Galactic plane in both the north and south with an order of magnitude lower energy threshold, a factor of 5–10 better sensitivity, and a superior angular resolution compared to HAWC. CTA's angular resolution in particular will allow it to probe morphological details not apparent in the larger HAWC sources.

6.1.3.2 *Synergies with other instruments*

The CTA GPS will have significant synergies with other MWL and MM facilities expected to operate contemporaneously with CTA, greatly enhancing the profile and scientific output of CTA. To help in the interpretation of the CTA results, it is necessary to measure the distribution of the interstellar gas (both atomic and molecular) in order to estimate the diffuse gamma-ray component arising from cosmic ray interactions on the gas. The gas is measured directly using radio and millimetre-wave telescopes (see Section 2.1), and thus collaboration between CTA and such instruments in both the southern and northern hemispheres is essential. On the particle detection

Table 6.2: Comparison of CTA and HAWC for surveying the Galactic plane at VHE.

Observatory	Hemisphere	Energy thresh.	Ang. resolution	Pt. source sensitivity	Ref.
CTA	N, S	125 GeV	∼0.07° at 1 TeV	2–4 mCrab	[201]
HAWC	N	2 TeV	0.30°	20 mCrab	[190]

Notes: The angular resolution is defined as the 68% confinement radius. The HAWC sensitivity assumes a livetime of five years. The sensitivity estimates for both instruments assume a power-law spectrum ($E^{-2.3}$ or $E^{-2.4}$) with no cutoff. Note that if a source cuts off at 5 TeV, the HAWC sensitivity degrades to ~ 50 mCrab while the CTA sensitivity is not greatly changed. The sensitivities for the CTA GPS were calculated for an energy threshold of 125 GeV; for a discussion of the unit "mCrab", unit of flux sensitivity, see Sect. 6.4.1.

side, the increasingly better localisation of sources of neutrinos and cosmic rays detected by, e.g., IceCube, Km3Net, and the Pierre Auger Observatory, makes a new searchable catalogue of TeV sources a valuable tool for MM analysis of potential cosmic-ray sources. The GPS will also be very relevant for the new and upcoming (on the same timescale as CTA early and full operations) optical and radio "Transient Factories" (e.g., *Gaia*, iPTF, ZTF, LSST, plus SKA and its pathfinders: LOFAR, MeerKAT, ASKAP, and MWA). For instance, a key step in the necessary automated decision-tree pipelines for further observation is to check coordinates against existing catalogues in order to identify the source. Given the propensity of VHE sources to vary also in radio and optical, it is important to provide access to some results of the GPS as soon as possible, ideally without waiting for the official public releases described above. This will require agreements between CTA and other facilities in order to share key source information from the GPS. Finally, GPS observations, spanning a large area of the sky and taken over a period of 10 years, could also prove useful in finding counterparts to sources of gravitational waves detected by LIGO and VIRGO.

6.2 Strategy

6.2.1 *Observation Requirements*

One of the most critical aspects of the GPS is the sensitivity goal for the observations — the sensitivity achieved will directly impact the number of detected sources and the quality of the determination of the source parameters (position, morphology, energy spectrum, and ability to detect variability). It will thus also impact the quality of the source identification. Because of the survey technique (i.e., many, separate pointings on a regular grid, where possible sources could be present anywhere in the field of view), a second key aspect is the requirement for good stability of CTA performance over different epochs. A third, critical aspect is to have the lowest-possible energy threshold (to measure spectra over the widest range and to reconstruct possibly soft-spectra sources; e.g., transients with durations of minutes, and pulsars). These various key aspects motivate the following general requirements for observing conditions:

- dark time (moonless) observations only,
- good (cloudless and low aerosol) weather conditions,
- zenith angles below 50°,
- use of both CTA-South and CTA-North, and

- full array observations for both CTA-South and CTA-North. Such operations are currently defined by having 80% of each telescope type deployed on a site.

6.2.2 *Targets, Observation Strategy, and Follow-ups*

For the GPS, the "target" is in principle the entire Galactic plane. Thus, when planning the GPS, the following parameters are of overall strategic importance:

(a) Galactic longitude and latitude,
(b) required sensitivity and observation time,
(c) yearly schedule for observations and reviews,
(d) pointing strategy,
(e) pointings, cadence, and schedule of observations, and
(f) follow-up observations: transients and PeVatrons.

We consider each of these aspects in turn.

(a) Galactic longitude and latitude

We consider longitude coverage first. Based on the scientific objectives and context presented in Section 6.1, there is good motivation for a survey of the entire Galactic plane, at least to a moderate depth. This approach has the benefits of maximising the discovery potential of CTA and also providing the long-lasting legacy of a full-plane survey. However, it is also clear that some regions of the Galactic plane (e.g., the inner region of $|l| < 60°$, the Sagittarius–Carina arm in the south and the Cygnus–Perseus arms in the north) will likely be more fruitful in VHE source discovery. This assumption is based on the density of currently known (e.g., PWNe, SNRs, binary systems, etc.) and prospective (e.g., globular clusters, star-forming regions, OB associations, novae, etc.) source types, as well as on our current knowledge from HE and VHE instruments. Thus, the survey should be carried out in both the southern and northern hemispheres and a graded approach should be implemented, i.e., the full plane should be surveyed to some moderate sensitivity while certain regions of the plane should receive significantly more observation time to achieve a deeper sensitivity.

In terms of Galactic latitude, we note that the large majority of current VHE sources lie within $|b| < 2°$. With the double-grid pointing strategy, discussed in (d) below, we can achieve relatively uniform sensitivity within 4° of the Galactic plane and additional, reduced sensitivity out to $\sim 6°$ due to CTA's relatively large field of view. Thus, the default double-grid pointing strategy should be sufficient for most of the Galactic plane.

(b) Required sensitivity and observation time

The scientific considerations in Sections 6.1.1 and 6.1.2 motivate that the CTA GPS achieve a point-source sensitivity in the 2–3 mCrab range. A minimal value of 4 mCrab is set by being able to achieve a substantial improvement over HAWC (see Table 6.2). As shown in Section 6.4, our current estimates predict a sensitivity of better than $\sim$3 mCrab over the entire Galactic plane in the south, with better than 2 mCrab in the inner region of $|l| < 60°$. In the north, we can reach a sensitivity better than 4 mCrab over the entire plane, and better than 3 mCrab in the Cygnus and Perseus regions.

To reach these sensitivities and achieve the scientific goals, a minimum of 1020 h is needed in the south and 600 h in the north, as determined by simulations (see Section 6.4). These times do not include follow-up time (e.g., pointed observations) for specific interesting regions of the plane.

The sensitivities quoted here are those for point sources, and it is important to note that the sensitivity will degrade for extended sources. For example, the sensitivity will be $\sim$3 times worse for an extended source with a radius of 0.25°. There will also be degradation in sensitivity from source confusion.

(c) Yearly schedule for observations and reviews

The GPS will be an important pathfinder for many other KSPs, and the probability of discovering many new VHE sources is very high. These considerations motivate a relatively rapid start to the GPS programme in the first two years of CTA, which will lead to important early scientific results for the project. On the other hand, we have also demonstrated that there is great scientific potential in going deeper to reach a few mCrab in sensitivity, and it is thus essential to continue the GPS throughout the nominal 10-year lifetime of the project. We define the short-term programme (STP) as years 1–2 and the long-term programme (LTP) as years 3–10. The STP starts in year 1 and the LTP starts in year 3. In Section 6.4, we give the projected sensitivities achieved in the STP and in the LTP as a function of Galactic longitude.

The high profile and importance of the GPS require both periodic assessments of the programme and regular data releases. The reviews are needed to assess the progress of the GPS and to consider other information gained from other CTA KSPs and from other instruments (e.g., HAWC, IceCube, X-ray and space gamma-ray missions, etc.). Scheduled reviews, possibly including external scientists, will be needed on a regular basis, e.g., approximately every two years. There may also be internal and more informal periodic assessments. We would also greatly benefit from input received from the broader GO community. In Section 6.3, we discuss the requirements and cadence of public data releases.

(d) Pointing Strategy

We considered two possible pointing strategies: a single-row raster scan and a double-row, offset raster scan. These schemes are described in Dubus *et al.* [9]. As shown in Figure 6.4, the single-row scheme uses a uniformly spaced single row of pointings that lie along the Galactic plane ($b = 0°$, or slightly adjusted in latitude, if need be). The double-row scheme uses pointings that lie above and below the $b = 0°$ line and that have a uniform spacing between adjacent points in the same row and between nearest points in different rows. The grid spacing in this scheme corresponds to the distance between nearest pointings that form an equilateral triangle.

Our simulations demonstrate that both pointing strategies will be satisfactory to achieve the desired sensitivities. However, the double-row scheme is preferred because it offers better performance at larger Galactic

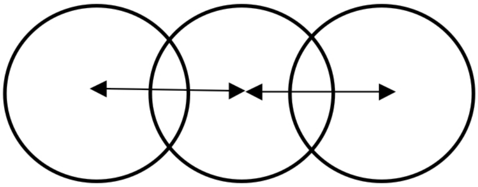

(a)

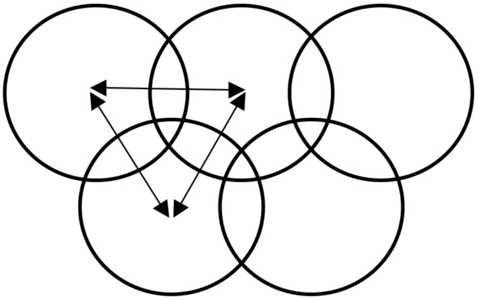

(b)

Figure 6.4: Pointing schemes considered for the Galactic Plane Survey. Single-row scheme (a) and double-row scheme (b). The grid spacing is illustrated by the arrows in both schemes.

latitudes ($|b| > 2°$) and more uniform sensitivity along the plane, and it may be more robust during background subtraction.

(e) Pointings, cadence, and schedule of observations

As outlined in the previous section, the pointing strategy will use the double-row scheme. We have simulated various separation distances (2°, 3°, and 4°) and find reasonable results with each of these possibilities; we select 3° as a good default choice. In determining a realistic schedule for the GPS observations, we keep the following guidelines in mind:

- Observations are carried out as close to culmination as possible, to minimise zenith angles. This will permit the best overall sensitivity and lowest energy threshold.
- We revisit fields on a recurring basis (e.g., on day, week, month, and year time scales) to improve our sensitivity to detecting periodic phenomena.

A tentative schedule has been developed for the first two years (STP) of the GPS. For the southern observatory, a total of 300 h spread over 120° of Galactic longitude has been simulated; for the north, it is a total of 180 h over 90° of Galactic longitude (see Table 6.3). The scheduling study indicates that the STP observations can be achieved during the first two years of CTA operations. Work is continuing on this topic, in particular to plan for re-scheduling of GPS observations affected by bad weather or data quality.

(f) Follow-up observations: Transients and PeVatrons

The GPS will discover many sources and regions of the plane for which follow-up observations will be highly motivated. Some of the follow-up observations will be carried within the KSP, but we expect that the majority will be done through the GO programme.

We define transients as sources whose VHE fluxes change by a significant amount over a relatively short period of time. Transients can occur anywhere in the field of view during any CTA observation in any portion of the sky. The definition for what a transient is (i.e., for the required flux change and the appropriate time interval) is defined globally for CTA and is discussed in detail in the *Transients KSP* (Chapter 9). Thus, in this regard, although the GPS and the Extragalactic Survey cover many more pointings than other KSPs, they are no different than other programs in how transients should be considered. Any transients discovered during a KSP pointing will be followed-up (or not), as discussed in Chapter 9.

It is expected that general follow-up observations of non-transient sources (including both steady sources and variable sources such as binaries) will be proposed and carried out in the GO programme. The one exception to this general strategy relates to PeVatron sources because of their high importance; these sources are discussed below.

One of the main science goals of the CTA Observatory is to discover the origin of Galactic cosmic rays. This goal is closely connected to the search for elusive PeVatrons, putative cosmic accelerators that accelerate particles up to PeV energies. The current theoretical consensus is that there should exist a small number ($\sim$2–3) of currently active PeVatrons somewhere in the Galaxy (see, e.g., Ref. [202]). The CTA GPS will provide an unparalleled data set which can be used to carry out this search. With its full-plane coverage and deep sensitivity — especially at multi-TeV energies, thanks to the inclusion of SSTs in the CTA-South array — it should be possible to identify at least several PeVatron candidates from the GPS data alone, by looking for source candidates with hard power-law spectra that extend up to $\sim$50 TeV and beyond, without evidence for a spectral cutoff. This work will be carried out in the context of of the Cosmic Ray PeVatrons KSP, which will follow-up with deeper, pointed observations to confirm the candidates' PeVatron nature.

6.2.3 *Relation/Importance to other KSPs*

As a pathfinder for a number of other KSPs, the GPS will cover some of the same sky using observations that will, in some cases, be taking place in the early phase of CTA operations. The synergies with other KSPs are briefly listed below:

- **Galactic Centre KSP:** The GPS will survey the region close to (i.e. within a few degrees of) the Galactic Centre, achieving a sensitivity of 2.7 mCrab in the first two years and 1.8 mCrab over 10 years. The region will be surveyed to a much deeper level in the context of the *Galactic Centre KSP*.
- **Cosmic Ray PeVatrons KSP:** The GPS will find the first evidence for PeVatrons which will be followed up by the *Cosmic Ray PeVatrons KSP* to confirm and subsequently characterise their nature in detail.
- **Star Forming Systems KSP:** The GPS will survey the Carina and Cygnus star-forming regions and the Westerlund 1 star cluster at a sensitivity level of a few mCrab. In particular, the GPS coverage will result in a complete survey of the Cygnus region ($65° < l < 85°$, $|b| < 3°$),

with a sensitivity of 4.2 mCrab in the first two years and 2.7 mCrab over 10 years. Specific regions-of-interest will be surveyed to deeper levels in the context of the *Star Forming Systems KSP*.

- **Transients KSP**: As discussed above, transients detected during GPS observations will be followed up in the context of the *Transients KSP*. Additionally, any AGN detected during the GPS will be of interest to the *Active Galactic Nuclei KSP*.
- **Extragalactic Survey KSP:** The spatial coverage of the Extragalactic Survey is such that it will be contiguous with the GPS, i.e., it will extend down to latitudes $b \sim 5°$, leaving no un-surveyed zone between them. This will provide information about possible Galactic sources, the Fermi Bubbles, and diffuse emission at high latitudes, which are less affected by Galactic MWL backgrounds (or foregrounds).

6.3 Data Products

It is essential for the CTA GPS to make regularly scheduled data releases. First, we discuss the results from the STP (years 1 and 2). The CTA data rights policy has the philosophy that data should be released to the community by, or before, one year after the completion of the programme associated with those data. It is natural to define the first two years of data taking as the initial program. We thus expect the main GPS data release for the STP to be done at the latest by the end of year 3; doing it earlier would be even better. However, three years is too long a time to hold off on releasing results from the GPS to the community. Thus, we need to also prepare for an intermediate data release of first GPS results on a time scale of 12–18 months after the start of data taking (i.e., in the middle of year 2). This intermediate release would be similar in intent to the Fermi-LAT bright gamma-ray source list [203].

Moving on to the LTP, if we define each successive two-year period as a successive program, subsequent data releases can be naturally made every two years, i.e., at the end of years 5, 7, 9, and 11 (assuming a 10-year nominal lifetime for CTA). If one of the CTA sites comes online significantly earlier than the other, the initial releases may only contain data from the first completed array.

Data products available to the outside community via an online searchable archive will include:

- source catalogue, including source position, morphology, spectrum, and light curve, all with appropriate errors,

- sky maps (FITS format), and
- scientific analysis tools (including *exclusion* maps, diffuse emission templates, etc.).

The catalogue/archive will provide information about sources extended beyond the CTA PSF, in terms of their preferred morphology (obtained with a likelihood analysis). For unidentified sources, the catalogue/archive will provide information about possible counterparts. The catalogue/archive will be published and available online, perhaps with web-browsing tools (e.g., along the lines of TeVCat [204]). The number and type of sky maps have not yet been determined, but they will likely include test significance maps and flux maps (units of photons $\mathrm{cm}^{-2}\ \mathrm{s}^{-1}\ \mathrm{pixel}^{-1}$). Legacy data products (FITS format) to the astronomical community will include high-resolution images, spectra, and light curves.

As discussed in Section 6.2, results from the CTA GPS will be of high importance to the general astronomical and astroparticle physics communities. Accordingly, prior to carrying out the GPS, we expect to develop coordinated efforts between CTA and other observatories and data archive centres to best leverage the worldwide expertise in MWL science and data preservation. For more information on CTA's MWL programme, see Chapter 2.

6.4 Expected Performance/Return

6.4.1 *Performance of the CTA GPS*

The first sensitive VHE survey of the Galactic plane was carried out by H.E.S.S. [205], resulting in the discovery of an unexpectedly large number of VHE gamma-ray sources. It is almost certain that the CTA GPS will also lead to the discovery of a larger (and likely even more diverse) population of VHE sources. Similarly, the full CTA GPS data set will comprise data taken during a period of 10 years. In total, 1620 h of observation time are requested for this programme.

The target point-source sensitivity is less than (better than) 4 mCrab throughout the plane generally, with a goal of achieving better sensitivity in key regions in the plane, i.e., less than 3 mCrab in the north and less than 2 mCrab in the south. Table 6.3 details the expected performance for the current plan, for both the south and north and for both the STP and LTP. For the approximate effective exposure *on-axis* for each region, see Table 6.4.

The sensitivities given in Table 6.3 were determined by updated simulation calculations. Two different methods to estimate sensitivity were used.

Table 6.3: Estimated point-source sensitivity reach of the CTA Galactic Plane Survey for various regions of the Galactic plane.

	STP (years 1–2)		LTP (years 3–10)	Total (years 1–10)	
Galactic Longitude	Hours	Sensitivity	Hours	Hours	Sensitivity
SOUTH					
300°–60°, Inner region	300	**2.7 mCrab**	480	780	**1.8 mCrab**
240°–300°, Vela, Carina			180	180	**2.6 mCrab**
210°–240°			60	60	**3.1 mCrab**
				1020	
NORTH					
60°–150°, Cygnus, Perseus	180	**4.2 mCrab**	270	450	**2.7 mCrab**
150°–210°, anti-Centre, etc.			150	150	**3.8 mCrab**
				600	

Notes: These sensitivities correspond to an energy threshold of 125 GeV. For the approximate effective exposure "on-axis" for each region, see Table 6.4.

Table 6.4: Estimated point-source sensitivity reach of the CTA Galactic Plane Survey and equivalent exposure times for various regions of the Galactic plane (within 2° of the Galactic plane for each portion of the survey).

	STP (years 1–2)		Total (years 1–10)	
Galactic Longitude	Sensitivity	Eq. exposure	Sensitivity	Eq. exposure
SOUTH				
300°–60°, Inner region	**2.7 mCrab**	**11.0 h**	**1.8 mCrab**	**28.6 h**
240°–300°, Vela, Carina			**2.6 mCrab**	**13.2 h**
210°–240°			**3.2 mCrab**	**8.8 h**
NORTH				
60°–150°, Cygnus, Perseus	**4.2 mCrab**	**6.3 h**	**2.7 mCrab**	**15.8 h**
150°–210°, anti-Centre, etc.			**3.8 mCrab**	**7.9 h**

The first (parametric) method uses the off-axis sensitivity distributions to estimate the effective exposure time for various representative positions in, and near, the Galactic plane. The sensitivities for these positions are then estimated from the curve of point-source sensitivity versus observation time. The second (full simulation) method uses the effective areas and background rates to simulate detected source and background events smoothly distributed in Galactic longitude and latitude. The detected events are fit to a combined source and background model, and the source flux is varied until a five standard deviation detection level is reached. The sensitivities are estimated for representative points on a grid of spacing 0.25°. The sensitivities estimated by the two methods are consistent with each other.

The "milliCrab" (mCrab) flux unit is used commonly in the VHE gamma-ray community but is not yet well-known outside that community. For these sensitivity calculations, the Crab flux determined by the HEGRA instrument was used. The trigger and reconstruction requirements resulted in an energy threshold of 125 GeV. The HEGRA Crab nebula spectrum is $\mathrm{dN/dE} = 2.83 \times 10^{-11}\ (\mathrm{E}/1\ \mathrm{TeV})^{-2.62}\,\mathrm{cm}^{-2}\,\mathrm{s}^{-1}\,\mathrm{TeV}^{-1}$. For an energy threshold of 125 GeV, $1\ \mathrm{mCrab} = 5.07 \times 10^{-13}\,\mathrm{cm}^{-2}\,\mathrm{s}^{-1}$ [197].

In this GPS implementation, during the first STP, we will achieve good sensitivity in the inner region $|l| < 60°$, as well as in Cygnus and Perseus. The STP sensitivities are shown graphically in Figure 6.5.

By the end of the LTP, very deep sensitivity will be achieved in the inner region, deep sensitivity is achieved in the Cygnus, Perseus, and the Sagittarius–Carina regions, and finally moderate sensitivity is achieved in the $150° < l < 240°$ (extended anti-Centre) region. Figure 6.6 shows the achieved sensitivity for the various regions of Galactic longitude. In these figures, the sensitivity appears more uniform than it will be in reality, since the effects of diffuse emission and source confusion were not taken into account in the simulations.

6.4.2 *Source Confusion*

As mentioned in Section 6.1.2, we expect source confusion to be a significant consideration, especially in the inner regions of the Galaxy. The main issues to consider are the unknown shapes of the sources, the unknown level of diffuse emission, the high source density in the inner Galaxy (so that many CTA sources will overlap), and the dependency of source identification on the analysis methods (e.g., maximum likelihood source detection and de-blending criteria). The added value of MWL information and the improved angular resolution of CTA will help resolve many instances of source confusion, but a large fraction of the sources detected in the GPS will naturally be relatively weak and thus inherently very difficult to resolve and identify.

Initial studies have been carried out to try to estimate the expected level of source confusion. In one of these, a Galactic population of sources was simulated based on our current understanding of the VHE source population, using an extrapolation of the source count (i.e., log N–log S), distributions

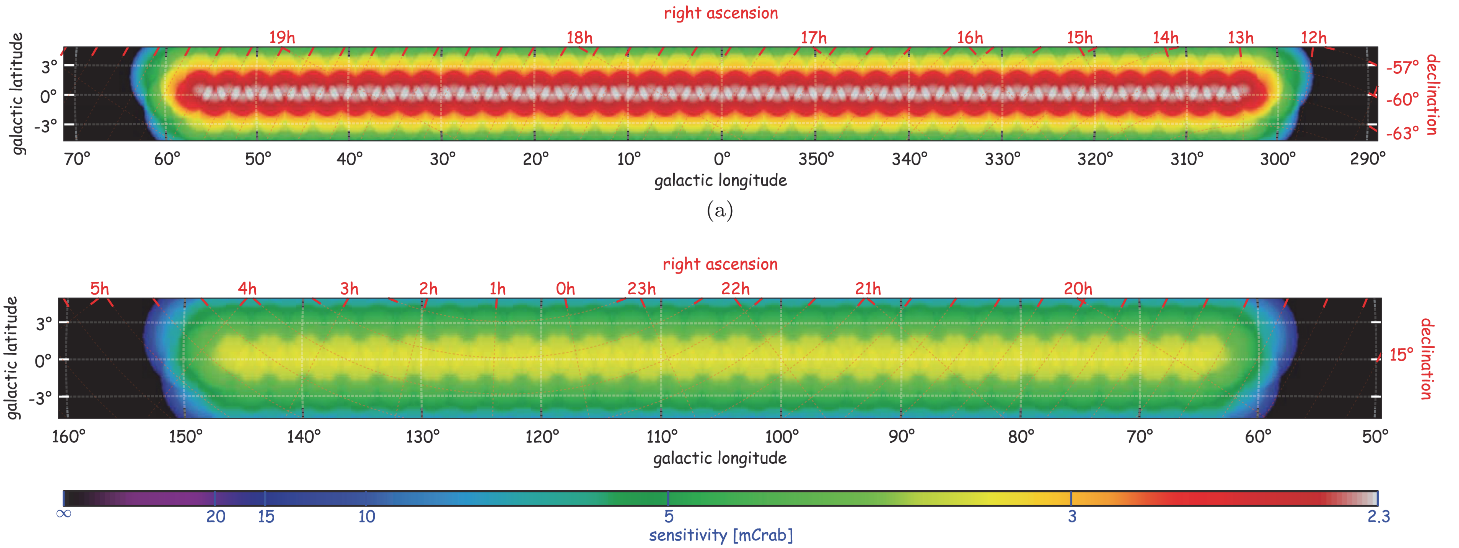

(a)

(b)

Figure 6.5: Point-source sensitivities (colour scale, in mCrab) achieved in the short-term programme (STP; years 1–2) of the CTA Galactic Plane Survey by the north (a) and south (b) observatories.

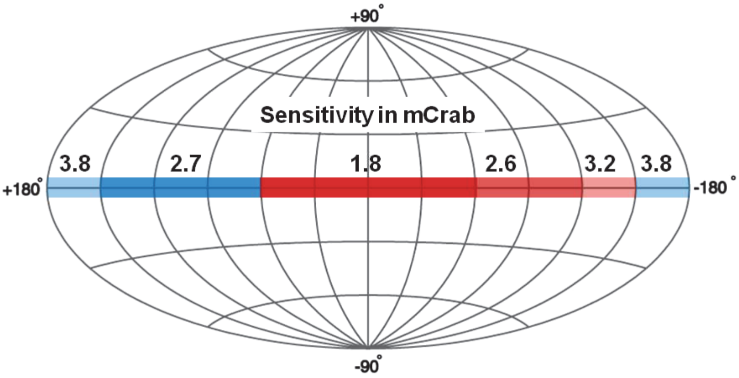

Figure 6.6: Point-source sensitivities (in mCrab) achieved in the full 10-year programme of the CTA Galactic Plane Survey for various regions along the Galactic plane. The survey carried out by the southern (northern) array is indicated by the red (blue) segments.

of source spectral indices and sizes consistent with existing data, and an assumed spatial distribution of sources around the Galactic Centre. No diffuse emission was included (except for the Galactic Centre ridge) and two different extrapolations of the log N–log S distribution were used to bracket the range of the expected source density. A position in the sky was considered confused if there was more than one simulated source within a radius of 1.3 times the CTA angular resolution. Using these assumptions leads to an approximate lower limit to the amount of source confusion. The estimated confusion lower limits range from 13–24% at 100 GeV to 9–18% at 1 TeV, for the region $|l| < 30°$ and $|b| < 2°$. Work on simulations will continue to better quantify this aspect of the CTA GPS.

6.4.3 *Summary*

The CTA GPS will produce guaranteed high-impact science returns and legacy products, as well as greatly expanded discovery potential in VHE astrophysics, due to its uniform, mCrab-deep coverage of the entire Galactic plane. PWNe and SNRs comprise the bulk of currently known VHE Galactic sources, and they will likely dominate the Galactic source populations for CTA as well. The log N–log S curves and representative models for source spectra and morphology can be used to estimate ranges in the expected number of source counts, as discussed in Section 6.1.2. Hundreds of sources will be detected and, for each of these sources, the GPS will provide spectra that can be used, in conjunction with MWL data and comparisons to theoretical models, to identify the particle acceleration scenarios most likely relevant for the VHE gamma-ray emission. Pulsars and binary systems will also feature prominently in the GPS data set, with their phaseograms and light curves, respectively, bringing additional physics to bear. With data taken over 10 years, the GPS will also be an important source of serendipitous discovery. Even non-detections will be of great importance to the astronomical and MM communities, with many constraining VHE upper limits expected.

All of this rich data will be provided to the broader community on a regular basis and will be an indispensable resource for follow-up proposals to the CTA GO program. The GPS will provide a source catalogue (listing e.g., flux and spectral index) and high-level sky maps, all accessible to the worldwide community. These data products will allow us to (a) perform VHE source population studies, (b) investigate VHE diffuse emission, and (c) carry out in-depth studies of individual sources through follow-up observations made by CTA and other observatories.

7

KSP: Large Magellanic Cloud Survey

The Large Magellanic Cloud (LMC) is a unique galaxy hosting extraordinary objects, including the star-forming region 30 Doradus (the most active star-forming region in the local group of galaxies), the super star cluster R136 (an exceptional cluster with a large concentration of very massive O and Wolf-Rayet stars), supernova SN1987A (the closest supernova in modern times), and the puzzling 30 Dor C superbubble (a rare superbubble with non-thermal emission). As a satellite of the Milky Way, it is one of the nearest star-forming galaxies, and a very active one; it has one-tenth of the star formation rate of the Milky Way, distributed in only about two percent of its volume. This activity is attested by more than 60 supernova remnants (SNRs), dozens to hundreds of HII regions, and bubbles and shells observed at various wavelengths, all of which promise fruitful gamma-ray observations. The LMC is seen nearly face-on at high Galactic latitude, and hence source confusion, line of sight crowding, and interstellar absorption do not hamper these studies, in contrast to the case for the plane of our Galaxy. It is therefore a unique place to obtain a significantly-resolved global view of a star-forming galaxy at very high energies. In addition, the distance to the LMC is known to the few percent level, thus allowing precise luminosity measurements to be made, something which is often very difficult for Galactic sources.

The current Fermi-LAT and H.E.S.S. instruments have opened the way for a study of the LMC by CTA. Observations with these telescopes have revealed a small number of sources, some of uncertain nature. With CTA, we would have a unique opportunity to further and deeper explore the entire LMC. With its unprecedented sensitivity and angular resolution, CTA will complement and extend these early results, and it will allow us to probe the origin of the VHE emission of a galaxy and its connection to global galactic properties.

This KSP has as many scientific objectives as an entire star-forming galaxy can offer: population studies on SNRs and pulsar wind nebulae (PWNe), transport of cosmic rays from their release into the interstellar medium to their escape from the system, and the search for signatures of the elusive dark matter component of the universe. These studies will be complementary to those done and planned for the Milky Way because they feature an unusual global perspective, different astrophysical settings due to the specific conditions in the LMC galaxy and data analysis with different uncertainties and systematics.

To make a significant contribution to the above-outlined science topics, the LMC KSP consists of an initial deep scan over a circular region of radius 3.5°. This will be achieved over the first four years of CTA from a small number of pointings with the southern array, for a total of 340 h of observations. Then, if SN1987A is detected in this deep scan, a second part of the project will consist of the monitoring of SN1987A over the following six years at a level of 50 h every two years.

The total of about 500 h spread over one decade is probably beyond what can be granted to individual Guest Observers. In addition, the observation of SN 1987A, if detected after the first deep scan, should be carried out over a decade on a regular basis, requiring a long-term granted observing program. The size of the LMC is about the size of the field of view of the CTA MSTs and SSTs, and the emission will likely be composed of several contributions, from point-like sources to extended and very extended objects. The determination of the best observing strategy and the analysis of the resulting observations will likely be very challenging. Therefore, this project is well suited to being led by the CTA Consortium. In return, the Consortium commits itself to the release of a source catalogue, spectra, light curves, and a complete emission model to the community at large.

The interpretation of TeV gamma-ray observations of the LMC will benefit from a large and comprehensive MWL context, and, in return, some results of the project may reach beyond the usual VHE topics, e.g., analyses of cosmic-ray populations in the LMC may be of interest for studies of the properties and evolution of the interstellar medium done from radio and infrared observations. Considering this, a deep scan of the LMC by CTA would be an appropriate and highly appreciated legacy to the astronomical community.

7.1 Science Targeted

The LMC is a nearby satellite galaxy that is visible from the southern hemisphere at a Galactic latitude of $b = -32.9^\circ$ and hence clearly off the Galactic plane. It is located at a distance $d = 50\,\mathrm{kpc}$ (with an uncertainty of $\sim$2%, see [206]) and it has the shape of a disk seen nearly face-on, with a small inclination angle of $i = 30$–40° [207]. Considering the typical angular resolution of gamma-ray telescopes, the LMC is perhaps the only object which can provide us with a global and significantly resolved view of an external galaxy at gamma-ray energies. Surveys of the LMC over the past few decades and across the electromagnetic spectrum have revealed a very active system in terms of star formation; it has one-tenth of the star formation rate of the Milky Way, distributed in only about two percent of its volume [208]. The LMC hosts:

- 30 Doradus, the largest star-forming region of the local group of galaxies [209],
- SN 1987A, the remnant of the nearest naked-eye supernova since Kepler in 1604 [210],
- about 60 well-established and 20 good-candidate SNRs [211],
- one of the densest stellar clusters known: R136 [212],
- the most massive stars known [212],
- hundreds of HII regions [213],
- more than a dozen superbubbles [214],
- about 20 supershells and a hundred giant shells [215],
- two of the most powerful pulsars known and their nebulae [216, 217], and
- a well-studied population of star clusters, with ages from a few Myr up to 10Gyr [218].

Since most of the gamma-ray emission of our Galaxy is due to massive star evolution, the activity and proximity of the LMC ensures fruitful gamma-ray observations. Indeed, after just one year of all-sky survey observations, Fermi-LAT detected significant emission from the LMC with several source components [148]. Using more than six years of data, Fermi-LAT revealed a much richer picture comprising four point-like sources, all being extreme objects, large-scale emission from the full extent of the LMC, and a handful of regions featuring extended emission of unclear origin [219]. Similarly, H.E.S.S. detected the first extragalactic PWN based on about 50 h of observations of the LMC [220]. With a data set of about 200 h available now, H.E.S.S. also detected SNR N132D and superbubble 30 Doradus C [149] and has started to probe the richness of a star-forming galaxy at TeV photon energies from an external viewpoint. In the future, CTA is expected to make a deeper exploration of the origin of the VHE emission of a galaxy and on how it connects to its global properties.

7.1.1 *Scientific Objectives*

The science objectives of this KSP can be grouped into three key questions:

- What are the processes and sites in which the bulk of the cosmic rays are accelerated?
- How do cosmic rays propagate away from sources and interact with the interstellar medium?
- What is the nature of dark matter?

The science case is introduced below in more detail. Quantitative prospects are addressed in Section 7.4 for cosmic-ray origin and transport, and in Chapter 4 for dark matter.

Cosmic-ray origin: SNRs are thought to be the main source of cosmic rays up to PeV energies; however, the whole picture is still incomplete. The maximum particle energy attainable, the influence of the SN progenitor and its environment on the non-thermal population produced, and the transport of particles away from the accelerator are all still active research topics. The very young SNR SN 1987A in the LMC is a unique target for studying the production and temporal evolution of the gamma-ray emission from cosmic-ray acceleration during the earliest SNR stages. The temporal evolution of this object was monitored from the very beginning, including the properties of the progenitor star. Given its nearby location, this is the only SNR spatially resolved by modern instruments at different wavelengths so early after the explosion (see [210] for a review). The non-thermal radio and hard X-ray emission from the remnant is evidence of particle acceleration in the supernova blast wave, which is impacting on the dense shell produced by the progenitor star in the current epoch [221, 222]. Long-term VHE monitoring of the target will thus provide a unique opportunity for studying the interaction between the SN shock wave and the circumstellar medium.

For studies of SNRs at a later stage in their evolution, the LMC harbours a rich population of 60 well-established SNRs and an additional 20 good SNR candidates (M. Filipovic, private communication; [223]). Such a rich sample enables the study of the impact of various properties on remnant evolution and its ability to accelerate particles. These properties include explosion types (thermonuclear versus core-collapse), environmental conditions (interaction with interstellar clouds or circumstellar material versus expansion in cavities), and the age of the remnant. From radio, optical, and X-ray analyses, several LMC objects seem to be very similar to famous Milky Way remnants. Studying the former could be a useful test of our models for the latter.

Cosmic-ray propagation: Milky Way studies of cosmic-ray origin and propagation have provided a wealth of information, from direct particle measurements in the Solar System to radio and gamma-ray diffuse emission observations from the entire Galaxy. Yet, we lack a global and resolved perspective on the phenomenon. What happens to cosmic rays freshly escaping from their sources? Are they confined for some time, and potentially reaccelerated in the highly turbulent medium of bubbles and superbubbles (such as hinted at by the detection of the Cygnus cocoon, see [224])? Are they advected into the Galactic halo after bubble breakout, thus contributing to the Galactic wind? In that context, some additional questions are specific to the LMC. Does the LMC have a galactic wind, and how is it connected or affected by cosmic-ray transport [225]? Can cosmic-ray transport be influenced by the wind of the Milky Way sweeping away particles?

Without line-of-sight confusion and with accurate estimates for the distance of the galaxy, observations of the LMC will allow us to test our understanding of the processes that rule the injection of cosmic rays and their subsequent propagation in the system. The usefulness of the LMC in that context was already demonstrated from Fermi-LAT observations, whereas the interstellar gamma-ray emission of the Milky Way is observed to be strongly correlated with the gas, the gamma-ray emission from the LMC is very poorly correlated with it. Apart from a large-scale emission component spread across the LMC disk, extended emission from smaller-size regions seems to be correlated with cavities in the interstellar medium and there is currently no explanation for this phenomenon. Continuing observations with Fermi-LAT will help to refine the picture, but CTA could well provide essential data needed to make real progress. Fermi-LAT observations probe ~GeV cosmic rays that accumulate in a galaxy over a 1–10 Myr duration, and are well suited to study the large-scale transport of cosmic rays. In contrast, CTA will probe ~TeV cosmic rays having a shorter residence time and will thus provide a view of cosmic-ray injection into the interstellar medium (ISM) and the small-scale transport around sources. The two instruments are therefore complementary to one another and should allow us to better understand the life cycle of cosmic rays, from injection and possible confinement around sources and in superbubbles to escape into the intergalactic medium.

The nature of dark matter: The LMC is an interesting and complementary target in the search for gamma rays from dark matter annihilation. The expected dark matter flux depends on the particle properties of dark matter and the dark matter distribution. The most favourable targets are nearby and have large concentrations of dark matter; this information about the dark matter distribution is expressed in terms of the "J-factor", which is the integral of the dark matter density squared along the line of sight. Targets with larger J-factors produce larger dark matter signals. The J-factor of the Galactic Centre can be as large as $\log_{10}(J) \sim 23$ (integrated in a cone with opening angle 0.5° in units of $\mathrm{GeV}^2\ \mathrm{cm}^{-5}$), but the central point source and other sources of gamma rays represent a large astrophysical background to a dark matter search. The J-factor of the LMC has been claimed to be as high as $\log_{10}(J) \sim 20.5$ [147]. Dwarf galaxies of the Milky Way, which have been considered extensively in dark matter searches because of their known locations, high dark matter densities, and low backgrounds, typically have smaller J-factors of $\log_{10}(J) \sim 18$–19. This simple comparison suggests that the LMC could yield a strong dark matter signal. However, the LMC is spatially extended and has significant astrophysical gamma-ray emission. Nevertheless, an LMC survey will complement the dark matter searches that will be performed in the Galactic Centre and in dwarf galaxies by providing a different target, albeit with larger analysis uncertainties and systematics.

Other science: Beyond the science topics addressed above, there may be side benefits from deep observations of an ~10° patch of the sky that includes an entire galaxy. For example, the scan of the LMC may reveal one or two additional gamma-ray binaries, which could be a useful addition to the handful we know already. The recent discovery in the LMC of the most luminous gamma-ray binary [226] is promising in that respect. The LMC survey should also lead to the detection of several active galactic nuclei (AGN). There are half a dozen Fermi-LAT sources in the LMC field, with some having hard spectra and at least one being an AGN with a high level of variability (PKS 0601-70, see [219]).

7.1.2 *Context/Advance beyond State of the Art*

The LMC was already covered by many surveys at different wavelengths: radio (ATCA, Parkes, Mopra, Planck, Herschel), infrared (AKARI, Spitzer, VISTA), optical, X-rays (ROSAT, XMM-Newton), MeV (INTEGRAL), GeV (Fermi-LAT), and TeV (H.E.S.S.). CTA observations and studies of the LMC will therefore benefit from a highly homogeneous MWL context.

The continuation of Fermi-LAT observations until 2020 (at least), combined with the continuous improvement in event reconstruction, will no doubt provide a better grasp of the emission morphology and the separation between diffuse and discrete objects. However, as mentioned previously, CTA will be complementary to Fermi for two reasons: first, it probes higher-energy cosmic rays and thus a different stage of the life cycle of cosmic rays (because higher-energy cosmic rays may be able to escape the system more easily, especially protons since they suffer much less severe radiative losses than electrons); second, with its better angular resolution, CTA will likely lead to a better and more complete picture of the gamma-ray emission of the LMC. A full understanding over the entire gamma-ray range will be achieved with a joint Fermi-LAT and CTA analysis (see Section 7.4).

In the meantime, the Planck collaboration will release the analysis of the dust and synchrotron polarised emission from the LMC. This will be complemented later by results from the second PILOT balloon flight (2016–2017), with a better sensitivity and angular resolution than Planck. The Square Kilometre Array (SKA) and its precursors will also contribute to these science topics. All instruments will provide information about the large-scale magnetic field structure and the leptonic component of the cosmic-ray population. They will also allow a deeper census of the populations of pulsars and PWNe in the LMC [227, 228], which could be responsible for extended emission as unresolved gamma-ray sources. The interpretation of the Fermi-LAT and CTA observations will necessarily have to include the information and constraints from these radio measurements.

ALMA is already operational and can indirectly probe the lower-energy cosmic rays ($<1\,\mathrm{GeV}$) because the latter ionise the gas and this process affects the chemistry and molecular line emission. Although no global project dedicated to the LMC yet exists for ALMA, SN 1987A was among the first objects to be imaged [229] and other LMC proposals were made. It is likely that by the beginning of CTA operations, we will have estimates of low-energy cosmic-ray density in at least a few prominent places such as 30 Doradus. This again will have to be considered in the analysis and interpretation of the CTA data.

7.2 Strategy

This KSP has one target: the LMC, which we define here as a disk centred on the position $(\alpha, \delta) = (80.0^\circ, -68.5^\circ)$ and having a radius of 3.5°. In order to maximise the scientific return and the possibility for discoveries, and to

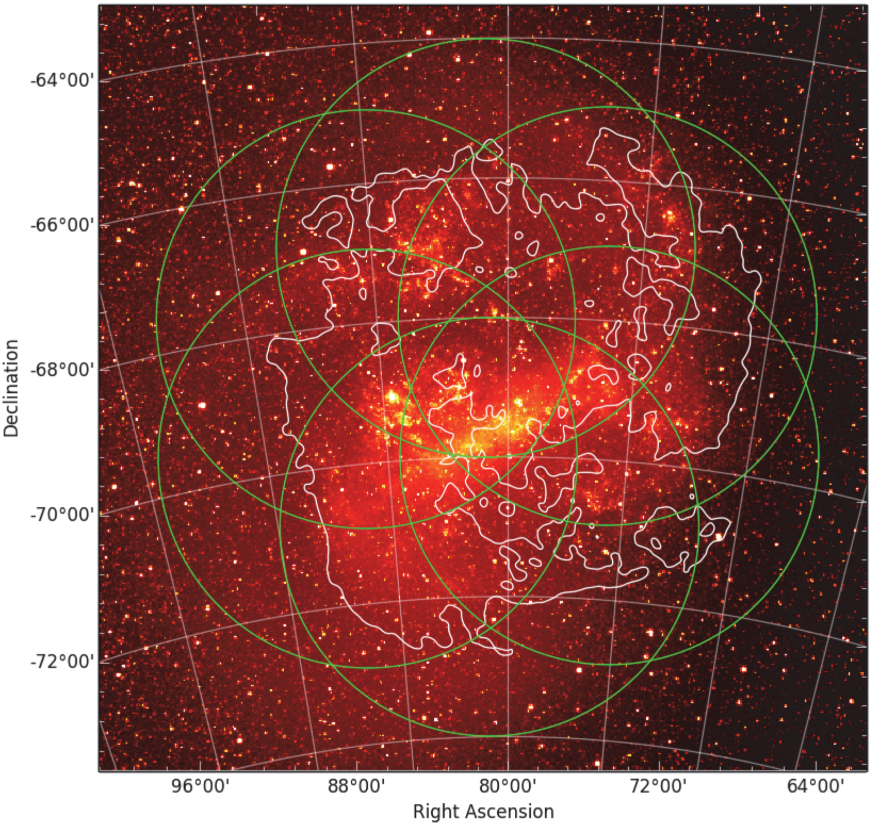

Figure 7.1: Illustration of a possible pointing pattern for the LMC deep scan. The pattern consists of six pointings evenly distributed around the LMC centre at a separation distance of 2.0° (green circles, for a typical field of view radius of 3°). The spacing of the pointings will depend on the actual off-axis performance of CTA and should provide enough empty field regions for sufficient control of the instrumental background. Credits: optical skymap from Ref. [230]; contour of H I distribution from Refs. [150, 231].

take full benefit of the global view that the LMC provides, it is planned to build a uniform sensitivity exposure over that region, and not just over the inner regions or 30 Doradus. This will be achieved with a small number of pointings (i.e. less than ten). A possible layout of the scan is shown in Figure 7.1, but the layout used will depend on the off-axis performance of CTA and it may need to be revised once the array is fully commissioned. As explained below, there could be a second phase of the project in order to monitor SN 1987A, in which case the observations would consist of a single pointing centred on SN 1987A (or wobble observations, or any other pattern motivated by discoveries made during the first phase of the program).

The project comprises two phases over a 10-year period, with the second one being optional (depending on whether SN 1987A is detected):

1. a deep scan of 340 h, ideally performed over the first four years in order to reach an effective exposure of 250 h over the entire LMC disk, as defined above, and
2. long-term monitoring of SN 1987A, totalling 150 h, at the level of 50 h every two years if the object is detected in the first phase.

Since the deep scan covers a region that is slightly larger than the effective field of view of the CTA MSTs and SSTs, reaching an exposure of 250 h over the LMC disk requires a total of about 340 h of observing time (assuming a field of view radius of 3° and a differential sensitivity above 400 GeV that is at least 60–70% of the on-axis value). The observations are planned to be performed by the full southern array after commissioning in order to get the best sensitivity for this very extended object. Current Monte Carlo simulation results indicate that the energy threshold would be around 200 GeV.

For CTA-South, the LMC is observable above an elevation of 40° for a total of about 280 h/yr, with the peak of the time distribution being in the November to January period. Performing the deep scan with CTA in four years imposes observing the LMC for 85 h/yr. This is far below the total available time, but there may be constraints from the schedule or from bad weather.

7.3 Data Products

The LMC in TeV gamma rays currently consists of a few objects: PWN N157B, SNR N132D, and the 30 Doradus C superbubble. Extrapolating the known Galactic TeV source population of the Milky Way to the LMC indicates that the 250 h exposure may provide the detection of ∼10 objects (see section 7.4). If this estimate turns out to be correct, a coherent catalogue of LMC sources listing their spectra, fluxes, and light curves should be produced; such a catalogue should also include upper limits on potential VHE emitters. If diffuse emission of interstellar origin can be detected and mapped, a complete emission model including the morphological and spectral properties of the various components should be released to the community; this may trigger transverse collaborations with groups interested in interstellar medium studies. Lastly, the long-term monitoring of SN 1987A may deserve two specific releases, at 250 h and 400 h of exposure, in the form of light curves and time-dependent spectra.

The schedule for data products and releases to the community is:

1. An initial release of results is planned based on the first 100 h of exposure, in order to inform the community and to keep a high interest in the LMC.
2. Once the 250 h effective exposure is achieved, products on individual sources, diffuse emission, and SN 1987A should be released within a year, or as soon as possible, to trigger and feed Guest Observer proposals.
3. Optionally, a final release of results on SN 1987A after 10 years of monitoring, along with an update on the other topics based on the additional 150 h exposure is envisioned.

7.4 Expected Performance/Return

We present below some of the simulations that were performed to assess the potential of the LMC as a target for CTA and to quantify the required amount of observing time. Cosmic-ray origin and propagation aspects are addressed here, while the prospects for dark matter searches are discussed in Chapter 4.

Cosmic-ray origin: Regarding the gamma-ray emission of SN 1987A, a time-dependent prediction of the VHE gamma-ray flux was proposed, based on nonlinear shock acceleration theory [232]. In this model, the VHE gamma-ray flux is expected to be rising (since the shock has entered the equatorial ring) and to have reached a level of $F(> 1\,\mathrm{TeV}) \simeq 2.5 \times 10^{-13}\,\mathrm{cm}^{-2}\,\mathrm{s}^{-1}$ (as of 2010), dominated by emission of hadronic origin. Given the uncertainties in the theoretical model and in the knowledge of the ambient target density structure, the predicted flux has an uncertainty of at least a factor of two. The time evolution of the flux strongly depends on the spatial distribution of the circumstellar medium. The flux is predicted to be increasing in the current epoch and to become a factor of two higher in the next 20 years, hopefully permitting the detection of this source. The extension of the SN shell of a few arc-seconds is much smaller than the achievable angular resolution of CTA . The target is thus expected to be point-like for CTA. Figure 7.2 shows the >1 TeV detection level provided by multiple 50 h observations distributed over several decades. The recent upper limit from H.E.S.S. observations, at a level of $5 \times 10^{-14}\,\mathrm{cm}^{-2}\,\mathrm{s}^{-1}$ [149], challenges this picture; it suggests that the rise to the maximum may be delayed and steeper or that the overall level of the emission is lower [233]. The prospects for the detection of TeV emission from SN 1987A will need to be reassessed,

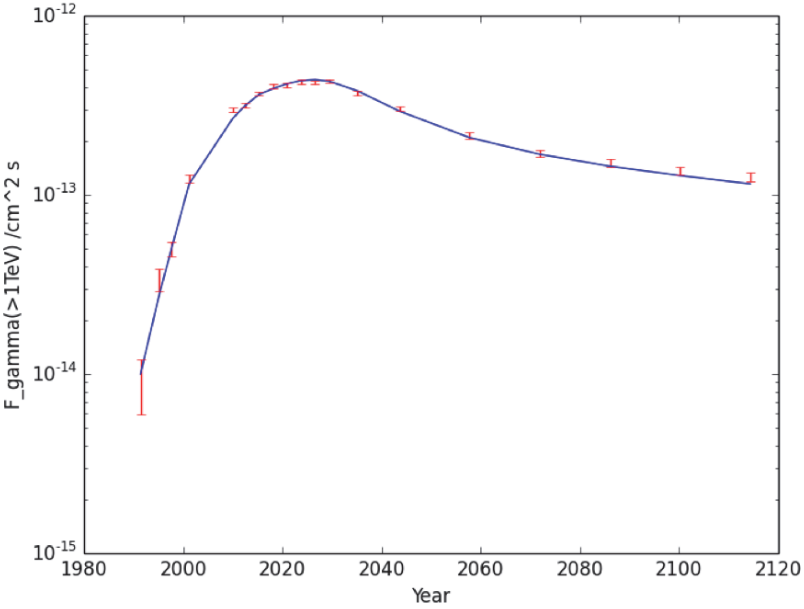

Figure 7.2: Predicted gamma-ray light curve for SN 1987A (blue, from E.G. Berezhko, private communication) and anticipated detections with CTA for several 50 h observations distributed over decades (red points). The recent upper limit from H.E.S.S. observations, at a level of $5 \times 10^{-14}\,\mathrm{cm}^{-2}\,\mathrm{s}^{-1}$ [149], contradicts this picture; it suggests that the rise to the maximum may be delayed and steeper or that the overall level of the emission is substantially lower.

especially in view of the lower energy threshold of CTA. In either case, it shows the potential of deep observations of SN 1987A to constrain models.

For more evolved accelerators, the expected number of TeV-emitting sources can be estimated from the known Galactic VHE gamma-ray source population and the sensitivity of CTA. For an integral energy flux sensitivity of 3×10^{-14} erg cm^{-2} s^{-1} above 1 TeV, in 250 h gamma-ray sources as luminous as 9×10^{33} erg/s would be detectable with CTA at the LMC distance of 50 kpc. Of all Galactic TeV emitters known in the Milky Way for which distance estimates exist, about 30 sources have a luminosity greater than this value. Correcting for the lower star-formation rate in the LMC (∼1/10 of the Milky Way), and assuming that ∼30% of the Milky Way has been surveyed to this luminosity limit with H.E.S.S., ∼10 LMC sources are expected to emit in VHE gamma rays at a level detectable by CTA. Note however that the environment in the LMC is different from the Milky Way. For instance, the radiation field energy densities and gas densities are higher, which would result in a higher gamma-ray flux on average, implying more sources to be detectable. N157B, the most luminous PWN known so far, is a prime example in that respect [220].

The current population of known SNRs in the LMC amounts to 60 objects, plus 20 plausible candidates. Not all of them are expected to be detected by CTA, but a selection based on simple criteria can provide a first-order quantitative estimate of the number of promising targets. Based on our knowledge of the Galactic population of TeV-emitting SNRs — namely the GeV-hard, TeV-bright young and isolated SNRs and the GeV-bright, TeV-soft middle-aged, interacting SNRs — we restrict ourselves to young to intermediate SNRs with an age <4000 yr (i.e., similar to the largest age estimates for Vela Jr and HESS J1731-347) and to interacting SNRs whatever their age (given that those known to emit TeV gamma rays in the Galaxy span nearly two orders of magnitude in age). A non-exhaustive list of candidates for TeV detection is given below:

1. Young/intermediate SNRs: SNR 0540-6919 (an O-rich SNR hosting the "Crab-twin" pulsar and its nebula), SNR 0509-67.5 and SNR 0519-69.0 (400 and 600 yr type Ia remnants with inferred efficient cosmic-ray acceleration, see [234]), DEM L71 (a $\sim$4000 yr type Ia remnant), N63A (a $\sim$4000 yr core-collapse remnant candidate).
2. Interacting SNRs: N132D (an O-rich SNR with similarities to Cas A and Puppis A), N49 (the third X-ray brightest in LMC, very energetic explosion, see [235]), possibly N49B, N103B (a 870 yr type Ia SNR with circumstellar interaction, a possible Kepler's older cousin, see [236]), DEM L249 and DEM L238 (10000–15000 yr type Ia remnants with denser than expected environment, see [237]).

These remnants have typical sizes below 3 arc-minutes and would likely appear as point-like objects even for CTA. We emphasise the very interesting opportunity to study type Ia remnants, from very young ones to those that seem to be interacting with circumstellar medium and might be the result of prompt explosions from young <100 Myr progenitors [237].

Regarding PWNe, the prospects are not as good, at least based on our present knowledge of the population of pulsars and their nebulae. We currently know 5 PWNe in the LMC: N157B, N158A, B0453-685, B0532-710, DEM L241 (the first one being already detected by H.E.S.S., the second one being associated with the Crab twin pulsar, also named B0540-693 [238], and the last now being confirmed as a gamma-ray binary). Prospects are good for the detection of N158A by CTA, especially considering the very high spin-down luminosity of its pulsar (1.5×10^{38} erg/s; see also [239]).

Beyond the exceptional pulsars in N157B and N158A, there are 17 other detected pulsars in the LMC [240]. For those listed in the ATNF catalogue, all have a spin-down luminosity $\leq 5 \times 10^{34}$ erg/s. This leaves little hope for the detection of the corresponding nebulae, but there is still the possibility to discover TeV PWNe associated with currently unknown pulsars.

Cosmic ray propagation: The current knowledge we have about the hadronic cosmic-ray population of the LMC comes from Fermi-LAT observations in the GeV range. The latest analysis revealed a background of cosmic rays spread over most of the disk of the LMC and having a density which is about three times lower than the local Galactic value. On top of that average, a few regions may have increased cosmic-ray densities by a factor of 2–3 or more and likely harder spectra, possibly resulting from a recent injection of cosmic rays [219]. As a consequence, we considered several objectives for the cosmic-ray population and associated interstellar emission in the CTA energy range. On large spatial scales, we would like to know: (i) whether we can detect the background interstellar emission from the large-scale cosmic-ray sea at TeV energies, (ii) if this emission is hadronic in origin or if the inverse-Compton process takes over at some point, and (iii) if we can gain knowledge about the efficiency with which 10 TeV cosmic-ray particles escape or diffuse away from the galaxy and how that efficiency compares with what we think takes place in the Milky Way. On smaller scales, we would like to constrain: (i) the level at which we can we probe the inhomogeneities of the LMC cosmic-ray population, (ii) the knowledge we can get on the transport of cosmic rays in and away from active star-forming regions, (iii) the escape of the higher-energy cosmic rays from their sources or their confinement around them, and (iv) the relation of the gamma-ray emission to star-formation activity and/or ISM conditions.

We simulated different scenarios to evaluate the potential of CTA for the study of cosmic-ray propagation and determine the observing time needed for a rich scientific potential. The properties of the background interstellar emission from the large-scale cosmic-ray sea at TeV energies are currently unknown and two options were therefore considered. As a first possibility, we considered hadronic emission, where the source spatial model was a gas column density map of the LMC and the source spectral model was a power law with a spectral index of 2.7, normalised to the level of the emission of the LMC disk at 10 GeV (as measured by the Fermi-LAT) and under the assumption that the emission results from old, accumulated cosmic rays interacting with interstellar gas. Alternatively, we considered leptonic emission, where the source spatial model consisted of a smeared out version of the IRAS far-infrared emission distribution, to account for the diffusion of short-lived >1 TeV cosmic-ray electrons around star-forming regions, and the source spectral model was taken from a model of the non-thermal emission from star-forming galaxies applied to a small-sized system similar to the LMC [241]. With an effective 250 h exposure over the LMC, the average detection significance obtained is above three standard deviations for the hadronic model and above seven standard deviations for the leptonic model. The background interstellar emission from the large-scale cosmic-ray sea could therefore be detected if the inverse-Compton process dominates the emission in the CTA energy range. However, the actual spatial and spectral distributions of this possible emission component are unknown and they would have to be determined from the data, which may eventually complicate the detection of such an extended signal.

A parametric study was performed to determine the extent to which CTA could probe active star-forming regions where young cosmic rays are released. Simulations were carried out for various region sizes (for radii of 100, 200, 500 pc) and for different densities for the cosmic-ray population in these regions. We used as reference the cosmic-ray sea density at 10 TeV, which was determined under the assumption that it has one-third of the local Galactic value at 10 GeV and follows a power-law spectrum with a spectral index of 2.7 up to at least 10 TeV. The emission was assumed to be of hadronic origin with an average hydrogen number density, N_H, over the region of $10^{22}\,\mathrm{cm}^{-2}$ (the densest, molecular regions in the LMC have N_H of a few $\times 10^{22}\,\mathrm{cm}^{-2}$ while the average over the LMC is $\sim 3 \times 10^{21}\,\mathrm{cm}^{-2}$). The spectrum of the emission was assumed to be that of a recently injected cosmic-ray population that homogeneously fills the region and does not diffuse away significantly; we therefore assumed a power-law spectrum with a spectral index of 2.2. The results are shown in Figure 7.3. It turns out that in 250 h of effective exposure, CTA would significantly detect regions of 100–200 pc in radius if they were recently enriched in cosmic rays by one supernova or more (a supernova is associated with 10^{51} erg of kinetic energy, of which 10^{50} erg are assumed to go into cosmic rays). Larger regions of 500 pc in radius would be significantly detected if enriched by about ten supernovae at least, which is probably a rare occurrence. CTA could therefore probe inhomogeneities in the cosmic-ray population down to small scales and few events. The high significance reached for 100 and 200 pc-sized regions enriched in cosmic rays by one or two supernova explosions suggests that spectral and morphological studies will be possible beyond the simple detection. Such numbers of supernovae in such volumes are consistent

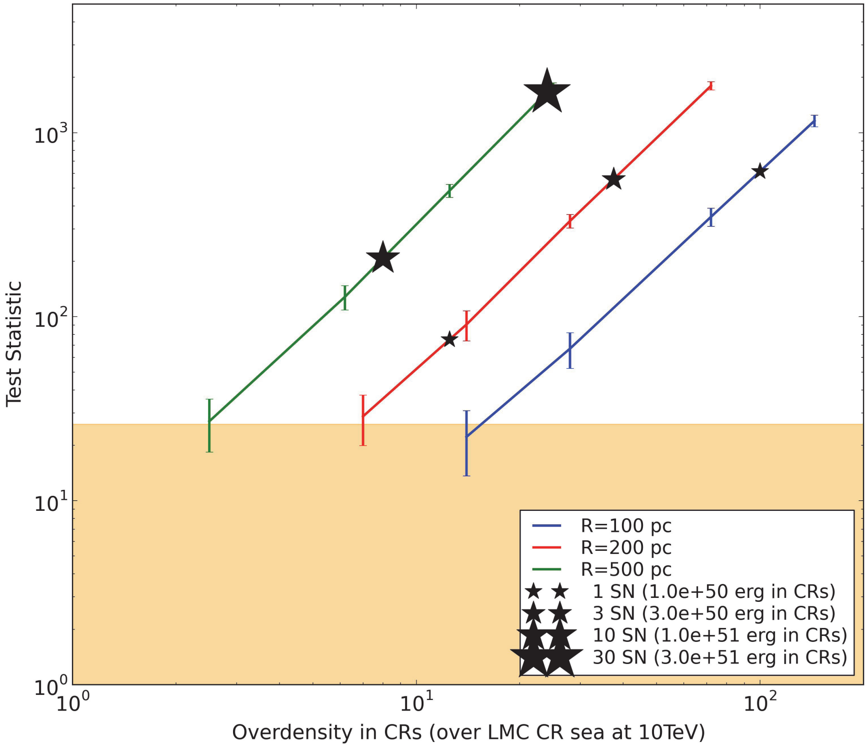

Figure 7.3: Detectability of a region in the LMC as a function of its size (100, 200, and 500 pc) and cosmic-ray density (given by reference to the large-scale background level of cosmic rays at 10 TeV). For a given region size and density, the black stars give the equivalent cosmic-ray density in numbers of supernovae, assuming each event releases 10% of 10^{51} erg into the kinetic energy of cosmic rays. The shaded area marks the area of detection significance below five standard deviations. The high significance reached for 100 and 200 pc-sized regions enriched in cosmic rays by one or two supernova explosions suggests that spectral and morphological studies will be possible beyond the simple detection.

with the characteristics of the 103 giant shell candidates listed in [215]. The estimated mechanical luminosities that inflated the shell structures are consistent with the numbers of SNe given above for the detectability of their non-thermal gamma-ray emission: shells with observed sizes of 100 and 170 pc require a mechanical luminosity corresponding to about 1–5 and 3–15 SNe, respectively (see [215, Figure 8]). Yet, the dynamical age of these structures is typically several Myr, a duration over which cosmic rays may have diffused away. On the other hand, there is still ample speculation about the role of such superbubbles in confining, accelerating, and reaccelerating cosmic rays [242]. With its ability to detect enhancements in the cosmic-ray

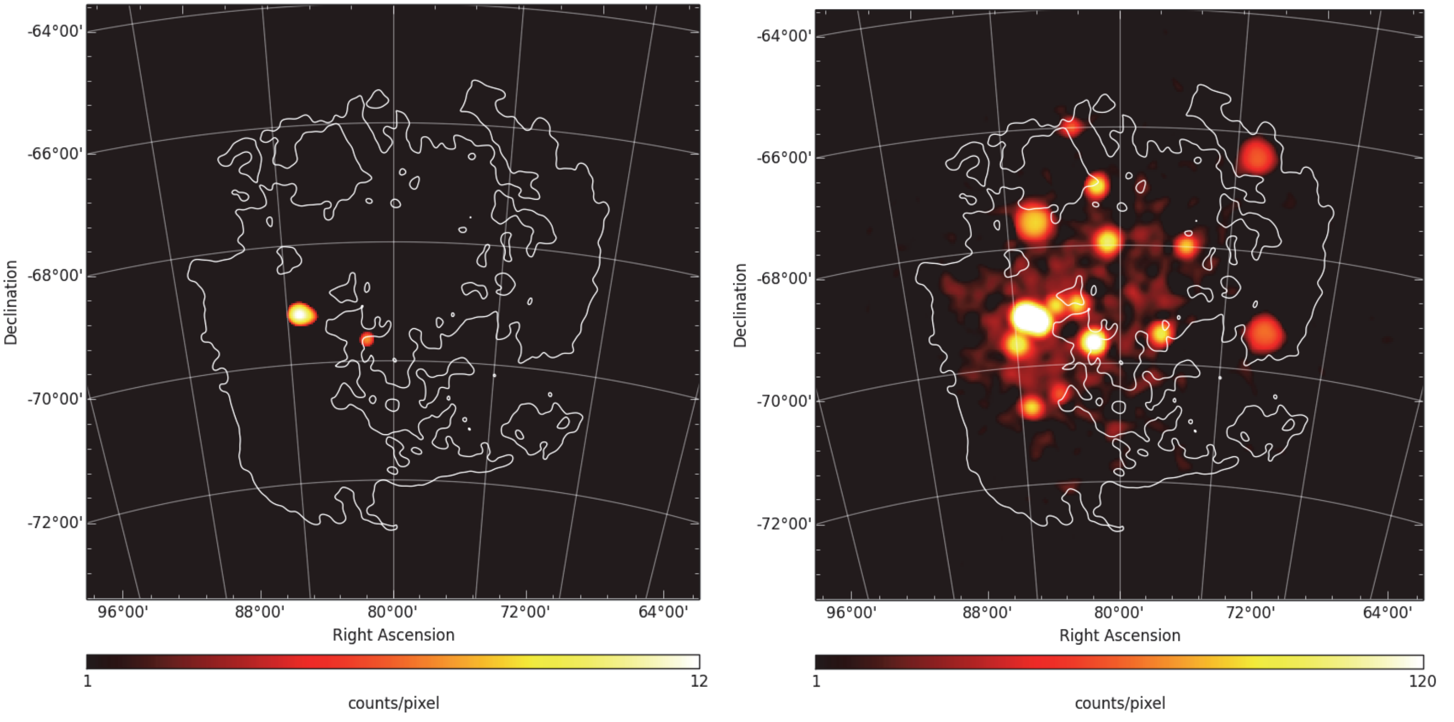
-64°00'
-66°00'
-68°00'
-70°00'
-72°00'
Declination
96°00'
88°00'
80°00'
72°00'
64°00'
Right Ascension
1
12
counts/pixel
-64°00'
-66°00'
-68°00'
-70°00'
-72°00'
Declination
96°00'
88°00'
80°00'
72°00'
64°00'
Right Ascension
1
120
counts/pixel

(a)

(b)

Figure 7.4: Comparison of the LMC as viewed in VHE gamma rays with current instruments (a) and with CTA (b). The panels show smoothed residual count maps after subtraction of the instrumental background counts to the simulated events. The emission model includes detected sources (N157B, 30DorC, and N132D), ten point-like sources with >1 TeV luminosities of $\sim 10^{34}\,\mathrm{erg\,s^{-1}}$, and a handful of regions enriched in cosmic rays. (a) mimics the current H.E.S.S. view of the LMC and was obtained from a simulated 16 h of CTA observations using a single pointing and selecting events with energies >800 GeV. (b) is a simulation of the full CTA survey of the LMC involving six pointings and 340 h of observations for energies >200 GeV, plus an additional source for the brightening SN 1987A. The diffuse glow in the bottom panel results from the large-scale emission. Credit: contour of H I distribution from Ref. [150, 231].

population down to small scales and few events, CTA may therefore provide a valuable view of what happens in the early stages of cosmic-ray propagation. The recent detection of superbubble 30 Doradus C with H.E.S.S. indicates the promise of this approach.

Figure 7.4 illustrates the breakthrough that a deep CTA survey of the LMC would allow, compared to the current view provided by existing instruments (H.E.S.S.). Observations were simulated based on an emission model comprising: the three sources detected so far, hadronic and leptonic large-scale diffuse emission, hadronic small-scale diffuse emission from a handful of regions enriched in freshly released cosmic rays, ten point-like sources with $>1\,\mathrm{TeV}$ luminosities of $\sim 10^{34}\,\mathrm{erg\,s^{-1}}$, and SN 1987A (in the case of CTA observations only, due to the rising flux of the source). For a simulation of a CTA survey using six pointings and a total of 340 h of observations, almost all sources appear in a residual counts map, even the relatively faint large-scale diffuse emission. The contrast with the simulated current H.E.S.S. view, which probed only the most extreme objects of the LMC, is striking.

This page intentionally left blank

8

KSP: Extragalactic Survey

This Key Science Project (KSP) consists of a blind survey of 25% of the total sky. The survey is aimed primarily at extragalactic science with the main objective to construct an unbiased VHE extragalactic source catalogue with an integral sensitivity limit of ∼6 mCrab above 125 GeV. At the moment there are about 60 extragalactic sources seen with the imaging atmospheric Cherenkov telescopes (IACTs) H.E.S.S., MAGIC, and VERITAS, most of these being BL Lacertae (BL Lac) objects. In addition there are five radio galaxies, six flat spectrum radio quasars (FSRQs) and two starburst galaxies (NGC 253 and M 82). The sample is, however, strongly biased since most of observations were motivated by high averaged flux at lower frequencies in optical, X-ray or gamma-ray wavebands. Moreover, about half of the detections have been made when alerted that the sources were in a flaring state. A second objective of this KSP is to provide a high resolution map of the extragalactic sky at gamma-ray energies between 50 GeV and 10 TeV. A third objective is to search for unexpected and serendipitous VHE phenomena over a large portion of the sky. The area covered by the Extragalactic Survey will connect to the Galactic Plane Survey (GPS) so that no Galactic latitude is left un-surveyed.

As shown in Section 8.4, with 1000 h of observation CTA will reach a flux sensitivity for point-like sources at the level of 6 mCrab flux for any sky point in the survey. For the definition of the mCrab unit see Section 6.4.1. This flux limit is on the level of the weakest sources detected with IACTs so far. When compared to Fermi-LAT (10-year exposure) and HAWC (five year exposure), the CTA extragalactic survey will be unique in the energy range between 100 GeV and 10 TeV.

The extragalactic survey of a large portion of the sky is expected to be considered as one of the main legacies of CTA. Given its scale and scientific importance, the survey fits well within the KSP concept and its results will have a large beneficial impact on the broader astronomical community. The survey also has strong synergies with fundamental physics (e.g., the dark matter search and electron spectrum anisotropy).

With the predicted sensitivity, it will be possible to construct an unbiased BL Lac sample in the nearby universe, up to a redshift of $z \approx 0.2$. Sources in quiescent as well as in flaring states will be detected and, depending on the number density (N) of sources as a function of their flux (S) (the log N–log S distribution, also called the luminosity function, LF) for the BL Lacs (which is largely unknown), 30–150 sources are expected to result from the survey; see below in Section 8.1.1 for justification of these numbers. Moreover, more distant ($z \gtrsim 0.2$) BL Lacs and FSRQs will be detected, but only when they will be in elevated or flaring flux states because in the quiescent flux state they would typically remain below the CTA detection threshold for short exposures. Also, several new radio galaxies will be discovered in VHE gamma rays. The list of potential discoveries is long and the highlights include:

- unbiased determination of the yet unknown log N–log S of gamma-ray AGN (BL Lacs and possibly FSRQs),
- discovery of extreme blazars peaking in the ∼100 GeV to 1 TeV region,
- serendipitous detection of fast flaring sources, not detectable in short observation time (hours) by lower sensitivity observatories like Fermi-LAT and HAWC,
- discovery of gamma-ray emission from yet undetected source classes such as Seyfert galaxies, ultraluminous infrared galaxies (ULIRGs), etc.,
- discovery of dark sources with no astrophysical counterpart, which would be a possible signal from dark matter annihilation,
- the possible detection of a gamma-ray burst (GRB) in the prompt phase (the probability for this is 2–4 times higher if the survey is performed in divergent pointing mode, see below), and
- the study of large-scale anisotropies in the electron spectrum at energies between 100 GeV and few TeV.

To ensure the uniformity of the survey, we propose to perform it with the full CTA Observatory in a period of time of not more than three years. In the present Monte Carlo simulations, the sensitivity of the southern array is about a factor of 1.5 better than the northern array in the energy range above 100 GeV because of the larger number of MSTs and the presence of the

SSTs in the south. A factor of approximately 2.2 longer exposure is needed to compensate for this difference in sensitivity. Nonetheless, it is proposed to utilise both CTA sites for the extragalactic survey since it will allow us to complete the survey to the required sensitivity within three years. To achieve a uniform sensitivity, it is proposed to cover 15% of the sky in the south using 400 h and the remaining 10% of the sky in the north using 600 h. Such coverage would ensure a 6 mCrab sensitivity over the whole area of the survey after 1000 h of observations in total.

It is anticipated that the divergent pointing mode (see Section 8.4.5) will be more effective for this survey than the standard mode. Because of its greatly improved capabilities for serendipitous flaring sources, the divergent pointing mode will be used for this KSP if it can be shown that the required flux sensitivity can be achieved within the same time (even if this results in a moderate worsening of the spectral and angular resolutions). However, detailed studies on the divergent mode are still ongoing and the estimates here are based on the performance of the normal pointing mode, which is a conservative choice.

8.1 Science Targeted

Through the unbiased survey of a significant part of the extragalactic sky, we mainly target a population study of the local ($z < 0.2$) universe in gamma rays in the energy range of 100 GeV to 10 TeV. It will be the first time that such a large portion (~25%) of the sky is observed uniformly and with high sensitivity at these energies. The uniqueness of the survey also enables the search for new source classes, as well as the search for large scale structures in the electron spectrum as outlined below. At the same time, such a survey will lead to an unbiased picture of the flaring sky in the 100 GeV to 10 TeV regime, which is vital for understanding the largely unknown duty cycles of blazar flaring activities. The other strength of this KSP is the ability to look for the unexpected discoveries (e.g., dark gamma-ray sources, new source classes, etc.).

8.1.1 *Scientific Objectives*

Blazars: Luminosity functions (or luminosity distributions, and their possible dependence on the redshift) are fundamental for understanding the main physics drivers within the sources and their evolution. An unbiased survey with a uniform exposure allows us to measure the luminosity function and the number density of sources depending on their flux (the so-called log N–log S distribution). To construct the log N–log S distribution, one needs a sufficient number of sources (>50), which are representative for the underlying population. The main source class of gamma rays in the extragalactic sky are blazars (BL Lacs and FSRQs), which are believed to produce gamma rays inside relativistic jets with large bulk Lorentz factors ($\sim$10 or larger) beaming the emission towards the observer. The mechanism of the gamma-ray production in blazars is not completely understood, with evidence that most of the emission has a leptonic origin and that flaring activity is associated with freshly accelerated electrons or rapid changes in the magnetic field. Determining the log N–log S of blazars is of fundamental importance as it is also crucial for determining the total gamma-ray background. The measurement of the extragalactic gamma-ray background (which does not yet exist for energies >700 GeV) is the ultimate way to verify the theory of gamma-ray production in AGN. Assuming the unified scheme of the AGN is correct — that the phenomenology of AGN mainly follows our viewing angle with respect to the jet orientation — the jets of the blazars have a small angle to the observer's line of sight, which means that blazars account for a few % of the total AGN gamma-ray emission [243, 244].

The number of detected blazars will determine the quality of the blazar LF. However, the problem for measuring the LF is not just the number of objects but the bias introduced in targeting. This bias can be solved with a wide survey. The number of sources will affect the uncertainties, i.e., the ability to discriminate between different LF distributions and eventually the contribution of the different sub-classes (FSRQ, BL Lac).

We foresee detecting 30–150 blazars within the survey. If we extrapolate Fermi-LAT sources with known redshifts into the CTA energy range assuming a reasonable intrinsic cutoff of 1 TeV on average, we obtain some 30–40 sources to be detected with the proposed sensitivity. When instead of extrapolating from Fermi-LAT, we use predictions by [12], who used IR and X-ray data to construct the log N–log S of blazars, we obtain approximately 75 sources. In Figure 8.1, the sensitivity of the survey is shown and compared to the 1 mCrab CTA 50 h sensitivity as well as the flux limit of the current VHE gamma-ray telescopes. The histogram in the upper left plot is for 27,000 deg^2, leading to a factor of 2.7 smaller predicted numbers for a 10,000 deg^2 (25% of the sky) survey. However, the catalogue is incomplete and can easily result in double as many sources, i.e., close to 150. Similarly high numbers are obtained by [245] based on the EGRET luminosity function [246]. There is also the possibility of detecting distant objects ($z \sim 1$) at energies $\gtrsim$300 GeV by including secondary gamma-ray emission from blazars in the presence of intergalactic magnetic fields of $(10^{-17} - 10^{-15})$ G [247]. In Ref. [13], the expected number of blazars emitting above 100 GeV is estimated based on Monte Carlo simulated surveys that reproduce the Fermi-LAT results well. They predict that the CTA extragalactic survey will detect between 110 and 180 blazars depending on different assumptions on the VHE spectrum (see Figure 8.1(b)).

Even if many of the sources detected will be the known ones, the slope of the log N–log S distribution can only be determined through an unbiased survey. Some sources will be detected during flaring gamma-ray states introducing a bias when studying the quiescent state of sources only. However, we estimate the bias to be in the order of ~10%,[a] and the result can be corrected for it. In addition, the detected unbiased flaring episodes (within the survey) are as important to characterise the gamma-ray sky as the sources detected in the quiescent state. One of the major unanswered questions of modern AGN physics is the existence or not of the blazar sequence. If the sequence exists, there should be no, or only a few, detections of high luminosity blazars that have their synchrotron peak in optical and UV wavebands. The survey will be able to probe this prediction.

Extreme blazars: The survey will reveal a population of extreme blazars, i.e., sources with hard spectra having their gamma-ray peak in the range of 100 GeV to more than 10 TeV. Extreme blazars are very interesting because of their use in studies of the extragalactic background light (EBL) and the intergalactic magnetic field (IGMF), as well as due to the fact that the gamma-ray emission in leptonic scenarios must be produced in a deep Klein–Nishina regime (which is unusual) or have a hadronic origin. The sources are usually too weak to be detected with Fermi-LAT even in 10 years exposure, making it hard to make predictions for CTA. In the local universe, two bright extreme blazars are known: Mrk 421 and Mrk 501 (at $z \sim 0.03$). A third extreme blazar is 1ES 0229+200 ($z = 0.14$). Typical VHE gamma-ray fluxes for Mrk 421 and Mrk 501 are on the order of 200 mCrab when in a quiescent state. Taking the envisioned sensitivity of 6 mCrab as the detection limit, sources 40 times weaker can be detected during the survey. This leads to an

---

[a] The uncertainty in the number of sources found in a flaring state is large due to unknown VHE gamma-ray duty cycles. A rough estimate can be made using the monthly duty cycles of Fermi-LAT. High-flux events above 1.5 standard deviation significance have a duty cycle of about 5–10% for FSRQs and BL Lacs in the GeV band [248]. Therefore, we assume that during the proposed survey 10% of the sources will be in a flaring state.

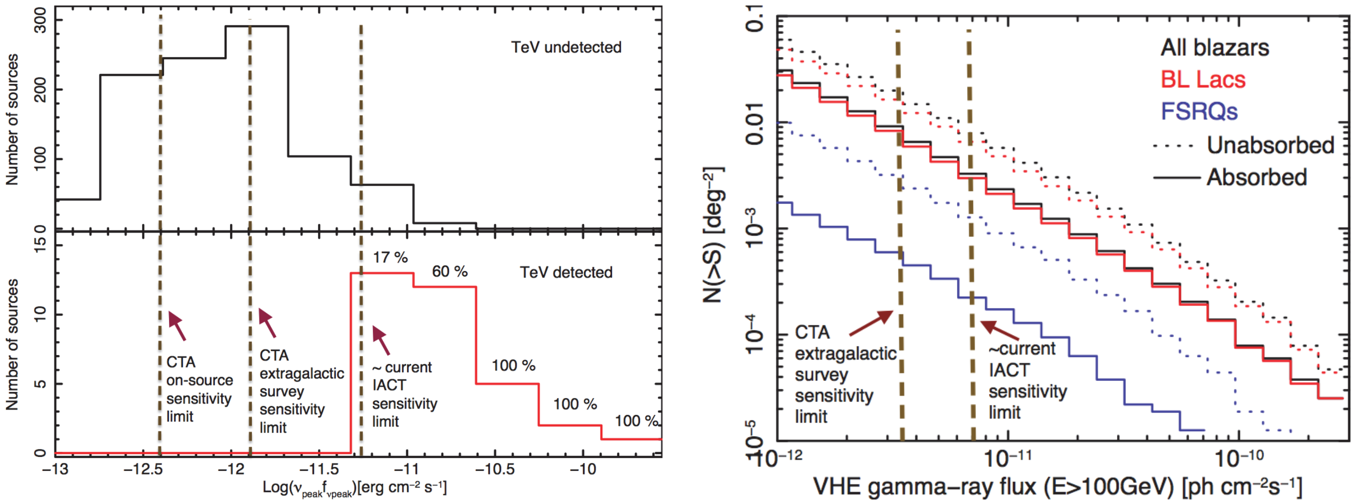

(a) (b)

Figure 8.1: Predictions for the number of blazars on the sky in the GeV–TeV gamma-ray domain. (a) Expected source counts as a function of the integral gamma-ray flux above 100 GeV in 27,000 deg^2. The upper panel shows predictions by [12] together with the current and envisioned sensitivity limits of imaging atmospheric Cherenkov telescopes (IACTs). The lower panel shows detected AGN with IACTs. The numbers above the red histogram give the fraction of expected sources detected by current instruments. (b) Simulated log N–log S distribution from Ref. [13]. The dashed (solid) lines represent the expected distributions without (with) taking into account the absorption by the EBL. According to this study, with the 6 mCrab sensitivity during the proposed survey CTA should detect around 100 sources in 10,000 deg^2.

increase in distance by a factor of ∼6 (out to $z \sim 0.2$), or to an increase in the accessible volume to Mrk-like sources by a factor of 200. The extrapolation from two sources has naturally a large uncertainty, but making a conservative estimate and taking EBL absorption into account (which is not relevant for energies below 300 GeV for these redshifts), we expect to detect 30–150 extreme blazars.

Radio galaxies: Nearby radio galaxies have also been found to be sources of gamma rays. However, the mechanisms by which radio galaxies produce their gamma-ray emission are not well understood, with several explanations currently possible. Gamma rays are possibly produced near the nucleus or in the knots along the jet, but radio lobes are also discussed as candidate sites. Only five radio galaxies have been detected in VHE gamma rays so far, and the flaring duty cycles are poorly known. The survey we suggest will help detecting more radio galaxies, which would boost our understanding of the emission mechanisms and the contribution of radio galaxies to the total production of gamma rays. Using the fact that the five radio galaxies have their TeV fluxes in the order of 20 mCrab when in a quiescent state, we estimate that within the survey sensitivity we will detect a few new radio galaxies.

Starburst galaxies: Two close starburst galaxies (M 82 and NGC 253) have been detected in VHE gamma rays. Both show weak emission at the flux level of 6 mCrab. With the suggested extragalactic survey, we will reach the sensitivity to detect further starburst galaxies at any location in the survey if their gamma-ray flux is at a similar level. However, since M 82 and NGC 253 are probably the brightest gamma-ray starburst galaxies, we foresee at most only a few new detections within the survey.

New source classes: An unbiased survey of ∼25% of the extragalactic sky enables the detection of new source classes. Clusters of galaxies, Seyfert 2 galaxies, and ULIRGs have been proposed to emit VHE gamma rays, but none have been detected so far. At GeV energies, Fermi-LAT did detect the Seyfert 2 galaxy Circinus [249]. Beyond this, the survey has chances to detect gamma-ray sources without clear association with known objects (dark sources) or sources where no strong non-thermal emission is detected. This can be a clear signature of unknown physics, for example, the decay of a new particle, such as dark matter, into gamma rays.

Gamma-Ray Bursts and other transients: Gamma-ray bursts (GRBs) are usually distant events with redshift $z > 1$, meaning that most of their VHE gamma-ray emission will be absorbed by the extragalactic background light. However, the universe is basically transparent to gamma rays with energies $E < 30\,\mathrm{GeV}$ and absorption is not severe up to 50 GeV even for large cosmological distances. This means that with the low-energy response of CTA, there will be a good chance to catch GRBs even if their redshift is $z \gg 1$, provided their central engine emits to sufficiently high energies. For more details on the prospects on GRB detection, see Chapter 9.

There is a chance of catching a GRB in the onset of the prompt phase if the burst occurs within the observed field. If the survey is performed in the normal pointing mode, the chances to catch a GRB during the survey are the same as during any other pointed observations and are quite low, $\sim 0.08\,\mathrm{yr}^{-1}$ in the 8° diameter field of view (FoV) of the MSTs. However, if the extragalactic survey can be conducted in divergent pointing mode with an instantaneous FoV considerably larger than in normal pointing, it would significantly enhance the prospects for studying cosmic transients at very high energies without relying on triggering the observations with an external alert. In particular, carrying out the survey in divergent pointing mode could enable:

- the detection of GRBs from their onset, including the prompt phase of short GRBs and realising the associated improvements for probing Lorentz invariance violation,
- unbiased searches for VHE transients in general, and
- MWL and/or MM spatio-temporal correlation studies with other observatories with wide FoV and/or limited localisation capabilities.

In the most optimistic case, CTA can cover up to $1{,}000\,\mathrm{deg}^2$ simultaneously when observing in divergent pointing mode, which is about a factor of 20 higher than the FoV when using normal pointing. This would boost the rate of GRBs observable by CTA in the prompt phase to about 2 per year. For the purpose of studying GRBs or transients, a FoV as large as possible is favoured, but this needs to be balanced with the sensitivity and energy threshold required for the other aims of the survey. More details on the unique prospects for studying transients with a divergent pointing survey are discussed in the Transients KSP (Chapter 9).

Large-scale electron anisotropy: The sensitivity of CTA is sufficient to detect the diffuse electron component of the cosmic-ray spectrum above 100 GeV in every survey pointing.[b] Thus, systematic errors permitting, the survey will allow the study of large-scale anisotropies in the electron background, which has not yet been possible at these energies.

---

[b] We assume here a single pointing of 30 min and normal pointing mode.

Diffuse gamma-ray background: Though, as stated before, the beamed gamma rays from blazars are estimated to account for about $\sim$1% of the total AGN gamma-ray emission, the extragalactic gamma rays with $E > 100\,\mathrm{GeV}$ are mainly from blazars. Therefore, through the construction of the log N–log S distribution of blazars, the survey will allow us to resolve the average diffuse gamma-ray background [250, 251] and compare it to the measurement of the gamma-ray background at lower energies. Such a comparison is vital to understand the completeness of the sample detected and thus the total amount of extragalactic gamma rays produced. A direct measurement of the gamma-ray background at very high energies will also be attempted by CTA using the survey data, but due to the electron background this will be a very challenging task, as discussed in Ref. [30].

Dark Matter clumps: Structure formation predicts gravitationally bound dark matter clumps down to much lower masses than for dwarf spheroidal galaxies. The total number of clumps within Galactic halos can be as high as 10^{15}. It is likely that a large population of lighter dark clumps exists with highly suppressed (or even negligible) baryonic content, hiding from detection in currently operating sky surveys. Because of the difficulty in the identification of clumps in optical surveys, the prime channel of detecting dark clumps are high-energy and VHE gamma rays resulting from annihilations or decays of dark matter particles in the clump. Such objects, if bright enough, could appear as unidentified sources in the proposed survey. Because of the limited sensitivity of Fermi-LAT, if the dark matter mass is above a few hundred GeV, these objects could have been missed by Fermi-LAT and could be detectable by CTA.

8.1.2 *Context/advance beyond state of the art*

There are about 70 extragalactic sources detected with the current generation of IACTs: H.E.S.S., MAGIC, and VERITAS. The majority of the sources belongs to the AGN subclass called BL Lacs. The sample is, however, strongly biased since most of the observations were motivated by high averaged flux at lower frequencies in the optical, X-ray or gamma-ray wavebands. Moreover, about half of the detections have been made following alerts that indicated that the sources were in a flaring state. The performance of the current generation of IACTs does not allow for an unbiased survey of a large portion of the extragalactic sky with a reasonable flux sensitivity. Assuming a survey time of 1000 h and a FoV for the current telescopes of around $10\,\mathrm{deg}^2$, one obtains a 1 h exposure for every sky point in a $10000\,\mathrm{deg}^2$

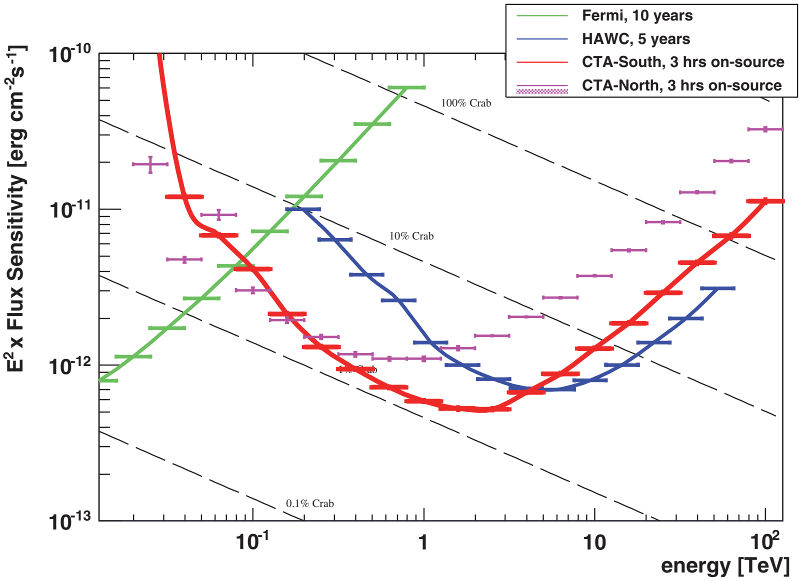

Figure 8.2: Differential sensitivities of instruments in the GeV–TeV range together with the CTA extragalactic survey sensitivity. The Fermi-LAT sensitivity is shown for 10 years exposure (dark green [252]). HAWC is shown for a five-year exposure (blue [190]). The CTA target sensitivity for the extragalactic survey is 6 mCrab and is similar to the 3 h sensitivity of the southern array (red). Sensitivity for the northern CTA array is also shown (magenta). See text for details.

survey (∼25% of the sky), which would allow the detection of only ∼10 of the brightest sources. Therefore, with the current IACTs no systematic survey can be performed over a large portion of the sky, and spending 1000 h on such a survey cannot be justified.

For CTA, the situation will be quite different because CTA will be much more capable than the present-day instruments. In Figure 8.2, the differential sensitivities of CTA and the current wide-field instruments (Fermi-LAT and HAWC) are shown. With a 6 mCrab integral sensitivity above 125 GeV (which would roughly correspond to the red curve in the plot for sources with Crab-like spectra), the CTA extragalactic survey will make a unique measurement between 100 GeV and 10 TeV. It is worth mentioning that the integral sensitivity of Fermi-LAT after an exposure of 10 years is expected to reach a level of 20 mCrab above 200 GeV, which makes Fermi-LAT competitive with CTA for steady sources up to that energy. In the southern sky, which HAWC does not access, the uniqueness of the survey extends to higher energies. In the north, HAWC is complementary to CTA at energies above 10 TeV. It is clear that the CTA-North array, with a smaller number of telescopes and no SSTs, will require a longer exposure to obtain the same target sensitivity.

8.2 Strategy

The CTA extragalactic survey is proposed to take 1000 h and cover 25% of the overhead sky. The survey is unique and in that it opens a new window for the search of extragalactic sources as well as it being the first attempt for a complete log N–log S study of close-by blazars in VHE gamma rays.

The normal, conservative, pointing scheme would be the default one. In case the simulations show that the divergent pointing mode is more sensitive than normal pointing for the survey, the survey would be performed using divergent pointing. In this case, the complexity of the event reconstruction and data analysis would require the set up of a special analysis pipeline and the unique expertise of the CTA Consortium.

8.2.1 *Possibility of Several Pointings for a given Field of View*

It will be shown later (Section 8.4) that the optimal strategy for the survey is a sequence of pointings at grid points of the survey area with a 3° separation between the points. This pointing strategy would result in approximately 3 h effective observation time for every point on the sky within the boundary of the survey. The default plan would be to observe at each grid point for the required amount of time (i.e., 0.51 h in the south and 1.11 h in the north, see Table 8.2). However, it may be better to have shorter pointings (e.g., 10 minutes in the south and 22 minutes in the north) for each grid point and to return to each grid point three times during the survey. This would increase the chances of catching flaring activity, while keeping the total observation time the same. Also, shorter exposures would enhance CTA's ability to detect short, bright transient phenomena. We will keep this possibility in mind for the optimisation of the survey strategy once the time needed for re-pointing CTA is known.

8.2.2 *Shallow survey versus deep survey*

We investigated different survey strategies. In particular, we focused on the comparison between a shallow and wide survey versus a deep and narrow one. According to the study made by [13], which is based on Monte Carlo simulations of blazar populations, observing a four times narrower field for, consequently, four times longer time would result in a detection of about 50% less sources. We, therefore, argue for a wide area shallow survey. However, the shallow survey should be deep enough to obtain a significantly (more than a factor of ten) better sensitivity than Fermi-LAT and HAWC for steady sources. A quarter-of-the-sky survey is a good compromise (see Section 8.4.3 for a discussion of the achievable sensitivities). We stress, however, that the survey area can be further optimised using results on the number of serendipitous sources found in pointed observations during the CTA construction phase (see Section 8.4.2).

8.2.3 *Targets*

We propose an extragalactic survey as shown by the light blue area of Figure 8.3. The survey would connect with the Galactic Plane Survey ($|b| < 5°$, dark blue area) and cover ~25% of the sky, over Galactic longitude $-90° < l < 90°$. The proposed survey would be performed using both CTA arrays for zenith angles of observations smaller than 45° to ensure uniformity in the energy threshold and resulting sensitivity. Several highly interesting regions, such as Cen A (south) and the Virgo cluster, Coma cluster, and Fermi bubbles (north), will be covered by the proposed survey.

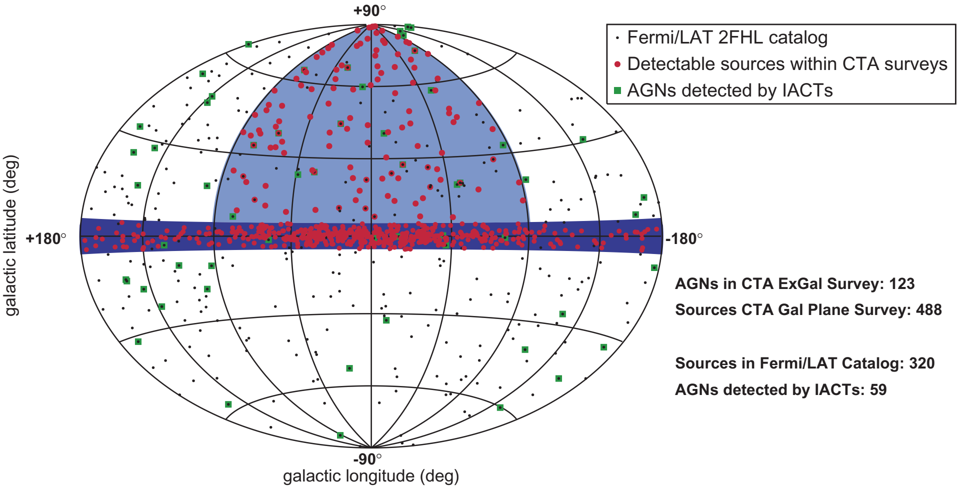
+90°
· Fermi/LAT 2FHL catalog
● Detectable sources within CTA surveys
🟩 AGNs detected by IACTs
galactic latitude (deg)
+180°
-180°
AGNs in CTA ExGal Survey: 123
Sources CTA Gal Plane Survey: 488
Sources in Fermi/LAT Catalog: 320
AGNs detected by IACTs: 59
-90°
galactic longitude (deg)

Figure 8.3: Proposed region of the extragalactic survey in Galactic coordinates: $b > 5°; -90° < l < 90°$, 25% of the sky, marked in light blue. The Galactic Plane Survey is indicated by darker blue. Red points show a hypothetical example of the sources to be detected in the extragalactic and Galactic CTA surveys. Extragalactic and unidentified Fermi-LAT hard-spectrum sources (2FHL catalogue [191]) are displayed as black dots, whereas green points show the AGN that have been detected so far by IACTs [204].

A hypothetical result of the survey is illustrated Figure 8.3 by the red dots. The black dots represent 2FHL sources (Galactic sources are not shown) from [191]. The red dots result from CTA simulations extrapolating 2FHL sources for a CTA exposure of 6 h, assuming an averaged flux state and that 5% of the sources will be found in a flaring state. The Galactic sources are simulated to follow the spatial distribution of pulsars in the ATNF pulsar catalogue. The green points show extragalactic sources already detected in the TeV gamma-ray regime from Ref. [204].

8.3 Data Products

This KSP will produce an extragalactic gamma-ray catalogue of detected sources. For each source, the catalogue will contain the:

- differential energy spectrum,
- significance of the detection,
- source location,
- integral flux,
- variability index,
- extension of the source, if applicable, and
- association with known objects, if made.

The catalogue will also contain the time intervals (modified Julian dates) for the observation periods and the time intervals for any detected flares.

The catalogue will be released one year after completion of the survey. In case of detection of a significant transient event, a public alert will be issued at the earliest possible moment (via, e.g., the Virtual Observatory network using VOEvent protocol, see the Transients KSP in Chapter 9).

Interrupting the survey for self-triggers and/or external triggers will be possible, but the conditions for such events should be carefully studied and covered by a separate proposal. Follow-up observations are not part of this KSP and are expected to be largely carried out through the GO Programme.

In order to maximise the scientific output of the extragalactic survey, we are planning to organise an extensive MWL effort to accompany the survey. We foresee obtaining simultaneous optical data and snapshots in the radio band. Since the optical and radio observations have a much smaller FoV than the CTA telescopes, we plan to observe potential sources within the CTA FoV only or make shallow scan observations. For the new detected TeV sources without well determined redshifts, we will launch follow-up optical spectroscopy observations to obtain the redshifts. In the X-ray band, we will launch ToO programmes for follow-ups on detected gamma-ray flares. We will complement our MWL efforts by the public Fermi-LAT data in the GeV gamma-ray band. It is planned that all available simultaneous MWL data will be published in the extragalactic gamma-ray catalogue as additional information.

8.4 Expected Performance/Return

In this section, we estimate the expected survey sensitivity. All numbers are given for a survey size of 25% of the sky. We focus on the estimation of what can be achieved through parallel pointing of the telescopes (i.e., where during each observation all telescopes are pointing in the same direction). The prospect of using the divergent pointing mode is also briefly discussed.

8.4.1 *Method*

The survey pattern considered is similar to that presented in an earlier paper on surveys with CTA [9]. We consider a pattern where the observation pointing directions are uniformly distributed on a grid of equilateral triangles. The observations are simulated using standard software used in the gamma-ray band (ctools and GammaLib) and the instrument response functions come from CTA simulations. A representative portion of the survey is considered and the sensitivity at each point is calculated by simulating a point source with 0.25 degree steps in the source position. The simulated source has a Crab-like spectrum, and its flux is adjusted so that the source is detected at a significance of five standard deviations above the background. That flux then corresponds to the detection sensitivity at that location in the survey. The sensitivities are given in comparison with the Crab nebula flux, as discussed in Section 6.4.1.

8.4.2 *Serendipitous Discoveries during the Construction Phase*

As stated above, there is a large spread in the theoretical predictions on the source numbers and their class types for the envisioned extragalactic survey with CTA. We investigated the chances for serendipitous discovery of new gamma-ray sources during the construction phase of CTA. We considered on-source observations that will be performed after completion of half of the CTA array and before the start of observations with the full array. It is reasonable to assume that there will be some 50 extragalactic fields observed with this half-CTA array, for 20 h each. Taking a reduced sensitivity of the half-array into account we assume that within a 20 h observation, a 6 mCrab integral sensitivity level will be achieved within a 3° radius of the centre of the field of view. Using these assumptions we performed two Monte Carlo simulations:

- optimistic scenario: assuming that there are 150 extragalactic sources detectable with CTA (flux higher than 6 m Crab) in 10,000 $\deg^2$, and
- pessimistic scenario: assuming that there are 30 extragalactic sources detectable with CTA (flux higher than 6 m Crab) in 10,000 $\deg^2$.

In each case, a population of sources was uniformly simulated in 10,000 $\deg^2$. Two cases of CTA pointings were considered: in the first one, all 50 pointings are random and not correlated with the simulated source positions. In a second one, we assumed that the 50 pointings are performed towards a subset of the simulated population (if there are more pointings than sources, the rest of the pointings are random). Each simulation was repeated 1,000 times and the mean value in the number of detections, as well as the spread, were obtained.

The results of the simulations are shown in Figure 8.4. In the plots on the left, we show one out of 1,000 simulations. In these plots, the small red dots indicate the random pointing positions of CTA. We count serendipitous discoveries in following cases:

- serendipitous detection of a source in a random pointing (Figure 8.4, big blue dots);
- serendipitous detection of a second source in a random pointing (Figure 8.4, big green dots);
- serendipitous detection of a second source in a pointing towards another source (Figure 8.4, big red dots);

In the histograms on the right, the distributions of the serendipitous detections are plotted. Depending on the assumptions made, we find that, in the optimistic case, 20–30 sources can be discovered serendipitously to pointed observations. In the pessimistic case, 2–5 sources will be discovered serendipitously.

These Monte Carlo simulations show us that with a partial CTA array during the construction phase we will be able to obtain a reasonable estimate on the number of expected sources in the extragalactic survey, which can be used to refine the survey strategy.

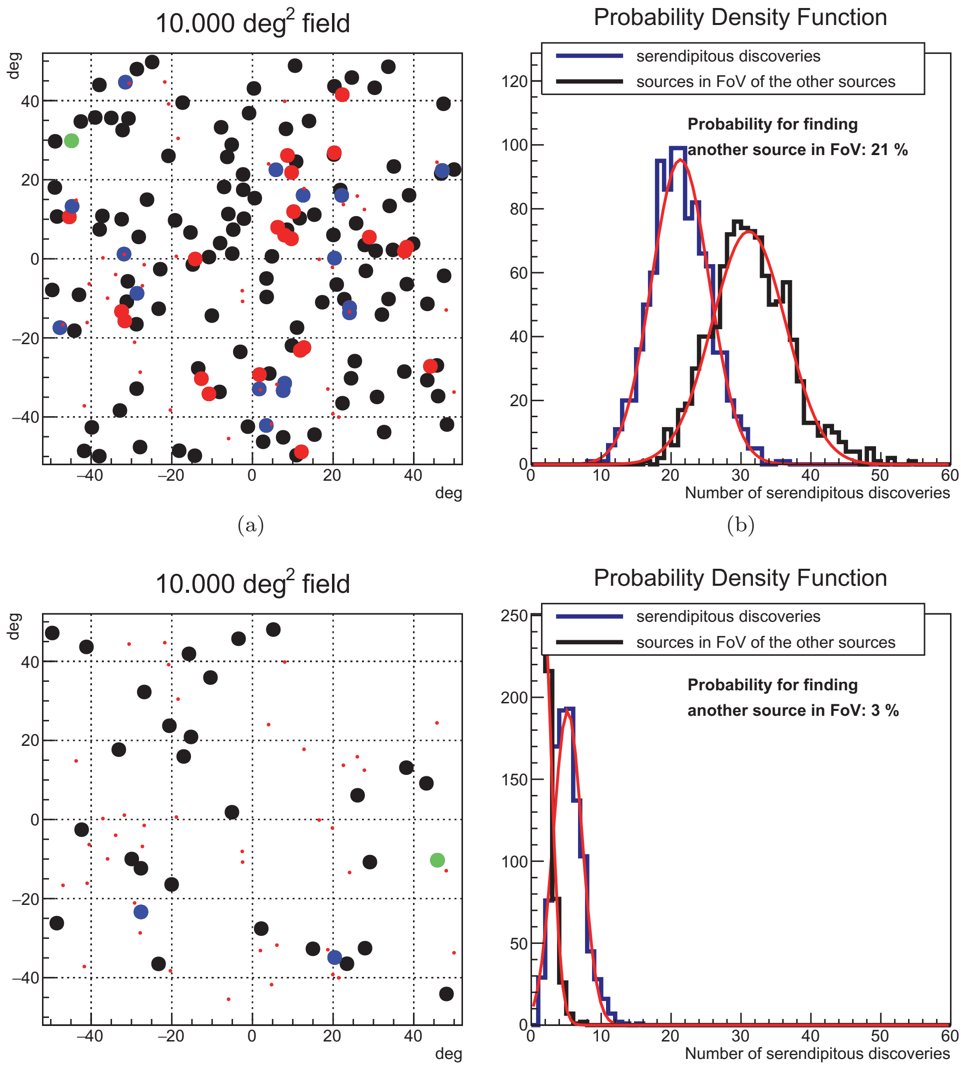

(a) (b)

(c) (d)

Figure 8.4: Results of the Monte Carlo simulation for serendipitous discoveries during the CTA construction phase. In the optimistic case ((a) and (b)), 20–30 sources can be discovered serendipitously, whereas in the pessimistic case ((c) and (d)), only 2–5 serendipitous discoveries can be made. See text for details.

8.4.3 *Results after the Completion of the Survey*

Sensitivities have been calculated for the south and north arrays using the CTA simulations. A preliminary study has shown that the instrument response functions obtained using a set of cuts optimised in 50 h observations and a Crab-like spectrum give the best results in terms of survey integral sensitivity compared to other available sets of cuts. The results presented here make use of the instrument response functions (IRFs) derived from these cuts. Nevertheless, since the cuts have not been optimised for the survey, the sensitivity quoted here may not be optimal.

For the CTA-South and CTA-North arrays, we use the configurations with 4 LSTs, 24 MSTs and 35 SSTs, and 4 LSTs and 15 MSTs, respectively. The same arrays without LSTs have also been considered. An optimisation is performed considering the spacing between the pointings (the smaller the spacing the more uniform the sensitivity) and the exposure per pointing, keeping the total exposure of the 10,000 deg^2 constant. Three different spacings have been considered: 2°, 3°, and 4°. An example of the resulting sensitivities and their variation is shown in Figure 8.5. This particular example shows the performance of the south array with a 3° spacing between the pointings. The integral sensitivities are colour-coded and the grid is in RA/Dec coordinates.

The results of the study for 600 h and 25% of the sky are summarised in Table 8.1. Note that here we assume that entire 600 h are spent in South or in North. A spacing of three degrees between the observations gives a better mean sensitivity compared to 4° or 2°. Using this spacing and pointing

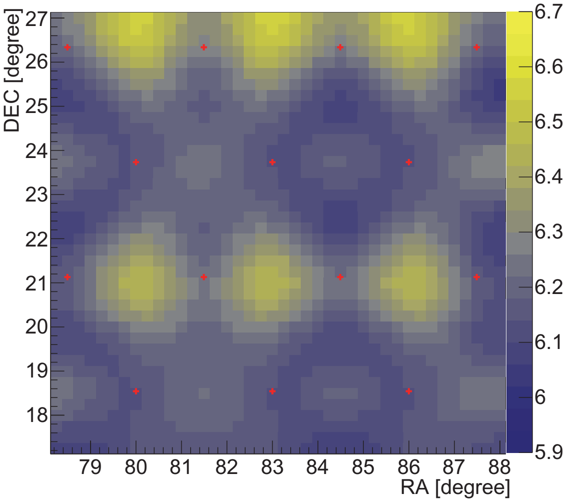

Figure 8.5: Sensitivity map (colour scale, integral sensitivities in units of mCrab for energies above 125 GeV) from simulations for a portion of the survey, assuming the southern array for 600 h and covering 10,000 deg^2. The grid is in approximate RA/Dec coordinates. Note that the colour scale is zero-suppressed to better illustrate sensitivity variations across the survey. Red crosses denote the actual pointing positions.

Table 8.1: Estimation of the survey sensitivity for a total of 600 h of observations and a coverage of 25% of the sky, for the south and north arrays and for various grid spacings (in degrees).

	Spacing between the observations					
	4 degree 0.83 h/obs.		3 degree 0.46 h/obs.		2 degree 0.21 h/obs.	
ARRAY	S	ΔS	S	ΔS	S	ΔS
South-noLST	5.4	0.9	4.8	0.4	5.0	0.5
North	8.61	1.2	8.0	0.8	8.1	0.8

Notes: The sensitivity, S, is given in units of mCrab, see Section 6.4.1. ΔS represents the survey sensitivity fluctuation; this is the standard deviation of the sensitivity distribution over the sampled survey field of view.

Table 8.2: Same as Table 8.1 but for the 3° spacing with the sensitivity numbers scaled for a total of 1000 h shared between CTA-South (400 h) and CTA-North (600 h), covering 60% and 40% of the survey area, respectively.

ARRAY	Time per pointing (h)	Integral sensitivity $S \pm \Delta S$
South-noLST	0.51	5.1 ± 0.5
North	1.11	5.4 ± 0.6

scheme, every sky point in the survey has an effective observation time about six times larger than that of a single pointing. In the south, the survey integrated sensitivity is on the order of 5 mCrab above 125 GeV. In the north, a sensitivity of 8 mCrab can be achieved. These numbers will only improve with an optimised array layout and advanced analysis techniques.

In order to obtain a uniform sensitivity between North and South, we propose to cover 15% of the sky (60% of the survey) from the south in 400 h and the remaining 10% of the sky (40% of the survey) from the north in 600 h. Such coverage would ensure a 6 mCrab sensitivity over the area of the whole survey after 1000 h observations from south and north in total. Having both CTA-S and CTA-N participating in the survey allows one to cover several regions of particular interest (e.g., the Coma cluster, Fermi bubbles, Cen A, and Virgo cluster) and complete the extragalactic sky survey within the first two years of operation, which would not be possible with one site alone. The sensitivities for the proposed shared survey for a total of 1000 h are shown in Table 8.2. We note that with improved data analysis techniques, a better sensitivity than the targeted one can be achieved in the same observation time.

8.4.4 *Participation of LSTs*

Including the LSTs into the extragalactic survey has some crucial advantages, including:

- a higher sensitivity to transients as most of them are distant sources with soft spectra (but the improvement factor is unclear and our best guess is that the number of detected transients would increase by a factor of two),
- the potential discovery of short-term variability for sources at energies below 100 GeV, as the LSTs provide several orders of magnitude better sensitivity than Fermi-LAT for exposures of less than one hour (see Figure 1.5),
- the measurement of the low-energy lever arm in the spectra for most of the detected sources, and
- the detection of a factor two more Fermi-LAT known sources (this is a difference between the 25 GeV threshold energy of the LSTs and 80 GeV for the MSTs).

There are, however, some caveats. One of them is that including LSTs into the survey does not change the overall sensitivity much because we evaluated the sensitivity above 125 GeV, which is dominated by the MSTs. A second point is that the LSTs have a narrower field of view than the MSTs, which means that the survey could be done more rapidly without the LSTs. Including the LSTs also adds some non-uniformity of the exposure. Finally, if the LSTs were excluded from the survey, they could be devoted to other programmes (done in parallel to the survey) that require a low-energy threshold and do not require a high sensitivity above 1 TeV. Nevertheless, we recommend to include the LSTs into the extragalactic survey arguing that the advantages outweigh the disadvantages.

8.4.5 *Prospects for Divergent Pointing*

In the divergent pointing mode, each telescope in the array is pointed to a location on the sky that is slightly offset from its neighbour in order to cover a larger portion of the sky at once.

Here, we briefly summarise the results of a preliminary study based on CTA simulations with no LSTs. The divergent pointing pattern considered resulted in a field of view of 14° in diameter with sensitivity fluctuations below a factor two across the field of view. Comparing divergent pointing and normal pointing indicates that a sensitivity gain of roughly 1.5 can be achieved if divergent pointing is used to do the survey.

An independent study on the prospects of the divergent pointing mode was made by [253] using early simulations of an array of 23 MSTs. The authors showed that the divergent mode will be significantly superior to the normal pointing mode for source detections, i.e., it will have a superior flux sensitivity. They calculated that by separating the telescope pointings by up to 6° (from the pointing of the inner telescopes to the outermost ones), the needed time for a given flux sensitivity can be reduced by a factor of 2.3, which confirmed the gain in sensitivity seen in the study discussed earlier. As expected, however, the angular and energy reconstruction accuracy for the divergent pointing mode is up to a factor of about two worse than for the normal pointing. Still, such an increase in flux sensitivity is very attractive for the survey, especially because of the increased chances of observing GRBs that occur within the field of view.

The studies of the divergent pointing mode are very promising and will be continued with the latest simulations using the final array layout for the northern and southern arrays in order to reach a robust conclusion on the use of this mode.

9

KSP: Transients

The universe hosts a diverse population of astrophysical objects, within our Galaxy and beyond, that explode or flare up in dramatic and unpredictable fashion across the electromagnetic spectrum and over a broad range of timescales spanning milliseconds to years. Collectively designated “transients”, many are known to be emitters of high energy gamma rays and are also potential sources of non-photonic signals that include cosmic rays, neutrinos, and/or gravitational waves (GWs). They are of great scientific interest, being associated with catastrophic events involving relativistic compact objects such as neutron stars (NSs) and black holes (BHs) that manifest the most extreme physical conditions in the universe. However, their dynamic nature has often hindered detailed observational characterisation and robust physical understanding. One of the key strengths of CTA is the unprecedented sensitivity in VHE gamma rays for transient phenomena and short timescale variability [18], which can revolutionise our knowledge of cosmic transients. Its relatively large field of view (FoV) is also a crucial asset in discovering transient events on its own, as well as in following up alerts of transients issued by monitoring instruments.

In this context, we propose follow-up observations of six classes of targets (denoted A-F) triggered by external or internal alerts, together with an unbiased survey for transients utilising divergent pointing observations (G).

(A) **Gamma-ray bursts** (GRBs), based on external alerts from monitoring facilities. Thought to be triggered by special types of stellar collapse and merger events involving NSs and/or BHs, these highly luminous and distant explosions in the universe are also one of its most mysterious phenomena, with many basic aspects still poorly understood [14, 254, 255]. In addition to addressing key issues regarding the physics of GRBs, CTA will use GRBs as probes of cosmic-ray physics, observational cosmology, and fundamental physics [14, 31, 256].

(B) **Galactic transients,** based on external alerts from monitoring facilities. A wide range of compact objects in our Galaxy exhibit different types of jets and winds that accelerate high energy particles in sporadic outbursts, whose production mechanisms can be greatly clarified through CTA observations [15, 20, 257]. These include flares from pulsar wind nebulae (PWNe; relativistic outflows driven by rotating NSs) [15, 258], flares from magnetars (NSs with anomalously high magnetic fields), jet ejection events from microquasars and other X-ray binaries (NSs or BHs accreting matter from a stellar companion) [20, 259], novae (explosions on the surfaces of white dwarfs) [259], etc.

(C) **X-ray, optical, and radio transients,** based on alerts from “transient factory” facilities. Large numbers of X-ray, optical, and radio transient phenomena will be newly identified by current and upcoming transient factories capable of regularly monitoring large areas of the sky in these wavebands [260], including tidal disruption events (TDEs) [261], supernova shock breakout (SSB) events [262], and fast radio bursts (FRBs) [263]. Observing a selected sample of such alerts with CTA offers new strategies for elucidating various known types of transients, as well as the potential for discovering completely new source classes.

(D) **High-energy neutrino transients,** based on alerts from neutrino observatories. Cosmic high-energy neutrinos are clear indicators of hadronic cosmic-ray production [264] and have begun to be detected by current facilities [45], although their origin is yet unclear [265]. CTA follow-up of appropriately selected alerts can determine their origin [266, 267] and can possibly give insight on extragalactic and/or Galactic cosmic rays as well.

(E) **GW transients,** based on alerts from GW observatories. GWs are most prominently expected from cosmic transients and were directly detected for the first time from binary BH merger events [7, 29] without any clear evidence of associated electromagnetic signals [268] (see however Ref. [269]). More GW detections are expected in the coming years, including those of NS mergers accompanied by electromagnetic emission [270], albeit often with large localisation uncertainties. Follow-up by CTA with suitable strategies can play a unique and essential role for identifying and understanding their sources [6, 271].

(F) **Serendipitous VHE transients,** identified via the CTA real-time analysis (RTA) during scheduled CTA observations. The RTA can recognise new transients or flaring states of known sources at very high energies anywhere in the FoV and automatically issue alerts within 30 s [272, 273]. As with transient factory events, follow-up of a selected sample will greatly advance studies of known and unknown transients.

(G) **VHE transient survey,** utilising divergent pointing and in conjunction with the CTA Extragalactic Survey KSP (Chapter 8). As a novel capability of CTA, observations in divergent pointing mode covering a large instantaneous FoV could offer not only more efficient surveying of the extragalactic sky [9, 253, 274], but also unique prospects for a VHE transient survey not biased by alerts. The potential discovery space includes detection of GRBs from their onset and consequently improved tests of Lorentz invariance violation (LIV), searches for new classes of VHE transients, and simultaneous MWL and/or MM studies with other wide FoV facilities of short-duration transients such as SSBs and FRBs.

Key science questions addressed by this KSP include:

- What are the physical mechanisms that drive jets and winds around neutron stars and black holes?
- What are the physical mechanisms that drive GRBs, the most luminous explosions in the universe?
- What is the origin of the ultra-high energy cosmic rays (UHECRs), the highest energy particles in the universe?
- What is the origin of the recently discovered cosmic high-energy neutrinos?
- What is the origin of the recently discovered fast radio bursts?
- What are the sources of GWs and the physical mechanisms that drive them?
- Is Einstein's theory of special relativity correct?
- Are there unknown types of explosive phenomena in the universe?

Validity as a key science project (KSP)

Suitability as a KSP is clear for all targets, as the observing programme proposed here demands:

- expertise of the CTA Consortium to optimise: (i) for A–E, the response to external alerts and MWL/MM co-ordination with other large-scale collaborations, often bound by memoranda of understanding (MoUs),

(ii) for F, internal data communication, and (iii) for G, the array pointing mode and coordination with the extragalactic survey strategy,
- starting observations using partial arrays, for A–F, and
- persistent, dedicated efforts for achieving positive detections for A–E and G, and possibly F as well.

Observing strategy and required time

The strategies and required times are given below for each target class, to be considered provisional guidelines subject to revision in the light of actual findings. At present, we anticipate aggregate observing times of 390 h/yr/site for the two-year early phase, 125 h/yr/site for the first two years of full-array operation, and 95 h/yr/site from the third year onwards, see Table 9.1.

(A) Gamma-ray bursts: We propose that all alerts during dark time with zenith angle less than 70° be followed up by the full array for 2 h each; if a positive detection is achieved, the observations are extended for as long as the target remains detectable. Together with some high-energy alerts not promptly accessible by CTA, the total estimated observing time is 50 h/yr/site, to be distributed equally for each site and each year, starting from the operation of the first large-sized telescopes (LSTs).

(B) Galactic transients: Different observing strategies (e.g., trigger criteria, observing times, site requirements, etc.) are warranted depending on the type of object, as summarised and prioritised. In all, 150 h/yr/site is proposed for the early phase, plus 30 h/yr/site for the first two years of full operation. Further continuation is contingent on the discovery of new sources with fast variability, except for automatic follow-up of magnetar giant flares as part of (A).

(C) X-ray, optical, and radio transients: Their follow-up hold great scientific promise but currently involves various unknowns that preclude the determination of explicit strategies. Nevertheless, to conduct exploratory science along with requisite tests of the alert system, 50 and 10 h/yr/site are proposed for the early and full phases, respectively.

(D) High-energy neutrino transients: Follow-up is proposed for alerts from IceCube and other high-energy neutrino observatories of candidate muon neutrino-induced track events, either multiplets of events that arrive sufficiently close together in time and sky position or single, well-reconstructed events that can be identified as neutrinos with high confidence. The observing time should not exceed 20 h/yr/site for the early phase and 5–10 h/yr/site for the full phase.

Table 9.1: Summary table of proposed maximum observation times for follow-up targets in the Transients KSP. Observations of Galactic transients could be extended beyond year 3 of regular operations if new source classes with fast variability are discovered. The early phase, prior to array completion, is assumed to last for two years.

		Observation times (h yr^{-1} site^{-1})			
Priority	Target class	Early phase	Years 1–2	Years 3–10	Years 1–10
1	GW transients	20	5	5	
2	HE neutrino transients	20	5	5	
3	Serendipitous VHE transients	100	25	25	
4	GRBs	50	50	50	
5	X-ray/optical/radio transients	50	10	10	
6	Galactic transients	150	30	0(?)	
	Total per site (h yr^{-1} site^{-1})	390	125	95	
	Total both sites (h yr^{-1})	780	250	190	
	Total in different CTA phases (h)	1560	500	1520	2020

(E) GW transients: Follow-up of low-latency GW alerts can entail covering large areas of the sky via tiling or divergent pointing for a modest number of expected events, albeit subject to sizeable uncertainties. As with neutrinos, we propose 20 h/yr/site for the early phase and 5–10 h/yr/site afterwards.

(F) Serendipitous VHE transients: Unpredictable by definition, they constitute important exploratory targets whose follow-up prospects depend on the performance of the RTA. Accounting for different possibilities and tests of the system, we propose 100 and 25 h/yr/site for the early and full phases, respectively.

(G) VHE transient survey: To be performed via divergent pointing and concurrently with parts of the extragalactic survey, and the associated observing time will be accounted for in the Extragalactic Survey KSP. Detailed plans for its implementation are to be decided after more comprehensive Monte Carlo predictions for the expected performance become available.

Key data products

Spectra and light curves for each positively detected object on timescales depending on the target class, plus upper limits for a fraction of alerts for A–E. For the most part, data rights can follow the proposed protocol of being proprietary for one year, but selected information should be communicated rapidly in the form of Gamma-ray burst Coordinates Network (GCN)

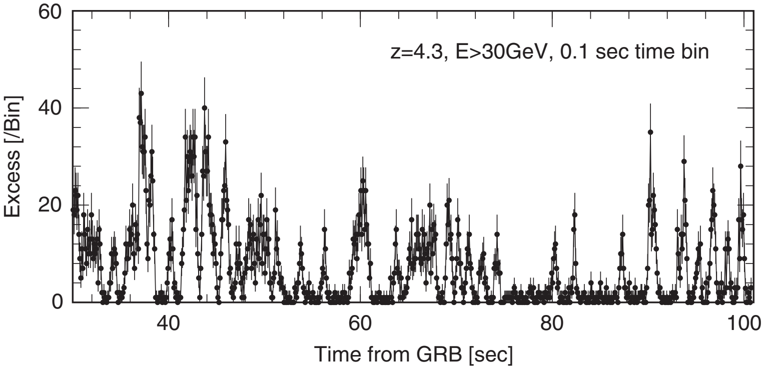

Figure 9.1: Simulated CTA light curve of GRB 080916C at $z = 4.3$, for observed photon energies above 30 GeV with 0.1 s time binning and plotted from $t_0 = 30$ s after burst onset. The assumed template is the measured Fermi-LAT light curve above 0.1 GeV for this burst, extrapolating the intrinsic spectra to very high energies with power-law indices as determined by Fermi-LAT in selected time intervals [275] and taking the EBL model of Ref. [276]. For more details, see Ref. [14].

notices, Astronomer's Telegrams, IAU circulars, etc. to ensure MWL/MM follow-up.

Summary of simulations

Detailed simulations demonstrate that CTA detections of bright GRBs allow measurements of their VHE light curves (Figure 9.1) and spectra (Figure 9.2) in unprecedented detail, from which invaluable information is expected concerning radiation mechanisms, hadronic cosmic-ray signatures, constraints relevant to cosmology and fundamental physics, etc. Simulated observations of PWN flares (Figure 9.3) and X-ray binary jet outbursts (Figure 9.4) exemplify the power of CTA for probing the pertinent mechanisms of emission and particle acceleration.

9.1 Science Targeted

9.1.1 *Scientific Objectives*

(A) Gamma-ray bursts: The most luminous cosmic explosions after the Big Bang are also one of the most enigmatic classes of transients [14, 254, 255]. Phenomenologically, they are defined by a "prompt" emission phase that is prominent in the MeV band with durations in the range T_{90} ~0.01–1000 s and rapid, irregular variability, followed by an "afterglow" phase with emission that decays gradually over hours to weeks or longer and spans all wavebands from radio to high energy gamma rays. Two populations can be distinguished in the distributions of duration and prompt spectra: "long, soft GRBs" with $T_{90} \gtrsim 2\,\mathrm{s}$ and "short, hard GRBs" with $T_{90} \lesssim 2\,\mathrm{s}$ [277]. Both are likely to originate from ultra-relativistic jets, the former triggered by certain types of stellar core collapse events that form NSs or BHs, and the latter widely discussed to be triggered by merger events of NS-NS or NS-BH binaries. However, many of the basic physical properties of GRBs remain poorly understood, such as the nature of the central engine and the mechanisms of jet formation, particle acceleration, and radiation, particularly for the prompt and early afterglow phases. Known to occur at cosmological distances (median redshifts $\bar{z} \sim 2$ and $\bar{z} \sim 0.5$ for long and short GRBs, respectively), they can also serve as important probes of the extragalactic background light (EBL), intergalactic magnetic fields (IGMF) [14, 31], and the fundamental nature of space-time [256, 271]. They are also one of the leading candidates for the currently mysterious sources of UHECRs, the highest energy particles known to exist in the universe [264].

GeV–TeV gamma rays provide crucial insight into all of these issues. Specific science goals that can be addressed by CTA observations of GRBs include:

- determining the velocity of the jet and location of the emission site via intrinsic gamma–gamma absorption features and short timescale variability,
- determining the mechanisms of particle acceleration and radiation for the prompt emission via time-resolved, broadband spectra,
- determining the mechanisms of particle acceleration and radiation for the early afterglow emission,
- testing the GRB origin of UHECRs by revealing hadronic gamma-ray signatures in time-resolved spectra,
- clarifying the global evolution of stars and supermassive black holes (SMBHs) in the universe via gamma–gamma attenuation features due to the EBL over a large range of redshifts, potentially beyond the reach of active galactic nuclei (AGN) at $z > 2$ [30], and
- testing LIV with high precision via energy dependence of photon arrival times.

Thus, outstanding contributions can be expected not only to the astrophysics of GRBs, but also for cosmic-ray physics, observational cosmology, and fundamental physics. For more details, see Section 9.4A and [14].

Note that automated follow-up of GRBs by CTA can occasionally hit upon completely different types of transients such as giant flares of magnetars [278] (see B), magnetar-like behaviour of gamma-ray binaries [279], relativistic SSB events [262], or relativistic TDEs [261] (see E), benefiting the studies of such source classes as well.

(B) Galactic transients: Various types of compact objects in our Galaxy are seen to produce jets, winds, or other kinds of outflows and then convert their energy into high energy particles and radiation, whose physical mechanisms are often not well understood. Although certain classes of such objects are persistent and/or periodically variable emitters, others, listed below, are transients that exhibit irregular and unpredictable variability in different wavebands. Some of the latter are known high-energy (HE; GeV band) gamma-ray sources, but none have been clearly detected so far in VHE gamma rays. CTA observations of these Galactic transients are expected to provide new, critical insight into the underlying physical processes [15, 20, 257].

- Pulsar wind nebulae (PWNe) flares: PWNe are bubbles of relativistic plasma that are energised by magnetically driven winds emanating from rotating NSs. While many are observed as steady sources spanning the radio to VHE bands, the unexpected discovery of bright, HE gamma-ray flares from the Crab nebula have revealed that they can also be transients [258, 280, 281]. CTA observations can discriminate different models that have been proposed and probe the physics of energy dissipation and particle acceleration in pulsar winds [15, 257, 258] (Section 9.4B).
- Magnetar giant flares: Magnetars are NSs thought to be powered by the energy of their anomalously high magnetic fields rather than their rotation [278]. On rare occasions, they trigger giant flares, primarily in MeV photons, which are the brightest bursts of extra-solar radiation ever observed. To date, only three such flares (one each in 1979, 1998, and 2004) are known, and (to our knowledge) none have been properly observed above GeV energies, despite some predictions for HE afterglow emission [282]. CTA follow-up may provide the first VHE coverage of such flares and offer fresh clues to their mysterious origin.
- Microquasars: NSs or BHs activated by accreting matter from their companion stars can be classified according to their companion mass into high-mass or low-mass X-ray binaries (HMXBs or LMXBs). A subset of them are observed to generate collimated jets of plasma in sporadic outbursts and are called microquasars [20, 259, 283]. Some HMXB microquasars such as Cyg X-3 and Cyg X-1 are known sources of HE gamma rays [203, 284, 285] whose emission mechanisms (e.g., leptonic or

hadronic) are still unclear, while some LMXB microquasars such as GRS 1915+105 have long been predicted to be gamma-ray emitters [283]. MWL observations featuring CTA will provide not only crucial tests of emission models (Section 9.4B), but also new insight into the long-standing problem of astrophysical jet formation [20, 259].

- Transient binary pulsars: Some X-ray binary pulsars that display transient behaviour may contain pulsar winds interacting with material from their stellar companions and emit GeV–TeV gamma rays in a way analogous to some known, periodic gamma-ray binaries [259]. These include Be/X-ray binary pulsars that show aperiodic X-ray outbursts [286] and transitional pulsars that switch between rotation-powered and accretion-powered phases [287]. Their study with CTA will shed new light on the physics of pulsar winds, accretion onto NSs, and binary pulsar evolution.
- Novae: Under certain conditions, matter accreting onto white dwarfs undergoes thermonuclear explosions and give rise to novae, with thermal optical emission lasting days to weeks. Unexpectedly, HE gamma rays were detected from several novae and interpreted as emission from particles accelerated by shocks in their expanding ejecta [259, 288]. Many uncertainties remain concerning the mechanisms of radiation and particle acceleration that can be clarified by CTA observations [259, 289].
- Unidentified HE transients: Wide-field instruments operating at GeV energies, such as Fermi-LAT, AGILE, DAMPE, or upcoming missions, are capable of discovering new HE transients in the Galactic plane that may not be immediately identifiable with known objects [290]. Follow-up with CTA can play a crucial role in clarifying their nature or possibly unravelling new types of Galactic transients.

(C) X-ray, optical, and radio transients: Wide-field monitoring facilities operating in the X-ray to soft gamma-ray bands (hereafter simply "X-rays" unless indicated otherwise), as exemplified currently by Swift and INTEGRAL and to be succeeded by SVOM, have proven to be effective transient factories, capable of discovering a large variety of transient phenomena over a broad range of timescales [291]. New and upcoming optical transient factories such as GAIA, Pan-STARRS, iPTF, ZTF, and LSST [292] as well as radio transient factories such as SKA and its pathfinders LOFAR, MeerKAT, MWA, and ASKAP [293] (see details in Chapter 2) guarantee a revolution in our physical understanding of the transient universe [260]. Besides GRBs and the Galactic transients mentioned above, thousands of sources of a very diverse nature are expected to be discovered, from nearby flaring stars with extreme non-thermal variability [294] to orphan GRB afterglows at cosmological distances [295]. Thus, following up properly selected alerts from X-ray/optical/radio transient factories with CTA will pave a new and unexplored path to study the universe in VHE gamma rays, with great promise for exciting results in widely disparate areas of astrophysics. Some particularly noteworthy classes of expected transients are as follows:

- Tidal disruption events (TDEs): All sufficiently massive galaxies are expected to harbour SMBHs in their central regions. They can occasionally brighten in the optical to soft X-ray bands via a transient accretion event lasting weeks to months caused by tidal disruption of an approaching star or gas cloud [261]. A fraction of them are relativistic TDEs that are transient versions of blazars, co-producing jets with prominent non-thermal radio to hard X-ray emission [296, 297]. HE/VHE emission has been predicted for such events as well as for non-relativistic TDEs [298], but the predictions are yet to be critically tested. CTA follow-up observations can bring forth fresh insight into the physics of tidal disruption, as well as new perspectives on jet formation by SMBHs that are complementary to observations of AGN [30].
- Supernova shock breakout (SSB): Besides their emission powered by radioactive decay on timescales of weeks, early UV to X-ray flashes are expected from supernovae due to shock-heated ejecta on timescales of hours. A subset of such events found by Swift on minute-timescales involve relativistic ejecta and may (or may not) be associated with low-luminosity GRBs [262, 299, 300]. Detection by CTA of correlated VHE emission [301], either via rapid follow-up or via a simultaneous VHE survey, can probe particle acceleration in radiation-rich environments, supernova explosion dynamics, and its connection with GRBs.
- Fast radio bursts (FRBs): Radio surveys with wide FoV and high time resolution have unexpectedly uncovered GHz-frequency, millisecond-duration FRBs [36, 37]. Apart from redshifts $z \sim 0.2$–1.3 inferred from their large dispersion measures, their origin is unclear, and a plethora of models have been proposed [263]. MWL follow-up of one FRB alert has led to the possible identification of a radio afterglow and an elliptical host galaxy, implying a progenitor akin to NS–NS mergers [302] and an intriguing potential link between FRBs, short GRBs, and GW events (see A, E above). However, doubts have been raised for this particular case [303]. Another FRB that is so far unique in exhibiting burst repetition [304] was recently localised to sufficient accuracy to be reliably associated

with a dwarf host galaxy at $z \sim 0.2$ and a persistent radio counterpart [305], potentially pointing a young NS origin. There may possibly be more than one class of FRBs. Notwithstanding the current ambiguities, CTA follow-up of selected FRBs can test their supposed connection with young NSs or NS–NS mergers and help to solve their mysterious origin. Note that correlated, millisecond VHE bursts expected in some models [306] can only be realistically tested by a simultaneous radio and VHE survey (see G).

(D) High-energy neutrino transients: Several types of transients covered in this KSP are also promising candidate sources of high-energy neutrinos, whose detection with currently operating or upcoming neutrino facilities would reveal their inner workings in novel ways that are complementary to photons and GWs. Follow-up of neutrino alerts can address the long-standing question of the origin of hadronic cosmic rays if they are transient sources [264]. A new mystery, possibly independent of the directly observed hadronic cosmic rays, is the origin of cosmic neutrinos with TeV–PeV energies discovered by IceCube [45, 265]. While they do not appear to be correlated with bright GRBs or AGN [267], it is possible that they are generated by fainter GRBs/transients or flaring states of persistent objects, some of them perhaps Galactic, that may give rise to VHE gamma rays via processes concurrent with neutrino production. Spatial and temporal coincidence studies between neutrinos and gamma rays can identify their sources, and unequivocally prove hadronic cosmic-ray acceleration therein [266, 267].

(E) GW transients: Cataclysmic transient events such as mergers of binary NSs and/or BHs are predicted to be the strongest sources of GWs. Their direct detection opens up a completely new window to probe the dynamical behaviour of relativistic compact objects, in a way complementary to photons or neutrinos. This long-awaited goal was recently achieved for BH–BH mergers by the LIGO-VIRGO collaboration [7, 29]. With the upcoming network of new-generation observatories comprising LIGO, VIRGO, KAGRA, and INDIGO, many more detections are expected including NS–NS or NS–BH mergers [307]. These are also leading candidates for the progenitors of short GRBs [270, 308] and probable VHE gamma-ray emitters under certain conditions, the nearest of which could occur within the expected detection horizon of GW observatories [6, 271]. However, for their first years of operation, the localisation errors of GW events are expected to be very large, typically spanning 100–1000 deg^2, as was indeed the case for the first detections [29, 268]. Even after the detectors reach full performance, large localisation errors can still be the case for events near the sensitivity limit. Thanks to the relatively large FoV, especially if divergent pointing can be employed, CTA follow-up of GW candidates may offer better localisation prospects compared to other wavebands through more efficient searches over larger areas of the sky for their electromagnetic counterparts. This will provide the impetus for further, extensive MWL follow-up that may reveal the source, distance, and energetics of these events.

(F) Serendipitous VHE transients: One of the key advantages of CTA is its high instantaneous sensitivity combined with its large FoV of several degrees. This offers the tantalising possibility of serendipitously discovering transient VHE sources within the FoV during any observation. In this context, the RTA system can identify flaring sources in the FoV in less than 30 s from data taking, with a sensitivity at most a factor of three worse than the final analysis [273]. Therefore, the RTA system will provide serendipitous discoveries of new VHE gamma-ray sources in the FoV, which should be observed more deeply by extending the observations being conducted at any time. The RTA will also automatically issue alerts to the outside community to promote MWL follow-up. The nature of such serendipitous VHE transients can be any of those described above, or, more interestingly, of a new and unexpected class.

(G) VHE transient survey: By virtue of the large number of its constituent telescopes, CTA offers the novel capability of observations in divergent pointing mode, whereby the telescopes (primarily MSTs) are pointed in progressively offset directions to allow simultaneous coverage of a considerably larger FoV compared to normal pointing mode [9, 253, 274]. While this entails some loss in energy resolution and angular resolution and some increase in energy threshold, the enlarged FoV can compensate for these losses and enable more efficient surveys for persistent point sources, a potentially crucial asset for the Extragalactic Survey (see Chapter 8). Furthermore, it can provide enhanced prospects and unique discovery space for elucidating cosmic transients at very high energies without relying on follow-up of alerts, in particular:

- detection of GRBs from their onset, including the prompt phase of short GRBs and associated improvements for probing LIV,
- unbiased searches for VHE transients in general, including new classes of transients, and
- MWL and/or MM spatio-temporal correlation studies with other observatories with wide FoV and/or limited localisation capabilities, including

simultaneous MWL observations of short-duration transients such as SSBs [262, 301] and FRBs [306, 309].

9.1.2 *Context/Advance beyond State of the Art*

(A) Gamma-ray bursts: Fermi-LAT has been detecting GeV-band emission from GRBs at a rate of $\gtrsim$10 yr^{-1}, totalling $\sim$120 as of December 2016, revealing a rich phenomenology [310]: (i) most MeV-bright GRBs are accompanied by GeV emission whose flux is generally consistent with extrapolations of the measured MeV spectra, (ii) the GeV emission often extends up to $\sim$10–30 GeV, and occasionally to $\sim$100 GeV, with no conspicuous spectral cutoffs (with one exception [311]), (iii) the few brightest GRBs clearly exhibit a hard spectral component that significantly exceeds simple extrapolations of the MeV spectra, (iv) GeV emission is generally observed during the prompt as well as the afterglow phase, lasting up to a few thousand seconds, and occasionally to $\sim$1 day, (v) GeV emission is seen in both long and short GRBs, and (vi) current observations are not inconsistent with the majority of GRBs possessing such high-energy emission, including fainter GRBs (although $\sim$20% of MeV-bright GRBs show indirect evidence for some sort of spectral break between MeV and GeV [312]).

These observations, particularly of photons at a few GeV and above, have led to some important physical insight, including significantly higher velocities of the emission zone than had been inferred previously [275], evidence for non-trivial mechanisms of emission and/or particle acceleration during the early afterglow [313, 314], constraints on the EBL at the highest redshifts so far [315], and the strongest limits to date on the violation of Lorentz invariance [316, 317]. Nevertheless, in many cases, the limited photon statistics achievable with Fermi-LAT at tens of GeV have prevented firm conclusions, and many competing theoretical models remain viable. Imaging atmospheric Cherenkov telescope (IACT) observations of GRBs can potentially provide significant progress through much higher photon statistics (see Figures 9.1, 9.2 and Section 9.4A for more details). However, the sensitivity and energy threshold of current IACTs imply a detection rate that is considerably less than $\sim$1 GRB yr^{-1}, and no GRB has been clearly detected so far despite efforts over the last decade [318–320]. CTA can lead to a major breakthrough by detecting GRBs at an appreciable rate of $\gtrsim$1 yr^{-1} with far superior photon statistics compared to Fermi-LAT in the pivotal energy range above 10 GeV [14, 321, 322].

HAWC may be able to detect GRBs at a rate of $\sim$1 yr^{-1} without external alerts from their onset, albeit with much higher energy threshold and lower sensitivity [323, 324]. CTA follow-up offers significant advantages with more sensitive observations down to considerably lower energies for studying long GRBs and the afterglows of short GRBs, the latter of which will also be key for identifying GW sources (see D below). Even the prompt emission of short GRBs may be accessible to CTA if they can be caught during a survey with divergent pointing, with particularly interesting implications for testing LIV (see G below). On the other hand, an intriguing prospect is follow-up of GRBs detected and alerted by HAWC, which would be almost guaranteed to be detectable by CTA as long as the alert is fast enough.

(B) Galactic transients: None of our proposed target classes have been unambiguously detected as transients at very high energies. Those observed by Fermi-LAT and/or AGILE as transient sources of HE gamma rays on timescales of hours to days include PWN flares from the Crab nebula [280, 281], the HMXB microquasars Cyg X-3 [203, 284] and Cyg X-1 [285, 325, 326], several novae [288], and the transitional pulsar PSR J1023 + 0038 [287]. A few unidentified HE transients have also been seen at low Galactic latitudes, although some, or all, of them may be extragalactic [290]. No signals have been seen yet in IACT observations of Crab nebula flares [327–329], Cyg X-3 [330], or novae [331] (see however tentative evidence for Cyg X-1 [332]). Except for some novae, current IACT upper limits are insufficient to constrain spectral turnovers between the HE and VHE bands, so more sensitive observations with CTA are warranted to characterise the maximum energy and nature (leptonic or hadronic) of the radiating particles.

Despite high expectations on both theoretical and empirical grounds [283], LMXB microquasars such as GRS 1915+105 have so far not been detected above GeV energies [326], nor have transient Be/X-ray binary pulsars such as 1A 0535+262 [286]. To our knowledge, no proper HE or VHE observations have been conducted yet for the rare giant flares from magnetars [282]. CTA observations of these objects may allow the first detailed exploration of their behaviour in the gamma-ray domain.

HAWC may be able to detect Crab nebula flares at multi-TeV energies [190] and possibly provide alerts to CTA for more sensitive follow-up observations. However, other types of transients may be more difficult for HAWC, especially if they have VHE spectral breaks that are expected for some objects. Through detailed coverage of the highest energy electromagnetic window, MWL studies of Galactic transients featuring CTA could clarify the relevant mechanisms of particle acceleration and radiation, as well as the associated physical conditions concerning magnetic fields, matter, and radiation density.

(C) X-ray, optical, and radio transients: So far, dozens of candidate TDEs have been observed in the optical and/or X-ray bands, but only a handful of them have been identified as relativistic TDEs with jets [261, 296, 297]. Although searches for a few such objects in the GeV [296, 333] and TeV [334, 335] bands have been negative, systematic and comprehensive studies of TDEs at these energies have yet to be conducted. Only a small number of SSB events have been discovered to date in the optical and/or X-ray bands [262], with proper coverage lacking above GeV. The situation is expected to improve with new optical and X-ray transient factories that can detect and provide alerts for many more TDEs and SSBs by the time of full CTA operation.

Real-time alerts of FRBs have begun to be issued only recently, with typical latency of a few hours [302]. A follow-up observation was conducted ∼15 h afterwards by H.E.S.S., yielding the first upper limits on VHE afterglow emission from an FRB [336]. Upcoming radio facilities with improved capabilities for FRB identification should allow more efficient follow-up for a larger number of events, critically constraining FRB models and helping to solve their mysterious origin.

More generally, new types of X-ray, radio, and optical transients are likely to be discovered by transient factories that will come online during the following years; these are not yet providing alerts for current IACTs (although some tests have already been conducted, e.g., LOFAR-MAGIC). The follow-up of sources triggered by transient factories will basically be a MWL effort, where CTA will play a key role in elucidating the high-energy end of the electromagnetic spectrum, significantly improving upon the capabilities of Fermi-LAT, AGILE, and/or HAWC for the detection of fast transient sources.

(D) High-energy neutrino transients: The IceCube observatory reported the first evidence for extraterrestrial high-energy neutrinos in the energy range of 30 TeV–2 PeV, with a diffuse flux significantly in excess of the expected atmospheric neutrino background [45, 265]. Their sky distribution is consistent with isotropy, and no significant correlations with known astrophysical objects have been found so far. The lack of a correlation is not surprising as the majority of the detections are cascade-type events with large positional uncertainties of $\sim 10^\circ$. The neutrinos are likely produced in inelastic interactions between hadrons accelerated to >PeV energies and ambient low-energy photons and/or hadrons. VHE photons are inevitably co-produced in these interactions and may be observable as long as they escape the source and propagate unattenuated.

Detection of such components would not only provide a critical means to identify and elucidate the neutrino sources, but also greatly contribute to solving the long-standing puzzle of the origin of UHECRs and/or Galactic cosmic rays. If the sources are transient, follow-up by CTA of appropriate alerts from neutrino facilities can achieve much better sensitivity compared to Fermi-LAT or HAWC [18].

MWL follow-up programmes of neutrino alerts from IceCube and ANTARES have been carried out by telescopes in the optical, X-ray, and VHE gamma-ray bands, including MAGIC [267], VERITAS [337], and H.E.S.S. [338], albeit with no positive detections to date. ANTARES alerts rely on real-time event reconstruction of single, upgoing candidates, whose detection threshold is tuned to give acceptable rates for optical or X-ray follow-up [339]. The first IceCube alert program, in operation since 2011, has been based on a predefined list of sources, mostly AGN, when an increase in the rate of upgoing neutrino candidate events (multiplets or clusters) is seen at a source position above a certain threshold, which is adjusted to yield a tolerable false alert rate of a few per year [266, 340]. Since 2016, new alert channels were activated based on real-time, online event reconstruction that identifies single-muon neutrino-induced track events with high confidence and localisation accuracies of order of one degree or better, caused by either extremely high-energy through-going events [266] or high-energy starting events with contained interaction vertices [267]. Under consideration is an unbiased, full-sky scan for upgoing multiplets without relying on a predefined source list. Availability of an equally sensitive installation in the northern hemisphere (e.g., KM3NeT [341] and GVD [342]) is still uncertain but would increase the sensitivity towards the southern sky and permit lower energy thresholds for Galactic sources. A substantial expansion of IceCube is also being proposed for the future [343].

(E) GW transients: The momentous discovery of GW150914 by LIGO-VIRGO heralded the birth of GW astronomy [7]. Quite surprisingly, this was a BH–BH merger event [27], in contrast to most predictions that the first GW detections would be coalescence events of NS–NS or NS–BH binaries. The event was followed up by numerous facilities covering the entire electromagnetic spectrum [268], as well as HE neutrinos [344], with almost all follow-ups yielding null results, as had been expected for BH–BH mergers. However, the report of a low-significance, time-coincident signal by Fermi-GBM [269] has provoked a number of new theoretical suggestions for potential electromagnetic signals from binary BH mergers (see, e.g., Ref. [345]) which must be tested through further observations.

Eventual GW detections of NS–NS or NS–BH mergers are also highly anticipated [307], as are associated electromagnetic signals [270]. These events are also the most promising progenitors of short GRBs, from which VHE afterglow emission is predicted for the fraction of events with their GRB-emitting jets pointing close to our line of sight [316], in contrast to the GW emission that should be nearly isotropic. Although GW alerts are expected to have large localisation errors with areas having non-trivial topology and spanning 100–1000 deg^2, especially for the first few years of LIGO-VIRGO, follow-up should still be manageable with CTA through either tiling or divergent pointing strategies [6].

In view of the difficulty of wide-field instruments at other wavebands in effectively covering sky regions as large as 1000 deg^2 and the relative brightness of the high energy afterglow from short GRBs compared to its optical counterpart, CTA may provide the best localisation prospects and enable subsequent MWL follow-up of a manageable region of the sky. Compact binary mergers can also eject a significant amount of fast material in directions away from the GRB jet axis [346]. The interaction of that material with ambient media may possibly induce additional high energy emission, even for non-GRB, off-axis GW events [347]. The detection of such components will provide unique information concerning the dynamics of these events, complementing potential electromagnetic counterparts at other wavelengths (e.g., optical/infrared "kilonovae" [348]). Follow-up is therefore warranted for all GW alerts that are accessible to CTA.

(F) Serendipitous VHE transients: To our knowledge, there has not been any new VHE transient that occurred serendipitously in the FoV during observations by existing IACTs. A systematic search in the Fermi-LAT data for variable sources on weekly timescales has identified numerous flaring sources, most of which can be associated with blazars and with no strong evidence for new Galactic transients beyond novae and the Crab nebula [290]. HAWC may discover VHE transients without external alerts by virtue of its wide FoV and high duty cycle, particularly GRBs and PWN flares (see A, B above). If alerts for such HAWC detections are available sufficiently rapidly, they can be followed up by CTA with its higher sensitivity and lower energy threshold to obtain much more information.

(G) VHE transient survey: Divergent pointing observations by CTA will be an unprecedented endeavour for IACTs. It will offer the prospects for an unbiased survey of GRBs and other transients at very high energies, beyond the energy range of Fermi-LAT and at much better sensitivity and lower energy threshold compared to HAWC [9, 253, 274]. This capability will be of special importance in the currently burgeoning era of time domain astronomy, with numerous other facilities already operating, or soon coming online, that are geared to surveying large areas of the sky for transient phenomena, particularly in the optical and radio bands (Chapter 2). An intriguing possibility is coordinated, simultaneous MWL observations of the same regions of the sky by CTA and such facilities which could enable the first comprehensive studies of transients with short durations.

9.2 Strategy

It is highly desirable to begin transient follow-up observations with CTA as soon as possible, including with partial arrays during construction. An early start is warranted due to the infrequent nature and uncertain flux of the transients, for example one should not miss a once per decade transient event due to incomplete telescope array commissioning and verification. Such observations are very suitable for early high-risk execution (unlike for example, precision measurements of known systems) and can be effectively managed by the CTA Consortium due to its extensive scientific and technical knowledge. It may be necessary to invest a significant amount of time before a successful detection, and trigger conditions will need to be modified based on experience. All of this makes the transient programme well suited to execution as a Key Science Project.

Described below are the observing strategies for each target class. In case follow-up demands arise simultaneously for different classes, we prioritise those that are expected to be rarer, less time consuming, and of potentially higher scientific impact, in the following order: (1) GW transients, (2) HE neutrino transients, (3) serendipitous VHE transients, (4) GRBs, (5) X-ray/optical/radio transients, and (6) Galactic transients. The proposed strategies and prioritisation are provisional and subject to change depending on what is actually observed and how the fields evolve scientifically.

(A) Gamma-ray bursts: Alerts during operation of CTA are expected primarily from soft gamma-ray instruments such as Swift, Fermi-GBM, and SVOM, the latter planned to be launched no later than 2021 [349]. Additional, albeit rarer, alerts can come from wide-field instruments in high energy gamma rays such as Fermi-LAT, DAMPE, HAWC, and LHAASO, and possibly also from instruments in other wavebands such as GAIA, LSST, etc. As cosmologically distant objects, they should be uniformly distributed across the entire sky with equal rates for the CTA southern and northern

Table 9.2: Summary of GRB follow-up strategy and observing time for one array site.

Strategy	Expected event rate (yr^{-1})	Exposure per follow-up (h)	Exposure per year (h yr^{-1})
Prompt follow-up of accessible alerts	∼12	2	25
Extended follow-up for detections	0.5–1.5	10–15	10–15
Late-time follow-up of HE GRBs Not accessible promptly	∼1	10	10

Note: The numbers are equal for the CTA-South and CTA-North sites.

sites. In view of EBL attenuation typically expected at higher energies, the LSTs will be vital for follow-up, having the lowest energy threshold and the fastest slewing capabilities of the three CTA telescope types. Nonetheless, the full array including MSTs and SSTs should be slewed to maximise the sensitivity at all energies. The full array will be particularly important if the redshift turns out to be $z \lesssim 1$ (see, e.g., Ref. [313]), in which case the detection of even multi-TeV photons may be feasible for a bright event [14].

We propose the following strategy for GRB observations, as summarised in Table 9.2:

1. Prompt follow-up by the full array of all 'accessible' GRB alerts, i.e., those occurring during dark time and having zenith angles less than 70 degrees, with exposure of 2 h for each alert. The expected alert rates are ∼5/yr/site for Swift or SVOM and ∼10/yr/site for Fermi-GBM [14, 321, 322], totalling ∼12/yr/site when accounting for some overlap. For Fermi-GBM alerts with localisation errors larger than the LST FoV, some form of scanning or multiple-pointing (tiling) observation may be advantageous [350], whereas the alternative possibility of employing divergent pointing of LSTs has been deemed less effective from preliminary studies. All available telescopes, particularly all LSTs, should always be employed to guarantee maximum sensitivity at the lowest energies, as the detailed properties of GRBs can vary greatly from burst to burst.
2. Extended observations for detected GRBs with the full array. The RTA system will clarify whether VHE photons are detected with a latency of 30 s, in which case the observation should continue for as long as the target is visible and detectable. The predicted GRB detection rates are of order ∼1/yr/site [321, 322].
3. Late-time follow-up of high-energy GRBs not accessible promptly with the full array. Cases may be expected where a bright GRB is detected

by Fermi-LAT, DAMPE, HAWC, or LHAASO but is not accessible immediately to CTA by occurring on the other side of the Earth at trigger time. These should be followed up as soon as the target becomes visible, for which we estimate a rate of ∼1/yr/site.

Some important caveats concerning the detection rate predictions quoted above are discussed in Section 9.4A. Note that additional follow-up observations during partial moon time is feasible and can increase the detection rate by ∼50%. Analysis of GRB data may be amenable to looser selection cuts for background rejection and correspondingly lower energy thresholds compared to standard analysis criteria, allowing access to spectral regions less affected by EBL absorption. On the other hand, some data may be taken while the telescopes are slewing; such data will need to be carefully calibrated on the basis of a good understanding of the behaviour of the telescopes under such conditions.

Contemporaneous MWL follow-up with available facilities covering the entire electromagnetic spectrum should be utilised whenever possible to obtain complementary data. A prime motivation is good characterisation of the time-dependent, broadband spectra of the afterglow, in order to pin down key physical quantities such the total burst energy, jet collimation angle, and ambient density. Of utmost importance is the determination of the GRB redshift by optical/infrared telescopes, the failure of which would seriously compromise the science return, especially in view of the modest expected detection rates. For this purpose, in addition to maximal cooperation with external observers, it is desirable to have an on-site telescope dedicated for CTA follow-up, which can localise a majority of the afterglows to sufficient accuracy so that larger telescopes can be alerted for spectroscopic follow-up. Infrared coverage is preferable to cope with optically dark GRBs that constitute a large fraction of all afterglows [351], but may only be viable with external telescopes in view of cost limitations.

The demand for ground-based localisation may become somewhat less urgent once SVOM is launched, whose on-board optical telescope with red coverage can localise up to ∼70% of afterglows by itself. Note that the probability of GRB redshift determination is currently higher in the north than the south by ∼50%, thanks to the prevalence of telescopes and astronomical communities available for follow-up [352]. GRBs may also be detected by GW or neutrino observatories (Sections 9.1.1C and 9.1.1D). Low significance (sub-threshold) detections may be useful for coincident searches among multiple observatories, and thus CTA should participate in relevant networks such as the Astrophysical Multi-messenger Observatory Network (AMON).[a]

(B) Galactic transients: The targets proposed for this KSP are listed in Table 9.3. We have tentatively provided prioritisation among them, in case multiple source classes happen to be active at the same time. Magnetar giant flares are placed first due to their rarity, short duration, extraordinary properties, and lack of precedent gamma-ray coverage. HE-detected source classes follow, roughly in order of their typical duration of activity: PWN (Crab) flares, HMXB microquasars (Cyg X-3 and Cyg X-1), and unidentified HE transients. LMXB microquasars are placed next in view of their high expectations despite not yet being clearly detected at high energies (see however Ref. [353]). Novae and transitional pulsars are given lower priority on account of their expected spectral turnovers above the HE band, followed by Be/X-ray binary pulsars. We emphasise that this ordering is provisional and is open to change in response to what is actually observed and how the field develops during the course of this KSP.

Since we are exploring the unknown for all of these sources, trigger criteria are not provided in detail here and will be determined based on the actual evolution of the transient phenomena. Approximate trigger rates for CTA follow-up, their urgency, and duration of activity are given, together with the total number of hours of observation per transient episode and sites to be used. For sources with priority rank 5–8, we propose to trigger only in 2–3 cases with good enough sensitivity. A total observation time of 150 h/yr/site is estimated for Galactic transients during the early phases of CTA, and of 30 h/yr/site during the first two years of regular operations. Extension of this observation time into years 3–10 of full operations is contingent on the discovery of new Galactic source classes that show fast variability. The general requirements for observations will be zenith angles below 50° (70° for PWN flares) and any weather conditions.

Simultaneous MWL follow-up observations should be arranged for all targets to maximise the scientific output. The best approach would be to collaborate with existing teams of experts (internal or external to CTA) that already have granted observing time in multiple facilities. Efforts are warranted to establish collaborations with such teams prior to the early science phase. Furthermore, a dedicated, on-site, 0.5–1 m class optical telescope can provide important benefits, including coordinated optical photometry to clarify various thermal and non-thermal processes and possibly polarimetry

---

[a] see http://amon.gravity.psu.edu/index.shtml

Table 9.3: Summary table of Galactic transients proposed within the Transient KSP during the early phase of CTA.

Follow-up priority	Target class	Detected @ HE	Trigger	Rate (yr^{-1})	Urgency	Activity duration	Obs. time (h) /night	Total time (h)	Site
1	Magnetar giant flares	–	MeV	0.1	1 min	1–2 d	Max. 1	10	A/B
2	PWN flares: Crab nebula	Y	HE	1	1 d	5–20 d (HE)	4	50	S&N
3	HMXB microquasars:								
	Cyg X-3	Y	HE/X-ray	0.5	1 d	50–70 d (HE)	Max. 1	50	N
	Cyg X-1	Y	HE/X-ray	0.2	1 d	1–10 d ?	Max. 1	30	N
4	Unidentified HE transients	Y	HE	1	1 d	?	2	20	A/B
5	LMXB microquasars	?	X-ray/radio	1	1 d	Weeks	2	20	A/B
6	Novae	Y	HE/opt.	2	1 d	Weeks	2	20	A/B
7	Transitional pulsars	Y	Radio/opt.	0.5	1 d	Weeks	2	20	A/B
8	Be/X-ray binary pulsars	N	X-ray	1	1 d	Weeks	2	20	A/B

Note: The codes for the last column are: S (south), N (north, A (any), and B (both, if possible).

to obtain valuable complementary information on magnetic fields, density of ambient gas, etc.

(C) X-ray, optical, and radio transients: To exploit the potential of X-ray, optical, and radio transient factories, we suggest 50 h/yr/site during the early phase to test and tune the filter and trigger response system based on responding to promising bright transients. Thereafter, we consider 10 h/yr/site during regular operations to use the tuned filters to follow-up on the many new transient alerts we expect to receive.

The systems for responding to X-ray alerts from Swift, INTEGRAL, or SVOM are already well established for current IACTs and can be generally followed for CTA as well. Based on existing data, we do not expect the rate of alerts for transients of interest such as TDEs or SSBs to exceed those of GRBs. On the other hand, planning concrete strategies at this moment for follow-up to optical or radio transient factory alerts is challenging, due to numerous uncertainties concerning the actual performance of each facility, the latency for receiving different types of alerts, and the extent of the information that will be available. This is especially the case for fast transients such as FRBs. Nevertheless, a sketch of some possible strategies can be outlined for the relatively slower, Galactic transients. For example, optical transient factories are expected to discover large numbers of novae. Several novae have been detected by Fermi-LAT in HE gamma rays [288], and current IACTs are searching for VHE gamma rays from these objects, as predicted in some hadronic models. We expect that observations conducted by these and other high-energy facilities during the following years will provide a clearer picture as to what the best trigger conditions may be for follow-up with CTA. Possible filtering criteria could be based on optical magnitude (to select nearby objects), nova type (nature of the companion and expected physical behaviour), properties of the HE gamma rays detected by Fermi, etc. Similar exercises will also be conducted for other types of objects during the following years and prior to the early science of CTA, such that the optimal methodology can be developed for selecting the particular types of transient factory alerts that are most interesting for our aims.

(D) High-energy neutrino transients: Follow-up with the full CTA is proposed for three different types of neutrino alerts, which are already being issued by IceCube for current IACTs:

1. *Upgoing multiplets:* The strategy that is already being pursued by IceCube and present IACTs is based on event multiplets for a predefined list of known objects, consisting mostly of AGN in the northern

hemisphere [338, 340]. Alerts to IACTs are issued whenever IceCube observes an increase in the rate of upgoing neutrino candidate events from the positions of the listed sources above a certain threshold, whose significance is adjusted to around three standard deviations so that the false alarm rate remains at a tolerable level of a few/year. The search algorithms analyse all time intervals ranging from seconds up to 3 weeks, covering the known range of AGN flare durations.

2. *Extremely high energy events:* A real-time, online system in operation since July 2016 that can identify through-going, track-type events induced by muon neutrinos of >160 TeV energy with very high confidence [266]. It is capable of issuing alerts with a latency of ∼30 s and localisation accuracy of a fraction of a degree (0.22° median angular resolution). The expected event rate is ∼4/year from the whole sky, about half of which will be of atmospheric origin.
3. *High-energy starting events:* An alternative system operating since April 2016 that is real-time, online and with relatively low background distinguishes track-type events due to $\gtrsim$100 TeV muon neutrinos whose primary interaction vertices are well-reconstructed within the IceCube detector volume, utilising the veto technique that enabled the first identification of astrophysical high-energy neutrinos [45]. The alert latency is similar to extremely high energy events, while the localisation accuracy is 0.4–0.6° (median angular resolution). The event rate is expected to be around 4 per year in all regions of the sky but with a higher expected atmospheric event rate of ∼75%.

Analogous to the strategy for GRBs, we propose follow-up of all alerts during dark time with zenith angle (at the CTA site) less than 70° for at least 2 h each. The exposure would be extended if RTA reveals a transient signal. The rate of all accessible neutrino alerts will be a few/year/site, consisting mostly of Types 2 and 3 with a small fraction of Type 1. Note that the frequency of alerts can be increased by relaxing the relevant threshold. In view of various uncertainties, during the early phase of CTA, we propose a total of 20 h/yr for each site in order to develop and fine tune the follow-up strategies with the IceCube collaboration. After full operations, a total of 5–10 h/yr for each site is deemed sufficient.

Depending on the extent of the information that will be publicly disclosed for the alerts, MoUs between IceCube and the CTA Consortium may be warranted. If the RTA uncovers a gamma-ray signal, further alerts should be sent out rapidly to the community in order to identify the source through

MWL follow-up in all possible wavebands (although some X-ray and optical facilities that have MoUs with IceCube may directly follow-up the alerts from IceCube).

Other strategies for follow-up of neutrino alerts from IceCube may be implemented, such as an unbiased, full-sky scan of upgoing multiplets without recourse to a predefined source list or online identification of UHE tau neutrino events. Several scenarios are under discussion to enhance the IceCube detector itself, many of which invoke an augmented fiducial volume to increase the sensitivity to TeV–PeV neutrinos [343], which would also increase the number of issuable triggers. Construction of northern observatories such as KM3NeT or GVD would also improve the prospects substantially. The CTA neutrino follow-up program should evolve in accordance with such future developments.

(E) GW transients: The CTA Consortium will receive GW alerts from LIGO-VIRGO as stipulated in the MoU that has already been signed. Follow-up strategies for GW alerts may involve tiling or divergent pointing strategies for localisations with large uncertainties, to be assessed in detail once Monte Carlo simulations of the corresponding sensitivity become available. For very large localisation errors, an alternative strategy may be to target nearby galaxies within the regions of highest probability for GW emission. Although the most plausible prediction for VHE emission is from short GRB afterglows in the fraction of NS–NS or NS–BH mergers with their GRB jet axes close to the line of sight [6], it is generally not possible to know before the alert whether this will be the case or not. Some VHE emission may also be possible from non-GRB, off-axis GW events due to interaction of fast ejecta and ambient media. Following the discovery of GW150914, various theoretical proposals have been put forth for electromagnetic signals accompanying BH–BH mergers and these should be observationally tested. This motivates the follow-up of all accessible GW alerts. The all-sky detection rate in GWs of binary NS mergers is quite uncertain, but is expected to be 40/yr (with a range of 0.4–400/yr) for full LIGO-VIRGO [49]. Initial LIGO results may suggest even higher rates for binary BH mergers [354]; these rates should become clearer within the next few years.

As with GRBs and neutrinos, we consider follow-up of all GW alerts during dark time with zenith angles less than 70° for 2 h each, with additional exposure in the case of positive detections. Taking only the higher range of rate estimates for binary NS mergers, the rate of real alerts would be $\sim$1–10/yr/site, with a corresponding observing time of $\sim$2–20 h/yr/site. The expected detection rate for on-axis, short GRB afterglows jointly with GWs is only $\lesssim$0.03/yr [6], while that for off-axis GW events is more difficult to predict. More relevant, and difficult to estimate at this stage, is the rate of false GW alerts. In a spirit similar to neutrino follow-up, we propose a total of 20 and 5–10 h/yr/site for GW follow-up in the early and full CTA phases, respectively.

(F) Serendipitous VHE transients: VHE transients in the FoV will be identified by the RTA system [272, 273], which will explore the data on different timescales from seconds up to hours. The sensitivity will vary as a function of the timescale considered and it will also depend on the VHE sources present in the FoV and the baseline flux in the case of a known source that is flaring. Once a transient source is detected, the short-term scheduler of CTA will allow extension of the observations. MWL follow-up should also be promoted via alerts to the community with a latency depending on its measured duration, especially for newly discovered objects. In the first stage, the serendipitous VHE transients should be observed for as long as possible during the same night. The decision on the continuation of the observations on the following night should be motivated with the obtained CTA and MWL data of the particular VHE transient. We note that, in general, the CTA on-site analysis performed ~10 h after data taking could also provide serendipitous VHE transients in the FoV. In such cases, follow-up observations could be conducted during the subsequent night.

If numerous serendipitous VHE transients are found, different patterns in the flux and spectral variability can be identified and the observation strategy can be correspondingly modified (e.g. number of hours observed in the first night, use of sub-arrays, etc.). Assuming five transients per site and 5 h of observations for each transient on average, we estimate a total observation time of 25 h/yr/site during regular operations. During the early phase, 100 h/yr/site will be needed to account for tests, possible fake alerts with the preliminary RTA system, etc. In general, the observations should be extended up to zenith angles of 60° in any weather conditions. After gaining some experience, this limit could be changed, and CTA sub-arrays could eventually be used for the follow-up observations.

In Table 9.1, we summarise the observation times proposed for each class of targets (A-F) in the different phases of CTA. The proposed times are equal for the northern and southern arrays. In total, we request 390 h/yr/site during the early phase, 125 h/yr/site during Years 1 and 2, and 95 h/yr/site during years 3–10 (2020 h during years 1–10 including both sites).

(G) VHE transient survey: The VHE transient survey via divergent pointing could be conducted in conjunction with some fraction of the Extragalactic Survey KSP, and the associated observing time is considered to be part of that KSP. In order to be effective for the aims of both the transient and survey KSPs, a judicious compromise must be struck between the gain in the FoV and the concomitant decrease in sensitivity and increase in energy threshold. The chances of a GRB serendipitously occurring in the 8° diameter FoV of the MSTs during normal pointing observations is once per $\sim 10^4$ h of dark time observations [14]. If the instantaneous FoV can be enlarged by a factor of a few, the probability of finding GRBs during the prompt phase in ∼1000 h of blind survey observations starts to become plausible. For example, a recent Monte Carlo simulation study [274] (see also Ref. [253]) showed that assuming an array of 18 MSTs and 56 SSTs with a suitable divergent pointing pattern, the survey efficiency for steady point sources is comparable to that achieved using normal pointing. In the same configuration, the sensitivity at a 10° offset remains within a factor of 3 of that at the center of the FoV, so it may be feasible to nominally consider a ∼20° diameter FoV for searches of relatively bright transients.

The annual all-sky rates for GRBs of the types detected by Swift-BAT and Fermi-GBM are, respectively, ∼800 and ∼600 when accounting for their instrumental FoV and the fraction of time capable of triggering. Thus, the number of such GRBs occurring in the aforementioned ∼20° diameter FoV during dark time with 10% duty cycle is ∼1/yr [14]. The rate of GRBs actually detectable by CTA in this mode requires more detailed knowledge of the corresponding sensitivity and threshold on short exposure times. It is possible that pointing modes that are divergent enough to be more interesting for GRBs may not be the ideal choice for other aims of the extragalactic survey. Discussions on precisely how to implement the survey will continue and will be helped by Monte Carlo predictions for the expected performance throughout the relevant parameter space.

Note that unlike follow-up of external alerts, no time delays are involved due to communication with alert facilities or telescope slewing, and inadequate localisations are not a concern. Although GRBs are expected to occur with equal probability anywhere in the sky, targeting regions at high Galactic latitudes is strongly favoured, as those near the Galactic plane are affected by interstellar absorption that hampers X-ray and optical follow-up required for good localisation and redshift determination [352]. The RTA will play a critical role by automatically identifying new transients, rapidly alerting the community to foster MWL follow-up, and allowing the option of switching to follow-up observations with normal pointing if the detected signal meets certain criteria. The scientific prospects can be significantly enhanced if the timing and/or FoV of the observation can be arranged to coincide with comparable surveys at other wavelengths. Close coordination with upcoming transient factory facilities may be particularly valuable, potentially allowing simultaneous MWL studies of short-duration transients for the first time.

9.3 Data Products

The data products expected from the Transients KSP are outlined below.

(A) Gamma-ray bursts: Measurements are foreseen of spectra and light curves for ∼1 GRB/yr/site with more than 100 photons above 30 GeV per event [14, 321, 322]. In addition, upper limits can be expected for ∼10 GRB/yr, also offering valuable information for constraining GRB physics, the EBL, and LIV, as long as the redshift of the GRB is determined. Data rights should follow the proposed protocol, but it is also essential that some information be disseminated immediately through GCN notices, particularly in the case of detections, so as to encourage MWL follow-up observations and maximise the science return. For example, similar to GCN notices from Fermi-LAT, we may communicate information such as *XXX photons are detected above XXX GeV.*

(B) Galactic transients: Information on CTA observations of Galactic transients will be published in Astronomer's Telegrams as soon as possible after the observations are made, typically on the timescale of a day to several days. Once the CTA performance is established, light curves and spectra may be published even during the early phase.

(C) X-ray, optical, and radio transients: The data products resulting from triggers by X-ray/optical/radio transient factories will be light curves and spectra (or upper limits). The schedule for the data release will depend on the agreements reflected in the corresponding MoUs.

(D) High-energy neutrino transients: Some types of alerts may be distributed via non-public channels, in which case the details of the specific requirements and data rights will be addressed in dedicated MoUs. These MoUs should provide the possibility to issue VOEvent alerts, GCNs, or Astronomer's Telegrams as soon as possible after the detection of a transient gamma-ray source in the vicinity of the neutrino trigger in order to ensure MWL coverage.

(E) GW transients: The most critical part of the CTA detection of counterparts to GW candidates is the source localisation. The CTA Consortium has signed an MoU with LIGO-VIRGO to permit the free exchange of information regarding GW detections and their localisations, counterpart detections by CTA, and counterpart detections by other follow-up partners who are signatories to the MoU. Joint GW-CTA observations of a GW candidate will be published according to the publication policy laid out in the MoU.

(F) Serendipitous VHE transients: The detection of serendipitous VHE sources in the CTA FoV should be announced to the community as soon as possible through the use of tools such as VOEvent.

(G) VHE transient survey: As with F, RTA will be essential to autonomously identify new transients and promptly alert the community for their MWL follow-up.

9.4 Expected Performance/Return

Here, we discuss the expected performance of the Transients KSP and potential scientific return from observations of the various target categories.

(A) Gamma-ray bursts: Simulations for selected aspects of GRB observations by CTA have been presented in Refs. [14, 31]; below, we provide a brief summary of the results.

- *Spectra.* Choosing as templates a few prominent Fermi-LAT bursts whose spectra and variability were relatively well characterised up to multi-GeV energies, we assume that their intrinsic spectra extend to very high energies with the power-law indices measured by LAT in specific time intervals. Selected models are used to account for the effect of the EBL. Figure 9.2 shows an example of the distant but bright GRB 080916C at redshift $z = 4.35$ [275], with particular attention on the effect of the EBL. Despite the high redshift, even for exposure times as short as 20 s, the detection of several hundred photons above 30 GeV can be expected, with significant differences in the number detected depending on the assumed level of the EBL. The VHE spectra of such GRBs will be extremely valuable for probing the uncertain EBL at high redshifts through their consequent attenuation features, potentially beyond the range feasible

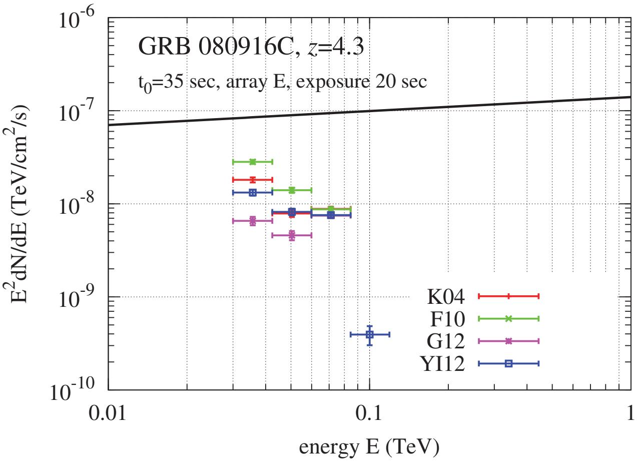

Figure 9.2: Simulated CTA energy spectrum of GRB 080916C at $z = 4.3$, with an assumed intrinsic flux $dN/dE = 1.4 \times 10^{-7}(E/\mathrm{TeV})^{-1.85}$ cm^{-2} s^{-1} TeV^{-1} (black line) corresponding to the time interval 55–100 s after burst onset [275], for an exposure time of 20 s. Compared are expectations for different EBL models: Kneiske *et al.* (2004) 'best fit' (K04, red) [355], Finke *et al.* (2010) (F10, green) [276], Gilmore *et al.* (2012) (G12, magenta) [356], and Inoue *et al.* (2013) (YI12, blue) [357]. See Refs. [14, 31] for more details.

through AGN observations, which would provide unique information on the cosmic history of star formation, black hole accretion, and intergalactic reionisation. Further physics insights can be obtained in combination with variability information, as discussed below.

- *Light curves.* As for simulations of spectra, we use as templates the Fermi-LAT data of selected bursts extrapolated into the CTA band, for which the example of GRB 080916C at $z = 4.35$ is shown in Figure 9.1. Despite the time delay required for follow-up (hence the plot being displayed only for times later than 30 s after burst onset), CTA is potentially capable of resolving the light curve in exquisite detail for such bright bursts (and to a lesser extent for bursts with more moderate brightness), especially if it can begin observations during the prompt phase. Of particular value for extracting crucial physics information is the energy dependence of the light curves, within the CTA band as well as within other bands from keV to GeV, which could: (i) elucidate the origin of the poorly understood mechanism of GRB prompt and/or early afterglow emission, (ii) reveal definitive signatures of hadronic emission processes through their characteristic delays at high energies, (iii) distinguish intrinsic spectral cutoffs from those due to EBL attenuation (of which the latter should remain time-independent), and (iv) probe LIV effects through their unique, expected energy dependence.

- *Detection rates.* Already discussed earlier, the predictions for the detection rate for CTA follow-up observations are based on a GRB population model tuned to match Swift observations, combined with assumptions on their VHE spectra from extrapolations of Fermi-LAT observations [14, 321, 322]. The general expectation is of the order of one CTA detection per year per site, the majority of which are for the early afterglow phase. One cautionary remark that must be made is that Fermi-LAT-detected GRBs reflect only the high-luminosity end of the GRB luminosity distribution [310]. CTA may have better chances of detecting GRBs with more moderate luminosities, whose high-energy properties are yet to be observationally constrained. Depending on whether their true power at very high energies relative to the MeV band is higher or lower than that deduced from LAT-detected bursts, the aforementioned detection rates could be either underestimates or overestimates, respectively. Given the lack of VHE detections so far, they are unlikely to be serious underestimates, although the reality will only become clear with further observations.

(B) Galactic transients: Using simulations of the CTA performance, we have estimated the observation times needed to detect selected types of known Galactic transient sources. Assuming that the Crab nebula high-energy flares are due to synchrotron emission, to detect the variable inverse-Compton component at multi-TeV energies we would need to monitor the source for 4 h/night during approximately 10 nights. With this strategy we could unveil the nature of these flares and, according to the model presented in [358], we could constrain the bulk Lorentz factor Γ of the putative moving plasma blobs. An example of different spectra obtained in the case of $\Gamma = 70$ is shown in Figure 9.3. The observations with the southern array would cover the multi-TeV emission, while with the northern array we could check if there is any contribution from the high-energy end of the synchrotron spectrum at low zenith angles and look for the multi-TeV variability at high zenith angles.

For Cygnus X-3, extrapolating the Fermi-LAT spectrum reported in [359] during the high flux state and assuming a photon index of -2.7, the northern array of CTA could detect the source at a five standard deviation confidence level in $\sim$10 h of observation (see Figure 9.4). Obtaining a spectrum could require up to 30 h. If the spectrum is harder during the flares, these numbers

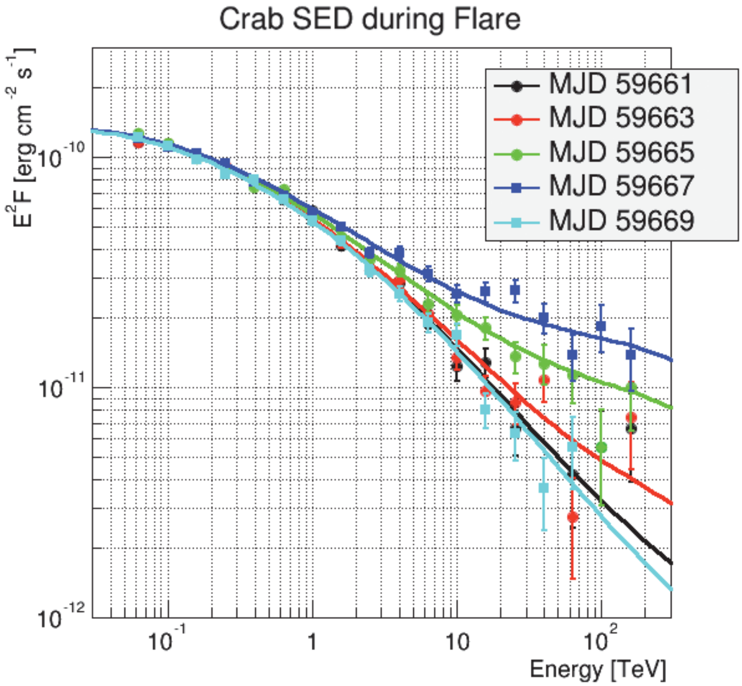

Figure 9.3: Simulated energy spectra of a Crab nebula flare observed with CTA. The model presented in [358], assuming a Lorentz factor Γ of 70, has been used to simulate the inverse-Compton component of the 2011 April flare observed with Fermi-LAT. A total of ten pointings of 4 h each separated by one day have been used. The variable tail from 10 to 100 TeV is clearly detectable.

could decrease significantly: a photon index of −2.2 would provide a detection in ∼1.5 h and a spectrum in ∼5 h. For Cygnus X-1, we use the possible VHE detection [332] to estimate that a five standard deviation detection could be obtained in 4 min and a good spectrum in ∼15 min (see Figure 9.4; also Fig. 7 of [285]). In summary, for some Galactic transients simulations have been conducted, but we would be mostly exploring the unknown.

(C) X-ray, optical, and radio transients: No simulations have been conducted for follow-up of X-ray, optical, or radio sources from transient factories, since in general, we will be exploring predominantly new phase space. However, as in the other transient cases, there is the potential to provide high-impact results with a moderate amount of observation time.

(D) High-energy neutrino transients: Detection of VHE gamma rays associated with high-energy neutrinos would be instrumental for revealing and understanding the sources of the neutrinos. If the parent hadrons can

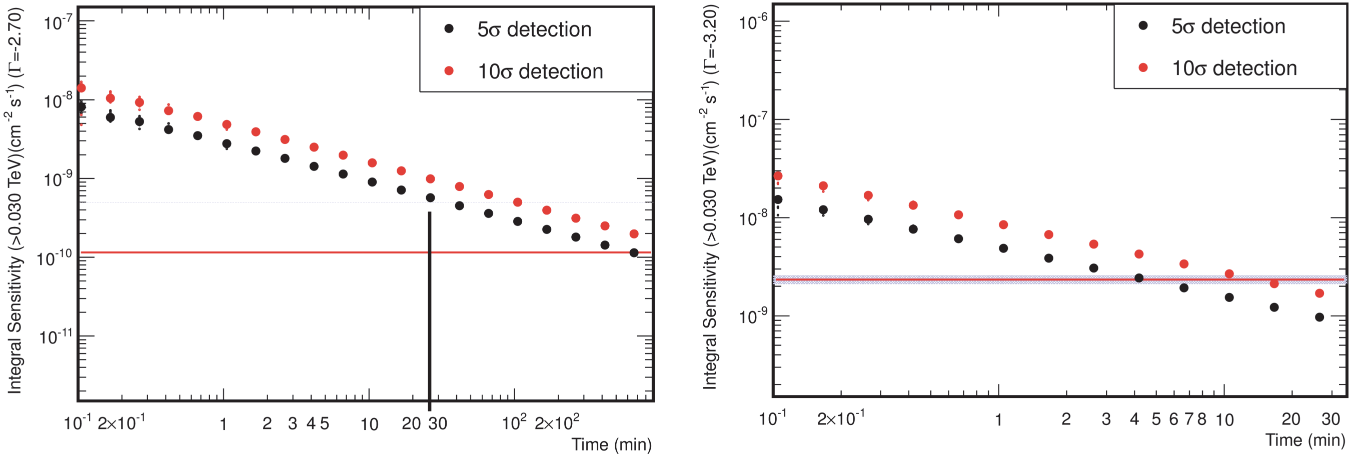

(a) (b)

Figure 9.4: (a) Simulated integral sensitivity above 30 GeV of a flare from Cygnus X-3 observed with the CTA northern array. The Fermi-LAT high flux reported in Ref. [359] has been extrapolated assuming a photon index of −2.7 and is represented by the horizontal red line. A five standard deviation detection could be obtained in ∼10 h of observations, while the determination of the spectrum could take up to 30 h of observations, denoted by the black vertical line. (b) Same as left panel but for Cygnus X-1. The possible VHE spectrum of Ref. [332] has been used as a template (pink horizontal line), resulting in a five standard deviation detection in 4 min and a good spectrum in ∼15 min for CTA (see also Ref. [285]).

also escape from the sources with reasonable efficiency and contribute to the observed cosmic rays, the neutrino plus gamma-ray signature could constitute the long-sought smoking gun of the sources of UHECRs. One model-independent way to estimate values for the VHE flux from potential sources of the IceCube neutrinos detected so far is discussed in Ref. [360]. Assuming that each detected neutrino originates from a distinct astrophysical object via pp or $p\gamma$ interactions, time-averaged fluxes of concomitant VHE gamma rays can be estimated for each object to be at the level of $0.6 - 1.7 \times 10^{-8}$ GeV cm^{-2} s^{-1} above several tens of TeV. At face value, this would be readily detectable in a few hours of CTA observation. However, this neglects EBL attenuation that can be severe depending on the photon energy and source redshift [31], as well as internal gamma–gamma absorption that can be significant in cases of $p\gamma$ production [265]. The true VHE gamma-ray flux can be higher if the sources are transient with durations shorter than the relevant IceCube exposure time and they will be lower if they are actually more numerous than the currently detected number of neutrinos.

(E) GW transients: The impact of CTA detecting a counterpart to GW radiation cannot be overstated. First, it would strengthen the significance of the GW candidate, particularly if the temporal coincidence was strong (as expected for short GRB afterglows). The association of a short GRB-like afterglow with a GW event can test the compact binary merger model for short GRBs and possibly discriminate between NS–NS or NS–BH progenitors. A good localisation of the VHE counterpart would permit follow-up observations by optical telescopes that could reveal the redshift and hence the energetics of these mergers. The sensitivity of CTA to on-axis GW events may be the same as that to short GRBs (see A above), but the effect of tiling and divergent pointing strategies that can improve the sensitivity to both has yet to be simulated and optimised. If VHE emission is limited to short-GRB-like beams, detection can only be expected for less than a few percent of all follow-up observations. However, as mentioned above (Section 9.1.2D), NS mergers may also possibly induce off-axis high-energy emission as a consequence of fast mass ejection in non-polar directions and associated particle acceleration [347]. Finally, observations of binary BH mergers will test newly proposed models for associated electromagnetic emission. Detection of such events will constitute a unique discovery and provide novel information on the dynamics of binary coalescence events.

(F) Serendipitous VHE transients: As stated earlier, there have been no new serendipitous VHE transients discovered so far in the FoV of currently existing VHE telescopes. On the other hand, transient sources are regularly discovered in the large fields of view of Fermi-LAT or AGILE, albeit being very bright objects (flaring AGN or GRBs in most cases). With our current limited knowledge, we can provide very approximate estimates for the probability of CTA to detect such objects in any given observation. The chances for serendipitous occurrence of GRBs during normal pointing observations is quite low, once per $\sim$35(13) yr in the 4.5(8)° diameter FoV of the LST(MST) array [14]. This rate can be increased with divergent pointing (see Section 9.2G). Of this, the fraction detectable by CTA may be still less, depending on the uncertain high-energy properties of GRBs with moderate to low luminosities that have not been well constrained by existing observations (see remarks in Section 9.2A). For flaring AGN, the prospects depend on the sensitivity reached in the particular observation. For example, at the sensitivity of 5 mCrab as envisaged for the Extragalactic Survey, we can scale the number of expected AGN detections for the survey and assume a 10% flare duty cycle to obtain a 2–10 (6–30)% probability of finding a flaring AGN in the FoV of the LST (MST) array, subject to uncertainties on the AGN luminosity function and duty cycle at very high energies. Expectations for other types of serendipitous transients are even more uncertain. The true situation should become clearer as actual observations proceed for the Extragalactic Survey as well as the flare programme of the AGN KSP (Chapter 12). Note that strategies for the Galactic Plane Survey KSP are currently being considered whereby the same regions of the Galactic plane are revisited over a range of timescales, enabling improved probes of variability in known objects as well as searches for new Galactic transients (Chapter 6). In any case, in view of the unprecedented sensitivity and FoV of CTA, discoveries of new types of VHE transients may be feasible and impactful.

(G) VHE transient survey: Divergent pointing observations would greatly increase the FoV of CTA, at the cost of reduced sensitivity and increased energy threshold compared to follow-up observations with normal pointing. However, these two techniques are complementary and would provide complete time coverage of the prompt emission phase of both long and short GRBs from their onset, which would address important questions concerning the physical mechanisms of jet formation, particle acceleration, and radiation in these objects. Divergent pointing would be the only way to detect or set limits on the VHE prompt emission of short GRBs, of great importance in view of their potential connection with NS–NS mergers, the most promising sources of GWs. While Fermi-LAT observation of the short

GRB 090510 has set the first limit beyond the Planck scale for LIV with a linear dependence on the mass scale [316], the much better photon statistics potentially offered by detecting a bright, short GRB with CTA in divergent mode can lead to a further, dramatic improvement by up to three orders of magnitude.

A VHE transient survey by CTA also opens up significant discovery space. As mentioned earlier, Fermi-LAT GRBs correspond only to the most luminous ones (i.e., the "tip of the iceberg") in the GRB luminosity distribution [310], and the high-energy properties of the great majority of GRBs with lower luminosities still remain unexplored. (For reference, blazars are well known to have SEDs that differ strongly and systematically with luminosity, with those of lower-luminosity BL Lac objects extending to much higher photon energies compared to the higher-luminosity flat-spectrum radio quasars.) Other potential, fast extragalactic VHE transients include relativistic SSB events [301]. The most exciting prospect would be the discovery of new and completely unexpected types of VHE transient sources.

MWL-coordinated surveys between CTA and upcoming transient factories can further advance the horizons of transient research. A prime candidate may be the recently discovered fast radio bursts (FRBs), i.e. bursts at GHz frequencies with millisecond duration of unknown origin but with clear signs of being extragalactic through radio dispersion effects, and with inferred all-sky rates approximately three orders of magnitude higher than GRBs [309]. Some models for FRBs predict correlated VHE bursts on similar timescales [306], which would be testable only by simultaneous observations involving CTA and suitable radio facilities. Note that $\sim$2 FRBs per day could be occurring in the FoV of CTA using the divergent pointing mode.

10

KSP: Cosmic Ray PeVatrons

Cosmic rays are primarily energetic nuclei which fill the Galaxy and carry on average as much energy per unit volume as that in starlight, in interstellar magnetic fields, or in motions of interstellar gas [361]. The confinement time of cosmic rays within the Galaxy is of the order of ∼10 million years [361], and this implies that cosmic-ray sources must provide $\sim 10^{41}$ erg/s in the form of accelerated particles in order to maintain the cosmic-ray intensity at the observed level. Moreover, the spectrum of cosmic rays observed at Earth is largely dominated by protons up to the so called *knee* in the spectrum at an energy of a few PeV. Above that energy, the differential power-law spectrum steepens from $\sim E^{-2.7}$ to $\sim E^{-3.0}$, where E is the particle energy, and its chemical composition becomes heavier [362]. Thus, the search for cosmic-ray sources has been focused on objects able to satisfy these requirements, i.e. *powerful cosmic-ray proton PeVatrons.*

It is well known that supernova remnants (SNRs) are able to satisfy the cosmic-ray energy requirement if they can somehow convert ∼10% of the supernova kinetic energy into accelerated particles [363]. In this context, particles are accelerated via diffusive shock acceleration at the expanding SNR shocks [364]. The acceleration of cosmic rays at SNR shocks is accompanied by an amplification of the magnetic field that can boost the acceleration of protons up to the energy of the knee and even beyond [365]. However, the details of such an amplification mechanism are not completely understood, and thus it is still unclear whether or not SNRs can act as cosmic-ray PeVatrons. To conclude, 100 years after their discovery, the question of the origin of cosmic rays is still open.

A tight connection exists between cosmic-ray physics and VHE gamma-ray astronomy. This comes about because if SNRs indeed are the sources of cosmic rays, they should also be bright VHE gamma-ray sources, due to the decay of neutral pions produced in the interactions between the accelerated cosmic rays and the gas swept up by the shock [366]. In fact, at GeV energies, clear evidence for the pion bump in the gamma-ray spectra of several SNRs has now been demonstrated [367]. At very high energies, a number of SNRs are now well-established gamma-ray emitters [368], but current observations do not allow us to unambiguously ascribe the gamma-ray emission to hadronic processes. This is because electrons can also be accelerated at SNR shocks and produce gamma rays through inverse-Compton scattering off soft ambient photons. An essential way to make progress would be to observe SNRs in the almost unexplored $>$10 TeV energy domain. The detection of an SNR whose spectrum extends without any appreciable attenuation up to energies of $\sim$100 TeV would imply that: (i) the emission is hadronic, because the leptonic emission is strongly suppressed at such high energies due to reduced Compton losses in the Klein–Nishina regime and (ii) the SNR is a PeVatron, because $\sim$100 TeV photons are produced by $\sim$PeV protons. It is thus of paramount importance to identify gamma-ray sources whose spectra extend, without any appreciable suppression, well beyond $\sim$10 TeV. This task is challenging for current atmospheric Cherenkov telescopes, due to their limited sensitivity in the $\gg$10 TeV energy domain, but it is well within the reach of CTA.[a]

This KSP proposes an observational strategy to search for PeVatrons with CTA. First, we suggest to perform deep observations of known sources with particularly hard spectra (i.e., not much steeper than $\approx E^{-2}$) and with hints for a possible spectral extension into the multi-TeV energy domain. Second, we also suggest to search for diffuse gamma-ray emission from the vicinity of prominent gamma-ray bright SNRs. This is motivated by the belief that PeV particles are expected to quickly escape the SNR shock [369] and then propagate diffusively in the ambient medium surrounding the remnant. The interactions of such runaway PeV particles with the ambient gas produce gamma rays with a characteristic hard spectrum extending up to $\sim$100 TeV [370]. An obvious target for this second kind of investigation is the SNR RX J1713.7$-$3946, which is one of the best-studied supernova remnants at very high energies. Though the leptonic or hadronic origin of its gamma-ray emission is still debated [23, 371], the steepening clearly observed in the gamma-ray spectrum at energies of ∼10 TeV suggests that the highest energy particles might have escaped the remnant. If this is the case, the diffuse gamma-ray emission one would expect to surround the SNR has been shown to be well within the reach of CTA [372].

---

[a] While this document was finalised, the H.E.S.S. Collaboration reported on the discovery of a cosmic PeVatron in the Galactic Centre region, possibly identified with the supermassive black hole Sgr A* [170]. Such a detection reveals possible new scenarios for the acceleration of PeV cosmic rays in the Galaxy and strengthens the case for deep searches with CTA.

The deep investigation of SNRs using CTA at full sensitivity, with special emphasis on the high-energy range, will allow us to address the basic questions listed above and will provide crucial information to the scientific community, in understanding both particle acceleration mechanisms and supernova remnants. The proposed observations also require an excellent understanding of the instrument, including an optimal angular resolution, high control of systematic effects at the highest energies in deep observations, and a good pointing strategy based on preliminary results of the CTA Galactic Plane Survey (GPS, see Chapter 6). Given the high-risk/high-gain and exploratory nature of these observations and its strong interest in developing the Small-Sized Telescope (SST) array, the CTA Consortium is in a good position to devote sufficient resources in the context of a Key Science Project to tackle this important unresolved question of cosmic-ray origins.

10.1 Science Targeted

10.1.1 *Scientific Objectives*

The scientific goals of this KSP appeal directly to the fundamental question of the origin of the cosmic-ray sea that fills our Galaxy.

1. Where and how in the Galaxy are cosmic rays accelerated up to PeV energies?
2. Are we sitting in a particular location of the Galaxy, or do the cosmic rays form a uniform sea within the whole Galaxy?
3. What is the distribution of PeVatrons in the Galaxy?
4. Do young shell-type SNRs accelerate hadronic cosmic rays up to PeV energies?
5. If so, up to which energies and how effective is this acceleration?

10.1.2 *Context/Advance beyond State of the Art*

10.1.2.1 *Hadronic mechanisms and the connection with cosmic-ray origin*

Very tight connections exist between cosmic-ray studies and gamma-ray astronomy, due to the fact that cosmic-ray protons can undergo hadronic interactions with the interstellar medium, producing neutral pions that in turn decay into gamma rays (see, e.g., [373, 374]). This is of particular relevance for the identification of cosmic-ray sources, since the production of gamma rays is expected, at some level, during cosmic-ray acceleration.

At GeV energies, the acceleration of hadrons at SNR shocks has now been clearly established [367]. At TeV energies, atmospheric Cherenkov telescope observations of SNRs interacting with molecular clouds show very strong hints of hadrons around them [375]. Finally, the >10 TeV energy domain is currently an important unexplored regime in the gamma-ray section of the electromagnetic spectrum, and opening this observational window would allow us to establish a link between the observed PeV Galactic cosmic rays and their astrophysical accelerators.

Below, we propose a number of observations to be performed by CTA that will shed light on the question of the origin of PeV cosmic rays:

- **PeVatrons:** Only a few bright VHE sources have been detected above ∼20 TeV so far. Although the newly commissioned HAWC air shower detector [2, 190] will have significantly improved sensitivity relative to its predecessor Milagro, CTA will be able to reach the same sensitivity as five years of HAWC in about 50 h and with much better spectroscopic capability ($\Delta E/E < 0.1$, 68% containment), thanks to the capabilities of the Small-Sized Telescopes (SSTs) in the southern array. This unique capability of CTA will enable the detection of the most energetic photons ever observed and the sampling of the highest energy particles in the Galaxy up to the PeV scale. Finding the extreme accelerators powering those particles is a goal that is within the reach of CTA.

  Moreover, at energies above 50 TeV, the problematic ambiguity between leptonic and hadronic origin is nearly completely resolved, since 100 TeV photons are produced preferentially by hadronic processes. This is a result of the Klein–Nishina effect, where the cross-section for inverse-Compton electron–photon interactions decreases very quickly above a few tens of TeV. The hadronic cosmic rays capable of producing photons of ∼100 TeV should have energies approximately an order of magnitude higher, i.e., in the PeV regime. Discovering the sites of cosmic-ray acceleration up to 1 PeV within the Galaxy would confirm the hypothesis that cosmic rays below the "knee" can be accelerated in the Galaxy and would finally shed light on the origin of Galactic cosmic rays. Within the SNR scenario for the origin of cosmic rays, only a handful of such PeVatrons are expected to be currently active in the Galaxy; here, we propose to follow-up promising high-energy candidates first seen in the CTA GPS.

We propose to trigger dedicated observations for sources detected in the CTA GPS which exhibit hard power-law spectra that extend up to extremely high energies, i.e., by requiring a detection at the three standard deviation level above 50 TeV. With the dedicated observations we will: (i) measure the extension of the spectrum to the highest energies CTA can reach and (ii) provide a precise localisation and measurement of the source size (extension beyond the point spread function (PSF), if any) to identify the MWL counterpart responsible for producing such radiation and thereby pinpointing the origin of the PeVatron. Even the discovery of only one Galactic PeVatron would represent a major breakthrough and allow us to understand the physics of the most extreme accelerators in the Galaxy.

- **RX J1713.7-3946:** is one of the brightest VHE gamma-ray sources detected. At a distance of 1 kpc [376], it is an ideal target to study the acceleration of cosmic rays in SNRs. Besides being the brightest SNR, numerous theoretical and observational studies at many different wavelengths have been performed, making RX J1713.7-3946 an ideal laboratory to understand hadronic acceleration in SNRs.

  At present, young SNRs are the most probable candidates for being the major accelerators of cosmic rays. The detections of non-thermal X-rays have already provided evidence for the acceleration of electrons to ultra-relativistic energies at SNR shocks [377], and previous VHE gamma-ray observations confirmed the existence of high-energy particles in the shocks of young SNRs (see, e.g., [378–382]). However, the leptonic or hadronic nature of those particles is still uncertain [23, 24].

  For RX J1713.7-3946, some evidence has been put forward to support a leptonic origin of the TeV gamma-ray emission [383]. However, a leptonic origin stands in contradiction to the high magnetic field required to explain the observed width of X-ray filaments. Radio observations of CO and HI gas have revealed, on the other hand, a highly inhomogeneous medium surrounding the SNR, such as clumpy molecular clouds [384, 385], whereas X-ray observations have revealed details of the particle acceleration (e.g., magnetic field amplification) via spectro-morphological characterisation of the remnant [16]. Spectro-morphological characterisation at very high energies, along with a complete comparison with the synchrotron X-ray emission and the CO material, is not yet feasible due to the lack of statistics and limited angular resolution of the present generation of atmospheric Cherenkov telescopes. Moreover, in the diffusive shock acceleration picture, the most energetic cosmic rays leave the shell at the beginning of the Sedov phase, while the less energetic ones are still confined today. These high-energy runaway protons can produce extended enhanced gamma-ray emission when colliding with atomic and molecular gas in the vicinity of the SNR. The well-studied molecular gas surrounding of RX J1713.7-3946 provides the perfect tracer to investigate this scenario, together with the improved CTA sensitivity and angular resolution [372]. Note that the presence of gamma-ray emission extending beyond the SNR shell of RX J1713.7-3946 has been recently reported by the H.E.S.S. Collaboration [386].

Simulations show that CTA will provide clear measurements of: (i) the extension of the gamma-ray bright shell, constraining the emission of the high-energy runaway particles interacting with the dense medium, (ii) the radial profile, which is expected to differ if the gamma rays are produced mainly by electrons or hadrons, and (iii) the spectral distribution in different regions of the shell, sampling differences in magnetic fields and/or in dense, clumpy regions. The spectral measurements will determine the maximum energy reached in the source, providing an unprecedented spectral characterisation to be compared with the low-energy radiation part.

10.2 Strategy

Deep observations of several selected sources are requested to investigate one of the basic questions that has driven the VHE gamma-ray field over the last few years, in particular, to understand the acceleration of Galactic cosmic rays to PeV energies. Despite considerable observation time devoted by the current generation of Cherenkov telescopes, it is clear that a significant breakthrough can be achieved only with the sensitivity of CTA over a large energy range and with superior angular resolution. In a conservative approach, and considering a supernova rate in our Galaxy of at most a few per century and the hypothesis that only young sources in the very early stages of their evolution (i.e., in the first $\sim$100 years) are able to accelerate particles to PeV energies, we expect a limited number of PeVatrons in the Galaxy in the present epoch. Accordingly, we propose to re-observe the five most promising hard-spectrum candidates, in which no evidence of a cutoff is detected from the shallower Galactic Plane Survey observations. These PeVatron candidates will be observed for 50 h each, increasing by a factor of 3–4 the exposure expected to be reached in the Galactic Plane Survey (see Chapter 6). The trigger criteria rely strongly on early results from the GPS

Table 10.1: Summary of objects proposed for observations in this Key Science Project.

Target	Type	Exposure (h)	Array	Year	Configuration
RX J1713.7-3946	SNR	50	S	1–3	Full array
PeVatrons	Unknown	5×50	S	>3	MSTs + SSTs

observations, and follow-up observations will be carried out on those sources that display an extension of their spectrum up to several tens of TeV.

Deep observations of the SNR RX J1713.7-3946 are also proposed based on its particular location and characteristics. RX J1713.7-3946 is one of the best studied SNRs at gamma-ray energies, and a considerable body of theoretical work has been devoted to it. Moreover, it is embedded in a dense, well-studied region that provides a large amount of target material. Thus, the source is an optimal one in which to investigate the interactions of cosmic rays, which are believed to escape from the acceleration region and collide with these clouds. This type of study requires a good understanding of the imaging atmospheric Cherenkov technique and of the instrument point spread function, when imaging the SNR surroundings at a few parsecs resolution.

10.2.1 *Targets*

Table 10.1 summarises the targets and required exposure for this Key Science Project.

10.3 Data Products

The data products produced in this KSP will consists of maps/datacubes and spectral information. We will provide large maps of 10° size with information on each selected source, along with morphological fits, including detailed analysis of any shell-type SNRs. With respect to the spectro-morphological studies, we will also provide spectral information in different regions of the (extended) sources, including spectral information in a few-arcminute-size wedges to investigate cosmic-ray escape in extreme accelerators. The pointing strategy depends on the preliminary results of the GPS observations. We will follow-up those sources for which an extension of a hard spectrum is detected, increasing the exposure to achieve improved statistics above 50 TeV. The results of these follow-up observations will be released simultaneously with the GPS ones, if possible.

10.4 Expected Performance/Return

To evaluate the capability of CTA to detect PeVatrons, we simulated the capability of CTA to detect 50-TeV photons in ∼15 h (an approximation for the effective observing time achieved in the inner Galaxy in the first several years of the GPS). For the differential energy spectrum of the PeVatron, we used a simple power-law with no cutoff, $\phi = \phi_0(E/\mathrm{TeV})^{-\Gamma}$, with $\phi_0 = 2.1 \cdot 10^{-11}\ \mathrm{TeV}^{-1}\ \mathrm{cm}^{-2}\ \mathrm{s}^{-1}$ (similar to the flux level of RX J1713.7-3946, a prototypical, bright VHE source) and took the spectral index $\Gamma = 2$ as proxy and calculated the minimum percentage of the flux ϕ detectable above 50 TeV at a significance of three standard deviations in a 15 h observation time. This significance level was chosen as a reasonable indication for a real excess which can be investigated with further observations. Simulations were performed assuming that the PeVatrons under examination are point sources and taking the background rate from the Monte Carlo simulations performed by the CTA Consortium to evaluate the instrument response. The results show that after 15 h of observation CTA will be able to detect enough photons to reconstruct a point at 50 TeV having a flux level of ∼7% of the flux ϕ_0, that is, of the order of $\sim 10^{-12}\,\mathrm{TeV}^{-1}\,\mathrm{cm}^{-2}\,\mathrm{s}^{-1}$, if there is no cutoff in the spectrum. If a cutoff is included in the spectrum, we estimate that a minimum of 50 h observation time is required to obtain enough statistics to determine an energy cutoff of ∼60 TeV for a source with a flux 10% of ϕ_0.

To test the capability of CTA to estimate spectral features, we show in Figure 10.1 the results of simulations of a powerful Crab-like source characterised by two hard photon indices (2.0 in solid lines and 2.2 in dashed lines). The different spectral features are clearly reconstructed even for the most extreme case, assuming an energy cutoff of 200 TeV (best-fit values are 203±23 TeV and 188±25 TeV for photon indices of 2.0 and 2.2, respectively). To compare with the case described above, the same simulations for a 7% of ϕ_0 spectrum in 50 h show that spectral points could be reconstructed up to 200 TeV, reproducing an energy cutoff as high as 135 ± 45 and 110 ± 35 TeV for the same 2.0 and 2.2 photon indices. More details on the impact of the different CTA configurations can be found in two dedicated papers [15, 24].

We also performed simulations of RX J1713.7-3946, the bright SNR proposed to study cosmic-ray acceleration. The gamma-ray emission from this object was simulated by assuming different emission mechanisms, supported

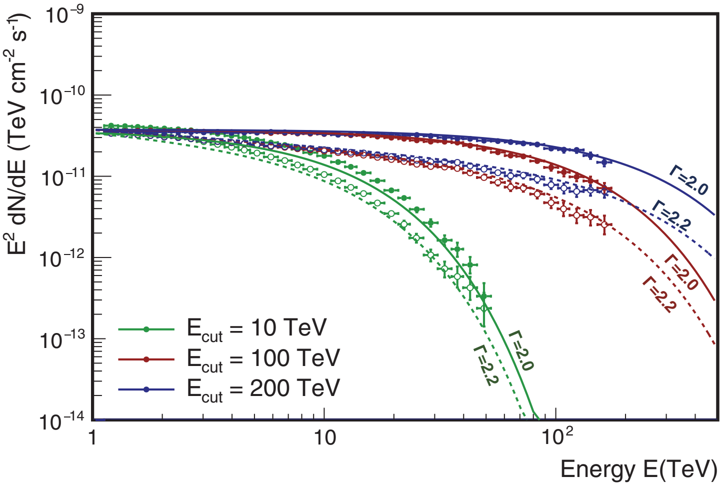

Figure 10.1: Simulated reconstructed spectra for CTA for a PeVatron source with a flux equal to the Crab nebula, using two photon indices (solid: 2.0, dashed: 2.2). Three different exponential energy cutoff values are used, as indicated by the colours.

by the extensive, existing MWL observations. To evaluate leptonic emission, we used an X-ray image of RX J1713.7-3946 from *XMM-Newton* observations as a template that traces the gamma-ray morphology. We considered a simplified case where the gamma-ray spectrum is spatially independent. For the hadronic case, we obtained the total target gas distribution based on CO and HI observations and used it as a template that traces the gamma-ray morphology. To evaluate different levels of hadronic and leptonic distributions, we considered several cases with different values of $A_{\rm p}/A_{\rm e}$, where $A_{\rm e}$ and $A_{\rm p}$ are the leptonic and hadronic normalisation parameters, respectively. The absolute values of these normalisation parameters were determined by requiring that the integration of the sum $N_{\rm e}(E) + N_{\rm p}(E)$ over the remnant equalled the total photon flux measured by H.E.S.S.

Figure 10.2(a) and (b) show the images for $A_{\rm p}/A_{\rm e} = 0.01$ and 100, respectively. Each image assumes 50 h observations with CTA. The lepton-dominated case (Figure 10.2(a)) shows a gamma-ray image similar to the X-ray image, and the hadron-dominated image is (Figure 10.2(b)) similar to the interstellar proton distribution including both CO and HI. The difference between the two cases is significant as shown in the subtracted image (Figure 10.2(c)). We note here that another obvious target for morphological investigations would be the SNR Vela Junior [388].

In addition to the morphological studies, the expected spectra for different scenarios were simulated for RX J1713.7-3946 [24] (Figure 10.3).

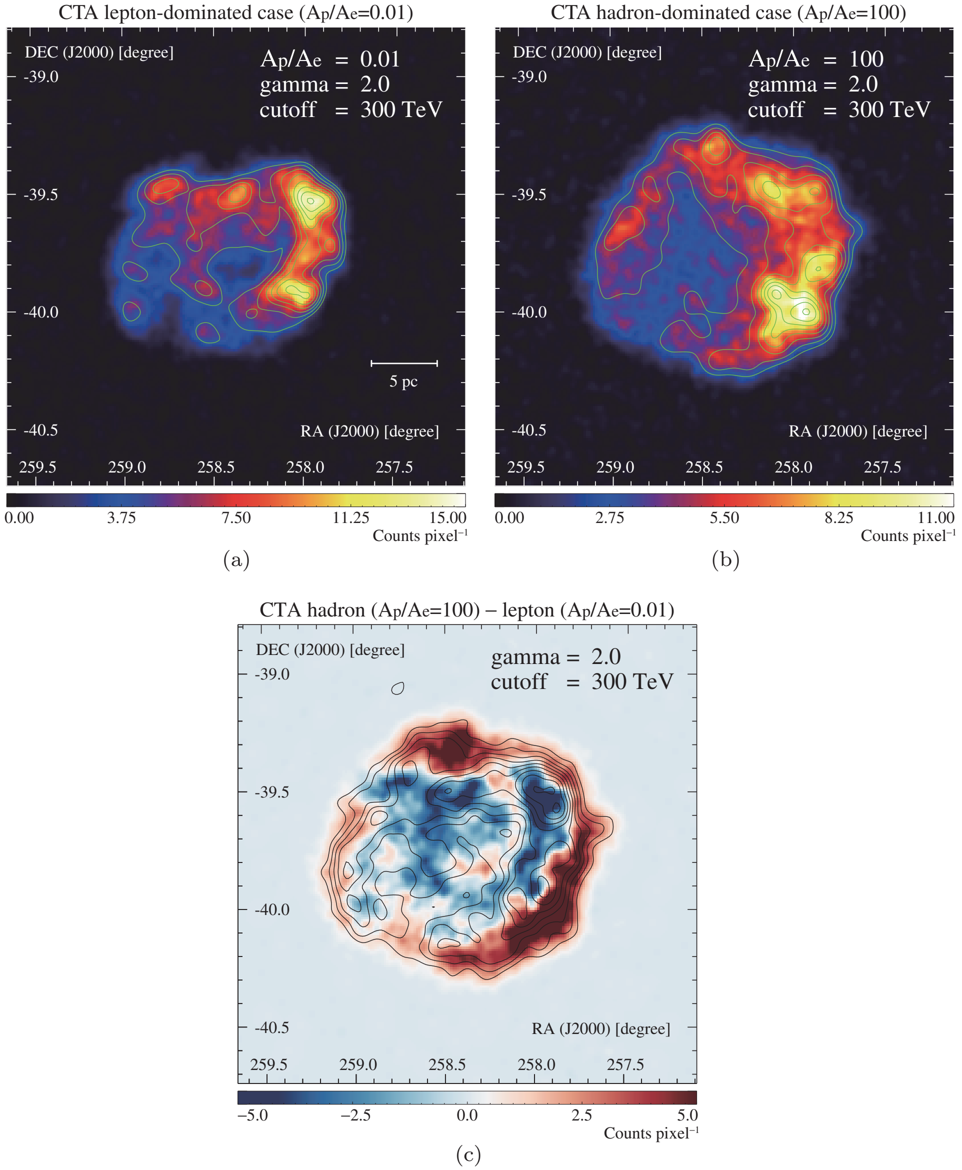

(a)

(b)

(c)

Figure 10.2: Simulated gamma-ray images of RX J1713.7-3946 in different scenarios: (a) $A_\mathrm{p}/A_\mathrm{e} = 0.01$ (lepton-dominated case) and (b) $A_\mathrm{p}/A_\mathrm{e} = 100$ (hadron-dominated case), with $\Gamma_\mathrm{p} = 2.0$ and $E_\mathrm{c}^\mathrm{p} = 300\,\mathrm{TeV}$. Reproduced from Ref. [25]. The green contours show: (a) *XMM-Newton* X-ray intensity [387] and (b) total interstellar proton column density [385], smoothed to match the PSF of CTA. The subtracted image of (a)−(b) is shown in (c). The black contours in (c) correspond to the VHE gamma-ray emission as reported by H.E.S.S. [379].

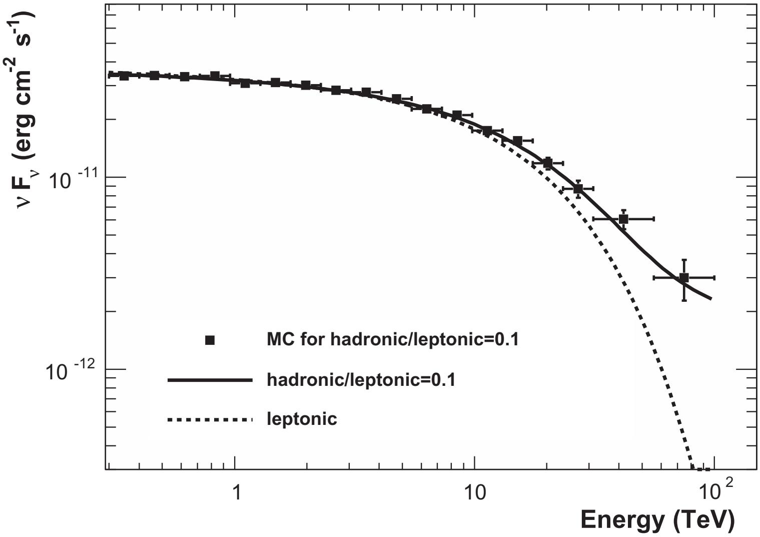

Figure 10.3: Simulation of the different spectral shapes resulting from different scenarios considered for SNR RX J1713.7-3946. Reproduced from Ref. [25]. The black squares show the total of the fluxes for the leptonic and hadronic spatial templates. The solid line shows the input spectra of the gamma-ray simulation. The dotted line is for the model where the emission is only due to leptonic processes.

The results show a clear discrepancy detected at high energies according to different origins of the gamma-ray radiation in the supernova.

As a further study, we simulated the response of CTA to the gamma-ray emission from a massive cloud ($\sim 10^5 M_\odot$) illuminated by a nearby, young SNR which injected in the interstellar medium $3 \cdot 10^{50}$ erg of kinetic energy in cosmic rays. The cloud was assumed to be located at different distances (50, 100, and 200 pc) from the SNR itself. Cosmic rays escaping from the accelerator can diffuse in the turbulent interstellar magnetic field and illuminate the cloud to produce gamma rays due to proton–proton collisions. Apart from being an indirect way to identify cosmic-ray sources, studies of illuminated molecular clouds are notable in that they can be used to estimate the cosmic-ray diffusion coefficient in the vicinity of the accelerators, since the properties of the expected gamma-ray emission depend on this value as well as its energy dependence [370]. Figure 10.4 shows results from these simulations, performed assuming a typical cosmic-ray diffusion coefficient equal to $10^{28}(E/\mathrm{GeV})^{0.5}$ and a distance to the SNR from Earth of 1 kpc. The expected spectra exhibit a concave shape that varies in a broad energy range between 100 GeV and tens of TeV and depends on the distance between the SNR and the cloud(s). The spectrum is further dependent on the SNR age

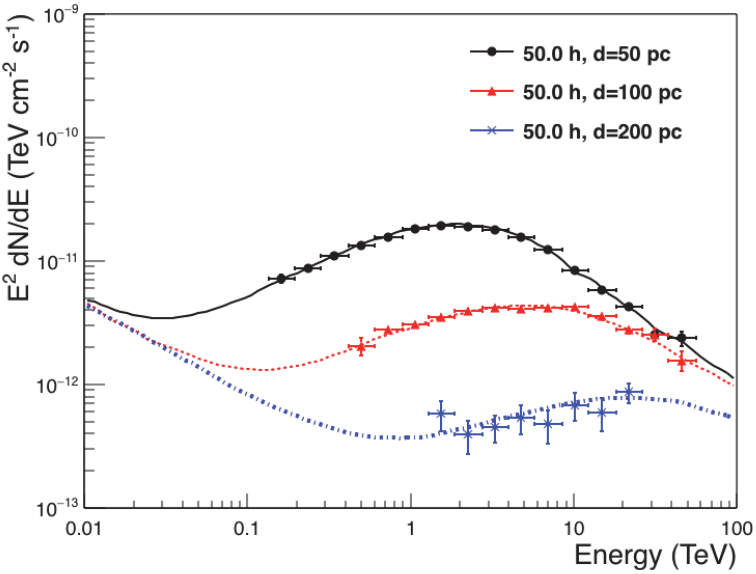

Figure 10.4: Gamma-ray spectra for a molecular cloud illuminated by cosmic rays coming from a nearby SNR (lines) and simulated observations (data points) for a 50 h CTA observation. See Ref. [24]. Black solid, red dashed, and blue dotted lines correspond to distances between the SNR and the cloud of 50, 100, and 200 pc, respectively. The distance of the cloud to Earth is 1 kpc, the cloud mass is $10^5 M_\odot$, and the SNR age is 2000 years.

and the assumed value of the diffusion coefficient. These dependencies can be parametrised and compared with future observations in order to extract or constrain physical parameters such as the cosmic-ray diffusion coefficient and the source's cosmic-ray acceleration efficiency [389]. For a nearby source ($d \sim 1\,\text{kpc}$), the cloud is detectable if located within a few hundred parsecs from the cosmic-ray accelerator. This corresponds to an angular distance of $\approx 6^\circ (l/100\ \text{pc})(d/\text{kpc})^{-1}$, where l is the distance between the SNR and the cloud and d is the distance to Earth. This angular scale is of the same order as the field of view of CTA. Thus, for nearby SNRs, illuminated clouds should be searched for in the GPS data and then repointed to with follow-up observations to obtain a deeper exposure and better determination of the spectrum and morphology.

11

KSP: Star Forming Systems

Cosmic rays are believed to be an important regulator of the star formation process. It is hence important to understand where cosmic rays are being accelerated, how they propagate, and where they interact in the interstellar medium (ISM). While travelling through the ISM, cosmic rays interact with the ambient gas and radiation fields to produce gamma rays, which trace directly the parental cosmic-ray population. Gamma rays are thus among the best tools to study cosmic-ray properties in star-forming environments. CTA observations of star-forming systems over six orders of magnitude in the star-formation rate (SFR) will help to unveil the relationship between high-energy particles and the star-formation process. The study of individual star-forming regions and star-forming galaxies will furthermore help to disentangle source-specific properties from global ones. By studying the gamma-ray emission in these systems, we can measure the fraction of interacting high-energy particles as a function of the SFR and hence investigate to which extent cosmic rays, magnetic fields, and radiation are in equipartition.

Within the Galaxy, observations of the Carina and Cygnus regions and the most massive stellar cluster Westerlund 1 will allow us to: (a) constrain the fraction of mechanical stellar wind energy transferred into gamma rays down to a level of 10^{-8}, (b) study particle acceleration in Galactic stellar clusters and superbubbles, and (c) search for signs of cosmic-ray propagation and interaction with the ISM via spectra-morphological studies.

Outside the Galaxy, the Large Magellanic Cloud (LMC) is the only other galaxy for which CTA will be able to resolve the VHE gamma-ray source population and study in detail the similarities and differences to our own Galaxy. Although important for the purpose of this KSP, the LMC is discussed separately in Chapter 7 and is only addressed here for modelling purposes. Observations of the Andromeda galaxy will provide important measurements and estimates of cosmic-ray properties and diffusion in the nearest spiral galaxy.

Long observations of the two starburst galaxies NGC 253 and M 82 will enable us to test how cosmic rays traverse the ISM, to distinguish between the truly diffuse emission and individual source populations such as pulsar wind nebulae (PWNe), and to possibly resolve the starburst nucleus in VHE gamma rays. Observations of the only ultraluminous infrared galaxy (ULIRG) likely within the reach of CTA, Arp 220, will for the first time allow us to test cosmic-ray properties in a system where all accelerated particles are expected to interact — i.e., a calorimetric system — and might establish ULIRGs as a new source class in VHE gamma rays.[a]

Deep observations of at least one object per decade in the SFR are required to investigate the relationship between star formation and gamma-ray emission and to study the impact of cosmic rays on their environment from the smallest to the largest scales. Table 11.1 summarises the list of objects proposed for observations within this KSP, of which four are also part of other KSPs. The observational program is well suited to be a KSP to be carried out by the CTA Consortium for a number of reasons. The total proposed observation time of 720 h could be difficult to obtain in a single

Table 11.1: Summary of targets proposed for observations in this Key Science Project, along with the expected extension of the gamma-ray emission and estimated supernova (SN) rates.

Target	Type	Extension	SN rate (yr^{-1})
Carina†	Star-forming region	$\sim 1.5°$	1.7×10^{-4}
Cygnus†	Star-forming region	$\sim 2.5°$	1.0×10^{-4}
Wd 1†	Stellar cluster	$\sim 2.2°$	1.0×10^{-4}
M 31	Galaxy	$\sim 2.0°$	2.5×10^{-3}
NGC 253	Starburst	$\sim 0.1° \times 0.5° (20'' \times 45'')$	0.03
M 82	Starburst	$\sim 4.8' \times 4.8' (15'' \times 50'')$	0.2
Arp 220	ULIRG	$\sim 2.5'' \times 1''$	4

†Objects that are also part of the Galactic Plane Survey KSP.
Note: SN rates in Galactic objects have been derived from the star-formation rate (Carina) and/or stellar remnants (Cygnus, Wd 1). The sizes for NGC 253 and M 82 are for the entire galaxy and the sizes of the starburst regions are in parentheses.

---

[a] See, e.g., the recent tentative detection of GeV gamma rays from the direction of Arp 220, reported in Ref. [390, 391].

Guest Observer (GO) program. Splitting observations into separate GO projects, with possible different foci and too low an exposure would require re-observation of targets and would significantly delay these timely studies. Furthermore, the proposed targets require excellent control of instrumental systematics. For example, the predicted emission from M 31 and Arp 220 is at the sensitivity limit of CTA, and the central molecular zones of NGC 253 and M 82 have sizes close to the CTA point spread function (PSF). The expected extension of sources in Cygnus covers a large fraction of the field of view (FoV) of CTA and mandates an excellent understanding of the residual cosmic-ray background. Moreover, the level of optical background light in the Carina region and in M 31 varies by more than an order of magnitude and will require the development of specialised analysis tools.

This KSP will provide legacy data products for the entire astronomical community such as catalogues of sources, flux maps, and data cubes (gamma-ray excess maps binned in energy) for the Cygnus and Carina regions. These will be useful to community members to prepare deeper observations for later, open time proposals.

11.1 Science Targeted

Understanding the fundamentals of the star-formation process is one of the great challenges in modern astrophysics (see, e.g., Ref. [392]). Through the ionisation of ISM material, cosmic rays affect astrochemistry and mediate the interaction of ISM material with magnetic fields, both of which are important influences on molecular cloud structure and star formation. Very massive stars undergo SN explosions at the end of their lives and enrich the ISM with heavy elements, necessary for the evolution of life on Earth. Supernova remnants (SNRs), the leftovers of SN explosions, are believed to be a major source of cosmic rays, which ionise the surrounding medium of SNRs, form a significant pressure component in the ISM, and amplify magnetic fields. Thereby, they can suppress or enhance star-formation in individual molecular clouds and entire galaxies [393, 394]. The acceleration, propagation, and interaction of cosmic rays are hence crucial to understanding the evolution of the building blocks of the universe on all scales: from stars to stellar clusters and from giant molecular clouds to galaxies and clusters of galaxies. Cosmic rays are believed to amplify magnetic field fluctuations upstream of the blast wave shock [365], and strong magnetic fields may hamper the star-formation process. Cosmic rays escape their acceleration sites, and low-energy cosmic rays are especially a dominant source of ionisation in the Galaxy. They penetrate deep into the dense cores of molecular clouds — much deeper than ultraviolet radiation. There they initiate a complex chemistry and influence the star-formation process [395, 396]. There is also increasing evidence that cosmic rays are dynamically important in galaxy formation and need to be considered in cosmological simulations [397, 398].

SNR shells are not the only sources discovered at TeV gamma-ray energies. The population of Galactic VHE gamma-ray sources to date comprises a variety of other object types: SNRs interacting with molecular clouds, pulsars, PWNe, and gamma-ray binary systems. All these objects are associated with late stages of stellar evolution, and they cluster tightly along the Galactic mid-plane with a scale height similar to that of the molecular gas and of the regions of star formation. Moreover, gamma-ray emission from massive star-forming regions and stellar clusters has been detected [399, 400], which can be seen as an indication for cosmic-ray acceleration in strong stellar winds as proposed in, e.g., Ref. [401].

Most of the light of young massive stars is radiated at ultraviolet wavelengths, absorbed by dust and re-emitted at infrared wavelengths. Kennicutt [403] has shown that the infrared luminosity and the star-formation rate of galaxies follow a linear relation. A similar scaling relation between infrared luminosity (and radio luminosity) and high-energy gamma-ray luminosity in a sample of nearby galaxies has recently been found [404], which suggests a direct connection between the process of star-formation and the high-energy particles. Although this relation is striking, the spread in gamma-ray luminosity of one order of magnitude indicates that the efficiency with which gas is channelled via massive stars into high-energy particles is different in individual objects. This points towards a complex interplay between star formation, particle acceleration, and escape and feedback with the ISM in these systems.

11.1.1 *Scientific Objectives*

Gamma rays provide a powerful tool to study cosmic-ray properties in star-forming environments and to thereby unveil the relationship between high-energy particles and the star-formation process. Although theoretical work has made major progress in recent years, in-depth studies of star forming systems on all spatial scales with the next-generation CTA are required to answer the most pressing questions, including:

1. What is the relationship between star-formation and particle acceleration in systems on all scales? Does a universal far-infrared/TeV luminosity relationship exist?

2. How does the calorimetric fraction change as a function of the SFR and does equipartition hold in star forming systems?
3. What is the contribution of different source classes to the cosmic-ray population in star forming systems? Where and when are particles accelerated, how do they leave, and what is their impact on the surrounding ISM?

CTA observations of Galactic and extragalactic massive stellar clusters and star-forming regions, of spiral and starburst galaxies, and ULIRGs will allow us to address these questions. The study of individual star-forming regions and entire systems will furthermore help to disentangle source-specific properties from global ones. For example, the starburst episode in starburst galaxies and ULIRGs only lasts for tens of millions of years, but it plays a key role in galaxy evolution and the star-formation history of the universe. By studying the gamma-ray emission in these systems we can measure the fraction of high-energy particles that interact as a function of the SFR and hence investigate to what extent cosmic rays, magnetic fields and radiation are in equipartition. Figures 11.1 and 11.2 illustrate the potential of CTA to study star forming systems on all scales and compares the predicted calorimetric flux from existing measurements to the sensitivity of CTA. To estimate the calorimetric limit, we follow Ref. [405] and assume that 10^{50} erg per SN explosion are transferred into protons, which interact and channel 1/6 of their energy into gamma rays that follow a power-law spectrum with differential index $\Gamma = 2.2$. The fraction that is then radiated at energies $E > 0.3\,\mathrm{TeV}$ is 5%. For the LMC and 30 Doradus, the 70μm flux is used to infer the SFR [213] and subsequently the SN rate. For Cygnus and Westerlund 1, the SN rate is derived from the number and ages of stellar remnants, and for Carina from the SFR alone.

11.1.2 *Context/Advance beyond State of the Art*

So far, only very few star forming systems have been discovered at TeV gamma-ray energies, and those that could be detected are at the limit of current-generation instruments. These systems are either at the sensitivity limit of H.E.S.S., MAGIC, or VERITAS, too extended for detailed spectro-morphological studies, or are not yet resolvable. Furthermore, several of the star forming systems seen at GeV energies with Fermi-LAT are as yet undetected in the TeV regime, with predicted flux levels at or just below the sensitivity of current-generation Cherenkov telescopes. For example, the starburst galaxy NGC 253 is the weakest VHE gamma-ray source detected so far [405], the massive stellar cluster Wd 1 is one of the largest TeV sources

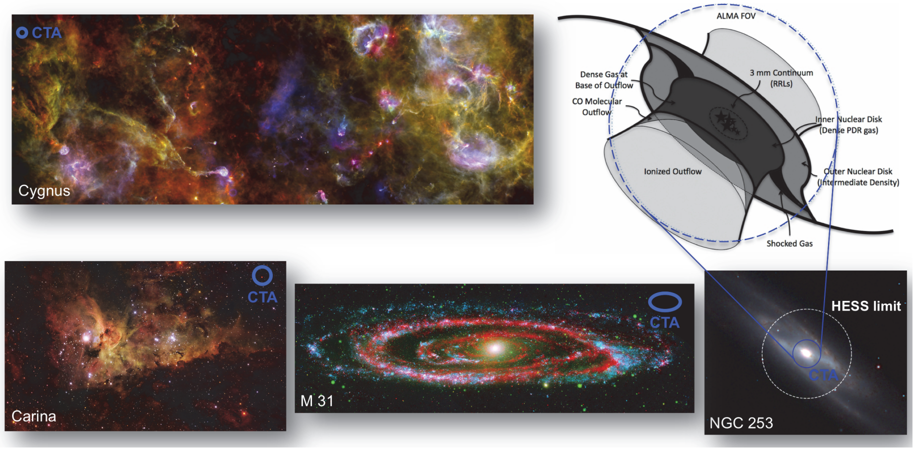
CTA
Cygnus
ALMA FOV
Dense Gas at Base of Outflow
CO Molecular Outflow
3 mm Continuum (RRLs)
Inner Nuclear Disk (Dense PDR gas)
Ionized Outflow
Outer Nuclear Disk (Intermediate Density)
Shocked Gas
CTA
Carina
CTA
M 31
HESS limit
CTA
NGC 253

Figure 11.1: Representative MWL images of four objects addressed in this KSP. For Carina and Cygnus, blue circles indicate the CTA resolution; for M 31, they indicate the maximum extension CTA will be able to detect and for NGC 253 the minimum extension CTA will be able to resolve. For NGC 253, the dashed white circle is the H.E.S.S. extension limit. Image credits: Cygnus — ESA/PACS/SPIRE, Martin Hennemann & Frédérique Motte; Carina — ESO/IDA/Danish 1.5 m/R.Gendler, J-E. Ovaldsen, C. Thöne, and C. Feron; M 31 — NASA/JPL-Caltech/K. Gordon (Univ. of Arizona) & GALEX Science Team; NGC 253 — 2MASS, WISE, [402].

in the sky [400], and the ULIRG Arp 220 has a predicted flux level which requires a long exposure, even with CTA.

Compared to observations at GeV energies, available for all the systems discussed here, observations with CTA are highly complementary. CTA will probe higher gamma-ray energies and hence higher particle energies that are crucial to understand the overall cosmic-ray population in star-forming systems. Thanks to the much higher photon statistics and superior point spread function above $\simeq$50 GeV, CTA will provide much more detailed gamma-ray spectra and high-resolution images than Fermi-LAT. Fermi-LAT is sensitive to large-scale interstellar emission in the Milky Way and nearby galaxies, whereas CTA will probe younger particles close to their acceleration sites.

11.1.2.1 *Star-forming regions*

The Carina nebula and the Cygnus region are exceptionally luminous and massive Galactic star-forming regions, and Wd 1 is the most massive stellar cluster in the Galaxy. As such, they are very unique systems, different in many respects, and their study at GeV and TeV energies will help to

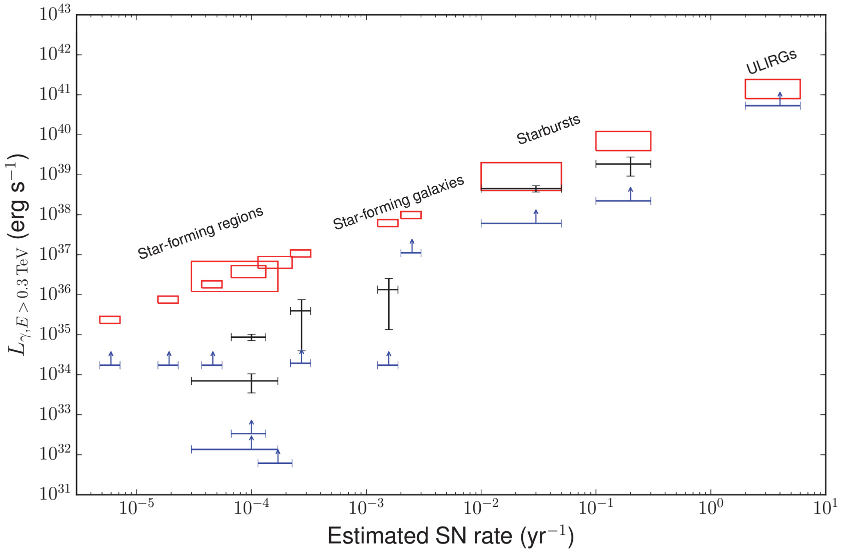

Figure 11.2: The expected calorimetric gamma-ray luminosity of star-forming regions, stellar clusters, star-forming galaxies, starbursts, and ULIRGs in red. The sizes of the boxes represent uncertainties in the SFR and the estimated calorimetric gamma-ray flux. Blue arrows indicate the expected CTA sensitivity for the anticipated observation time. Black points indicate measurements in the TeV domain, or, where objects are only detected in GeV gamma rays, extrapolations to VHE gamma rays, based on the Fermi-LAT spectra. In case SN rate estimates do not exist, the 70 μm flux is used to infer the SFR [213] and subsequently translated into a SN rate based on the scaling relation $\nu_{\mathrm{SN}} = (0.010 \pm 0.002) \cdot \mathrm{SFR}(M_\odot/\mathrm{yr})$.

Notes: (1) The 30 Doradus and LMC estimates have been derived by extrapolating the Fermi-LAT measurement with a broken power-law ($\Gamma_1 = 2.0, \Gamma_2 = 2.4$, $E_\mathrm{c} = 1\,\mathrm{TeV}$) and assuming a 90% error on the integral flux.

(2) The M 82 flux has been estimated by combining the VERITAS and Fermi-LAT measurements and assuming a 50% error on the integral flux.

(3) The Cygnus flux has been derived by extrapolating the Fermi-LAT measurement, assuming a power-law spectrum with index $\Gamma = 2.2$ and a 50% error on the integral flux.

understand where particles in star-forming regions are accelerated and how they escape, and, along with MWL observations, the observations will reveal what their impact on the ISM is.

The **Carina nebula** is one of the largest, most active, and best studied H II regions in our Galaxy and is a place of ongoing star formation. It harbours eight open stellar clusters with more than 60 O-type stars, three Wolf-Rayet stars, and Eta Carinae, the only colliding-wind binary (CWB) firmly established to emit GeV gamma rays (see, e.g., Ref. [406]). The age estimates of the Carina clusters, Tr14, Tr15, and Tr16, indicate several past episodes of star formation in the northern region and more recent star formation ongoing in the southern part of the nebula [407]. The study of extended X-ray emission as seen with Suzaku, XMM-Newton, and Chandra [408–410] suggests that the diffuse plasma originates in one or several unrecognised SNRs and/or may be attributed to stellar winds from massive stars. Based on the gas content in the Carina nebula and a limit on the gamma-ray flux, H.E.S.S. constrained the cosmic-ray enhancement factor in this region to be less than one order of magnitude above the cosmic-ray sea [411].

The Carina arm region also hosts the very young, but as yet undetected at gamma-ray energies, starburst cluster NGC 3603, where no SN explosion is expected to have occurred. The second most massive Galactic stellar cluster, Westerlund 2, is associated with a TeV source, and it harbours many massive stars and remnants of a few stellar explosions [412]. Westerlund 2, NGC 3603, and Eta Carinae provide complementary information on how much kinetic stellar wind energy is channelled into cosmic rays. The proposed CTA observations will provide the required spatial coverage and flux sensitivity (in a comparably "clean" environment) to constrain the fraction of input mechanical stellar wind energy that is converted into gamma-ray emission in stellar clusters to a level of 2×10^{-8} in NGC 3603, 5×10^{-8} in Tr16, and 2×10^{-7} in Tr14. Furthermore, the observations will allow us to probe the high-energy end of the Eta Carinae spectrum and to answer the question to what extend CWBs contribute to the Galactic cosmic-ray population.

Cygnus can be seen as a small-scale version of a starburst, harbouring all types of known Galactic TeV sources. Cygnus is one of the most promising parts of the Galactic plane to address questions related to particle acceleration and high-energy phenomena in massive star-forming regions. Cygnus has a total mass in molecular gas of a few million solar masses and a total mechanical stellar wind energy of $\gtrsim 10^{39}\,\mathrm{erg\,s^{-1}}$. This corresponds to several percent of the kinetic energy input by SNe into the entire Galaxy. A wealth of gamma-ray sources discovered by the Fermi-LAT, HEGRA, Milagro, VERITAS, MAGIC, HAWC, and ARGO-YBJ collaborations prove that ongoing particle acceleration proceeds in the Cygnus region up to hundreds of TeV energies. The first ever unidentified source discovered at TeV energies, TeV J2032+4130, is located in the direction of the Cygnus OB2 association [399]. Fermi and VERITAS discovered GeV and TeV emission towards the Gamma Cygni SNR, respectively. Most importantly, Fermi-LAT data revealed the presence of a cocoon of freshly accelerated cosmic rays stretching between Cygnus OB2, the NGC 6910 open cluster, and Gamma Cygni [224]. The cocoon provides evidence of particles escaping a close-by accelerator and being confined by the magnetic fields in the extreme environment of massive stellar clusters. The ARGO-YBJ collaboration claimed the identification of the source ARGO J2031+4157 (associated with the Milagro source MGRO J2031+41) with the cocoon [413].

Next to Orion, Cygnus is possibly the best studied star-forming region in the Milky Way across the entire electromagnetic spectrum, and it has been targeted in large Herschel, Spitzer, and Chandra programmes. At VHE gamma-ray energies, a survey of the region to a flux level of a few percent of the Crab nebula was made by VERITAS [414]. Once CTA is operational, HAWC will have collected 4–5 years of data on the Cygnus region and should reveal even more TeV emitters. CTA will provide the necessary angular resolution, flux sensitivity, and energy coverage above $\sim$50 GeV to disentangle the gamma-ray sources that pile up and overlap in this region and to identify their low-energy counterparts. CTA will furthermore study the propagation of cosmic rays in the ISM, map the spatial cosmic-ray energy density distribution, and thereby study the correlation between cosmic rays and active star-formation sites. Given the proximity of Cygnus to Earth, CTA observations will provide the best linear resolution and energy flux sensitivity compared to any other star-forming region in the Galaxy or the LMC.

Westerlund 1 (Wd 1) is the most massive stellar cluster in the Milky Way and contains a very rich population of massive stars, including a magnetar. H.E.S.S. observations have revealed an emission region twenty times larger than the size of the cluster. The detailed spectral and morphological studies demonstrated that a significant part of the emission may well originate from Wd 1 and that protons are most likely responsible for the emission [400]. The apparent size of the emission region also supports the idea that particles are accelerated in the cluster, and then escape and interact with the surrounding material and a nearby HII region. This scenario is further supported by the morphology of the HI gas in the region, which shows a bubble-like structure where dense gas partly overlaps with regions of strong TeV emission [400, 415]. The analysis of Fermi-LAT data revealed an extended emission region, offset from Wd 1, and only partly overlapping with the TeV emission [416]. This could imply that energy-dependent and anisotropic diffusion and advection are at work in this system, or that this region harbours multiple particle accelerators. The very large amount of energy in cosmic rays of 10^{51} erg required to explain the H.E.S.S. data can easily be provided by the stellar winds and multiple supernovae that went off in Wd 1.

Deep CTA observations of this region will provide the required spatial and energy coverage to perform a high-resolution study of the energy-dependent morphology of the emission and to compare Wd 1 to the Cygnus X superbubble (which is detected at GeV energies) and to 30 Dor C (the TeV detected superbubble in the LMC). Furthermore, the VHE gamma-ray spectrum shows no indication of a cutoff up to 10 TeV, although the spectrum could only be reconstructed with limited precision given the large size of the emission region. CTA observations are crucial to reconstruct the spectrum with much higher precision, determine the maximum energy to which particles can be accelerated in stellar clusters, and probe if these objects are potential PeV accelerators. In the same field of view, the most luminous TeV-emitting Galactic SNR, HESS J1640-465, HESS J1641-463, and the gamma-ray pulsar PSR B1706-44 are located. Early observations of the Wd 1 region will demonstrate the great potential of CTA for the study of very extended objects with complex morphologies and for the separation of close-by sources.

11.1.2.2 *Star-forming galaxies*

The **Andromeda galaxy (M 31)** is the nearest spiral galaxy at a distance of ∼780 kpc to Earth. It has a similar SFR as the Milky Way and can hence be considered as its twin. Studying the similarities and differences in gamma rays will provide important insights on the global cosmic-ray properties of M 31 and our own Galaxy. M 31 is detected by Fermi-LAT and is consistent with a point-like source but with an indication of a marginal spatial extension (see Figure 11.1 for the CTA capabilities to detect such an extension) [417]. The GeV spectrum is noticeably harder than for the Milky Way, and the ratio of gamma-ray luminosity over SFR is higher by a factor of three. The clear advantages compared to our own Galaxy are the outside, unbiased view and the fact that the SFR is much better known for M 31. Observations of the Andromeda galaxy with CTA within this KSP will provide invaluable insights into cosmic-ray properties in a spiral galaxy, allowing us to extend the measured gamma-ray spectrum to TeV energies and to search for truly diffuse emission and for diffuse emission from individual source populations such as PWNe.

11.1.2.3 *Starburst galaxies*

The enhanced star-formation activity seen in starburst galaxies is often triggered by a close fly-by of galaxies, a galaxy merger, or galactic bar instabilities. The extremely high thermal and non-thermal particle pressure in the central regions of starburst galaxies often leads to the formation of a galactic wind that enriches the intra-cluster medium with heavy elements and that is proposed to be a re-acceleration site of particles to energies beyond 10^{15} eV [418]. The high star-formation activity results in a highly increased SN rate. This increased SN rate is predicted to lead to an increased production of cosmic rays, which can then interact in the starburst region to produce gamma rays [419]. Indeed, the emission of GeV and TeV gamma rays from the starburst galaxies **NGC 253 and M 82** was detected, demonstrating that cosmic rays and the star-formation process are connected on galactic scales [405, 420, 421]. These observations finally provided evidence for proton acceleration in the two archetypal starburst galaxies. The gamma-ray luminosity of starbursts depends on the efficiency with which energy in cosmic rays is converted into gamma-ray emission. If all the hadronic cosmic-ray energy is lost in proton–proton collisions, the system can be considered *calorimetric*. Non-fully-calorimetric systems on the other hand may indicate a strong influence of winds. Indeed, only ∼40% of the cosmic rays in NGC 253 and M 82 seem to interact in the starburst nucleus, with the remainder being advected away in the starburst wind. The study of starburst galaxies at TeV energies will test the details of the cosmic-ray physics.

Measuring the calorimetric fraction as a function of the SFR in different starbursts and in ULIRGs tells us how much gamma-ray luminosity is produced per given input cosmic-ray and inner starburst gas density. Gamma rays are especially well-suited for this study since starburst galaxies are an order-of-magnitude brighter in gamma rays than in radio. A second key question is whether or not equipartition holds in starburst environments and what the mechanism is if it does. It is expected that the denser the starburst the less in equipartition the environment will be. Equipartition may perhaps hold in M 82 and NGC 253 (e.g., [422, 423]), but it might not be realised in the ULIRG Arp 220 (e.g., Ref. [424, 425]). Third, CTA observations of star forming systems will also shed light on how mixing of cosmic rays with ambient gas works. Models of non-thermal emission from starbursts assume that cosmic rays experience the volume-averaged gas density. But, this can only happen if the cosmic rays leave the hot phase and enter the molecular gas and HII regions. Additionally, we know that the ISM, the magnetic field, and the injection of cosmic rays are not necessarily homogeneous. Some works have expanded from these assumptions by correlating radio emission, gamma-ray emission, and star-formation to constrain cosmic-ray diffusion [426], by creating three-dimensional steady-state models of cosmic rays in M 82 and NGC 253 [423, 427] or by considering the time- and space-dependent contributions of individual injectors of cosmic rays [428].

CTA observations will help to determine how cosmic rays traverse the different gas phases in starbursts and which one regulates its transport, or provides target material for hadronic interactions, or contains the magnetic fields responsible for the radio emission. Observations of both starbursts are important, as M 82 is brighter, located in the northern hemisphere, and is unique as it exhibits a strong wind. NGC 253 on the other hand is located in the south, has a weaker wind, and offers the possibility to detect the disk. For both galaxies, we can potentially spatially resolve the starburst core. Most importantly, the two starbursts have star-formation rates (and SN rates) that differ by a factor of ten, and hence they probe different regimes in the radio-gamma-ray relation. Finally, the detailed spectral study of the brightest nearby starbursts M 82 and NGC 253 may help distinguishing the diffuse starburst emission from gamma-ray emission produced by individual populations of sources. This is of particular importance for the more abundant Galactic TeV sources such as PWNe, for which spectral features can appear [429, 430].

11.1.2.4 *ULIRGs*

ULIRGs are mergers of galaxies, where much of the gas from the spiral disks falls into a common centre of gravity. The merger creates an extreme molecular environment ($> 1000\,\mathrm{cm}^{-3}$) within a small region of a few hundred parsecs size, triggering a huge burst of star formation [431]. The interstellar medium in an ULIRG is similar to the inner parts of giant molecular clouds and photon energy densities in the infrared can reach up to $1000\,\mathrm{eV\,cm}^{-3}$, leading to strong radiative losses. ULIRGs are relatively rare objects [431], with **Arp 220** being the only ULIRG within 100 Mpc ($z = 0.018$) of Earth. Arp 220 is also a very extreme object; a SN explosion is expected to occur every six months, compared to ~1 per century in the Milky Way or in Andromeda (e.g., Ref. [432]), and several individual SNRs are visible at any time [433]. The SN rate in Arp 220 is the highest known in the local universe, making it the perfect object to study cosmic-ray production, interaction with gas, escape, and environmental feedback on galactic scales. Arp 220 would be the first object of this source class to be detected at gamma-ray energies (and, in fact, at any energy beyond 10 keV). The radio spectrum of Arp 220 is explained as synchrotron and free-free emission and absorption from primary and secondary electrons [434, 435]. The inferred magnetic fields can reach the mG range in the most extreme star-formation regions. The predicted gamma-ray emission of Arp 220 is at the limit of detection by current instruments. Fermi-LAT [404], MAGIC [436], and VERITAS [437] have reported upper limits. For the former, the galaxy is expected to be detected within the 10-year mission duration, and indeed [390, 391] report a tentative detection using more than seven years of Fermi data. Moreover, all correlations between star-formation indicators and gamma-ray luminosity place Arp 220 in a detectable range for Fermi-LAT and in line with measured values for the Small Magellanic Cloud, the LMC, M 31, M 82, NGC 253, and others given sufficient integration time. At TeV gamma-ray energies, CTA should detect Arp 220 after a deep exposure, although its distance will limit the detection to a point-like source.

The timeline of CTA matches the launches of recent and upcoming major instruments in radio, optical, millimetre, and X-ray wavelengths. The next generation of radio surveys in HI and CO transition lines with the upgraded ATCA system and the SKA pathfinder ASKAP are underway; they will map the three-dimensional neutral gas distribution of our Galaxy with unmatched spatial and velocity resolution and will cover the Galactic stellar clusters and star-forming regions discussed in this KSP. Millimetre and sub-millimetre instruments such as APEX, IRAM, and ALMA will provide measures of the ionisation level of dense molecular clouds induced by cosmic rays [395]. All these instruments will add information about the thermal energy content of the hot gas and about the energy input from massive stars; in this way, they will complement CTA in the study of ultra-relativistic electrons via synchrotron radiation.

11.2 Strategy

A summary of the proposed targets, their exposure, and observation conditions are given in Table 11.2. Given the angular size of the expected gamma-ray emission, the proposed targets will typically fit into the CTA field of view, but more extended, Galactic star-forming regions such as Cygnus may require a mini-scan.

11.3 Data Products

The proposed deep observations of star forming systems within this KSP will provide numerous data products that will, according to the proposed CTA data rights policy, be released to the public one year after the data have been taken. Although the entire program will be only finished by the

Table 11.2: Summary of observation times and conditions for the proposed targets.

Target	Exposure (h)	Array	Year	Zenith	Moonlight fraction (%)
Carina†	100	S	1–3	<45°	0
Cygnus (OB1/OB2)†	130	N	1–2	<50°	0
Wd 1†	40	S	0–1	<50°	25
M 31	150	N	2–5	<45°	0
NGC 253	100	S	1–3	<40°	0
M 82	100	N	1–3	<55°	0
Arp 220	100	S/N	2–5	<50°	0

Notes: Observation times for objects that are also part of the Galactic Plane Survey (GPS) KSP (marked with a †; Chapter 6), have been corrected for the effective exposure achieved by the GPS in the respective years.

end of year 5, data products on individual targets will be released sooner. Since Wd 1 is a strong source, observations of the Wd 1 region will be performed early on and could be used to publish first science results in year 2, demonstrating the potential of CTA. Data will be released to the public in the form of maps (flux, hardness ratio) and data cubes (gamma-ray excess). The Carina and Cygnus region have been observed in basically all wavelength bands. CTA observations will provide rich legacy products that are of great interest to a broad scientific community and will be released in year 4. CTA data will also in this case be released in the form of maps (flux) and data cubes (gamma-ray excess). Additionally, source catalogues, including spectral and morphological information and spectra and upper limits for source populations (PWNe, SNe, HII regions), will be released. Data obtained in observations of M 82 and NGC 253 will provide spectral and morphological information that will be released to the community in year 4 in the form of maps and data cubes. The same data products will be released for M 31 and Arp 220 towards the end of the program in year 6.

11.4 Expected Performance/Return

The expected performance and science return has been evaluated with simulations, utilising internal CTA tools for M 31 and using the gammalib/ctools framework [438] for all other sources.

11.4.1 *Star-forming Regions*

Simulations of two deep Cygnus pointings towards: (a) Cygnus OB2 and the cocoon of freshly accelerated cosmic rays and (b) Cygnus OB1 and

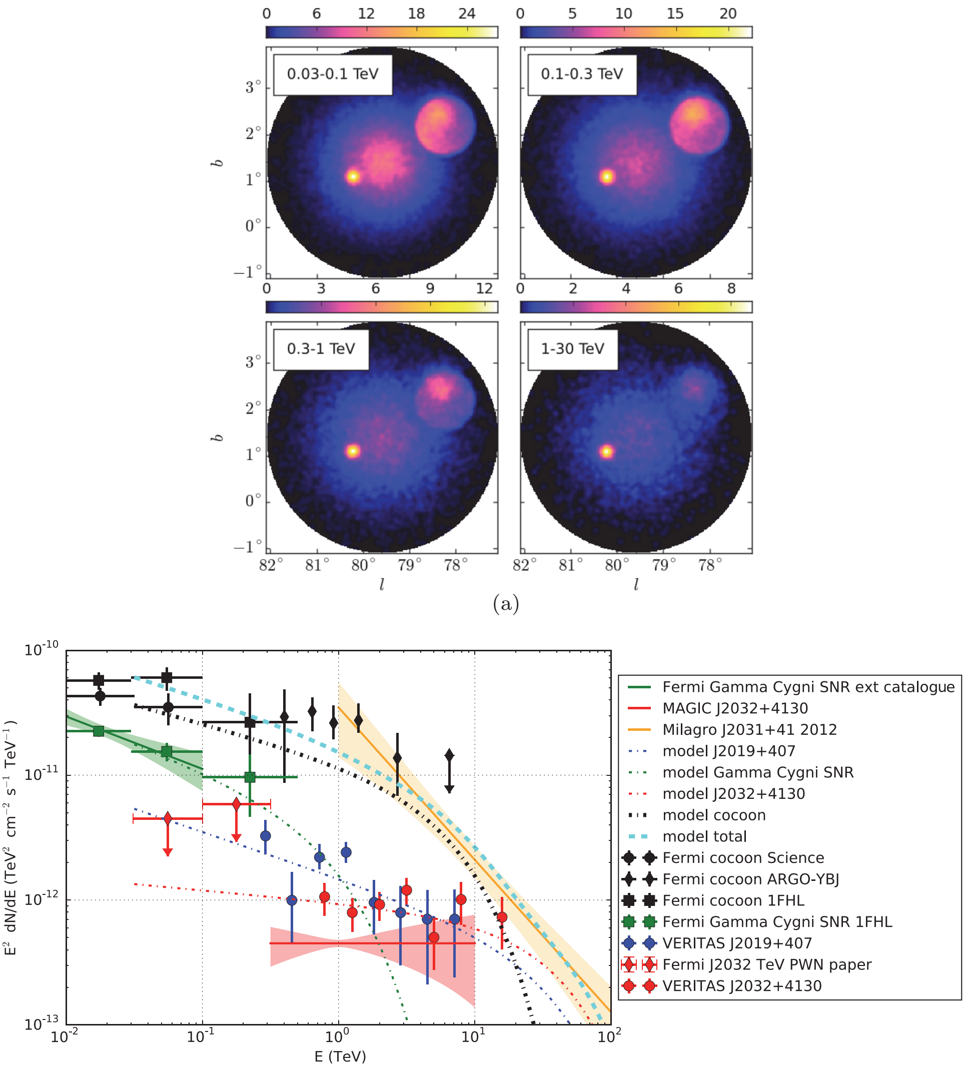

(a)

(b)

Figure 11.3: Simulated gamma-ray count map for CTA of the Cygnus OB2 region in four different energy bands (a) and spectra for gamma-ray sources in Cygnus OB2 (b), based on the observations proposed in this KSP.

VER J2019+407 have been performed. With the proposed observation time and based on the known sources as shown in Figure 11.3, the diffuse cocoon component can be detected at the 18 standard deviation significance level. This exposure is necessary, but also sufficient, to study the energy-dependent morphology of this complex region in detail. It furthermore provides the gamma-ray statistics required to detect sub-structures in the cocoon, to separate faint sources from the truly diffuse emission and to determine maximum particle energies in all objects. The Cygnus OB1 region shows strong diffuse emission and is proposed for a medium–deep exposure to find the counterparts to the Milagro and VERITAS sources and to investigate their relationship to the numerous stellar clusters and HII regions. Simulations show that all sources can be detected at a level that will allow for a detailed spectro-morphological study and a search for faint sources, embedded in the strong diffuse emission. Cutoff energies of the known sources can be reconstructed with high precision; in the case of the very hard source VER J2019+368 (spectral index $\Gamma = 1.75$), the cutoff energy can be reconstructed even up to energies of 80 TeV.

The **Carina region** hosts several stellar clusters and a huge reservoir of gas. With the proposed CTA observations, cosmic-ray enhancement factors in this region down to the cosmic-ray sea that fills the Galaxy will be probed. Additionally, these observations will test how much energy is channelled from stellar winds into gamma-ray emission. For individual clusters, the fraction of wind-kinetic energy going into gamma-ray emission will be measured down to a level of 2×10^{-8} for NGC 3603, 5×10^{-8} for Tr16, and 2×10^{-7} for Tr14. Simulations have been performed to investigate the CTA potential to determine the Eta Carinae spectral cutoff. Although a detection is possible within less than the proposed observation time, multi-year coverage is required to constrain the phase-dependent cosmic-ray escape into the ISM and the maximum energy in this CWB.

Simulations for **Westerlund 1** have been performed using the HI data in that region as a tracer for the TeV emission, adding a two-dimensional Gaussian source component as found in the Fermi-LAT energy band [416]. As indicated in Figure 11.4, CTA should be able to detect an energy-dependent morphology, resolve substructures and, if the GeV and TeV emissions are indeed connected, probe cosmic-ray propagation effects. The gamma-ray spectrum can be reconstructed with significant spectral points extending up to 100 TeV, if the Wd 1 spectrum has no intrinsic cutoff. The observations can hence establish whether or not Wd 1 is a Galactic PeVatron (see, e.g., Ref. [242]).

Additionally, the mechanical stellar wind energy input of the star-forming regions correspond to ∼0.1%, for Carina, ∼1% for Wd 1, and a few percent for Cygnus OB2 of the total mechanical energy input by SNe in the entire Galaxy. If no emission is detected, the CTA observations will

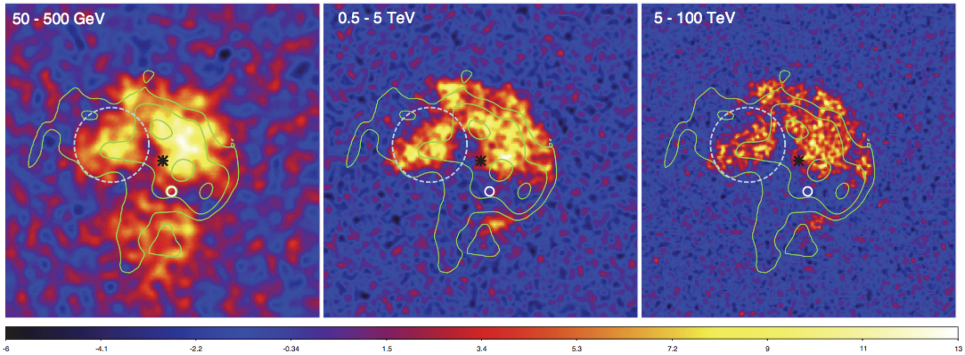

Figure 11.4: Expected Westerlund 1 gamma-ray excess maps for CTA in three different energy bands, smoothed with the CTA point spread function. H.E.S.S. contours are shown in green [400], the black star indicates the optical stellar cluster, and the magenta circle is the Fermi-LAT-detected PSR J1648-4611. The light blue dashed circle shows the star-forming region G 340.2-0.2. See also Ref. [416].

put strong constraints on the contribution of stellar winds as accelerators of Galactic cosmic rays.

11.4.2 *Star-forming Galaxies*

Simulations of **M 31** have been performed assuming different spectra and morphologies. If the Fermi-LAT measurement is extrapolated to TeV energies, a point-like signal can be detected by CTA for gamma-ray spectral indices of $\Gamma = (2.2 - 2.4)$ in the proposed observation time. A maximum extension of $(0.1 \times 0.2)^\circ$ can be detected only in the case that the diffuse emission has an index of $\Gamma = 2.2$ (or harder). If the diffuse gamma-ray spectrum of M 31 extends to higher energies, has a steeper index, or exhibits a cutoff (as, e.g., seen in the Milky Way), CTA will not be able to measure the true diffuse emission. However, it will be possible to measure an extended emission region of up to $(1.2 \times 0.3)^\circ$, in the case of an additional source population that peaks in the TeV domain (such as PWNe) and contributes to the gamma-ray signal (see Figures 11.1 and 11.2). In this case, an integrated signal of 4% of the Crab nebula flux with average source index $\Gamma_s = 2.2$ could be detected.

11.4.3 *Starburst Galaxies*

Simulations of NGC 253 have been performed to study the CTA potential to measure the extent of the starburst nucleus. ALMA and SMA observations of the core of NGC 253 indicate an extension of the central molecular zone of $\sim 0.35' \times 0.75'$. Resolving the starburst region in NGC 253 would prove that the gamma-ray emission correlates with regions of dense gas and hence increased star-formation and SN activity. With the proposed observations, a gamma-ray emission region as small as the ALMA field of view, as indicated in Figure 11.1, could be detected with three standard deviation statistical significance. This estimate does not include systematic uncertainties, but it is also not optimised for a high-resolution analysis. The same study will be performed for M 82, which has a slightly higher flux than NGC 253, but it will need to be observed with the northern array (where the sensitivity is somewhat worse than in the south). Simulations have also been performed to test if the disk component of NGC 253 could be resolved. For an asymmetric Gaussian-shaped region with corresponding widths $\sigma_1 = 13.8'$ and $\sigma_2 = 3.4'$, the disk can be detected if it exhibits a flux higher than 50% of the core emission as seen by H.E.S.S. The cutoff (or gamma–gamma absorption feature) in the gamma-ray spectra of NGC 253 and M 82 will be probed with high precision up to energies of ~ 5 TeV — the energy where gamma–gamma absorption features should appear (Figure 11.5(a); [24, 439]).

11.4.4 *ULIRGs*

Simulations of **Arp 220** have been performed and reveal that if the system is fully calorimetric as predicted by theory, the source will be detected with CTA. A simulated energy spectrum of Arp 220 is shown in Figure 11.5(b).

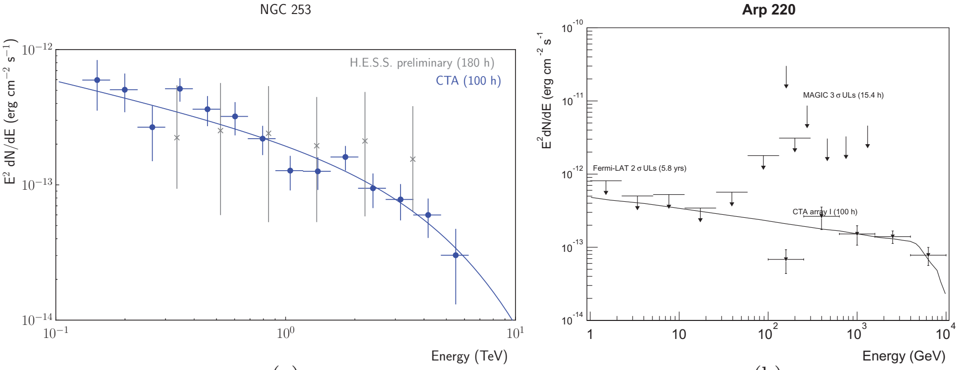

(a) (b)

Figure 11.5: Expected performance for CTA observations of NGC 253 (a) and Arp 220 (b). H.E.S.S. data are shown for NGC 253 as gray points (H.E.S.S. Collaboration, paper in preparation). For Arp 220, the MAGIC limits and theoretical model presented in Ref. [436] are depicted. The Fermi-LAT limits are obtained using 5.8 years of data.

In summary, the simulations show that the CTA observations proposed in this KSP will significantly expand our knowledge of cosmic-ray accelerators in the Milky Way and in nearby galaxies and hence allow us to study the connection between particle acceleration and star formation as function of SFR and SN rate.

This page intentionally left blank

12

KSP: Active Galactic Nuclei

VHE observations of active galaxies harbouring supermassive black holes (SMBHs) and ejecting relativistic outflows represent a unique tool to probe the physics of extreme environments, including accretion physics, jet formation, interaction of the black hole magnetosphere with the accretion disk corona, relativistic interaction processes, and general relativity. The same observations also allow us to search for signatures of ultra high-energy cosmic rays (UHECRs) and to characterise the evolution and differentiation (through intrinsic diversity or interaction within the host galaxy) of some of the brightest cosmic sources through space and time. The use of gamma-loud active galactic nuclei (AGN) as beacons provides insights into the cosmological evolution of star and galaxy formation through constraints on photon fields and magnetic fields along the line of sight. In addition, the study of VHE signals from extragalactic sources has a strong impact on the search for new fundamental physics.

AGN are known to emit variable radiation across the entire electromagnetic spectrum up to multi-TeV energies, with fluctuations on timescales from several years down to a few minutes. At present, AGN make up about 40% of the ∼180 sources detected at very high energies with ground-based telescopes. Apart from five nearby radio galaxies, all VHE AGN are blazars, i.e., their jets are closely aligned with the line of sight to Earth. The non-thermal MWL emission from blazars is characterised by two broad spectral bumps peaking in the optical to X-ray range and in the MeV to VHE gamma-ray range. Almost three quarters of blazars emitting in the VHE band are classified as high-frequency peaked BL Lac objects (HBLs), but there are also a few VHE blazars of other classes: flat-spectrum radio quasars (FSRQs), low- and intermediate-frequency peaked BL Lac objects (LBLs and IBLs, respectively), and a newly defined class of ultra high-frequency peaked BL Lac objects (UHBLs, EHBLs or "extreme blazars"), with spectral peaks of the high-energy bump above ∼1 TeV. The highest redshift of this sample of VHE detected sources is $z \sim 0.9$, and there is some evidence of the detection of photons above 100 GeV for redshifts as large as 1.5 [440]. The currently known population of VHE AGN is still very limited with respect to the coverage of different classes and redshifts.

CTA has the potential to substantially improve this coverage and increase the population of VHE sources at high redshifts. Extrapolations of averaged spectra from the high-energy (HE) gamma-ray band covered with Fermi-LAT show that more than 200 blazars of different classes and several radio galaxies should be detectable with acceptable exposure times, up to redshifts of $z \sim 2$ [30]. A much larger number should be accessible when accounting for sources with very hard spectra (see also the Extragalactic Survey Key Science Project, Chapter 8) and sources in flaring states. The targeting of flaring states will increase considerably our access to low-frequency peaked objects and help us constrain their emission process, which is currently supposed to differ from the processes in HBLs due to interactions with stronger photon fields in LBLs. In addition, CTA will allow us for the first time to study the VHE variability of numerous sources during their quiescent or low-flux states, of which very little is known up to now.

The AGN Key Science Project plays a crucial role in addressing the three CTA key science themes:

- **Probing Extreme Environments:** Data from the AGN KSP, together with MWL and possibly MM data, will bring us closer to a comprehensive understanding of the different types of blazars and their supposed parent population of radio galaxies, through the exploitation of a reference sample of high-quality spectra and light curves from different AGN classes. The signals detected from AGN over a large range of redshifts will also be used as beacons for a precise measurement of the extragalactic background light (EBL) [31] and to constrain the strength of the intergalactic magnetic field (IGMF) [444].
- **Understanding the Origin and Role of Relativistic Cosmic Particles:** This KSP aims at probing the nature of the gamma-ray emitting particles in AGN, by comparing leptonic and hadronic emission models against steady and time-resolved spectra over an unprecedented energy range. High-quality VHE spectra of a population of sources and

complementary MWL data will enable searches for signatures of UHECRs that will be distinguishable from other propagation or internal effects due to an extensive coverage of redshifts, classes, and activity states.

- **Exploring Frontiers in Physics:** VHE observations from AGN will provide important data for searches for Lorentz invariance violation (LIV) and axion-like particles (ALPs) which should leave discernible signatures in the gamma-ray spectra and light curves, with repercussions on our knowledge of general relativity, quantum gravity, and dark matter.

In terms of guaranteed science, data from this KSP will provide a wealth of information on the physics of gamma-loud AGN, with direct implications on our understanding of e.g., acceleration and emission processes, characteristics of relativistic jets, and accretion regimes of the SMBH. As an example, Figure 12.1 shows the expected CTA spectra for two simple emission scenarios — a leptonic and a hadronic model — in comparison with the currently available data. A set of high-quality spectra from different blazar types and different redshifts is needed to confidently distinguish intrinsic

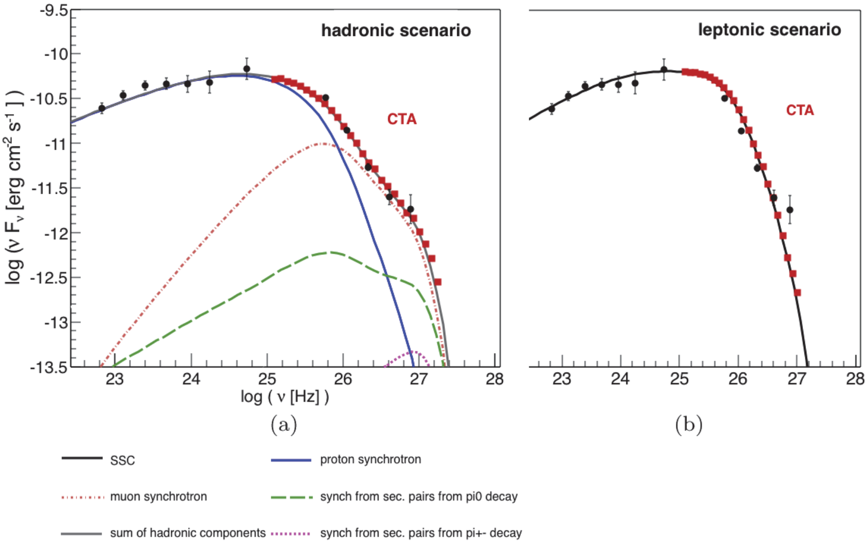

(a) (b)

Figure 12.1: A comparison of the expected CTA spectra for two specific (simple) emission models for the blazar PKS 2155-304. A hadronic scenario, where high-energy emission is caused by proton- and muon-synchrotron photons and secondary emission from proton–photon interactions, is shown on (a), and a standard leptonic synchrotron self-Compton (SSC) model on (b). The exposure time assumed for the simulations (33 h) is the same as the live time for the H.E.S.S. observations (black data points above 3×10^{25} Hz). The statistical uncertainties in the CTA data points are smaller than the red squares. For more details see Ref. [441–443].

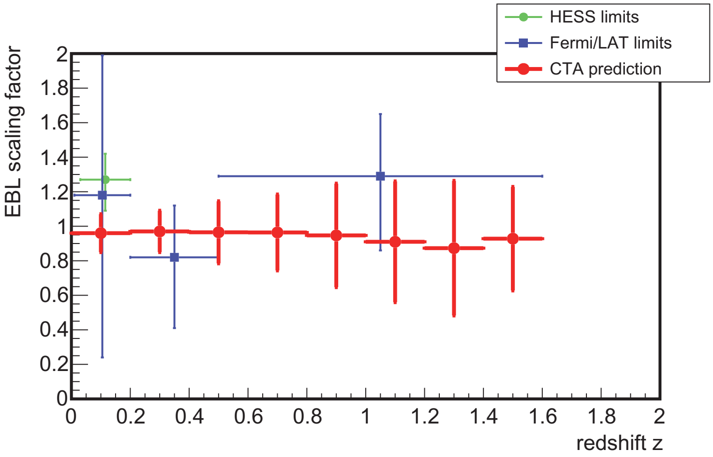

Figure 12.2: Potential for CTA to resolve the EBL density. The normalisation of the EBL density with respect to a state-of-the-art EBL model [446] is reconstructed as a function the distance of the sources used as gamma-ray beacons. Assumed are quiescent and flare states of ten sources per redshift bin and an average flux level of 25% of the Crab nebula at 100 GeV prior to absorption. The assumed exposure time takes into account that at higher redshifts the CTA data will be dominated by short flare states. Results obtained by H.E.S.S. [447] and Fermi-LAT [448] are shown for comparison. It should be noted that so far only a handful of sources above a redshift of 0.4 have been detected with ground-based gamma-ray telescopes.

spectral features of multi-component models, such as the hadronic model shown here, from external absorption on standard leptonic models. The AGN KSP will also lead to a precision measurement of the EBL spectrum at $z \sim 0$, down to the far-infrared and to a determination of its evolution up to $z \sim 1$ (cf. Figure 12.2). These data will also place strong constraints on the strength of the IGMF, informing us on conditions in the early universe and on predictions of fundamental physics.

In addition, the AGN KSP carries a great discovery potential for new VHE AGN classes, e.g., Narrow Line Seyfert 1 (NLSy1) galaxies or radio-quiet AGN classes, such as Seyfert galaxies or low-luminosity AGN (LLAGN). Estimates of the detectability of extended emission from the Centaurus A kpc jet, from its radio lobes, or from the radio lobes of M 87 are model dependent [30, 445]. If detected, such an extended signal would be a major breakthrough in the study of emission mechanisms in these sources and in the unification of different radio-loud AGN in general. Naturally, the possible detection of signatures from UHECR, the IGMF (in the form of “pair halos” or “pair echoes”), ALPs, or LIV are of great interest for the wider scientific community.

To this aim, we want to observe a reference sample of VHE AGN, which should cover all different gamma-loud classes and a large range of redshifts in a homogeneous way (in terms of required signal strength for each source and observation mode). The currently available VHE data on AGN have clearly shown the necessity of accessing not only high-quality spectra, but also flux and spectral variability on all timescales, together with simultaneous or contemporaneous (depending on the timescales under study) MWL coverage. Carrying out these observations in the form of a Key Science Project will provide the community with a homogeneous data set from a reference sample of VHE AGN, selected using well-defined criteria and including various archetypal AGN. The AGN KSP includes multi-annual observations (up to at least ten years for long-term monitoring of a few selected sources), which are difficult to propose and follow-up for individual observers. With the aim of self-triggering the CTA arrays on AGN flares, special "snapshot" observation modes, i.e., very short exposures on a large number of candidate flaring sources with small CTA sub-arrays, will be tested and optimised.

There are several arguments for carrying out this scientific programme in the context of a Key Science Project done by the CTA Consortium. As mentioned above, the AGN KSP will provide legacy data products (spectra, light curves, etc.) from a homogeneous sample of AGN that will be of great value to the community. The KSP is designed to guarantee coverage of a minimum number of sources at different redshifts and of different classes, as well as to ensure the long-term monitoring of a few prominent sources for at least 10 consecutive years. It is important that data from the long-term monitoring are released promptly to constitute a useful data set for the community. In addition, the snapshot programme requires very frequent short observations with multiple sub-arrays, where it can profit from flexible scheduling. To optimise the scheduling of these observations and their rapid evaluation, and to guarantee the timely emission of alerts, this programme is ideally suited to be carried out by the CTA Consortium. Finally, it is scientifically important that a maximum number of observations of flaring events be done with simultaneous Fermi-LAT coverage; therefore, an essential part of the AGN KSP is concerned with observations made in the pre-operational and early phases of CTA. The organisation of the proposed observations in the context of a KSP will greatly facilitate the necessary coordination with many different MWL and MM instruments.

Key data products will include legacy data sets of high-quality spectra, long-term light curves, time-varying spectra and high-resolution flare light curves. Furthermore, CTA will be able to send outgoing alerts for AGN flares to MWL facilities based on the snapshot programme, which monitors the VHE flux state of a large number of AGN.

Both the northern and southern arrays are needed to successfully implement this observational programme, otherwise the sample of accessible sources would be too limited, especially in the case of sources with soft spectra or at high redshifts which are difficult to detect. Observations will be carried out in dark time and under partial moonlight. Part of the programme can begin with partially complete arrays. It is strongly recommended to begin the targeted observations and the flare programme as soon as possible (i.e., in the period before the start of operations of the full CTA facility) to profit from simultaneous coverage with the Fermi-LAT detector before the end of its mission.

12.1 Science Targeted

12.1.1 *Relativistic Jets from Supermassive Black Holes*

12.1.1.1 *What are the relevant particle acceleration and emission processes in VHE blazars? How are different blazar types related?*

AGN studies in the nearby universe have indicated that their diversity may be understood by varying a few physical parameters (e.g., jet orientation and power; properties of accretion disk, corona and torus; spin and mass of the SMBH). Theoretical models predict that the jet power in AGN arises from the spin and mass of the central SMBH, as well as from the magnetic field at its horizon [449]. Although some VHE observations seem to favour a link between accretion physics, jet formation and VHE gamma-ray production, no universal connection has been established so far. Measurements of the gamma-ray spectra of blazars can be used to estimate their jet power. This provides insight into the energetics of the source and can be compared to the estimated accretion rate to confirm or dismiss potential connections (see, e.g., Ref. [450]). VHE data in particular can complete our present understanding with information from low-luminosity, high-frequency peaked blazars, which are supposed to probe a different accretion regime and possibly a different black hole spin range than the softer sources with spectral peaks in the Fermi-LAT range.

Results from modelling of blazar spectral energy distributions (SEDs) indicate that the presence or absence of thermal photons, emitted from the accretion disk and reflected from the dust torus or broad line region (BLR) and thus linked to the accretion process, could be responsible for the different shapes of the SED observed from different classes (see, e.g., [451–454]). High-quality spectra at very high energies are crucial to distinguish between the components of the SED due to inverse-Compton up-scattering of these different photon fields and to search for discernible spectral features from photon–photon absorption (see, e.g., Refs. [455, 456]). The interaction of VHE gamma rays with thermal photons also constrains the possible locations of their emission, e.g., to be within or outside the BLR (see, e.g., Refs. [457, 458]). Thanks to the improved capabilities of CTA (i.e., wider energy covered, improved energy resolution and improved sensitivity) and with complementary MWL information, we will be able to better constrain the theoretical models and discriminate between the different seed photon sources.

At present, the available emission models are generally not sufficiently well constrained, although in certain cases the basic one-zone synchrotron self-Compton (SSC) model has already shown its limitations when confronted with available data (e.g. discussion in [442]). To distinguish between different acceleration mechanisms, source parameters (such as the size of the emitting region and the magnetic field strength) and underlying particle populations, both spectral and temporal information are needed. Detection of flares, as well as long-term monitoring of sources, together with simultaneous MWL data, enables the reconstruction of time-dependent SEDs, which would put our current models to a serious test.

High-quality VHE spectra of different sources, as part of carefully organised MWL coverage, will help us characterise the nature of different blazar classes (addressing blazar unification and redshift evolution) and allow us to disentangle the origin (leptonic- or hadronic-dominated emission) and sites of the non-thermal radiation seen at highest energies, with direct implications for *in-situ* particle acceleration mechanisms (shock, shear, turbulence, magnetic reconnection), as well as jet power and jet dynamics.

Given the large dominance of low-redshift HBLs in the currently known VHE AGN sample, we want to widen the VHE coverage to include more low-frequency peaked objects (FSRQs, LBLs, and IBLs), as well as more sources at higher redshifts. Except for a few cases, FSRQs are difficult to detect during quiescent states, but their characteristically large VHE flux variations, up to a factor of 100 on short time scales (days/hours), make them good targets for detections during flaring states (see, e.g., Ref. [459]). There is increasing evidence that many LBLs and maybe IBLs share common properties with FSRQs (see, e.g., Ref. [460]). Observing flaring events from such objects can help to understand the links between FSRQs and the bulk of the VHE blazars known to date and to pinpoint the conditions for efficient particle acceleration and radiation within blazar jets. In addition, it will also be necessary to observe some objects of each class during their quiescent states to gain unbiased access to their emission mechanisms, which might well be different between quiescent and high states.

On the other end of the supposed "blazar sequence", we also want to gain access to a larger sample of "extreme blazars" or UHBLs [456, 461, 462]. This new class of BL Lac objects, of which only a handful of sources have been detected so far, is characterised by a very hard intrinsic VHE spectrum, with a peak of the high-energy spectral bump around 1 TeV or higher, and little or no flux variability. The interpretation of their multi-band emission with the standard SSC scenarios requires extreme parameter values (see, e.g., Ref. [463]). More complex leptonic scenarios (see, e.g., Refs. [464, 465]) or hadronic scenarios (see, e.g., Refs. [442, 466]) are required for a convincing description of their emission.

12.1.1.2 *What causes the observed variability in AGN from time scales of a few years down to a few minutes?*

Variability at all wavelengths is one of the defining properties of AGN. The most rapid variations in gamma rays are on the scale of only a few minutes. The very rapid variability of flares puts strong constraints on the size of the emitting region and its bulk velocity due to light crossing-time arguments. The power spectra of AGN light curves show flicker-noise or red-noise behaviour on time scales ranging from minutes to years, which points to a stochastic origin of their emission. The cause, additive or multiplicative processes, and the source of these variations, intra-jet or disk-modulated, remain largely debated (see, e.g., Ref. [467]). In both source scenarios, flaring events are rare, but contribute significantly to the total time-averaged emission of the source. Monthly observations with Fermi-LAT indicate that the most probable value of the duty cycle of high-flux events (i.e., above 1.5 standard deviations) is about 5–10% for BL Lac objects and FSRQs [248]. The long-term variability and duty cycle of AGN in VHE gamma rays are largely unknown. Most of the known VHE AGN are detectable on daily time scales only during flares for current instruments. Light curves with shorter time intervals are only available for a handful of sources in extreme flaring states.

One can roughly distinguish three typical time scales relevant for AGN physics:

- **Slow: Annual timescale** — The annual time scales are related to the duty cycle of the sources, and the claimed periodicities and quasi-periodicities have yearly timescales. There does not seem to be a significant difference between gamma-ray (detected by Fermi-LAT) and non gamma-ray blazars (see, e.g., the Roma BZB catalogue[a]), indicating that the duty cycles are long (>6 years of Fermi-LAT observations) also in gamma rays. The (quasi-)periodicities could be related to binary supermassive black holes, jet precession, or processes in the accretion disk. Finally, breaks in the power spectra of X-ray light curves have been observed on such long time scales for a wide range of black-hole masses and have been shown to scale with the ratio of black hole mass to the accretion rate (see, e.g., Ref. [468]). On the other hand, the absence of variability even on relatively long time scales could be an indication in favour of scenarios where gamma-ray emission stems from cosmic-ray induced cascades that develop outside of the source, as will be discussed below.
- **Intermediate: Timescale of days, weeks, months** — These time scales are related to the macrophysics of the emission region in the AGN jet such as its size, location, geometry, and dynamics. A better understanding of the emission region is directly linked to information about the possible acceleration and emission mechanisms. Sampling of the light curves at these time scales is crucial for comparison with light curves at other wavelengths to distinguish different emission components.
- **Rapid: Timescale of hours, minutes** — Sampling blazar fluxes below the light-crossing time scale of the SMBH, $T_G \sim 3\,\mathrm{h} \times (M/10^9 M_\odot)$ and during the whole visibility window of a night is a key strategy to understand the flickering behaviour of blazars on short time scales. Such measurements put strong constraints on the bulk Doppler factor, as well as on particle acceleration and cooling processes. Very rapid variability has so far only been studied in a few extreme flares, which have shown the limitations of standard emission models and given rise to more sophisticated scenarios, e.g., turbulent, multi-zone emission [469], or magnetic reconnection (see, e.g., Refs. [470, 471]) inside the jet or in the jet launching region (see, e.g., Refs. [472–474]), or pulsar-like acceleration in the black-hole magnetosphere (see, e.g., Refs. [475, 476]). To illustrate

---

[a] see `http://www.asdc.asi.it/bzcat`

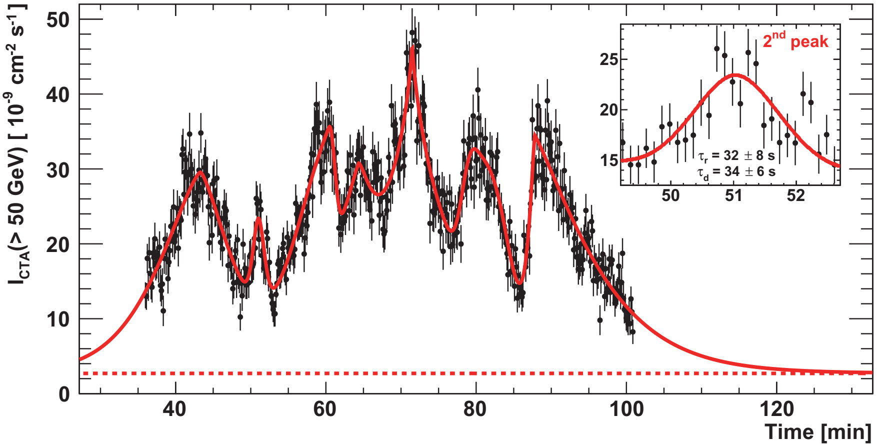

Figure 12.3: Simulated light curve based on an extrapolation of the power spectrum of the 2006 flare from PKS 2155-304 [30]. Error bars indicate the statistical uncertainty at one standard deviation. The doubling rise time and decay time are indicated for the second peak in insert.

the expected performance of CTA, Figure 12.3 shows the simulated CTA light curve of a hypothetical AGN flare modelled on a flare detected from the blazar PKS 2155-304 in 2006. As can be seen, CTA will for the first time probe sub-minute timescales.

The observations of the AGN KSP cover flux variations on these three different time scales. The slow and intermediate time scales will be probed with the "long-term monitoring" programme, which will provide light curves with regular (weekly) sampling over several years. The intermediate variability will also be tested with observations of relatively bright sources as part of the "high-quality spectra" programme. Rapid variability will be probed with the dedicated "AGN flares" programme. In conjunction with other MWL data, these programmes will provide unprecedented data sets for detailed time series analyses.

12.1.1.3 *From where does the VHE emission of radio galaxies originate?*

In standard AGN unification models, blazars are thought to be a sub-class of a larger parent population of radio galaxies, distinguished by a close alignment of their jets with the line of sight to Earth. The observation of radio galaxies at very high energies is of special interest with respect to understanding the unification of different blazar and radio galaxy classes. Since their jets are not pointing directly towards us, radio galaxies can be mapped in the radio band and at other frequencies, and they provide data which are less biased by strong relativistic beaming effects.

The number of radio galaxies detected at very high energies is still very small (this is also true for the GeV band). Only the most nearby sources have been detected at very high energies so far, namely M 87, Centaurus A ("Cen A"), NGC 1275, and PKS 0625-35; these are all FR-I radio galaxies, which are often interpreted as "misaligned BL Lacs".[b] The small sample of known TeV radio galaxies do not exhibit any common features at wavelengths below the gamma-ray band [30]. This might indicate that the VHE emission is not directly related to a specific property of those sources and is rather a general characteristic of radio galaxies. It raises the question whether the VHE emission in radio galaxies is generated in the jet, as is generally assumed for blazars, or in the core region, possibly due to magnetic processes. This latter possibility would naturally correlate their radio and VHE properties with those of micro-quasars (see, e.g., Ref. [478]).

Results from Fermi-LAT observations of Cen A have shown that the extended emission from the giant lobes in radio galaxies is visible in gamma rays [479].[c] Even if a simple extrapolation of the Fermi-LAT spectrum from this emission does not seem easily accessible for CTA, an additional VHE emission component is not ruled out and prospects for another nearby radio galaxy, M 87, are more promising [30]. In Cen A, emission from the kpc jet provides another challenging target that could lead to an important VHE discovery [445].

To indisputably determine the exact location of the VHE emission, simultaneous or contemporaneous VLBI coverage of VHE flares, with an angular resolution able to image the flaring region, will be essential. The power of such observations is very well illustrated by the observations of M 87 [481]. VLBI observations of this radio galaxy have shown that different episodes of VHE flares may be related to different emission regions, in this case the radio core and the HST-1 radio knot [482]. Such unexpected results strengthen the case for further studies.

An open problem is also presented by the mismatch seen between the Fermi-LAT and H.E.S.S. spectra from the core of Cen A [483]. A high-quality measurement of the spectrum in the overlap region will be able to verify the indication of a spectral hardening towards the high energy end of the Fermi-LAT spectrum [484, 485] and to distinguish between different leptonic or lepto-hadronic scenarios trying to explain the origin of the GeV and TeV emission [483, 486–488].

---

[b] The VHE emission from IC 310, another radio galaxy candidate, is most likely linked to the blazar core of this source [477].

[c] Extended emission has also been recently detected with Fermi-LAT from the radio galaxy Fornax A [480].

12.1.1.4 *Do other classes of AGN emit VHE gamma rays?*

After the recent detections with Fermi-LAT [489–492], it is clear that NLSy1s are a class of AGN that should be within the reach of CTA during flaring states. While TeV blazars and radio galaxies tend to be hosted by giant ellipticals with a SMBH of $10^{8-9} M_\odot$, NLSy1s are thought to be hosted by spiral galaxies and to lie in the low range of the SMBH mass spectrum ($10^{6-8} M_\odot$), while exhibiting very efficient accretion (but see Refs. [493, 494]). VHE gamma rays detected from NLSy1s could provide crucial insights into the unification of various classes of AGN and on the conditions for jet formation as a function of the SMBH mass and accretion rate, as well as the role of the host galaxy. Several NLSy1s are included in our list of targets to survey for flares.

Even more challenging targets are Seyfert galaxies or low-luminosity AGN (LLAGN). Several models for the direct production of gamma-ray emission in the vicinity of SMBH have been proposed (see, e.g., Refs. [475, 476, 495–497] and references therein). No VHE gamma-ray emission has been detected from such objects so far, although at GeV energies Fermi-LAT has detected the Seyfert II galaxy Circinus [249]. Given the weakness of the expected signal from such sources, a stacking analysis of several candidates seems the most promising approach, with nearby galaxy clusters being the best targets. The deep observation of M 87, included in the AGN KSP, will at the same time provide coverage of the centre of the Virgo cluster, while observations of other clusters are foreseen within the dedicated Cluster of Galaxies Key Science Project (Chapter 13). In addition, a stacking analysis can also be carried out on the fields of view of all other observations of AGN.

12.1.2 ***Blazars as Probes of the Universe***

12.1.2.1 *What is the spectrum of the EBL at redshift $z \sim 0$ and how does it evolve at higher redshifts?*

The EBL encodes important information on the star formation history of the universe and it constitutes a major research area in observational gamma-ray cosmology. Direct measurements of the EBL are difficult, due to strong foregrounds from our Solar System and the Galaxy, with current constraints from galaxy counts and direct observations leaving the absolute level of the EBL density uncertain by a factor of two to ten. The excellent "spectral lever arm" of CTA, covering both intrinsic (with optical depth $\tau = 0$) and absorbed ($\tau \approx 3$) ranges of the energy spectra from blazars, will allow an unprecedented (indirect) precision measurement of the EBL density, particularly in the poorly constrained low-frequency range (mid to far infrared).

The potential of EBL studies with CTA has been discussed in detail [31]. With CTA, we aim for a substantial improvement over current measurements of the EBL performed with Fermi-LAT [448] and current atmospheric Cherenkov telescopes (see e.g., Refs. [447, 498]). We will take advantage of the unique capability of CTA to measure simultaneously and with high precision both the unabsorbed intrinsic (GeV) and attenuated (TeV) parts of the blazar spectra and thereby disentangle intrinsic physical processes from external absorption features, which will be essential for a precise EBL density determination.

For this purpose, we will observe a large sample of blazars located at different redshifts. Many of the targets are already discovered TeV emitters, others are seen with Fermi-LAT so far only, and others will only be seen by CTA when in flaring states. In addition, the exceptional statistics from extreme flaring states of, e.g., Mrk 421, Mrk 501 or PKS 2155-304, is of utter importance for the study of pair-creation on the far-infrared EBL, for which gamma rays are needed above 10 TeV, requiring observations of nearby hard-spectrum sources. The detection of high-redshift sources, more likely during flares, would allow us to measure the evolution of the cosmic optical background. Flares also help us distinguish the effects of EBL absorption from internal spectral variations.

The first goal of this part of the AGN KSP is a measurement of the EBL spectrum from the mid ultraviolet to the far infrared at $z \sim 0$ with an uncertainty of 10% on the overall flux, which can be reached with a sufficient number of sources, evenly spread over redshifts up to $z \sim 1$. The expected "scaling factor", a measure of the sensitivity to differences between the assumed and actual EBL density, for measurements with CTA is shown in Figure 12.2. The second goal is the characterisation of the EBL evolution up to a redshift of $z \sim 1$, which can be directly compared to models of galaxy evolution.

In addition, we note that the measurement of gamma-ray absorption on the EBL may also be used for the determination of the expansion rate of the universe, i.e., the Hubble constant, as has been shown in Refs. [498, 499]. The value adopted for the Hubble constant has an influence on the evolution of the EBL density and on the gamma-ray propagation that should lead to a measurable effect on the detected spectrum. Sources at redshifts between $z = 0.04$ and $z = 0.1$ seem particularly constraining for such a measurement. This method would present an approach that is independent from more established methods such as Cepheids, supernovae, the cosmic microwave background and baryon acoustic oscillations. Its accuracy will increase with an improved understanding of the EBL and new VHE data.

12.1.2.2 *What is the strength of the IGMF?*

The origin of the IGMF, be it structure formation, inflation, or primordial phase transitions, is still widely discussed. For recent overviews see, e.g., Refs. [500–504]. The actual detection of a non-zero IGMF, if primordial, could shed new light on conditions in the early universe and could complete the dynamo description for the origin of cosmic magnetic fields, by providing magnetic seed fields for dynamo amplification processes in turbulent flows during the formation of large-scale structures. On the other hand, an origin of the IGMF through astrophysical mechanisms, e.g., bulk outflows of magnetised material from radio galaxies, could explain young magnetised large-scale structures, with little time for dynamo growth, such as the magnetic bridge identified in the Coma supercluster [505]. The importance of a characterisation of the IGMF for our understanding of the evolution of the universe and the development of galactic magnetic fields has been outlined (see, e.g., Ref. [30] and the references therein).

Indirect detection methods, using a subset of the target selection for the EBL measurement, are our best approach towards a first measurement of the strength of the IGMF. There are two possible strategies to adopt when studying the IGMF using gamma rays above a few TeV:

- **Imaging analysis** searches for extended “pair halos” around blazars, which are expected for IGMF strengths $\gtrsim 10^{-16}$ G. Such searches will profit from the improved angular resolution and wide field of view of CTA (see Figure 12.4(a)). A first hint for the existence of pair halos in stacked Fermi-LAT data of blazars has recently been reported [508].
- **Time-resolved spectral analysis** explores a different parameter space, for IGMF strengths $\lesssim 10^{-16}$ G, which lead to so-called “pair echoes” (see Figure 12.4(b)) in the intergalactic medium, resulting in delayed signals at reduced energies. Rapid flux variations should be washed out by the cascade-like reprocessing of gamma rays towards lower energies. The ability of CTA to disentangle spectral components that are time-dependent

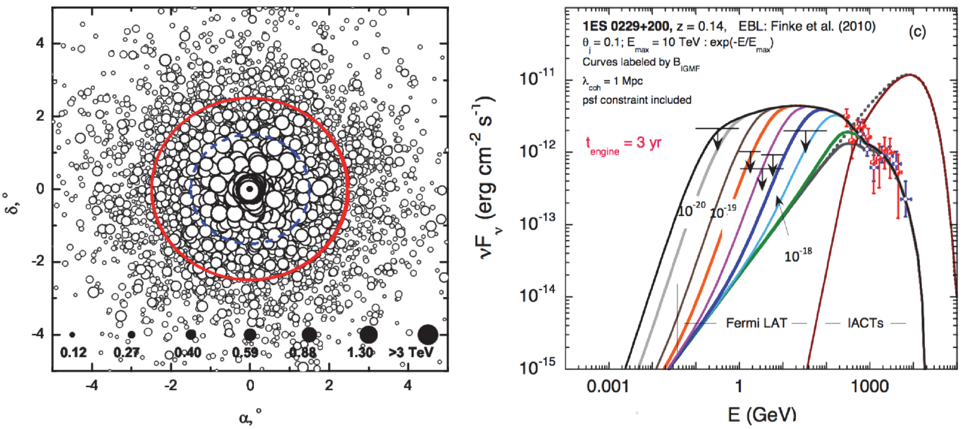

(a) (b)

Figure 12.4: (a) The arrival directions of primary and secondary gamma rays (black circles) from a source at a distance $D = 120$ Mpc with an IGMF strength of 10^{-14} G. The sizes of the black circles are proportional to the photon energies. The AGN intrinsic gamma-ray spectrum is described as a power law with an exponential cutoff. The blue dashed and red solid circles have radii of 1.5° and 2.5°, respectively, to indicate the extension of the pair halo image. Figure taken from Ref. [506]. (b) A model of the cascade radiation spectrum in a pair echo, applied to observations of the blazar 1ES 0229+200. The cascade spectra assume persistent TeV emission for different values of the magnetic field strength and coherence length. Figure taken from Ref. [507].

from those that are constant, especially in the low-energy range, will be of special importance.

12.1.3 *UHECRs and Fundamental Physics*

12.1.3.1 *AGN as potential sources of UHECRs*

In a similar way to the important advances that were made in the search for Galactic cosmic-ray emitters with GeV and TeV observations of supernova remnants and molecular clouds, one may expect that CTA will lead to an insight into the origin of UHECRs through high-quality data from extragalactic sources. Indirect evidence for cosmic-ray acceleration in such sources, from observations of gamma rays and possibly neutrinos, might indeed be the only way to solve this question, given the difficulties of direct searches for UHECR sources due to the low event statistics and the deviation of charged particles in extragalactic and Galactic magnetic fields.

Although the detection of very rapid variability of the high-energy flux during flares from a few bright sources such as PKS 2155-304, Mrk 421, or Mrk 501 seems to favour leptonic emission scenarios in blazars (but see, e.g., Ref. [509]), a significant contribution from hadrons during low states is not excluded. We will collect information on the occurrence of rapid flares in different AGN classes, as well as on the flux variability during low states, which will constrain current hadronic emission models. Simultaneous MWL observations will be crucial for such studies. A possible signature of UHECRs in gamma rays is a hard spectrum at energies beyond the characteristic gamma-ray absorption energy by the EBL. UHECRs interact with photons of the cosmic microwave background and the EBL during propagation in intergalactic space to produce UHE photons and leptons, which trigger electromagnetic cascades. If the IGMF is sufficiently weak, their cascaded secondary photons contribute to the gamma-ray flux from the source. Models based on this scenario reproduce successfully the SED of hard-spectrum blazars (see, e.g., Refs. [466, 510, 511]). Figure 12.5 shows the expected spectral hardening from UHECR-induced intergalactic cascades for a high-redshift blazar observable by CTA.

Another signature for the presence of relativistic hadrons in AGN is the occurrence of synchrotron-pair cascades in the emission region, which can lead, under certain conditions, to a visible spectral "bump" in the TeV range ([441, 443, 452, 513], see Figure 12.1). In addition, models of gamma-ray

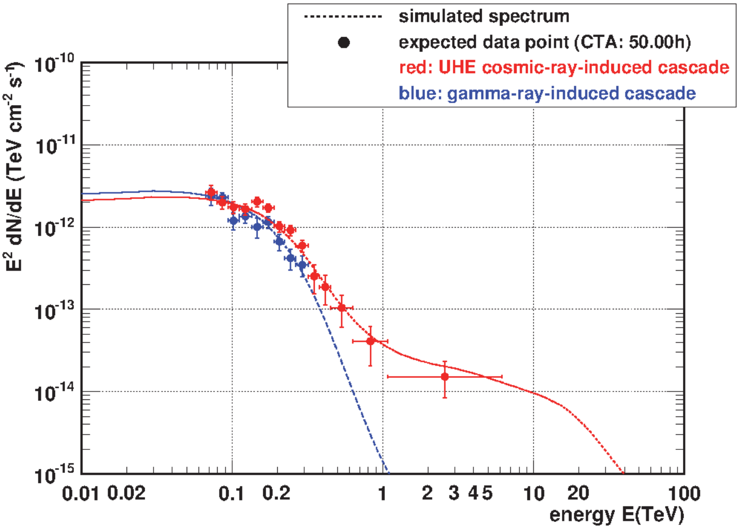

Figure 12.5: The expected CTA spectrum for the distant blazar KUV0031-1938, based on an extrapolation from current measurements and the addition of gamma-ray-induced cascades (blue curve), is compared to the spectrum from the same source when including UHECR-induced cascade emission (red curve). Error bars indicate the statistical uncertainty of one standard deviation. See also Refs. [466, 512].

emission close to the central SMBH, which can best be probed in LLAGN, provide yet another scenario for the acceleration of hadrons to ultra-high energies.

The search for such signatures requires high-quality spectra covering a wide spectral range for a sample of different VHE AGN classes and redshifts, together with information on the source variability. This will be achieved with the data gathered from the "high-quality spectra" and "AGN flare" programmes that are detailed below. In addition, several emission scenarios based on different acceleration sites have been proposed for radio galaxies, especially Cen A. These scenarios can be tested with the deep VHE observations we propose for this source (see, e.g., Refs. [486, 514–516] and many others).

12.1.3.2 *Can we find signatures for the existence of axion-like particles?*

An issue with wide ranging implications for fundamental physics that can be probed in several ways with measurements of VHE gamma rays from distant sources is the existence of ALPs (for more information, see Chapter 1). EBL absorption of VHE photons would be considerably reduced by $\gamma \leftrightarrow$ ALP oscillations taking place in ambient magnetic fields [517–524]. First hints for a reduced gamma-ray opacity might have been observed in the form of a pair-production anomaly at the four standard deviation level [525] and of unusually hard gamma-ray spectra compared to what is expected from standard EBL absorption [526, 527]. (These hints do not seem to be confirmed however, see [498, 528, 529]). Photon-ALP oscillations would provide a natural solution to these problems if they are confirmed [518, 522, 530].

Alternatively, the $\gamma \rightarrow$ ALP conversion could occur inside the blazar or in its direct environment, and the ALP $\rightarrow \gamma$ reconversion could take place in the Milky Way magnetic field [518]. One possibility is that the blazar resides inside a group of galaxies or a galaxy cluster, where the $\gamma \rightarrow$ ALP conversion is triggered by the cluster magnetic field [530, 531]. It should be noted that these environments will be extensively studied by SKA using Faraday rotation measurements to achieve a better parametrisation of the magnetic fields.

As far as completely isolated BL Lac objects are concerned, the $\gamma \rightarrow$ ALP conversion probability strongly depends on the uncertain position of the VHE gamma-ray emission region along the jet and on the strength of the magnetic field therein [531, 532]. On the other hand, the turbulent magnetic field in radio lobes at the termination of AGN jets could lead to a significant proportion of ALPs in the beam [532]. Photon-ALP mixing could also explain the observation of VHE gamma ray in FSRQs if the emission zone is located inside the BLR (e.g., Ref. [533]).

Due to the expected spectral signatures of photon-ALP mixing, a search for ALPs suggests an observational strategy closely related to that of EBL studies. In order to detect a reduced opacity, observations at high optical depths are necessary. Dedicated studies [531, 534] show that flaring episodes of distant blazars at redshifts $0.2 \lesssim z \lesssim 0.5$ are best suited for this work. At the same time, the intrinsic spectrum emitted by the blazar has to be determined as precisely as possible. To this end, MWL coverage, especially with X-ray telescopes, is of importance since it can provide insights on the particle distribution inside the source and thus help constrain the intrinsic spectrum in the CTA energy range.

Observations of bright FSRQs at any redshift offer an additional opportunity to search for ALPs and to test the hypothesis that ALPs facilitate the escape of gamma rays from the BLR. Promising targets coincide with the sources selected for EBL studies. The search for oscillations in the spectra are best carried out with bright sources located in regions where the magnetic field is known to be strong. Thus, bright AGN in galaxy clusters are ideal targets [535, 536]. Examples are PKS 2155-304, M 87, and NGC 1275 (see also the Clusters of Galaxies KSP, Chapter 13). Blazars in isolated environments could serve as a control sample in case indications for ALP-induced oscillation features in spectra are found.

12.1.3.3 *Can we rule out Lorentz Invariance Violation?*

The significance of LIV searches as a motivation in the development of quantum gravity theories has been discussed in Chapter 1. CTA observations of AGN would enable multiple tests of LIV to break the degeneracy between intrinsic source physics and propagation-induced effects, given the balance of variability, distance, and VHE emission [271]. The duration of AGN flares is sufficient for atmospheric Cherenkov telescopes to slew to them, but still retains the potential to observe rapidly varying features to provide constraining limits on LIV effects. The AGN we target are regularly spaced in redshift so that propagation-induced versus source intrinsic dispersion effects can be tested for.

Recent observations of GRBs with Fermi-LAT have provided stringent constraints on the linear term in generic models that break Lorentz invariance [537], and measurements of VHE photons from AGN flares with

H.E.S.S. [538] have shown that atmospheric Cherenkov telescope data from AGN flares can put strong constraints on the quadratic term, which is not yet well constrained.

Even if the AGN light curve does not have sufficiently rapid features to determine dispersion for any single flaring episode, a LIV-induced dispersion will mean that the higher energy photons will always be shifted with respect to the lower energy ones in the light curve. The accumulation of long-term monitoring data means that we can still potentially determine time delays with high confidence through the use of cross-power spectral analysis methods [271]. This will be the first time that routine AGN observations, i.e. not at exceptional flux levels, will allow us to constrain LIV parameters.

The LIV that modifies the dispersion relation for gamma rays could also affect the kinematics in the pair-production with the EBL, changing the threshold for interaction and allowing VHE photons to be detected that would not normally arrive at the observer [498, 539, 540]. A study with deep observations of suitably hard-spectrum, distant AGN testing for any changes in EBL absorption, akin to the ALPs study, would enable a probe of new physics with relevance to LIV studies also.

12.1.4 *Advance beyond State of the Art*

One of the main difficulties in all the studies discussed above with current-generation instruments lies in the separation of intrinsic spectral features from propagation-induced effects. The strength of the observing strategy of CTA's AGN KSP lies in the observation of a large set of sources of different classes and at different redshifts with high gamma-ray statistics. In addition, variability leads to different patterns for intrinsic and propagation-induced effects. With the AGN KSP, we will for the first time gather information from a selection of sources at all time scales. This will allow us to distinguish signatures of the EBL, IGMF, and modified fundamental interactions from source physics.

AGN observations will profit greatly from the improved performance of CTA compared to current instruments. CTA will provide better access to low-frequency peaked sources (FSRQs, LBLs, IBLs, and probably NLSy1s) due to its wider energy coverage. The improved sensitivity will allow us to measure variability, even in quiescent source states and to record time-resolved spectra for many bright sources. Measurements of the EBL will, for the first time, make use of the access to absorbed and un-absorbed components in a single gamma-ray spectrum, which will reduce greatly the systematic uncertainties. Similarly, IGMF measurements will use the original and reprocessed components in a single spectrum. Improved energy resolution and sensitivity will lead to high-quality spectral measurements. The improved angular resolution will be useful for the search for extended emission from radio galaxies and halos. There is also, for the first time, the possibility of carrying out snapshots with sub-arrays to increase the probability of detecting flares.

A complementary approach to CTA in the VHE band is represented by ground-based air-shower detectors such as HAWC, Argo YBJ, or the future LHAASO. These detectors have the advantage of a very large duty cycle and wide sky coverage, which will be useful for continuous monitoring of bright AGN, but they suffer from a higher energy threshold and poorer sensitivity at a comparable exposure time for a given field of view.

When comparing its expected performance with that of Fermi-LAT, the great advantage of CTA in the overlap region of energies (a few tens of GeV) lies in its much better sensitivity to rapid variability. Furthermore, the higher energy reach of CTA is important to detect features at the end of the observed spectrum, such as breaks or cutoffs, which can originate from acceleration and radiation mechanisms or from absorption effects. CTA has limited sensitivity to the majority of FSRQs and LBLs in low states, but, on the other hand, the high energy emission from UHBLs, which are very difficult to detect with Fermi-LAT, falls almost exclusively into CTA's energy range. IBLs and HBLs will be well covered due to the wide energy range of CTA. The overall accessible source statistics will be less than for Fermi-LAT, given the difference in the energy bands and the steeply declining spectra of AGN, but observations with CTA will provide much higher resolution in light curves and variable spectra for the detected sources.

12.2 Strategy

Current advances in AGN physics rely to a large extent on the simultaneous measurement of the AGN SED and its time variation across all wavebands, from radio to VHE. In the context of the AGN KSP, the CTA Consortium will:

- set up coordinated — where appropriate long-term — programmes of AGN observations, involving observation proposals, target of opportunity (ToO), and MoU-based co-operations with other facilities and instruments, enabling coherent and consistent MWL coverage and joint data analysis (see Section 12.2.2 for details),

- ensure effective and consistent follow-up of AGN flares reported by other facilities and instruments, under MoUs where appropriate, and set up programmes for flare monitoring and alert generation, and
- help to implement observation modes and scheduling for the most efficient monitoring of variable sources, by flexibly dividing the arrays into multiple subsystems as appropriate.

The following observation programmes will be carried out under the AGN KSP:

1. **Long-term monitoring** of a few prominent VHE AGN up to at least 10 years:
    - *Guaranteed science*: long-term light curves and time-resolved spectra for all studies involving AGN variability on medium and long-time scales, addressing quiescent states, duty cycles, and spectral variability.
    - *Discovery potential*: disk-jet connection, (quasi-)periodic oscillations, and LIV.
2. Search for, and follow-up of, short-term **AGN flares** based on external ToOs and internal snapshot monitoring of a large number of AGN:
    - *Guaranteed science*: effectively sampling the high states of AGN and high-statistics, high-temporal resolution spectra for studies of short-term variability; EBL/IGMF measurements at $z > 0.5$.
    - *Discovery potential*: TeV emission from NLSy1s and others; LIV and ALPs.
3. **High-quality spectra** for a systematic coverage of redshifts and AGN typology:
    - *Guaranteed science*: a comprehensive data set, obtained under uniform conditions, for AGN classification and evolution studies; high-precision spectra for a precise measurement of the EBL, studies of emission scenarios for VHE blazars and of the IGMF.
    - *Discovery potential*: extended VHE emission from two nearby radio galaxies; UHECR signatures; LIV and ALPs.

Data from long-term monitoring will be released immediately in the form of light curves. The "AGN flare" programme will produce regular alerts to the community, e.g., in the form of VOEvents. High-quality spectra will be compiled in a catalogue that will be available to the community after the usual proprietary period.

The long-term source monitoring and snapshot programmes can make use of observations under moonlight. In general, extraction of high-quality spectra with energy coverage down to the lowest energies will require observations taken at small zenith angles. Specific developments are under way for an efficient online real-time analysis during the snapshot programme.

12.2.1 *Target Selection*

12.2.1.1 *Long-term monitoring*

In the long-term monitoring programme, which will provide long-term VHE light curves, we want to cover all known types of VHE AGN (UHBL, HBL, IBL, LBL, FSRQs, and radio galaxies). To arrive at a representative sample, we want to observe two to three sources per class. As an example, a list of 15 potential targets, including some of the most prominent TeV sources, is given in Table 12.1.

Each target should be observed on average ~30 min once a week during its period of detectability with the full array (possibly less for the bright UHBLs and HBLs and more for soft-spectrum sources). This would result in <12 h/yr per target, leading to greater than seven standard deviation ($>7\sigma$) detections of all sources in their quiescent state, sufficient for spectral measurements. For the brighter sources, spectra can be extracted on a weekly or monthly basis. The regular observations will permit tracking of the flux variability of all sources in the form of long-term light curves. If a source is found in a flaring state, more intensive coverage can be triggered as part of the "AGN flare programme" (see below).

The total exposure time for 15 fields of view would be <180 h/yr. With the currently proposed list of targets, this time would be split into 132 h of yearly observation time for the north and 48 h for the south. Observations would fall naturally into dark time (~50%) and moon time (~50%). Note that even though the main objective of this programme, i.e., studying the long-term flux variation, can be achieved with LSTs and MSTs, an additional

Table 12.1: Example list of targets for long-term monitoring.

UHBLs	1ES 0229+200 (N), 1ES 1426+428 (N), 1ES 1101-232 (S)
HBLs	Mrk 421 (N), Mrk 501 (N), PKS 2155-304 (S)
IBLs	1ES 1011+496 (N), 3C 66A (N), W Comae (N)
LBLs	AP Librae (S), BL Lacertae (N)
FSRQs	PKS 1510-089 (S), PKS 1222+216 (N)
Radio Galaxies	M 87 (N), NGC 1275 (N)

Note: The labels "(N)" and "(S)" indicate observations with the northern and southern array, respectively.

(currently not foreseen) SST component in the north would be very useful for extending the spectral coverage of HBLs and UHBLs during flaring states above 10 TeV with good sensitivity,

The list of targets will be reviewed after five years and reduced to the 10 most interesting objects (in terms of variability patterns) for further monitoring over at least 10 years, and ideally over the full CTA lifetime.

12.2.1.2 *AGN flare programme*

Given the central importance of variable phenomena for VHE research with CTA, an extended programme needs to be set up to target AGN flares. The expected number of external alerts, based on our experience from current experiments (with, e.g., Fermi-LAT or Swift), would be roughly 25 per year, about half of which will be followed up with a full CTA array. This would lead to ∼10−15 external flare alerts to be followed up per year. An on-site optical facility with photometric and polarimetric facilities would be extremely useful in this respect, as discussed below (cf. Section 12.2.2). Future "transient factories" as well as ground-based VHE detectors, discussed in Section 12.2.2 and Chapter 2, might increase this rate slightly. One should note that ground-based VHE detection will provide rapid alerts only for very bright hard-spectrum sources. The alerts from optical and radio transient factories will be more numerous, but as the time scales of the flares from the transient factories are very different than VHE flares, only a few of these alerts will be followed with the full CTA arrays. However, these alerts can be used as a selection criterion for potential targets for the snapshot programme.

Thus, although they are very important, it is not sufficient to rely on external alerts from MWL facilities, since different variability behaviour is seen even when comparing VHE data from current atmospheric Cherenkov telescopes to HE data from Fermi-LAT. In addition to external alerts, plus some flares expected from the long-term monitoring targets and from the selection of targets for high-quality spectra (see below), we will carry out snapshots, i.e., very short exposures of a large list of targets, using CTA sub-arrays, to self-trigger full-array observations in the case of flares. This method is already being used successfully by current atmospheric Cherenkov telescopes.[d]

---

[d] Alternatively, one might consider to extend the lifetime of certain of the current atmospheric Cherenkov telescopes to serve as dedicated VHE monitoring facilities for CTA.

The selection of potential targets for snapshots should be large, given the limited rate of detectable flares. An example of sources that should be included are:

- FSRQs and soft-spectrum BL Lac type objects (LBL, IBL). A selection can be based on Fermi-LAT average spectra, by computing the "flux enhancement" needed to reach 30% of the Crab nebula flux in the CTA energy range. When the enhancement factor is within the typical variation for such sources (factor of 10–40), the source is selected,
- a selection of ~20 known VHE gamma-ray emitting HBLs/UHBLs (see TeVCat [204]), giving preference to bright sources with well established redshifts,
- a selection of ~10 radio galaxies detected with Fermi-LAT, and
- NLSy1s detected with Fermi-LAT (eight sources with high significance so far [541, 542]).

The above selection of ~80 AGN will be followed with CTA sub-arrays with a sensitivity of ~20% of the Crab nebula flux.

- **Soft-spectrum sources** (FSRQs, NLSy1s, LBLs, certain IBLs, and certain radio galaxies) will be observed with the large-sized telescopes (LSTs). Setting the threshold for triggering a flaring alert to 20% of the flux from 3C 279 during its 2006 flare [543] (corresponding to roughly 20% of the Crab nebula flux), four LSTs will need ~10 min of exposure time plus an overhead (pointing, stopping, and starting the observation) of ~2 min per pointing.[e] Five targets could be covered in one hour, i.e., covering ~20 targets twice a week would require ~4 h per week per site. A total of ~200 h of LST observation time would be needed per year per site to cover 40 sources.[f]
- **Hard-spectrum sources** (HBLs, UHBLs, certain IBLs, and certain radio galaxies) will be observed preferably with sub-arrays of medium-sized telescopes (MSTs), or small-sized telescopes (SSTs) in the case of very bright, very hard sources observed from the southern hemisphere. Sub-arrays of four MSTs are estimated to provide a sensitivity of 20% of the Crab nebula flux in roughly 3 min. If CTA is divided into ten such sub-arrays (in total, 4 for the northern plus 6 for the southern array[g]),

---

[e] The use of sub-arrays with two LSTs is less efficient in terms of the total time needed.

[f] Each source is assumed to be visible for about half a year.

[g] Given the currently simulated configurations, one of the northern sub-arrays would contain only 3 MSTs and would be pointed to the brightest targets.

> only ∼10 min would be needed to cover 20 sources. This would lead to an estimated average observation time of ∼20 min per week per site and ∼17 h/yr per site for the full MST sub-array, to cover 40 sources.

Observations with the northern site will be given preference, where possible, due to the smaller overlap with Galactic observation programmes. With this in mind, the total observation time could be split roughly into 300 h/yr with the northern LSTs, 22 h/yr with the northern MSTs, 100 h/yr with the southern LSTs, and 11 h/yr with the southern MSTs. The requirement for observation time with the LSTs is rather high and one should try to target most sources, except for the ones with the softest spectra, with MST sub-arrays. Work on such an optimisation is under way.

To estimate the overall rate of triggers from snapshots, we assume the flaring probability for the brightest events to be ∼1%, based on past observations. If we monitor ∼20 sources twice a week at each site, this corresponds to roughly 7 sources observed each night per site and to less than one hour per night per site. For any night, the probability to catch a flare would be about 7%, leading to about 20 flares per year per site triggered with snapshots. As will be discussed below, the number of snapshots will be reduced after the first two years of full operation, which should lead to a reduction to roughly half of this number in the third year and to a further reduction in the following years.

Once a CTA array has been successfully triggered, the average observation time to follow-up on a trigger is estimated to be roughly 4 h. Based on these estimates, we foresee the total follow-up observing time per year with the full arrays (sum for two sites) for snapshot triggers, triggers from the other observation programmes of the AGN KSP, and accepted external triggers to be roughly 200 h, with a larger fraction for the northern site.

In addition, some more observing time needs to be allotted to sub-array observations that verify external triggers and to perform periodically spaced observations to verify the state of the source once an external trigger has been issued, to search for delayed flares. The verification should require about 10 min for each of the estimated 25 external triggers, i.e., ∼4.5 h/yr. The follow-up verifications, on average 10 per year, would add ∼40 h of observing time per sub-array per year.

Given the nature of these observations, a large fraction will be carried out during moon time. The impact on data quality, especially on the low-frequency peaked objects due to the higher energy threshold during observations with moonlight, will be evaluated during the first year of observations.

12.2.1.3 *High-quality spectra*

This last observation programme consists of two distinct groups of targets:

(a) Coverage of redshifts and VHE AGN classes

A set of targets has been selected to maximise the population in redshift space with VHE AGN of different classes. We have extracted spectra of known TeV emitters and promising source candidates from the Fermi-LAT 1FHL catalogue [544] and extrapolated their spectra to the TeV range, while applying a redshift- and energy-dependent absorption on the EBL following the model of Ref. [446]. For those sources for which no redshift was provided in the catalogue, we have used the lower limits determined by Refs. [545, 546]. The resulting spectra were then compared against the CTA performance curves.

We selected our targets among those sources with an expected significance above 5σ in 20 h of observations in the energy region where EBL absorption is significant, i.e., at energies where the optical depth is larger than 1. To sample both the intrinsic and absorbed parts of the spectrum, we additionally required at least five spectral points, with at least two points in the absorbed ($\tau > 1$) regime and at least one point with $\tau > 2$, and a significance of 20σ above 60 GeV for most targets ($10\,\sigma$ above 60 GeV for a few sources with relatively low fluxes). For very hard sources, we introduced a spectral break at 500 GeV.

An example selection list of such sources is given in Table 12.2. Due to unpredictable long-term variations in the blazar flux states, this list is preliminary and will be updated with the most promising targets once CTA operations begin. If a source shows no signal after the exposure time expected for a detection at a predefined significance, it will be replaced with a new source in the same redshift band and of the same class, if possible. The distribution of expected integral fluxes (above 60 GeV) against redshift can be seen in Figure 12.6.

About 10 sources have been selected in each of the two intervals of $\Delta z = 0.1$ from $z = 0$ to $z = 0.2$; these sources are particularly constraining for far-infrared measurements of the EBL and a determination of the Hubble constant. Ideally, at least five sources would then be needed in each interval of $\Delta z = 0.2$ from $z = 0.2$ to $z = 1.0$ for a precision measurement of the EBL and its evolution and for a study of the evolution of blazars with redshift. Care was taken to include sources of different gamma-ray loud AGN classes, wherever available. For the IGMF study, we will select a subset of sources for which the spectral region where EBL absorption is significant ($\tau > 1$) is

Table 12.2: Example selection list of sources for high-quality spectra. Sources are ordered by redshift.

Object	RA	DEC	Class	σ(20 h)	Redshift	TeVCat	t [h] (20σ)	N/S
IC 310	49.169	41.322	HBL	35.63	0.019	Yes	6	N
Mrk 421 (lt)	166.121	38.207	HBL	212.50	0.031	Yes	(1)	N
Mrk 501 (lt)	253.489	39.754	HBL	101.46	0.034	Yes	(1)	N
1ES 2344+514	356.759	51.705	HBL	66.95	0.044	Yes	2	N
Mrk 180	174.100	70.159	HBL	27.55	0.046	Yes	11	N
1ES 1959+650	300.007	65.158	HBL	28.60	0.047	Yes	10	N
PKS 0521-36	80.85	−36.34	RG	9.25	0.06	No	23 (10σ)	S
PKS 0548-322	87.669	−32.260	HBL	14.34	0.069	Yes	39	S
PKS 0625-35	96.704	−35.479	RG	26.14	0.055	Yes	12	S
PKS 1440-389	221.011	−39.145	HBL	27.28	0.065 (?)	No	11	S
PKS 2005-489	302.360	−48.830	HBL	60.83	0.071	Yes	2	S
MS 13121-4221	198.749	−42.696	HBL	85.52	0.108	Yes	1	S
VER J0521+211	80.449	21.220	IBL	53.45	0.108	Yes	3	N
VER J0648+152	102.225	15.281	HBL	18.10	0.179	Yes	24	N
PKS 2155-304 (lt)	329.721	−30.219	HBL	131.71	0.116	Yes	(1)	S
1ES 1215+303	184.460	30.104	HBL	22.34	0.130 (?)	Yes	16	N
1H 1914-194	289.441	−19.365	HBL	25.37	0.137	No	12	S
1ES 0229+200 (lt)	38.20250	20.29	UHBL	—	0.14	Yes	(1)	N
TXS 1055+567	164.666	56.459	IBL	22.78	0.143	No	15	N
PG 1218+304	185.337	30.194	HBL	32.22	0.184	Yes	8	N
1ES 0347-121	57.3458	−11.97	UHBL	—	0.188	Yes	1	S
1H 1013+498	153.773	49.427	HBL	21.59	0.212	Yes	17	N
PKS 0301-243	45.868	−24.128	HBL	39.46	0.260	Yes	5	S
PMN J1936-4719	294.214	−47.356	BLL	20.10	0.265	No	20	S
PMN J0816-1311	124.091	−13.177	HBL	18.17	0.290 (ll)	No	24	S
3C 66A (lt)	35.669	43.035	IBL	49.64	0.33 (ll)	Yes	(3)	N
1ES 0502+675	77.038	67.624	HBL	41.65	0.340	Yes	5	N
TXS 0506+056	77.394	5.714	IBL	13.17	0.210 (ll)	No	46	N
MS 1221.8+2452	186.146	24.628	HBL	13.09	0.218	Yes	47	N
PG 1553+113	238.942	11.190	HBL	67.27	0.43 (ll)	Yes	2	N
4C +21.35	186.220	21.377	FSRQ	13.74	0.434	Yes	42	N
1ES 0647+250	102.712	25.081	HBL	24.75	0.490 (ll)	Yes	13	N
KUV 00311-1938	8.407	−19.361	HBL	22.07	0.506 (ll)	Yes	16	S
PMN J1610-6649	242.726	−66.849	HBL	14.70	0.447 (ll)	No	37	S
PKS 1424+240	216.766	23.790	HBL	29.33	0.600 (ll)	Yes	9	N
PKS 1958-179	300.28	−17.87	FSRQ	7.0	0.65	No	41 (10σ)	S
B3 0133+388	24.147	39.100	HBL	14.22	0.750 (ll)	Yes	40	N
PKS 0537-441	84.714	−44.088	LBL/FSRQ	19.33	0.892	No	21	S
4C +55.17	149.421	55.377	FSRQ	8.53	0.899	No	27 (10σ)	N
PKS 0426-380	67.178	−37.937	LBL/FSRQ	10.63	1.111	No	18 (10σ)	S

Notes: Those sources that are already covered in the selection for long-term monitoring are labelled “(lt)”. Lower redshift limits are marked with “(ll)” and uncertain redshifts with “(?)”. The column labelled “TeVCat” indicates if a source is an already known TeV emitter or not [204].

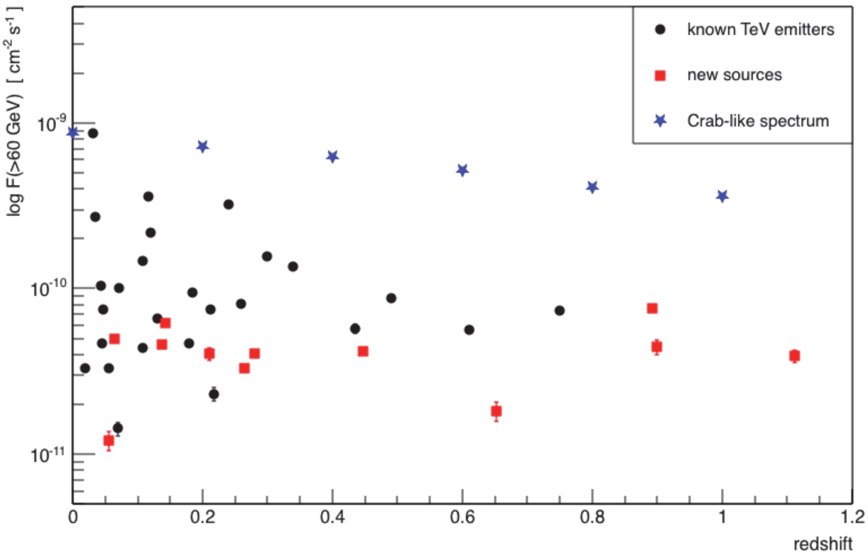

Figure 12.6: Expected integral fluxes above 60 GeV (from extrapolations of Fermi-LAT spectra) versus redshift for the selection of sources for the high-quality spectra programme. The flux from a source with a Crab nebula-like spectrum, shifted to different redshifts, is shown for comparison. For studies of the EBL, IGMF, and blazar evolution, this sample will be completed with observations from the AGN flare programme at high redshifts.

located at TeV energies, to ensure that the bulk of the reprocessed emission is detectable with CTA.

Several hard-spectrum, high-redshift sources in this selection have been identified to be particularly well suited for ALP searches. We also foresee deep observations of at least two hard-spectrum sources from the above selection for the study of LIV effects in the interactions between gamma rays and diffuse extragalactic background radiation and for the search for UHECR-induced cascade features. A source with $z < 0.15$ and with an intrinsic spectral cutoff above 10 TeV would be required to obtain limits of above 10^{11} GeV on a quadratic LIV term. It should be noted that the energy range above 10 TeV will be targeted mostly with southern sources, due to the SST component in the southern array.

The total estimated observation time would be ∼343 h for the northern array and ∼283 h for the southern array, given the current source selection. It should be noted that the difference between CTA-North and CTA-South sensitivity (roughly a factor 4 in sensitivity above 10 TeV) was taken into account in the target selection and required observation time estimation. Given the importance of observing high-quality spectra over a maximum energy range, we ask for low zenith angle observations using the full array, except for the soft-spectrum targets (FSRQs and LBLs), where VHE emission above a few TeV is not expected and the SST component can be used to observe other targets. Observations should be performed where possible within one month to avoid mixing different states. Given the amount of exposure time required, this campaign can begin during the (late) construction phase of CTA, where we would focus on those targets that require the least exposure, and it could extend over the first three years of full operations. We estimate that roughly half of the total observation time could be covered during the phase before the start of full CTA operations.

(b) Deep exposures of two radio galaxies

The two nearest radio galaxies, both known TeV emitters, are proposed for deep observations to extract high-quality spectra and to search for extended emission:

- **Cen A:** To probe extended emission from Cen A, either from its radio lobes or its kpc jet, a deep scan is foreseen. Three deep exposures with the southern CTA array will be necessary to completely cover the central part of Cen A, including the kpc jet and the southern extended radio lobe, with sufficient overlap between the fields of view and allowing for a significant exposure away from the lobe for background subtraction. The three fields of view will be centred on the central core and on the lateral edges of the southern radio lobe. Data will be taken in wobble mode, where the telescopes are pointed at small offsets from the targeted position, usually 0.5° to 1.5°, in alternating directions to facilitate background subtraction (cf. Figure 12.7 for a schematic view of the pointings).

  The exposure of the core region will provide a high-quality spectrum of the emission from the central source and will allow us to distinguish between different proposed interpretations of the mismatch seen between the Fermi-LAT and H.E.S.S. spectra. If this first exposure shows an indication for a signal from the lobes, two dedicated exposures of the southern lobe will be carried out. We choose the southern lobe since it is seen to be brighter than the northern one at other wavelengths. An observing time of 50 h (dark time) will be needed for each of the three exposures, resulting in a total of 150 h of observing time with the southern array. All telescopes should be included in these observations. In the case of discovery of extended emission from the southern lobe, this observational programme could be extended to both radio lobes, either in the form of an updated KSP or in the form of a GO proposal, which would profit from the technical expertise

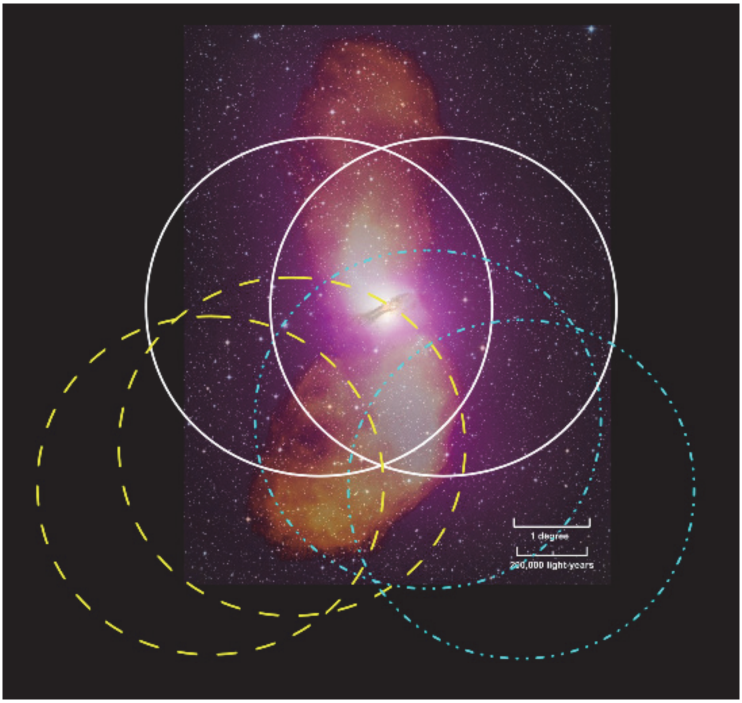

Figure 12.7: Scheme of a possible pointing pattern for a scan of the Cen A central core and southern lobe. The circles correspond to the size of the LST field of view (4.5° in diameter), which is the smallest field of view of the three CTA telescope types. Different colours and line styles indicate the three different exposures with pointings in wobble mode (see text for discussion). Credits for the skymap: NASA/DOE/Fermi-LAT Collaboration, Capella Observatory, and Ilana Feain, Tim Cornwell, and Ron Ekers (CSIRO/ATNF), R. Morganti (ASTRON), and N. Junkes (MPIfR).

that we will have acquired, especially concerning estimates of systematic errors.

- **M 87:** Given its smaller extension in the sky, M 87 can be covered with a single deep observation. A total observing time of 100 h of dark time is foreseen for the full northern array. This observation will produce a high-quality spectrum and might lead to the detection of extended emission from the radio lobes [30]. In addition, a possible extension of the hard power-law of M 87 to a few tens of TeV would allow for a very good probe of the EBL in the regime of a few tens of micrometer, although significant statistics in this energy range would probably require data from flaring states due to the foreseen absence of an SST component in the northern array. It should be noted that M 87 is also a prime target for monitoring, due to its high variability. Exposure time spent on the source

Table 12.3: Summary of required observing times for the northern site ("N") and the southern site ("S") for the different parts of the observation programme.

Programme	Total N [h]	Total S [h]	Duration [yr]	Observation mode
Long-term monitoring	1110	390	$10^{\dagger}$	Full array
AGN flares				
Snapshots	1200	475	10^{*}	LSTs
Snapshots	138	68	10^{*}	MSTs (assuming 10 sub-arrays)
Verification ext. trig.	300	150	10^{*}	LSTs or MST sub-arrays
Follow-up of triggers	725	475	10^{*}	Full array
High-quality spectra				
Redshift sample	195	135	3	Full array
M 87 and Cen A	100	150	3	Full array

Note: The total duration of each programme is given in the fourth column, where a "$*$" ("†") indicates a reduction of the yearly exposure time after 2 (5) years.

with the long-term monitoring programme during the first three years will contribute to the deep exposure.

12.2.1.4 *Time distribution model for the AGN KSP*

A summary of the required observation times for the different parts of the AGN KSP is given in Table 12.3. The current time distribution model foresees that the high-quality spectrum, long-term monitoring and the AGN flare programmes begin during the construction phase of CTA. Spectrum measurements will be completed by the end of the third year of operations with the full arrays. However, with the estimated rate of flares it will take about five years to collect the 30–50 flares needed to cover the high-redshift bins for the EBL measurement. It should be noted that $<50\%$ of flares are estimated to provide sufficiently high-quality spectra to be used for this purpose. For FSRQs, NLSy1s, and high-redshift sources, the programme should continue beyond the first five years. After the first two years, the trigger threshold will be increased to progressively reduce the observing time dedicated to ToOs and snapshots. Long-term monitoring should continue for at least 10 years, with a reduction in the number of targets to the 10 most interesting ones (given their past record of observations) after the first five years.

Based on 10 years of operation with the full arrays, the AGN KSP would require a total of about 3300 h full-array exposure, not accounting for observations with sub-arrays (i.e., snapshots and verification of external triggers). However, the use of moonlight time for the observation of hard-spectrum sources would reduce the amount of required dark time for full-array observations to about 2000 h. For example, targets from the EBL/IGMF selection with redshifts $z < 0.2$ can in general be observed with moderate moonlight, given the existence of data points at several TeV. About 1000 additional hours of observations could be carried out during the construction phase, split in equal parts between the high-quality spectra programme, the long-term monitoring programme, and the AGN flare programme. Data for several targets (e.g. PKS 2155-304, PG 1553+113, etc.) will also be available from the science verification observations. A time distribution model for exposures with the full array during the first 10 years of full operations is shown in Figure 12.8.

The observation time with partial arrays must also be considered. An estimated 1350 h (550 h) of LST exposure time and 290 h (140 h) of MST exposure time are required over 10 years for the northern (southern) array for snapshots and verification of external triggers. About half of these observations will be carried out under moonlight, leading to a total of about

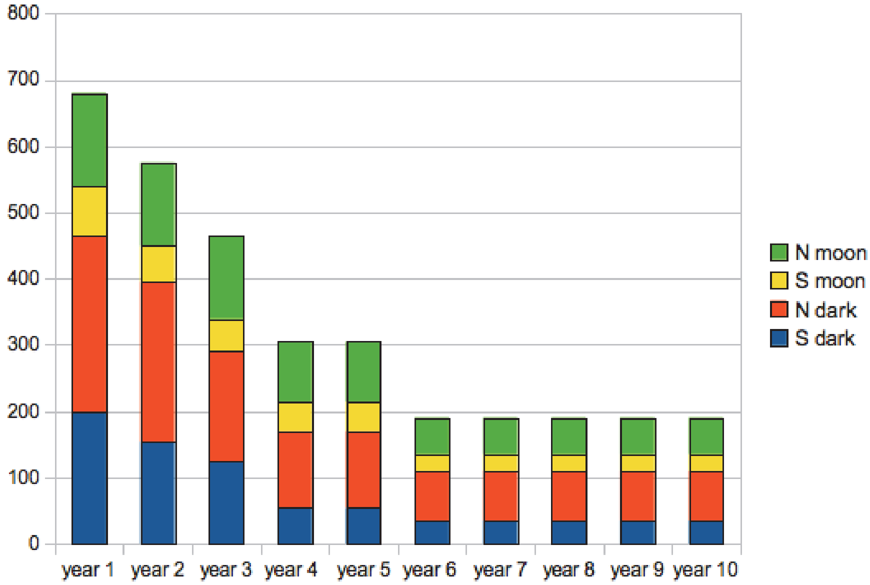

Figure 12.8: Distribution of the required full-array observation times (in hours) for the AGN KSP over the first 10 years of full operation, including all observation programmes, except for snapshots and verification of external triggers, which will not necessitate the full array (cf. Table 12.3). The different colours in each column indicate, from top to bottom, the exposure during moon time for the northern and the southern arrays and the exposure during dark time for the northern and the southern arrays.

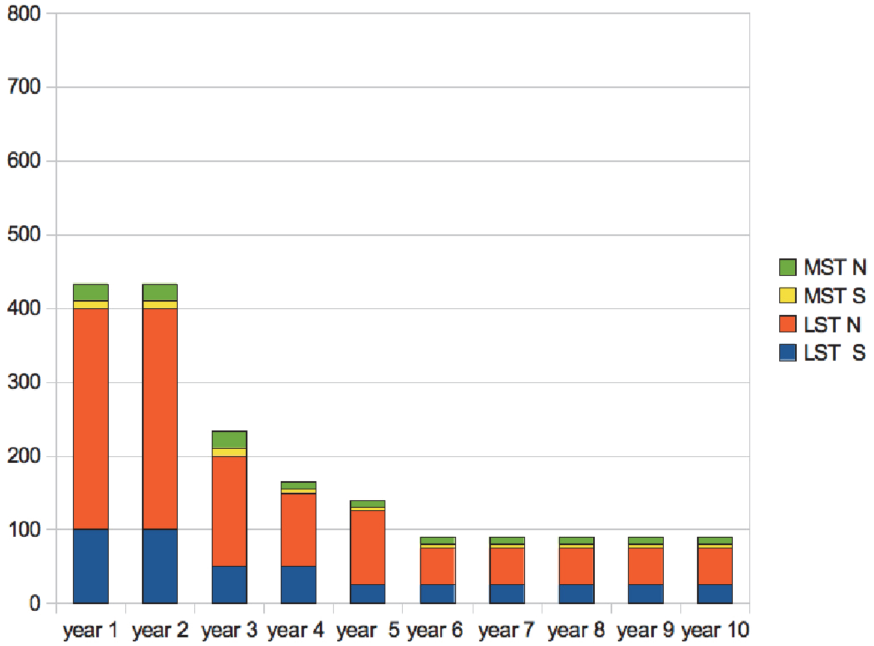

Figure 12.9: Distribution of the proposed sub-array observation times (in hours) for the snapshot programme over the first 10 years of full operation (see Table 12.3). The different colours in each column indicate, from top to bottom, the exposure with MST sub-arrays with the northern site and southern site and the exposure with LST sub-arrays with the northern site and southern site. It should be noted that about half of these observations will make use of moonlight.

950 h of required dark time for the LST sub-array and about 220 h of required dark time for the MST sub-arrays over 10 years of full operation. Snapshots with LSTs could be carried out while the MST and SST component of the array are used for observations that do not require very low energy reach. MST snapshots could also be run in parallel with other observations. A study on optimising the usage of LST sub-arrays is under way. A time distribution model for snapshot exposures with LST and MST sub-arrays during the first 10 years of full operations is shown in Figure 12.9.

12.2.2 *Multi-wavelength and Multi-messenger Coverage*

The unique advantage of observations of AGN in the VHE band is that they provide information on the most energetic particles inside those sources and probe the shortest variability time scales. However, to maximise the scientific return from such observations, a combination with data from other wavebands and messengers is of great importance. Simultaneous MWL observations have proven of great value in the past to constrain emission scenarios through correlated flux variations and detailed SEDs. The main reason is that different components in the blazar spectra vary on different time scales and are thought to be produced in different places along the jet.

The availability of dedicated optical instruments in close proximity to the two CTA sites, with photometric and polarimetric capabilities, would be an important advantage for this KSP. As discussed in Chapter 2, this would permit a continuous monitoring of all targeted sources, providing complementary data simultaneous to the VHE observations. Candidate sources in the search for flaring states could be monitored for high optical states, which seem generally linked to increased VHE activity (see, e.g., Refs. [42, 547]).

In addition, the optical polarisation monitoring of blazars has proven to be a powerful tool for locating the emission region within the jet in luminous quasars (see, e.g., Refs. [548, 549]). Polarisation traces the ordered magnetic field of the jet and can be modified by shocks. Rotations of the optical polarisation vector or shifts in the polarisation fraction have been found to coincide with gamma-ray outbursts and can be used to trigger VHE observations. A good example is the RoboPol project[h] that monitored a sample of 100 gamma-loud blazars in the optical band, requiring 60% of the time of the dedicated facility [38]. A large statistical sample of sources in different activity states enabled the assessment of the statistical connection between the optical polarisation and high energy events. During its three first seasons, RoboPol detected 40 optical polarisation angle rotations indicating a physical connection to gamma-ray flares, possibly based on several distinct underlying mechanisms [550]. Based on these results, it is already clear that a dedicated instrument is needed to provide triggers for CTA based on optical rotations and to systematically monitor AGN observed with CTA.

All of the observation programmes of this KSP require at least some MWL support to guarantee an optimal impact of the resulting data:

- **Long-term monitoring of a few prominent AGN**
  Well-sampled, simultaneous light curves at different wavelengths (X-ray, optical, radio) are necessary to allow us to search for correlations and time-lags between different bands. This is most efficiently organised via dedicated long-term monitoring programmes. Current examples are the Tuorla blazar monitoring (in optical) and Metsähovi Radio Observatory

---

[h] See `http://robopol.org`

programmes, the data of which are being used by the MAGIC collaboration, or the systematic follow-up of H.E.S.S. observations with the on-site optical ATOM telescope and joint observation programmes with the Nançay Radio Telescope. For CTA, the optical flux and polarisation monitoring may make use of dedicated telescopes. In the radio band, several facilities exist and coordination of long-term programmes seems feasible. While no direct correlations between the low-frequency radio band and the higher frequency bands are expected, follow-up at low frequencies (e.g., with MWA, LOFAR, etc.) is still interesting to study long-term variations. Organising the long-term coverage in the X-ray band is more challenging and needs to be explored in the near future.

- **AGN flare programme**
  MWL coverage is crucial, at least for the most prominent flares, for variability studies and dynamical spectral modelling of flaring states. The most relevant instruments for CTA are discussed in Chapter 2. The organisation of MWL campaigns should include: spectral information from X-ray telescopes (currently operational: Chandra, XMM, Swift, NuStar; planned: Athena+ etc.); photometry and polarimetry from optical telescopes; flux densities and polarimetry from radio and sub-millimetre telescopes (currently operational: OVRO, Metsähovi and Nançay radio telescopes, GMRT, JVLA, SMA, ASKAP, MeerKAT, eMerlin, ATCA, ALMA, VLBI facilities; soon operational: SKA, Event Horizon Telescope, etc.). Simultaneous observations with Fermi are of great interest for flaring AGN and should be given high priority during the first years of operation of CTA, as long as Fermi is operational.

  A network of exchanges with MWL and MM facilities will also be very important for incoming and outgoing alerts associated with AGN flares. In addition to wide-field VHE detectors (especially HAWC and the future LHAASO) and Fermi, X-ray instruments with very wide field of view, e.g., the ASTROSAT telescope or the planned SVOM satellite, are very interesting for incoming triggers. Optical telescopes will provide another source of alerts triggered by high flux states and changes in polarisation. Although such external triggers will be very useful, the fact that variability patterns are not the same in different wavebands, and the limited sensitivity and modest low-energy reach of the wide-field VHE detectors, still mean that the internal snapshot programme remains essential to fully profit from the timing capabilities of CTA.

  On the other hand, CTA will provide outgoing alerts to the MWL and MM communities. Exchanges with MM experiments (currently operational: IceCube, ANTARES, VIRGO, LIGO, Pierre Auger Observatory, Telescope Array; planned: KM3Net, eLISA, JEM/EUSO, etc.) to trigger mutual alerts already exist for the current generation of atmospheric Cherenkov telescopes (e.g. MoUs with IceCube and ANTARES) and should be continued and intensified with CTA.

- **High-quality spectra**
  MWL coverage is needed for the interpretation of SEDs, but since we are dealing mostly with low states, simultaneous observations will not always be crucial and contemporaneous/archival data will suffice for some sources. High-coverage optical data will be very useful to compare the state of sources at low energies against archival data. In the case of significant flux variations, however, MWL campaigns for simultaneous coverage will need to be arranged quickly, as discussed for the AGN flare programme. Simultaneous Fermi-LAT data would be very complementary to CTA data on the intrinsic high-energy spectra for EBL and IGMF studies.

  Contrary to the low-state blazar observations, the deep exposures of the radio galaxies M 87 and Cen A should be accompanied by MWL campaigns. Spectra from instruments with high angular resolution (X-rays: Chandra, later Athena+, etc.; optical: the future JWST; sub-millimetre and radio: ALMA and VLBI facilities) are especially interesting to probe different scenarios for the location of the VHE emission region(s), as has been seen in previous campaigns on M 87.

Another aspect of complementary MWL observations concerns the early organisation of redshift campaigns. A significant fraction of the AGN detected with CTA, especially BL Lac objects, will have no spectroscopic redshift and sometimes only poor photometric redshift estimates. For example, about 50% of AGN from the 1FHL catalogue [544] that will be detectable with CTA have currently no reliable redshift. This puts a serious limit on our selection of sources for the "high-quality spectra" programme and will also be a challenge for the exploitation of AGN flares. The problem is more acute at redshifts $z > 0.2$. To increase the fraction of AGN with well-known redshifts, efforts are currently underway to set up dedicated campaigns.

To summarise, the organisation of MWL observations can be divided into two types of campaign: long-term monitoring and targeted campaigns (both ToOs and pre-planned observations). For the latter, we envisage the use of proposal-driven observatories and time granted via ToOs and MoUs. Guaranteeing long-term monitoring observations via proposal-driven observatories is much more challenging. In the optical band, a dedicated automatic telescope at each CTA site would be ideal, while in the radio band, MoUs with existing telescopes (such as Metsähovi, Nançay, MWA, etc.) could be sufficient. The possibility of long-term campaigns including X-ray facilities will need to be explored.

12.3 Data Products

The data products that will result from the different parts of the AGN KSP are the following:

1. **Long-term monitoring** will provide high-resolution light curves and time-resolved spectra in different source states for 15 archetypal sources of different classes. The light curves will be released immediately in an online catalogue and will be continuously updated. All data will be released in such a format as to allow external users to extract spectra for time periods of their choice.
2. Data from the **AGN flare programme** will result in time-resolved spectra and light curves from flaring states of all different types of VHE AGN. Flares detected with CTA snapshots will trigger alerts to inform the community and to enable MWL follow-ups. Such alerts can take the form of Astronomer's Telegrams or VOEvents. Data from flares that are detected under this programme will generally be released after the proprietary period for each flare observation. Mutual agreements with other collaborations will permit joint publications and the exchange of data from specific flares before the end of the proprietary period.
3. **High-quality spectra** of about 40 blazars and radio galaxies will be published, together with the complete data sets, after the proprietary period for this programme. The spectra will form a homogeneous catalogue to be used for source statistics and modelling by the wider community.
4. Deep exposures of **M 87** and **Cen A** will potentially result in maps tracing the VHE emission in those sources, if an extended component is found. These maps will be published together with the complete data sets from these observations after the proprietary period for this programme.

12.4 Expected Performance/Return

The expected scientific results from the AGN KSP can be separated into guaranteed results and potential discoveries.

12.4.1 *Guaranteed Science Return*

The main deliverable of the AGN KSP will be a homogeneous collection of high-quality spectra and light curves, which will be exploited for spectral fitting, variability studies, and comparison against emission models. As was seen with the results from Fermi-LAT and the current generation of atmospheric Cherenkov telescopes, the knowledge gained from such an increased quality and quantity of available data will be profound and not restricted to a single science question. Figure 12.10 shows a sky map of the current target selection for the extraction of high-quality spectra. Simulated spectra for a few sources are shown in Figure 12.11 (as well as in Figures 12.1 and 12.5) to illustrate how different physical assumptions on the mechanism of the observed emission can be distinguished using data from the AGN KSP.

The systematic search for flaring events with snapshots will lead to the detection of the order of 200 flares with fluxes above 20% of the Crab nebula flux from all different known types of gamma-loud AGN during the first 10 years of full operation. External triggers will lead to an expected number of about 10–15 additional flare detections per year. This advance in time-domain VHE observations will be unequalled by other instruments. VHE air shower arrays, such as HAWC and LHAASO, have a much larger duty

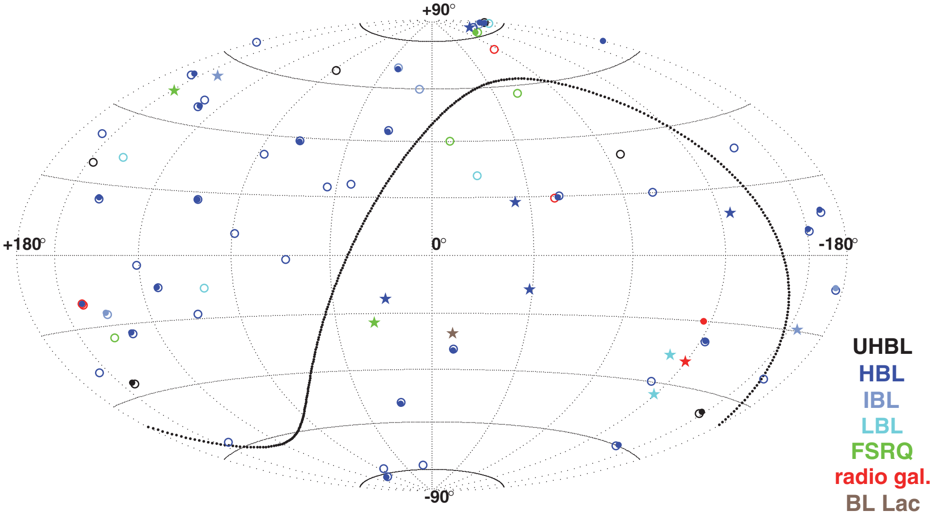

Figure 12.10: Skymap of potential sources from the "high-quality-spectra" programme in Galactic coordinates. In the map, the already known VHE AGN are marked with open circles. Targets for the AGN KSP are marked with full circles (known VHE emitters) or stars (new candidate sources). Different colours in the map correspond to different AGN classes. The solid black line indicates the celestial equator.

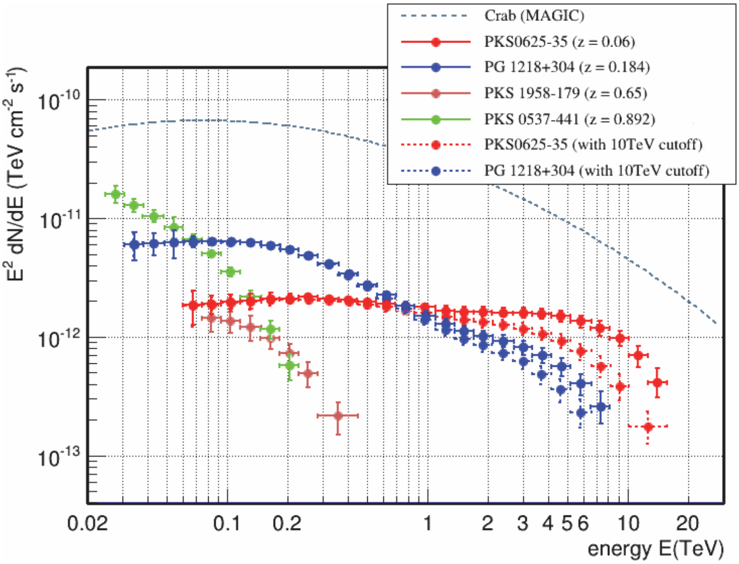

Figure 12.11: Four examples of simulated CTA spectra at different redshifts based on extrapolations from Fermi-LAT and absorption by the EBL [446]. For the two hardest source spectra, alternative scenarios with an exponential cutoff at 10 TeV are shown for comparison. Error bars indicate the statistical uncertainty of one standard deviation.

cycle and sky coverage, but will only be sensitive to the brightest flares from hard-spectrum sources. The source populations probed with CTA and with air shower arrays are thus complementary.

A certain number of serendipitous source detections (on the order of 10) is also guaranteed, based on our experience with the current generation of atmospheric Cherenkov telescopes. It should be noted that the "high-quality spectrum" observations alone will cover a non-negligible fraction of the sky. If CTA points to ~40 separate fields of view with the MSTs, a total geometrical field of view of more than 4% of the sky will be covered.

A precision measurement of the EBL and its evolution with an unprecedented accuracy of ~10% will be carried out, thanks to the observations of steady sources and flares, (see Figure 12.2). Observations with atmospheric Cherenkov telescopes are among the only means for making such a measurement, which is closely linked to our understanding of the evolution of the universe and its star-forming history.

12.4.2 *Discovery Potential*

Based on Fermi-LAT observations of flaring events, the high energy end of the spectrum from NLSy1s will be accessible to CTA with high probability,

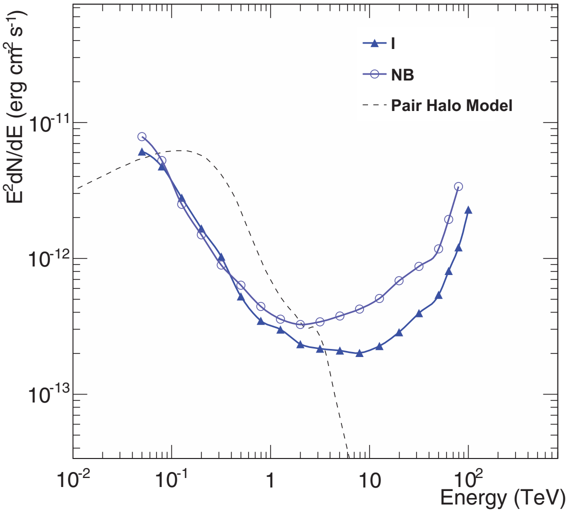

Figure 12.12: Estimate of the flux for the expected pair halo emission compared to sensitivity curves for the southern ("I") and northern ("NB") sites. A differential angular distribution of a pair halo at $z = 0.129$ and $E_\gamma > 100\,\mathrm{GeV}$ was used for the theoretical model and an observation time of 50 h was assumed. For more details see Ref. [30].

and a few of these sources should be detectable by CTA. The measurement of their spectra will profit from the very good time resolution of CTA and will constrain the conditions in the emission region of these still poorly understood objects.

Other AGN types, such as radio-quiet Seyfert galaxies or low-luminosity AGN, will be probed for VHE emission through a stacking analysis. In the absence of a signal, such studies will put stringent upper limits on theories that require particle acceleration in the magnetosphere linked to the SMBH.

Extended VHE emission from radio galaxies would be a major discovery as it would prove that particles can be accelerated to very high energies in the extended jets or radio-lobes of AGN, thus constraining the energetics and the magnetic fields in these structures and providing us with a first direct view of the location of the VHE emission regions in AGN.

Another major discovery would be the detection of gamma-ray signatures from the IGMF in the form of pair halos or pair echoes. This would be the first (indirect) measurement of the strength of the IGMF, leading to important implications on its origin. Clearly, the derivation of reliable constraints will already be an important step. Figure 12.12 shows the expected signal from a pair halo model compared to CTA sensitivity curves.

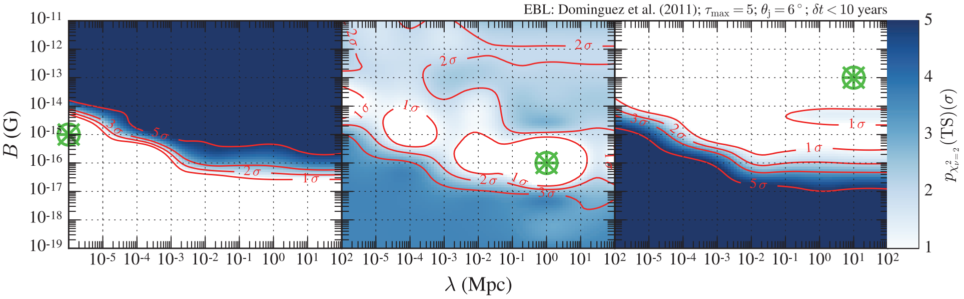

Figure 12.13: Possible constraints on the IGMF field strength (B) and coherence length (λ) for three different assumptions on the true IGMF (green markers). Colours and contour lines give the significance with which IGMF parameters can be rejected in units of the standard deviation (σ). The constraints are derived from a combined likelihood analysis of simulated CTA spectra of four UHBLs using the non-observation of a pair echo. Only cascade photons that arrive within the 80% containment radius and a time delay of less than 10 years are included in the analysis. For more information, see Ref. [551].

Expected results of searches for pair echos with CTA are shown in Figure 12.13 for three different assumptions on the magnetic field strength and coherence length of the IGMF. These results are derived for the observation of several known blazars with hard spectra in the TeV band ([551]).

CTA might also identify the sources of UHECRs, through indirect signatures of protons or nuclei in the gamma-ray spectra. The long-standing question of UHECR origin has been difficult to tackle using data from UHECR particle detectors alone. Apart from neutrino detectors, gamma-ray telescopes seem to provide the only other means of attacking this open problem. A possibility to investigate physics beyond the Standard Model is given by the search for ALPs, the discovery of which would have profound implications for particle physics. The existence of such particles would also imply that the "gamma-ray horizon" for TeV detection is far less constraining than what is currently assumed. On the other hand, if no ALP signatures are found, strong constraints on their parameters are possible that could rule out certain ALP dark-matter scenarios.

The search for LIV will lead either to the verification of the theory of general relativity at a new level of sensitivity or possibly to the discovery of new physics, again with profound implications for fundamental physics. With data from this KSP, we will match the Fermi-LAT sensitivity at the Planck scale on the linear term with a different type of astrophysical object. We will also improve the sensitivity on the quadratic term by a factor of two compared to current results, i.e., at a scale of a few times 10^{11} GeV. These results will be largely independent of the source physics since they will be based on data from sources at different redshifts and in different states. While transient events will still provide the best constraints, the observations in the AGN KSP will be capable of providing competitive sensitivity independent of flaring events, through a mixture of routine observations of many sources and deeper exposures of a few suitable hard-spectrum sources.

13

KSP: Clusters of Galaxies

Galaxy clusters are expected to be reservoirs of cosmic rays accelerated by structure formation processes, galaxies, and active galactic nuclei (AGN). The detection of diffuse synchrotron radio emission in several clusters confirms the presence of cosmic-ray electrons and magnetic fields permeating the intra-cluster medium (ICM). While there is no direct proof for proton acceleration yet, gamma rays can prove it as cosmic-ray protons can yield high-energy (HE) gamma-ray emission through neutral pion decay. Additionally, some of the galaxies hosted in clusters could be detected in gamma rays individually, if harbouring AGN, or via their summed output, e.g., in the case of star-forming galaxies. Finally, about 80% of the mass of clusters is in the form of dark matter, and therefore they are considered prime targets for indirect dark matter searches.

Focusing on the diffuse gamma-ray emission in clusters coming from proton–proton interactions, and based on both theoretical studies and hydrodynamical simulations, Perseus should be the brightest cluster of galaxies in gamma rays. Perseus also hosts two gamma-ray-bright AGN: NGC 1275, one of the few radio galaxies known to emit gamma rays, and IC 310, potentially one of the closest known blazars. These two objects prevent Fermi-LAT from studying the ICM itself in Perseus because of its modest angular resolution (especially at low energies). At very high energies, MAGIC performed a deep observation campaign and put constraints on the cosmic-ray-to-thermal pressure in the cluster at the few percent level [554]. Currently, the best limits on the proton content in clusters comes from Fermi-LAT observations [556]. Our simulations for CTA show that a 300 h observation will potentially allow a detection of the Perseus cluster in gamma rays or,

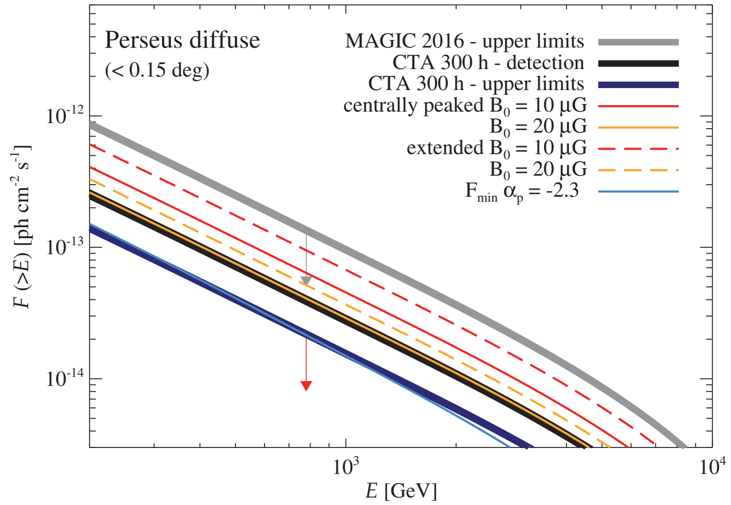

Figure 13.1: Theoretical parameter space for the predicted intensity of cosmic-ray-induced gamma-ray emission in the Perseus cluster integrated within a region of radius 0.15° from the cluster centre. The models refer to centrally peaked (solid line) and extended (dashed line) cosmic-ray profiles [552–554]. We show them for two different values of the central magnetic field for which the models fit the radio mini-halo of Perseus assuming it has an hadronic origin. The grey band shows current upper limits on the diffuse emission from the MAGIC observations [554]. The dark blue band is an estimate of the 95% upper limit level reachable with 300 h of observation by CTA-North, while the black band represents an estimate of the corresponding detectability level. All these three bands refer to the adopted models, with the upper and lower boundaries corresponding to the extended and centrally peaked models, respectively. We additionally show, with a light blue line, the so-called minimum gamma-ray flux, for a cosmic-ray proton spectral index of 2.3, assuming that the Perseus radio mini-halo is of hadronic origin [554].

alternatively, set unprecedented limits on the cosmic-ray proton content — potentially triggering a substantial revision of the current paradigm of proton acceleration and confinement in galaxy clusters (see Figures 13.1 and 13.2). Additionally, due to the large mass of this cluster, CTA can significantly improve the constraints on decaying dark matter with respect to those from Fermi-LAT observations of the Galactic halo (see Section 4.2.4).

The high-risk/high-gain character of this work makes it a worthy Key Science Project. Additionally, the long observation time needed to achieve our scientific goals calls for a Consortium effort. Perseus is observable in optimal conditions, i.e., low zenith angles (<60°), only by the northern array. Here we refer to the fully complete northern array, as we need the best achievable sensitivity to aim for a detection of the diffuse gamma-ray emission. The data products will depend on whether we get a detection or

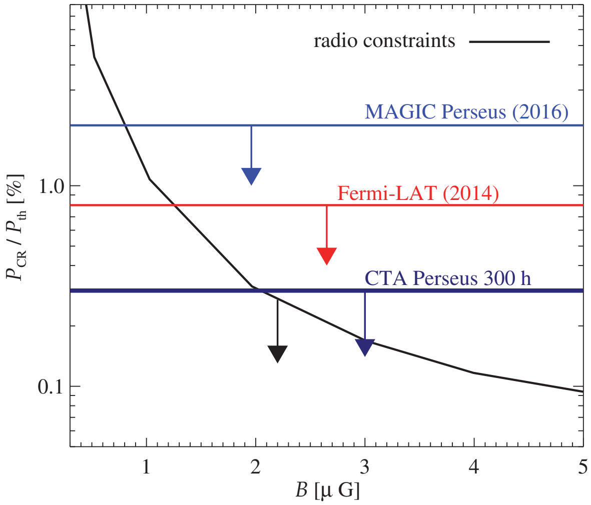

Figure 13.2: Upper limits on the cosmic-ray-to-thermal pressure in clusters. We show the upper limits obtained from GMRT radio observations (black line), which depend on the assumed magnetic field value [555], together with the latest upper limits from the MAGIC observations (blue line, [554]) and the Fermi-LAT observations (red line, [556]). The thick dark blue line is an estimate of the level reachable with the proposed CTA observation of Perseus. All the gamma-ray limits refer to the case of the centrally peaked cosmic-ray profile.

not. They will range from maps/datacubes (excess, flux, spectral hardness) to morphological analysis of the possible diffuse emission and detailed analysis on point-like sources. Special care will be given to examine the parameter space of cosmic-ray physics in clusters of galaxies.

The detection of diffuse gamma-ray emission from clusters of galaxies would establish a new class of gamma-ray sources. Thus, it would constitute a significant achievement and would be potentially groundbreaking for the study of cosmic-ray acceleration and its relation to large-scale structure formation processes, the ICM and magnetic fields.

13.1 Science Targeted

Clusters of galaxies represent the latest stage of structure formation. They are the most massive gravitationally bound systems in the universe, characterised by radii of a few Mpc and masses of the order of $10^{14} - 10^{15}\, M_\odot$. About 80% of their mass is in the form of dark matter, while galaxies and gas contribute roughly 5% and 15%, respectively [557]. While there has been no detection of diffuse gamma-ray emission in clusters so far, these objects are expected to be gamma-ray emitters for several reasons that are explained below.

Clusters are being assembled today and are actively developing in this latest, and most energetic, phase of structure formation [558]. It follows that they should dissipate energies of the order of the final gas binding energy via merger and accretion shocks as well as via turbulence (e.g., Ref. [559]). These processes are also likely to accelerate electrons and protons to high energies (see Ref. [560] for a review). While the presence of non-thermal electrons is confirmed by the detection of diffuse synchrotron radio emission from several clusters (see Ref. [561] for a review), there is no direct proof of proton acceleration yet. However, cosmic-ray protons in the ICM have a long cooling time and should accumulate in clusters over cosmological times [26, 562]. Therefore, they are expected to contribute to the relativistic particle content of clusters. If protons are present in significant amounts, their hadronic interactions with the ICM will generate gamma-ray emission via neutral pion decays (see, e.g., Refs. [563, 564]), which should dominate over inverse-Compton scattering or bremsstrahlung emission [552, 565]. Additionally, protons can be accelerated to ultra-high energies by high Mach number shocks, such as accretion shocks around galaxy clusters [566, 567], or they can be directly injected into the ICM by the clusters' AGN [568, 569]. The interaction of these ultra-high energy protons with both the ICM and the background (cosmic microwave background and infrared) photons [570] could produce secondary electrons that would also yield significant gamma-ray emission via inverse-Compton scattering. The production and confinement of cosmic rays at very high energies is uncertain, as is the contribution of galaxy clusters to the high energy part of the observed cosmic-ray spectrum.

Large-scale diffuse synchrotron radio emission is observed in several galaxy clusters. The existence of these so-called radio halos and relics proves the presence of relativistic cosmic-ray electrons, as mentioned above, and of μG magnetic fields permeating the ICM [561]. The short cooling length of synchrotron-emitting electrons at radio frequencies ($\sim$10 kpc) represents a challenge for theoretical models that aim at explaining diffuse radio emission extending over several Mpc. In the hadronic model, radio-emitting electrons are produced by cosmic-ray protons interacting with the protons of the ICM. Alternatively, in the re-acceleration model, cosmic-ray electrons can be re-accelerated by merger-induced turbulence and produce the observed radio emission during cluster mergers. See Ref. [560] for a review of these processes.

Peripheral radio relics show irregular morphology and highly polarised emission, and they appear to trace merger shocks. Radio halos, which are generally characterised by unpolarised radio emission (or with a low level of polarisation), are centred on clusters and show a more regular morphology. The latter can be divided in two classes. Giant radio halos are typically associated with merging clusters and have large extensions; e.g., the halo in Coma has an extension of about 2 Mpc. Radio mini-halos are associated with relaxed clusters that harbour a cool core and typically extend over a few hundred kpcs, e.g., the Perseus radio mini-halo has an extension of about 0.3 Mpc. The observed morphological similarities with the thermal X-ray emission suggests radio halos may be of hadronic origin. In fact, cool-core clusters are characterised by high thermal X-ray emissivities and ICM densities that are more peaked in comparison to non cool-core clusters that often show signatures of cluster mergers (see, e.g., Ref. [571]).

We know now that giant radio halos cannot be purely of hadronic origin [553, 572]. The challenge is to determine what the exact contribution of secondaries is to the observed radio emission, if any, and, therefore, the origin of the observed radio-emitting electrons (e.g., Ref. [573]). On the other hand, current observations do not allow us to favour any model for radio mini-halos as both turbulent and hadronic scenarios fit current observations well (e.g., Refs. [574, 575]). There is also the problem of the connection between giant and mini-halos (e.g., Ref. [553]). Understanding the nature of these halos and their possible connection will allow fundamental constraints on cosmic-ray acceleration and transport in galaxy clusters to be derived. Only adequately deep gamma-ray observations of massive nearby systems hosting diffuse radio emission can ultimately break the degeneracy of radio observations in solving the problem of the cosmic-ray electron/proton fraction in the ICM.

In addition to cosmic-ray protons accelerated by structure formation shocks in the ICM, galaxies and AGN activity can also inject and accelerate protons into the cluster environment. Based on the current theoretical paradigm, these contributions are thought to be about an order of magnitude lower compared to those from structure formation shocks [560]. However, as clusters host hundreds of galaxies, gamma-ray observations could detect their combined emission as a sum of discrete sources, as, e.g. in the case of star-forming galaxies in clusters [576, 577]. From estimates of the star-forming galaxy population, it is possible to determine the minimum pion-decay-induced gamma-ray emission expected from galaxy clusters. Rough estimates [576] give integral flux lower limits above 1 TeV of the order of 10^{-14} cm^{-2} s^{-1} for Virgo and 10^{-16} cm^{-2} s^{-1} for Perseus for typical radii of several degrees (about 7.6° for Virgo and 1.3° for Perseus). However, such an extended signal strongly challenges detection possibilities for CTA. Additionally, AGN (both aligned and misaligned) in clusters can be individually studied as in the case of NGC 1275 and IC 310 in Perseus [477, 578–581]. For all these reasons, CTA observations of clusters of galaxies are imperative; they will pave the road to VHE studies of member galaxies and open up a completely new window on clusters.

Galaxy clusters are also interesting environments in which to study axion-like particles (ALPs) [582]. For example, the strong magnetic field in the centre of the Perseus cluster (see Ref. [578] for a discussion) would offer an ideal environment for photon-ALP conversion. Therefore, NGC 1275 is an optimal target to search for irregular features in the gamma-ray spectrum possibly connected to this phenomenon [536] (see also Chapter 12). Finally, galaxy clusters present very high mass-to-light ratio environments and should also be considered as targets for indirect dark matter searches, in particular for dark matter decay (see Chapter 4).

13.1.1 *Scientific Objectives*

The scientific goals of this Key Science Project are to:

1. detect, for the first time, diffuse gamma-ray emission from clusters of galaxies,
2. determine the cosmic-ray proton content of clusters and its dynamical impact on the cluster environment,
3. study the clusters' cosmic-ray proton acceleration, propagation, and confinement properties,
4. study the origin of the radio-emitting relativistic electrons and the connected particle acceleration mechanisms in galaxy clusters, and
5. study the magnetic field distribution in clusters, in synergy with radio and X-ray observations.

13.1.2 *Context/Advance beyond State of the Art*

There have been many gamma-ray observations of clusters over the last 20 years from EGRET, WHIPPLE, CANGAROO, VERITAS, H.E.S.S., MAGIC, and Fermi-LAT [554, 556, 578, 583–607]. The MAGIC observations of Perseus [554, 578, 605] and the Fermi-LAT results on Coma as well as the combined-likelihood analysis of 50 clusters [556, 590, 596] represent some of the key accomplishments in this area. These observations limit the cosmic-ray-to-thermal pressure in galaxy clusters to be less than a few percent, assuming that the spatial distribution of cosmic-ray protons follows that of the ICM. They also constrain several models for the production of gamma rays from structure formation processes in clusters. However, a large amount of parameter space is still available and many fundamental quantities, such as the cosmic-ray spectral and spatial distributions, acceleration efficiency, and transport properties, remain to be clearly determined.

Detection of gamma rays from galaxy clusters will be of high importance, if realised. Even a null detection will result in exclusion limits significantly more constraining than those currently available. In turn, they will produce a significant change in our view of cosmic-ray proton acceleration and transport in the ICM, and will provide fundamental constraints on the contribution to the proton population in clusters by galaxies and AGN. A precise assessment of the total proton content is of paramount importance also for cosmological studies done using the cluster mass function, as the presence of cosmic rays induces a bias on the hydrostatic mass estimates [554, 608]. To determine whether CTA observations will be able to bring a major breakthrough in this field, below we compare CTA prospects with the results of Fermi-LAT which is now in its ninth year of observations and which will likely continue to operate for a few more years.

As explained in the next section, the best target for this program is the Perseus cluster of galaxies. The presence in the cluster field of two gamma-ray bright AGN, NGC 1275 and IC 310, prevents Fermi-LAT from studying the cluster environment itself. This is due to the poor angular resolution of Fermi-LAT at low energies and to its limited sensitivity at very high energies. Therefore, in the case of Perseus, CTA has a clear advantage over Fermi-LAT thanks to its excellent angular resolution. Perseus is the best studied cool-core cluster [609] and it hosts the archetypal radio mini-halo that is the brightest known to date [610, 611]. The high ICM density in the centre of the cluster implies a very high density of target protons for hadronic interactions. CTA is in a unique position to unravel the high-energy properties of the Perseus cluster and its member galaxies. In Figure 13.3, we show the gamma-ray skymap of the Perseus cluster as observed by MAGIC [554].

The CTA observations of the Perseus galaxy cluster will dramatically improve upon the current MAGIC results. We discuss this in detail in Section 13.4, where we explain how the proposed observations will improve the current limits by about a factor of six.

Perseus is the most promising target for this program and the proposed CTA observations will represent a major leap forward in our understanding

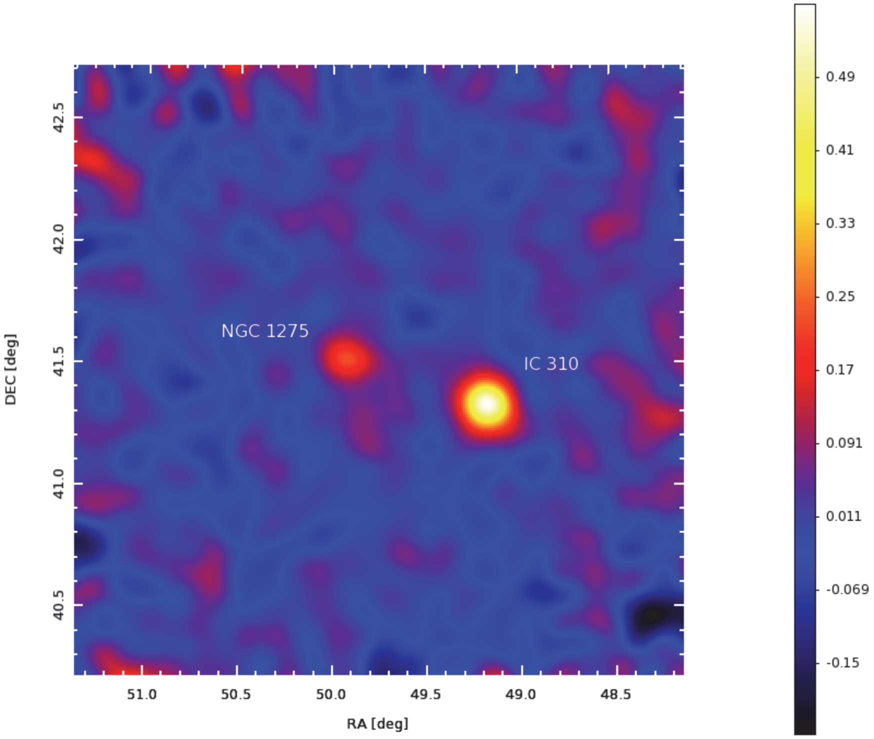

Figure 13.3: Skymap of the Perseus cluster as observed by MAGIC above 250 GeV (253 h of observation; figure adapted from Ref. [554]). The colour scale shows the relative flux in signal-to-background ratio. Both NGC 1275, at the centre of the cluster, and IC 310 can be clearly seen.

of this cluster and its non-thermal activity. The observation of a second target and its selection is a more complex matter and will be re-evaluated over the next few years, particularly taking into account the final results of Fermi-LAT [612] and advances in radio astronomy.

13.2 Strategy

The first step of the target selection is based upon the cluster's distance and mass as measured in X-rays [613]. Due to the cosmic-ray proton confinement and accumulation over cosmological times, gamma-ray emission should scale with the cluster's mass [552, 560], although this scaling may have a significant scatter depending on the merging history of a given target [614]. Here, we consider different predictions for gamma rays generated by structure formation processes in clusters [156, 552, 572, 615], and we obtain a first selection of candidates, in order of preference, as follows: Perseus, Ophiuchus, Coma, Norma, and Centaurus, where the first three targets host well-known radio halos. The Virgo cluster is also an excellent candidate, but its large angular size, more than 10° across, represents a serious observational challenge [597]. Perseus is expected to be the brightest cluster in gamma rays due to a combination of distance, mass, and high ICM density in the cluster's centre, implying a high density of target protons for hadronic interactions.

It is hard to provide precise predictions of the gamma-ray emission in clusters due to the uncertainties on cosmic-ray acceleration efficiencies and transport properties in these unique environments. Here, we follow two complementary strategies by considering: (i) expectations based on radio constraints assuming an hadronic origin for the observed diffuse radio emission, where present, and (ii) expectations based on hydrodynamical simulations that provide predictions for the cosmic-ray spatial and spectral distributions. In particular, we base our simulations on the hadronic model predictions given in Refs. [552, 553, 590].

The gamma-ray flux induced by secondaries from hadronic interactions must respect the measured radio synchrotron emission, as electrons are also produced from charged pion decays. Therefore, the magnetic field strength and distribution in clusters is also an important ingredient and is usually parametrised as $B = B_0\,(n/n_0)^{\alpha_B}$, where n is the ICM gas density. Generally we have limited knowledge of cluster magnetic fields, apart from very detailed work on Faraday rotation measurements of the Coma cluster [616, 617], which provide good estimates for the Coma magnetic field ($B_0 \approx 5\ \mu$G, $\alpha_B \approx 0.5$). In this sense, the synergy with radio observations of clusters by the Low-Frequency Array (LOFAR; [618]) and other Square Kilometre Array (SKA) precursors will be crucial. By the same token, SKA itself is expected to shed new light on the magnetic field in clusters of galaxies and will therefore significantly narrow down the available parameter space [619, 620].

While Ophiuchus seems *a priori* to be a good target, the extremely low-surface-brightness radio emission of its central region lowers significantly the prediction for gamma rays, independent of the exact value of the magnetic field strength [553]. The same is true for Norma, Centaurus, and Virgo, where the absence of bright diffuse radio emission also suggests a low level of gamma-ray emission. On the contrary, both Perseus and Coma host very bright diffuse radio emission allowing for higher hadronically induced gamma-ray emission. Therefore, in the following, we consider only these last two objects for CTA observations.

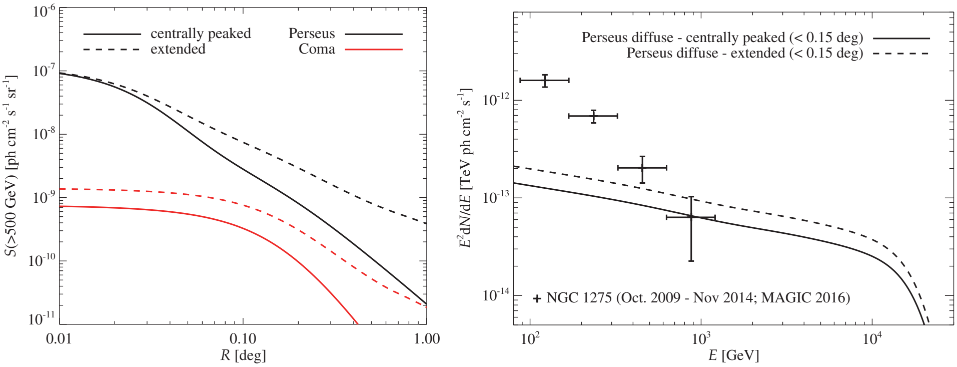

(a) (b)

Figure 13.4: (a) Predicted surface brightness of the hadronic-induced gamma-ray emission (above 500 GeV) from the Perseus and Coma galaxy clusters for two models with centrally peaked and extended cosmic-ray profiles, as described in the text [552–554, 590]. The luminosity distance and radius of Perseus are 78 and 1.9 Mpc, respectively, while for Coma they are 101 and 2.3 Mpc, respectively [613]. In both cases, the angular radius is approximately 1.3°. (b) Differential spectra for the two models adopted for the hadronic-induced diffuse gamma-ray emission of Perseus integrated within a radius of 0.15° from the centre. The effect of the EBL absorption is clear above 10 TeV. Additionally shown is the spectrum of NGC 1275, the central radio galaxy of Perseus, as measured by MAGIC [554]. Note that the higher energy data point of the NGC 1275 spectrum is only marginally significant and is in agreement with the current upper limits on the diffuse emission [554].

In Figure 13.4(a), we show the surface brightness of the predicted hadronically induced gamma-ray emission from the Perseus and Coma clusters. For each cluster, two sets of models are shown. The difference in the models comes from the assumption on how the cosmic-ray protons are distributed in the cluster, varying from a centrally peaked [552] to a more radially extended distribution in order to account for possible variations in the cosmic-ray transport properties [553, 621, 622]. In the case of Coma, the flat cosmic-ray profile is the maximum allowed hadronic contribution that still respects the Fermi-LAT constraints [590]. The peaked one is the maximum possible emission for which the radio counterpart does not overshoot the measured radio flux at the cluster centre (under the above-mentioned assumption for the Coma magnetic field) [590]. In the case of the Perseus cluster, both models fit well the radio data of the mini-halo at 1.4 GHz [610] assuming a central magnetic field of $B_0 = 10\ \mu$G and $\alpha_B = 0.3$ and 0.5 for the centrally peaked and extended models, respectively. Note that, in the case of mini-halos that are in cool-core clusters, current observations favour relatively high values of magnetic fields [623–626]. These two models for Perseus are the same that have been explored in the latest

MAGIC publication [554] (the centrally peaked model is referred to there as the semi-analytical model [552]).

The total gamma-ray flux above 500 GeV within the virial radius[a] predicted for Perseus is $0.2-1.0\times10^{-12}$ cm^{-2} s^{-1}, while, for comparison, for Coma it is $1.3-6.3\times10^{-14}$ cm^{-2} s^{-1}. We emphasise that these models adopt a cosmic-ray spectral index (equal to the photon spectral index) of about 2.2 in the energy range of interest for Cherenkov telescopes, as suggested by simulations [552]. A harder cosmic-ray component would dramatically increase our detection chances, while a softer one would obviously worsen them. In the case of Coma, where we know that the hadronic contribution represents at most only a part of the observed radio emission, both cases could be realistic. However, in the case of Perseus, we assume that the observed radio emission is of hadronic origin and the adopted spectral distribution matches well the observed radio spectral shape [610] (see also the discussion in Ref. [605]). Note that, following Ref. [627], we apply the correction due to the attenuation by the extragalactic background light (EBL) on our spectra. As a consequence, for example, our Perseus spectrum appears as a power law with an index of 2.33 above 300 GeV and a cutoff above 10 TeV [554], as shown in Figure 13.4(b) for the two adopted models.

Our simulations suggest that the models adopted for Coma would need more than a thousand hours of observation to be detectable by CTA, while the models adopted for Perseus are within reach in a few tens of hours.[b] In particular, we search for the integral energy range, starting with energies above 100 GeV, and the angular region size, from 0.05° to 1°, that minimise the number of hours needed to reach a detection. Not surprisingly, the minimum is typically reached using the full energy range, which maximises the total flux, and the smallest angular region size, which minimises the background event counts. In this case, the models predict that Perseus would be detectable with 40 and 50 h of observation by the northern CTA array for the extended and centrally peaked cases, respectively. However, these numbers are based on the assumption that we can perfectly model the two bright point-sources in the Perseus field of view, NGC 1275 and IC 310. The presence of IC 310 will not be a major obstacle in the search for the diffuse emission as it is located about 0.6° away from the centre of the cluster from where we expect the bulk of the diffuse emission (see Figure 13.3). However, NGC 1275 is located right in the centre and it dominates the gamma-ray emission up to a few hundred GeV as shown in Figure 13.4(b). In order to account for this, we use the conservative strategy of excluding the lowest energies from the detection criteria and find that, considering only energies above 780 GeV where the contribution of NGC 1275 should be negligible, the extended and centrally peaked models should be detectable in 60 and 100 h, respectively.

---

[a] The cluster virial radius is defined here with respect to an average density that is 200 times the critical density of the universe. Values are taken from Ref. [613].

[b] The detection criteria is a statistical significance greater than five standard deviations, the number of excess events >10 and a signal/background ratio >0.03.

We can foresee three ways to disentangle the possible diffuse emission from that of NGC 1275:

- The first method relies on the spectral characteristics of the two emissions. The NGC 1275 spectrum at the energies of interest has a very soft index of about 4 [581], and the corresponding gamma-ray emission becomes undetectable above a few hundred GeV. On the contrary, the spectrum of the possible hadronic-induced diffuse emission should be much harder and should show no cutoff except at the highest energies (due to EBL absorption). The predicted spectrum is shown in Figure 13.4(b).
- The second method relies on the extension of the emission. NCG 1275 is a point-like source while the predicted hadronic-induced emission is expected to be quite extended, as can be seen in Figure 13.4(a). The excellent angular resolution of CTA should permit a clean disentangling of the two. Figure 13.5 shows the simulated gamma-ray flux skymaps above 780 GeV for 100 h of observations for the two considered models of cosmic-ray-induced emission in the Perseus cluster. The 68% containment radius for the CTA-North array at 780 GeV is about 0.06°. For both models considered, the detected diffuse emission extends beyond the 68% containment radius.
- The third potential discriminator is variability as the diffuse emission is not expected to exhibit any.

In conclusion, if diffuse gamma-ray emission is present at a level suggested by the adopted models, we will have the means to disentangle it from the point-like emission. A more complex matter will be to disentangle it from a possible dark matter induced component. While the discrimination strategy would be based on the difference in the emission morphology and the shape of the energy spectrum, how well the discrimination could be done would critically depend on the significance of the detection. We leave a more detailed study of all the gamma-ray components possibly observable by CTA in the Perseus cluster for future work.

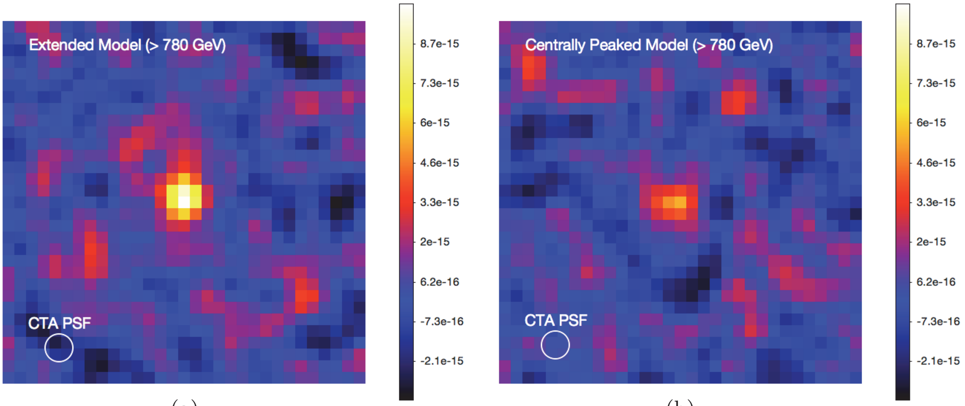

(a) (b)

Figure 13.5: Simulated gamma-ray flux ($\mathrm{cm}^{-2}\ \mathrm{s}^{-1}$) skymaps above 780 GeV for 100 h of observation of a region of 1.55° × 1.55° around the Perseus cluster centre. (a) Shows the result for the extended cosmic-ray profile, while (b) shows the result for the centrally peaked cosmic-ray profile. The white circles indicate the expected CTA 68% containment radius at 780 GeV (of about 0.06°). We simulated the signal and background event counts in the region with a pixel size of 0.05°. The maps were obtained by calculating the corresponding flux and subtracting the background from the signal (resulting in some areas having negative flux values) and then smoothing the final map with a Gaussian function with $\sigma = 0.06°$.

We eventually plan to observe the Perseus cluster region for 300 h with CTA-North. This amount of observation time is necessary for two reasons: (i) to ensure enough event counts, in the case of detection of the adopted models, for a detailed morphology study that will be mandatory, e.g., to enable disentangling the point-like and diffuse emissions, and (ii) to allow a deeper reach in the parameter space of theoretical models, in the context of relaxing the strongest assumption made in this section, i.e., the hadronic origin of the Perseus radio mini-halo (see further discussion in Section 13.4).

Note that we used the 1.4 GHz observations of the radio mini-halo of the Perseus cluster [610] to calibrate our models. However, results at 327 MHz [611, 628] suggest that the high-frequency observations may be missing some of the flux. Depending on the exact value of the magnetic field at the radii where the bulk of the emission is coming from, this could boost the corresponding allowed gamma-ray emission. This boost factor can range from about 1.1, for the magnetic field model adopted here, to more than 1.2, for magnetic field models considering the effect of ICM compression in the cooling-flow region [611]. Such boosts would imply that CTA would need about 20%-30% less observation time to report a detection of the adopted models.

Table 13.1: Galaxy cluster selected for this key science project along with the basic requirements.

Target	Time [h]	Hemisphere	Array configuration	Special requirements
Perseus	300	North	Full array	Low zenith angles

13.2.1 *Targets*

Table 13.1 shows the selected cluster target. We expect the Perseus cluster to host the brightest gamma-ray emission coming from proton-proton interactions. Additionally, Perseus hosts two extremely interesting gamma-ray point-sources: NGC 1275, one of the few radio galaxies known to emit gamma rays and the galaxy IC 310. As mentioned earlier, the Perseus field of view is observable in optimal conditions, i.e. at zenith angles $<60°$, only by the northern array. Note that while in Table 13.1 we ask for low zenith angle observations to maximise sensitivity, medium and large zenith angle observations could provide a larger effective area at high energies, increasing the corresponding event counts and, therefore, possibly improving morphological studies. We leave the detailed study of this latter possibility for future work.

13.3 Data Products

The data products produced will clearly depend on whether a significant detection of the diffuse gamma-ray emission in Perseus is made or not. In the case of a detection, the data products will include maps/data-cubes (excess, flux, and spectral hardness) for the whole cluster, morphological analysis of the diffuse emission, spectra and light curves of NGC 1275 and IC 310, and a model for their subtraction from the whole cluster emission. We will additionally provide a detailed analysis of the cosmic-ray physics parameter space matching the observed emission and other possible diffuse contributions from, e.g., dark matter. In the case where no diffuse gamma-ray emission is detected, the analysis will be focused on the constraints that can be made on the cosmic-ray physics in clusters.

We plan to release the data products related to the diffuse emission in two steps: the first after 100 h of observation have been performed and the second at the end of the programme after 300 h of observation. We note that the results on the point sources, including possible serendipitous discoveries, will be released before the completion of the cluster campaign following the strategy outlined for the AGN KSP (see Section 12.4).

13.4 Expected Performance/Return

We estimate here the parameter space accessible to the proposed CTA observations for the Perseus cluster. In Figure 13.1, we show the predicted gamma-ray integral spectrum from hadronic-induced emission for the adopted models, including the effect of EBL absorption. In particular, we show the centrally peaked and extended models corresponding to $B_0 = 10\ \mu$G which, according to our estimates, should be detectable in 100 and 60 h of observations, respectively. We also show the cases corresponding to $B_0 = 20\ \mu$G. We estimate the detection level reachable in 300 h of observation for these two models simply by scaling by the square root of the time that is obtained with our detection criteria. The detection level is shown with a black band in Figure 13.1 and while it suggests that we could be able to detect also the cases corresponding to $B_0 = 20\ \mu$G, we recall that this optimistically assumes no contribution from the central radio galaxy NGC 1275, which will become larger for longer observation times. Nevertheless, if the Perseus mini-halo is (mostly) of hadronic origin and the adopted models are correct, CTA observations will achieve a detection in about 100 h of observation. In this case, with the proposed 300 h of observation, we will be able to determine critical cosmic-ray parameters such as the spectral and spatial distributions (connected to cosmic-ray transport properties) and to study the acceleration efficiency. Taking into account currently available radio data, and future data from LOFAR and SKA precursors, we will also be able to provide a complementary measure of the magnetic field strength and distribution in the cluster.

Figure 13.1 also shows, with a grey band, the current constraints on the parameter space for the centrally peaked and extended models obtained from MAGIC observations [554]. We stress that the figure does not mean to show the real gamma-ray flux excluded by observations but rather the theoretical parameter space for the diffuse emission models. In fact, the low energies will always be dominated by the emission from NGC 1275, as shown in Figure 13.4(b). For comparison with current upper limits by MAGIC, we show, with a dark blue band, an estimate of the 95% upper limit level reachable with 300 h of observations by CTA, assuming zero excess events, for the two adopted models. This shows that CTA observations could improve by about a factor of six on the current MAGIC constraints.

We additionally estimate the so-called minimum gamma-ray emission expected from Perseus in the hadronic scenario (taking the radio flux at 1.4 GHz as a reference value [610]). This lower-limit is obtained by assuming that the observed radio emission is of hadronic origin and that the magnetic field is much higher than the equivalent magnetic field strength of the cosmic microwave background throughout the radio-emitting region (see [554, 605] for details). A non-detection at this level would rule out the secondary origin of the Perseus diffuse radio emission, independent of the exact value of the cluster's magnetic field. Figure 13.1 shows, with a light blue line, the case for a proton spectral index of $\alpha_{\rm p} = 2.3$. The comparison with the upper limit level reachable with 300 h of observations suggests that a hadronic origin of the Perseus radio mini-halo for $\alpha_{\rm p} \leq 2.3$ could be excluded independently of magnetic field values.

The proposed 300 h of observation are motivated by the goal of making scientific statements which go beyond the assumption of the hadronic origin of the observed non-thermal emission in Perseus and, instead, aim to measure the cosmic-ray proton spectrum and energy density in the ICM. Although the cosmic-ray proton spectrum in clusters is uncertain, indications from hydrodynamical simulations and observations of discrete sources in clusters (i.e., AGN, whose ejecta also contribute to the cosmic-ray proton population in the ICM) suggest reasonable values between 2.0 and 2.5 [560]. Assuming that the cosmic-ray pressure scales as the thermal ICM pressure in the cluster — as a result of cosmic-ray proton advection on cosmic times and as suggested by several simulations — and recalling the MAGIC results on Perseus [554], the proposed CTA observation will push the cosmic-ray-to-thermal pressure limits down to 0.1–2.5% for proton spectral indices of 2.1–2.5, respectively. We show the case for the model with a centrally peaked cosmic-ray profile in Figure 13.2, together with current limits from both gamma-ray and radio observations, noting that the latter constraints depend on the adopted magnetic field values. CTA observations will not only provide unprecedented constraints on the cosmic-ray acceleration efficiency at structure formation shocks, potentially below 10% according to Refs. [552, 556], but they will also strongly constrain the contribution to the cluster proton population from galaxies and AGN. In fact, such low values of the cosmic-ray-to-thermal pressure can potentially put constraints on the cosmic-ray electron/proton fraction in the cluster's AGN (NGC 1275 in this case) or, alternatively, on how these protons are transported from the central AGN to the cluster periphery (an issue also connected to the confinement of such protons in AGN bubbles [560]). Last but not least, CTA observations will eventually constrain the cosmic-ray bias on the hydrostatic mass estimates [554, 608] down to the $<5\%$ level, independent of assumptions on cosmic-ray spectral and spatial distributions. Models with extended cosmic-ray profiles imply a growing cosmic-ray-to-thermal pressure in cluster outskirts. While the current constraints from MAGIC are only below $\sim 15\%$, the proposed CTA observations could potentially constrain these models to $\leq 3\%$.

To summarise, the observation campaign on Perseus proposed in this Key Science Project will lead to a major step forward in our understanding of cosmic rays and non-thermal phenomena in clusters. Additionally, as mentioned above, we will be studying the emission from the galaxies NGC 1275 and IC 310 and exploring the nature of dark matter (see Chapter 4) and the existence of ALPs (see Chapter 12). The proposed programme represents a major opportunity for CTA to make a significant contribution to galaxy cluster science and it will be a very significant step forward compared to the results from Fermi-LAT and current atmospheric Cherenkov telescopes. Therefore, this KSP will lead to a long-lived legacy in the study of non-thermal phenomena in clusters of galaxies.

This page intentionally left blank

14

Capabilities beyond Gamma Rays

Although designed as a gamma-ray observatory, CTA is a powerful tool for a range of other astrophysics and astroparticle physics. For example, CTA can make precision studies of charged cosmic rays in the energy range from ∼100 GeV up to PeV energies, and it can be used as an instrument for optical intensity interferometry, to provide unprecedented angular resolution in the optical for bright sources. Below, we briefly summarise these possibilities. Most of the topics we discuss can be explored in parallel with gamma-ray data-taking, without interfering with the major science operations of CTA. Those studies (such as intensity interferometry) which require specific observations can likely make use of bright moonlight time, thus enhancing the CTA science return without negative impact on the key science goals.

14.1 Cosmic-Ray Nuclei

The origin of cosmic rays remains one of the most important questions in astrophysics. Over the past few decades, a consensus has emerged that supernova remnants (SNRs) are likely to be the main sources of cosmic rays up to energies of the cosmic-ray knee (∼3 PeV). Finding out if SNRs are indeed the dominant accelerators of cosmic rays is a major science goal of CTA. While gamma-ray observations provide a view of the accelerators themselves, CTA will also address this question by directly detecting cosmic rays which reach the Earth.

The elemental composition and energy spectrum of cosmic rays provide important clues about their acceleration and diffusion through the Galaxy. For example, composition measurements at lower energies (<100 GeV) indicate that the cosmic-ray spectrum observed at the Earth is significantly steeper than in the sources [629] and that cosmic rays spend most of their lifetime in the Galactic halo [630]. Particularly interesting is the elemental composition around the knee of the energy spectrum. The steepening of the cosmic-ray spectrum at this point is still not understood; it is expected to be related to the maximum energy to which particles can be accelerated inside Galactic cosmic-ray accelerators. This maximum energy should increase with increasing rigidity of the particle (rigidity = momentum/charge) and therefore lead to an enhancement of heavier nuclei with increasing energy at the knee. Experimental evidence for this has been reported by the KASCADE collaboration [631], although the analysis is challenging due to its dependence upon hadronic interaction models, leading to significant systematic uncertainties.

Cosmic-ray composition measurements above 100 TeV will give us further insights into this question. Balloon and space-born measurements have measured the composition of cosmic rays up to $\approx$100 TeV. It is difficult to extend these measurements to higher energies because of the limited collection area and observation time of these instruments, although the CALET and ISS-CREAM instruments should significantly extend the reach of the satellite technique. At energies of a few PeV, detection of the secondary shower particles from the ground becomes possible, allowing for larger collection areas and composition measurements at these energies. These measurements are, however, affected by severe systematic uncertainties related to the simulation of hadronic showers.

CTA will be able to perform composition measurements in the TeV to PeV domain by measuring the Cherenkov light emitted by cosmic-ray nuclei prior to their first interaction [632]. As was shown by the H.E.S.S. [633] and VERITAS [634] collaborations, this emission can be detected by atmospheric Cherenkov telescopes, enabling the reconstruction of the charge of the primary. Using this technique, CTA is expected to measure the iron spectrum of cosmic rays up to, and beyond, 1 PeV. For lighter nuclei down to oxygen, the measurement of the spectrum is expected to extend up to a few hundred TeV. Techniques based on shower properties rather than direct Cherenkov emission of the primary will provide further capability for composition measurements, in particular for light nuclei. Such studies will also be carried out by the LHAASO instrument (see Section 2.5).

14.2 Cosmic-Ray Electrons

Electrons form only a small fraction of the cosmic rays — at GeV energies the fraction is around 1% — yet they are important for a wide range of scientific questions. In the VHE regime, the lifetime of cosmic-ray electrons is severely limited by radiative losses due to synchrotron emission in interstellar magnetic fields and inverse-Compton scattering on star light, IR light, and the cosmic microwave background. The lifetime of a cosmic-ray electron with energy E can be expressed as

$$t \approx 5 \times 10^5 (E/1\mathrm{TeV})^{-1} ((B/5\mu\mathrm{G})^2 + 1.6(w/1\mathrm{eVcm}^{-3}))^{-1} \text{ years},$$

where w is the energy density in low frequency photons in the interstellar medium and B is the mean interstellar magnetic field [375]. This restricts the distances that VHE cosmic-ray electrons can propagate and implies a local origin of TeV electrons (<1 kpc distance) as discussed in, e.g., Refs. [635, 636]. In the TeV range, therefore, only a few local sources are able to contribute and the spectrum can differ dramatically from the power-law form seen at lower energies, revealing the imprint of nearby sources. Thus, VHE cosmic-ray electrons offer a unique tool to study our local neighbourhood in terms of single electron accelerators, rather than testing the averaged contribution of the whole population of sources in the Galaxy, as visible in cosmic-ray protons.

In addition to the limited propagation distance, the cooling of cosmic-ray electrons also leads to a steepening of the electron spectrum far from acceleration sites, i.e., as observed at the Earth. This steepening, from a $\sim E^{-2.7}$ to $\sim E^{-3}$ power-law form, is not observed in the cosmic-ray protons, and has the effect of further reducing the flux and poses a severe challenge for direct balloon or satellite measurements. While balloon measurements generally suffer from short exposures, a new generation of satellite experiments recently provided high-statistics electron measurements up to several hundred GeV [637–640]. Still, the energy regime above ∼2 TeV is not yet accessible to these instruments due to either limited detector area or the lack of sufficient detector depth for energy measurement at higher energies.

The multi-TeV energy regime is of particular interest because it has the unique feature of reflecting the situation in our local neighbourhood. Exploring this energy range would provide a new perspective on local particle accelerators. Another frequently discussed possibility is the potential signature of dark matter annihilation in the electron spectrum (see, e.g., Ref. [641] and references therein), which was fueled by the observation of a rise in the positron fraction by PAMELA [642] and AMS-02 [643].

Imaging atmospheric Cherenkov telescopes (IACTs), such as CTA, detect VHE cosmic-ray electrons through the same air shower technique that they detect VHE gamma rays. Electrons initiate air showers very similar to those originating from gamma rays, and so special data-taking conditions are not required. Furthermore, due to the isotropic nature of cosmic-ray electrons, their measurement does not need targeted observations but can be performed with any data set where significant gamma-ray emission regions can be readily excluded (i.e., away from the Galactic Plane). This makes a cosmic-ray electron measurement at TeV energies an excellent by-product of regular observations made by CTA.

A proof-of-principle measurement of cosmic-ray electrons with IACTs was made by H.E.S.S. [375] and later confirmed by MAGIC [644] and VERITAS [645]. The H.E.S.S. data extended the measured energy range of cosmic-ray electrons up to 6 TeV and revealed a break in the spectrum at around 1 TeV, with a $\sim E^{-4}$ spectrum at higher energies. As there are almost certainly no regions of the sky from which cosmic ray electrons do not arrive, the contamination of IACT measurements by the residual background of hadronic cosmic rays must be estimated with the aid of simulations rather than control regions within the field of view. Limitations of the measurement therefore arise due to our limited understanding of hadronic physics in air showers, introducing systematic uncertainties into the estimation of the level of hadronic contamination. Additionally, to obtain a sufficiently large data set, long observations are required by the current generation of instruments, which introduces significant systematic uncertainties to account for the wide variety of observing conditions. At the highest energies, electron statistics become the limiting factor, due to the steeply declining spectrum at TeV energies.

Significant improvements can be expected from a CTA measurement of the electron spectrum, compared to the results from present instruments. With the CTA design optimised for a broad energy coverage and high sensitivity at TeV energies, an electron measurement will cover a similarly broad energy range, starting at $\sim$100 GeV. At high energies, a measurement of the spectrum is possible up to 20 TeV in the case that there is no contribution from a local source and that the spectrum continues with an index of -4.1. In the case of a local source contribution (see Figure 14.1), the electron spectrum may be measurable with CTA up to $\sim$100 TeV.

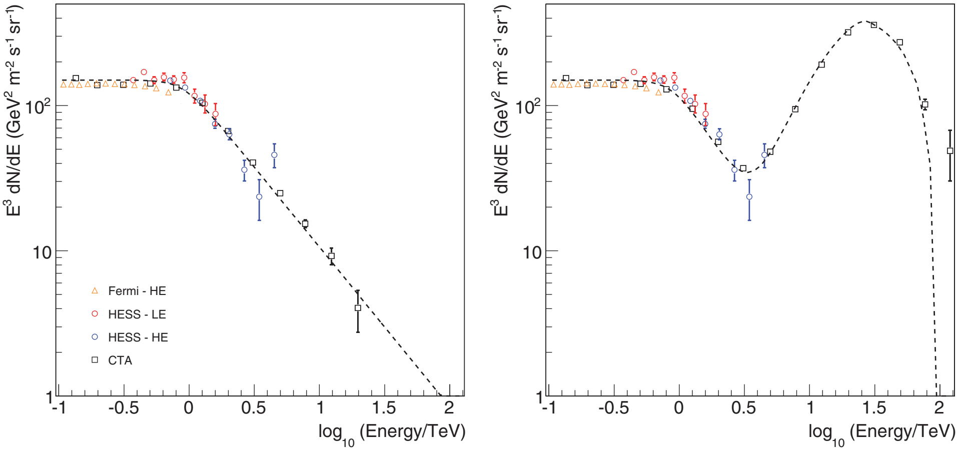

(a) (b)

Figure 14.1: Predictions for the measurement of the high-energy electron spectrum using 1000 h of CTA-South data: (a) without any local source and (b) with an injection of 5×10^{48} ergs in cosmic-ray electrons at 500 parsec distance 5000 years ago, plausibly comparable to the case of the Vela PWN. The differential energy spectrum multiplied by a factor of E^3 is plotted as a function of energy. Note that these studies were done with no Galactic diffuse component present. Reproduced from Ref. [646].

In addition to the greatly increased sensitivity and effective area of CTA, the energy resolution will also be significantly enhanced, aiding the identification of local source signatures in the spectrum. Furthermore, with the expected level of systematic uncertainties, the measurement of anisotropy in the electron arrival directions may be possible with CTA and would provide, together with spectral features at TeV energies, a probe of cosmic-ray electron source characteristics and propagation. A proper understanding of atmospheric variations is the key to such an anisotropy measurement, and again CTA will improve dramatically on the situation for current IACTs. A complete monitoring and correction scheme is under development for CTA [647], aiming to greatly reduce systematic variations in measured flux. Once cosmic-ray electron anisotropy is measured or constrained, cosmic-ray electrons are expected to play an important role in the calibration and monitoring of CTA [648].

Current ground-based measurements are dominated by the systematic errors arising from uncertainties in the simulations of hadronic air showers (necessary for the discrimination between electrons and the hadronic background) and from atmospheric conditions. For the case of the simulations, differences between hadronic interaction models are currently a leading source of uncertainty. CTA will be able to reduce these uncertainties by exploiting a new and (especially at TeV energies) improved generation of hadronic models. The increase in the centre-of-mass energy of hadronic collisions to ∼14 TeV for proton–proton collisions at the LHC is clearly a significant step towards a better understanding of this energy regime. Furthermore, the experiments LHCf and TOTEM are dedicated specifically to the measurement of cross-sections in the forward direction, thus providing key input to models and hopefully leading to a significant reduction in the uncertainties of the hadronic models used in air showers [649].

The measurement of the electron spectrum with CTA will be complementary to observations by the CALET instrument, which was recently mounted on the International Space Station and is able to measure cosmic-ray electrons up to 10 TeV [650]. In combination, these instruments will provide detailed observations of the electron spectrum at never before seen energies, potentially discovering and characterising powerful cosmic-ray accelerators in the local Galactic neighbourhood.

14.3 Optical Measurements with CTA

CTA will provide unprecedented telescopic light-collecting area — of the order of 10,000 m^2 distributed over a few square kilometres — far exceeding the mirror area of all of the world's large (>3 m) optical telescopes combined. Although mainly devoted to detecting Cherenkov light, other applications can be envisioned. These include searching for very rapid events from compact astrophysical sources, observing occultations of stars by distant Kuiper-belt objects, searching for optical signals from nearby civilisations (OSETI), or serving as a terrestrial ground station for optical communication with distant spacecraft. Since most such operations could be carried out during nights with bright moonlight which would not normally be used for regular gamma-ray observations, such additional applications would enable a more efficient use of CTA, enhance scientific contacts with other fields, and yield unique science not achievable at any other observatory. One area which has been explored in detail for CTA is operation as an optical intensity interferometer.

Diffraction-limited optical aperture synthesis over kilometre baselines, operating optical telescopes in a similar way as radio interferometers, is a long-held astronomical vision. This would enable imaging of stellar surfaces and their environments, explore their evolution over time, and reveal interactions of stellar winds and gas flows in binary star systems. The current best resolution in optical astronomy is offered by amplitude (phase-) interferometers which combine light from telescopes separated by up to a few hundred metres. Several concepts have been proposed to extend such facilities to scales of a kilometre or more, but their realisation remains challenging either on the ground or in space. Limiting parameters include the requirement of optical and atmospheric stability to a small fraction of an optical wavelength and the need to cover many interferometric baselines, given that optical light (as opposed to radio) cannot be copied with retained phase but has to be split up by beam-splitters to achieve interference among multiple telescope pairs.

The atmospheric and optical stability requirements of amplitude interferometers can be circumvented by *intensity interferometry*, a technique once developed for measuring stellar sizes (originally using an instrument at Narrabri in Australia [651, 652]). What is observed is the second-order coherence of light (i.e., that of intensity, not of amplitude or phase), by measuring temporal correlations of arrival times between photons recorded in different telescopes. The variation of that correlation with increasing telescopic distance provides the second-order spatial coherence of starlight, corresponding to the square of the visibility observed in any classical amplitude interferometer. Thus, one obtains [the square of] the Fourier transform of the brightness distribution of the source, from which its spatial properties and its two-dimensional image can be retrieved.

The great observational advantage is that the method is practically insensitive to either atmospheric turbulence or to telescope optical imperfections, enabling very long baselines, as well as observing at short optical wavelengths. Since telescopes are connected only electronically, error budgets and required precisions relate to electronic timescales of nanoseconds and to light-travel distances of tens of centimetres or meters rather than small fractions of an optical wavelength. However, the method requires very good photon statistics and therefore large telescopes, even in observing bright stars. These requirements for large and widely distributed optical flux collectors, equipped with fast detectors and high-speed electronics, have caused intensity interferometry not to be further pursued in a significant way since the early attempts.

The technical specifications for atmospheric Cherenkov telescopes are remarkably similar to the requirements for intensity interferometry (and conversely, the original telescopes at Narrabri were once used for pioneering experiments in observing Cherenkov light flashes). In the original Narrabri instrument, the telescopes were moved during observations to maintain their projected baseline; however, electronic time delays can now be used instead to compensate for different arrival times of the wavefront to various telescopes, removing the need for mechanical mobility. The potential of using modern Cherenkov telescope arrays for optical intensity interferometry has been explored recently [22, 653]. Pairs of 12 m Cherenkov telescopes of the VERITAS array in Arizona were connected to test electronics for intensity interferometry [654]; theoretically simulated observations, including subsequent reconstruction of source images, have been carried out [655]; laboratory measurements with arrays of small telescopes mimicking the CTA array have been made [656].

The "easiest" targets for interferometry are bright and hot, single or binary stars of spectral types O and B or Wolf–Rayet stars with their various circumstellar emission-line structures. The stellar disk diametres of the brightest such objects in the sky are typically 0.2–0.5 mas and thus lie (somewhat) beyond what can be resolved with existing amplitude interferometres. In addition, rapidly rotating oblate stars, circumstellar disks, winds from hot stars, blue super-giants and extreme objects such as η Carinae, interacting binaries, the hotter parts of (super)nova explosions, and pulsating Cepheids are clear candidates [22].

While initial experiments will likely use only a subset of the telescopes in the CTA array, best performance will be reached if the full CTA is equipped for interferometry at the shortest optical wavelengths. In the violet ($\lambda \sim$350 nm), the spatial resolution of CTA would then approach $\approx$30 μas. Such resolutions have hitherto been reached only in the radio and open up significant discovery space in the most well-established waveband of astronomy.

In addition to this interferometry possibility, CTA's huge collection area and extremely fast photo-detection and processing results in significant potential for the detection of transient optical phenomena, especially on relatively short timescales (of seconds or less). Examples include detecting counterparts to gamma-ray transients such as GRBs, radio transients, and gravitational wave events, studying outer Solar System bodies [657], and the search for optical SETI signals [658, 659]. These capabilities will be explored in detail in the near future.

15

Appendix: Simulating CTA

The expectations for the scientific capabilities of CTA presented in this document are based on sensitivity and response functions derived from detailed Monte Carlo simulations of the CTA observatory. The simulations model extensive air showers initiated by high-energy (HE) primary particles (gamma rays or background cosmic-ray nuclei and electrons), the Cherenkov light production by the shower particles, and the measurement processes of imaging atmospheric Cherenkov telescopes.

The air shower simulations are based on the CORSIKA code [660] and include realistic assumptions of the atmospheric conditions at the two CTA sites in the southern and northern hemispheres. The absorption and scattering of the Cherenkov photons due to atmospheric aerosols and molecules and the response of the telescopes are simulated with the tool sim_telarray [661]. The telescope simulations include the ray-tracing of the photons through the optical structure and a detailed simulation of the focal plane detector, trigger system, and detector readout. The simulations also include the noise photons coming from the expected night-sky background light at each site, with a level equivalent to dark-sky observations towards an extragalactic field. The telescope array assumed for the southern site consists of four large-sized telescopes (LST), 25 medium-sized telescopes (MST) and 70 small-sized telescopes (SST), with an area covered by the array of $\sim$4 km^2. The northern array consists of four LSTs and 15 MSTs, with area covered by the array of $\sim 0.4\,\mathrm{km}^2$. For a more detailed description of the simulation parameters see Ref. [662].

For all performance estimations, a gamma-ray source with a power-law shaped energy spectrum with a differential spectral index of 2.57 is assumed.

The sensitivity calculations require a large number of simulated events from cosmic-ray protons and electrons/positrons, due to the excellent gamma-hadron separation capabilities of CTA. The simulation set for each CTA site comprises about one billion simulated gamma-ray and electron showers and about 100 billion proton showers.

Two independent analyses of the Monte Carlo samples have been carried out, yielding consistent results. The analysis codes used are derived from tools developed in the MAGIC and the VERITAS collaborations. These analyses apply imaging cleaning algorithms to remove channels with signals dominated by background light, a geometrical image parametrisation, and stereoscopic methods. Most events observed by CTA will have shower cores that lie inside the area of the array. Compared to presently operating observatories, these so-called contained events will lead to much better sampled showers by CTA with a larger number of telescopes and will result in significantly improved reconstruction accuracy for the gamma-ray direction and energy. The gamma-hadron separation will also be much more powerful in CTA, resulting in improved sensitivity in the background-limited energy range of CTA. The gamma-hadron separation methods applied are based on multivariate methods (random forests and boosted decision trees) and separation cuts are optimised for the given observation time that is typically 50 h, 5 h, or 30 min. All analyses are optimised for the best point-source sensitivity per differential energy bin (five logarithmic bins per decade of energy); better energy and angular resolution can be expected for dedicated high-resolution selection criteria.

References

[1] http://www.slac.stanford.edu/exp/glast/groups/canda/lat_Performance.htm.

[2] Abeysekara A.U., Albert A., Alfaro R. *et al.* (2017). Observation of the Crab Nebula with the HAWC Gamma-Ray Observatory. *ApJ*, **843**, 39.

[3] Holler M., Berge D., van Eldik C. *et al.* (2015). Observations of the Crab Nebula with H.E.S.S. Phase II. arXiv:1509.02902.

[4] Aleksić J., Ansoldi S., Antonelli L.A. *et al.* (2016). The major upgrade of the MAGIC telescopes, Part II: A performance study using observations of the Crab Nebula. *Astropart. Phys.*, **72**, 76.

[5] https://veritas.sao.arizona.edu/about-veritas-mainmenu-81/veritas-specifications-mainmenu-111.

[6] Bartos I., Veres P., Nieto D. *et al.* (2014). Cherenkov Telescope Array is well suited to follow up gravitational-wave transients. *MNRAS*, **443**, 738.

[7] Abbott B.P., Abbott R., Abbott T.D. *et al.* (2016). Observation of gravitational waves from a binary black hole merger. *Physical Review Letters*, **116**, 6, 061102.

[8] https://www.cta-observatory.org/science/cta-performance/.

[9] Dubus G., Contreras J.L., Funk S. *et al.* (2013). Surveys with the Cherenkov Telescope Array. *Astropart. Phys.*, **43**, 317.

[10] Abdo A.A., Allen B., Berley D. *et al.* (2007). TeV gamma-ray sources from a survey of the Galactic plane with Milagro. *ApJ*, **664**, L91.

[11] Amenomori M., Ayabe S., Chen D. *et al.* (2005). A northern sky survey for steady tera-electron volt gamma-ray point sources using the Tibet Air Shower Array. *ApJ*, **633**, 1005.

[12] Arsioli B., Fraga B., Giommi P. *et al.* (2015). 1WHSP: An IR-based sample of ˜1000 VHE γ-ray blazar candidates. *A&A*, **579**, A34.

[13] Padovani P. & Giommi P. (2015). A simplified view of blazars: the very high energy γ-ray vision. *MNRAS*, **446**, L41.

[14] Inoue S., Granot J., O'Brien P.T. *et al.* (2013). Gamma-ray burst science in the era of the Cherenkov Telescope Array. *Astropart. Phys.*, **43**, 252.

[15] de Oña-Wilhelmi E., Rudak B., Barrio J.A. *et al.* (2013). Prospects for observations of pulsars and pulsar wind nebulae with CTA. *Astropart. Phys.*, **43**, 287.

[16] Uchiyama Y., Aharonian F.A., Tanaka T. *et al.* (2007). Extremely fast acceleration of cosmic rays in a supernova remnant. *Nature*, **449**, 576.

[17] Bulgarelli A., Fioretti V., Contreras J.L. *et al.* (2013). The real-time analysis of the Cherenkov Telescope Array Observatory. arXiv:1307.6489.

[18] Funk S., Hinton J.A. & CTA Consortium (2013). Comparison of Fermi-LAT and CTA in the region between 10-100 GeV. *Astropart. Phys.*, **43**, 348.

[19] Begelman M.C., Fabian A.C. & Rees M.J. (2008). Implications of very rapid TeV variability in blazars. *MNRAS*, **384**, L19.

[20] Paredes J.M., Bednarek W., Bordas P. *et al.* (2013). Binaries with the eyes of CTA. *Astropart. Phys.*, **43**, 301.

[21] Picozza P. & Boezio M. (2013). Multi messenger astronomy and CTA: TeV cosmic rays and electrons. *Astropart. Phys.*, **43**, 163.

[22] Dravins D., LeBohec S., Jensen H. *et al.* (2013). Optical intensity interferometry with the Cherenkov Telescope Array. *Astropart. Phys.*, **43**, 331.

[23] Gabici S. & Aharonian F.A. (2014). Hadronic gamma-rays from RX J1713.7-3946? *MNRAS*, **445**, L70.

[24] Acero F., Bamba A., Casanova S. *et al.* (2013). Gamma-ray signatures of cosmic ray acceleration, propagation, and confinement in the era of CTA. *Astropart. Phys.*, **43**, 276.

[25] The CTA Consortium: Acero, F, Aloisio R., Amans J. *et al.* (2017). Prospects for Cherenkov Telescope Array observation of the young supernova remnant RX J1713.73946. *ApJ*, **840**, 2, 74.

[26] Völk H.J., Aharonian F.A. & Breitschwerdt D. (1996). The nonthermal energy content and gamma-ray emission of starburst galaxies and clusters of galaxies. *Space Sci. Rev.*, **75**, 279.

[27] Abbott B.P., Abbott R., Abbott T.D. *et al.* (2016). Astrophysical implications of the binary black hole merger GW150914. *ApJ*, **818**, L22.

[28] Abbott B.P., Abbott R., Abbott T.D. *et al.* (2016). GW151226: Observation of gravitational waves from a 22-solar-mass binary black hole coalescence. *Physical Review Letters*, **116**, 24, 241103.

[29] Abbott B.P., Abbott R., Abbott T.D. *et al.* (2016). Binary black hole mergers in the first Advanced LIGO observing run. *Phys. Rev. X*, **6**, 4, 041015.

[30] Sol H., Zech A., Boisson C. *et al.* (2013). Active galactic nuclei under the scrutiny of CTA. *Astropart. Phys.*, **43**, 215.

[31] Mazin D., Raue M., Behera B. *et al.* (2013). Potential of EBL and cosmology studies with the Cherenkov Telescope Array. *Astropart. Phys.*, **43**, 241.

[32] Broderick A.E., Chang P. & Pfrommer C. (2012). The cosmological impact of luminous TeV blazars. I. Implications of plasma instabilities for the intergalactic magnetic field and extragalactic gamma-ray background. *ApJ*, **752**, 22.

[33] Hinton J., Sarkar S., Torres D. *et al.* (2013). A new era in gamma-ray astronomy with the Cherenkov Telescope Array. *Astropart. Phys.*, **43**, 1.

[34] Bourke T.L., Braun R., Fender R. *et al.* (editors) (2015). *Proceedings, Advancing Astrophysics with the Square Kilometre Array (AASKA14)*, volume AASKA14. SISSA, SISSA.

[35] Ray P.S., Abdo A.A., Parent D. *et al.* (2012). *Radio Searches of Fermi LAT Sources and Blind Search Pulsars: The Fermi Pulsar Search Consortium*. Proc. Fermi Symposium.

[36] Lorimer D.R., Bailes M., McLaughlin M.A. *et al.* (2007). A bright millisecond radio burst of extragalactic origin. *Science*, **318**, 777.

[37] Thornton D., Stappers B., Bailes M. *et al.* (2013). A population of fast radio bursts at cosmological distances. *Science*, **341**, 53.

[38] Pavlidou V., Angelakis E., Myserlis I. *et al.* (2014). The RoboPol optical polarization survey of gamma-ray-loud blazars. *MNRAS*, **442**, 1693.

[39] Blinov D., Pavlidou V., Papadakis I. *et al.* (2015). RoboPol: First season rotations of optical polarization plane in blazars. *MNRAS*, **453**, 1669.

[40] Reinthal R., Lindfors E.J., Mazin D. *et al.* (2012). Connection between optical and VHE gamma-ray emission in blazar jets. *J. Phys. Conf. Ser.*, **355**, 1, 012013.

[41] Lindfors E. & MAGIC Collaboration (2012). Recent results from MAGIC observations of AGN. *J. Phys. Conf. Ser.*, **355**, 1, 012003.

[42] Aleksić J., Alvarez E.A., Antonelli L.A. *et al.* (2012). Discovery of VHE γ-rays from the blazar 1ES 1215+303 with the MAGIC telescopes and simultaneous multi-wavelength observations. *A&A*, **544**, A142.

[43] Tepe A. & HAWC Collaboration (2012). HAWC — The high altitude water Cherenkov detector. *J. Phys. Conf. Ser.*, **375**, 5, 052026.

[44] Di Sciascio G. on behalf of the LHAASO Collaboration (2016). The LHAASO experiment: From gamma-ray astronomy to cosmic rays. arXiv:1602.07600.

[45] Aartsen M. *et al.* (2013). Evidence for high-energy extraterrestrial neutrinos at the IceCube detector. *Science*, **342**, 1242856.

[46] Razzaque S. (2013). Galactic Center origin of a subset of IceCube neutrino events. *Phys. Rev. D*, **88**, 8, 081302.

[47] Katz U.F. (2006). KM3NeT: Towards a km^3 Mediterranean neutrino telescope. *NIM A*, **567**, 457.

[48] Aasi J., Abadie J., Abbott B.P. *et al.* (2013). Prospects for localization of gravitational wave transients by the Advanced LIGO and Advanced Virgo observatories. arXiv:1304.0670.

[49] Abadie J., Abbott B.P., Abbott R. *et al.* (2010). Topical review: Predictions for the rates of compact binary coalescences observable by ground-based gravitational-wave detectors. *Classic. Quant. Grav.*, **27**, 17, 173001.

[50] Punturo M., Abernathy M., Acernese F. *et al.* (2010). The Einstein Telescope: A third-generation gravitational wave observatory. *Classic. Quant. Grav.*, **27**, 19, 194002.

[51] Abdallah H. *et al.* (2016). Search for dark matter annihilations towards the inner Galactic halo from 10 years of observations with H.E.S.S. *Phys. Rev. Lett.*, **117**, 11, 111301.

[52] Ackermann M., Albert A., Anderson B. *et al.* (2015). Searching for dark matter annihilation from Milky Way dwarf spheroidal galaxies with six years of Fermi Large Area Telescope data. *Physical Review Letters*, **115**, 23, 231301.

[53] Roszkowski L., Sessolo E.M. & Williams A.J. (2015). Prospects for dark matter searches in the pMSSM. *JHEP*, **2**, 14.

[54] Roszkowski L., Sessolo E.M. & Williams A.J. (2014). What next for the CMSSM and the NUHM: Improved prospects for superpartner and dark matter detection. *JHEP*, **1408**, 067.

[55] Abramowski A. *et al.* (2011). Search for a dark matter annihilation signal from the Galactic Center halo with H.E.S.S. *Phys. Rev. Lett.*, **106**, 161301.

[56] Zwicky F. (1933). Die Rotverschiebung von extragalaktischen Nebeln. *Helv. Phys. Acta*, **6**, 110.

[57] Clowe D., Gonzalez A. & Markevitch M. (2004). Weak lensing mass reconstruction of the interacting cluster 1E0657-558: Direct evidence for the existence of dark matter. *ApJ*, **604**, 596.

[58] Bradac M., Allen S.W., Treu T. *et al.* (2008). Revealing the properties of dark matter in the merging cluster MACSJ0025.4-1222. *ApJ*, **687**, 959.

[59] Clowe D., Bradac M., Gonzalez A.H. *et al.* (2006). A direct empirical proof of the existence of dark matter. *ApJ*, **648**, L109.

[60] Alcock C. *et al.* (2000). The MACHO project: Microlensing results from 5.7 years of LMC observations. *ApJ*, **542**, 281.

[61] Tisserand P. *et al.* (2007). Limits on the MACHO content of the galactic halo from the EROS-2 Survey of the Magellanic Clouds. *A&A*, **469**, 387.

[62] Ade P. *et al.* (2014). Planck intermediate results. XVI. Profile likelihoods for cosmological parameters. *A&A*, **566**, A54.

[63] Planck Collaboration, Ade P.A.R., Aghanim N. *et al.* (2016). Planck 2015 results. XIII. Cosmological parameters. *A&A*, **594**, A13.

[64] Springel V., Wang J., Vogelsberger M. *et al.* (2008). The Aquarius Project: The subhalos of galactic halos. *MNRAS*, **391**, 1685.

[65] Diemand J., Kuhlen M., Madau P. *et al.* (2008). Clumps and streams in the local dark matter distribution. *Nature*, **454**, 735.

[66] Navarro J.F., Frenk C.S. & White S.D. (1996). The structure of cold dark matter halos. *ApJ*, **462**, 563.

[67] Graham A.W., Merritt D., Moore B. *et al.* (2006). Empirical models for dark matter halos. III. The Kormendy relation and the $log(\rho_e)$–$log(R_e)$ relation. *Astron. J.*, **132**, 2711.

[68] Navarro J.F., Ludlow A., Springel V. *et al.* (2010). The diversity and similarity of cold dark matter halos. *MNRAS*, **402**, 21.

[69] Walker M.G., Mateo M., Olszewski E.W. *et al.* (2009). A universal mass profile for dwarf spheroidal galaxies. *ApJ*, **704**, 1274.

[70] Walker M.G. & Penarrubia J. (2011). A method for measuring (slopes of) the mass profiles of dwarf spheroidal galaxies. *ApJ*, **742**, 20.

[71] Zeldovich Y., Klypin A., Khlopov M.Y. *et al.* (1980). Astrophysical constraints on the mass of heavy stable neutral leptons. *Sov. J. Nucl. Phys.*, **31**, 664.

[72] Blumenthal G.R., Faber S., Flores R. *et al.* (1986). Contraction of dark matter galactic halos due to baryonic infall. *ApJ*, **301**, 27.

[73] Merritt D. (2004). Evolution of the dark matter distribution at the Galactic Center. *Phys. Rev. Lett.*, **92**, 201304.

[74] Merritt D., Harfst S. & Bertone G. (2007). Collisionally regenerated dark matter structures in galactic nuclei. *Phys. Rev. D*, **75**, 043517.

[75] Gondolo P. & Silk J. (1999). Dark matter annihilation at the Galactic Center. *Phys. Rev. Lett.*, **83**, 1719.

[76] Merritt D., Milosavljevic M., Verde L. *et al.* (2002). Dark matter spikes and annihilation radiation from the Galactic Center. *Phys. Rev. Lett.*, **88**, 191301.

[77] Gnedin N.Y., Tassis K. & Kravtsov A.V. (2009). Modeling molecular hydrogen and star formation in cosmological simulations. *ApJ*, **697**, 55.

[78] Wise J.H. & Abel T. (2011). Enzo+Moray: Radiation hydrodynamics adaptive mesh refinement simulations with adaptive ray tracing. *MNRAS*, **414**, 3458.

[79] Teyssier R. (2002). Cosmological hydrodynamics with adaptive mesh refinement: A new high resolution code called RAMSES. *A&A*, **385**, 337.

[80] Keres D., Vogelsberger M., Sijacki D. *et al.* (2012). Moving mesh cosmology: Characteristics of galaxies and haloes. *MNRAS*, **425**, 2027.

[81] Ackermann M. *et al.* (2014). Dark matter constraints from observations of 25 Milky Way satellite galaxies with the Fermi Large Area Telescope. *Phys. Rev. D*, **89**, 4, 042001.

[82] Susskind L. (1984). The gauge hierarchy problem, technicolor, supersymmetry, and all that. (Talk). *Phys. Rept.*, **104**, 181.

[83] Bertone G., Hooper D. & Silk J. (2005). Particle dark matter: Evidence, candidates and constraints. *Phys. Rept.*, **405**, 279.

[84] Cushman P., Galbiati C., McKinsey D. *et al.* (2013). Snowmass CF1 summary: WIMP dark matter direct detection. arXiv:1310.8327.

[85] Tulin S., Yu H.B. & Zurek K.M. (2013). Beyond collisionless dark matter: Particle physics dynamics for dark matter halo structure. *Phys. Rev. D*, **87**, 11, 115007.

[86] Cahill-Rowley M., Cotta R., Drlica-Wagner A. *et al.* (2013). Complementarity and searches for dark matter in the pMSSM. arXiv:1305.6921.

[87] Bringmann T., Calore F., Vertongen G. *et al.* (2011). On the relevance of sharp gamma-ray features for indirect dark matter searches. *Phys. Rev. D*, **84**, 103525.

[88] Arina C., Hambye T., Ibarra A. *et al.* (2010). Intense gamma-ray lines from hidden vector dark matter decay. *JCAP*, **1003**, 024.

[89] Bringmann T., Bergstrom L. & Edsjo J. (2008). New gamma-ray contributions to supersymmetric dark matter annihilation. *JHEP*, **0801**, 049.

[90] Birkedal A., Matchev K.T., Perelstein M. *et al.* (2005). Robust gamma ray signature of WIMP dark matter. arXiv:0507194.

[91] Bergstrom L., Bringmann T., Eriksson M. *et al.* (2005). Gamma rays from Kaluza-Klein dark matter. *Phys. Rev. Lett.*, **94**, 131301.

[92] Bergstrom L., Bringmann T., Eriksson M. *et al.* (2005). Gamma rays from heavy neutralino dark matter. *Phys. Rev. Lett.*, **95**, 241301.

[93] Bergstrom L. (1989). Radiative processes in dark matter photino annihilation. *Phys. Lett. B*, **225**, 372.

[94] Toma T. (2013). Internal bremsstrahlung signature of real scalar dark matter and consistency with thermal relic density. *Phys. Rev. Lett.*, **111**, 091301.

[95] Mayer L. (2010). Environmental mechanisms shaping the nature of dwarf spheroidal galaxies: the view of computer simulations. *Adv. Astron.*, **2010**, 278434.

[96] Aharonian F. *et al.* (2006). H.E.S.S. observations of the Galactic Center region and their possible dark matter interpretation. *Phys. Rev. Lett.*, **97**, 221102.

[97] Iocco F., Pato M., Bertone G. *et al.* (2011). Dark matter distribution in the Milky way: microlensing and dynamical constraints. *JCAP*, **1111**, 029.

[98] Schaye J., Crain R.A., Bower R.G. *et al.* (2015). The EAGLE project: Simulating the evolution and assembly of galaxies and their environments. *MNRAS*, **446**, 521.

[99] Wyrzykowski L., Rynkiewicz A.E., Skowron J. *et al.* (2015). The largest sample of microlensing events and the structure of the Galactic bulge from the OGLE-III Survey. *ApJS*, **216**, 12.

[100] Freeman K., Ness M., de Boer E.W. *et al.* (2013). ARGOS II: The Galactic bulge survey. *MNRAS*, **428**, 3660.

[101] Howard C.D., Rich R.M., Reitzel D.B. *et al.* (2008). The bulge radial velocity assay (BRAVA): I. Sample selection and a rotation curve. *ApJ*, **688**, 1060.

[102] GAIA: http://sci.esa.int/gaia/.

[103] Zoccali M., Gonzalez O.A., Vasquez S. *et al.* (2014). The GIRAFFE inner bulge survey (GIBS). I. Survey description and a kinematical map of the Milky Way bulge. *A&A*, **562**, A66.

[104] Lefranc V., Moulin E., Panci P. *et al.* (2015). Prospects for annihilating dark matter in the inner Galactic halo by the cherenkov telescope array. *Phys. Rev. D*, **91**, 12, 122003.

[105] Cabrera-Catalan M.E., Ando S., Weniger C. *et al.* (2015). Indirect and direct detection prospect for TeV dark matter in the nine parameter MSSM. *Phys. Rev. D*, **92**, 3, 035018.

[106] Pierre M., Siegal-Gaskins J.M. & Scott P. (2014). Sensitivity of CTA to dark matter signals from the Galactic Center. *JCAP*, **6**, 024.

[107] Silverwood H., Weniger C., Scott P. *et al.* (2015). A realistic assessment of the CTA sensitivity to dark matter annihilation. *JCAP*, **1503**, 03, 055.

[108] Ackermann M. *et al.* (2012). Fermi LAT search for dark matter in gamma-ray lines and the inclusive photon spectrum. *Phys. Rev. D*, **86**, 022002.

[109] Abramowski A. *et al.* (2013). Search for photon line-like signatures from dark matter annihilations with H.E.S.S. *Phys. Rev. Lett.*, **110**, 041301.

[110] Bringmann T., Huang X., Ibarra A. *et al.* (2012). Fermi LAT search for internal bremsstrahlung signatures from dark matter annihilation. *JCAP*, **1207**, 054.

[111] Weniger C. (2012). A tentative gamma-ray line from dark matter annihilation at the Fermi Large Area Telescope. *JCAP*, **1208**, 007.

[112] Martinez G.D. (2015). A robust determination of Milky Way satellite properties using hierarchical mass modeling. **451**, 2524.

[113] DES Collaboration, Bechtol K. *et al.* (2015). Eight new Milky Way companions discovered in first-year dark energy survey data. *ApJ*, **807**, 50.

[114] Koposov S.E., Belokurov V., Torrealba G. *et al.* (2015). Beasts of the Southern Wild: Discovery of nine ultra faint satellites in the vicinity of the Magellanic Clouds. *ApJ*, **805**, 130.

[115] Bonnivard V., Combet C., Maurin D. *et al.* (2015). Dark matter annihilation and decay profiles for the Reticulum II dwarf spheroidal galaxy. *ApJ*, **808**, 2, L36.

[116] Bringmann T. (2009). Particle models and the small-scale structure of dark matter. *New J. Phys.*, **11**, 105027.

[117] Zackrisson E. & Riehm T. (2010). Gravitational lensing as a probe of cold dark matter subhalos. *Adv. Astron.*, **2010**, 478910.

[118] Chen J. & Koushiappas S.M. (2010). Gravitational nanolensing from subsolar mass dark matter halos. *ApJ*, **724**, 400.

[119] Garsden H., Bate N. & Lewis G. (2012). Probing planetary mass dark matter in galaxies: gravitational nanolensing of multiply imaged quasars. *MNRAS*, **420**, 3574.

[120] Geringer-Sameth A. & Koushiappas S.M. (2012). Detecting unresolved moving sources in a diffuse background. *MNRAS*, **425**, 862.

[121] Carlberg R.G. & Grillmair C.J. (2013). Gaps in the GD-1 star stream. *ApJ*, **768**, 171.

[122] Grillmair C.J., Cutri R., Masci F.J. *et al.* (2013). Detection of a nearby halo debris stream in the WISE and 2MASS surveys. *ApJ*, **769**, L23.

[123] Grillmair C.J. (2014). Two new halo debris streams in the Sloan Digital Sky Survey. *ApJ*, **790**, L10.

[124] Hargis J., Willman B., Sand D. *et al.* (2014). Milky Way stellar streams: A window to purely dark subhalos. *NOAO Proposal*.

[125] Sesar B., Banholzer S.R., Cohen J.G. *et al.* (2014). Stacking the invisibles: A guided search for low-luminosity Milky Way satellites. *ApJ*, **793**, 135.

[126] Erkal D. & Belokurov V. (2015). Forensics of subhalo-stream encounters: The three phases of gap growth. *MNRAS*, **450**, 1136.

[127] Pieri L., Bertone G. & Branchini E. (2008). Dark matter annihilation in substructures revised. *MNRAS*, **384**, 1627.

[128] Buckley M.R. & Hooper D. (2010). Dark matter subhalos in the Fermi first source catalog. *Phys. Rev. D*, **82**, 063501.

[129] Zechlin H., Fernandes M., Elsaesser D. *et al.* (2012). Dark matter subhaloes as gamma-ray sources and candidates in the first Fermi-LAT catalogue. *A&A*, **538**, A93.

[130] Smith G.P. (1963). A peculiar feature at $l^{II} = 40^\circ.5$, $\mathrm{b}^{II} = -15^\circ.0$. *Bull. Astron. Inst. Netherlands*, **17**, 203.

[131] Saul D.R., Peek J., Grcevich J. *et al.* (2012). The GALFA-HI compact cloud catalog. *ApJ*, **758**, 44.

[132] Hill A.S., Haffner L.M. & Reynolds R.J. (2009). Ionized gas in the Smith cloud. *ApJ*, **703**, 1832.

[133] Bonnivard V., Combet C., Maurin D. *et al.* (2015). Spherical Jeans analysis for dark matter indirect detection in dwarf spheroidal galaxies — impact of physical parameters and triaxiality. *MNRAS*, **446**, 3002.

[134] Geringer-Sameth A., Koushiappas S.M. & Walker M. (2015). Dwarf galaxy annihilation and decay emission profiles for dark matter experiments. *ApJ*, **801**, 74.

[135] Koch A., Kleyna J., Wilkinson M. *et al.* (2007). Stellar kinematics in the remote Leo II dwarf spheroidal galaxy — Another brick in the wall. *AJ*, **134**, 566.

[136] Walker M.G., Mateo M. & Olszewski E. (2009). Stellar velocities in the Carina, Fornax, Sculptor and Sextans dSph galaxies: Data from the Magellan/MMFS Survey. *AJ*, **137**, 3100.

[137] Walker M. (2013). Dark matter in the galactic dwarf spheroidal satellites, in Oswalt T.D., Gilmore G. (eds.), *Planets, Stars and Stellar Systems* (Springer, Dordrecht), p. 1039.

[138] http://sumire.ipmu.jp/pfs/intro.html. (2011).

[139] Charbonnier A., Combet C., Daniel M. *et al.* (2011). Dark matter profiles and annihilation in dwarf spheroidal galaxies: Prospectives for present and future gamma-ray observatories — I. The classical dSphs. *MNRAS*, **418**, 1526.

[140] Strigari L.E., Koushiappas S.M., Bullock J.S. *et al.* (2008). The most dark matter dominated galaxies: Predicted gamma-ray signals from the faintest Milky Way dwarfs. *ApJ*, **678**, 614.

[141] Strigari L.E. (2013). Galactic searches for dark matter. *Phys. Rept.*, **531**, 1.

[142] Koposov S., Belokurov V., Evans N. *et al.* (2008). The luminosity function of the Milky Way satellites. *ApJ*, **686**, 279.

[143] Tollerud E.J., Bullock J.S., Strigari L.E. *et al.* (2008). Hundreds of Milky Way satellites? Luminosity bias in the satellite luminosity function. *ApJ*, **688**, 277.

[144] Bullock J.S. (2010). Notes on the missing satellites problem. arXiv:1009.4505.

[145] Hargis J.R., Willman B. & Peter A.H.G. (2014). Too many, too few, or just right? The predicted number and distribution of Milky Way dwarf galaxies. *ApJ*, **795**, L13.

[146] Tasitsiomi A., Siegal-Gaskins J.M. & Olinto A.V. (2004). Gamma-ray and synchrotron emission from neutralino annihilation in the Large Magellanic Cloud. *Astropart. Phys.*, **21**, 637.

[147] Buckley M.R., Charles E., Gaskins J.M. *et al.* (2015). Search for gamma-ray emission from dark matter annihilation in the Large Magellanic Cloud with the Fermi Large Area Telescope. *Phys. Rev. D*, **91**, 10, 102001.

[148] Abdo A.A., Ackermann M., Ajello M. *et al.* (2010). Observations of the Large Magellanic Cloud with Fermi. *A&A*, **512**, A7+.

[149] H.E.S.S. Collaboration, Abramowski A., Aharonian F. *et al.* (2015). The exceptionally powerful TeV γ-ray emitters in the Large Magellanic Cloud. *Science*, **347**, 406.

[150] Kim S., Staveley-Smith L., Dopita M.A. *et al.* (1998). An H I aperture synthesis mosaic of the Large Magellanic Cloud. *ApJ*, **503**, 674.

[151] van der Marel R.P. & Kallivayalil N. (2014). Third-Epoch Magellanic Cloud proper motions II: The Large Magellanic Cloud rotation field in three dimensions. *ApJ*, **781**, 2, 121.

[152] van der Marel R.P., Alves D.R., Hardy E. *et al.* (2002). New understanding of Large Magellanic Cloud structure, dynamics and orbit from carbon star kinematics. *AJ*, **124**, 2639.

[153] Combet C., Maurin D., Nezri E. *et al.* (2012). Decaying dark matter: Stacking analysis of galaxy clusters to improve on current limits. *Phys. Rev. D*, **85**, 6, 063517.

[154] Sanchez-Conde M.A. & Prada F. (2014). The flattening of the concentration-mass relation towards low halo masses and its implications for the annihilation signal boost. *MNRAS*, **442**, 2271.

[155] Pinzke A., Pfrommer C. & Bergstrom L. (2009). Gamma-rays from dark matter annihilations strongly constrain the substructure in halos. *Phys. Rev. Lett.*, **103**, 181302.

[156] Pinzke A., Pfrommer C. & Bergström L. (2011). Prospects of detecting gamma-ray emission from galaxy clusters: Cosmic rays and dark matter annihilations. *Phys. Rev. D*, **84**, 12, 123509.

[157] Cirelli M., Moulin E., Panci P. *et al.* (2012). Gamma ray constraints on decaying dark matter. *Phys. Rev. D*, **86**, 083506.

[158] Sánchez-Conde M.A., Cannoni M., Zandanel F. *et al.* (2011). Dark matter searches with cherenkov telescopes: Nearby dwarf galaxies or local galaxy clusters? *JCAP*, **12**, 011.

[159] Aleksić J., Rico J. & Martinez M. (2012). Optimized analysis method for indirect dark matter searches with imaging air Cherenkov telescopes. *JCAP*, **10**, 032.

[160] Ackermann M. *et al.* (2012). Constraints on the Galactic halo dark matter from Fermi-LAT diffuse measurements. *ApJ*, **761**, 91.

[161] Cembranos J.A.R., de La Cruz-Dombriz A., Dobado A. *et al.* (2011). Photon spectra from WIMP annihilation. *Phys. Rev. D*, **83**, 8, 083507.

[162] Ponti G., Morris M.R., Terrier R. *et al.* (2015). The XMM-Newton view of the central degrees of the Milky Way. *MNRAS*, **453**, 172.

[163] LaRosa T.N., Kassim N.E., Lazio T.J.W. *et al.* (2000). A wide-field 90 centimeter VLA image of the Galactic Center region. *AJ*, **119**, 207.

[164] Molinari S., Bally J., Noriega-Crespo A. *et al.* (2011). A 100 pc elliptical and twisted ring of cold and dense molecular clouds revealed by Herschel around the Galactic Center. *ApJ*, **735**, L33.

[165] van Eldik C. (2015). Gamma rays from the Galactic Centre region: A review. *Astropart. Phys.*, **71**, 45.

[166] Aharonian F., Akhperjanian A.G., Anton G. *et al.* (2009). Spectrum and variability of the Galactic Center VHE γ-ray source H.E.S.S. J1745-290. *A&A*, **503**, 817.

[167] Archer A., Barnacka A., Beilicke M. *et al.* (2014). Very-high energy observations of the Galactic Center region by VERITAS in 2010–2012. *ApJ*, **790**, 149.

[168] Aharonian F., Akhperjanian A.G., Bazer-Bachi A.R. *et al.* (2006). Discovery of very-high-energy γ-rays from the Galactic Centre ridge. *Nature*, **439**, 695.

[169] Archer A., Benbow W., Bird R. *et al.* (2016). TeV gamma-ray observations of the Galactic Center ridge by VERITAS. *ApJ*, **821**, 129.

[170] H.E.S.S. Collaboration, Abramowski A., Aharonian F. *et al.* (2016). Acceleration of petaelectronvolt protons in the Galactic Centre. *Nature*, **531**, 476.

[171] Aharonian F., Akhperjanian A.G., Aye K.M. *et al.* (2005). Very high energy gamma rays from the composite SNR G 0.9+0.1. *A&A*, **432**, L25.

[172] Jones P.A., Burton M.G., Cunningham M.R. *et al.* (2012). Spectral imaging of the central molecular zone in multiple 3-mm molecular lines. *MNRAS*, **419**, 2961.

[173] Johnson S.P., Dong H. & Wang Q.D. (2009). A large-scale survey of X-ray filaments in the Galactic Centre. *MNRAS*, **399**, 1429.

[174] Kosack K. *et al.* (2004). TeV gamma-ray observations of the Galactic Center. *ApJ*, **608**, L97.

[175] Tsuchiya K. *et al.* (2004). Detection of sub-TeV gamma-rays from the Galactic Center direction by CANGAROO-II. *ApJ*, **606**, L115.

[176] Figer D.F., Rich R.M., Kim S.S. *et al.* (2004). An extended star formation history for the Galactic Center from Hubble Space Telescope/NICMOS observations. *ApJ*, **601**, 319.

[177] Crocker R.M., Jones D.I., Aharonian F. *et al.* (2011). Wild at heart:-The particle astrophysics of the Galactic Centre. *MNRAS*, **413**, 763.

[178] Yoast-Hull T.M., Gallagher J. & Zweibel E.G. (2014). The cosmic ray population of the Galactic central molecular zone. *ApJ*, **790**, 86.

[179] Yang H.Y., Ruszkowski M., Ricker P. *et al.* (2012). The Fermi bubbles: Supersonic AGN jets with anisotropic cosmic ray diffusion. *ApJ*, **761**, 185.

[180] Law C. (2010). A multiwavelength view of a mass outflow from the Galactic Center. *ApJ*, **708**, 474.

[181] Nakashima S., Nobukawa M., Uchida H. *et al.* (2013). Discovery of the recombining plasma in the south of the Galactic Center; a relic of the past Galactic Center activity? *ApJ*, **773**, 20N.

[182] Borkowski K.J., Reynolds S.P., Green D.A. *et al.* (2014). Nonuniform expansion of the youngest galactic supernova remnant G1.9+0.3. *ApJ*, **790**, L18.

[183] Aharonian F. *et al.* (2006). The H.E.S.S. survey of the inner Galaxy in very high-energy gamma-rays. *ApJ*, **636**, 777.

[184] Aharonian F., Akhperjanian A.G., Barres de Almeida U. *et al.* (2008). Exploring a SNR/molecular cloud association within H.E.S.S. J1745-303. *A&A*, **483**, 509.

[185] Aharonian F. *et al.* (2006). H.E.S.S. observations of the Galactic Center region and their possible dark matter interpretation. *Phys. Rev. Lett.*, **97**, 221102.

[186] Zubovas K., Nayakshin S. & Markoff S. (2012). Sgr A^* flares: Tidal disruption of asteroids and planets?. *MNRAS*, **421**, 1315.

[187] Wommer E., Melia F. & Fatuzzo M. (2008). Diffuse TeV emission at the Galactic Centre. *MNRAS*, **387**, 987.

[188] Melia F. & Fatuzzo M. (2011). Diffusive cosmic-ray acceleration at the Galactic Centre. *MNRAS*, **410**, L23.

[189] Amano T., Torii K., Hayakawa T. *et al.* (2011). Stochastic acceleration of cosmic rays in the central molecular zone of the Galaxy. arXiv:1110.3140.

[190] Abeysekara A.U., Alfaro R., Alvarez C. *et al.* (2013). Sensitivity of the high altitude water Cherenkov detector to sources of multi-TeV gamma rays. *Astropart. Phys.*, **50**, 26.

[191] Ackermann M., Ajello M., Atwood W.B. *et al.* (2016). 2FHL: The second catalog of hard Fermi-LAT sources. *ApJS*, **222**, 5.

[192] Carrigan S., Brun F., Chaves R.C.G. *et al.* (2013). Charting the TeV Milky Way: H.E.S.S. Galactic plane survey maps, catalog and source populations. arXiv:1307.4868.

[193] Ong R. *et al.* (2013). Recent VERITAS results on VHE gamma-ray sources in Cygnus. *Proc. 33rd ICRC*, Rio de Janiero, Brazil.

[194] Bartoli B., Bernardini P., Bi X.J. *et al.* (2013). TeV gamma-ray survey of the northern sky using the ARGO-YBJ detector. *ApJ*, **779**, 27.

[195] Aharonian F. *et al.* (2002). A search for TeV gamma-ray emission from SNRs, pulsars and unidentified GeV sources in the Galactic plane in the longitude range between −2 deg and 85 deg. *A&A*, **395**, 803.

[196] Atkins R. *et al.* (2004). TeV gamma-ray survey of the northern hemisphere sky using the Milagro Observatory. *ApJ*, **608**, 680.

[197] Aharonian F. *et al.* (2004), The Crab nebula and pulsar between 500 GeV and 80 TeV: Observations with the HEGRA stereoscopic air Cherenkov telescopes. *ApJ*, **614**, 897.

[198] H.E.S.S. Collaboration, Abramowski A. *et al.* (2014). Diffuse Galactic gamma-ray emission with H.E.S.S. arXiv:1411.7568.

[199] Renaud M. (2009). Latest results on Galactic sources as seen in VHE gamma-rays. *Proc. 44th Recontres de Moriond*, 2009.

[200] Abdo A.A., Allen B.T., Aune T. *et al.* (2009). Milagro observations of multi-TeV emission from Galactic sources in the Fermi bright source list. *ApJ*, **700**, L127.

[201] Acharya, B. *et al.* (2013). Introducing the CTA concept. *Astropart. Phys.*, **43**, 3.

[202] Schure K.M. & Bell A.R. (2013). Cosmic ray acceleration in young supernova remnants. *MNRAS*, **435**, 1174.

[203] Abdo A. *et al.* (2009). Fermi Large Area Telescope bright gamma-ray source list. *ApJS*, **183**, 46.

[204] TeVCat: http://tevcat.uchicago.edu/.

[205] Aharonian F. *et al.* (2006). The H.E.S.S. survey of the inner Galaxy in very high-energy gamma-rays. *ApJ*, **636**, 777.

[206] Pietrzyński G., Graczyk D., Gieren W. *et al.* (2013). An eclipsing-binary distance to the Large Magellanic Cloud accurate to two per cent. *Nature*, **495**, 76.

[207] van der Marel R.P. (2006). The Large Magellanic Cloud: Structure and kinematics. In M. Livio & T.M. Brown (eds.), *The Local Group as an Astrophysical Laboratory* (Cambridge University Press), pp. 47–71.

[208] Hughes A., Staveley-Smith L., Kim S. *et al.* (2007). An Australia telescope compact array 20-cm radio continuum study of the Large Magellanic Cloud. *MNRAS*, **382**, 543.

[209] Walborn N.R., Sana H., Simón-Díaz S. *et al.* (2014). The VLT-FLAMES tarantula survey. XIV. The O-type stellar content of 30 Doradus. *A&A*, **564**, A40.

[210] McCray R. (1993). Supernova 1987A revisited. *ARA&A*, **31**, 175.

[211] Bozzetto L.M., Filipović M.D., Vukotić B. *et al.* (2017). Statistical analysis of supernova remnants in the Large Magellanic Cloud. *ApJS*, **230**, 2.

[212] Crowther P.A., Schnurr O., Hirschi R. *et al.* (2010). The R136 star cluster hosts several stars whose individual masses greatly exceed the accepted $150M_{\rm solar}$ stellar mass limit. *MNRAS*, **408**, 731.

[213] Lawton B., Gordon K.D., Babler B. *et al.* (2010). Spitzer analysis of H II region complexes in the Magellanic Clouds: Determining a suitable monochromatic obscured star formation indicator. *ApJ*, **716**, 453.

[214] Dunne B.C., Points S.D. & Chu Y.H. (2001). X-rays from superbubbles in the Large Magellanic Cloud. VI. A sample of thirteen superbubbles. *ApJS*, **136**, 119.

[215] Kim S., Dopita M.A., Staveley-Smith L. *et al.* (1999). H I shells in the Large Magellanic Cloud. *AJ*, **118**, 2797.

[216] Marshall F.E., Gotthelf E.V., Zhang W. *et al.* (1998). Discovery of an ultrafast X-ray pulsar in the supernova remnant N157B. *ApJ*, **499**, L179.

[217] Seward F.D., Harnden Jr. F.R. & Helfand D.J. (1984). Discovery of a 50 millisecond pulsar in the Large Magellanic Cloud. *ApJ*, **287**, L19.

[218] de Grijs R. & Anders P. (2006). How well do we know the age and mass distributions of the star cluster system in the Large Magellanic Cloud?. *MNRAS*, **366**, 295.

[219] Ackermann M., Albert A., Atwood W.B. *et al.* (2016). Deep view of the Large Magellanic Cloud with six years of Fermi-LAT observations. *A&A*, **586**, A71.

[220] H.E.S.S. Collaboration, Abramowski A., Acero F. *et al.* (2012). Discovery of gamma-ray emission from the extragalactic pulsar wind nebula N 157B with H.E.S.S.. *A&A*, **545**, L2.

[221] Chevalier R.A. & Dwarkadas V.V. (1995). The presupernova H II region around SN 1987A. *ApJ*, **452**, L45.

[222] Zanardo G., Staveley-Smith L., Ball L. *et al.* (2010). Multifrequency radio measurements of supernova 1987A over 22 years. *ApJ*, **710**, 1515.

[223] Maggi P., Haberl F., Kavanagh P.J. *et al.* (2016). The population of X-ray supernova remnants in the Large Magellanic Cloud. *A&A*, **585**, A162.

[224] Ackermann M., Ajello M., Allafort A. *et al.* (2011). A cocoon of freshly accelerated cosmic rays detected by Fermi in the Cygnus superbubble. *Science*, **334**, 1103.

[225] Barger K.A., Lehner N. & Howk J.C. (2016). Down-the-barrel and transverse observations of the Large Magellanic Cloud: Evidence for a symmetric galactic wind on the near and far sides of the galaxy. *ApJ*, **817**, 91.

[226] Corbet R.H.D., Chomiuk L., Coe M.J. *et al.* (2016). A luminous gamma-ray binary in the Large Magellanic Cloud. *ApJ*, **829**, 105.

[227] Gelfand J., Breton R., Ng C.Y. *et al.* (2015). Pulsar Wind Nebulae in the SKA era. *Advancing Astrophysics with the Square Kilometre Array (AASKA14)*, 46.

[228] Keane E., Bhattacharyya B., Kramer M. *et al.* (2015). A cosmic census of radio pulsars with the SKA. *Advancing Astrophysics with the Square Kilometre Array (AASKA14)*, 40.

[229] Indebetouw R. & SN1987A ALMA Cycle 0 Team (2014). ALMA resolves SN 1987A's dust factory and particle accelerator. In *American Astronomical Society Meeting Abstracts #223*, volume 223 of *American Astronomical Society Meeting Abstracts*, p. 354.37.

[230] Mellinger A. (2009). A color all-sky panorama image of the Milky Way. *PASP*, **121**, 1180.

[231] Kim S., Staveley-Smith L., Dopita M.A. *et al.* (2003). A neutral hydrogen survey of the Large Magellanic Cloud: Aperture synthesis and multibeam data combined. *ApJS*, **148**, 473.

[232] Berezhko E.G., Ksenofontov L.T. & Völk H.J. (2011). Expected gamma-ray emission of supernova remnant SN 1987A. *ApJ*, **732**, 58.

[233] Berezhko E.G., Ksenofontov L.T. & Völk H.J. (2015). Re-examination of the expected gamma-ray emission of supernova remnant SN 1987A. *ApJ*, **810**, 63.

[234] Williams B.J., Borkowski K.J., Reynolds S.P. *et al.* (2011). Dusty blast waves of two young Large Magellanic Cloud supernova remnants: Constraints on post-shock compression. *ApJ*, **729**, 65.

[235] Park S., Hughes J.P., Slane P.O. *et al.* (2012). An X-ray study of supernova remnant N49 and soft gamma-ray repeater 0526-66 in the Large Magellanic Cloud. *ApJ*, **748**, 117.

[236] Williams B.J., Borkowski K.J., Reynolds S.P. *et al.* (2014). Spitzer observations of the Type Ia supernova remnant N103B: Kepler's older cousin? *ApJ*, **790**, 139.

[237] Borkowski K.J., Hendrick S.P. & Reynolds S.P. (2006). Dense, fe-rich ejecta in supernova remnants DEM L238 and DEM L249: A new class of Type Ia supernova? *ApJ*, **652**, 1259.

[238] Brantseg T., McEntaffer R.L., Bozzetto L.M. *et al.* (2014). A multi-wavelength look at the young plerionic supernova remnant 0540-69.3. *ApJ*, **780**, 50.

[239] Martin J., Torres D.F., Cillis A. *et al.* (2014). Is there room for highly magnetized pulsar wind nebulae among those non-detected at TeV? *MNRAS*, **443**, 138.

[240] Bozzetto L.M., Filipović M.D., Crawford E.J. *et al.* (2012). Multifrequency study of the Large Magellanic Cloud supernova remnant J0529-6653 near pulsar B0529-66. *MNRAS*, **420**, 2588.

[241] Martin P. (2014). Interstellar gamma-ray emission from cosmic rays in star-forming galaxies. *A&A*, **564**, A61.

[242] Bykov A.M. (2014). Nonthermal particles and photons in starburst regions and superbubbles. *A&AR*, **22**, 77.

[243] Urry C.M. & Padovani P. (1995). Unified schemes for radio-loud active galactic nuclei. *PASP*, **107**, 803.

[244] Henri G. & Saugé L. (2006). The bulk Lorentz factor crisis of TeV blazars: Evidence for an inhomogeneous pileup energy distribution?. *ApJ*, **640**, 185.

[245] Inoue Y., Totani T. & Mori M. (2010). Prospects for a very high-energy blazar survey by the next-generation Cherenkov telescopes. *PASJ*, **62**, 1005.

[246] Inoue Y. & Totani T. (2009). The blazar sequence and the cosmic gamma-ray background radiation in the Fermi era. *ApJ*, **702**, 523–536.

[247] Inoue Y., Kalashev O.E. & Kusenko A. (2014). Prospects for future very high-energy gamma-ray sky survey: Impact of secondary gamma rays. *Astropart. Phys.*, **54**, 118.

[248] Ackermann M. *et al.* (2011). The second catalog of active galactic nuclei detected by the Fermi Large Area Telescope. *ApJ*, **743**, 171.

[249] Hayashida M., Stawarz Ł., Cheung C.C. *et al.* (2013). Discovery of GeV emission from the Circinus galaxy with the Fermi Large Area Telescope. *ApJ*, **779**, 131.

[250] Di Mauro M., Calore F., Donato F. *et al.* (2014). Diffuse γ-Ray emission from misaligned active galactic nuclei. *ApJ*, **780**, 161.

[251] Inoue Y. & Tanaka Y.T. (2016). Lower bound on the cosmic TeV gamma-ray background radiation. *ApJ*, **818**, 187.

[252] Atwood W., Albert A., Baldini L. *et al.* (2013). Pass 8: Toward the full realization of the Fermi-LAT scientific potential. arXiv:1303.3514.

[253] Szanecki M., Sobczyńska D., Niedźwiecki A. *et al.* (2015). Monte Carlo simulations of alternative sky observation modes with the Cherenkov Telescope Array. *Astropart. Phys.*, **67**, 33.

[254] Mészáros P. (2013). Gamma ray bursts. *Astropart. Phys.*, **43**, 134.

[255] Kumar P. & Zhang B. (2015). The physics of gamma-ray bursts and relativistic jets. *Phys. Rep.*, **561**, 1.

[256] Ellis J. & Mavromatos N.E. (2013). Probes of Lorentz violation. *Astropart. Phys.*, **43**, 50.

[257] Bednarek W. (2013). High energy γ-ray emission from compact Galactic sources in the context of observations with the next generation Cherenkov telescope arrays. *Astropart. Phys.*, **43**, 81.

[258] Bühler R. & Blandford R. (2014). The surprising Crab pulsar and its nebula: A review. *Rep. Prog. Phys.*, **77**, 6, 066901.

[259] Dubus G. (2015). Gamma-ray emission from binaries in context. *Comptes Rendus Physique*, **16**, 661.

[260] O'Brien P.T. & Smartt S.J. (2013). Interpreting signals from astrophysical transient experiments. *Royal Society of London Philosophical Transactions Series A*, **371**, 20498.

[261] Komossa S. (2015). Tidal disruption of stars by supermassive black holes: Status of observations. *Journal of High Energy Astrophysics*, **7**, 148.

[262] Brown P.J., Roming P.W.A. & Milne P.A. (2015). The first ten years of Swift supernovae. *Journal of High Energy Astrophysics*, **7**, 111.

[263] Katz J.I. (2016). Fast radio bursts, A brief review: Some questions, fewer answers. *Mod. Phys. Lett. A*, **31**, 1630013.

[264] Halzen F. (2013). Pionic photons and neutrinos from cosmic ray accelerators. *Astropart. Phys.*, **43**, 155.

[265] Ahlers M. & Halzen F. (2015). High-energy cosmic neutrino puzzle: A review. *Rep. Prog. Phys.*, **78**, 12, 126901.

[266] IceCube Collaboration, Aartsen M.G., Abbasi R. *et al.* (2013). The IceCube neutrino observatory part I: Point source searches. arXiv:1309.6979.

[267] IceCube Collaboration, Aartsen M.G., Abraham K. *et al.* (2015). The IceCube neutrino observatory — Contributions to ICRC 2015 Part I: Point source searches. arXiv:1510.05222.

[268] Abbott B.P., Abbott R., Abbott T.D. *et al.* (2016). Localization and broadband follow-up of the gravitational-wave transient GW150914. arXiv:1602.08492.

[269] Connaughton V., Burns E., Goldstein A. *et al.* (2016). Fermi GBM observations of LIGO gravitational wave event GW150914. *ApJ*, **826**, L6.

[270] Fernández R. & Metzger B.D. (2015). Electromagnetic signatures of neutron star mergers in the Advanced LIGO era. arXiv:1512.05435.

[271] Doro M., Conrad J., Emmanoulopoulos D. *et al.* (2013). Dark matter and fundamental physics with the Cherenkov Telescope Array. *Astropart. Phys.*, **43**, 189.

[272] Bulgarelli A., Fioretti V., Zoli A. *et al.* (2015). The on-site analysis of the Cherenkov Telescope Array. arXiv:1509.01963.

[273] Fioretti V., Bulgarelli A., Zoli A. *et al.* (2015). Real-time analysis sensitivity evaluation of the Cherenkov Telescope Array. *Proc. 34th ICRC*, The Hague, Netherlands.

[274] Gerard L. (2015). Divergent pointing with the Cherenkov Telescope Array for surveys and beyond. arXiv:1508.06197.

[275] Abdo A.A., Ackermann M., Arimoto M. *et al.* (2009). Fermi observations of high-energy gamma-ray emission from GRB 080916C. *Science*, **323**, 1688.

[276] Finke J.D., Razzaque S. & Dermer C.D. (2010). Modeling the extragalactic background light from stars and dust. *ApJ*, **712**, 238.

[277] Kouveliotou C., Meegan C.A., Fishman G.J. *et al.* (1993). Identification of two classes of gamma-ray bursts. *ApJ*, **413**, L101.

[278] Mereghetti S., Pons J.A. & Melatos A. (2015). Magnetars: Properties, origin and evolution. *Space Sci. Rev.*, **191**, 315.

[279] Torres D.F., Rea N., Esposito P. *et al.* (2012). A magnetar-like event from LS I+61 303 and its nature as a gamma-ray binary. *ApJ*, **744**, 106.

[280] Tavani M., Bulgarelli A., Vittorini V. *et al.* (2011). Discovery of powerful gamma-ray flares from the Crab Nebula. *Science*, **331**, 736.

[281] Abdo A.A., Ackermann M., Ajello M. *et al.* (2011). Gamma-ray flares from the Crab Nebula. *Science*, **331**, 739.

[282] Taylor G.B. & Granot J. (2006). The giant flare from SGR 1806-20 and its radio afterglow. *Mod. Phys. Lett. A*, **21**, 2171.

[283] Dubus G. (2013). Gamma-ray binaries and related systems. *A&A Rev.*, **21**, 64.

[284] Tavani M., Bulgarelli A., Piano G. *et al.* (2009). Extreme particle acceleration in the microquasar Cygnus X-3. *Nature*, **462**, 620.

[285] Zanin R., Fernández-Barral A., de Oña Wilhelmi E. *et al.* (2016). Gamma rays detected from Cygnus X-1 with likely jet origin. *A&A*, **596**, A55.

[286] Acciari V.A., Aliu E., Araya M. *et al.* (2011). Gamma-ray observations of the Be/pulsar binary 1A 0535+262 during a giant X-ray outburst. *ApJ*, **733**, 96.

[287] Stappers B.W., Archibald A.M., Hessels J.W.T. *et al.* (2014). A state change in the missing link binary pulsar system PSR J1023+0038. *ApJ*, **790**, 39.

[288] Ackermann M., Ajello M., Albert A. *et al.* (2014). Fermi establishes classical novae as a distinct class of gamma-ray sources. *Science*, **345**, 554.

[289] Metzger B.D., Caprioli D., Vurm I. *et al.* (2016). Novae as Tevatrons: Prospects for CTA and IceCube. *MNRAS*, **457**, 1786.

[290] Ackermann M., Ajello M., Asano K. *et al.* (2013). The first Fermi-LAT gamma-ray burst catalog. *ApJS*, **209**, 11.

[291] Gehrels N. & Cannizzo J.K. (2013). High-energy transients. *Philosophical Transactions of the Royal Society of London Series A*, **371**, 20120270.

[292] Kulkarni S.R. (2012). Cosmic explosions (optical transients). arXiv:1202.2381.

[293] Fender R.P. & Bell M.E. (2011). Radio transients: An antediluvian review. *Bulletin of the Astronomical Society of India*, **39**, 315.

[294] Fender R.P., Anderson G.E., Osten R. *et al.* (2015). A prompt radio transient associated with a gamma-ray superflare from the young M dwarf binary DG CVn. *MNRAS*, **446**, L66.

[295] Ghirlanda G., Salvaterra R., Campana S. *et al.* (2015). Unveiling the population of orphan γ-ray bursts. *A&A*, **578**, A71.

[296] Bloom J.S., Giannios D., Metzger B.D. *et al.* (2011). A possible relativistic jetted outburst from a massive black hole fed by a tidally disrupted star. *Science*, **333**, 203.

[297] van Velzen S., Anderson G.E., Stone N.C. *et al.* (2016). A radio jet from the optical and X-ray bright stellar tidal disruption flare ASASSN-14li. *Science*, **351**, 62.

[298] Chen X., Gómez-Vargas G.A. & Guillochon J. (2016). The gamma-ray afterglows of tidal disruption events. *MNRAS*, **458**, 3314–3323.

[299] Campana S., Mangano V., Blustin A.J. *et al.* (2006). The association of GRB 060218 with a supernova and the evolution of the shock wave. *Nature*, **442**, 1008.

[300] Soderberg A.M., Berger E., Page K.L. *et al.* (2008). An extremely luminous X-ray outburst at the birth of a supernova. *Nature*, **453**, 469.

[301] Kashiyama K., Murase K., Horiuchi S. *et al.* (2013). High-energy neutrino and gamma-ray transients from trans-relativistic supernova shock breakouts. *ApJ*, **769**, L6.

[302] Keane E.F., Johnston S., Bhandari S. *et al.* (2016). The host galaxy of a fast radio burst. *Nature*, **530**, 453.

[303] Williams P.K.G. & Berger E. (2016). No precise localization for FRB 150418: Claimed radio transient is AGN variability. *ApJ*, **821**, L22.

[304] Spitler L.G., Scholz P., Hessels J.W.T. *et al.* (2016). A repeating fast radio burst. *Nature*, **531**, 202.

[305] Chatterjee S., Law C.J., Wharton R.S. *et al.* (2017). A direct localization of a fast radio burst and its host. *Nature*, **541**, 58.

[306] Lyubarsky Y. (2014). A model for fast extragalactic radio bursts. *MNRAS*, **442**, L9.

[307] Andersson N., Baker J., Belczynski K. *et al.* (2013). The transient gravitational-wave sky. *Classic. Quant. Grav.*, **30**, 19, 193002.

[308] Berger E. (2014). Short-duration gamma-ray bursts. *ARA&A*, **52**, 43.

[309] Keane E.F. & SUPERB Collaboration (2016). Fast radio bursts: Searches, sensitivities and implications. arXiv:1602.05165.

[310] Ackermann M., Ajello M., Albert A. *et al.* (2013). The Fermi all-sky variability analysis: A list of flaring gamma-ray sources and the search for transients in our Galaxy. *ApJ*, **771**, 57.

[311] Ackermann M. *et al.* (2011). Detection of a spectral break in the extra hard component of GRB 090926A. *ApJ*, **729**, 114.

[312] Fermi Large Area Telescope Team, Ackermann M., Ajello M. *et al.* (2012). Constraining the high-energy emission from gamma-ray bursts with Fermi. *ApJ*, **754**, 121.

[313] Ackermann M., Ajello M., Asano K. *et al.* (2014). Fermi-LAT observations of the gamma-ray burst GRB 130427A. *Science*, **343**, 42.

[314] Kouveliotou C., Granot J., Racusin J.L. *et al.* (2013). NuSTAR observations of GRB 130427A establish a single component synchrotron afterglow origin for the late optical to multi-GeV emission. *ApJ*, **779**, L1.

[315] Atwood W.B., Baldini L., Bregeon J. *et al.* (2013). New Fermi-LAT event reconstruction reveals more high-energy gamma rays from gamma-ray bursts. *ApJ*, **774**, 76.

[316] Abdo A.A., Ackermann M., Ajello M. *et al.* (2009). A limit on the variation of the speed of light arising from quantum gravity effects. *Nature*, **462**, 331.

[317] Vasileiou V., Jacholkowska A., Piron F. *et al.* (2013). Constraints on Lorentz invariance violation from Fermi-Large Area Telescope observations of gamma-ray bursts. *Phys. Rev. D*, **87**, 12, 122001.

[318] Acciari V.A., Aliu E., Arlen T. *et al.* (2011). VERITAS observations of gamma-ray bursts detected by Swift. *ApJ*, **743**, 62.

[319] Aleksić J., Ansoldi S., Antonelli L.A. *et al.* (2014). MAGIC upper limits on the GRB 090102 afterglow. *MNRAS*, **437**, 3103.

[320] H.E.S.S. Collaboration, Abramowski A., Aharonian F. *et al.* (2014). Search for TeV gamma-ray emission from GRB 100621A, an extremely bright GRB in X-rays, with H.E.S.S. *A&A*, **565**, A16.

[321] Gilmore R.C., Bouvier A., Connaughton V. *et al.* (2013). IACT observations of gamma-ray bursts: Prospects for the Cherenkov Telescope Array. *Experimental Astronomy*, **35**, 413.

[322] Kakuwa J., Murase K., Toma K. *et al.* (2012). Prospects for detecting gamma-ray bursts at very high energies with the Cherenkov Telescope Array. *MNRAS*, **425**, 514.

[323] Abeysekara A.U., Aguilar J.A., Aguilar S. *et al.* (2012). On the sensitivity of the HAWC observatory to gamma-ray bursts. *Astropart. Phys.*, **35**, 641.

[324] Taboada I. & Gilmore R.C. (2014). Prospects for the detection of GRBs with HAWC. *NIM A*, **742**, 276.

[325] Malyshev D., Zdziarski A.A. & Chernyakova M. (2013). High-energy gamma-ray emission from Cyg X-1 measured by Fermi and its theoretical implications. *MNRAS*, **434**, 2380.

[326] Bodaghee A., Tomsick J.A., Pottschmidt K. *et al.* (2013). Gamma-ray observations of the microquasars Cygnus X-1, Cygnus X-3, GRS 1915+105, and GX 339-4 with the Fermi Large Area Telescope. *ApJ*, **775**, 98.

[327] Mariotti M. (2010). No significant enhancement in the VHE gamma-ray flux of the Crab Nebula measured by MAGIC in September 2010. *The Astronomer's Telegram*, **2967**, 1.

[328] Ong R.A. (2010). Search for an enhanced TeV gamma-ray flux from the Crab Nebula with VERITAS. *The Astronomer's Telegram*, **2968**, 1.

[329] H.E.S.S. Collaboration, Abramowski A., Aharonian F. *et al.* (2014). H.E.S.S. observations of the Crab during its March 2013 GeV gamma-ray flare. *A&A*, **562**, L4.

[330] Aleksić J., Antonelli L.A., Antoranz P. *et al.* (2010). Magic constraints on γ-ray emission from Cygnus X-3. *ApJ*, **721**, 843.

[331] Ahnen M.L., Ansoldi S., Antonelli L.A. *et al.* (2015). Very high-energy γ-ray observations of novae and dwarf novae with the MAGIC telescopes. *A&A*, **582**, A67.

[332] Albert J., Aliu E., Anderhub H. *et al.* (2007). Very high energy gamma-ray radiation from the stellar mass black hole binary Cygnus X-1. *ApJ*, **665**, L51.

[333] Peng F.K., Tang Q.W. & Wang X.Y. (2016). Search for high-energy gamma-ray emission from tidal disruption events with the Fermi Large Area Telescope. *ApJ*, **825**, 47.

[334] Aliu E., Arlen T., Aune T. *et al.* (2011). VERITAS observations of the unusual extragalactic transient Swift J164449.3+573451. *ApJ*, **738**, L30.

[335] Aleksić J., Antonelli L.A., Antoranz P. *et al.* (2013). Very high energy gamma-ray observation of the peculiar transient event Swift J1644+57 with the MAGIC telescopes and AGILE. *A&A*, **552**, A112.

[336] H.E.S.S. Collaboration, Abdalla H., Abramowski A. *et al.* (2017). First limits on the very-high energy gamma-ray afterglow emission of a fast radio burst. H.E.S.S. observations of FRB 150418. *A&A*, **597**, A115.

[337] Santander M., VERITAS & IceCube Collaborations (2015). Searching for TeV gamma-ray emission associated with IceCube high-energy neutrinos using VERITAS. *Proc. 34th ICRC*, The Hague, Netherlands.

[338] Schüssler F., Balzer A., Brun F. *et al.* (2015). The H.E.S.S. multi-messenger program. *Proc. 34th ICRC*, The Hague, Netherlands.

[339] Adrián-Martínez S., Ageron M., Albert A. *et al.* (2016). Optical and X-ray early follow-up of ANTARES neutrino alerts. *JCAP*, **2**, 062.

[340] IceCube Collaboration, Aartsen M.G., Abraham K. *et al.* (2016). Very high-energy gamma-ray follow-up program using neutrino triggers from IceCube. arXiv:1610.01814.

[341] Km3NeT Technical Design Report. http://www.km3net.org/TDR/TDRKM3NeT.pdf.

[342] BAIKAL-GVD Scientific-Technical Report. http://baikalweb.jinr.ru/gvd/BAIKAL-GVD_En.pdf.

[343] IceCube-Gen2 Collaboration, Aartsen M.G. *et al.* (2015). IceCube-Gen2 — The next generation neutrino observatory at the South Pole: Contributions to ICRC 2015. arXiv:1510.05228.

[344] ANTARES Collaboration, IceCube Collaboration, LIGO Scientific Collaboration *et al.* (2016). High-energy neutrino follow-up search of gravitational wave event GW150914 with ANTARES and IceCube. arXiv:1602.05411.

[345] Perna R., Lazzati D. & Giacomazzo B. (2016). Short gamma-ray bursts from the merger of two black holes. *ApJ*, **821**, L18.

[346] Lehner L. & Pretorius F. (2014). Numerical relativity and astrophysics. *ARA&A*, **52**, 661.

[347] Kyutoku K., Ioka K. & Shibata M. (2014). Ultrarelativistic electromagnetic counterpart to binary neutron star mergers. *MNRAS*, **437**, L6.

[348] Tanvir N.R., Levan A.J., Fruchter A.S. *et al.* (2013). A ‘kilonova’ associated with the short-duration γ-ray burst GRB 130603B. *Nature*, **500**, 547.

[349] Godet O., Nasser G., Atteia J. *et al.* (2014). The X-/gamma-ray camera ECLAIRs for the gamma-ray burst mission SVOM. In *Society of Photo-Optical Instrumentation Engineers (SPIE) Conference Series*, Vol. 9144.

[350] Finnegan G. for the VERITAS Collaboration (2011). Orbit mode observation technique developed for VERITAS. *Proc. Fermi Symposium 2011.*

[351] Greiner J., Krühler T., Klose S. *et al.* (2011). The nature of “dark” gamma-ray bursts. *A&A*, **526**, A30.

[352] Bagoly Z., Balázs L.G., Horváth I. *et al.* (2008). Different satellites-different GRB redshift distributions?. In Y.F. Huang, Z.G. Dai & B. Zhang (editors), *American Institute of Physics Conference Series*, Vol. 1065, pp. 119–122.

[353] Loh A., Corbel S., Dubus G. *et al.* (2016). High-energy gamma-ray observations of the accreting black hole V404 Cygni during its 2015 June outburst. *MNRAS*, **462**, L111.

[354] Abbott B.P., Abbott R., Abbott T.D. *et al.* (2016). The rate of binary black hole mergers inferred from Advanced LIGO observations surrounding GW150914. arXiv:1602.03842.

[355] Kneiske T.M., Bretz T., Mannheim K. *et al.* (2004). Implications of cosmological gamma-ray absorption. II. Modification of gamma-ray spectra. *A&A*, **413**, 807.

[356] Gilmore R.C., Somerville R.S., Primack J.R. *et al.* (2012). Semi-analytic modelling of the extragalactic background light and consequences for extragalactic gamma-ray spectra. *MNRAS*, **422**, 3189.

[357] Inoue Y., Inoue S., Kobayashi M.A.R. *et al.* (2013). Extragalactic background light from hierarchical galaxy formation: Gamma-ray attenuation up to the epoch of cosmic reionization and the first stars. *ApJ*, **768**, 197.

[358] Kohri K., Ohira Y. & Ioka K. (2012). Gamma-ray flare and absorption in the Crab nebula: Lovely TeV-PeV astrophysics. *MNRAS*, **424**, 2249.

[359] Fermi LAT Collaboration, Abdo A.A., Ackermann M. *et al.* (2009). Modulated high-energy gamma-ray emission from the microquasar Cygnus X-3. *Science*, **326**, 1512.

[360] Padovani P. & Resconi E. (2014). Are both BL Lacs and pulsar wind nebulae the astrophysical counterparts of IceCube neutrino events? *MNRAS*, **443**, 474.

[361] Gaisser T.K. (1990). *Cosmic Rays and Particle Physics* (Cambridge University Press).

[362] Antoni T., Apel W.D., Badea A.F. *et al.* (2005). KASCADE measurements of energy spectra for elemental groups of cosmic rays: Results and open problems. *Astropart. Phys.*, **24**, 1.

[363] Hillas A.M. (2005). Can diffusive shock acceleration in supernova remnants account for high-energy galactic cosmic rays? *Journal of Physics G Nuclear Physics*, **31**, 95.

[364] Drury L.O. (1983). An introduction to the theory of diffusive shock acceleration of energetic particles in tenuous plasmas. *Rep. Prog. Phys.*, **46**, 973.

[365] Bell A.R. (2004). Turbulent amplification of magnetic field and diffusive shock acceleration of cosmic rays. *MNRAS*, **353**, 550.

[366] Drury L.O., Aharonian F.A. & Voelk H.J. (1994). The gamma-ray visibility of supernova remnants. A test of cosmic ray origin. *A&A*, **287**, 959.

[367] Ackermann M., Ajello M., Allafort A. *et al.* (2013). Detection of the characteristic pion-decay signature in supernova remnants. *Science*, **339**, 807.

[368] Aharonian F.A. (2013). Gamma rays from supernova remnants. *Astropart. Phys.*, **43**, 71.

[369] Bell A.R., Schure K.M., Reville B. *et al.* (2013). Cosmic-ray acceleration and escape from supernova remnants. *MNRAS*, **431**, 415.

[370] Gabici S. & Aharonian F.A. (2007). Searching for Galactic cosmic-ray PeVatrons with multi-TeV gamma rays and neutrinos. *ApJ*, **665**, L131.

[371] Ellison D.C., Patnaude D.J., Slane P. *et al.* (2010). Efficient cosmic ray acceleration, hydrodynamics, and self-consistent thermal X-ray emission applied to supernova remnant RX J1713.7-3946. *ApJ*, **712**, 287.

[372] Casanova S., Jones D.I., Aharonian F.A. *et al.* (2010). Modeling the gamma-ray emission produced by runaway cosmic rays in the environment of RX J1713.7-3946. *PASJ*, **62**, 1127.

[373] Stecker F.W. (1971). Cosmic gamma rays. *NASA Special Publication*, **249**.

[374] Dermer C.D. (1986). Secondary production of neutral pi-mesons and the diffuse Galactic gamma radiation. *A&A*, **157**, 223.

[375] Aharonian F., Akhperjanian A.G., Barres de Almeida U. *et al.* (2008). Energy spectrum of cosmic-ray electrons at TeV energies. *Physical Review Letters*, **101**, 26, 261104.

[376] Fukui Y., Moriguchi Y., Tamura K. *et al.* (2003). Discovery of interacting molecular gas toward the TeV gamma-ray peak of the SNR G 347.3–0.5. *PASJ*, **55**, L61.

[377] Koyama K., Petre R., Gotthelf E.V. *et al.* (1995). Evidence for shock acceleration of high-energy electrons in the supernova remnant SN1006. *Nature*, **378**, 255.

[378] Enomoto R., Tanimori T., Naito T. *et al.* (2002). The acceleration of cosmic-ray protons in the supernova remnant RX J1713.7-3946. *Nature*, **416**, 823.

[379] Aharonian F.A., Akhperjanian A.G., Aye K.M. *et al.* (2004). High-energy particle acceleration in the shell of a supernova remnant. *Nature*, **432**, 75.

[380] Aharonian F., Akhperjanian A.G., Bazer-Bachi A.R. *et al.* (2005). Detection of TeV γ-ray emission from the shell-type supernova remnant RX J0852.0-4622 with HESS. *A&A*, **437**, L7.

[381] Acciari V.A., Aliu E., Arlen T. *et al.* (2011). Discovery of TeV gamma-ray emission from Tycho's supernova remnant. *ApJ*, **730**, L20.

[382] Albert J., Aliu E., Anderhub H. *et al.* (2007). Observation of VHE γ-rays from Cassiopeia A with the MAGIC telescope. *A&A*, **474**, 937.

[383] Abdo A.A., Ackermann M., Ajello M. *et al.* (2011). Observations of the young supernova remnant RX J1713.7-3946 with the Fermi Large Area Telescope. *ApJ*, **734**, 28.

[384] Fukui Y. (2013). Molecular and atomic gas in the young TeV γ-Ray SNRs RX J1713.7-3946 and RX J0852.0-4622; Evidence for the hadronic production of γ-rays. In D.F. Torres & O. Reimer (editors), *Cosmic Rays in Star-Forming Environments*, Advances in Solid State Physics, Vol. 34, p. 249.

[385] Sano H., Fukuda T., Yoshiike S. *et al.* (2014). A detailed study of non-thermal X-ray properties and interstellar gas toward the γ-ray supernova remnant RX J1713.7-3946. arXiv:1401.7418.

[386] H.E.S.S. Collaboration, Abdalla H., Abdalla H. *et al.* (2016). H.E.S.S. observations of RX J1713.7-3946 with improved angular and spectral resolution; evidence for gamma-ray emission extending beyond the X-ray emitting shell. arXiv:1609.08671.

[387] Berezhko E.G., Pühlhofer G. & Völk H.J. (2009). Theory of cosmic ray and γ-ray production in the supernova remnant RX J0852.0-4622. *A&A*, **505**, 641.

[388] H.E.S.S. Collaboration, Abdalla H., Abramowski A. *et al.* (2016). Deeper H.E.S.S. observations of Vela Junior (RX J0852.0-4622): Morphology studies and resolved spectroscopy. arXiv:1610.01863.

[389] Pedaletti G., Torres D.F., Gabici S. *et al.* (2013). On the potential of the Cherenkov Telescope Array for the study of cosmic-ray diffusion in molecular clouds. *A&A*, **550**, A123.

[390] Peng F.K., Wang X.Y., Liu R.Y. *et al.* (2016). First detection of GeV emission from an ultraluminous infrared galaxy: Arp 220 as seen with the Fermi Large Area Telescope. *ApJ*, **821**, L20.

[391] Griffin R.D., Dai X. & Thompson T.A. (2016). Constraining gamma-ray emission from luminous infrared galaxies with Fermi-LAT; Tentative detection of Arp 220. *ApJ*, **823**, L17.

[392] Kennicutt R.C. & Evans N.J. (2012). Star formation in the Milky Way and nearby galaxies. *ARA&A*, **50**, 531.

[393] Socrates A., Davis S.W. & Ramirez-Ruiz E. (2008). The Eddington limit in cosmic rays: An explanation for the observed faintness of starbursting galaxies. *ApJ*, **687**, 202.

[394] Jubelgas M., Springel V., Enßlin T. *et al.* (2008). Cosmic ray feedback in hydrodynamical simulations of galaxy formation. *A&A*, **481**, 33.

[395] Ceccarelli C., Hily-Blant P., Montmerle T. *et al.* (2011). Supernova-enhanced cosmic-ray ionization and induced chemistry in a molecular cloud of W51C. *ApJ*, **740**, L4.

[396] Papadopoulos P.P. & Thi W.F. (2013). The initial conditions of star formation: Cosmic rays as the fundamental regulators. In D.F. Torres & O. Reimer (editors), *Cosmic Rays in Star-Forming Environments*, Advances in Solid State Physics, Vol. 34, p. 41.

[397] Booth C.M., Agertz O., Kravtsov A.V. *et al.* (2013). Simulations of disk galaxies with cosmic ray driven galactic winds. *ApJ*, **777**, L16.

[398] Salem M., Bryan G.L. & Hummels C. (2014). Cosmological simulations of galaxy formation with cosmic rays. *ApJ*, **797**, L18.

[399] Aharonian F., Akhperjanian A., Beilicke M. *et al.* (2002). An unidentified TeV source in the vicinity of Cygnus OB2. *A&A*, **393**, L37.

[400] Abramowski A., Acero F., Aharonian F. *et al.* (2012). Discovery of extended VHE γ-ray emission from the vicinity of the young massive stellar cluster Westerlund 1. *A&A*, **537**, A114.

[401] Casse M. & Paul J.A. (1980). Local gamma rays and cosmic-ray acceleration by supersonic stellar winds. *ApJ*, **237**, 236.

[402] Meier D.S., Walter F., Bolatto A.D. *et al.* (2015). Alma multi-line imaging of the nearby starburst NGC 253. *ApJ*, **801**, 1, 63.

[403] Kennicutt Jr. R.C. (1998). Star formation in galaxies along the Hubble sequence. *ARA&A*, **36**, 189.

[404] Ackermann M., Ajello M., Allafort A. *et al.* (2012). GeV observations of star-forming galaxies with the Fermi Large Area Telescope. *ApJ*, **755**, 164.

[405] Abramowski A., Acero F., Aharonian F. *et al.* (2012). Spectral analysis and interpretation of the γ-ray emission from the starburst galaxy NGC 253. *ApJ*, **757**, 158.

[406] Reitberger K., Reimer A., Reimer O. *et al.* (2015). The first full orbit of η Carinae seen by Fermi. *A&A*, **577**, A100.

[407] Preibisch T., Ratzka T., Kuderna B. *et al.* (2011). Deep wide-field near-infrared survey of the Carina Nebula. *A&A*, **530**, A34.

[408] Hamaguchi K., Petre R., Matsumoto H. *et al.* (2007). Suzaku observation of diffuse X-ray emission from the Carina Nebula. *PASJ*, **59**, 151.

[409] Ezoe Y., Hamaguchi K., Gruendl R.A. *et al.* (2009). Suzaku and XMM-Newton observations of diffuse X-ray emission from the eastern tip region of the Carina Nebula. *PASJ*, **61**, 123.

[410] Townsley L.K., Broos P.S., Chu Y.H. *et al.* (2011). The Chandra Carina Complex Project: Deciphering the enigma of Carina's diffuse X-ray emission. *ApJS*, **194**, 15.

[411] H.E.S.S. Collaboration, Abramowski A., Acero F. *et al.* (2012). H.E.S.S. observations of the Carina nebula and its enigmatic colliding wind binary Eta Carinae. *MNRAS*, **424**, 128.

[412] Abramowski A., Acero F., Aharonian F. *et al.* (2011). Revisiting the Westerlund 2 field with the H.E.S.S. telescope array. *A&A*, **525**, A46+.

[413] Bartoli B., Bernardini P., Bi X.J. *et al.* (2014). Identification of the TeV gamma-ray source ARGO J2031+4157 with the Cygnus Cocoon. *ApJ*, **790**, 152.

[414] Popkow A. for the VERITAS Collaboration (2015). The VERITAS survey of the Cygnus region of the Galaxy. arXiv:1508.06684.

[415] Kothes R. & Dougherty S.M. (2007). The distance and neutral environment of the massive stellar cluster Westerlund 1. *A&A*, **468**, 993.

[416] Ohm S., Hinton J.A. & White R. (2013). γ-ray emission from the Westerlund 1 region. *MNRAS*, **434**, 2289.

[417] Abdo A.A., Ackermann M., Ajello M. *et al.* (2010). Fermi Large Area Telescope observations of Local Group galaxies: Detection of M 31 and search for M 33. *A&A*, **523**, L2.

[418] Dorfi E.A. & Breitschwerdt D. (2012). Time-dependent galactic winds. I. Structure and evolution of galactic outflows accompanied by cosmic ray acceleration. *A&A*, **540**, A77.

[419] Völk H.J., Klein U. & Wielebinski R. (1989). M82, the Galaxy, and the dependence of cosmic ray energy production on the supernova rate. *A&A*, **213**, L12.

[420] VERITAS Collaboration, Acciari V.A., Aliu E. *et al.* (2009). A connection between star formation activity and cosmic rays in the starburst galaxy M82. *Nature*, **462**, 770.

[421] Abdo A.A., Ackermann M., Ajello M. *et al.* (2010). Detection of gamma-ray emission from the starburst galaxies M82 and NGC 253 with the Large Area Telescope on Fermi. *ApJ*, **709**, L152.

[422] Domingo-Santamaría E. & Torres D.F. (2005). High energy γ-ray emission from the starburst nucleus of NGC 253. *A&A*, **444**, 403.

[423] Rephaeli Y., Arieli Y. & Persic M. (2010). High-energy emission from the starburst galaxy NGC 253. *MNRAS*, **401**, 473.

[424] Thompson T.A., Quataert E., Waxman E. *et al.* (2006). Magnetic fields in starburst galaxies and the origin of the FIR-radio correlation. *ApJ*, **645**, 186.

[425] Lacki B.C., Thompson T.A., Quataert E. *et al.* (2011). On the GeV and TeV detections of the starburst galaxies M82 and NGC 253. *ApJ*, **734**, 107.

[426] Murphy E.J., Porter T.A., Moskalenko I.V. *et al.* (2012). Characterizing cosmic-ray propagation in massive star-forming regions: The case of 30 Doradus and the Large Magellanic Cloud. *ApJ*, **750**, 126.

[427] Persic M., Rephaeli Y. & Arieli Y. (2008). Very-high-energy emission from M82. *A&A*, **486**, 143.

[428] Torres D.F., Cillis A., Lacki B. *et al.* (2012). Building up the spectrum of cosmic rays in star-forming regions. *MNRAS*, **423**, 822.

[429] Mannheim K., Elsässer D. & Tibolla O. (2012). Gamma-rays from pulsar wind nebulae in starburst galaxies. *Astropart. Phys.*, **35**, 797.

[430] Ohm S. & Hinton J.A. (2013). Non-thermal emission from pulsar-wind nebulae in starburst galaxies. *MNRAS*, **429**, L70.

[431] Sanders D.B. & Mirabel I.F. (1996). Luminous infrared galaxies. *ARA&A*, **34**, 749.

[432] Pavlidou V. & Fields B.D. (2002). The guaranteed gamma-ray background. *ApJ*, **575**, L5.

[433] Smith H.E., Lonsdale C.J., Lonsdale C.J. *et al.* (1998). A starburst revealed — luminous radio supernovae in the nuclei of Arp 220. *ApJ*, **493**, L17.

[434] Torres D.F. (2004). Theoretical modeling of the diffuse emission of gamma rays from extreme regions of star formation: The case of Arp 220. *ApJ*, **617**, 966.

[435] Torres D.F. & Domingo-Santamaría E. (2005). Some comments on the high energy emission from regions of star formation beyond the Galaxy. *Mod. Phys. Lett. A*, **20**, 2827.

[436] Albert J., Aliu E., Anderhub H. *et al.* (2007). First bounds on the very high energy γ-ray emission from Arp 220. *ApJ*, **658**, 245.

[437] Fleischhack, H. for the VERITAS Collaboration (2015). Upper limits on the VHE gamma-ray flux from the ULIRG Arp 220 and other galaxies with VERITAS. *Proc. 34th ICRC*, The Hague, Netherlands.

[438] Knödlseder J., Mayer M., Deil C. *et al.* (2016). GammaLib and ctools. A software framework for the analysis of astronomical gamma-ray data. *A&A*, **593**, A1.

[439] Inoue Y. (2011). High energy gamma-ray absorption and cascade emission in nearby starburst galaxies. *ApJ*, **728**, 11.

[440] Armstrong T., Brown A.M., Chadwick P.M. *et al.* (2017). DBSCAN re-applied to Pass 8 Fermi-LAT data above 100 GeV. *AIP Conf. Proc.*, **1792**, 1, 070001.

[441] Zech A., Cerruti M. & for the CTA consortium (2013). Signatures of relativistic protons in CTA blazar spectra. *Proc. 33rd ICRC*, Rio de Janeiro, Brazil. arXiv: astro-ph/1307.2232.

[442] Cerruti M., Zech A., Boisson C. *et al.* (2015). A hadronic origin for ultra-high-frequency-peaked BL Lac objects. *MNRAS*, **448**, 910.

[443] Zech A., Cerruti M. & Mazin D. (2017). Expected signatures from hadronic emission processes in the TeV spectra of BL Lacertae objects. *A&A*, **602**, A25.

[444] Sol H., Zech A., Boisson C. *et al.* (2013). Prospect on intergalactic magnetic field measurements with gamma-ray instruments. In A.G. Kosovichev, E. de Gouveia Dal Pino & Y. Yan (editors), *Solar and Astrophysical Dynamos and Magnetic Activity, 294th IAU Symposium*, pp. 459–470.

[445] Hardcastle M.J. & Croston J.H. (2011). Modelling TeV γ-ray emission from the kiloparsec-scale jets of Centaurus A and M87. *MNRAS*, **415**, 133.

[446] Franceschini A., Rodighiero G. & Vaccari M. (2008). Extragalactic optical-infrared background radiation, its time evolution and the cosmic photon-photon opacity. *A&A*, **487**, 837.

[447] H.E.S.S. Collaboration, Abramowski A., Acero F. *et al.* (2013). Measurement of the extragalactic background light imprint on the spectra of the brightest blazars observed with H.E.S.S.. *A&A*, **550**, A4.

[448] Ackermann M. *et al.* (2012). The imprint of the extragalactic background light in the gamma-ray spectra of blazars. *Science*, **338**, 1190.

[449] Blandford R.D. & Znajek R.L. (1977). Electromagnetic extraction of energy from Kerr black holes. *MNRAS*, **179**, 433.

[450] Ghisellini G., Tavecchio F., Maraschi L. *et al.* (2014). The power of relativistic jets is larger than the luminosity of their accretion disks. *Nature*, **515**, 376.

[451] Ghisellini G., Tavecchio F., Foschini L. *et al.* (2010). General physical properties of bright Fermi blazars. *MNRAS*, **402**, 497.

[452] Böttcher M., Reimer A., Sweeney K. *et al.* (2013). Leptonic and hadronic modeling of Fermi-detected blazars. *ApJ*, **768**, 54.

[453] Cerruti M., Dermer C.D., Lott B. *et al.* (2013). Gamma-ray blazars near equipartition and the origin of the GeV spectral break in 3C 454.3. *ApJ*, **771**, L4.

[454] Dermer C.D., Cerruti M., Lott B. *et al.* (2014). Equipartition gamma-ray blazars and the location of the gamma-ray emission site in 3C 279. *ApJ*, **782**, 82.

[455] Poutanen J. & Stern B. (2010). GeV breaks in blazars as a result of gamma-ray absorption within the broad-line region. *ApJ Lett*, **717**, L118.

[456] Senturk G.D., Errando M., Boettcher M. *et al.* (2013). Gamma-ray observational properties of tev-detected blazars. *ApJ*, **764**, 119.

[457] Brown A.M. (2013). Locating the γ-ray emission region of the flat spectrum radio quasar PKS 1510-089. *MNRAS*, **431**, 824.

[458] Abeysekara A.U., Archambault S., Archer A. *et al.* (2015). Gamma-rays from the quasar PKS 1441+25: Story of an escape. *ApJ*, **815**, L22.

[459] Lindfors E., Nilsson K., Barres de Almeida U. *et al.* (2013). VHE gamma-ray emission from the FSRQs observed by the MAGIC telescopes. *Proc. Fermi Symposium 2012*. arXiv: astro-ph/1303.2102.

[460] Abdo A.A., Ackermann M., Ajello M. *et al.* (2010). Spectral properties of bright Fermi-detected blazars in the gamma-ray band. *ApJ*, **710**, 1271.

[461] Costamante L., Ghisellini G., Giommi P. *et al.* (2001). Extreme synchrotron BL Lac objects. Stretching the blazar sequence. *A&A*, **371**, 512.

[462] Bonnoli G., Tavecchio F., Ghisellini G. *et al.* (2015). An emerging population of BL Lacs with extreme properties: Towards a class of EBL and cosmic magnetic field probes? *MNRAS*, **451**, 611.

[463] Katarzyński K., Ghisellini G., Tavecchio F. *et al.* (2006). Hard TeV spectra of blazars and the constraints to the infrared intergalactic background. *MNRAS*, **368**, L52.

[464] Lefa E., Rieger F.M. & Aharonian F. (2011). Formation of very hard gamma-ray spectra of blazars in leptonic models. *ApJ*, **740**, 64.

[465] Asano K., Takahara F., Kusunose M. *et al.* (2014). Time-dependent models for blazar emission with the second-order Fermi acceleration. *ApJ*, **780**, 64.

[466] Murase K., Dermer C.D., Takami H. *et al.* (2012). Blazars as ultra-high-energy cosmic-ray sources: Implications for TeV gamma-ray observations. *ApJ*, **749**, 63.

[467] Biteau J. & Giebels B. (2012). The minijets-in-a-jet statistical model and the rms-flux correlation. *A&A*, **548**, A123.

[468] McHardy I. (2011). The origin of high energy variability in blazars. *Proc. "AGN Physics in the CTA Era" Workshop*, Toulouse, France.

[469] Marscher A.P. (2014). Turbulent, extreme multi-zone model for simulating flux and polarization variability in blazars. *ApJ*, **780**, 87.

[470] de Gouveia Dal Pino E.M., Piovezan P.P. & Kadowaki L.H.S. (2010). The role of magnetic reconnection on jet/accretion disk systems. *A&A*, **518**, A5.

[471] Giannios D. (2013). Reconnection-driven plasmoids in blazars: Fast flares on a slow envelope. *MNRAS*, **431**, 355.

[472] Kadowaki L.H.S., de Gouveia Dal Pino E.M. & Singh C.B. (2015). The role of fast magnetic reconnection on the radio and gamma-ray emission from the nuclear regions of microquasars and low luminosity AGNs. *ApJ*, **802**, 113.

[473] Singh C.B., de Gouveia Dal Pino E.M. & Kadowaki L.H.S. (2015). On the role of fast magnetic reconnection in accreting black hole sources. *ApJ*, **799**, L20.

[474] Khiali B., de Gouveia Dal Pino E.M. & Sol H. (2015). Particle acceleration and gamma-ray emission due to magnetic reconnection around the core region of radio galaxies. arXiv:1504.07592.

[475] Osmanov Z. (2010). On the simultaneous generation of high energy emission and submillimeter/infrared radiation from active galactic nuclei. *ApJ*, **721**, 318.

[476] Levinson A. & Rieger F.M. (2011). Variable TeV emission as a manifestation of jet formation in M87? *ApJ*, **730**, 123.

[477] Aleksić J., Antonelli L.A., Antoranz P. *et al.* (2014). Rapid and multiband variability of the TeV bright active nucleus of the galaxy IC 310. *A&A*, **563**, A91.

[478] Khiali B., de Gouveia Dal Pino E.M. & del Valle M.V. (2015). A magnetic reconnection model for explaining the multiwavelength emission of the microquasars Cyg X-1 and Cyg X-3. *MNRAS*, **449**, 34.

[479] Abdo A.A., Ackermann M., Ajello M. *et al.* (2010). Fermi gamma-ray imaging of a radio galaxy. *Science*, **328**, 725.

[480] Ackermann M., Ajello M., Baldini L. *et al.* (2016). Fermi Large Area Telescope detection of extended gamma-ray emission from the radio galaxy Fornax A. *ApJ*, **826**, 1.

[481] Acciari V.A., Aliu E., Arlen T. *et al.* (2009). Radio imaging of the very-high-energy γ-ray emission region in the central engine of a radio galaxy. *Science*, **325**, 444.

[482] Cheung C.C., Harris D.E. & Stawarz L. (2007). Superluminal radio features in the M87 jet and the site of flaring TeV gamma-ray emission. *ApJ*, **663**, L65.

[483] Abdo A.A., Ackermann M., Ajello M. *et al.* (2010). Fermi Large Area Telescope view of the core of the radio galaxy Centaurus A. *ApJ*, **719**, 1433.

[484] Sahakyan N., Yang R., Aharonian F.A. *et al.* (2013). Evidence for a second component in the high-energy core emission from Centaurus A? *ApJ*, **770**, L6.

[485] Brown A.M., BÅ'hm C., Graham J. *et al.* (2017). Discovery of a new extragalactic population of energetic particles. *Phys. Rev. D*, **95**, 6, 063018.

[486] Sahu S., Zhang B. & Fraija N. (2012). Hadronic-origin TeV gamma-rays and ultrahigh energy cosmic rays from Centaurus A. *Phys. Rev. D*, **85**, 4, 043012.

[487] Petropoulou M., Lefa E., Dimitrakoudis S. *et al.* (2014). One-zone synchrotron self-Compton model for the core emission of Centaurus A revisited. *A&A*, **562**, A12.

[488] Cerruti M., Zech A., Emery G. *et al.* (2016). Hadronic modeling of TeV AGN: Gammas and neutrinos. arXiv:1610.00255.

[489] Abdo A., Ackermann M., Ajello M. *et al.* (2009). Radio-loud narrow-line Seyfert 1 as a new class of gamma-ray active galactic nuclei. *ApJ*, **707**, L142.

[490] D'Ammando F., Orienti M., Finke J. *et al.* (2012). SBS 0846+513: A new γ-ray-emitting narrow-line Seyfert 1 galaxy. *MNRAS*, **426**, 317.

[491] Foschini L. *et al.* (2011). The July 2010 outburst of the NLS1 PMN J0948+0022. *Proc. 3rd Fermi Symposium*, Rome, Italy. arXiv: astro-ph/1110.5649.

[492] D'Ammando F., Tosti G., Orienti M. *et al.* (2013). Four years of Fermi LAT observations of narrow-line Seyfert 1 galaxies. arXiv:1303.3030.

[493] Marconi A. *et al.* (2008). Weighing black holes from zero to high redshift. *ApJ*, **678**, 693.

[494] Calderone G., Ghisellini G., Colpi M. *et al.* (2013). Black hole mass estimate for a sample of radio-loud narrow-line Seyfert 1 galaxies. *MNRAS*, **431**, 210.

[495] Neronov A. & Aharonian F.A. (2007). Production of TeV gamma radiation in the vicinity of the supermassive black hole in the giant radio galaxy M87. *ApJ*, **671**, 85.

[496] Rieger F.M. & Aharonian F.A. (2008). Variable VHE gamma-ray emission from non-blazar AGNs. *A&A*, **479**, L5.

[497] Istomin Y.N. & Sol H. (2009). Acceleration of particles in the vicinity of a massive black hole. *Ap&SS*, **321**, 57.

[498] Biteau J. & Williams D.A. (2015). The extragalactic background light, the Hubble constant, and anomalies: Conclusions from 20 years of TeV gamma-ray observations. *ApJ*, **812**, 60.

[499] Domínguez A. & Prada F. (2013). Measurement of the expansion rate of the universe from γ-ray attenuation. *ApJ*, **771**, L34.

[500] Widrow L.M. (2002). Origin of galactic and extragalactic magnetic fields. *Rev. Mod. Phys.*, **74**, 775.

[501] Kulsrud R.M. & Zweibel E.G. (2008). On the origin of cosmic magnetic fields. *Rep. Prog. Phys.*, **71**, 4, 046901.

[502] Kandus A., Kunze K.E. & Tsagas C.G. (2011). Primordial magnetogenesis. *Phys. Rep.*, **505**, 1, 1.

[503] Widrow L.M., Ryu D., Schleicher D.R.G. *et al.* (2012). The first magnetic fields. *Space Sci. Rev.*, **166**, 37.

[504] Ryu D., Schleicher D.R.G., Treumann R.A. *et al.* (2012). Magnetic fields in the large-scale structure of the universe. *Space Sci. Rev.*, **166**, 1.

[505] Kim K.T., Kronberg P.P., Giovannini G. *et al.* (1989). Discovery of intergalactic radio emission in the Coma-A1367 supercluster. *Nature*, **341**, 720.

[506] Elyiv A., Neronov A. & Semikoz D.V. (2009). Gamma-ray induced cascades and magnetic fields in the intergalactic medium. *Phys. Rev. D*, **80**, 2, 023010.

[507] Dermer C.D., Cavadini M., Razzaque S. *et al.* (2011). Time delay of cascade radiation for TeV blazars and the measurement of the intergalactic magnetic field. *ApJ*, **733**, L21.

[508] Chen W., Buckley J.H. & Ferrer F. (2015). Search for GeV γ-ray pair halos around low redshift blazars. *Physical Review Letters*, **115**, 21, 211103.

[509] Barkov M.V., Aharonian F.A., Bogovalov S.V. *et al.* (2012). Rapid TeV variability in blazars as a result of jet-star interaction. *ApJ*, **749**, 119.

[510] Essey W. & Kusenko A. (2010). A new interpretation of the gamma-ray observations of distant active galactic nuclei. *Astropart. Phys.*, **33**, 81.

[511] Essey W., Kalashev O., Kusenko A. *et al.* (2011). Role of line-of-sight cosmic-ray interactions in forming the spectra of distant blazars in tev gamma rays and high-energy neutrinos. *ApJ*, **731**, 51.

[512] Takami H., Murase K. & Dermer C.D. (2013). Disentangling hadronic and leptonic cascade scenarios from the very-high-energy gamma-Ray emission of distant hard-spectrum blazars. *ApJ*, **771**, L32.

[513] Abdo A.A., Ackermann M., Ajello M. *et al.* (2011). Fermi Large Area Telescope observations of Markarian 421: The missing piece of its spectral energy distribution. *ApJ*, **736**, 131.

[514] Joshi J.C. & Gupta N. (2013). Testing hadronic models of gamma ray production at the core of Cen A. *Phys. Rev. D*, **87**, 2, 023002.

[515] Rieger F.M. & Aharonian F.A. (2009). Centaurus A as TeV gamma-ray and possible UHE cosmic-ray source. *A&A*, **506**, L41.

[516] Yang R., Sahakyan N., de Ona Wilhelmi E. *et al.* (2012). Deep observation of the giant radio lobes of Centaurus A with the Fermi Large Area Telescope. *A&A*, **542**, 19.

[517] de Angelis A., Roncadelli M. & Mansutti O. (2007). Evidence for a new light spin-zero boson from cosmological gamma-ray propagation? *Phys. Rev. D*, **76**, 12, 121301.

[518] Simet M., Hooper D. & Serpico P.D. (2008). Milky way as a kiloparsec-scale axionscope. *Phys. Rev. D*, **77**, 6, 063001.

[519] Sánchez-Conde M.A., Paneque D., Bloom E. *et al.* (2009). Hints of the existence of axionlike particles from the gamma-ray spectra of cosmological sources. *Phys. Rev. D*, **79**, 12, 123511.

[520] de Angelis A., Mansutti O., Persic M. *et al.* (2009). Photon propagation and the very high energy γ-ray spectra of blazars: How transparent is the Universe? *MNRAS*, **394**, L21.

[521] de Angelis A., Galanti G. & Roncadelli M. (2011). Relevance of axionlike particles for very-high-energy astrophysics. *Phys. Rev. D*, **84**, 10, 105030.

[522] Domínguez A., Sánchez-Conde M.A. & Prada F. (2011). Axion-like particle imprint in cosmological very-high-energy sources. *JCAP*, **11**, 020.

[523] De Angelis A., Galanti G. & Roncadelli M. (2013). Transparency of the Universe to gamma-rays. *MNRAS*, **432**, 3245.

[524] Galanti G., Roncadelli M., De Angelis A. *et al.* (2015). Axion-like particles explain the unphysical redshift-dependence of AGN gamma-ray spectra. arXiv:1503.04436.

[525] Horns D. & Meyer M. (2012). Indications for a pair-production anomaly from the propagation of VHE gamma-rays. *JCAP*, **2**, 33.

[526] Horns D. & Meyer M. (2013). Pair-production opacity at high and very-high gamma-ray energies. DESY-PROC-2013-04. arXiv: Astro-ph/1309.3846.

[527] Rubtsov G.I. & Troitsky S.V. (2014). Breaks in gamma-ray spectra of distant blazars and transparency of the universe. *Soviet Journal of Experimental and Theoretical Physics Letters*, **100**, 355.

[528] Sanchez D.A., Fegan S. & Giebels B. (2013). Evidence for a cosmological effect in gamma-ray spectra of BL Lacs. *A&A*, **554**, A75.

[529] Domínguez A. & Ajello M. (2015). Spectral analysis of Fermi-LAT blazars above 50 GeV. *ApJ*, **813**, L34.

[530] Horns D., Maccione L., Meyer M. *et al.* (2012). Hardening of TeV gamma spectrum of active galactic nuclei in galaxy clusters by conversions of photons into axionlike particles. *Phys. Rev. D*, **86**, 7, 075024.

[531] Meyer M., Montanino D. & Conrad J. (2014). On detecting oscillations of gamma rays into axion-like particles in turbulent and coherent magnetic fields. *JCAP*, **9**, 3, 003.

[532] Tavecchio F., Roncadelli M. & Galanti G. (2015). Photons to axion-like particles conversion in active galactic nuclei. *Phys. Lett. B*, **744**, 375.

[533] Tavecchio F., Roncadelli M., Galanti G. *et al.* (2012). Evidence for an axion-like particle from PKS 1222+216? *Phys. Rev. D*, **86**, 8, 085036.

[534] Meyer M. & Conrad J. (2014). Sensitivity of the Cherenkov Telescope Array to the detection of axion-like particles at high gamma-ray opacities. *JCAP*, **12**, 016.

[535] Abramowski A., Acero F., Aharonian F. *et al.* (2013). Constraints on axionlike particles with H.E.S.S. from the irregularity of the PKS 2155-304 energy spectrum. *Phys. Rev. D*, **88**, 10, 102003.

[536] Ajello M., Albert A., Anderson B. *et al.* (2016). Search for spectral irregularities due to photon-axionlike-particle oscillations with the Fermi Large Area Telescope. *Physical Review Letters*, **116**, 16, 161101.

[537] Abdo A.A., Ackermann M., Ajello M. *et al.* (2009). A limit on the variation of the speed of light arising from quantum gravity effects. *Nature*, **462**, 331.

[538] H.E.S.S. Collaboration, Abramowski A., Acero F. *et al.* (2011). Search for Lorentz invariance breaking with a likelihood fit of the PKS 2155-304 flare data taken on MJD 53944. *Astropart. Phys.*, **34**, 738.

[539] Kifune T. (1999). Invariance violation extends the cosmic ray horizon? *ApJ*, **518**, L21.

[540] Fairbairn M., Nilsson A., Ellis J. *et al.* (2014). The CTA sensitivity to Lorentz-violating effects on the gamma-ray horizon. *JCAP*, **6**, 005.

[541] D'Ammando F., Orienti M., Larsson J. *et al.* (2015). The first γ-ray detection of the narrow-line Seyfert 1 FBQS J1644+2619. *MNRAS*, **452**, 520.

[542] D'Ammando F., Orienti M., Finke J. *et al.* (2016). A panchromatic view of relativistic jets in narrow-line Seyfert 1 galaxies. *Galaxies*, **4**, 11.

[543] MAGIC Collaboration, Albert J., Aliu E. *et al.* (2008). Very-high-energy gamma rays from a distant quasar: How transparent is the Universe? *Science*, **320**, 1752.

[544] Ackermann M. *et al.* (2013). The first FERMI-LAT catalog of sources above 10 GeV. *ApJS*, **209**, 34.

[545] Shaw M.S., Romani R.W., Cotter G. *et al.* (2013). Spectroscopy of the largest ever γ-ray-selected BL Lac sample. *ApJ*, **764**, 135.

[546] Pita A., Goldoni P., Boisson C. *et al.* (2014). Spectroscopy of high-energy BL Lacertae objects with X-shooter on the VLT. *A&A*, **565**, A12.

[547] H.E.S.S. Collaboration, Abramowski A., Acero F. *et al.* (2012). A multiwavelength view of the flaring state of PKS 2155-304 in 2006. *A&A*, **539**, A149.

[548] Marscher A.P., Jorstad S.G., D'Arcangelo F.D. *et al.* (2008). The inner jet of an active galactic nucleus as revealed by a radio-to-γ-ray outburst. *Nature*, **452**, 966.

[549] Marscher A.P., Jorstad S.G., Larionov V.M. *et al.* (2010). Probing the inner jet of the quasar PKS 1510-089 with multi-waveband monitoring during strong gamma-ray activity. *ApJ*, **710**, L126.

[550] Blinov D., Pavlidou V., Papadakis I. *et al.* (2016). RoboPol: Do optical polarization rotations occur in all blazars? *MNRAS*, **462**, 1775.

[551] Meyer M., Conrad J. & Dickinson H. (2016). Sensitivity of the Cherenkov Telescope Array to the detection of intergalactic magnetic fields. *ApJ*, **827**, 147.

[552] Pinzke A. & Pfrommer C. (2010). Simulating the γ-ray emission from galaxy clusters: A universal cosmic ray spectrum and spatial distribution. *MNRAS*, **409**, 449.

[553] Zandanel F., Pfrommer C. & Prada F. (2014). On the physics of radio haloes in galaxy clusters: Scaling relations and luminosity functions. *MNRAS*, **438**, 124.

[554] Ahnen M.L., Ansoldi S., Antonelli L.A. *et al.* (2016). Deep observation of the NGC 1275 region with MAGIC: Search of diffuse γ-ray emission from cosmic rays in the Perseus cluster. *A&A*, **589**, A33.

[555] Brunetti G., Venturi T., Dallacasa D. *et al.* (2007). Cosmic rays and radio halos in galaxy clusters: New constraints from radio observations. *ApJl*, **670**, L5.

[556] Ackermann M., Ajello M., Albert A. *et al.* (2014). Search for cosmic-ray-induced gamma-Ray emission in galaxy clusters. *ApJ*, **787**, 18.

[557] Voit G.M. (2005). Tracing cosmic evolution with clusters of galaxies. *Rev. Mod. Phys.*, **77**, 207.

[558] Forman W., Churazov E., David L. *et al.* (2003). A high angular resolution view of hot gas in clusters, groups, and galaxies. arXiv:0301476.

[559] Miniati F. & Beresnyak A. (2015). Self-similar energetics in large clusters of galaxies. *Nature*, **523**, 59.

[560] Brunetti G. & Jones T.W. (2014). Cosmic rays in galaxy clusters and their nonthermal emission. *Int. J. Mod. Phys. D*, **23**, 1430007.

[561] Feretti L., Giovannini G., Govoni F. *et al.* (2012). Clusters of galaxies: Observational properties of the diffuse radio emission. *A&A Rev.*, **20**, 54.

[562] Berezinsky V.S., Blasi P. & Ptuskin V.S. (1997). Clusters of galaxies as storage room for cosmic rays. *ApJ*, **487**, 529.

[563] Blasi P. & Colafrancesco S. (1999). Cosmic rays, radio halos and nonthermal X-ray emission in clusters of galaxies. *Astropart. Phys.*, **12**, 169.

[564] Pfrommer C., Enßlin T.A. & Springel V. (2008). Simulating cosmic rays in clusters of galaxies — II. A unified scheme for radio haloes and relics with predictions of the γ-ray emission. *MNRAS*, **385**, 1211.

[565] Blasi P. (2001). The non-thermal radiation-cluster merger connection. *Astropart. Phys.*, **15**, 223.

[566] Inoue S., Aharonian F.A. & Sugiyama N. (2005). Hard X-ray and gamma-ray emission induced by ultra-high-energy protons in cluster accretion shocks. *ApJl*, **628**, L9.

[567] Vannoni G., Aharonian F.A., Gabici S. *et al.* (2011). Acceleration and radiation of ultra-high energy protons in galaxy clusters. *A&A*, **536**, A56.

[568] Armengaud E., Sigl G. & Miniati F. (2006). Secondary gamma rays from ultrahigh energy cosmic rays produced in magnetized environments. *Phys. Rev. D*, **73**, 8, 083008.

[569] Kotera K., Allard D., Murase K. *et al.* (2009). Propagation of ultrahigh energy nuclei in clusters of galaxies: Resulting composition and secondary emissions. *ApJ*, **707**, 370.

[570] Kelner S.R. & Aharonian F.A. (2008). Energy spectra of gamma rays, electrons, and neutrinos produced at interactions of relativistic protons with low energy radiation. *Phys. Rev. D*, **78**, 3, 034013.

[571] Croston J.H., Pratt G.W., Böhringer H. *et al.* (2008). Galaxy-cluster gas-density distributions of the representative XMM-Newton cluster structure survey (REXCESS). *A&A*, **487**, 431.

[572] Brunetti G., Blasi P., Reimer O. *et al.* (2012). Probing the origin of giant radio haloes through radio and γ-ray data: The case of the Coma cluster. *MNRAS*, **426**, 956.

[573] Pinzke A., Oh S.P. & Pfrommer C. (2016). Turbulence and particle acceleration in giant radio haloes: The origin of seed electrons. arXiv:1611.07533.

[574] ZuHone J.A., Markevitch M., Brunetti G. *et al.* (2013). Turbulence and radio minihalos in the sloshing cores of galaxy clusters. *ApJ*, **762**, 78.

[575] Jacob S. & Pfrommer C. (2016). Cosmic ray heating in cool core clusters II: Self-regulation cycle and non-thermal emission. arXiv:1609.06322.

[576] Storm E.M., Jeltema T.E. & Profumo S. (2012). Gamma rays from star formation in clusters of galaxies. *ApJ*, **755**, 117.

[577] Persic M. & Rephaeli Y. (2012). Cosmic rays in star-forming galaxies. *J. Phys. Conf. Ser.*, **355**, 1, 012038.

[578] Aleksić J., Antonelli L.A., Antoranz P. *et al.* (2010). MAGIC gamma-ray telescope observation of the Perseus cluster of galaxies: Implications for cosmic rays, dark matter, and NGC 1275. *ApJ*, **710**, 634.

[579] Aleksić J., Antonelli L.A., Antoranz P. *et al.* (2010). Detection of very high energy γ-ray emission from the Perseus cluster head-tail galaxy IC 310 by the MAGIC telescopes. *ApJL*, **723**, L207.

[580] Aleksić J., Alvarez E.A., Antonelli L.A. *et al.* (2012). Detection of very-high energy γ-ray emission from NGC 1275 by the MAGIC telescopes. *A&A*, **539**, L2.

[581] Aleksić J., Ansoldi S., Antonelli L.A. *et al.* (2014). Contemporaneous observations of the radio galaxy NGC 1275 from radio to very high energy γ-rays. *A&A*, **564**, A5.

[582] Wouters D. & Brun P. (2013). Constraints on axion-like particles from X-ray observations of the Hydra galaxy cluster. *ApJ*, **772**, 44.

[583] Reimer O., Pohl M., Sreekumar P. *et al.* (2003). EGRET upper limits on the high-energy gamma-ray emission of galaxy clusters. *ApJ*, **588**, 155.

[584] Ackermann M., Ajello M., Allafort A. *et al.* (2010). Constraints on dark matter annihilation in clusters of galaxies with the Fermi large area telescope. *JCAP*, **5**, 025.

[585] Ackermann M., Ajello M., Allafort A. *et al.* (2010). GeV gamma-ray flux upper limits from clusters of galaxies. *ApJL*, **717**, L71.

[586] Jeltema T.E. & Profumo S. (2011). Implications of Fermi observations for hadronic models of radio halos in clusters of galaxies. *ApJ*, **728**, 53.

[587] Han J., Frenk C.S., Eke V.R. *et al.* (2012). Constraining extended gamma-ray emission from galaxy clusters. *MNRAS*, **427**, 1651.

[588] Ando S. & Nagai D. (2012). Fermi-LAT constraints on dark matter annihilation cross section from observations of the Fornax cluster. *JCAP*, **7**, 017.

[589] Huber B., Tchernin C., Eckert D. *et al.* (2013). Probing the cosmic-ray content of galaxy clusters by stacking Fermi-LAT count maps. *A&A*, **560**, A64.

[590] Zandanel F. & Ando S. (2014). Constraints on diffuse gamma-ray emission from structure formation processes in the Coma cluster. *MNRAS*, **440**, 663.

[591] Prokhorov D.A. & Churazov E.M. (2014). Counting gamma rays in the directions of galaxy clusters. *A&A*, **567**, A93.

[592] Vazza F. & Brüggen M. (2014). Do radio relics challenge diffusive shock acceleration? *MNRAS*, **437**, 2291.

[593] Griffin R.D., Dai X. & Kochanek C.S. (2014). New limits on gamma-ray emission from galaxy clusters. *ApJL*, **795**, L21.

[594] Selig M., Vacca V., Oppermann N. *et al.* (2015). The denoised, deconvolved, and decomposed Fermi γ-ray sky. An application of the D^{3}PO algorithm. *A&A*, **581**, A126.

[595] Vazza F., Eckert D., Brüggen M. *et al.* (2015). Electron and proton acceleration efficiency by merger shocks in galaxy clusters. *MNRAS*, **451**, 2198.

[596] Ackermann M., Ajello M., Albert A. *et al.* (2016). Search for gamma-ray emission from the Coma cluster with six years of Fermi-LAT data. *ApJ*, **819**, 149.

[597] Ackermann M., Ajello M., Albert A. *et al.* (2015). Search for extended gamma-ray emission from the Virgo galaxy cluster with Fermi-LAT. *ApJ*, **812**, 159.

[598] Perkins J.S., Badran H.M., Blaylock G. *et al.* (2006). TeV gamma-ray observations of the Perseus and Abell 2029 galaxy clusters. *ApJ*, **644**, 148.

[599] Perkins J.S. (2008). VERITAS observations of the Coma cluster of galaxies. In F.A. Aharonian, W. Hofmann & F. Rieger (editors), *American Institute of Physics Conference Series*, Vol. 1085, pp. 569–572.

[600] Aharonian F., Akhperjanian A.G., Anton G. *et al.* (2009). Very high energy gamma-ray observations of the galaxy clusters Abell 496 and Abell 85 with H.E.S.S. *A&A*, **495**, 27.

[601] Domainko W., Nedbal D., Hinton J.A. *et al.* (2009). New results from H.E.S.S. observations of galaxy clusters. *Int. J. Mod. Phys. D*, **18**, 1627.

[602] Galante N. for the VERITAS Collaboration (2009). Observation of radio galaxies and clusters of galaxies with VERITAS. arXiv:0907.5000.

[603] Kiuchi R., Mori M., Bicknell G.V. *et al.* (2009). CANGAROO-III search for TeV gamma rays from two clusters of galaxies. *ApJ*, **704**, 240.

[604] Acciari V.A., Aliu E., Arlen T. *et al.* (2009). VERITAS upper limit on the very high energy emission from the radio galaxy NGC 1275. *ApJL*, **706**, L275.

[605] Aleksić J., Alvarez E.A., Antonelli L.A. *et al.* (2012). Constraining cosmic rays and magnetic fields in the Perseus galaxy cluster with TeV observations by the MAGIC telescopes. *A&A*, **541**, A99.

[606] Arlen T., Aune T., Beilicke M. *et al.* (2012). Constraints on cosmic rays, magnetic fields, and dark matter from gamma-ray observations of the Coma cluster of galaxies with VERITAS and Fermi. *ApJ*, **757**, 123.

[607] Abramowski A., Acero F., Aharonian F. *et al.* (2012). Constraints on the gamma-ray emission from the cluster-scale AGN outburst in the Hydra A galaxy cluster. *A&A*, **545**, A103.

[608] Ando S. & Nagai D. (2008). Gamma-ray probe of cosmic ray pressure in galaxy clusters and cosmological implications. *MNRAS*, **385**, 2243.

[609] Churazov E., Forman W., Jones C. *et al.* (2003). XMM-newton observations of the Perseus Cluster. I. The temperature and surface brightness structure. *ApJ*, **590**, 225.

[610] Pedlar A., Ghataure H.S., Davies R.D. *et al.* (1990). The radio structure of NGC1275. *MNRAS*, **246**, 477.

[611] Gitti M., Brunetti G. & Setti G. (2002). Modeling the interaction between ICM and relativistic plasma in cooling flows: The case of the Perseus cluster. *A&A*, **386**, 456.

[612] Charles E., Sánchez-Conde M., Anderson B. *et al.* (2016). Sensitivity projections for dark matter searches with the Fermi Large Area Telescope. *Phys. Rep.*, **636**, 1.

[613] Reiprich T.H. & Böhringer H. (2002). The mass function of an X-ray flux-limited sample of galaxy clusters. *ApJ*, **567**, 716.

[614] Vazza F., Brüggen M., Wittor D. *et al.* (2016). Constraining the efficiency of cosmic ray acceleration by cluster shocks. *MNRAS*, **459**, 70.

[615] Kushnir D. & Waxman E. (2009). Nonthermal emission from clusters of galaxies. *JCAP*, **8**, 002.

[616] Bonafede A., Feretti L., Murgia M. *et al.* (2010). The Coma cluster magnetic field from Faraday rotation measures. *A&A*, **513**, A30+.

[617] Bonafede A., Vazza F., Brüggen M. *et al.* (2013). Measurements and simulation of Faraday rotation across the Coma radio relic. *MNRAS*, **433**, 3208.

[618] Röttgering H., Afonso J., Barthel P. *et al.* (2011). LOFAR and APERTIF surveys of the radio sky: Probing shocks and magnetic fields in galaxy clusters. *J. Astrophys. Astron.*, **32**, 557.

[619] Govoni F., Murgia M., Xu H. *et al.* (2013). Polarization of cluster radio halos with upcoming radio interferometers. *A&A*, **554**, A102.

[620] Bonafede A., Vazza F., Brüggen M. *et al.* (2015). Unravelling the origin of large-scale magnetic fields in galaxy clusters and beyond through Faraday Rotation Measures with the SKA. *Advancing Astrophysics with the Square Kilometre Array (AASKA14)*, 95.

[621] Enßlin T., Pfrommer C., Miniati F. *et al.* (2011). Cosmic ray transport in galaxy clusters: Implications for radio halos, gamma-ray signatures, and cool core heating. *A&A*, **527**, A99+.

[622] Wiener J., Oh S.P. & Guo F. (2013). Cosmic ray streaming in clusters of galaxies. *MNRAS*, **434**, 2209.

[623] Govoni F. & Feretti L. (2004). Magnetic fields in clusters of galaxies. *Int. J. Mod. Phys. D*, **13**, 1549.

[624] Clarke T.E. (2004). Faraday rotation observations of magnetic fields in galaxy clusters. *Journal of Korean Astronomical Society*, **37**, 337.

[625] Enßlin T.A. & Vogt C. (2006). Magnetic turbulence in cool cores of galaxy clusters. *A&A*, **453**, 447.

[626] Kuchar P. & Enßlin T.A. (2011). Magnetic power spectra from Faraday rotation maps. REALMAF and its use on Hydra A. *A&A*, **529**, A13+.

[627] Domínguez A., Primack J.R., Rosario D.J. *et al.* (2011). Extragalactic background light inferred from AEGIS galaxy-SED-type fractions. *MNRAS*, **410**, 2556.

[628] Sijbring L.G. (1993). *A Radio Continuum and HI Line Study of the Perseus Cluster*. Ph.D. thesis, Groningen University.

[629] Juliusson E., Meyer P. & Müller D. (1972). Composition of cosmic-ray nuclei at high energies. *Physical Review Letters*, **29**, 7, 445.

[630] Garcia-Munoz M., Mason G.M. & Simpson J.A. (1975). The isotopic composition of Galactic cosmic-ray lithium, beryllium, and boron. *ApJ*, **201**, L145.

[631] KASCADE-Grande Collaboration, Apel W.D. *et al.* (2013). KASCADE-Grande measurements of energy spectra for elemental groups of cosmic rays. *Astropart. Phys.*, **47**, 54.

[632] Kieda D., Swordy S. & Wakely S. (2001). A high resolution method for measuring cosmic ray composition beyond 10 TeV. *Astropart. Phys.*, **15**, 3, 287.

[633] Aharonian F., Akhperjanian A., Bazer-Bachi A. *et al.* (2007). First ground-based measurement of atmospheric Cherenkov light from cosmic rays. *Phys. Rev. D*, **75**, 4, 042004.

[634] Wissel S.A. (2010). Observations of direct Cerenkov light in ground-based telescopes and the flux of iron nuclei at TeV energies. ProQuest Dissertations And Theses; Thesis (Ph.D.) — The University of Chicago.

[635] Aharonian F.A., Atoyan A.M. & Voelk H.J. (1995). High energy electrons and positrons in cosmic rays as an indicator of the existence of a nearby cosmic tevatron. *A&A*, **294**, L41.

[636] Kobayashi T., Komori Y., Yoshida K. *et al.* (2004). The most likely sources of high-energy cosmic-ray electrons in supernova remnants. *ApJ*, **601**, 340.

[637] Abdo A.A., Ackermann M., Ajello M. *et al.* (2009). Measurement of the cosmic ray $e^+ + e^-$ spectrum from 20 GeV to 1 TeV with the Fermi Large Area Telescope. *Physical Review Letters*, **102**, 18, 181101.

[638] Adriani O., Barbarino G.C., Bazilevskaya G.A. *et al.* (2011). Cosmic-ray electron flux measured by the PAMELA Experiment between 1 and 625 GeV. *Physical Review Letters*, **106**, 20, 201101.

[639] Aguilar M., Aisa D., Alvino A. *et al.* (2014). Electron and positron fluxes in primary cosmic rays measured with the Alpha Magnetic Spectrometer on the International Space Station. *Physical Review Letters*, **113**, 12, 121102.

[640] Abdollahi S., Ackermann M., Ajello M. *et al.* (2017). Cosmic-ray electron-positron spectrum from 7 GeV to 2 TeV with the Fermi Large Area Telescope. *Phys. Rev. D*, **95**, 082007.

[641] Malyshev D., Cholis I. & Gelfand J. (2009). Pulsars versus dark matter interpretation of ATIC/PAMELA. *Phys. Rev. D*, **80**, 6, 063005.

[642] Adriani O., Barbarino G.C., Bazilevskaya G.A. *et al.* (2009). An anomalous positron abundance in cosmic rays with energies 1.5-100GeV. *Nature*, **458**, 607.

[643] Aguilar M., Alberti G., Alpat B. *et al.* (2013). First result from the Alpha Magnetic Spectrometer on the International Space Station: Precision measurement of the positron fraction in primary cosmic rays of 0.5-350 GeV. *Physical Review Letters*, **110**, 14, 141102.

[644] Borla Tridon D. (2011). Measurement of the cosmic electron spectrum with the MAGIC telescopes. *International Cosmic Ray Conference*, **6**, 47.

[645] Staszak D. for the VERITAS Collaboration (2015). A cosmic-ray electron spectrum with VERITAS. *Proc. 34th ICRC*, The Hague, Netherlands.

[646] Parsons R.D. (2011). *Towards a Measurement of the Cosmic Ray Electron Spectrum at the Highest Energies, using the Next-Generation Cherenkov Array CTA*. Ph.D. thesis, University of Leeds.

[647] Gaug M., Berge D., Daniel M. *et al.* (2014). Calibration strategies for the Cherenkov Telescope Array. In *Observatory Operations: Strategies, Processes, and Systems V*, *Proc. SPIE*, Vol. 9149, p. 914919.

[648] Parsons R.D., Hinton J.A. & Schoorlemmer H. (2016). Calibration of the Cherenkov Telescope Array using cosmic ray electrons. *Astropart. Phys.*, **84**, 23.

[649] d'Enterria D., Engel R., Pierog T. *et al.* (2011). Constraints from the first LHC data on hadronic event generators for ultra-high energy cosmic-ray physics. *Astropart. Phys.*, **35**, 98.

[650] Marrocchesi P.S. (2015). CALET: A high energy astroparticle physics experiment on the ISS. arXiv:1512.08059.

[651] Brown R.H. (1974). *The Intensity Interferometer: Its Application to Astronomy*, (Halsted Press).

[652] Tuthill P.G. (2014). The narrabri stellar intensity interferometer: A 50th birthday tribute. *Proc. SPIE*, Vol. 9146, pp. 91460C–91460C–7.

[653] Le Bohec S. & Holder J. (2006). Optical intensity interferometry with atmospheric Cerenkov telescope arrays. *ApJ*, **649**, 399.

[654] Dravins D. & LeBohec S. (2008). Toward a diffraction-limited square-kilometer optical telescope: Digital revival of intensity interferometry. In *Society of Photo-Optical Instrumentation Engineers (SPIE) Conference Series*, Vol. 6986.

[655] Nuñez P.D., Holmes R., Kieda D. *et al.* (2012). High angular resolution imaging with stellar intensity interferometry using air Cherenkov telescope arrays. *MNRAS*, **419**, 172.

[656] Dravins D. & Lagadec T. (2014). Stellar intensity interferometry over kilometer baselines: Laboratory simulation of observations with the Cherenkov Telescope Array. In *Optical and Infrared Interferometry IV*, *Proc. SPIE*, Vol. 9146, p. 91460Z.

[657] Lacki B.C. (2014). On the use of Cherenkov telescopes for outer solar system body occultations. *MNRAS*, **445**, 1858.

[658] Hanna D.S., Ball J., Covault C.E. *et al.* (2009). OSETI with STACEE: A search for nanosecond optical transients from nearby stars. *Astrobiology*, **9**, 345.

[659] Abeysekara A.U., Archambault S., Archer A. *et al.* (2016). A search for brief optical flashes associated with the SETI target KIC 8462852. *ApJ*, **818**, L33.

[660] Heck D., Knapp J., Capdevielle J. *et al.*. *Corsika a monte-carlo code to simulate extensive air showers*. Report FZKA 6019 (1998), Forschungszentrum Karlsruhe; https://web.ikp.kit.edu/corsika/physics_description/corsika_phys.pdf.

[661] Bernlöhr K. (2008). Simulation of imaging atmospheric Cherenkov telescopes with CORSIKA and sim_ telarray. *Astropart. Phys.*, **30**, 149.

[662] Hassan T., Arrabito L., Bernlör K. *et al.* (2015). Second large-scale Monte Carlo study for the Cherenkov Telescope Array. arXiv:1508.06075.

Glossary

AGILE	Astro-rivelatore Gamma a Immagini LEggero
AGN	Active Galactic Nuclei
ALMA	Atacama Large Millimetre/Submillimetre Array
ALP	Axion-like Particle
AMON	Astrophysical Multimessenger Observatory Network
AMS	Alpha Magnetic Spectrometer
ANTARES	Astronomy with a Neutrino Telescope and Abyss environmental RESearch
APEX	Atacama Pathfinder EXperiment
ARGO-YBJ	Astrophysical Radiation with Ground-based Observatory at YangBaJing
ARGOS	Advanced Rayleigh Guided Ground Layer Adaptive Optics System
ASKAP	Australian Square Kilometre Array Pathfinder
ATCA	Australia Telescope Compact Array
ATNF	Australia Telescope National Facility
ATOM	Automated Telescope for Optical Monitoring
BH	Black Hole
BL Lac	BL-Lacertae
BLR	Broad Line Region
BRAVA	Bulge Radial Velocity Assay
CANGAROO	Collaboration of Australia and Nippon (Japan) for a GAmma Ray Observatory in the Outback
CAS	Chinese Academy of Sciences
CDM	Cold Dark Matter

CMB	Cosmic Microwave Background
CMR	Circum-nuclear Ring
CMZ	Central Molecular Zone
CP	Charge Parity
CR	Cosmic Ray
CREAM	Cosmic Ray Energetics and Mass
CSM	Circumstellar Medium
CTA	Cherenkov Telescope Array
CTAC	CTA Consortium
CWB	Colliding-Wind Binary
DATE5	Dome A Terahertz Explorer 5 m
DM	Dark Matter
dSph	Dwarf Spheroidal Galaxy
E-ELT	European Extremely Large Telescope
EAGLE	Evolution and Assembly of GaLaxies and their Environments
EBL	Extragalactic Background Light
EGRET	Energetic Gamma Ray Experiment Telescope
EGS	Extragalactic Survey
EHBL	Extremely-high-frequency peaked BL Lacertae
EM	Electromagnetic
eMERLIN	Multi-Element Radio Linked Interferometer Network
eROSITA	extended ROentgen Survey with an Imaging Telescope Array
ESA	European Space Agency
Fermi-GBM	Fermi Gamma-ray Burst Monitor
Fermi-LAT	Fermi Large Area Telescope
FITS	Flexible Image Transport System
FoV	Field of View
FP7	Framework Programme 7
FRB	Fast Radio Burst
FSRQ	Flat Spectrum Radio Quasar
GAIA	Globales Astronomisches Interferometer für die Astrophysik
GC	Galactic Centre
GCN	Gamma-ray Burst Coordinate Network
GIBS	GIRAFFE Inner Bulge Survey
GMRT	Giant Metrewave Radio Telescope
GMT	Giant Magellan Telescope

GO	Guest Observer
GPS	Galactic Plane Survey
GRB	Gamma-ray Burst
GVD	Gigaton Volume Detector
GW	Gravitational Wave
H.E.S.S.	High Energy Stereoscopic System
HAWC	High Altitude Water Cherenkov
HBL	High-frequency peaked BL Lac
HE	High Energy
HEASARC	High Energy Astrophysics Science Archive Research Center
HEAT	High Elevation Antarctic Terahertz telescope
HEGRA	High Energy Gamma Ray Astronomy
HST	Hubble Space Telescope
HXMT	Hard X-ray Modulation Telescope
IACT	Imaging Atmospheric Cherenkov Telescope
IBL	Intermediate-frequency peaked BL Lacertae
IC	Inverse Compton
ICM	Intra-cluster Medium
IGMF	Intergalactic Magnetic Field
INTEGRAL	International Gamma-Ray Astrophysics Laboratory
iPTF	intermediate Palomar Transient Factory
IR	Infrared
IRAM	Institut de Radioastronomie Millimétrique
IRAS	Infrared Astronomical Satellite
IRF	Instrument Response Functions
ISM	Interstellar Medium
ISS	International Space Station
JEM/EUSO	Japanese Experiment Module/Extreme Universe Space Observatory
JVLA	Jansky Very Large Array
JWST	James Webb Space Telescope
KAGRA	Kamioka Gravitational Wave Detector
KASCADE	Karlsruhe Shower Core and Array Detector
KM3Net	Cubic Kilometre Neutrino Telescope
KSP	Key Science Project
LBL	Low-frequency peaked BL Lacertae
LEP	Large Electron-Positron Collider
LF	Luminosity Function

LHAASO	Large High Altitude Air Shower Observatory
LHC	Large Hadron Collider
LIGO	Laser Interferometer Gravitational-wave Observatory
LIV	Lorentz Invariance Violation
LLAGN	Low-luminosity Active Galactic Nucleus
LMC	Large Magellanic Cloud
LOBO	Low Band Observatory
LOBSTER	Large-angle OBServaTory with Energy Resolution
LOFAR	Low Frequency Array
LOFT	Large Observatory for X-ray Timing
LOS	Line of Sight
LSP	Lightest Supersymmetric Particle
LSST	Large Synoptic Survey Telescope
LST	Large Sized Telescope
LTP	Long-term Program
MAGIC	Major Atmospheric Gamma-Ray Imaging Cherenkov Telescopes
MAXI	Monitor of All-sky X-ray Image
MC	Monte Carlo
MeerKAT	Karoo Array Telescope
Milagro	Milagro Gamma Ray Observatory
MM	Multi-messenger
MOPRA	Mopra Radio Telescope
MoUs	Memoranda of Understanding
MST	Medium Sized Telescope
MUSE	Multi Unit Spectroscopic Explorer
MW	Milky Way
MWA	Murchison Widefield Array
MWL	Multi-wavelength
NASA	National Aeronautics and Space Administration
NFW	Navarro, Frenk and White
NICER	Neutron star Interior Composition ExploreR
NIR	Near Infrared
NLSy1	Narrow-Line Seyfert 1 Galaxy
NS	Neutron Star
NuSTAR	Nuclear Spectroscopic Telescope Array
OIR	Optical/Infrared
OSETI	Optical Search for Extraterrestrial Intelligence
OVRO	Owens Valley Radio Observatory

PAMELA	Payload for Antimatter Matter Exploration and Light-nuclei Astrophysics
Pan-STARRS	Panoramic Survey Telescope and Rapid Response System
PANGU	PAir-productioN Gamma-ray Unit
PILOT	Polarized Instrument for Long Wavelength Observations of the Tenuous ISM
pMSSM	Phenomenological Minimal Supersymmetric Model
PSF	Point Spread Function
PWN	Pulsar Wind Nebula
QCD	Quantum Chromodynamics
RA/Dec	Right Ascension/Declination
RoboPol	ROBOtic POLarimeter
ROSAT	ROntgen SATellite
RTA	Real-time Analysis
RXTE	Rossi X-ray Timing Explorer
SCT	Schwarzschild-Couder Telescope
SED	Spectral Energy Distribution
SFR	Star-Formation Rate
SFS	Star-Forming System
SKA	Square Kilometre Array
SM	Standard Model
SMBH	Supermassive Black Hole
SMC	Small Magellanic Cloud
SMEX	Small Explorer
SN	Supernova
SNR	Supernova Remnant
SSC	Synchrotron Self Compton
SST	Small Sized Telescope
STAC	Scientific and Technical Advisory Committee
STP	Short-term Program
SUSY	Supersymmetry
SVOM	Space Variable Objects Monitor
Swift-BAT	Swift Burst Alert Telescope
TA	Telescope Array
TDE	Tidal Disruption Event
TF	Transient Factory
TMT	Thirty Meter Telescope
ToO	Target of Opportunity
TOTEM	Total, elastic and diffractive cross-section measurement

UHBL	Ultra High-frequency peaked BL Lacertae
UHECR	Ultra High-Energy Cosmic Ray
ULIRG	Ultraluminous Infrared Galaxy
UV	Ultraviolet
VERITAS	Very Energetic Radiation Imaging Telescope Array System
VHE	Very High-Energy
VIB	Virtual Internal Bremsstrahlung
VISTA	Visible and Infrared Survey Telescope for Astronomy
VLBI	Very Long Baseline Interferometry
VLITE	VLA Low Frequency Ionosphere Transient Experiment
VLT	Very Large Telescope
VOEvent	Virtual Observatory Event
WHIPPLE	Fred Lawrence Whipple Observatory
WIMP	Weakly Interacting Massive Particle
WMAP	Wilkinson Microwave Anisotropy Probe
WSRT	Westerbork Synthesis Radio Telescope
XMM	X-ray Multi Mirror
XTP	X-ray Timing and Polarization mission
ZTF	Zwicky Transient Facility